VOLUME 14 NUMBERS 1, 2, 3 and 4

REACTOR SCIENCE AND TECHNOLOGY

JOURNAL OF NUCLEAR ENERGY PARTS A & B

Editor-in-chief

J. V. DUNWORTH

OL.
14
961

GENERAL EDITORS

J. GUÉRON G. RANDERS

EXECUTIVE EDITORS

G. W. K. FORD (U.K.) D. J. LITTLER (U.K.) W. K. ERGEN (U.S.A.)

EDITORIAL ADVISORY BOARD

T. E. ALLIBONE—Aldermaston
J. P. BAXTER—Sydney
H. J. BHABHA—Bombay
T. BJERGE—Röskilde
H. BRYNIELSSON—Stockholm
Sir JOHN COCKCROFT—Cambridge
Sir WILLIAM COOK—London
R. C. DALZELL—Washington
S. EKLUND—Stockholm
H. M. FINNISTON—Newcastle
J. GOENS—Mol-Donk
M. DE HEMPTINNE—Louvain
N. HILBERRY—Argonne
J. HOROWITZ—Saclay
F. IPPOLITO—Rome
G. C. LAURENCE—Chalk River
W. B. LEWIS, Chalk River
J. F. LOUTIT—Harwell
P. NOWACKI—Warsaw
J. M. OTERO—Madrid
Sir LEONARD OWEN—Risley
R. E. PEIERLS—Birmingham
F. PERRIN—Paris
L. ROTHERHAM—London
C. SALVETTI—Vienna
C. STARR—Canoga Park
J. F. ULRICH—Lisbon
ALVIN M. WEINBERG—Oak Ridge
J. J. WENT—Arnhem
K. WIRTZ—Karlsruhe
W. H. ZINN—Florida
W. J. ZUNTI—Zürich

Pergamon Press

LONDON OXFORD NEW YORK PARIS

REACTOR SCIENCE AND TECHNOLOGY

(Journal of Nuclear Energy Parts A & B)

EDITOR-IN-CHIEF

J. V. DUNWORTH: *Atomic Energy Establishment, Winfrith, Dorchester, Dorset*

GENERAL EDITORS

J. GUÉRON: *Brussels* G. RANDERS: *Lillestrøm*

EXECUTIVE EDITORS

G. W. K. FORD: (Engineering) *Atomic Energy Establishment, Winfrith, Dorchester, Dorset*
D. J. LITTLER: (Physics) *Central Electricity Generating Board, Friars House, Blackfriars Road, London S.E. 1*
W. K. ERGEN: *Oak Ridge National Laboratory, Oak Ridge, Tenn., U.S.A.*

EDITORIAL ADVISORY BOARD

T. E. ALLIBONE—Aldermaston
J. P. BAXTER—Sydney
H. J. BHABHA—Bombay
T. BJERGE—Röskilde
H. BRYNIELSSON—Stockholm
SIR JOHN COCKCROFT—London
Sir WILLIAM COOK—London
R. C. DALZELL—Washington
S. EKLUND—Stockholm
H. M. FINNISTON—Newcastle
J. GOENS—Brussels
L. J. HAWORTH—Brookhaven
M. DE HEMPTINNE—Louvain
N. HILBERRY—Argonne
J. HOROWITZ—Saclay
F. IPPOLITO—Rome
G. C. LAURENCE—Chalk River
W. B. LEWIS—Chalk River
J. F. LOUTIT—Harwell
P. NOWACKI—Warsaw
J. M. OTERO—Madrid
Sir LEONARD OWEN—Risley
R. E. PEIERLS—Birmingham
F. PERRIN—Paris
L. ROTHERHAM—London
C. SALVETTI—Vienna
C. STARR—Canoga Park
J. F. ULRICH—Lisbon
ALVIN M. WEINBERG—Oak Ridge
J. J. WENT—Arnhem
K. WIRTZ—Karlsruhe
W. H. ZINN—Florida
W. J. ZUNTI—Zürich

Sub-editor: P. C. GROOMS, Journals Dept., Pergamon Press Ltd., 4 Fitzroy Square, London W.1

Pergamon Press also publish the following International Research Journals of interest to persons associated with the fields of Nuclear Energy and Thermonuclear Research

J.N.E. 'C' JOURNAL OF NUCLEAR ENERGY PART C: PLASMA PHYSICS—ACCELERATORS—THERMONUCLEAR RESEARCH*
J.A.R.I. INTERNATIONAL JOURNAL OF APPLIED RADIATION AND ISOTOPES
J.I.N.C. JOURNAL OF INORGANIC AND NUCLEAR CHEMISTRY
HEALTH PHYSICS (*The official Journal of the Health Physics Society*)

* This Journal also publishes translations of the relevant papers of *Atomnaya Energiya* on behalf of the Pergamon Institute, a Division of the Pergamon International Corporation at Headington Hill Hall, Headington, Oxon.

Pergamon Press are also the publishers of the following journals

TETRAHEDRON (*The International Journal of Organic Chemistry*)
TETRAHEDRON LETTERS
TALANTA (*An International Journal of Analytical Chemistry*)
BIOCHEMICAL PHARMACOLOGY
†BIOPHYSICS
†JOURNAL OF MICROBIOLOGY, EPIDEMIOLOGY, AND IMMUNOBIOLOGY
†PROBLEMS OF ONCOLOGY
†PROBLEMS OF VIROLOGY
†PROBLEMS OF HEMATOLOGY AND BLOOD TRANSFUSION
†SECHENOV PHYSIOLOGICAL JOURNAL OF THE U.S.S.R.
†ELECTRIC TECHNOLOGY, U.S.S.R.
†RADIO ENGINEERING
†RADIO ENGINEERING AND ELECTRONICS
†TELECOMMUNICATIONS
†PHYSICS OF METALS AND METALLOGRAPHY
†THE ABSTRACTS JOURNAL OF METALLURGY
†APPLIED MATHEMATICS AND MECHANICS
†PAVLOV JOURNAL OF HIGHER NERVOUS ACTIVITY
†SOVIET TECHNOLOGY DIGEST
CHEMICAL ENGINEERING SCIENCE
JOURNAL OF ATMOSPHERIC AND TERRESTRIAL PHYSICS
PLANETARY AND SPACE SCIENCE
GEOCHIMICA ET COSMOCHIMICA ACTA
ANNALS OF THE INTERNATIONAL GEOPHYSICAL YEAR
SPECTROCHIMICA ACTA
JOURNAL OF THE MECHANICS AND PHYSICS OF SOLIDS
ACTA METALLURGICA
(*for the Board of Governors of Acta Metallurgica*)
INTERNATIONAL JOURNAL OF THE PHYSICS AND CHEMISTRY OF SOLIDS
DEEP-SEA RESEARCH
JOURNAL OF NEUROCHEMISTRY
JOURNAL OF PSYCHOSOMATIC RESEARCH
JOURNAL OF INSECT PHYSIOLOGY
JOURNAL OF AIR POLLUTION
INTERNATIONAL ABSTRACTS OF BIOLOGICAL SCIENCES
(*for Biological and Medical Abstracts Ltd.*)
RHEOLOGY ABSTRACTS
GEOLOGICAL ABSTRACTS
VACUUM
OPERATIONAL RESEARCH QUARTERLY
ANNALS OF OCCUPATIONAL HYGIENE
ARCHIVES OF ORAL BIOLOGY
ELECTROCHIMICA ACTA
HUMAN FACTORS
SOLID-STATE ELECTRONICS
JOURNAL OF SMALL ANIMAL PRACTICE
JOURNAL OF CHILD PSYCHOLOGY AND PSYCHIATRY
COMPARATIVE BIOCHEMISTRY AND PHYSIOLOGY

† Translations of Russian journals published on behalf of the Pergamon Institute, a Division of the Pergamon International Corporation

Leaflets giving further details and subscription rates for each of these journals are available on request

PERGAMON PRESS LTD.

4 FITZROY SQUARE, LONDON W.1
122 EAST 55TH STREET, NEW YORK 22, N.Y.
HEADINGTON HILL HALL, OXFORD
24 RUE DES ECOLES, PARIS V^e

VOL
14
196

LIST OF CONTENTS

NUMBER 1

W. S. BLACKBURN: Creep buckling of stacked fuel elements 1

R. S. BRUCE and T. E. F. CARR: Studies in the metabolism of carrier-free radioruthenium—I. Preliminary investigations 9

M. REIER and J. A. DE JUREN: Diffusion length of thermal neutrons in water from 23°C to 244°C . . 18

E. R. MOSBURG, JR. and W. M. MURPHEY: A recalibration of the NBS standard thermal neutrón flux . 25

L. R. BLAKE: Achieving high burn-up in fast reactors 31

Letters to the Editors

R. BERTRAND: Dosage au moyen de la spectrométrie alpha du ^{239}Pu dans un échantillon d'uranium naturel irradié 49

D. S. POPPLEWELL: The specific alpha activity and half-life of ^{233}U 50

J. ADAM and M. D. ROGERS: X-ray diffraction studies of fission fragment damage in uranium carbide and nitride 51

R. DAHLBERG, K. JIRLOW and E. JOHANSSON: Measurements of some resonance activation integrals . . 53

Translations from *Atomnaya Energiya*

I. I. BONDARENKO and YU. YA. STAVISSKII: Pulsed operation of a fast reactor 55

Letters to the Editors

V. P. SHVEDOV, M. I. ZHILKINA, V. K. ZINOV'EVA, L. M. IVANOVA, T. P. MAKAROVA and N. A. PAVLOVA: Fall-out of ^{90}Sr in the Leningrad region 59

V. P. SHVEDOV, G. V. YAKOVLEVA, M. I. SHILKINA and T. P. MAKAROVA: The dose of external gamma-radiation from the fall-out of certain fission products 59

A. A. BIBERGAL: A new graphical method of calculating the dose field of extended sources 60

W. SANTHOLZER: Fall-out after the cessation of nuclear weapon tests 63

L. I. GEDEONOV, V. P. SHVEDOV and G. V. YAKOVLEVA: Calculation of the dose of external γ-radiation from the fall-out of radioactive fission products 64

Abstracts and Titles of Future Papers (*Atomnaya Energiya*) 67

NUMBERS 2/3

J. L. PERKIN and R. F. COLEMAN: Cross-sections for the $(n,2n)$ reactions of ^{232}Th, ^{238}U and ^{237}Np with 14 MeV neutrons 69

N. T. KASHUKEEV, YU. P. POPOV and F. L. SHAPIRO: Measurements of the energy dependence of the cross-section of the $Cl(n,\gamma)$ reaction 76

B. ADAMS, R. BATCHELOR and T. S. GREEN: The energy dependence of the fission cross-sections of ^{238}U, ^{233}U and ^{239}Pu for neutrons in the energy range 12·6 to 20 MeV 85

J. W. WEALE, H. GOODFELLOW, M. H. MCTAGGART and M. L. MULLENDER: Measurements of the reaction rate distribution produced by a source of 14 MeV neutrons at the centre of a uranium metal pile . . . 91

K. W. ALLEN, P. BOMYER and J. L. PERKIN: The interaction of 14 MeV neutrons with uranium . . . 100

W. S. BLACKBURN: The effect of internal stresses due to irradiation growth and thermal cycling on the creep of uranium, in the cases of both elastic and plastic behaviour 107

Book Review 117

Translations from *Atomnaya Energiya*

L. V. GROSHEV and A. M. DEMIDOV: $M1$ transitions from highly-excited states 118

T. N. ZUBAREV: Stability of the heat output from a pulsed reactor 124

A. G. SAMARTSEVA: Electrolytic separation of small quantities of uranium, neptunium, plutonium and americium 127

Letters to the Editors

N. P. GALKIN, N. E. GORIAINOV, V. B. TIKHOMIROV and V. D. FEDOROV: The mechanism of distribution of liquids in a plate extractor 132

S. L. RIVKIN: The density of heavy water 133

D. L. TIMROT and K. F. SHUISKAIA: The viscosity of heavy water 135

VOL. 14 1961

S. L. Rivkin and B. N. Egorov: The specific heat of heavy water 137
M. Z. Maksimov: A possible method of increasing the yields of nuclear reactions in thin targets . . 139
Iu. V. Gofman, O. F. Nemets and V. V. Tokarevskii: The spectra of neutrons scattered by oxygen, antimony and chromium 140
V. S. Grammatikati, U. Ya. Margulis and V. G. Khrushchev: The dose field of a line source . . 141
Errata 143

NUMBER 4

R. S. Bruce and T. E. F. Carr: Studies in the metabolism of carrier-free radioruthenium—II. The uptake of nitrosyl-ruthenium complexes from the gastrointestinal tract 145
A. C. Chamberlain, R. J. Garner and D. Williams: Environmental monitoring after accidental deposition of radioactivity 155
R. W. Deutsch: Method for analysing low-enrichment, light-water cores 168
A. V. Cohen: The non-elastic neutron cross-section for uranium at 13–19 MeV and beryllium at 14 MeV 180
M. Reier: The diffusion length of thermal neutrons in poisoned water 186
D. B. Wehmeyer and K. E. Roach: Nuclear safety of UO_3-ThO_2-H_2O systems 189
M. H. McKay: Resonance absorption in ^{239}Pu and its effect on the temperature coefficient of irradiated uranium rods 200
F. T. Adler and Y. D. Naliboff: A direct method for the evaluation of the resonance line shape functions 209

Letter to the Editors

M. H. McTaggart: The absorption of neutrons by the $^{16}O(n,\alpha)^{13}C$ reaction in an extended water moderator 212
Book Review 214
Abstracts and Titles of Future Papers (*Atomnaya Energiya*) 215
Notice 216

AUTHOR INDEX TO VOLUME 14

Adam, J. p. 51
Adams, B. p. 85
Adler, F. T. p. 209
Allen, K. W. p. 100
Batchelor, R. p. 85
Bertrand, R. p. 49
Bibergal, A. A. p. 60
Blackburn, W. S. pp. 1, 107
Blake, L. R. p. 31
Bomyer, P. p. 100
Bondarenko, I. I. p. 55
Bruce, R. S. pp. 9, 145
Carr, T. E. F. pp. 9, 145
Chamberlain, A. C. p. 155
Cohen, A. V. p. 180
Coleman, R. F. p. 69
Dahlberg, R. p. 53
Demidov, A. M. p. 118
Deutsch, R. W. p. 168
Egorov, B. N. p. 137
Fedorov, V. D. p. 132
Fonda, A. p. 118 (B.R.)
Galkin, N. P. p. 132
Garner, R. J. p. 155
Gedeonov, L. I. p. 64
Gofman, Iu. V. p. 140
Goodfellow, H. p. 91
Goriainov, N. E. p. 132
Grammatikati, V. S. p. 141
Green, T. S. p. 85
Groshev, L. V. p. 118
Guth, E. p. 214 (B.R.)
Ivanova, L. M. p. 59
Jirlow, K. p. 53
Johansson, E. p. 53
Juren, J. A. de p. 18
Kashukeev, N. T. p. 76
Khrushchev, V. G. p. 141
Makarova, T. P. p. 59
Maksimov, M. Z. p. 139
Margulis, U. Ya. p. 141
McKay, M. H. p. 200
McTaggart, M. H. pp. 91, 212
Mosburg, E. R. Jr. p. 25
Mullender, M. L. p. 91
Murphey, W. M. p. 25
Naliboff, Y. D. p. 209
Nemets, O. F. p. 140
Pavlova, N. A. p. 59
Perkin, J. L. pp. 69, 100
Popov, Yu. P. p. 76
Popplewell, D. S. p. 50
Reier, M. pp. 18, 186
Rivkin, S. L. pp. 133, 137
Roach, K. E. p. 189
Rogers, M. D. p. 51
Samartseva, A. G. p. 127
Santholzer, W. p. 63
Shapiro, F. L. p. 76
Shilkina, M. I. p. 59
Shuiskaia, K. F. p. 135
Shvedov, V. P. pp. 59, 64
Stavisskii, Yu. Ya. p. 55
Tikhomirov, V. B. p. 132
Timrot, D. L. p. 135
Tokarevskii, V. V. p. 140
Weale, J. W. p. 91
Wehmeyer, D. B. p. 189
Williams, D. p. 155
Yakovleva, G. V. pp. 59, 64
Zhilkina, M. I. p. 59
Zinov'eva, V. K. p. 59
Zubarev, T. N. p. 124

Note: (B.R.) indicates Book Review.

VOL
14
196

Reactor Science and Technology (J.N.E. Parts A/B), 1961, Vol. 14, pp. 1 to 8. Pergamon Press Ltd. Printed in Northern Ireland

CREEP BUCKLING OF STACKED FUEL ELEMENTS

W. S. BLACKBURN
Nuclear Research Centre, C. A. Parsons & Co. Ltd., Newcastle-upon-Tyne

(*Received* 30 *March* 1960)

Abstract—Equations are deduced from which bow in a rod forming part of an approximately vertical, pin-jointed column may be determined when there is slight tilt and initial bow in the rod and if the creep of the material under an applied load is known. The effect of the distribution of the weight and temperature is included. Using the experimentally determined form of the creep law for uranium being thermally cycled through ± 10°C, values are obtained for the time for uranium rods stacked approximately vertically in a channel to press tangentially against the side.

NOTATION

(χ, y, z)	Cartesian axes such that z-axis passes through the centroids of the cross-sections
t	time
T	temperature
λ, m	functions of z and t
v	displacement of a point parallel to the χ axis
P, X	vertical and horizontal forces
M	moment
S, I_z	area of the cross-section and its moment of inertia about the y-axis
w	applied uniaxial stress
$\dot{\epsilon}_{zz}$	rate of strain parallel to the z-axis
f	function of w and T
n, N, C, B	experimentally determined creep constants
L, a, c	length, radius and tilt of rod
ζ	z/L
K	function of ζ
V, V_0	$\int_0^\zeta v\,d\zeta, \int_0^\zeta v_0\,d\zeta$
d_i	constants representing initial bow
α_i	constants effecting increase of initial bow
f_i	eigenfunctions corresponding to α_i
β_i, γ	arbitrary constants
Λ	function of T
W	weight of rod
I_1, I_2	integrals defined by HANNAH (1956)
k	$B/(NT_1)$
μ	constant
T_1	centre temperature
V_A, V_B	solutions of equation (7) with $c = 0$, and with $V_0 = 0$ respectively
V_A^*, V_B^*	corresponding solutions of equation (18)
v_0	initial displacement
E	Young's modulus
r	number of rods whose weights are acting on the bottom of the rod under consideration.

INTRODUCTION

IN reactors such as those at Bradwell, creep deformation of the fuel elements may make it difficult to extract them from a channel after a time. To obtain an estimate of this time we are led to investigate the behaviour of a cylinder slightly tilted and with some small initial bow.

The buckling of columns due to creep has been treated by MARIN (1947) HOFF (1954) and other writers (further references are given by ODQUIST (1954)). For nuclear reactors the problem is complicated by:

(a) variations in macroscopic properties due to neutron irradiation or thermal cycling;

(b) non-uniform temperature distribution within the element; and

(c) the weight distribution of the element itself.

The first and second effects have been considered in several reports (ROBERTS and COTTRELL, 1956; ANDERSON and BISHOP, 1960; BLACKBURN *et al.*, 1960; KELLER, 1956; HANNAH, 1956) while the third was mentioned by GREENOUGH *et al.* (1958) for the case of uniform temperature.

In this report a differential equation is deduced which relates transverse displacement to a function, K, of the creep properties of a cross-section of the cylinder and a solution is obtained employing a general form of the creep law. To use this solution directly one would need a detailed knowledge of the distribution of the initial bow along the element and this is not normally available. One term of the solution, however, may be used to give the worst possible case for the buckling. From this simplification and the experimentally determined form of the creep law of uranium, results are obtained for a constant temperature distribution and for a ± ten degree thermal cycle on elements stacked in a vertical channel. The effects of elasticity are dealt with in an Appendix.

The theory may be applied to the case of uranium fuel elements tilted from one wall to the other of a channel when the angle of tilt is small and the end fittings are assumed to be incapable of sustaining bending moments.

When the initial bow is in the form of a sine wave,

and an element has a uniform cross-section there is initially point contact at the ends, but subsequently the top point of contact travels down the tube and hence contact may be lost at the bottom.

If spiders are added to the end fittings, the initial stage is similar to before, but it should be followed by a period in which there is point contact in a central region at a position which may move down the channel before splitting into two.

For given initial conditions of bow and tilt, the theory predicts the bow for times until the contact is no longer only at the ends. Since the initial conditions are not normally completely known we confine ourselves here to answering the question, for a given tilt and maximum initial bow: what is the shortest time it could take to attain another bow? For a bar of length L without spiders, the shapes of bow that increase at the greatest rate and that are formed due to the tilt of an initially straight rod resemble sine waves of period $2L$. Hence if the initial bow is of this form and the angle of tilt is c/L, it is of interest to know when its maximum will become c/π, since the bar cannot subsequently remain in contact only at the ends.

The problem should be approached in an inverse manner by plotting for appropriate times the maximum displacements v_A and v_B due to the initial bow and the tilt respectively. It is shown that v_A equals $\varepsilon e^{t/(\alpha_1 K)}$ where K is a constant depending on the geometry and creep behaviour and α_1, is an eigenvalue presented in Table 2 for several values of N and r, while v_B/C (where $v_B = \partial V_B/\partial\zeta$) is presented in Fig. 4 as a function of t/K for these values.

N is a constant such that under an applied stress w, the creep rate is Λw^N where Λ is a function of the temperature. Under thermal cycling or in conditions of appreciable irradiation growth N should be taken as 1, while if these effects are small it has been found to be 2·52. r is the position of the rod down the channel. If values are required when r exceeds the tabulated range, α, may be replaced by $\pi^2/(r - \frac{1}{4})$ while v_B/c may be obtained from the less accurate graph in Fig. 3.

Thus with ε, c, N and r known the maximum bow at any time may be obtained in terms of t/K, and hence the time to attain a given bow may be written as a constant divided by K.

With the above creep law K is,

$$\frac{\left\{\int\int_S \Lambda^{-1/N}\,dS\right\}^{N-1}\int\int_S x^2\Lambda^{-1/N}\,dS}{\{NL^2W^N(r-\frac{1}{4})^{N-1}\}}$$

where W is the weight of the element (minus its aerodynamic lift), S is its cross-section, and x is the distance of a point from a line in the cross-section in which it lies, perpendicular to the plane in which the bow under consideration is occurring provided this is along a principal axis. If the bar has a circular cross-section of radius a, and the material is elastic so that Λ is $Ce^{-B/T}$, then,

$$K = 4^N a^{2+2N} I_1 I_2^{N-1}/\{NcL^2W^N(r-\tfrac{1}{4})^N\}$$

where I_1 and I_2 are functions evaluated by HANNAH (1956) of the proportionate temperature drop from the centre to the surface of the uranium and N/B times the maximum temperature. If due to axial temperature variation K is found to vary appreciably along the axis, the mean of several values should be used.

For uranium in which the stress does not exceed the yield stress, and in which irradiation effects may be neglected, B should be taken as 25,300/°C and C as 8·415/hr p.s.i.$^{2\cdot52}$ if thermal cycling is negligible and otherwise as,

$$9\cdot492\left(\frac{E\alpha\Delta}{1+\nu}\right)^{1\cdot52}\Big/\text{hr p.s.i.}$$

where E is Young's modulus, ν is Poisson's ratio, α is the difference in coefficients of thermal expansion along the a and b crystal axes and Δ is the mean temperature deviation of the cycle provided it is not too large.

The times for a bar without spiders to reach bows of c/π when the initial bow is 0·032 in. are given in Table 1 for $c = 0\cdot1$ in., 0·2 in., 0·4 in.

GENERAL THEORY

When a cylinder of any homogeneous material, whose rate of deformation is an isotropic function of the stress, begins to deform in a radial temperature distribution under the action of a small constant longitudinal force and a bending couple, the rate of normal strain parallel to the axis at a point on a principal axis of the cross-section whose distance from the centroid of the cross-section is x, is given by $\lambda + mx$. λ and m are constants such that $m = -\dfrac{\partial^3 v}{\partial t\partial z^2}$, where t is the time, z the longitudinal co-ordinate measured from the bottom of the rod being considered and v the displacement of the centroid in the direction of the principal axis. The usual hypothesis of beam theory is that when the rod has a small deviation from a cylindrical shape and the force, couple and temperature are functions of z and t, λ and m vary with z and t also. We use this assumption throughout.

We consider a cylinder of length L and cross-section S and a general rate of strain/applied stress relationship $\dot{\varepsilon}_{33} = f(w, T)$ where T is the temperature and w a

TABLE 1

r	$\alpha_1(N=1)$	$\alpha_1(N=2{\cdot}52)$	Time to reach bow of c/π from initial bow of 0 032 in. ($N=1$)				
			$c=0{\cdot}1$ in.	$c=0{\cdot}2$ in.	$c=0{\cdot}4$ in.	Using values of K(est.) for Bradwell	
						$c=0{\cdot}2$ in.	$c=0{\cdot}4$ in.
1	18·568726	16·5286	0	$6{\cdot}23K$	$10{\cdot}47K$	50,000 hr	84,000 hr
2	6·53174	6·3563	0	$3{\cdot}21K$	$5{\cdot}7K$	5,600 hr	10,000 hr
3	3·9372903	3·8893	0	$2{\cdot}2K$	$4{\cdot}07K$	3,500 hr	6,500 hr
4	2·815903	2·797	0	$1{\cdot}67K$	$3{\cdot}14K$	6,900 hr	13,000 hr
5	2·192006	2·1823	0	$1{\cdot}33K$	$2{\cdot}54K$	72,000 hr	137,000 hr

uniaxial stress along the z-axis, and denote w as a function of $\dot{\epsilon}_{33}$ by $f^{-1}(\dot{\epsilon}_{33}, T)$. If P and M are the longitudinal force and the component of bending moment perpendicular to the direction of v, they are given by:

$$P = \int\int_S f^{-1}(\lambda + mx, T)\, dS,$$

$$M = \int\int_S xf^{-1}(\lambda + mx, T)\, dS. \qquad (1)$$

It is to be expected that $\frac{mx}{\lambda}$ should be small. To investigate the size of the error made in neglecting it compared with unity, we take the first four terms in the series expansions when the temperature is constant, the cylinder is circular of radius a and $f = (Cw)^n$. Transformed to polar co-ordinates equation (1) then becomes:

$$P/C = \int_0^{2\pi}\int_0^a (\lambda + mr\cos\theta)^{1/n}\, r\, dr\, d\theta$$

$$= \lambda^{1/n}\pi a^2\left\{1 - \frac{(n-1)m^2a^2}{8\lambda^2n^2} + \ldots\right\};$$

$$M/C = \int_0^{2\pi}\int_0^a (\lambda + mr\cos\theta)^{1/n}\, r^2\cos\theta\, dr\, d\theta$$

$$= \frac{\lambda^{1/n}\pi a^4 m}{4\lambda n}\left\{1 + \frac{(n-1)(2n-1)m^2a^2}{12\lambda^2n^2} + \ldots\right\}$$

These equations imply that:

$$m = \frac{4\lambda nM}{a^2P}\left\{1 + \frac{(1-n)(1+4n)m^2a^2}{24\lambda^2n^2} + \ldots\right\}$$

$$= \frac{4nP^{n-1}M}{C^n\pi^n a^{2(1+n)}}\left\{1 + \frac{2(1-n^2)M^2}{3a^2P^2} + \ldots\right\} \qquad (2)$$

Thus if only two terms are retained in the series expansions and the maximum displacement is a tenth of the radius, the average error in m is approximately $\frac{1}{3}(n^2-1)$ per cent.

We therefore take only the first two terms in the series in the general case, thus obtaining:

$$P = \int\int_S f^{-1}(\lambda, T)\, dS, \quad M = \int\int_S \frac{mx^2}{\frac{df}{dw}}\, dS \qquad (3)$$

The latter equation can be rewritten as,

$$\frac{\partial^3 v}{\partial t\partial z^2}\int\int_S \frac{x^2 dS}{\frac{df}{dw}} + M = 0. \qquad (4)$$

We now neglect inertia effects and determine P and M statically. The assumption that the connexions are equivalent to a hinge means that the rods will tilt through a small angle till they rest on the supports.

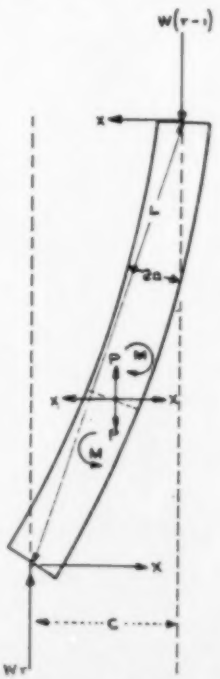

FIG. 1.—Forces acting on tilted and bowed rod.

All subsequent displacements are measured relative to the position now taken up. We denote the distance that the top of the rod tilts relative to the bottom in the direction of the displacement v by c (Fig. 1), the weight of the rod by W and the horizontal force on a cross-section by X. Then it is found by resolving forces and taking moments for the parts $(0, L)$ and $(0, z)$ of the r^{th} rod down a channel and neglecting v and c in comparison with a and L, that:

$$\begin{aligned} P &= W\left(r - \frac{z}{L}\right), \quad X = \frac{W}{L^2}\left\{(r - \tfrac{1}{2})cL + \int_0^L v\,dz\right\} \\ M &= P\left(v + \frac{cz}{L}\right) - Xz + \frac{W}{L^2}\int_0^z (Lv + cz)\,dz \\ &= W\left\{\left(r - \frac{z}{L}\right)v - \frac{z}{L^2}\int_0^L v\,dz + \frac{1}{L}\int_0^z v\,dz \right. \\ &\qquad \left. - \frac{c}{2L^2}(z^2 - Lz)\right\}. \end{aligned} \tag{5}$$

On substituting for M from equation (5) in equation (4) we deduce that:

$$\frac{\partial^3 v}{\partial t \partial z^2}\int\int_S \frac{x^2 dS}{\dfrac{df}{dw}} + W\left\{\left(r - \frac{z}{L}\right)v - \frac{z}{L^2}\int_0^L v\,dz + \frac{1}{L}\times\int_0^z v\,dz - \frac{c}{2L^2}(z^2 - Lz)\right\} = 0 \tag{6}$$

On writing $\dfrac{z}{L}$ as ζ, $\displaystyle\int_0^\zeta v\,d\zeta$ as V and $\dfrac{1}{WL^2}\displaystyle\int\int_S \frac{x^2\,dS}{\dfrac{df}{dw}}$ as $K(\zeta)$ this may be written as:

$$K(\zeta)\frac{\partial^4 V}{\partial t \partial \zeta^3} + (r - \zeta)\frac{\partial V}{\partial \zeta} + V - \zeta V(1) + \frac{c}{2}(\zeta - \zeta^2) = 0 \tag{7}$$

The boundary conditions that the displacements are zero at the hinges and the definition of V as an integral from zero imply that:

$$V(0) = \frac{\partial V(0)}{\partial \zeta} = \frac{\partial V(1)}{\partial \zeta} = 0.$$

We require a solution V, such that when $t = 0$, $V = V_0(\zeta)$ where $V_0(\zeta) = \displaystyle\int_0 v_0(\zeta)\,d\zeta$ and $v_0(\zeta)$ is the initial bow in that direction.

Since the equation is linear this solution may be expressed as $V_A + V_B$, where the equation and boundary conditions are satisfied by V_A when $c = 0$ and by V_B when $v_0(\zeta) = 0$. To obtain V_A we write it as:

$$V_A = \sum_{i=1}^{\infty} d_i \exp\left(\frac{t}{\alpha_i K(\frac{1}{2})}\right) f_i(\zeta) \tag{8}$$

where α_i and $f_i(\zeta)$ are unknown and d_i is such that $V_0(\zeta) = \displaystyle\sum_{i=1}^{\infty} d_i f_i(\zeta)$. Substitution in equation (7) with $c = 0$ yields:

$$\begin{aligned} &\frac{K(\zeta)}{K(\frac{1}{2})}\sum_{i=1}^{\infty}\frac{d_i}{\alpha_i}\exp\left(\frac{t}{\alpha_i K(\frac{1}{2})}\right) f_i'''(\zeta) + (r - \zeta) \\ &\quad \times \sum_{i=1}^{\infty} d_i \exp\left(\frac{t}{\alpha_i K(\frac{1}{2})}\right) f_i'(\zeta) \\ &\quad + \sum_{i=1}^{\infty} d_i \exp\left(\frac{t}{\alpha_i K(\frac{1}{2})}\right) f_i(\zeta) \\ &\quad - \zeta\sum_{i=1}^{\infty} d_i \exp\left(\frac{t}{\alpha_i K(\frac{1}{2})}\right) f_i(1) = 0. \end{aligned}$$

Thus the expression (8) satisfies the equation provided

$$\frac{1}{\alpha_i}\frac{K(\zeta)}{K(\frac{1}{2})} f_i''' + (r - \zeta) f_i' + f_i - \beta_i \zeta = 0 \tag{9}$$

where $f_i(0) = f_i'(0) = f_i'(1) = 0$, $f_i(1) = \beta_i$.

The values α_i for which a solution f_i exists may be determined successively by steadily increasing α and investigating whether the current value is such that the boundary conditions are satisfied. Functions f_A and f_B may be evaluated numerically by integrating equation (9) with the current value of α, $f_i(0) = f_i'(0) = 0$ and $f_i(0) = \pm\gamma$ respectively. We note that any linear combination of these functions satisfies equation (9) and that β_i and γ may be chosen arbitrarily.

We wish to find the combination which satisfies the boundary conditions at $\zeta = 1$. From the conditions that $f_i(1) = 0$ and $f_i(1) = \beta_i$ respectively, we deduce that:

$$f_i''(0) = 2\gamma\left\{\frac{1}{2} - \frac{f_A'(1)}{f_A'(1) - f_B'(1)}\right\}$$

and

$$2\gamma\left\{\frac{1}{2} + \frac{\beta_i - f_A(1)}{f_A(1) - f_B(1)}\right\},$$

since the equation is linear. Thus the values of α for which solutions of (9) exist satisfying the required boundary conditions are those for which these two expressions agree. The functions f_i can be determined by integrating equation (9) with these values for α_i and $f_i''(0)$ (and $f_i(0) = f_i'(0) = 0$).

As the imperfection represented by V_0 is unknown the distribution of d_i is arbitrary. The distribution of greatest interest will be that which causes the greatest

VOL. 14 196

increase in r. The greatest constant rate of proportionate creep occurs when $d_1 = \varepsilon$, $d_i = 0 (i \neq 1)$. Any non-constant proportionate rate is a sum of two or more constant proportionate rates less than or equal to this one. We therefore restrict attention to finding α_1.

The function V_B may be approximately calculated by replacing partial derivatives with respect to ζ by finite differences. If we divide the range (0, 1) into n equal intervals and denote the value of V_B at the end of the jth interval by V_j we obtain:

$$K\left(\frac{j}{n}\right) n^3 \left\{\frac{\partial V_{j+2}}{\partial t} - 3\frac{\partial V_{j+1}}{\partial t} + 3\frac{\partial V_j}{\partial t} - \frac{\partial V_{j-1}}{\partial t}\right\} + (nr - j)(V_{j+1} - V_j) + V_j - \left(\frac{j}{n}\right) V_n \quad (10)$$

$$= \tfrac{1}{2} C\left(\frac{j^2}{n^2} - \frac{j}{n}\right), \quad (j = 1, \ldots, n-1),$$

with $V_0 = V_1 = 0$, $V_{n+1} = V_n$. When $K\left(\frac{j}{n}\right)$ is known these equations may be integrated simultaneously.

The displacement at $\zeta = jL/n$ is then determined as:

$$n(V_{j+1} - V_j) + \sum_{i=1}^{\infty} d_i f_i'\left(\frac{j}{n}\right) \exp\left(\frac{t}{\alpha_i K(\frac{1}{2})}\right) \quad (11)$$

if d_i is known explicitly, and in general is known to be less than or equal to:

$$n(V_{j+1} - V_j) + \varepsilon f_1'\left(\frac{j}{n}\right) \exp\left(\frac{t}{\alpha_1 K(\frac{1}{2})}\right) \quad (12)$$

where $\max\{\varepsilon f_1(\zeta)\}$ is the greatest initial bow.

DETERMINATION OF K FROM EXPERIMENTAL CREEP LAWS

If the temperature in the rod varies and the creep response to a uniaxial stress is complicated, the determination of K involves finding λ such that

$$\iint_S f^{-1}(\lambda, T)\, dS = W(r - \zeta)$$

and computing the corresponding values of w and hence of df/dw throughout the body. However in cases of practical interest, the response can be closely approximated by $\dot{\varepsilon}_{zz} = \Lambda w^N$ and the calculation of K thus simplifies considerably when Λ is a function of T and N is a constant. On writing the strain rate as $\lambda + mx$, equations (3) and (4) reduce to:

$$P = \lambda^{1/N} \iint_S \Lambda^{-1/N}\, dS, \frac{\partial^3 v}{\partial t \partial z^2} + \frac{NM}{\iint_S \frac{x^2\, dS}{\Lambda w^{N-1}}} = 0 \quad (13)$$

and thus, using the same approximation as before, we obtain:

$$\frac{\partial^3 v}{\partial t \partial z^2} + \frac{NM\lambda^{1-1/N}}{\iint_S \Lambda^{-1/N} x^2\, dS} = 0,$$

and hence,

$$\frac{\partial^3 v}{\partial t \partial z^2} + \frac{NMP^{N-1}}{\iint_S \Lambda^{-1/N} x^2\, dS \left\{\iint_S \Lambda^{-1/N}\, dS\right\}^{N-1}} = 0 \quad (14)$$

$K(\zeta)$ is therefore given by:

$$\frac{\left\{\iint_S \Lambda^{-1/N}\, dS\right\}^{N-1} \iint_S \Lambda^{-1/N} x^2\, dS}{NL^2 W^N (r - \zeta)^{N-1}}. \quad (15)$$

We note that if T is independent of z, $K(\zeta) = \left(\frac{r - \frac{1}{2}}{r - \zeta}\right)^{N-1} K(\frac{1}{2})$ and hence both V_A and V_B can be written as functions of ζ and $K(\frac{1}{2})t$. In the opposite case where T is a function of z only:

$$K(\zeta) = S^{N-1} I_x / \{N\Lambda L^2 W^N (r - \zeta)^{N-1}\}$$

where S is the area of the cross-section and I_x its moment of inertia about a line through the centroid in the direction of the couple.

We now obtain K more explicitly for circular rods. It is usually considered adequate to take $T = T_1(1 - \mu r^2/a^2)$ where μ is constant, T_1 is the temperature at the centre and r is the distance from the axis. When the stresses are such that the material does not become plastic, Λ has been found experimentally to be of the form $Ce^{-B/T}$ where B and C are constant. Substitution of these formulae in (15) yields:

$$K(\zeta) = \frac{4^N a^{2+2N} I_1(k, \mu)\, I_2^{N-1}(k, \mu)}{NCL^2 W^N (r - \zeta)^{N-1}} \quad (16)$$

where $k = B/(NT_1)$,

$$I_1 = \frac{1}{4a^4} \iint_S x^2 \exp\left(\frac{k}{1 - \mu r^2/a^2}\right) dS$$

and

$$I_2 = \frac{1}{4a^2} \iint_S \exp\left(\frac{k}{1 - \mu r^2/a^2}\right) dS.$$

I_1 and I_2 have been evaluated by HANNAH (1956) and presented as functions of μ for several values of k in the form of graphs of $(\log_e I_1 - k)/\log_e 10$ and $(\log_e I_2 - k)/\log_e 10$. When μ is zero, equation (16) simplifies further to:

$$K(\zeta) = \frac{\pi^N e^{B/T} a^{2+2N}}{4NCL^2 W^N (r - \zeta)^{N-1}} \quad (17)$$

TABLE 2.—GENERAL CONSTANTS

r	$\pi^2/(r-\frac{1}{2})$	α_1 $(N=1)$	α_1 $(N=2{\cdot}52)$	Time for maximum displacement due to misalignment to reach 30% of end clearance		
				Using eqn. (18)	Using eqn. (7) $(N=1)$	Using eqn. (7) $(N=2{\cdot}52)$
1	19·73921	18·568726	16·5286	$14{\cdot}7K$	$15{\cdot}5K$	$13{\cdot}17K\ (\frac{1}{2})$
2	6·579736	6·53174	6·3563	$9{\cdot}85K$	$9{\cdot}96K$	$9{\cdot}73K\ (\frac{1}{2})$
3	3·947841	3·9372903	3·8893	$7{\cdot}56K$	—	$7{\cdot}5K\ (\frac{1}{2})$
4	2·819887	2·815903	2·797	$6{\cdot}23K$	—	$6{\cdot}19K\ (\frac{1}{2})$
5	2·1932454	2·1920061	2·1823	$5{\cdot}34K$	—	$5{\cdot}31K\ (\frac{1}{2})$
6	1·7944735	1·79527	1·789	$4{\cdot}69K$	—	

where B, C and N are experimental constants. These constants take the values, $B = 25{,}300°\text{C}$, $C = 8{\cdot}415/\text{hr p.s.i.}^{2{\cdot}52}$, $N = 2{\cdot}52$ for uranium in the natural state and $B = 25{,}300°\text{C}$, $C = 1{,}560{,}000/\text{hr p.s.i.}$, $N = 1$ for uranium which is being thermally cycled 10°C each way.

In Table 1 the values of K corresponding to the rods in the Bradwell reactor are presented and the times taken for the upper rods to press tangentially against the wall.

GENERAL NUMERICAL RESULTS

When the longitudinal temperature gradient is neglected, and the response to a uniaxial stress is given by $\dot{\varepsilon}_{zz} = Ce^{-B/T}W^N$ (as in most practical cases), K may be determined as in the last section. Both the integrated displacement V_B due to misalignment and the integrated displacement V_A due to initial bow may be derived, as shown, in terms of ζ and $K(\frac{1}{2})t$. For the practically important values of N (1, corresponding to large thermal cycling or irradiation growth, and 2·52, corresponding to the natural state,) the function V_B and the dominant coefficient α_1 in the function

$$V_A = \sum_{i=1}^{\infty} d_i \exp\left(\frac{t}{\alpha_i K(\frac{1}{2})}\right)$$

have been computed on a digital computer for integral values r up to 6.

For $N = 1$, equation (7) was replaced by:

$$K(\tfrac{1}{2})\frac{\partial^4 V}{\partial t \partial \zeta^3} + (r-\tfrac{1}{2})\frac{\partial V}{\partial \zeta} + \tfrac{1}{2}c(\zeta - \zeta^2) = 0 \quad (18)$$

since its solutions, V_A^* and V_B^*, differ from V_A and V_B by less than 1 per cent for $r > 1$.

A table of α_1 for $r = 1, \ldots, 6$ (Table 2) is presented for $N = 1$ and 2·52 and values $\pi^2/(r-\frac{1}{2})$, which correspond to α_1 for V_A^*, are included for comparison. The function $f_1(\zeta)$ is plotted in Fig. 2 for $N = 1$ and $r = 1$, 2 and 4 and is shown to differ from a sine wave by about 12 per cent in the first case and less than 2 per cent in the last.

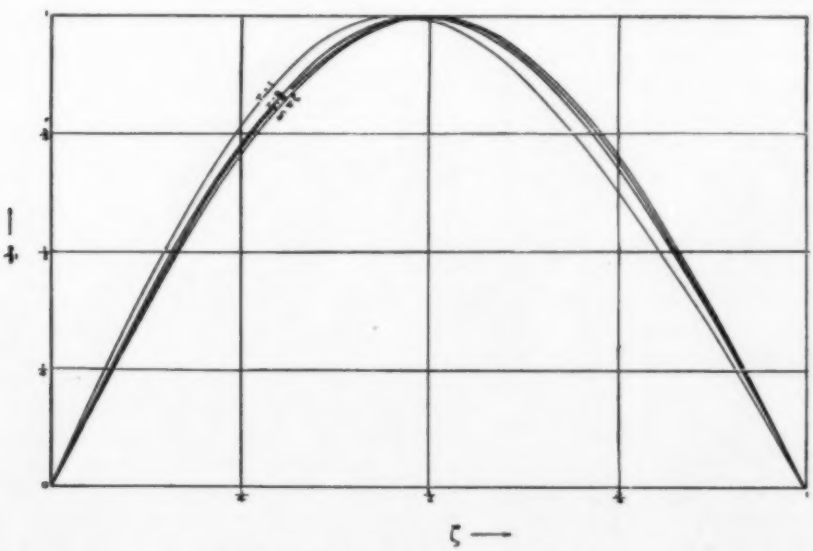

FIG. 2.—$f_1(\zeta)$ for $N = 1$, $r = 1$, 2, 4 and $\sin \pi\zeta$.

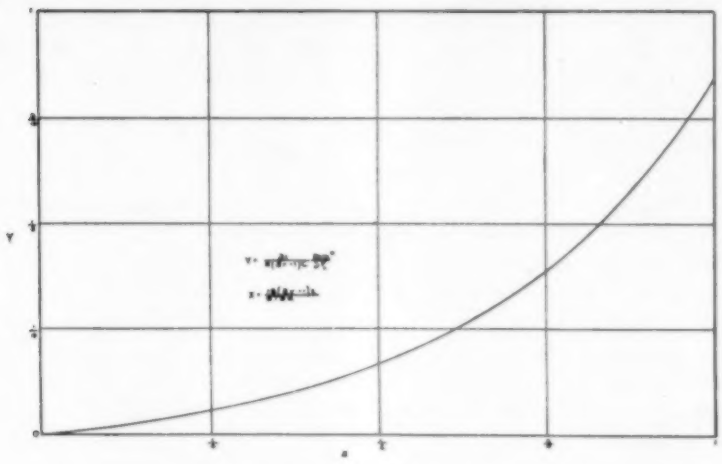

FIG. 3.—Maximum value of $\frac{\partial V_B^*}{\partial \zeta}$ as a function of t.

Fig. 3 displays the maximum values of Y as a function of X when $Y = \frac{21}{2(2r-1)c} \frac{\partial V_B^*}{\partial \zeta}$ and $X = \frac{16(2r-1)t}{875K}$.

In Fig. 4, graphs of the maximum displacement due solely to misalignment $\partial V_B/\partial \zeta$ are presented for $N = 1$ with $r = 1$ and 2, and for $N = 2{\cdot}52$ for integral values of r less than 6, until the maximum displacement is $0{\cdot}32c$ which is sufficiently large for certain designs of fuel element. The range (0, 1) was split into 16 for the difference approximation and the accuracy checked by confirming to five significant figures that with $c = 0$, $N = 1$, $r = 4$, a displacement f_1 increases exponentially at the rate $1/(K\alpha_1)$.

The shape of the rod resulting from the deformations due to the misalignment has also been investigated. $\partial V_B/\partial \zeta$ was considered as a function of ζ when the central displacement was approximately $0{\cdot}3c$. When $N = 1$ it was found to differ from a sine wave for $r = 1$ by slightly more than f_1(with $N = 1$) differed when $r = 2$ and 4 respectively. For $N = 2{\cdot}52$ the computed displacements indicated a local maximum displacement near the top, but the division into 16 intervals was insufficiently fine to yield reliable figures for this effect.

The times for the maximum bow near the centre of an initially straight rod to reach $0{\cdot}3c$ have been read from Figs. 2 and 3 for all cases considered and are included in Table 2.

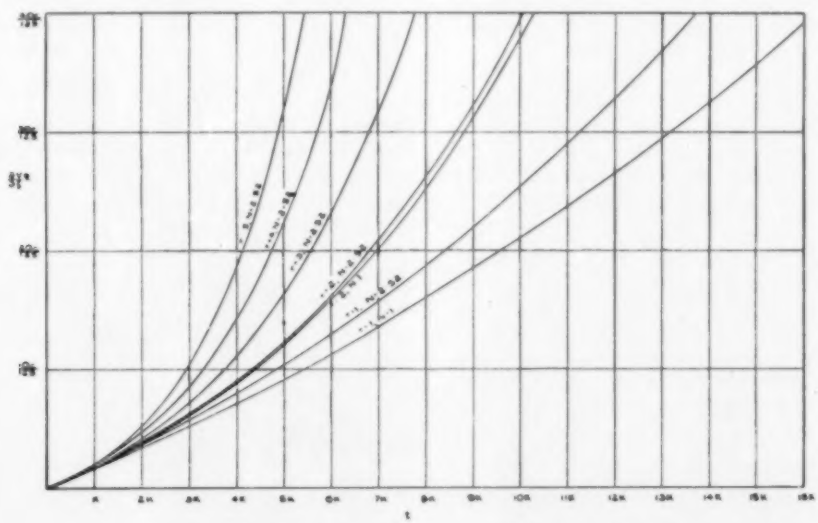

FIG. 4.—Maximum value near centre of $\frac{\partial V_B}{\partial \zeta}$ as a function of t for $N = 2{\cdot}52$, $r = 1, 2, 3, 4, 5$ $N = 1$, $r = 1, 2$.

CONCLUSIONS

Equations are deduced from which the bow may be determined due to a slight tilt and initial bow in a rod in an approximately vertical pin-jointed column, if the creep of the material under an applied stress is known. Non-dimensional graphs are presented from which the maximum bow may be obtained.

Owing to the non-coincidence in general of the planes of tilt and initial bow, the plane through the centres of the ends and the point of greatest bow of a rod in a channel will not generally remain fixed.

The time for the top rod in a channel to press tangentially against the side due to its tilt if initially straight is only about twenty per cent greater than the doubling time of a bow if initially vertical.

With creep laws of the type applicable to uranium, the distributed weight of a rod may be approximated by half the weight acting at each end, without affecting the displacement by more than 4 per cent except in the case of the top rod.

The shapes of the initial bow which increases at the greatest rate, and of the bow formed due to the tilt of an initially straight rod are found to resemble a sine wave.

Acknowledgement—The author is grateful to C. A. Parsons & Co. Ltd. for permission to publish this work.

REFERENCES

ANDERSON R. G. and BISHOP J. F. W. (1960) *Effect of Neutron Irradiation and Thermal Cycling on the Permanent Deformation of Uranium*. To be published.

BLACKBURN W. S., HARNBY G. and STOBO J. J. (1960) *J. Nucl. Energy* Part A: *Reactor Science* **12**, 162.

GREENOUGH G. B., SKINNER J., STUTTARD A., BISHOP J. and LAWTON H. (1958) *Irradiation Creep of Calder Fuel Elements*. Confidential U.K.A.E.A. Report IGRR/W.279.

HANNAH J. M. (1956) *Numerical Evaluation of Two Integrals Occurring in Creep Buckling of Fuel Element Rods*. Confidential AEI–JT. Report IGC–NPCC/FEWP/P.86.

HOFF N. J. (1954) *J. Roy. Aero. Soc.* **58**, 3.

KELLER A. Z. (1956) *Expansions for Two Integrals Occurring in Creep Buckling*. Confidential AEI–JT. Report IGC–NPCC/FEWP/P.70.

MARIN J. (1947) *J. Appl. Phys.* **18**, 103.

ODQUIST F. K. G. (1954) *Appl. Mech. Rev.* **7**, 517.

ROBERTS A. C. and COTTRELL A. H. (1956) *Phil. Mag.* **1**, 711.

APPENDIX

Effect of elasticity

The effect of the elasticity of the material can be taken into account when the temperature distribution is axial. The basic equation is now:

$$\lambda + m\dot{\chi} = f(w) + \frac{1}{E}\frac{dw}{dt} \tag{19}$$

where E is Young's modulus. In accordance with the assumptions of page 3, we write w as $w_0 + \overset{*}{w}x + \ldots$ and subsequently neglect x in comparison with a. Thus we obtain $w_0 = P/S$, $\overset{*}{w} = M/I_x$. Using these results we may deduce also that $\lambda = f(w_0)$ and by integrating equation (19) and x times equation (19) over a cross-section that:

$$mI_x = Mf'(P/S) + \frac{1}{E}\cdot\frac{dM}{dt}. \tag{20}$$

The equation:

$$\frac{\partial^4 V}{\partial t\,\partial\zeta^2} + \frac{WL^2}{EI_x}\left\{(r-\zeta)\frac{\partial^2 V}{\partial t\,\partial\zeta} + \frac{\partial V}{\partial t} - \zeta\frac{\partial V(1)}{\partial t}\right\} + \frac{1}{K}\left\{(r-\zeta)\frac{\partial V}{\partial\zeta} + V - \zeta V(1) + \tfrac{1}{2}c(\zeta-\zeta^2)\right\} = 0 \tag{21}$$

can be derived from equations (20) and (5). It may be solved in the same way as equation (7).

Normally however, we expect the difference to be negligible. When $c = 0$, the temperature is uniform throughout and the weight of the rod is approximated by half its magnitude acting at the top, equation (21) reduces to:

$$K\left(\frac{\partial^3 v}{\partial t\,\partial\zeta^2} + \frac{(r-\tfrac{1}{2})WL^2}{EI_x}\frac{\partial v}{\partial t}\right) + (r-\tfrac{1}{2})v = 0. \tag{22}$$

This equation is satisfied by $v = \sum_{i=1}^{\infty} d_i \sin \pi i\zeta \exp\left(\frac{\alpha_i t}{K}\right)$ where:

$$\alpha_i = \frac{r-\tfrac{1}{2}}{\pi^2 i^2 - (r-\tfrac{1}{2})WL^2/(EI_x)}.$$

The second term in the denominator would always be small compared with the first since the rod would be designed so as not to buckle elastically. Neglecting this term is equivalent to putting E as infinity. Thus we can generally expect the effect of the elasticity to be negligible.

Reactor Science and Technology (J.N.E. Parts A/B), 1961, Vol. 14, pp. 9 to 17. Pergamon Press Ltd. Printed in Northern Ireland

STUDIES IN THE METABOLISM OF CARRIER-FREE RADIORUTHENIUM—I

PRELIMINARY INVESTIGATIONS

R. S. BRUCE and T. E. F. CARR
Medical Research Council Radiobiological Research Unit, Harwell, Berks.

(*Received* 30 *June* 1960)

Abstract—Carrier-free radioruthenium (^{106}Ru) in different chemical forms has been administered orally to rabbits and rats and the uptake and distribution in the body has been determined. Derivatives of nitrosyl-ruthenium were absorbed to the greatest extent, uptake averaging 13 per cent by rabbits and 8 per cent by rats. The uptake of ruthenium chloride was lower and did not differ significantly from that of the dioxide in the absence of carrier. Uptake of all forms was rapid but a high proportion of the dose absorbed was excreted in the urine within 3 days. While the chemical nature of ruthenium considerably affected absorption, it did not influence the subsequent distribution. For the first few days after ingestion of ruthenium, the gastro-intestinal tract and the kidneys are subjected to the highest concentrations of ruthenium.

RUTHENIUM is a comparatively rare and little known element and there is no evidence that it occurs in detectable amounts in animals. Interest in the metabolism of ruthenium arose following its occurrence in the wide range of radioactive isotopes resulting from nuclear fission. ^{103}Ru and ^{106}Ru are two of these isotopes with physical half-lives of 40 and 365 days respectively. In view of the high fission yield and long half-life, particularly of ^{106}Ru, it became important to know something of the biological behaviour of the element in order to assess possible hazards arising from exposure to it.

The metabolism of a form of radioactive ruthenium in rats was investigated by HAMILTON (1947) who concluded that absorption from the gastro-intestinal tract was negligible. DAILEY *et al.* (1945) studied the uptake and distribution of ^{105}Ru following intrapulmonary administration. They found that the ruthenium was distributed fairly evenly throughout the body and that the rate of disappearance from the body was rapid compared with the half-life of the longer lived isotope, ^{106}Ru.

In view of the limited amount of information available and because ruthenium was one of the major components of effluent from the processing of reactor fuel in Britain, a more detailed investigation was initiated in this laboratory in 1953. An attempt has been made to follow the uptake, distribution and excretion of ^{106}Ru administered in different chemical forms which might occur in effluent or in fall-out following a nuclear explosion. The three chemical forms chosen for study were (a) the chloride, in which ruthenium occurs as Ru^{III} and Ru^{IV}, (b) the sparingly soluble dioxide and hydrated oxides, and (c) derivatives of nitrosyl-ruthenium. This latter group is formed by solutions of ruthenium when nitric oxide is present, for example in nitric acid solutions and is very stable under both acid and alkaline conditions.

METHODS AND MATERIALS

Animals

Sandylop rabbits, about six months old and weighing between 2 and 3 kg were used in the earlier experiments. Later, male Dutch rabbits weighing about 1·8 kg were used. The rabbits were kept in standard metabolism cages which allowed the separation of urine and faeces.

Wistar strain inbred male albino rats were also used at 3 months old when they weighed about 300 g. The rats were kept on stainless steel grids in aluminium cages. A second grid of finer mesh separated the faeces and urine.

The animals were fed on standard diets throughout: Rowett Diet No. 1 (North Eastern Agricultural Co-operative Society Ltd., Aberdeen) was used for rats and Diet 18, according to BRUCE and PARKES, for the rabbits.

Feeding procedure

To facilitate feeding, the solution of ruthenium was evaporated onto a carrier material: at first dried heart-muscle was used but during chromatographic investigation of the ruthenium compounds for homogeneity it was found that the ruthenium combined with the muscle powder. When acid-washed kieselguhr was employed as carrier, solutions of ruthenium

could be evaporated to dryness on it and later redissolved to give solutions behaving in the same way chromatographically as the original solution.

The aim has always been to cause as little disturbance to the animal as possible. The powder with ruthenium on it was fed in gelatine capsules to rabbits and to rats as a moist paste directly into the back of the mouth or the oesophagus from a tube of small diameter with a plunger.

Ruthenium compounds

It is impossible to characterize definite compounds of carrier-free ruthenium and the chemical nature of the compounds can only be inferred from their behaviour in solution. This is made difficult first by the lack of information on ruthenium chemistry, which was even more acute at the outset of the investigation, and second, because of the variation in behaviour in solutions due to slow changes from one compound to another.

The ruthenium was obtained by distillation of aged fission products and supplied by R. C. C. Amersham as a solution of ruthenium tetroxide in hydrochloric or nitric acid with a specific activity of about 18 curies/g. Ruthenium tetroxide in strong hydrochloric acid reacts to give predominantly Ru^{III} and Ru^{IV} chlorides. The solution of chlorides was checked for the presence of the nitrosyl form. A paper chromatographic method was employed using n-butanol saturated with 3N hydrochloric acid as a solvent. Under these conditions ruthenium chloride moves very little from the point of application while nitrosyl-ruthenium moves with the solvent on the paper. From a strongly acid solution, the nitrosyl form moves just behind the solvent front but in more dilute acid solutions, hydrolysis products are formed and the nitrosyl complex moves more slowly. (The behaviour of ruthenium in nitric acid solutions is discussed by BROWN, FLETCHER and WAIN, 1957). If there appeared to be any contamination of the chloride by nitrosyl forms it was purified either by redistillation or by extraction of the tetroxide into carbon tetrachloride followed by re-solution in hydrochloric acid.

Ruthenium dioxide was prepared by neutralizing a solution of the chloride in the presence of kieselguhr, boiling for a few minutes and then evaporating to dryness. Under these conditions, macro-amounts of ruthenium gave a granular black precipitate of the dioxide and it was assumed that at micro-levels, the dioxide would be formed similarly. Dialysis with a cellulose membrane (Visking casing) was used to assess the result of the neutralisation.

Solutions of nitrosyl-ruthenium were prepared from nitric acid solutions in which there was sufficient nitric oxide present to convert the ruthenium to the nitrosyl complex. The solution was evaporated *in vacuo* onto kieselguhr giving predominantly nitrosyl-ruthenium trinitrate, $Ru\,NO(NO_3)_3(H_2O)_2\;2H_2O$, (MARTIN, 1953). In some experiments ruthenium chloride was converted quantitatively to the nitrosyl complex by bubbling nitric oxide through the solution for a few seconds.

Method of assay

Ruthenium-106 is a β-emitter (maximum energy 0·04 MeV) decaying with a half-life of one year to rhodium-106 which in turn decays by β-emission (maximum energy 3·5 MeV) with a half-life of 30 seconds to stable palladium. Thus in the assay of ^{106}Ru, it is the β-emission of the rhodium with its higher energy which is measured, but in view of the short half-life of the daughter product, the two isotopes may be considered to be in equilibrium.

In the early experiments, biological samples were dried and ashed in a muffle furnace at 500°C. At this temperature no loss of ruthenium could be detected but the sample temperature should not be allowed to rise appreciably above this value or ruthenium would be lost as the volatile oxide. A weighed amount of ash was placed on an aluminium tray for assay under a thin end-window Geiger-Müller counter.

In later work it was found more convenient to dissolve the samples in concentrated nitric acid, make up to a known volume and count in an M6H halogen quenched Veall counter (20th Century Electronics Ltd.). While organic matter remained in solution and provided that the acid concentration was not excessive due to evaporation, no loss of ruthenium occurred.

RESULTS

A. *Uptake and Distribution of Ruthenium following Oral Administration to Rabbits*

1. *Preliminary experiments in which ruthenium was on dried heart muscle powder*

(a) *Elimination of ingested ruthenium chloride on muscle powder.* Three sandylop rabbits were fed with ruthenium chloride and sacrificed after 3, 22, and 113 days. Urine and faeces were collected daily up to 22 days, blood samples were taken at intervals and several tissues were assayed for retained activity when the animals were sacrificed. The results are summarized in Figs. 1 and 2 and Table 1.

It will be seen (Fig. 1(a)) that the total ruthenium retained in the animal decreased logarithmically with time but that the rate of elimination differed from

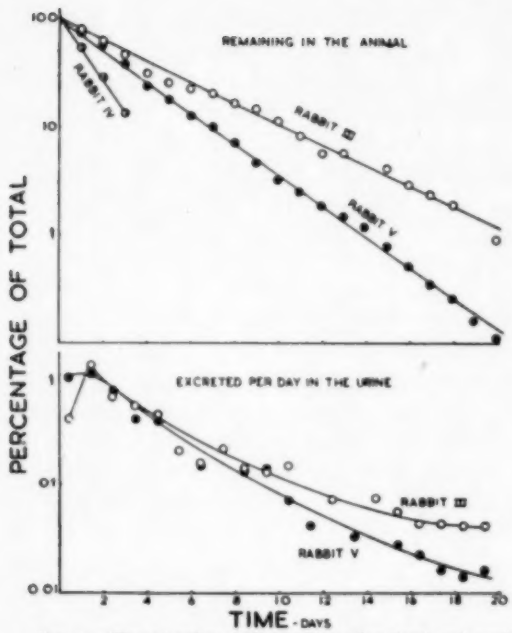

FIG. 1.—The retention and excretion of ruthenium by rabbits following a single oral dose of the chloride evaporated on to dried muscle powder. (a) The total remaining in the animal. (b) The amount excreted per day in the urine.

TABLE 1(a).—EFFECT OF TIME ON THE DISTRIBUTION OF RUTHENIUM CHLORIDE FED ON MUSCLE POWDER TO SANDYLOP RABBITS

	Time from administration		
	3 days	22 days	113 days
	Percentage of dose		
Stomach + contents	4·6	0·013	
Small intestine + contents	1·1	0·020	
Caecum + contents	4·9	0·53	0·006
Colon + contents	1·6	0·062	
Rectum + contents	1·7	0·001	
Liver	0·024	0·013	0·0025
Kidneys	0·019	0·010	0·0007
Faeces	82	94	95
Urine	4·0	4·9	4·5

TABLE 1(b).—CONCENTRATION OF RUTHENIUM IN SELECTED TISSUES

	Time from administration		
	3 days	22 days	113 days
	Percentage of dose/g tissue × 10^4		
Liver	2·7	1·7	0·28
Kidney	9·3	5·6	0·21
Muscle	0·20	0·12	0·12
Blood	0·76	0·18	—
Bone	V. low	0·62	V. low

animal to animal. The two curves showing the percentage of ruthenium in the urine per day (Fig. 1(b)) are similar in form but are not parallel to the retention curves.

Fig. 2 shows that the ruthenium content of the blood rose rapidly following administration and reached a maximum within 12 hours. The level of activity then fell rapidly for the first 4–6 days and more slowly subsequently. Of the activity remaining in the animal even after 22 days, most was in the gastro-intestinal tract and particularly in the caecum (Table 1a). The liver and kidneys were the only other tissues which contained a significant proportion of ruthenium. The concentration of ruthenium per gramme (Table 1b) was highest in the kidneys, with liver second; muscle content was very low and in the 3-day and 113-day animals ruthenium was barely detectable in the bone. With these animals the material to be assayed was

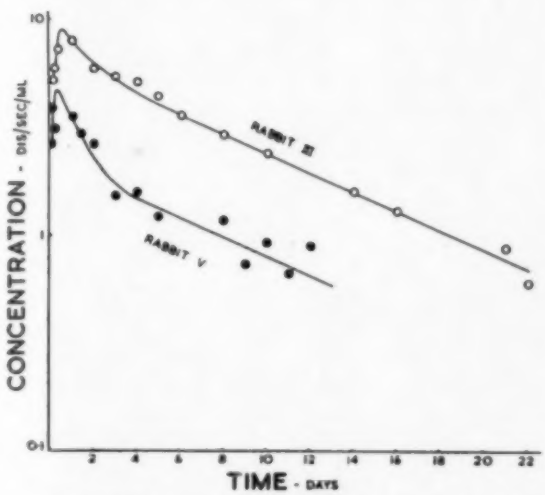

FIG. 2.—The concentration of ruthenium in the blood of rabbits after a single oral dose of the chloride evaporated on to dried muscle powder.

dry-ashed and trayed for solid counting. Consequently it was only possible to take small amounts of bone for counting and the method was not sensitive for very low levels of activity.

(b) *Comparison of uptake and distribution of ruthenium as chloride and as nitrosyl complex administered on muscle powder.* Ruthenium, as the chloride and as the nitrosyl complex evaporated onto muscle powder, was administered to two sandylop rabbits which were sacrificed after 3 days, the tissues dry-ashed and counted. The results, shown in Table 2, do not indicate any marked difference between the two compounds. The amount absorbed from the gut, (i.e. in the urine and in the carcass excluding the gut)

Table 2(a).—Distribution of ruthenium 3 days after feeding ruthenium chloride and nitrosyl-ruthenium on muscle powder to sandylop rabbits

	Percentage of Dose	
	Chloride	Nitrosyl complex
Stomach + contents	1·2	2·6
Small intestine + contents	2·6	1·1
Caecum + contents	42	34
Appendix + contents	1·0	0·22
Colon + contents	6·7	8·3
Rectum + contents	9·5	4·3
Remainder of tissues	0·24	0·24
Urine	3·1	2·8
Faeces	34	46

Table 2(b).—Distribution of ruthenium retained in the animal (excluding the gut) 3 days after administration

	% of total ruthenium retained		% of total ruthenium retained per gramme	
	Chloride	Nitrosyl complex	Chloride	Nitrosyl complex
Liver	11	17	0·13	0·24
Kidneys	27	22	1·5	1·2
Pancreas	5·8	4·9	1·1	0·88
Spleen	0·14	0·29	0·078	0·15
Gall bladder	—	0·49	—	0·47
Heart	0·40	0·49	0·059	0·068
Lungs	0·59	0·61	0·045	0·057
Trachea	0·17	0·14	0·064	0·050
Thyroid	0·005	0·003	0·025	0·012
Thymus	0·10	0·08	0·048	0·022
Salivary glands	—	0·06	—	0·040
Brain	0·22	0·08	0·022	0·008
Adrenals	0·034	0·023	0·19	0·096
Ovaries	0·053	0·015	0·11	0·079
Pelt	14	7·9	0·070	0·047
Skeleton*	11	13	—	—
Fore leg bones	—	—	0·065	0·058
Hind leg bones	—	—	0·068	0·051
Pelvis	—	—	0·044	0·060
Muscle	—	—	0·010	0·017
Blood	—	—	0·064	0·085

* Estimate based on mean concentration in bone samples and assuming that skeletal weight is 10 per cent of the total body weight.

in both cases amounted to about 3 per cent, and of the ruthenium remaining in the animal at sacrifice, most was in the caecum. The ruthenium was distributed generally throughout the tissues, with the highest concentration in the kidney and the lowest in the brain and muscle.

2. *Experiments in which ruthenium was fed on kieselguhr*

(a) *Comparison of the absorption by sandylop rabbits of ruthenium administered on kieselguhr as chloride, dioxide and nitrosyl complex.* Ruthenium chloride, dioxide and nitrosyl complex, each evaporated onto kieselguhr, were fed to male sandylop rabbits which were sacrificed after 3 days. The dioxide in this instance was prepared by neutralization of ruthenium chloride to which a small amount of carrier was added (approximately 2 mg/mc Ru) because carrier-free chloride neutralized under identical conditions still contained about 10 per cent of dialysable ruthenium. With the carrier present only 0·2 per cent of the radioactive ruthenium was dialysable.

The most striking feature of the results (Table 3) was the very high absorption of the nitrosyl complex

Table 3(a).—Distribution of ruthenium 3 days after administration in different chemical forms to sandylop rabbits

	Percentage of dose		
	Chloride	Dioxide	Nitrosyl complex
Stomach + contents	1·7	0·61	3·5
Small intestine + contents	0·57	0·24	2·6
Caecum + contents	22	6·4	7·9
Colon + contents	2·6	1·6	2·5
Rectum + contents	4·4	0·91	7·1
Liver	0·038	0·012	0·41
Kidneys	0·058	0·015	0·25
Muscle (estd. as 50% total body weight)	0·19	0·058	0·28
Bone*	0·12	0·015	0·36
Urine	2·6	0·99	11
Faeces	65	89	65

* Estimate based on mean concentration in bone samples and assuming the skeletal weight is 10 per cent of the total weight.

Table 3(b).—The relative concentrations of ruthenium in rabbit tissues 3 days after administration in different chemical forms

	Percentage of dose/g tissue × 10^4		
	Chloride	Dioxide	Nitrosyl complex
Liver	5·2	1·2	37
Kidneys	25	4·9	105
Muscle	1·0	0·31	1·8
Blood	1·6	0·68	9·1
Bone	3·2	0·41	12
Gall bladder	2·7	9·7	67
Spleen	1·8	0·94	7·4

VOL. 14 196

compared with the other compounds, while conversion of ruthenium from the chloride to the dioxide reduced the uptake. The concentration of ruthenium was high in the kidneys and liver while it was low for all compounds in muscle. The amount of ruthenium in the gall bladder appeared high but the values are based on counts of very small weights of ash and too great importance should not be attached to them.

(b) *Comparison of the absorption by Dutch rabbits of ruthenium administered on kieselguhr as chloride, dioxide and nitrosyl complex.* Three male Dutch rabbits were fed with ruthenium chloride, dioxide and nitrosyl trinitrate respectively and sacrificed after 4 days. The rabbits were litter-mates and the experiment was repeated with two further litters. In this comparison the ruthenium dioxide was prepared without carrier added but under conditions which would have given a precipitate of dioxide had macro-amounts of ruthenium been present. Dialysis experiments indicated that about 1–2 per cent was soluble though the amount increased slowly with time implying that at these very low ruthenium concentrations, the dioxide had a finite solubility.

TABLE 4.—A COMPARISON OF THE METABOLISM OF RUTHENIUM 4 DAYS AFTER ADMINISTRATION IN DIFFERENT CHEMICAL FORMS TO DUTCH RABBITS

(a). Ruthenium absorbed as a percentage of dose

Litter	Dioxide	Chloride	Nitrosyl complex
I	4·0	3·4	9·7
II	2·5	3·1	11
III	3·2	1·7	19
Mean	3·2	2·7	13

(b). Ruthenium retained as a percentage of dose

Litter	Dioxide	Chloride	Nitrosyl complex
I	0·53	0·51	1·0
II	0·22	0·59	1·6
III	0·31	0·18	1·8
Mean	0·35	0·43	1·5

(c). Ruthenium retained as a percentage of that absorbed

Litter	Dioxide	Chloride	Nitrosyl complex
I	13	15	11
II	8·6	19	14
III	9·7	10	10
Mean	10	15	12

TABLE 5.—THE RELATIVE LEVELS OF RUTHENIUM CONCENTRATION IN RABBIT TISSUES 4 DAYS FOLLOWING ADMINISTRATION IN DIFFERENT CHEMICAL FORMS

(a). Concentration as percentage of dose/g tissue × 10^3

	Dioxide	Chloride	Nitrosyl complex
Blood	0·34	0·28	1·8
Muscle	0·06	0·08	0·24
Bone	0·41	0·48	1·2
Pelt	0·43	0·68	1·5
Liver	0·77	0·66	7·2
Kidney	5·0	3·9	17
Residual carcass	0·17	0·19	0·65

(b). Concentration as percentage of dose absorbed/g tissue × 10^3

	Dioxide	Chloride	Nitrosyl complex
Blood	9·9	10	14
Muscle	1·6	2·9	1·8
Bone	11	16	10
Pelt	12	23	12
Liver	22	23	56
Kidney	145	141	131
Residual carcass	4·9	6·5	5·2

The results are summarized in Tables 4 and 5. Table 4(a) again shows the much higher uptake of nitrosyl-ruthenium compared with the other forms, which in this comparison did not differ appreciably. The amount retained as a percentage of that administered (Table 4b) shows a higher retention of nitrosyl-ruthenium but no significant difference between dioxide and chloride. However when the retained activity is expressed as a percentage of the ruthenium absorbed,* differences between compounds are relatively small (Table 4c). Similarly when individual tissues are considered, those of animals fed nitrosyl-ruthenium show higher concentrations in relation to the activity administered than tissues of animals fed the chloride or dioxide (Table 5a), but little difference when considered in relation to the ruthenium absorbed (Table 5b). A possible exception is the liver which does appear to have a consistently high level in animals fed nitrosyl-ruthenium.

It will be seen from Table 4 that there were considerable differences in the uptake of a compound by

* No account has been taken of ruthenium absorbed and subsequently excreted into the gastro-intestinal tract.

Table 6.—The percentage of administered ruthenium eliminated per day in faeces and urine by Dutch rabbits

		Faeces				Remaining in gut	Urine			
		Day after administration					Day after administration			
		1	2	3	4		1	2	3	4
Dioxide	Litter I	3	19	33	23	19	0·25	2·1	0·81	0·39
	II	57	14	14	5	8	1·3	0·53	0·34	0·20
	III	15	11	24	18	27	1·3	—	1·4	—
	Mean	25	15	24	15	18	0·94	0·87	0·84	0·20
Chloride	I	29	26	14	17	10	0·68	1·2	0·66	0·33
	II	41	13	15	12	16	1·0	0·61	0·59	0·28
	III	30	38	14	6	11	0·82	0·32	0·24	0·14
	Mean	34	26	14	12	12	0·84	0·71	0·50	0·25
Nitrosyl complex	I	19	23	16	14	19	3·0	3·3	1·6	0·72
	II	17	23	16	8	24	5·4	2·2	1·3	0·84
	III	21	13	22	10	15	8·7	4·7	2·0	1·4
	Mean	19	20	18	11	19	5·7	3·4	1·6	1·0

Table 7.—The effect of chemical form on the absorption and 24 hour retention of ruthenium by rats

Dioxide		Chloride		Nitrosyl complex	
% Absorbed	% Retained	% Absorbed	% Retained	% Absorbed	% Retained
0·88	0·42	0·76	0·33	7·2	2·6
0·97	0·34	0·70	0·35	4·8	1·8
1·4	0·28	5·4	0·11	7·5	2·6
1·4	0·43	2·3	0·16	4·5	1·7
0·54	0·26	1·2	0·31	5·3	1·9
0·73	0·32	0·84	0·29	7·8	2·9
Mean 0·98	0·34	1·9	0·26	6·2	2·2

individual animals and it was thought possible that these might be due to differences in the rate of movement of food and ruthenium through the gastro-intestinal tract. Taking faecal excretion as an indication of rate of movement, Table 6 shows variation between animals but there does not appear to be any direct correlation with percentage uptake. For instance in the case of rabbits fed nitrosyl-ruthenium, there is a factor of two in the amount metabolized yet the rates of faecal excretion were almost identical. It is of interest to note that even four days after administration, up to a quarter of the ruthenium remained in the gut, predominantly in the caecum.

B. *Uptake and Distribution of Ruthenium Compounds Administered Orally to Rats*

A comparison has been made of the extent and rate of uptake of ruthenium by rats when the ruthenium was given as the dioxide, chloride and nitrosyl complex. The absorption and retention of these three forms of ruthenium 24 hours after administration is given in Table 7, from which it can be seen that though there is considerable variation between individual rats, the average absorption and retention of the nitrosyl complex was much greater.

The overall distribution of ruthenium at different intervals from feeding is given in Table 8. Again there

TABLE 8.—THE GROSS DISTRIBUTION OF THREE RUTHENIUM COMPOUNDS AT DIFFERENT TIMES AFTER ORAL ADMINISTRATION TO RATS

		Percentage of dose*							
		Time from administration (hr)						Range for individual rats	Mean for all rats
		1	2	4	8	24	48		
Dioxide	Gut	99	99	97	68	16	3·8		
	Faeces	—	—	1·5	30	81	95		
	Carcass	1·2	0·68	1·3	1·1	0·78	0·23		
	Urine	0·18	0·27	0·32	0·18	1·6	0·65		
	Total absorbed	1·4	0·95	1·6	1·3	2·4	0·88	0·2–3·9	1·4
Chloride	Gut	96	98	95	59	6·9	0·6		
	Faeces	—	—	—	40	83	98		
	Carcass	3·3	1·6	4·8	0·95	8·1	0·44		
	Urine	0·59	0·11	0·52	0·31	2·3	0·48		
	Total absorbed	3·9	1·7	5·3	1·3	10·4	0·92	0·9–18·6	3·8
Nitrosyl complex	Gut	95	92	93	69	16	7·1		
	Faeces	—	—	—	22	73	86		
	Carcass	4·8	6·2	4·8	5·2	5·1	3·3		
	Urine	0·44	1·6	2·3	3·9	5·1	3·5		
	Total absorbed	5·2	7·8	7·0	9·1	10·2	6·8	2·1–12·6	7·9

* Mean value from two rats.

VOL. 14 1961

were large differences between individual rats but the nitrosyl-complex was absorbed to the greatest extent. The proportion absorbed did not change regularly with increasing time from administration and the values suggest that uptake was substantially complete within the first hour. The rate of movement through the gut was similar for each compound. Nearly all the ruthenium remained in it for four hours but by eight hours some was excreted in the faeces and after twenty-four hours only about one-tenth remained.

In view of the large differences in the absorption of ruthenium by individual animals a comparison of the concentrations in the various tissues corrected for a standard dose is not very enlightening. Concentrations in the tissues of animals fed the nitrosyl complex were higher than in those fed the other two compounds and in general rats which exhibited high absorption had high concentrations in the tissues.

When the concentrations in the tissues are adjusted for a standard amount absorbed, differences between animals and between compounds are much reduced. (Table 9). The effect of the chemical form of the ruthenium administered was only noticeable in the case of the kidneys and liver where the nitrosyl form consistently gave higher concentrations. In all the tissues examined the maximum concentration was reached within a few hours of receiving the ruthenium.

Discussion

It is evident from the foregoing results that ruthenium can no longer be considered as an element which is absorbed to a negligible extent from the gastro-intestinal tract. It is clear moreover that the chemical form of the administered ruthenium has a marked influence on the degree of absorption. The metabolism of nitrosyl-ruthenium derivatives has been studied for the first time and the most notable feature of this investigation is the very high absorption of ruthenium administered in this form. Though the percentage absorbed varies from animal to animal, for rabbits it is about 10–15 per cent while for rats the average is somewhat less.

The proportion of ruthenium chloride absorbed by both rabbits and rats is much smaller and agrees quite well with the value of 3 per cent found for chickens by HANSON and BROWNING (1954) and for rats by THOMPSON *et al.* (1958). THOMPSON *et al.* using carrier-free chlorides found that retention after 24 hours was the same when the ruthenium was administered intragastrically in solutions of pH 1, 2 and 4 but was reduced at pH 6. They did not find a marked influence of specific activity on 24 hour retention though inspection of their data shows that when the concentration of ruthenium was increased tenfold over the carrier-free concentration, retention

Table 9.—The concentration of ruthenium in rat tissues at different times from feeding, corrected for equal amounts absorbed

		Percentage of dose absorbed/g tissue × 10					
		Time from administration (hr)					
		1	2	4	8	24	48
Blood	Dioxide	2·1	3·4	1·5	1·3	0·54	0·52
	Chloride	1·3	1·5	4·1	1·7	2·1	0·60
	Nitrosyl complex	3·5	4·1	3·3	2·6	0·91	1·1
Bone	Dioxide	3·9	7·0	2·9	1·3	1·3	1·4
	Chloride	5·8	2·5	1·6	1·8	1·4	1·7
	Nitrosyl complex	3·1	2·3	1·9	1·8	0·75	1·5
Muscle	Dioxide	0·93	1·2	0·95	0·27	0·24	0·27
	Chloride	1·2	0·64	0·71	0·52	0·51	0·35
	Nitrosyl complex	0·93	0·89	0·76	0·62	0·26	0·48
Liver	Dioxide	6·3	3·7	2·3	2·1	0·85	1·2
	Chloride	0·80	1·1	2·4	2·3	1·7	1·1
	Nitrosyl complex	7·3	10	7·7	7·2	2·4	3·9
Kidney	Dioxide	24	29	15	13	8·3	12
	Chloride	5·5	7·4	15	17	17	11
	Nitrosyl complex	54	85	69	79	28	39
Pelt	Dioxide	3·7	5·1	3·9	5·2	1·8	1·8
	Chloride	3·2	5·8	3·6	5·8	2·0	2·0
	Nitrosyl complex	4·9	3·3	2·6	1·3	2·3	1·8
Residual Carcass	Dioxide	1·9	1·7	2·5	2·7	0·84	0·50
	Chloride	3·4	3·1	2·6	1·6	2·7	1·5
	Nitrosyl complex	2·0	1·7	1·3	1·4	1·6	1·1

was halved. If it is assumed that retention is closely related to total absorption, then this data is in accordance with the present findings for ruthenium dioxide fed to rabbits.

When the chloride with carrier ruthenium added was neutralized to give a precipitate of the dioxide, uptake was reduced but when no carrier was added and no visible precipitate was formed, there was no significant difference in uptake between the dioxide and chloride by rabbits, though in the case of rats the average uptake of dioxide was slightly less. Dialysis of the dioxide showed that the presence of carrier considerably reduced the proportion of diffusible ruthenium, suggesting that although ruthenium dioxide normally may be regarded as insoluble, it has a very low but measurable solubility in the absence of carrier. This degree of solubility would not in itself account for the availability of the ruthenium to the animal. However when the carrier-free dioxide is dialysed against dilute hydrochloric acid (N/100–N/10) much more ruthenium diffuses. It seems likely therefore that, when fed to an animal, the acid gastric juices readily re-dissolve the dioxide when no carrier is present, but have less effect when the dioxide is in the form of a granular precipitate.

Although something is known of the chemistry of these ruthenium compounds *in vitro* it is very difficult to assess what reactions may occur once they have been fed to the animal. Chromatographic and electrophoretic investigations (unpublished results)

VOL 14 196

have shown that ruthenium will combine with dried muscle powder or protein in solution. This behaviour may account for the reduced absorption of the nitrosyl compound when administered on muscle powder to the rabbit. It seems very probable that ruthenium will also combine with the contents of the stomach. Consequently the amount of ruthenium absorbed will depend on many factors such as the pH of the stomach contents, the degree of dilution with food in the stomach and its rate of movement from the stomach into the intestine. These factors may well account for the variation in the absorption of a single ruthenium compound by individual animals, which was particularly noticeable in the case of rats.

The chemical state of the ruthenium administered has a major effect on the degree of absorption but the distribution of the absorbed ruthenium does not appear to be greatly influenced. Although the absorption of nitrosyl-ruthenium is four to five times that of the dioxide or chloride, the proportion of absorbed ruthenium which is retained is almost the same for all compounds (Table 4 c). Similarly the concentrations of ruthenium in the tissues depend on the chemical form administered but if the concentrations are adjusted for a standard amount absorbed, then differences between compounds are much reduced (Tables 5 and 9). On this basis nitrosyl-ruthenium gives relatively higher concentrations in the liver of rabbits and the liver and kidneys of rats than the chloride or dioxide. For the other tissues examined there are no real differences between compounds.

With all the compounds, uptake is rapid and the maximum concentration in the tissues is reached within an hour or two of feeding the ruthenium. Thereafter the concentration falls, rapidly at first and then more slowly so that more than half of the absorbed ruthenium is excreted in the urine in the first two days and for rabbits 80–90 per cent is excreted in the first four days.

In the consideration of absorption and excretion, no account has been taken of ruthenium which has been absorbed from the gastro-intestinal tract and later re-excreted into it. THOMPSON *et al.* (1958) estimate that this endogenous excretion amounts to some 20 per cent of total absorption and consequently the values for absorption based on the ruthenium found in the tissues and urine should be increased by 25 per cent. This estimate of endogenous excretion does not differ appreciably from values found during the course of further studies yet to be reported.

The highest concentration of ruthenium, apart from that in the gastro-intestinal tract, is invariably found in the kidneys. The concentrations in the liver and pelt are also relatively high. The value for muscle is low and though there is evidence that retention occurs in bone, longer-term experiments are required to decide whether the ruthenium is permanently incorporated or whether it is readily removed. The gall bladder in rabbits appears to have a high concentration of ruthenium which may be associated with the prevailing alkaline conditions.

In conclusion it may be said that the chemical state of ruthenium has a great effect on absorption from the gastro-intestinal tract but a much smaller effect on subsequent distribution. For the first few days after ingestion of ruthenium, the gastro-intestinal tract and kidneys are subjected to the highest concentrations of ruthenium. Further studies are required to determine longer term effects and since uptake of nitrosyl-ruthenium is much higher than any results reported previously for the element, this chemical form has been chosen for further investigation.

Acknowledgement—The authors wish to acknowledge the helpful discussions on the chemistry of ruthenium which they have had with members of the Chemistry Division, A.E.R.E., Harwell.

REFERENCES

BROWN P. G. M., FLETCHER J. M. and WAIN A. G. (1957) *Nitrato Nitrosylruthenium Complexes and their Extraction from Nitric Acid Systems by Tributyl Phosphate.* A.E.R.E. C/R 2260.

DAILEY M., WENDER I. and ABRAMS R. (1945) *Tracer Studies with Inhaled 1·0 Year Ruthenium.* MDDC–420.

HAMILTON J. G. (1947) *Radiology* **49**, 325.

HANSON W. C. and BROWNING R. L. (1954) *Absorption and Distribution of Ruthenium in the Fowl.* Biology Research—Annual Report, 1953. HW–30437, 95.

MARTIN F. S. (1953) *Chem. Industr.* 824.

THOMPSON R. C., WEEKS M. H., HOLLIS O. L., BALLOU J. E. and OAKLEY W. D. (1958) *Amer. J. Roentgenol.* **79**, 1026.

Reactor Science and Technology (J.N.E. Parts A/B), 1961, Vol. 14, pp. 18 to 24. Pergamon Press Ltd. Printed in Northern Ireland

DIFFUSION LENGTH OF THERMAL NEUTRONS IN WATER FROM 23°C to 244°C

M. REIER and J. A. DE JUREN
Bettis Laboratory, Pittsburgh, Pa.*

(*First received* 30 *January* 1960 *and in revised form* 30 *June* 1960)

Abstract—The diffusion length, L, of thermal neutrons has been measured in water at 23°, 49°, 70°, 90°, 165·6° and 244·4° centigrade using an ^{124}Sb–Be (25 keV) source. The technique for correcting the data for the presence of a source term in the diffusion equation is outlined. The values reported are compared with a theoretical model which calculates the transport mean free path and the absorption cross-section averaged over the velocity weighted neutron spectrum. The values for L (corrected to a water density of one) found in this experiment are:

T°C	$L\rho/\rho_0$
23	2·775 ± 0·006
49	2·862 ± 0·011
70	2·957 ± 0·013
90	3·051 ± 0·006
166	3·302 ± 0·016
244	3·497 ± 0·020

1. INTRODUCTION

THE diffusion properties of a medium are of particular importance in the design of thermal reactors. As the diffusing neutrons are in thermal contact with the medium, one should expect a temperature dependence of the diffusion parameters. The one-group, steady-state, source-free diffusion equation has the form:

$$\nabla^2 n - \frac{v\Sigma_a n}{D_0} = 0, \tag{1}$$

where n is the thermal neutron density, v the velocity, D_0 the diffusion constant and Σ_a the macroscopic absorption cross-section. The diffusion length may be defined as

$$L = \left(\frac{D_0}{v\Sigma_a}\right)^{1/2} = \left(\frac{\lambda_{tr}\lambda_a}{3}\right)^{1/2}, \tag{2}$$

since $D_0 = v\lambda_{tr}/3$ and $\Sigma_a = 1/\lambda_a$. Several measurements of L have been made in water at room temperature (WILSON *et al.*, 1944; WRIGHT and FROST, 1956; SISK, 1951; HEINTZE, 1956; DE JUREN and ROSENWASSER, 1953; and BARKOV *et al.*, 1957) using a technique which depends on the solution of equation (1). WILSON *et al.*, FROST and WRIGHT, SISK, and HEINTZE measured the relaxation length in water of neutrons emerging from the thermal column of a reactor along the axis of a tank. This value must be corrected for a buckling effect in planes perpendicular to the axis. WILSON (1944) pointed out that although L is only 2 per cent larger than the measured axial relaxation length for this geometry, the error in this difference might be as high as 100 per cent. Both WILSON *et al.*, (1944) and FROST and WRIGHT (1956) appear to have difficulties due to neutrons leaking into the tank from the sides. The effect of these additional source terms leads to uncorrected systematic errors.

Another method of measuring L consists of pulsing neutrons into moderators of different sizes and measuring the thermal decay constants of the leakage neutrons after the higher harmonics have died out (VON DARDEL and SJÖSTRAND, 1954; ANTONOV *et al.*, 1956; BRACCI and COCEVA, 1956; CAMPBELL and STELSON, 1956). The general solution of the time-dependent diffusion equation is

$$n(t) = \sum_{lmn} A_{lmn} f_{lmn} e^{-\lambda_{lmn} t}, \tag{3}$$

where

$$\lambda_{lmn} = v\Sigma_a + D_0 B^2_{lmn}, \tag{4}$$

and f is the eigenfunction and B^2 are the eigenvalues of the equation

$$\nabla^2 f - B^2 f = 0.$$

This method has the advantage that Σ_a and D_0 can be determined separately; however, experimentally, λ does not appear to be a linear function of B^2. This may be caused by preferential leakage of the faster neutrons (diffusion cooling). In addition, the extrapolation length may be a function of the buckling.

* Operated for the U.S. Atomic Energy Commission by Westinghouse Electric Corporation.

OL.
14
961

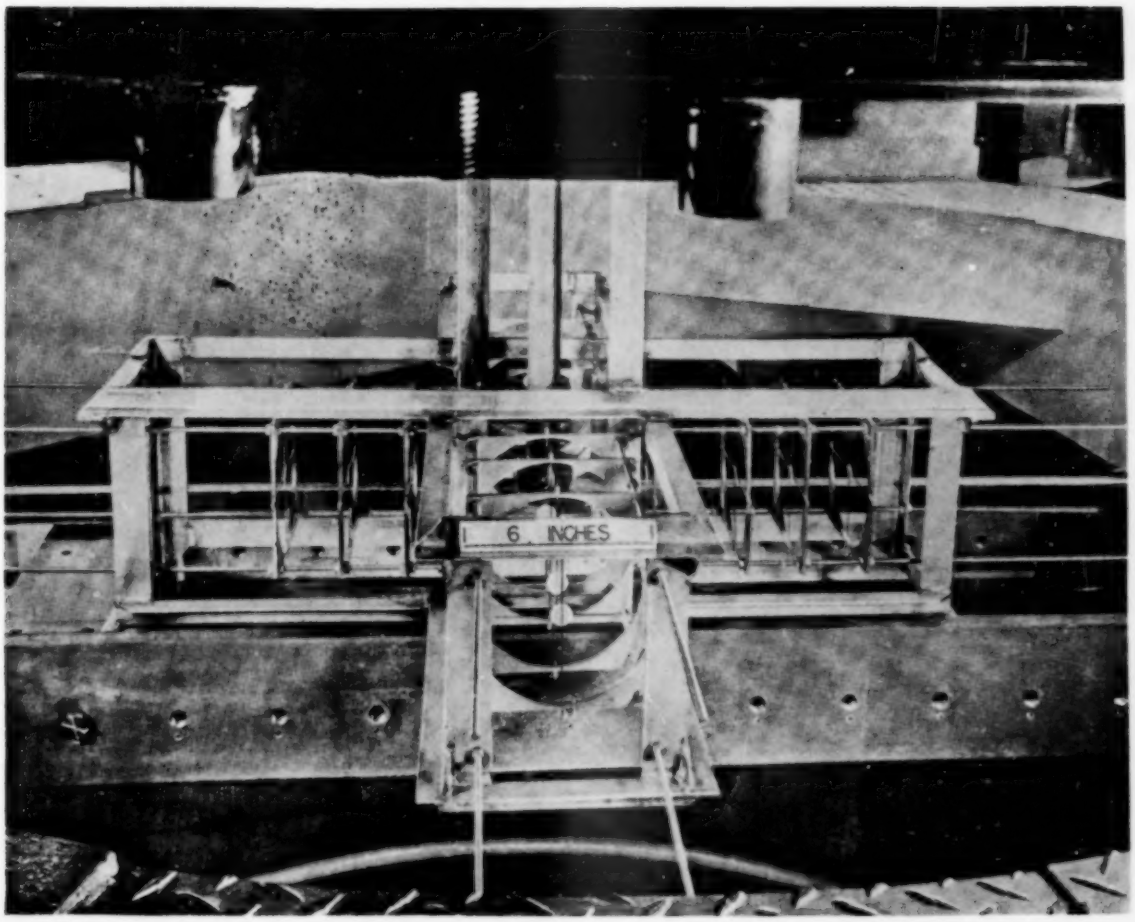

FIG. 1.—Foil holding mechanism for the 166°C and 244°C measurements.

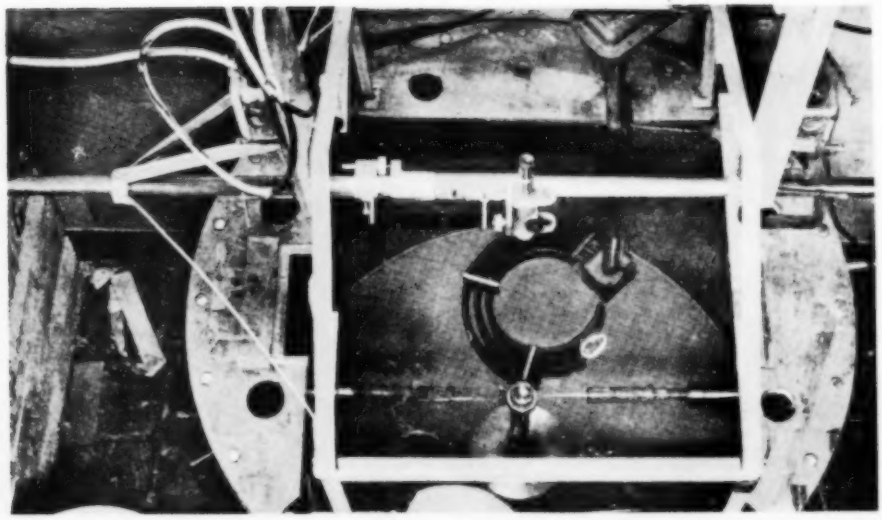

FIG. 3.—Tank and cathetometer used for measurements from 23 C to 90°C.

VOL
14
196

The technique chosen for this experiment involves the measurement of the relaxation length of thermal neutrons using a point source of ^{124}Sb–Be (25 keV) neutrons. DE JUREN and ROSENWASSER (1953) and BARKOV *et al.* (1957) used this technique. Equation (1) is modified by the addition of a source term. DE JUREN and ROSENWASSER solved the inhomogeneous equation in general form but did not evaluate the constant in the solution. Therefore, they did not correct their value of L for the source term and represented their value as an upper limit. BARKOV *et al.* (1957) stated that only diffused thermal neutrons are present beyond 15 cm and did not correct their data for thermalization in this region. They used the solution of the source-free diffusion equation for a distribution which exhibits spherical symmetry.

$$n = Ge^{-r/L}/r. \tag{5}$$

Actually, even though the cadmium ratios are greater than 100, the source term correction is not insignificant.

2. EXPERIMENTAL ARRANGEMENTS

The measurements were performed at two different facilities. One was a cylindrical vessel which was larger than two metres in all dimensions and which could be pressurized. The measurements at 165·6°C and 244·4°C were done in this facility. In addition, several runs were made at lower temperatures as a check against the values obtained earlier using the other system. An ^{124}Sb–Be neutron source was suspended in a tube from the top cover of the pressure vessel. This source emitted between 5×10^7 and 10^8 neutrons/sec initially. Each foil was held between the centres of two crossed 0·060 in. zirconium wires which were reduced to 0·040 in. at the centre to provide a shoulder for the foils (Fig. 1). These wires were secured to zirconium frames having a 7-in. diameter circular opening. The frame positioned the plane of the foils perpendicular to the source direction. The frames were mounted in a right-angle cross array with respect to the source with four frames on each arm of the cross. The same source to frame spacing was used on each arm during an irradiation. The saturated activities of opposite foils at the same distance from the source were averaged. Distances were measured with a micrometer and corrected for the thermal expansion of the holding mechanism. The distance between foils was 7 cm at 165·6°C and 244·4°C and 5 cm at 90°C and 23°C. The foils were ceramic disks 2 cm in diameter and about 0·030 cm thick composed of 12·5 weight per cent DyO_2 in an Al_2O_3 matrix.

The other facility was a cylindrical tank having a diameter and height of one meter. Indium-tin foils were mounted in slots in a lucite frame which was clamped to a solid lucite rod (Fig. 2). The rod was inserted into a moveable stainless steel cylinder in the same horizontal plane as the source. The distance of the lucite rod from the centre of the tank could be adjusted by a screw mechanism outside the tank. The foils could be viewed by a cathetometer which was mounted horizontally above the top of the tank. The tank cover had a glass panel for viewing the foil-holding mechanism. When the cover was in place, the glass was in contact with the water and prevented surface ripple. Also, the distances of the foils could be measured at elevated temperatures without the inconvenience of water vapour fogging the telescope lens. The frame which held the foils during irradiation had numerous holes cut out to reduce as much as possible the effect of the presence of a foreign substance

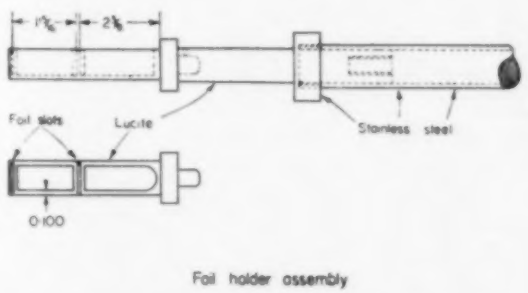

FIG. 2.—Lucite foil holders used for measurements from 23°C to 90°C.

in the medium. The solid lucite rod was at least two diffusion lengths from the nearest foil. The foils were 2×2 cm and 0·005 in. thick and contained 50 per cent indium and 50 per cent tin for rigidity. They were sandwiched between slots which had 0·100 in. of lucite in front and back of two 0·015 in. vinylite spacers.

The tank and cathetometer are shown in Fig. 3. Two identical foil-holding mechanisms, each holding two foils, were mounted on opposite sides of the source so that four foils could be irradiated simultaneously. In addition to the bare foil data, foils covered with 0·040 in. cadmium were irradiated to determine the contribution to the activation from capture at the indium resonances and in order to correct for the source term. A thermostatically controlled immersion heater maintained the desired temperature of the demineralized water in both facilities to within ± 1°C. Measurements in the vicinity of the source and foils indicated no appreciable temperature gradients.

3. FOIL COUNTING

After irradiation, the foils were counted on both sides successively in two continuous flow proportional gas counters. The pulses from the detectors were fed to non-overloading linear amplifiers and then to binary scalers. Operating the amplifiers at a high gain resulted in high voltage plateaus about 300 volts long. The usual corrections were applied to the counting rates to obtain the counting rate at saturation. A half-life of 60·9 days was used for the source. The four values for each foil were averaged.

4. DISCUSSION AND RESULTS

The foils used to measure the distribution are thin $1/r$ detectors. The thermal activity, A_{th}, is proportional to the thermal neutron density. The epithermal resonance activity was subtracted from the saturated indium bare foil activity. The former is 1·1 A_{Cd} where A_{Cd} is the saturated activity of cadmium-covered foils. The additional 10 per cent is due to the absorption of resonance neutrons by cadmium.* Cadmium ratios could not be taken at high temperatures; however, since dysprosium has extremely high cadmium ratios, the cadmium activity will be less than 0·1 per cent of the bare foil activity and can be neglected. An additional correction must be made for the shielding of a foil by foils between it and the source. The derivation of this correction is given in the Appendix. Self-shielding corrections are not necessary because only relative neutron densities are involved. Bare foil data were usually taken between about 15 and 25 cm for indium and up to about 38 cm for dysprosium at high temperatures and L (uncorrected for source term) calculated by a weighted least square fit to log $A_{th}r$. Finally, a correction must be made for the source term.

The steady-state diffusion equation is

$$D_0\nabla^2 n - nv\Sigma_a + q = 0, \tag{6}$$

where q is the neutron slowing down density into the thermal region. At large distances from the source, the slowing down density should decrease with distance as

$$q = Ke^{-r/b}/r^2. \tag{7}$$

With this source term the general solution is (DE JUREN and ROSENWASSER, 1953):

$$n = \frac{KL}{2D_0}\frac{e^{-r/L}}{r}\left[C - \int_{\alpha_I r}^{\infty}\frac{e^{-x}}{x}dx + e^{2r/L}\int_{\alpha_{II} r}^{\infty}\frac{e^{-x}}{x}dx,\right] \tag{8}$$

where $\int_{\alpha r}^{\infty}\frac{e^{-x}\,dx}{x}$ is the exponential integral $E_1(\alpha r)$,

and $\alpha_I = 1/b - 1/L$,

$\alpha_{II} = 1/b + 1/L$.

The relaxation length, b, has been obtained by measurements of the indium resonance activity with 0·040 in. cadmium covers at radii beyond 12 cm from the source. Its value is 1·58 ± 0·02 cm. To evaluate C, a relationship is needed between n and q. As $q = Ke^{-r/b}/r^2$, equation (8) becomes

$$\frac{n}{q} = \frac{rL}{2D_0}e^{\alpha_I r}[C - E_1(\alpha_I r) + e^{2r/L}E_1(\alpha_{II} r)].$$

Substituting $D_0 = L^2 v\Sigma_a$, we obtain

$$\frac{nv\Sigma_a}{q} = \frac{r}{2L}e^{\alpha_I r}[C - E_1(\alpha_I r) + e^{2r/L}E_1(\alpha_{II} r)]. \tag{9}$$

If the left-hand term can be evaluated at a radius r and a value L is assumed, C can be determined. The evaluation proceeds in the following manner. Measurements had been made previously of the cadmium-covered and thermal neutron distributions in water at room temperature from a Po–Be source. The ratio of the spatial integrals, which is independent of the initial source energy, may be calculated,

$$\frac{\int_0^{\infty} A_{2Cd}r^2\,dr}{\int_0^{\infty} A_{2th}r^2\,dr} = \gamma = 0{\cdot}0840 \text{ for } 0{\cdot}040 \text{ in. Cd covers.} \tag{10}$$

The foil activities are proportional to q and n.

Let $A_{2Cd} = C_{Cd}q_2$, $A_{1Cd} = C_{Cd}q_1$,

$A_{2th} = C_{th}n_2$, and $A_{1th} = C_{th}n_1$,

where subscript 2 applies to the Po–Be measurement and subscript 1 applies to measurements with the Sb–Be source. After substituting and dividing by $v\Sigma_{a2}$,

$$\frac{C_{Cd}\int_0^{\infty} q_2 r^2\,dr}{C_{th}\int_0^{\infty} n_2 v\Sigma_{a2} r^2\,dr} = \frac{\gamma}{v\Sigma_{a2}}.$$

From conservation of neutrons the two integrals must be equal. Therefore, the ratio of the coefficients becomes

$$\frac{C_{Cd}}{C_{th}} = \frac{\gamma}{v\Sigma_{a2}}. \tag{11}$$

For the Sb–Be measurements,

$$\frac{n_1 v\Sigma_{a1}}{q_1} = \frac{C_{Cd}}{C_{th}}\frac{A_{1th}}{A_{1Cd}}v\Sigma_{a1} = \gamma\frac{A_{1th}}{A_{1Cd}}\frac{\Sigma_{a1}}{\Sigma_{a2}}. \tag{12}$$

* Absorption of resonance neutrons by cadmium may vary with distance from the source because of the change in the neutron angular distribution with distance. However, because of the high (>120) Cd ratios in the region of interest, this effect is negligible.

VOL 14 196

For the Sb–Be measurements in water as a function of temperature,

$$\frac{n_1 v \Sigma_{a1}}{q_1} = \gamma \frac{A_{1th}}{A_{1Cd}} \frac{\rho(T)}{\rho(23°C)}.$$

A_{1th}/A_{1Cd} was measured at either 14 or 15 cm. C is evaluated by assuming an approximate value of L in equation (9). $A_{th}r$ divided by the evaluated bracketed expression then falls off as $e^{-r/L}$, and a second value of L is obtained from a least square fit of the logarithms of these corrected values. A second value of C may then be determined and iteration continues until a unique value of L is reached. As the convergence is quite rapid, a judicious estimate of the first value of L results in a bracketed term which changes negligibly after iteration. Figure 4 shows the correction factors (bracket of equation (8)) normalized to one at 30 cm which have been applied to the data at room temperature. Figure 5 is a sample of the data using indium foils at room temperature illustrating the effect of the correction term in changing the shape of the curve. These data taken over a wider radial range than an earlier set yielded a value of $2{\cdot}776 \pm 0{\cdot}009$ cm for the diffusion length as compared with the first value of $2{\cdot}783 \pm 0{\cdot}010$. The correction at 23° and 49° reduced the uncorrected value of L by 0·8 per cent. At 70° and 90°, the correction was 0·6 per cent. Because of the difficulty of measuring the cadmium ratio at high temperatures, the values at 165·5°C and 244·4°C are uncorrected for the source term and represent an upper limit which should not be more than 0·3 per cent too high.

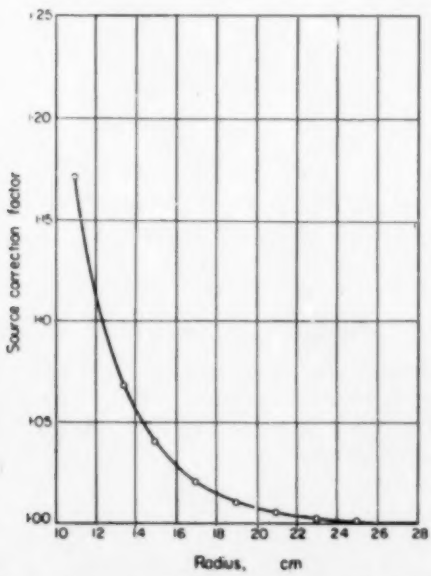

FIG. 4.—Source correction factor vs. r at room temperature. (F was arbitrarily normalized to unity at 30 cm. The value of C in equation (8) was 0·06060.)

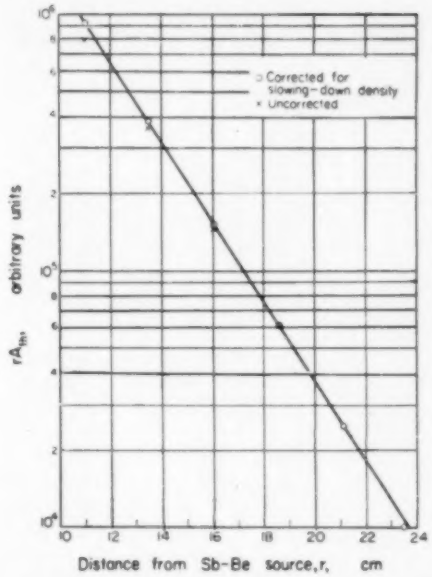

FIG. 5.—Effect of source correction term at room temperature. (The points are averaged values of several measurements at the indicated radii.)

The error in b from counting statistics was about 1 per cent. This results in a negligible error in L. However, because of the limitations of source strength, b could be measured only to 15 cm although the correction was applied in the range of 15 to 25 cm. The possibility exists that b becomes smaller as r increases. Data taken from 10 to 14 cm show definite curvature in b. If b were 10 per cent lower between 15 and 25 cm than where it was measured (12 to 15 cm), L at room temperature would be reduced by 0·6 per cent instead of 0·8 per cent. The effect at higher temperatures would be even less.

Figure 6 is a set of indium data taken at 90°C. Table 1 is a summary of the results obtained in this experiment compared with the results of other experiments and theoretical calculations. Measurements using a steady-state source are not directly comparable with those using a pulsed neutron source since the neutrons detected in the two cases may not have the same spectral distribution. VON DARDEL and SJÖSTRAND (1954) estimate that pulsed neutron measurements should give values of L in water about 1 per cent lower than steady-state source experiments.

The theoretical calculation is based on a model suggested by RADKOWSKY (1950) and has been incorporated into the Bettis SOFOCATE code (AMSTER and SUAREZ, 1957). This model calculates

TABLE 1

Temp. (°C)	L (cm)		$L\rho/\rho_0$*	Theoretical value of $L\rho/\rho_0$ using Maxwell spectrum
23°	2·779 ± 0·007†	Present expt. (In)	2·773 ± 0·007	
23°	2·786 ± 0·012	Present expt. (Dy)	2·780 ± 0·012	
23°	2·781 ± 0·006	Present expt. (aver. In + Dy)	2·775 ± 0·006	2·801
49°	2·895 ± 0·011	Present expt. (In)	2·862 ± 0·011	2·918
70°	3·024 ± 0·013	Present expt. (In)	2·957 ± 0·013	3·010
90°	3·172 ± 0·009	Present expt. (In)	3·062 ± 0·009	
90°	3·151 ± 0·009	Present expt. (Dy)	3·041 ± 0·009	
90°	3·162 ± 0·006	Present expt. (aver. In + Dy)	3·051 ± 0·006	3·095
166°	3·653 ± 0·017	Present expt. (Dy, no source corr.)	3·302 ± 0·016	3·393
244°	4·328 ± 0·025	Present expt. (Dy, no source corr.)	3·497 ± 0·020	3·678
23°	2·784 ± 0·042‡	(WILSON *et al.*, 1944)	2·777 ± 0·042	
25°	2·714 ± 0·010	(WRIGHT and FROST, 1956)	2·706 ± 0·010	
24°	2·74§	(SISK, 1951)	2·73	
21°	2·86 ± 0·03	(HEINTZE, 1956)	2·85 ± 0·03	
22°	2·763 ± 0·015	(DE JUREN and ROSENWASSER, 1953)	2·757 ± 0·015	
19°	2·69 ± 0·02	(BARKOV *et al.*, 1957)	2·69 ± 0·02	
22°	2·725 ± 0·03	(VON DARDEL and SJÖSTRAND, 1954)	2·718 ± 0·03	
22°	2·7 ± 0·1	(ANTONOV *et al.*, 1956)	2·7 ± 0·1	
22°	2·66 ± 0·11	(BRACCI and COCEVA, 1956)	2·65 ± 0·11	
22°	2·69	(CAMPBELL and STELSON, 1956)	2·68	
190°	3·927 ± 0·023	(WRIGHT and FROST, 1956)	3·436 ± 0·020	3·43
276·7°	5·360 ± 0·037	(WRIGHT and FROST, 1956)	4·116 ± 0·028	3·73

* ρ/ρ_0 is the ratio of the density of water at the specified temperature to unit density.
† Standard errors quoted in the present experiment are based on actual deviations of measured points from the least square fit and are slightly larger than errors based on counting statistics.
‡ Based on the relation $L = 2{\cdot}644 + 0{\cdot}0061\ t_c$ from the best linear fit to the data from 27·2° to 93·0°C.
§ The quoted value of 2·67 ± 0·02 cm was corrected for the finite geometry of the experiment.

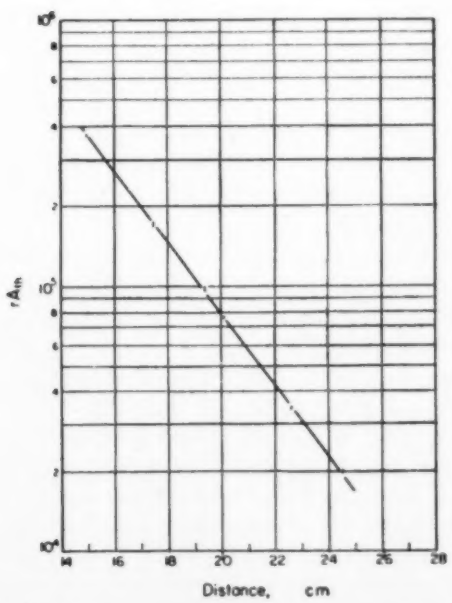

FIG. 6.—A set of indium data taken at 90°C. (Several of the points represent two or more points which are too close to be distinguished separately on the graph.)

D_0/v and Σ_a averaged over the flux-weighted Maxwellian distribution in order to obtain L^2.

$$\frac{D_0}{v} = \frac{\lambda_{tr}}{3} = \frac{\lambda_{sc}}{3(1 - \overline{\cos\theta})},$$

where $\overline{\cos\theta}$ is given by $2/3A$. A is the effective mass of the scattering centre and, in this model, is assumed to be a continuously varying function of the neutron energy. We may write, using the Born approximation,

$$\sigma_{sc}(E) = k\mu^2(E),$$

where μ is the reduced mass of the neutron and k is proportional to the matrix element for the scattering event and is not a function of energy. We further assume that the proton scatters as a free particle of mass one at energies where $\sigma_{sc} = 20b$. Therefore,

$$\frac{\sigma_{sc}}{20} = \frac{\left(\frac{A}{A+1}\right)^2}{\frac{1}{4}}.$$

Figure 7 is a plot of our experimental values of L compared with calculated values. The Maxwell-Boltzmann spectrum should give a lower limit to the calculated value of L since diffusion may harden the spectrum. The Selengut-Goertzel approximation inherent in the calculations may cause the calculated value at 23°C to be high by about 1 per cent (GELBARD, private communication). In addition, the values of the input cross-sections may cause an error of the order of 1 per cent in the diffusion length. The experimental data were fitted to the function $L\rho/\rho_0 = A(T + 273{\cdot}2)^{0{\cdot}4343}$, where T is the centigrade temperature and the exponent was determined by arbitrarily normalizing the data at 23°C and 166°C. The fit is slightly less

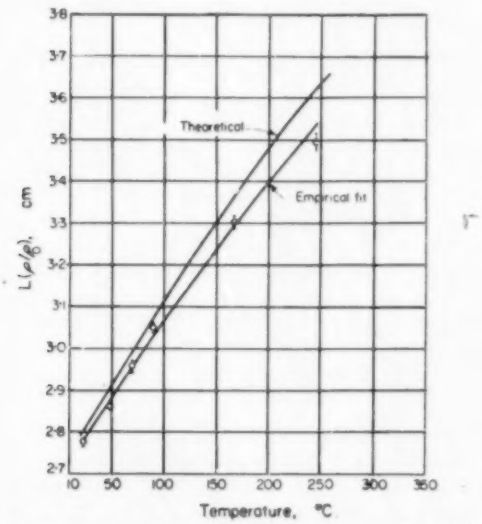

FIG. 7.—A comparison between the measured values of L from 23° to 244°C are those calculated using the Maxwell spectrum.

than one per cent from the data between 23 and 166 degrees and slightly more than one per cent greater than the experimental value at 244 degrees.

This work is being continued for several different concentrations of boron and cadmium in water at room temperature and will appear in a separate report.

Acknowledgements—It is a pleasure to express our gratitude to MR. W. D. OGLETHORPE and MR. E. A. HOOPER of the Bettis Laboratory for their assistance in taking data and to various members of the High Temperature Test Facility for their assistance and co-operation in the irradiation of foils for the high temperature measurements.

REFERENCES

AMSTER H. and SUAREZ R. (1957) WAPD–TM–39.

ANTONOV A. V., ISAKOV A. I., MURIN I. D., NEUPOKOEV B. A., FRANK I. M., SHAPIRO F. L. and SHTRANIKH I. V. (1956) *Proceedings of the First International Conference on the Peaceful Uses of Atomic Energy, Geneva*, 1955, Vol. 5, p. 3. United Nations, N.Y.

BARKOV L. M., MAKARIN V. K. and MUKHIN K. N. (1957) *J. Nucl. Energy* **4**, 94.

BRACCI A. and COCEVA C. (1956) *Nuovo Cimento* **4**, 59.

CAMPBELL E. C. and STELSON P. H. (1956) ORNL–2076.

DARDEL G. F. VON and SJÖSTRAND N. G. (1954) *Phys. Rev.* **96**, 1245.

GELBARD E. Private communication.

HEINTZE L. R. (1956) *Nucleonics* **14**, 108.

JUREN J. A. DE and ROSENWASSER H. (1953) *J. Res. Nat. Bur. Stand.* **51**, 203.

RADKOWSKY A. (1950) ANL–4476, p. 89.

SISK F. J. (1951) ORNL–933.

TITTLE C. W. (1951) *Nucleonics* **9**, 60.

WILSON V. C., BRAGDON E. W. and KANNER H. (1944) CP 2306.

WRIGHT W. B. and FROST T. R. (1956) KAPL–M–WBW–2.

APPENDIX

Neutron depression correction

In measurements of induced foil activities as a function of distance from a neutron source in a moderating medium, the absorption of neutrons by a foil may affect the neutron flux in the vicinity of a neighbouring foil. In principle, the effect of one foil on the thermal neutron absorption rate of the second is estimated by regarding the first foil as a negative source of neutrons equal to its neutron absorption rate. If the flux at the second foil due to this negative source is small compared with the flux with the first foil absent, separation is deemed satisfactory and, if necessary, a small correction is made to the foil activity. When no thermal source terms are present in the medium from thermalization of fast neutrons, the effect of one foil on a second foil on the same radial line from the source may be considerable even at large separations.

For the case of a point thermal neutron source in an absorbing medium such as water, the neutron flux, ϕ, as a function of distance from the source is given by

$$\phi(r) = \frac{3Qe^{-r/L}}{4\pi\lambda_{tr}r}, \tag{13}$$

where Q is the source strength in neutrons per second.

If a foil of area S is placed at a distance r from the source, its absorption rate of thermal neutrons, C_1, is given by

$$C_1 = \frac{\alpha\phi S}{2}, \tag{14}$$

where α is the probability of absorbing a thermal neutron from an isotropic flux (TITTLE, 1951). This negative sink prevents captured neutrons from diffusing to r_2 along the radial line through r_1. Assuming the dimensions of the foil are small compared to the radial separation, the flux decrease at r_2 is given by

$$-\Delta\phi(r_2) = \frac{3\alpha S\,\phi(r_1)\exp -\dfrac{(r_2 - r_1)}{L}}{8\pi\lambda_{tr}(r_2 - r_1)}. \tag{15}$$

If no sink were present, the flux at r_2 relative to r_1 would be

$$\phi(r_2) = \phi(r_1)\frac{r_1}{r_2}\exp -\frac{(r_2 - r_1)}{L} \tag{16}$$

Division of equation (15) by equation (16) gives

$$\frac{-\Delta\phi(r_2)}{\phi(r_2)} = \frac{3\alpha S r_2}{8\pi\lambda_{tr} r_1 (r_2 - r_1)}. \quad (17)$$

If a heavily absorbing foil is used at r_1, the flux in its vicinity is depressed by a factor $1/F$ and equation (17) becomes

$$\frac{-\Delta\phi(r_2)}{\phi(r_2)} = \frac{3\alpha S r_2}{8\pi\lambda_{tr} F (r_2 - r_1) r_1}. \quad (18)$$

F is the Bothe self-depression factor and is given by the following expressions for a circular foil of radius R:

$$F = 1 + \frac{\alpha}{2}\left[\frac{3R}{2\lambda_{tr}}\frac{L}{R+L} - 1\right] \text{ if } R \gg \lambda_{tr}, \text{ (TITTLE, 1951)} \quad (19)$$

$$F = 1 + \frac{0{\cdot}34\,\alpha R}{\lambda_{tr}} \text{ if } R \ll \lambda_{tr}. \quad (20)$$

For a square foil having an area of 4 cm², a circular foil of equal area has a radius of 1·128 cm. Equation (19) more nearly represents the experimental case for the indium foils where

$$R = 1{\cdot}128 \text{ cm},$$

$$\lambda_{tr} = 0{\cdot}425 \text{ cm},$$

and $L = 2{\cdot}77$ cm

are the values used for water at room temperature. Actually, both equations give nearly the same result.

$F = 1 + 0{\cdot}91\,\alpha$ from equation (19), and

$F = 1 + 0{\cdot}90\,\alpha$ from equation (20).

To test equation (18), two sets of measurements were taken with the 2 × 2 cm indium-tin foils at 20·07 cm with and without a 0·051 cm thick cadmium foil of the same area at 14·92 cm. The results are given in Table 2.

TABLE 2.—FOIL DEPRESSION DATA

Front Foil	Rear Foil	Rear Foil Activity
Blank	In–Sn	2308 (±1·4%)
Cd	In–Sn	1959 (±1·4%)

From equation (18), where $\alpha = 1$ for cadmium,

$$\frac{-\Delta\phi(r_2)}{\phi(r_2)} = 0{\cdot}154.$$

Experimentally, the depression is

$$\frac{-\Delta\phi(r_2)}{\phi(r_2)} = \frac{349}{2308} = 0{\cdot}151 \ (\pm 11 \text{ per cent}).$$

For this extreme case the agreement is quite good and the formulation should introduce negligible error in the practical case. For the indium-tin foils, α, the probability of absorption from an isotropic flux, is given by

$$\alpha = 1 - e^{-\Sigma_a d}(1 - \Sigma_a d) - \Sigma_a^2 d^2 E_1(\Sigma_a d). \text{ (TITTLE, 1951)} \quad (21)$$

The foils have an indium thickness of 44·15 mg/cm², and using 190 barns for the cross-section at 2200 m/sec, $\alpha = 0{\cdot}072$, and $F = 1{\cdot}065$. Substituting into equation (6) gives

$$\frac{-\Delta\phi(r_2)}{\phi(r_2)} = 0{\cdot}0198.$$

The effective thickness of the dysprosium in the foils was 13·2 mg/cm². Using 950 barns for the 2200 m/sec cross-section, $\alpha = 0{\cdot}075$, and $F = 1{\cdot}05$. This results in a cumulative depression of about 2 per cent at the last foil at the two highest temperatures where the foil separation was 7 cm and about 3 per cent at the other temperatures where the foil separation was 5 cm.

Note added in proof: During the period our paper was being revised to include the data at 166° and 244°C, ROCKEY K. S. and SKOLNIK W. (1960) *Nucl. Sci. Eng.* **8**, 62 published a set of diffusion length measurements in water at 25·9°, 122·7°, 218·5° and 295·3°C. Their technique was similar to ours but did not include a source term correction. The result at 218·5° was consistent with our empirical fit but the other three values are higher by amounts greater than the statistical errors.

VOL. 14 196

Reactor Science and Technology (J.N.E. Parts A/B), 1961, Vol. 14, pp. 25 to 30. Pergamon Press Ltd. Printed in Northern Ireland

A RECALIBRATION OF THE NBS STANDARD THERMAL NEUTRON FLUX

E. R. MOSBURG, JR. and W. M. MURPHEY
National Bureau of Standards, Washington 25, D.C.

(*Received* 4 *August* 1960)

Abstract—The Standard Thermal Neutron Flux of the National Bureau of Standards has been recalibrated in terms of the thermal neutron absorption cross-section of gold. This was accomplished by β–γ coincidence counting of activated gold foils approximately 0·001 in. and 0·00025 in. thick in a 4π-scintillation counter geometry. The value obtained was 4167 ± 1·5 per cent neutrons/cm² sec (October 1959). When averaged with a previous calibration made with boron foils the final value for the cadmium difference flux was 4203 ± 1·5 per cent neutrons/cm² sec. Measurement of the cadmium ratio for various thicknesses of gold led to a value of 0·0235 ± 2 per cent for the epithermal flux parameter, r, of WESTCOTT's convention. Using this convention the value of the flux is 4225 ± 1·5 per cent neutrons/cm² sec.

1. INTRODUCTION

THE NBS Standard Thermal Neutron Flux hereafter referred to as the Standard Flux, was calibrated originally in terms of the $B(n, \alpha)$ cross-section (DE JUREN and ROSENWASSER, 1954). As a result of an increased demand for the calibration of unknown fluxes by foil activation, a recalibration of the Standard Flux by an independent method was desired. A recent redetermination of the thermal absorption cross-section of gold (GOULD, TAYLOR, RUSTAD, MELKONIAN and HAVENS, 1957) has yielded the new value, 98·8 ± 0·3 barns (HUGHES and SCHWARTZ, 1958). For gold, the absorption cross-section equals the activation cross-section since (n, p) and (n, α) reactions are forbidden by the Coulomb barrier. This increased precision allows the recalibration of the Standard Flux directly in terms of the gold cross-section. The β–γ coincidence method was used and, because of the low specific activity available with the flux (about 1 dps per mg), 4π-scintillation detection was employed in each channel.

Thin gold foils (0·001 in. and 0·00025 in. thick) were irradiated for several half-lives in the Standard Flux and subsequently inserted between two concentric cylinders of plastic scintillator (see Fig. 1). This assembly was then coupled optically by a light pipe to the photomultiplier of the β-channel and was inserted into a well-type NaI(Tl) scintillator mounted on the photomultiplier of the γ-channel. Thus the foils were counted in essentially 4π geometry for both β- and γ-radiation. This was important in obtaining sufficient count rates.

The decay scheme of ^{198}Au is shown in Fig. 2. Because some of the 960 keV β-particles may penetrate

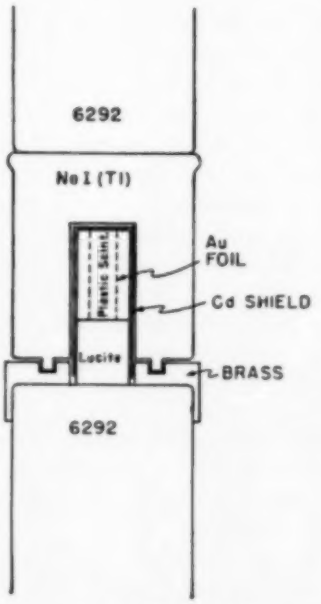

FIG. 1.—Geometry for 4π, β–γ coincidence counting of irradiated gold foils.

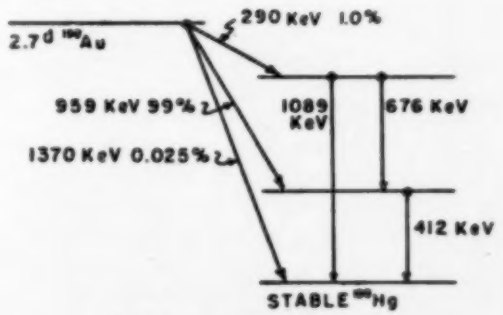

FIG. 2.—Decay scheme of ^{198}Au.

the plastic scintillator and enter the NaI, a β-shield was inserted between the plastic scintillators and the inner wall of the NaI in order to eliminate the possibility of β–β coincidences. No difference in the measurements was observed when this shield was changed from 0·004 in. of aluminium to 0·010 in. of cadmium. The cadmium together with the plastic scintillator and inner aluminium wall of the NaI scintillator provided a thickness well in excess of the extrapolated range for 1 MeV electrons. It was concluded therefore, that β–β coincidences due to β-particles entering the NaI were not possible in this geometry (the small amount of β-Bremsstrahlung is discussed below).

Because of the low count rates, good shielding of the scintillators was required. An annular, one-inch thick, mercury shield provided a decrease in background by a factor of five below the level obtained with the four-inch thick outer shield of lead. Inside the mercury shield, a layer of 0·060 in. of cadmium removed the K-fluorescence radiation from lead and mercury. Under these conditions the background counting rate in the γ-channel ranged from 1 to 2½ c/sec for γ-discrimination levels in the region 20–30 keV. The ratio of background to gold count rate was approximately 0·03 for the γ-channel. The pulses from the 6292 photomultipliers were applied to linear amplifiers. The discriminator outputs of these amplifiers were scaled and simultaneously fed to a coincidence circuit with a resolving time of 2 μsec. The settings of these discriminators allowed some control of the efficiencies of the β- and γ-channels.

2. THEORY

Throughout the article the following definitions will be used (STEYN and HAASBROEK, 1958):

e_β = probability* for detection of β-particles in the inner detector,

e_γ = probability* for detection of γ-rays in the inner detector (due to Compton scattering),

E_γ = probability* for detection of 412 keV γ-rays in the outer detector,

kE_γ = probability* for detection in the outer detector of γ-rays which have undergone Compton scattering in the inner detector.
No β-particles are allowed to reach the outer detector.

D = absolute disintegration rate of the foil,

σ = probability of Compton scattering of 412 keV γ-rays before reaching the outer detector,

c_β = measured count rate of pulses from the inner detector,

c_γ = measured count rate of pulses from the outer detector.

c_e = measured coincidence count rate.

Using the above definitions, we have for the count rate in the β-channel in terms of the disintegration rate:

$$\frac{c_\beta}{D} = e_\beta(1 - e_\gamma) + e_\gamma(1 - e_\beta) + e_\gamma e_\beta$$
$$= e_\beta + (1 - e_\beta)e_\gamma \qquad (1)$$

and for the γ-channel:

$$\frac{c_\gamma}{D} = (1 - \sigma)E_\gamma + \sigma k E_\gamma = [\sigma(k - 1) + 1]E_\gamma. \qquad (2)$$

The coincidence rate is similarly

$$\frac{c_e}{D} = [\sigma(k - 1) + 1]e_\beta E_\gamma + (1 - e_\beta)e_\gamma k E_\gamma \qquad (3)$$

where the first term represents β–γ coincidences and the second term represents γ–γ coincidences. Coincidences of the type β–β are excluded by the β-shielding between the two scintillators.

Combining the above equations we obtain

$$\frac{c_\beta c_\gamma}{c_e D} = \frac{e_\beta + (1 - e_\beta)e_\gamma}{e_\beta + (1 - e_\beta)e_\gamma \dfrac{k}{\sigma(k - 1) + 1}} \cdot \qquad (4)$$

The right side of the equation becomes unity for $e_\beta = 1$ or for $k = 1$, in which case $D = \frac{c_\beta c_\gamma}{c_e}$. Because of the thickness of the gold foil the maximum obtainable values of e_β are about 0·70 for 1 mil foils and 0·85 for 1/4 mil foils. Much thinner foils could not be used because of the low specific activity. The technique is therefore to adjust the γ-discrimination level so that k is close to unity. Then, with k fixed, the β-discrimination level is changed to vary e_β, extrapolating to $e_\beta = 1$. For the geometry used in this experiment we calculate $e_\gamma \simeq 0{\cdot}064$. We assume that $\sigma \simeq e_\gamma$. Then plotting $\frac{c_\beta c_\gamma}{c_e D}$ against e_β we obtain a family of curves with parameter, k, shown in Fig. 3. An accurate extrapolation to β-efficiency of 1·0 is impractical for any curves except those with k closely approximate to one. The hyperbola-like behaviour of the curves suggests a plot vs. $\frac{1}{e_\beta}$. Fig. 4 shows that $\frac{c_\beta c_\gamma}{c_e D}$ plotted vs. $\frac{1}{e_\beta} - 1$ extrapolates fairly well to $e_\beta = 1{\cdot}0$ even for values of k differing considerably from one, especially if points are limited to the region for which the value of $\frac{1}{e_\beta} - 1$ is between zero and six.

* The probabilities include the appropriate geometrical factors and circuit discrimination levels.

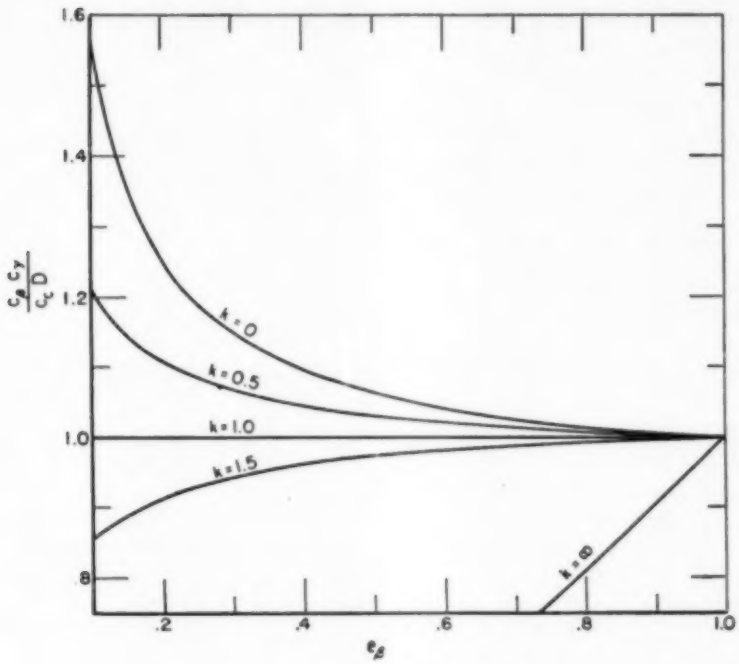

FIG. 3.—Plot of $\frac{c_\beta c_\gamma}{c_c D}$ versus e_β.

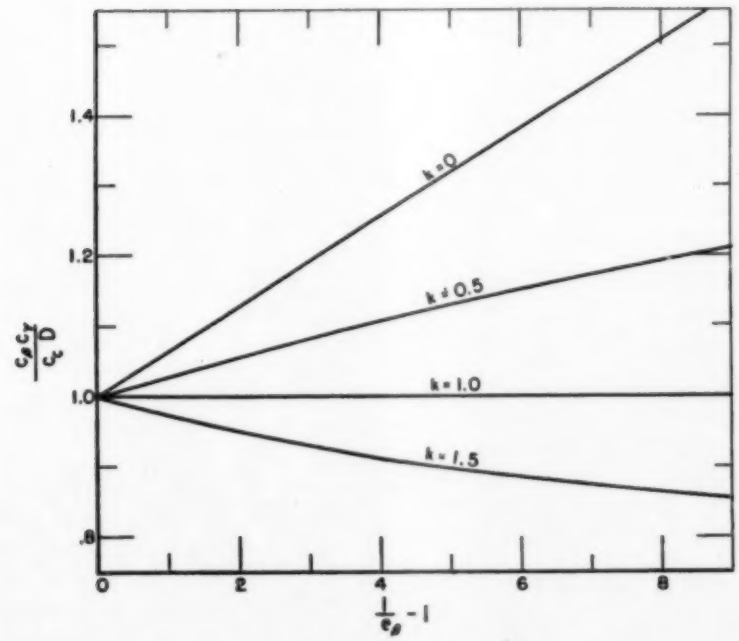

FIG. 4.—Plot of $\frac{c_\beta c_\gamma}{c_c D}$ versus $\frac{1}{e_\beta} - 1$.

Up to this point we have not considered the spatial extension of the gold source. If we proceed to do this in the simple case where γ–γ coincidences as well as β–β coincidences are neglected, then averaging over the foil volume gives (PUTMAN, 1957):

$$\frac{c_\beta c_\gamma}{c_e D} = \frac{\overline{e_\beta} \cdot \overline{E_\gamma}}{\overline{e_\beta E_\gamma}}. \tag{5}$$

If either E_γ or e_β is independent of position within the foil then

$$\frac{c_\beta c_\gamma}{c_e D} = 1. \tag{6}$$

This condition is not rigorously satisfied in the present experiment so we have estimated the error involved under the assumption that the variation of detection probability is linear over the position within the foil (PUTMAN, 1957). The maximum error amounts to 0·005 per cent under this assumption.

3. THE MEASUREMENTS

The value of the absolute decay rate of each set of foils was based on a series of 15-min counts taken over several days following removal from the flux. For the count rates involved, accidental coincidences are negligible. After correction for the background and the decay of gold activity with time, the values of $\frac{c_\beta c_\gamma}{c_e}$ were plotted vs. $\frac{1}{e_\beta} - 1$ for which we took $\frac{1}{e_\beta} = \frac{D}{c_\beta} = \frac{c_\gamma}{c_e}$. Theoretically, some curvature in $\frac{c_\beta c_\gamma}{c_e}$ vs. $\frac{1}{e_\beta} - 1$ can be expected for large values of $\frac{1}{e_\beta} - 1$. Hence only data with $\frac{1}{e_\beta} - 1$ less than 6 were used for the straight line extrapolation to $\frac{1}{e_\beta} - 1 = 0$. Data with very low levels of beta discrimination were also disregarded because the beta background is high and unstable in this region. The line of best fit was always close to horizontal indicating a value of k close to one. The intercept was taken as the first approximation to the absolute decay rate, D. From the intercept, new values of e_β, and hence $\frac{1}{e_\beta} - 1$, were determined as before for each experimental point. A final extrapolation to $\frac{1}{e_\beta} - 1 = 0$ with these new values was then calculated by the method of least squares. This extrapolation is based in each case on about 36 experimental points with weights assigned according to the count rate of the foil on the day of measurements. The statistical spread of these measurements around the line of best fit is approximately ± 1 per cent.

The measurements were repeated using the same foils activated inside a 0·040 in. thick cadmium cover.

The relation between the thermal neutron flux and the disintegration rates of the foil, corrected to saturation, is given by

$$\varphi = \frac{A}{N_0 \sigma_0} \frac{(D_0 - D_{ep})}{m} \cdot \frac{t}{f(t)} \tag{7}$$

where

D_0 = disintegration rate at saturation for bare activation,

D_{cd} = disintegration rate at saturation for cadmium covered activation,

$D_{ep} = F_{Cd} D_{Cd}$ where F_{Cd} is a correction (= 1·048 for 0·040 inches of Cd) for the shielding of epithermal flux by the cadmium (TITTLE, 1951),

$t = 0{\cdot}3021 \frac{m}{s}$ (dimensionless) $= \frac{N_0 \sigma_0 m}{As}$,

m = mass of the foil (g),

N_0 = Avogadro's number,

s = area of the foil (cm²),

A = atomic weight, and

σ_0 = 98·8 ± 0·3 barns (HUGHES and SCHWARTZ, 1958) (the 2200 m/sec absorption cross-section).

Since the gold foil is irradiated in an air slot, the flux depression at the surface of the foil can be shown to be negligible. The factor $\frac{t}{f(t)}$ is thus simply the self-shielding correction, where

$$f(t) = 1/2\left[1 - e^{-t} + te^{-t} - t^2 \int_t^\infty \frac{e^{-s}}{s}\, ds\right] \tag{8}$$

for an isotropic flux.

The correction factor for the 1 per cent of the ^{198}Au decay which does not lead to the first excited state of ^{198}Hg (Fig. 2) was calculated, using the simplified assumption of no γ–γ coincidences (i.e. $k = 0$), by considering the relative detection probabilities for all the different γ- and β-radiations involved. Such a modification of the detection probabilities in equations (1), (2), and (3) gave a correction factor of 0·998 to be applied to the value of D determined from equation (4) which assumes that all the decay occurs to the first excited state of ^{198}Hg.

To determine the effect of internal conversion of the 412 keV γ-rays, equations (1), (2), and (3) are rewritten to include the internal conversion probability,

I, and the detection efficiency of the resulting electron, ce_β, (e_β is as defined above).

$$\frac{c_\beta}{D} = (1 - I)[e_\beta + (1 - e_\beta)e_\gamma] + I[ce_\beta(1 - e_\beta) + e_\beta(1 - ce_\beta) + e_\beta ce_\beta] \quad (1')$$

$$\frac{c_\gamma}{D} = (1 - I)[\sigma(k - 1) + 1]E_\gamma \quad (2')$$

$$\frac{c_c}{D} = (1 - I)\{[\sigma(k - 1) + 1]E_\gamma e_\beta + (1 - e_\beta)e_\gamma kE_\gamma\} \quad (3')$$

This treatment leads to an equation identical with equation (4) except for the addition of a second term on the right equal to

$$I\frac{(1 - e_\beta)(ce_\beta - e_\gamma)}{e_\beta + (1 - e_\beta)e_\gamma \dfrac{k}{\sigma(k - 1) + 1}} . \quad (9)$$

Unlike the first term, this second term is not monotonic and reaches a peak value near $\frac{1}{e_\beta} = 3$. This results in an error in our linear extrapolation. Thus the correction to be made depends on the ratio, c, of the probability for detection of the resulting conversion electrons relative to the average detection probability for the whole β-spectrum. This latter quantity is known experimentally. The detection probability for the internal conversion electrons was calculated for several foil thicknesses, using the data of FLEEMAN (1954) by integrating graphically over angle and foil thickness. This indicated that c is a function of foil thickness. The resulting correction factors are shown in Table 1.

Effects on which only upper limits could be placed were for β-Bremsstrahlung due to the 0·96 MeV β-rays in the gold ($< +0{\cdot}04$ per cent) (determined experimentally by measuring the β-Bremsstrahlung of ^{204}Tl β-particles in gold taking due account of the X-rays in ^{204}Tl decay), for variations over position within the foil of the solid angle subtended by the γ-detector ($< +0{\cdot}005$ per cent) (calculated), for edge effects in the self-absorption correction ($< -0{\cdot}25$ per cent) (calculated) and for non-isotropy of the neutron flux ($< 0{\cdot}04$ per cent) (determined experimentally by activating foils parallel and perpendicular to the axis of symmetry of the sources in the flux). The sum of these upper limits is 0·3 per cent which will be considered as an uncertainty in the final flux value. The standard deviation of the measurements of 5 foil activities is 1·2 per cent so that the standard deviation of the average is about 0·6 per cent. The largest correction for self-shielding was 4·6 per cent and should be more precise than the error due to edge effects mentioned above. The correction for the internal conversion of 412 keV γ-ray should be good to within 0·4 per cent. The error in the absorption cross-section of gold is reported in BNL-325 2nd ed. (HUGHES and SCHWARTZ, 1958) as 0·3 per cent. Combining these uncertainties yields an overall accuracy of slightly less than 1·5 per cent.

4. CONCLUSIONS

The value of the Standard Flux as measured by gold foil activation when all corrections and errors have been considered is $4167 \pm 1{\cdot}5$ per cent neutrons/cm^2 sec (October, 1959).

In order to compare this determination of the Standard Flux, using gold foils, with that made by DE JUREN and ROSENWASSER (1954) in terms of the boron cross-section, a few corrections must first be made. The difference in the shielding of the aluminium holders used in the two experiments, measured with manganese foils, leads to a factor of 1·064 by which the flux determined with boron must be multiplied to obtain the flux present during the gold calibration.

TABLE 1

Foil thickness (mg/cm^2)	Total activity of foil (dps/mg)	Correction for epithermal activity $\left(1 - \frac{1}{R_{Cd}}\right)$	Thermal activity of foil (dps/mg)	Self-shielding correction	Internal conversion correction	Thermal flux (n/cm^2 sec)	Average value (n/cm^2 sec)	Final value corrected for gold decay scheme (n/cm^2 sec)
56·6	1·414	·8696	1·230	1·0455	·9884	4211		
56·6	1·420	·8696	1·235	1·0455	·9884	4228		
56·6	1·406	·8696	1·223	1·0455	·9884	4187	4175	4167
47·8	1·398	·8623	1·205	1·0395	·9874	4097		
14·6	1·563	·8033	1·256	1·0140	·9843	4153		

Subsequent to the calibration with boron, the Standard Flux was dismantled during a move to a new location. This caused the flux to increase by a factor of 1·018. During the time between the calibration with boron (Sept. 1952) and the calibration with gold (Oct. 1959) the growth of ^{210}Po had increased the flux by a factor of 1·021. Finally as reported by STAFFORD *et al.* (1960) the neutron absorption cross-section of the Argonne-Brookhaven standard boron has been redetermined as 764 ± 3 barns which involves a correction of the flux determined with boron by a factor of 0·987. When all these corrections are made, the flux determined with boron becomes, under the present conditions, 4276 ± 2 per cent neutrons/cm² sec. Thus the gold and boron determinations agree within 2·6 per cent. Combining the boron and gold determinations using arbitrary weights of 1 : 2 respectively, yields for the NBS Standard Thermal Neutron Flux a value of 4203 ± 1·5 per cent neutrons/cm² sec.

In a series of papers by WESTCOTT (1958) a convention for neutron flux is proposed which does not involve a cadmium difference measurement. However, in cases such as the present one where appreciable self-shielding occurs, the activity must be separated into $1/v$ and resonance components before self-shielding corrections can be applied and the convenience of such a convention is lost. In WESTCOTT's notation the relation between the thermal flux as defined by a cadmium difference, φ_{th}, and the flux of Westcott's convention, φ_w, is:

$$\varphi_{th} = \left(g - \frac{r}{K}\right)\varphi_w. \qquad (10)$$

For gold, WESTCOTT calculates $g = 1{\cdot}005$. K is a parameter depending on the thickness of cadmium used, which for 0·040 in. of cadmium is 2·2931. In order to calculate φ_w from the value of φ_{th} we must, therefore, measure the value of r for the Standard Flux. By correcting the resonance component for Doppler broadening and self-shielding according to the equation of ROE (1954) and the $1/v$ component for self-shielding according to equation (8) of this article, it is found that a value of $r = 0{\cdot}0235 \pm 2$ per cent gives the best agreement with the cadmium ratios for gold foils of approximately 0·00025, 0·001, 0·002, 0·003 and 0·006 in. thicknesses, as measured by β–γ coincidence. With this value of r, the value of the Standard Flux using WESTCOTT's convention becomes 4225 ± 1·5 per cent neutrons/cm² sec.

REFERENCES

FLEEMAN J. (1954) *Electron Physics* NBS Circular 527, p. 93.

GOULD F., TAYLOR T. I., RUSTAD B. M., MELKONIAN E. and HAVENS W. W. (1957) *Bull. Amer. Phys. Soc. II* **2**, 42.

HUGHES D. J. and SCHWARTZ R. B. (1958) *Neutron Cross-Sections* (2nd ed.) BNL 325.

JUREN J. DE and ROSENWASSER H. (1954) *J. Res. Nat. Bur. Stand.* **52**, 93.

PUTMAN J. L. (1957) AERE I/M 26.

ROE G. M. (1954) KAPL–1241.

STAFFORD G. S., TAYLOR T. I., RUSTAD B. M. and HAVENS W. W. JR. (1960) *Bull. Amer. Phys. Soc. II* **5**, 288.

STEYN J. and HAASBROEK F. J. (1958) *Proceedings of the Second International Conference on the Peaceful Uses of Atomic Energy, Geneva*, A/Conf. 15/P1 1104. United Nations, N.Y.

TITTLE C. W. (1951) *Nucleonics* **9**, 60.

WESTCOTT C. H. (1958) *Proceedings of the Second International Conference on the Peaceful Uses of Atomic Energy, Geneva*, A/Conf. 15/P/202; (1958) CRRP/787; (1959) CRRP/662. United Nations, N.Y.

Reactor Science and Technology (J.N.E. Parts A/B), 1961, Vol. 14, pp. 31 to 48. Pergamon Press Ltd. Printed in Northern Ireland

ACHIEVING HIGH BURN-UP IN FAST REACTORS

L. R. BLAKE*
Dounreay Experimental Reactor Establishment, Dounreay, Thurso, Caithness

(*First received* 9 *May* 1960 *and in final form* 16 *September* 1960)

Abstract—A theory is proposed, relating irradiation swelling in metal fuel with burn-up, and used to predict fuel-element behaviour under various fast reactor conditions; good agreement is obtained with known behaviour sufficient to substantiate the general conclusion that fission-product gas accumulation is chiefly responsible. It would appear impossible to eliminate such swelling, only to reduce and accommodate it. Based on this principle, a fast reactor fuel-element is suggested using unalloyed uranium, with substantial void-space in a strong can. This should be capable of 4 per cent average burn-up at 700°C centre temperature under practical fast reactor conditions, which should be sufficient to ensure economic power.

With oxide fuel it would appear that, in order to satisfy the essential safety and economic requirements in a fast reactor, it is also necessary to incorporate considerable voidage in the fuel and to employ a strong can; safety requirements could also lead to double-canning. Such an arrangement could possibly attain 10 per cent burn-up, which is comparable to 4 per cent with metal fuel. A cermet of UO_2–PuO_2 dispersed in uranium metal, again in a strong can and with void space in the fuel, appears a suitable way of combining the good properties of both oxide and uranium fuel, and could result in an excellent high burn-up fuel for fast reactors, though its behaviour is more uncertain to predict.

OL.
14
961

1. INTRODUCTION

COMPETITIVE power production from a fast-reactor and convenient operation without too many shut-downs for reloading depends upon obtaining a fuel element of high burn-up, of the order 1 per cent to 5 per cent according to the type of fuel. Until recently, hope of achieving this with metal fuel centred around the use of high alloy additions to uranium-plutonium, such as 14w/o molybdenum or fissium. So far this approach has been only partially successful for, although about 1 per cent average burn-up in a fast-reactor may be achieved with these fuels, this is still too low for economic power, particularly in view of the associated disadvantages: (1) high burn-up can only be obtained with a low centre-temperature of about 600 to 650°C maximum; (2) the alloying additions reduce thermal conductivity and this together with the low centre-temperature makes fuel elements small and expensive at the high power ratings necessary for low fuel-investment; (3) presence of the alloy reduces nuclear performance in particular reducing the internal (core) breeding ratio; and (4) aqueous reprocessing costs are considerably increased.

These rather disappointing results with metal-fuels have increased interest in oxide fuels, chiefly UO_2 and PuO_2, and oxide-fuel dispersed in a metal matrix such as Fe or ^{238}U-Mo; interest in carbide fuels has also increased though these are still in the very early stages of development. Although these fuels are certain to have a burn-up greater than 1 per cent, again this is not without additional disadvantages, particularly: lower overall breeding-ratio, lower internal breeding-ratio, larger reactivity changes with burn-up, and, possibly lower specific power; moreover, the implications on fast reactor safety of using oxide or carbide fuels has not yet been studied in any detail, especially the safety implications of high burn-up itself. However, economic power from fast reactors unequivocally demands high burn-up so that, despite these limitations, there is now a significant movement away from metal fuel as used in Dounreay Fast Reactor, EBR 1 and 2, and Enrico Fermi Reactor: for example, oxide-fuel is being used in the Russian BR5 and French 'Rapsodie' fast reactors and 25 v/o UO_2 in stainless-steel is intended for the second charge of the Enrico Fermi reactor.

As economic power from fast reactors requires about a 10-fold increase in burn-up over the best current thermal reactor practice, and under more severe power-rating and temperature conditions, it is evident that this extrapolation of irradiation data to predict fast-reactor fuel behaviour, and the most suitable fast-reactor fuel, can only be made with some theoretical justification. This paper attempts to provide this in order to bring out the important factors and to estimate the likely maximum burn-up

* Present address: Brush Electrical Co., Loughborough, Leics.

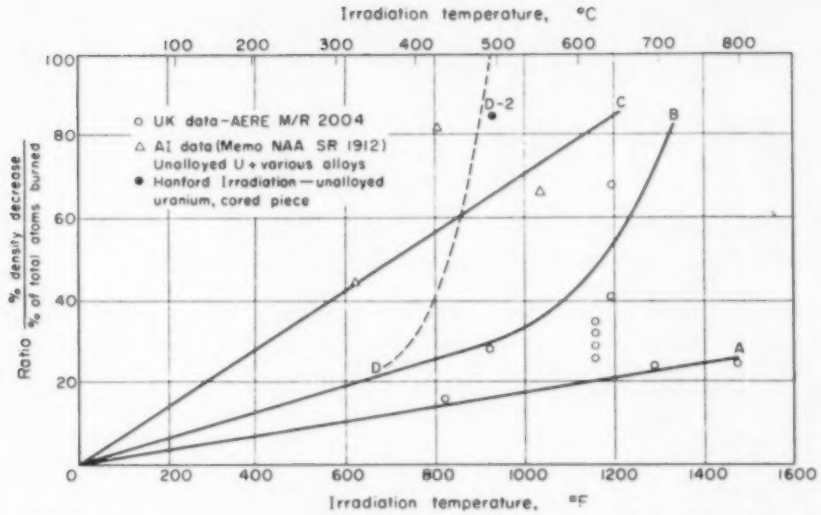
Irradiation temperature, °C
100 200 300 400 500 600 700 800
o UK data-AERE M/R 2004
△ Al data (Memo NAA SR 1912) Unalloyed U + various alloys
● Hanford Irradiation — unalloyed uranium, cored piece
D-2
C
B
A
D
Ratio % density decrease / % of total atoms burned
0 200 400 600 800 1000 1200 1400 1600
Irradiation temperature, °F

FIG. 1.—Effect of irradiation temperature on volume change of uranium and uranium alloys. *A*—lower limit and *B*—best fit of AERE M/R 2004 data; *C*—data from M. F. FINNISTON, (DIETRICH and ZINN, 1958).

achievable with various fuels under practical fast reactor conditions with due regard to safety requirements. In particular, the possibility of achieving high burn-up in metal-fuel is examined in detail.

Factors limiting burn-up in metal fuel

Irradiation data on metal fuel, canned and uncanned, shows an enormous spread in the ratio of fuel swelling to burn-up, v/b, where burn-up,

$$b = \frac{\text{atoms fissioned}}{\text{total fissile and fertile atoms present}}, \quad (1.1)$$

swelling, $$v = (V_b - V_0)/V_0, \quad (1.2)$$

and where V_0 = original fuel volume and V_b = volume at burn-up, b.

As indicated in Fig. 1 with unrestrained uranium at 0·3 per cent burn-up and about 500°C temperature, the spread of v/b is 9 to 450, with average values between 15 and 50. For uranium, strengthened by 10w/o molybdenum, there appears a threshold below which swelling is substantially restricted and above which it is rapid, again with v/b values between 15 and 50 (see Fig. 2). The threshold appears to depend upon burn-up and temperature, being approximately 1·7 per cent burn-up at 550°C and 0·5 per cent burn-up at 650°C.

It appears generally recognized that the main factors which control swelling under irradiation are:

(i) Solid fission fragments are larger than the parent fissile atom; up to 2 per cent volume increase per 1 per cent burn-up is probably necessary to accommodate this.

(ii) Gaseous fission products (chiefly Xe and Kr), collect in cavities and build up pressure sufficient to deform the fuel; the cavities and the fuel consequently increase in volume.

(iii) Irradiation is also accompanied by temperature change and usually some degree of temperature cycling. This alone will cause fuel growth in many alloys due to anisotropy, but it could also open up cracks between adjacent grains of different orientation and assist item (ii).

The main methods at present employed to restrict swelling are:

(i) Alloy the fuel, with the chief object of increasing creep strength or tensile strength at the working

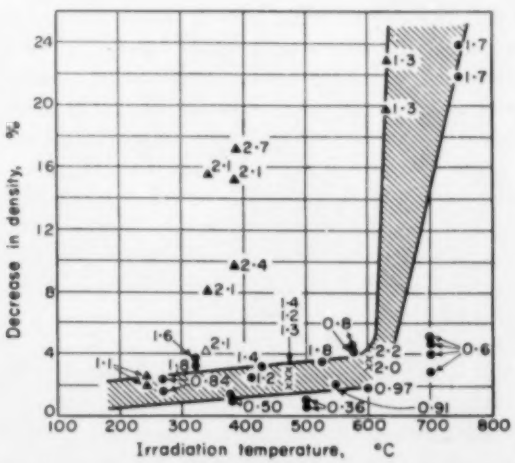

FIG. 2.—Density change as a function of irradiation temperature and burn-up in uranium-10 wt. per cent molybdenum alloy. (*Reactor Core Materials*, 1959).

temperature, so that the fuel can resist the gas pressure in the cavities and keep their size small.

(ii) Surround the fuel in a strong can which has a similar effect.

(iii) Control grain size and orientation by alloying, and heat treatment; control size, shape and distribution of gas cavities by control of impurities.

Present metallurgical development of fast-reactor metal-fuels centres around method (i). It seems unlikely that a major gain can be achieved over 10 w/o molybdenum or fission alloy, since creep strength is unlikely to be improved substantially and then not without corresponding economic disadvantages. However, it is possible that a major improvement might be possible by permitting and accommodating swelling, rather than putting the burden on the metallurgist to prevent it by high alloy additions. This approach seems particularly necessary to achieve a high burn-up of over 2 per cent in metal fuel at realistic temperatures. The implications of this principle will now be considered.

2. THEORIES OF IRRADIATION GROWTH

WYATT (1955) proposed a theory of irradiation swelling based on the assumption that fission product gases (krypton and xenon) migrate to and collect in voids, the fuel distorting by creep under the resulting gas pressure. As model for calculation he assumes the fuel to be composed of a lattice of cubes with a spherical bubble of fission product gas at the centre of each.

Equating forces due to gas pressure in the bubble with tensile force in the fuel, WYATT derives an expression for the swelling, v, in the form

$$v = 21(vT)^{3/2} \cdot (t/K)^{\frac{1}{3}} \qquad (2.1)$$

where T is the fuel temperature (°K), t is the time (hours) to burn-up, b (fraction), and K is a constant in an equation used to relate stress, creep rate and temperature, the value of K employed being given by $\log_{10}K = 12{\cdot}500/T$. To this value of growth due to fission product gas must be added a term to account for solid fission fragments. At a burn-up of 1 per cent attained in 300 days, equation (2.1) gives a value of voidage v of only 0·14 per cent to 500°C and 1·8 per cent at 600°C. This is evidently much too low, even considering the wide spread of experimental results.

FOREMAN (1956) extended WYATT's theory with a more rigorous treatment taking interactions between the spherical cavities into account. His final solution for swelling due to fission gas only is

$$v = 12{\cdot}6vT(t/K)^{\frac{1}{3}} \qquad (2.2)$$

which gives negligibly higher values than equation (2.1). ENDERBY (1956) further extended the calculation to take into account: (1) yielding around a cavity beyond the yield point; (2) departure from perfect gas laws of the gas in the cavities. With 1 per cent burn-up in 300 days at 575°C fuel temperature, modification (1) raised FOREMAN's figure for v from 1 per cent to 1·3 per cent; modification (2) raised it to 2·2 per cent. This is still much too low, as swelling of irradiated uranium centres around 30 per cent at 1 per cent burn-up (when incidentally the gas pressure is moderate and the perfect gas laws do hold).

Although these theories do not give quantative agreement with experimental results, there is little doubt from metallurgical examination of irradiated specimens that the general picture of fuel distortion under pressure of fission product gases is correct. CHURCHMAN, BARNES and COTTRELL (1958) and SYKES, HADDRELL and PFEIL (1956) report such examinations on specimens irradiated to 0·3 per cent burn-up at about 500°C. In each case the observed porosity agreed with the swelling, the results being summarized in Table 1.

CHURCHMAN (1958) suggests a theory of nucleation of cavities and indicates that the mobility of gas atoms varies with irradiation temperature so that at low temperature of up to 200°C, many bubbles of small size form and, at 500°C, gas atoms migrate to existing defects and cavities, such as oxide inclusions and grain boundaries.

3. EXTENSION OF THEORY OF IRRADIATION GROWTH

A full explanation of irradiation swelling must necessarily be complicated, since it is not only necessary to predict volume increase v as a function of

TABLE 1.—RESULTS OF METALLURGICAL EXAMINATION OF IRRADIATED SPECIMENS (CHURCHMAN, BARNES AND COTTRELL, 1958; SYKES, HADDRELL AND PFEIL, 1956)

Specimen	U	U − 10 w/o Zr	U − 7·5 w/o Nb
Specimen size before irradiation (mm³)	50	2·5	2·5
Average porosity after irradiation (%)	4·5	17·7	58·7
Main size of pores	98%, ·05 −2μ 2%, 100μ	1 − 15μ spherical & 1 × 3μ rods	mainly 4 × 10μ irregular some 1 × 4μ

burn-up b, temperature T and time t, but also the very great variation of v with different fuels and even with ostensibly identical specimens (DIETRICH and ZINN, 1958; SYKES, HADDRELL and PFEIL, 1956). Despite the low predictions of the WYATT-FOREMAN theory, it is difficult to picture a mechanism of substantial swelling other than that fission product gases collect in cavities and build up a pressure until the fuel yields. A full explanation, however, must include:

(1) Showing that the swelling v agrees with the volume of gas cavities. This has been done already by SYKES and CHURCHMAN.
(2) Calculating the pressure in the gas cavities, and showing that, with the particular cavity geometry and material properties, the stress distribution in the fuel is the right order to produce the observed deformation.
(3) Explaining how fuel anisotropy and temperature cycling influences results, for example, by helping to create cavities and to cause surface defects which reduce fuel strength, as well as causing growth in itself.
(4) Showing the factors which control cavity geometry and distribution in the fuel, for example: the role of impurity distribution; defects in the crystal or between grain boundaries; the factors controlling migration of gas in the lattice and the assembly of gas atoms in cavities; how the temperature and pressure during irradiation affects cavity nucleation and growth and also the effect of alloy additions and heat treatment prior to irradiation.
(5) Predicting swelling at a given burn-up for different alloy fuels, unrestrained and restrained in cans of differing materials and geometry, or with other forms of restraint, at a given temperature distribution in fuel and can.

An attempt will now be made to predict irradiation behaviour assuming that fission-product gas collects in irregular shaped cavities, which swell as more gas is added. The amount of gas released is assumed to be stable xenon and krypton isotopes only, which, from ANL-5742 and assuming appropriate irradiation conditions, is as shown in Table 2.

TABLE 2.—FISSION PRODUCT GAS RELEASE IN ^{235}U AND ^{239}Pu FAST FISSION (DEDUCED FROM ANL-5742)

Fast fission of	(Gas vol. at N.T.P.)/(Vol. of fuel completely fissioned)		
	Xe	Kr	(Xe + Kr)
^{235}U	391	53	444
^{239}Pu	428	16	444

The gas pressure at temperature $T(°K)$, burn-up b, and voidage v is, therefore,

$$p = 14{\cdot}7\,\frac{T}{273}\cdot\frac{444b}{v} = \frac{24Tb}{v}\ (\text{lb/in.}^2) \qquad (3.1)$$

The work done by the gas in deforming fuel and can is

$$W_g = \int_{v_0}^{v} p\,dv,\ (\text{in.-lb/in.}^3\ \text{fuel}), \qquad (3.2)$$

where v_0 is the initial voidage and v its value at burn-up b. Irradiation data suggests that up to a critical burn-up b_c where swelling increases markedly v is approximately proportional to b hence from equation (3.1) the gas pressure is constant and

$$\begin{aligned} W_g &= p(v - v_0) \\ &\to pv, \text{ if } v \gg v_0 \\ &= 24Tb. \end{aligned} \qquad (3.3)$$

In previous theories of irradiation swelling (WYATT, 1955; FOREMAN, 1956; ENDERBY, 1956; CHURCHMAN, BARNES and COTTRELL, 1958), emphasis has been placed on equilibrium conditions in the fuel, when forces due to gas pressure are equated with tensile forces in the fuel. It would appear more reasonable to assume that not only is the fuel stress limited everywhere to an appropriate creep stress, σ_c, but that when the fuel strain anywhere exceeds a limiting value, ε_r, (similar to that at rupture in a tensile test), that portion of the fuel is no longer capable of resisting by tension the gas pressures. As the fuel strain ε is maximum near a cavity and minimum at the fuel surface, this implies that internal regions of the fuel will reach its critical deformation before that of the surface. It would appear, therefore, that an energy balance, equating the work done by the gas with the maximum work of deformation to rupture of the fuel, would be more significant in predicting critical burn-up than a balance of forces. If the maximum work of deformation of the fuel is assumed to be similar to that in a creep test at appropriate strain rate, then at the critical burn-up and swelling, when the surface layer of fuel ruptures,

$$pv_c = 24Tb_c = \sigma_c\varepsilon_r. \qquad (3.4)$$

It is difficult to decide the strain rate to employ in determining the creep stress, σ_c. At the fuel surface the strain rate will be (assuming linear growth v until the critical growth v_c)

$$\dot{\varepsilon} = \dot{b}(\varepsilon_r/b_c), \qquad (3.5)$$

where $\dot{b}$ is the rate of burn-up. Assuming a cylindrical

fuel-element, with the surface skin having the properties of a thin-walled tube, then the fuel swelling v will be related to the surface strain by

$$v = 2\varepsilon_1 + \varepsilon_2$$

where ε_1 = hoop strain and ε_2 = longitudinal strain. Since $\varepsilon_2 = 0{\cdot}24\varepsilon_1$, then,

$$v = 2{\cdot}24\varepsilon_1 = 2{\cdot}24\varepsilon, \qquad (3.6)$$

if the fuel surface strain is identified with the hoop strain.

For the present estimate it is probably sufficiently accurate to assume that the work-to-rupture of internal fuel is the same as that of the surface fuel, so that although the strain rate $\dot{\varepsilon}$ is higher at the cavity surface, and hence the creep stress there is also higher, its strain at rupture ε_r is correspondingly less. This appreciably simplifies the calculation and enables values of σ_c, ε and $\dot{\varepsilon}$ appropriate to the surface layer of fuel to be assumed typical of all fuel. Equations (3.4) to (3.6) are readily solved iteratively to determine the critical burn-up b_c, the critical swelling v_c and $(v/b)_c$, provided the rate of burn-up, $\dot{b}$ and the fuel creep properties are known. Results are summarized below for the case of unrestrained uranium and for 10w/o molybdenum-uranium, at 500°C and 1 per cent burn-up per year ($\dot{b} = 1{\cdot}14 \times 10^{-6}$ hr^{-1}) assuming creep properties as in Fig. 3 and 2 per cent surface strain at rupture.

At a burn-up greater than b_c, runaway swelling can be expected, like runaway strain in a tensile test of ductile material. Under irradiation conditions, runaway swelling is accelerated due to reduced thermal conductivity and higher temperatures caused by the increased porosity, and is offset by the reducing gas pressure with increased voidage.

Because of runaway swelling it is necessary when comparing actual and predicted results to discard irradiation results beyond a critical swelling, v_c. If this is done, Table 3 shows remarkable agreement with the test data of Fig. 1, in fact, better than could be expected in view of the approximate nature of the analysis and possible errors in creep data. That this good agreement is partly fortuitous is apparent from the low gas pressure p_c in Table 3, which could not have remained constant at this low value during the whole of the irradiation period up to b_c, but must have been much higher during the early stages of swelling. This is inconsistent with the assumption that p is constant in deriving equation (3.3) and implies that $Wg > p_c v_c$. Hence the good agreement achieved may be the result of self-cancelling factors, the work of deformation of the fuel being correspondingly higher than the value $\sigma_c\varepsilon_r$ assumed. However, this analysis appears to have shown up the main controlling factors, and as long as it is recognized that equations (3.4) to (3.6) are subject to appreciable error, there would appear no point in further refining them, as any extension of the theory cannot be put to the test, due to the wide spread of irradiation and creep data.

TABLE 3.—IRRADIATION SWELLING PREDICTIONS USING EQUATIONS (3·4)–(3·6)

			Uranium	10w/o Mo-U
Critical burn-up	b_c	%	0·24	0·71
Critical swelling	v_c	%	4·5	4·5
Ratio (v/b) at critical point	$(v/b)_c$	—	19	6·3
Fuel creep stress	σ_c	lb/in.^{2}	2250	6600
Gas pressure in cavities $= \sigma_c/2{\cdot}24$	p_c	lb/in.^{2}	1000	3000

Equation (3.4) can readily be extended to include the effect of the can in restraining swelling. If the can is assumed to become effective at or near the critical burn-up of the fuel itself, then the fuel may be regarded as a hydrostatic fluid, and the pressure in the can will be that of the gas pressure in the cavities. Under these conditions, equation (3.4) becomes

$$p_c v_c = 24Tb_c = \sigma_c\varepsilon_r + v\sigma_c'\varepsilon_r', \qquad (3.7)$$

where v = (volume of can)/(original fuel volume) and the prime denotes can properties. Equations (3.5) and (3.6) will also apply to the can giving

$$\varepsilon' = v/2{\cdot}24,$$

so

$$\dot{\varepsilon}' = \dot{v}/2{\cdot}24 = \dot{b}(\varepsilon_r'/b_c). \qquad (3.9)$$

Substituting equations (3.6) in (3.7) gives an expression for the gas pressure in the cavities at the critical swelling

$$p_c = (\sigma_c + v\sigma_c')/2{\cdot}24. \qquad (3.10)$$

Equations (3.7) to (3.10) will now be applied to canned fuel elements.

4. IRRADIATION GROWTH PREDICTIONS

Dounreay fast reactor fuel element

Table 4 summarizes calculations for the niobium canned, ½ per cent Cr-U alloy, D.F.R. fuel element at a typical power rating, obtained solving equations (3.7) to (3.9) iteratively in conjunction with the creep data of Figs. 3 and 4. It shows that the niobium, if it retains the good mechanical properties assumed in Fig. 4(a), is at least as effective as the fuel itself in opposing swelling (compare contribution $v\sigma_c'$ from can with σ_c from fuel).

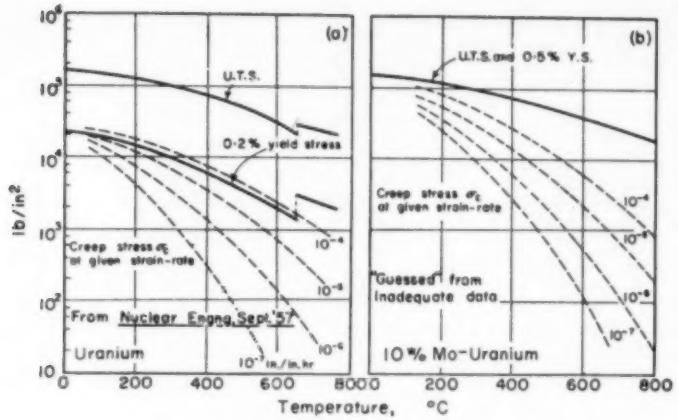

FIG. 3. (a, b).

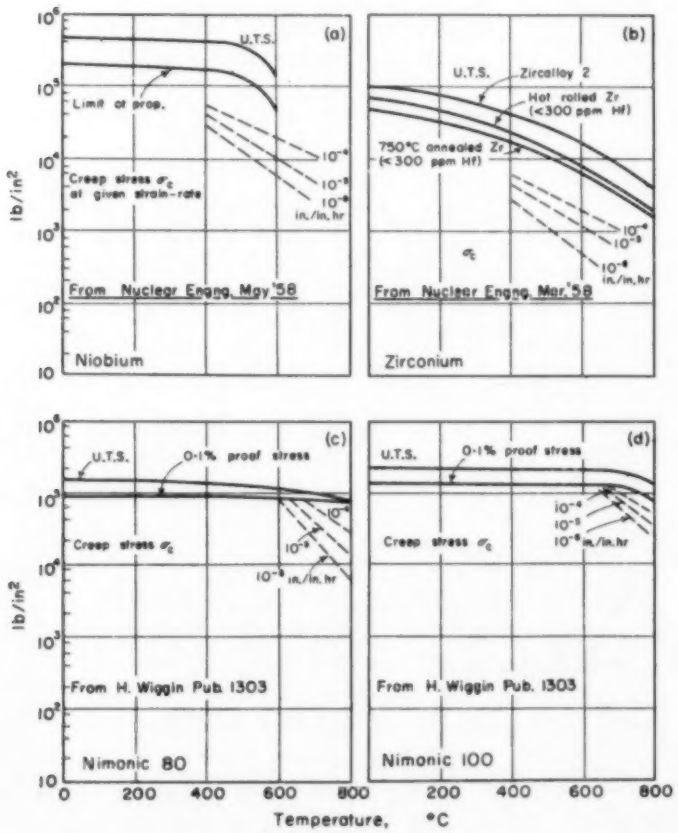

FIG. 4. (a–d).

FIGS. 3(a, b) and 4(a–d).—Tensile data on fuel and canning materials.

Enrico Fermi fuel pin

Fuel pin for first charge. The Enrico Fermi fuel pin is 0·148 in. dia. 10 w/o Mo-U fuel clad in 0·005 in. thick zirconium. Its predicted behaviour using equations (3.7) to (3.9) is given in Table 5.

Critical burn-up predictions agree reasonably well with test results, particularly showing up the strong temperature dependence of b_c. For interest, Fig. 5 shows the variation of swelling of the fuel with burn-up, as suggested by the theory proposed.

Alternative Enrico Fermi fuel design with strong can

The Enrico fuel pin for the first reactor charge, as shown above, relies on the 10 w/o Mo to strengthen

TABLE 4.—PREDICTED IRRADIATION BEHAVIOUR OF D.F.R. FUEL ELEMENT

Aver. power density	KW/in.³ (U5 + 8)		17·8	
Rate of burn-up, $\dot{b}$	hr⁻¹		$2{\cdot}5 \times 10^{-6}$	
Can/fuel vol. ratio, ν	—	·512	—	·512
Can and fuel strain at rupture, ϵ_r	%	2	2	2
Irradiation growth estimate	units	Case 1 Can sound, fuel sound	Case 2 Can defective, fuel sound	Case 3 Fuel defective, can sound
Can & fuel strain rate. $\dot{\epsilon} = 2\dot{b}/b_c$	hr⁻¹	7×10^{-6}	$1{\cdot}7 \times 10^{-5}$	$8{\cdot}8 \times 10^{-6}$
Fuel creep stress (Fig. 3), σ_c	lb/in.²	2,000	2,700	—
Can creep stress (Fig. 4), σ_c'	lb/in.²	30,000	—	35,000
$\nu\sigma_c'$	lb/in.²	4,600	—	5,310
Gas pressure at b_c, p_c	lb/in.²	3,000	1,200	2,400
$b_c = (\sigma_r + \nu\sigma_c')(\epsilon_r/24T)$	%	·7	·29	·57

TABLE 5.—PREDICTED IRRADIATION BEHAVIOUR OF ENRICO FERMI PIN AT VARIOUS TEMPERATURES

Rate of burn-up, $\dot{b}$	hr⁻¹		7×10^{-6}	
Can/fuel vol. ratio, ν	—		0·14	
Can temperature,	°C		500	
Max. strain $\epsilon_r = \epsilon_r'$	%		2	
Centre fuel temp.	°C	560	670	820
Aver. fuel temp.	°C	500	600	700
	°K	773	873	973
Strain rate $\dot{\epsilon} = \dot{\epsilon}' = 2\dot{b}/b_c$	hr⁻¹	$1{\cdot}3 \times 10^{-5}$	$3{\cdot}2 \times 10^{-5}$	7×10^{-5}
Fuel creep stress, σ_c	lb/in.²	10,000	4,200	2,000
Can creep stress, σ_c'	lb/in.²	2,000	2,500	3,000
$\nu\sigma_c'$	lb/in.²	280	350	420
Gas pressure (at b_c)	lb/in.²	4,600	2,000	1,100
$b_c = (\sigma_r + \nu\sigma_c')(\epsilon_r/24T)$	%	1·1	·44	·21
JENS (1958) value for b_c (based on test data)	%	1·7	·7	·3

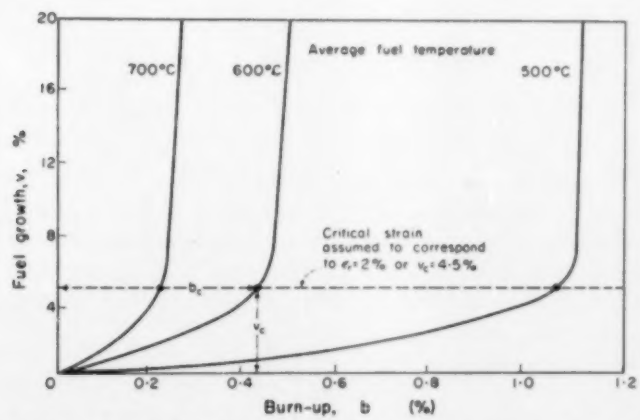

FIG. 5.—Predicted Enrico Fermi Fast Reactor fuel-pin behaviour at various temperatures. The critical point b_c, v_c, is calculated as in Table 5; the shape of the remainder of the curves is only a suggestion based on the general implications of the theory proposed.

TABLE 6(a).—COMPARISON OF 10w/o Mo-U ENRICO FERMI FUEL PIN WITH A PIN IN WHICH THE CAN IS STRENGTHENED BY 10w/o Mo EQUIVALENT AND THE FUEL CORRESPONDINGLY WEAKENED

Assumptions					
Can heat flux, h		w/in.^{2}	1900		
Sodium heat transfer coeff., h_s		w/in.^{2} °C	100		
Thermal cond. 10w/o Mo-U		w/in.°C	·73		
(K)	U	w/in.°C	·87		
	Zr	w/in.°C	·33		
	Nb	w/in.°C	1·6		
Nimonic	80	w/in.°C	·5		
Case No.			1	2	3
Description			Strong fuel, weak can	Weak fuel, strong can	
Fuel			10w/oMo-U	U	
Can material			Zr	Nb	Nim. 80
Fuel dia.	d	in.	·148	·134	
Can thickness	t	in.	·005	·012	
Can/fuel vol. ratio, $v = 4t/d\,(1 + t/d)$		—	·14	·39	
Temperatures					
Sodium		°C	450	450	450
Average can		°C	485	478	495
Average fuel		°C	562	539	583
		°K	835	812	856
Centre fuel		°C	617	582	626
Results					
Rate of burn-up $\dot{b} = hd_0/1{\cdot}8 \times 10^9\, d^2$		hr^{-1}	$7{\cdot}6 \times 10^{-6}$	$9{\cdot}3 \times 10^{-6}$	$9{\cdot}3 \times 10^{-6}$
Strain at rupture, $\dot{\varepsilon}_r = \dot{\varepsilon}_r'$		%	2	2	2
Strain rate, $\dot{\varepsilon} = \dot{\varepsilon}' = 2\dot{b}/b_c$		hr^{-1}	$2{\cdot}5 \times 10^{-6}$	$1{\cdot}5 \times 10^{-5}$	5×10^{-6}
Fuel creep stress σ_c		lb/in.^{2}	6200	1900	800
	σ_c'	lb/in.^{2}	2500	26,000	90,000
	$v\sigma_c$	lb/in.^{2}	350	10,100	39,000
Gas pressure at b_c, $p_c = (\sigma_c + v\sigma_c')/2{\cdot}24$		lb/in.^{2}	2900	5,300	18,000
$b_c = (\sigma_c + v\sigma_c')(\varepsilon_r/24T)$		%	·65	1·2	3·4

TABLE 6(b).—EFFECT ON b_c AND P_c OF REDUCING CAN THICKNESS, THE VOLUME SO SAVED BEING USED FOR ADDITIONAL FUEL VOIDAGE

Fuel voidage/net fuel volume	v	%	10	20	30	40	50	60	70
Can wall thickness	t	in.	·0234	·0200	·0166	·0136	·0106	·0076	·0047
Average fuel temperature	T	°K	892	883	877	875	881	896	934
Maximum burn-up	b_c	%	4·1	7·1	9·5	11·3	12·2	11·8	9·4
Max. can internal pressure	P_c	klb/in.^{2}	21	18	14·5	12	9·0	6·3	3·8

the fuel, the can offering no restraint to fuel swelling. It is interesting to examine the alternative possibility of using unalloyed uranium in a can containing the same amount of material as the molybdenum content of the fuel plus the zirconium content of the can, that is, having the same amount of uranium and the same outside dimensions as the E.F. 1 fuel-pin. The high strength materials niobium and Nimonic 80 are considered as canning material; their tensile properties are given in Figs. 3 and 4. The results of the calculation are given in Table 6. They indicate that better irradiation performance would appear to be achievable by using the 10w/o molybdenum to strengthen the can rather than the fuel, especially in the form of a very high creep-strength can material like Nimonic.

The effect of providing fuel expansion space inside can

The above theory of irradiation growth emphasizes the fact that 4·4 in.^{3} of fission product gas is generated per in.^{3} of fuel per 1 per cent burn-up and that this has

to be accommodated. If no space is provided for this gas, the pressure necessary to deform the fuel and can are developed at a low burn-up; if space is provided within the can, larger quantities of gas can be accommodated and the burn-up is correspondingly increased. Consider the case, therefore, of a strong can containing weak fuel with room for it to expand. Several methods of providing this expansion space, and at the same time splitting-up and weakening the fuel, are shown in Fig. 6.

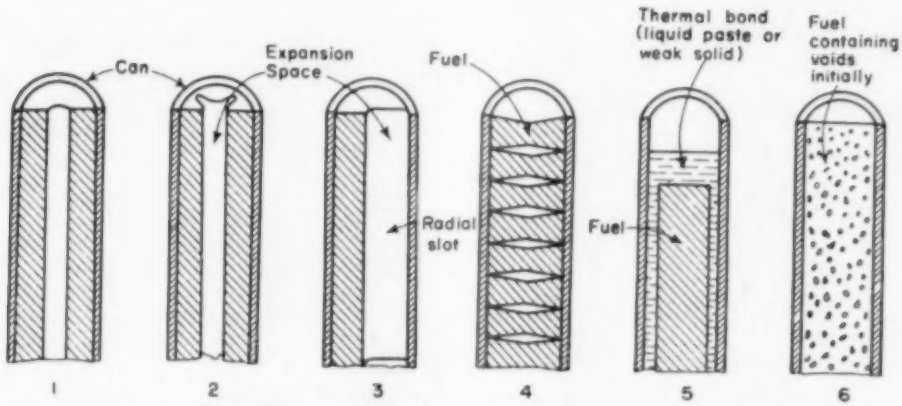

FIG. 6.—Some methods of introducing expansion space within can. (a) Axial hole in fuel, (b) radial slot, (c) and (d) separated fuel-pellets, (e) space between fuel and can, filled with liquid thermal bond with expansion space above, (f) fuel containing distributed voidage initially.

Even in Case 3, Table 6, the strength of the fuel is negligible compared with the strength of the can; when appreciable fuel expansion space is provided (say $v_0 > 5$ per cent), the fuel will be strained beyond its breakaway point, so the fuel strength is even less and can be neglected entirely. The behaviour of the fuel element under these conditions can be calculated quite accurately, since the can acts as a pressure vessel, the fission-product gas occupying the expansion volume provided, distributed in cavities uniformly within the fuel. If an expansion space of the order 20 per cent of the fuel volume is provided, this will fill up with the 'honey-combed' fuel after a burn-up of about 0·3 per cent–0·5 per cent is achieved, based on irradiation data of unrestrained uranium. Thereafter, the can restrains further swelling.

Consider a thin can of internal diameter d and wall thickness t, containing an internal pressure, p. Let the fuel creep strength σ_c be assumed to be zero. As additional refinements to the previous theory, assume that the fuel is incompressible (which is valid) and that the initial voidage v_0 (assumed to apply at the appropriate fuel and can temperatures) is supplemented by can strain and reduced by an assumed irresistible swelling due to solid fission fragments proportionate to burn-up, say of value $2b$. Then the volume ratio of void to fuel (excluding void) at burn-up b and can hoop strain ε_1, is

$$v = v_0 + 2{\cdot}23\ \varepsilon_1(1 + v_0) - 2b \qquad (4.1)$$

Substituting the expression for v of equation (4.1) in equation (3.1), we have,

$$b = \frac{v_0 + 2{\cdot}23\ \varepsilon_1(1 + v_0)}{2 + 24T/p_c}. \qquad (4.2)$$

Maximum burn-up b_c may be defined to occur at a critical pressure in the can, p_c. This may be the can bursting pressure or at that pressure occurring at a defined can strain ε_r', related as before to a creep stress σ_c' at a consistent strain rate $\varepsilon_r'\ b/b_c$. For all practical purposes the hoop stress can be taken as σ_c' so that

$$p_c = 2(t/d)\sigma_c'. \qquad (4.3)$$

$$b_c = \frac{v_0 + 2{\cdot}23\ \varepsilon_1(1 + v_0)}{2 + 12T/\sigma_c'(t/d)}. \qquad (4.4)$$

For thick overstrained cans, JORGENSON (1960) gives a more refined calculation of the bursting pressure and of the relation of internal pressure with external surface strain.

Consider Case 3, Table 6 modified in that an initial voidage $v_0 = 30$ per cent is introduced in the fuel. Fig. 7 indicates that this raises the effective fuel temperature from 856°K to 885°K. At a can hoop strain $\varepsilon_1 = 2$ per cent, the consistent value of can creep stress (obtained by iterative solution of equation (4.4) with Fig. 3b), σ_c', is 80;000 lb/in.^{2} and with $t/d = 0{\cdot}09$, equation (4.4) gives

$$b_c = \frac{30 + 5{\cdot}8}{2 + 1{\cdot}18} = 10 \text{ per cent.}$$

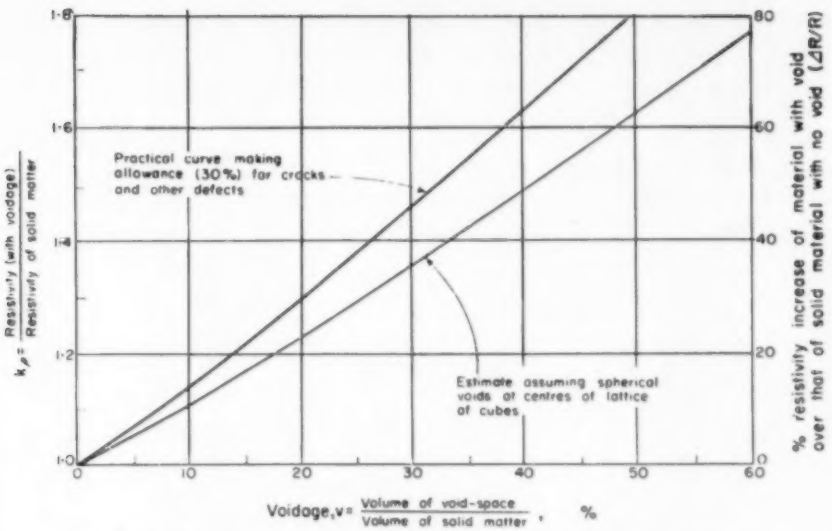

FIG. 7.—Thermal resistivity variation of porous material with voidage.

$$K\rho = \frac{\text{resistivity with voidage}}{\text{resistivity of solid matter}}.$$

A—resistivity increase proportional to voidage.
B—estimate assuming spherical voids at centres of lattice of cubes.
C—practical curve making 30 per cent allowance for cracks and similar defects.

This extremely high figure indicates that the fission product limitation to high burn-up in metal fuel due to fission gas can be overcome. The accuracy of equation (4.5) should be adequate as the most doubtful term is that which accounts for fuel growth due to solid fission fragments. There are a number of irradiation experiments where the total growth/burn-up ratio, r/b, is 2 or less: for example LEESER (1958), Table 1 lists results of 10w/o Mo-U in which, in four samples irradiated to 1 to 2 per cent burn-up at 400 to 600°C, the value for r/b is 1·8; in another specimen irradiated to 1 per cent at 200°C, r/b is only 1·5. Thus the term 2 is likely to be a conservative figure and might be as low as unity, which would raise the burn-up from 10 to 14 per cent. Apart from this, the only other assumption is the fission product gas production figure, which has now been verified both theoretically and experimentally. If the high figure of 80 klb/in.^{2} for the can creep stress cannot be realized under irradiation conditions, this will of course lower the burn-up; however, irradiation tests on materials similar to Nimonic 80 to 10^{20} n/cm^2 have shown a tendency for strength to increase rather than decrease; ductility appears to suffer most under irradiation which suggests that the can may rupture at a low maximum strain. The can will also suffer damage from fission fragments but this is not expected to be significant since damage is restricted to a few microns only on the inner side of the can.

The previous discussion is intended mainly to determine the factors controlling high burn-up and Nimonic 80 was used only as an example of a high creep strength material. Other factors also control its use as a fast reactor canning material are: its compatibility with sodium (which should be adequate); its compatibility with fuel (which is becoming doubtful above 600°C and definitely very bad above 700°C with uranium, and poor at 500°C with some plutonium-uranium alloys); limitations on heat flux due to thermal stresses (Nimonic has a poor thermal conductivity and a fairly large coefficient of thermal expansion); its high cost of about £5/lb. With a refractory metal liner, Nimonic 80—and the more exotic variants Nimonic 90 to 105, remain practical possibilities (or a high creep strength refractory metal could be used). Such alloys are being developed and results to date are encouraging (DE MASTRY *et al.*, 1960; WAGNER and KLINE, 1959).

Figure 8 shows the build-up of pressure in a fuel can, calculated using equations (4.1) and (4.5) and taking a normal tensile-test stress-strain curve for Nimonic 80 to relate ε' and σ_e'. It is seen that the pressure build-up is non-linear which makes it practical to introduce a substantial factor of safety, say by limiting burn-up to a figure where the can stress is half the yield stress.

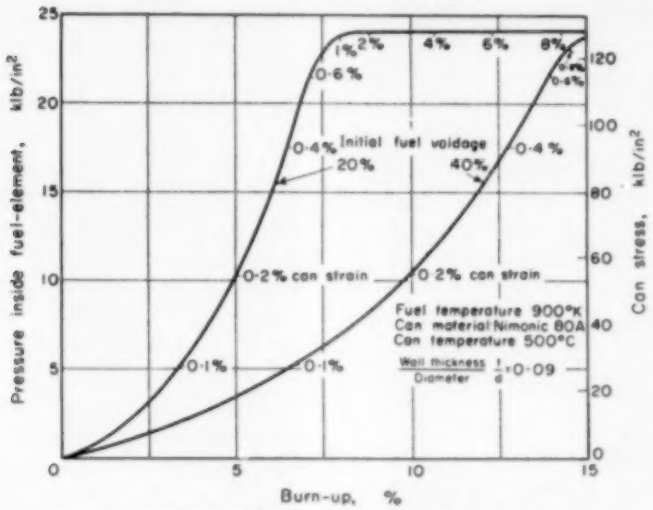

FIG. 8.—Variation of fuel pressure inside can with burn-up.

The value of a large voidage for high burn-up is also indicated. The optimum value of initial voidage will now be estimated.

Assume the following are held constant:

can outside diameter	$d_0 = 0{\cdot}200$ in.
can surface heat flux	$h = 2$ kw/in.^{2}
can outer surface temp.	$= 450°C$
can creep stress	$\sigma_c' = 80$ klb/in.^{2}
can thermal conductivity,	$K_c = 0{\cdot}5$ in.

fuel thermal conductivity, $K_f = 0{\cdot}65$ w/°C in.

voided fuel conductivity, $K_v = K_f \times$ factor K_ρ in Fig. 7.

Assume that the initial fuel voidage fraction v and can wall thickness t are varied together, as one is increased the other being correspondingly reduced to keep

$$\text{fuel volume} = \frac{\pi}{4}\frac{(d_0 - 2t)^2}{(1+v)} = \text{constant}.$$

Hence
$$\frac{1+v}{(d_0-2t)^2} = \frac{1+v_1}{(d_0-2t_1)^2}.$$

Take as one case, $v_1 = 0{\cdot}20$ and $t = 0{\cdot}020$ in. With $d_0 = 0{\cdot}20$, we have

$$(1+v) = 187{\cdot}5(0{\cdot}1 - t)^2.$$

Given the voidage v, the can wall thickness can be deduced, the voided fuel thermal conductivity K_v can be estimated, then the temperature drops and mean fuel temperature T°K. Equation (4.4) (with assumed 1 per cent) gives the maximum burn-up and equation (4.3) the maximum fuel pressure. Table 6 summarizes the results.

The most interesting result from Table 6 is that burn-up is a maximum at about 50 per cent initial voidage. As more canning material means more neutron losses by capture and degradation of spectrum by inelastic scattering, void is preferable to increased can thickness; however, particularly in small cores, increased voidage means increased neutron losses to offset this. For example, in the Enrico Fermi Fast Reactor, stainless-steel introduced into the core increases reactivity by 0·3 cents/kg or 2·4 cents/litre averaged over core (*Enrico Fermi Atomic Power Plant*, 1959), which could amount to a total increased reactivity of 1 per cent for a core with 10 per cent stainless-steel. A further effect is the change in breeding gain with voidage, particularly of core internal breeding. Thus it depends on the size of the reactor core whether in practice it is desirable to operate with a voidage greater or less than the optimum calculated as above. Another complicating factor is that increased voidage could lead to a greater tendency for fuel slumping and, under melt-down conditions, to a greater excess reactivity. Thus safety considerations could impose a limit to voidage, though in general, safety requirements would be met by other means. In practice an initial voidage of 30 to 40 per cent would appear reasonable.

To summarize, the theory proposed in this paper suggests that high burn-up should be achievable in metal fuel provided a strong can is employed and expansion space is provided for fuel swelling within the can. The voidage should be introduced in a way to encourage good thermal bonding between fuel and can, even in the absence of a bonding agent, and at the same time to weaken the fuel so as to prevent it from overstressing the can from its own thermal expansion

and also to permit the fuel to grow into the void so that the void is effectively available for the fission gases at all stages of burn-up. If this can be achieved it would appear that 4 per cent average burn-up should be practical in a fast reactor with centre fuel temperature of 700 to 750°C. If this is so there is little doubt that a power fast reactor would be extremely attractive economically, better than any thermal reactor yet proposed. Preparations are being made to test the theory by irradiating in Dounreay Materials Testing Reactor unalloyed uranium with 30 per cent to 50 per cent void space at 450°C can temperature, 700°C centre fuel temperature at 500 W/g or 1 per cent burn-up in 20 days.

The accommodating can concept

The previous method proposed to achieve high burn-up in metal fuel is to permit fuel-growth within the can. Another possibility is to permit the can to expand, with the fuel kept under pressure through the walls of the can. One possible arrangement is a flat plate element which can expand like a concertina, with pressure applied through ribs so that coolant passages remain constant in width. It is readily shown on the basis of the previous theory, that if an external pressure p_e(lb/in.^{2}) is applied to the fuel surface

$$\frac{v}{b} = \frac{24T}{\sigma_c + p_e}. \tag{4.5}$$

This expression can be assumed to apply up to a critical growth of about 5 per cent, above which the fuel strength will fall drastically. If a maximum growth as large as 20 per cent is permitted $\sigma_c \to 0$ and $v/b \to 24T/p_e$.

For fuel at 600°C and with an external pressure of 1000 lb/in.^{2}, v/b is likely to be in the range 10 to 20 and the maximum burn-up, at $v_{max} = 20$ per cent is 1 to 2 per cent. On the whole this arrangement would appear inferior to the previous method in achieving high burn-up and also more complicated to apply.

5. COMPARISON OF METAL, OXIDE AND CERMET FUELS UNDER FAST REACTOR OPERATING CONDITIONS

Fuel irradiation conditions in a fast reactor differ markedly from that of most thermal reactors and fuel development will probably progress on quite different lines. For example, a high power density of about 100 W/g (or MW/T) is essential in a power fast reactor to minimize fuel inventory cost and to prevent spectrum softening which reduces breeding gain. For economic power, an average burn-up of 2 to 5 per cent is necessary from the fuel. Temperatures and temperature gradient also are high. These severe irradiation conditions must not be achieved at the expense of safety standards, since any substantial concentration of the fuel could lead to dangerous power excursions; in particular, it must be ensured that the failure of one fuel element cannot affect its neighbour and lead to progressive failure. On the other hand, capture cross-sections are very low in a fast flux, which permits a wide selection and large amounts of canning, structural or alloying materials to be used. Although fuel element costs need to be as low as possible, nevertheless they can be very much higher than in thermal reactors, particularly if they are capable of high burn-up. Other factors are the high enrichment of the fuel in fast reactors and the fact that ultimately the fissile fuel must be based on ^{239}Pu rather than ^{235}U.

A large number of different fuels are possible for fast reactors, such as: high alloy metal, including 10w/o molybdenum and fissium alloys; unalloyed metal with void space in a strong can, as proposed in Section 4 of this paper; oxide fuel; carbide fuel; dispersions of oxide or carbide fuel in stainless-steel or some other metal matrix including uranium itself (possibly in one of the metal fuel element forms above to encourage breeding in the core); and liquid or paste fuels. At this stage where data is so limited, attention will be given to metal fuel (with expansion space in a strong can), oxide fuel, and a dispersion of oxide in metal fuel (again with expansion space and in a strong can).

As fuel-element swelling becomes catastrophic beyond a critical burn-up (as indicated in Figs. 2 and 5), it is evidently necessary to employ a considerable margin of safety, keeping maximum operating burn-up, b_m, well below the critical value. Moreover, conservative design is even more necessary as fuel-element failure in a fast reactor could lead to starving coolant from adjacent elements leading to their failure also, which in turn could cause significant reactivity changes.

To enable a fair comparison to be made of different fuels and to help put in perspective the conservative design philosophy necessary, the following fuel specification which each must meet will be assumed.

(1) It will be assumed that fuel element failure occurs at a burn-up b_f where a defect develops in a can allowing ingress of coolant or ejection of fuel, or where the fuel-element distorts in shape so as to affect core stability, coolant flow or fuel-element removal, or allows fission products or fuel itself to contaminate the coolant.

(2) Maximum safe burn-up in a fuel element (b_s)

VOL 14 196

will be assumed to be 50 per cent of that value at fuel element failure (i.e. $b_s = \frac{1}{2}b_f$).

(3) In predicting b_f, can failure will be assumed to occur at a pressure corresponding to the worst can tested from a significant selection (>5 per cent) of completed cans (excluding rejects) in a production batch, that is, after all inspection tests and rejects have been made. If predicting b_f assumes knowledge of fission-product gas-release, this will be under the most pessimistic conditions realized in tests of the fuel used. Similarly, most pessimistic operating conditions must be employed both for fuel and can, and worst can and fuel material properties assumed, appropriate to the production batch under consideration.

(4) No fuel-element in a core must exceed its maximum safe burn-up at the worst reactor over-load condition (say, 1·5 nominal maximum power at a flow corresponding to the lowest value at nominal maximum power); this restricts the maximum burn-up under normal operating conditions b_m to less than b_s.

(5) It is permissible to extend the maximum operating burn-up, b_m, by design or operation changes, such as double-canning of fuel elements or fuel shuffling during reloading, provided the same criterion is satisfied.

This conservative approach conflicts sharply with the strong economic incentives in a fast reactor which demand high burn-up fuel-elements. Achieving high burn-up will probably not only depend on finding a good fuel but will also depend on how consistently this can be maintained. Similarly, can defects must be made negligible in manufacture, and the highest inspection standards attained to ensure that, should they occur, they will be spotted and defects rejected. Also the factors controlling maximum burn-up must be understood and the fuel-element design be such that there is no chance of excessive temperatures, thermal stresses, or other operating conditions that will produce fuel-element failure. These high standards are necessary not only to prevent any nuclear incident but to prevent any damage to the reactor or prevent unnecessary, costly, shut-downs.

The special design development problems of a metal-fuelled fast reactor fuel-element, with 500°C maximum sodium temperature, to guarantee the above specification and that 4 per cent average burn-up is achievable is approximately as follows:

(1) A can must be developed, compatible with fuel and sodium coolant (up to 700°C at least for short periods). The can will be required in sizes 0·15 in. o.d. up to 0·30 in. o.d. with a wall thickness 0·010 in. to 0·040 in., defects in it must be reduced to the extent that 40,000 lb/in. creep strength can be guaranteed at up to 650°C average can temperature (this assuming to cover 50 per cent power overload condition) and after full irradiation. With uranium fuel, Nimonic 80 would appear just capable of this, but with plutonium fuel it is likely that the Nimonic 80 would need a refractory metal inner liner or be replaced altogether by a high creep-strength refractory-metal alloy.

(2) A method has to be found to introduce distributed voidage in the metal in a way to ensure that it is available for fission product gases, that does not increase thermal resistivity of the fuel excessively, that allows a good thermal bond to be made between fuel and can under all operating conditions so that hot spots in the fuel is avoided, that weakens the fuel or at least prevents a significant proportion of it to use its strength (in conjunction with the fission product gases) to work against the can rather than with the can to resist swelling. These points anticipate difficulty, for example with a hollow fuel rod as in Fig. 6(a), in that the compressive strength of the fuel prevents fuel being forced into the central hole so that the effective voidage is much less than that provided, whilst fuel thermal expansion could over-strain the can.

(3) Assurance must be provided that excessive centre temperature cannot develop, permitting fuel to melt and slump to the bottom of the can. If there is any possibility that this can happen, then it must be arranged that the reactivity change is acceptable. Generally these conditions can be met if a good thermal bond can be assured and centre temperatures limited to less than 900°C and the fuel subdivided up in sealed or semi-sealed compartments (e.g. separated with a refractory metal disk).

(4) The fuel-element design must be such that should a can leak and on shut-down permit entry of sodium, this cannot fill the void space and prevent its use by fission product gas. Moreover, should the sodium enter at shut-down, the expansion or vaporization of the sodium as the fuel temperature rises must not cause severe fracture of the can, so permitting fuel to be ejected into and blocking a coolant passage. These considerations suggest that it is best to provide the voidage in the fuel in the form of distributed porosity not interconnected or having connexion with the surface. Also a central void should be avoided, and operating the centre fuel above the boiling point of sodium (880°C) is undesirable.

(5) The voidage should also be introduced into the fuel in a way to weaken it in compression so that the thermal expansion and anisotropic expansion effects

of the fuel does not overstrain the can. For example, if a can is swaged on to fuel so that at room temperature it is in intimate contact, then, at power with the centre fuel temperature at 800°C for example and the can at 400°C and assuming the fuel to be incompressible, the can strain is $(18–10)10^{-6} \times 400 \times 100 + 20{\cdot}10^{-6} \times 400 \times 100 = 0{\cdot}32 + 0{\cdot}8 = 1{\cdot}12$ per cent, which is undoubtedly excessive and in the plastic range. On cooling a gap can be opened up between fuel and can. On reheating, imperfect thermal contact can create hot spots and high local thermal stresses in the can, at least temporarily until thermal expansion again closes the gap and maintains thermal contact. Fuel-elements with a sodium bond suffer particularly in this way since the sodium can be squeezed out as power rising leaving an uneven thermal bond on the second and subsequent rise to power. As the fuel swells due to anisotropy or irradiation, it later becomes capable of over-straining the can by thermal mechanism. In this respect, the introduction of appreciable voidage gives the designer more scope in controlling can strain due to differential thermal expansion. For example, if uniformly distributed porosity does not sufficiently weaken the fuel to prevent excessive can strain, part at least of the voidage could be provided by slotting the fuel axially in the form of a 'C'; this has the desirable effect of increasing the diametric expansion of the fuel to maintain it at all times in close contact with the can yet in a way to keep can strain limited to a prescribed amount. Tests to date at an irradiation rate of 500 w/g have shown that it is possible in this way to obtain good thermal bond and with only moderate can strain.

(6) Even assuming high quality canning material and high quality inspection techniques, it is desirable to ensure that no serious consequences result even if defects escape detection. This requires that fuel burn-up and temperature be restricted so that fuel is not extruded through the defect to block a coolant channel and that pressures are not sufficient to open up the defect further. As a further line of defence, even should fuel block a coolant channel, the power ratings should be restricted so that progressive fuel melting would not then occur. An alternative approach if this is too limiting on burn-up temperating and power density is to doubly-can with a thermal bond between the two cans so that should the inner-can fail, the outer-can can be relied upon. This has the disadvantages that the inter-can bond must be wholly reliable and that the fuel and inner-can temperatures are raised.

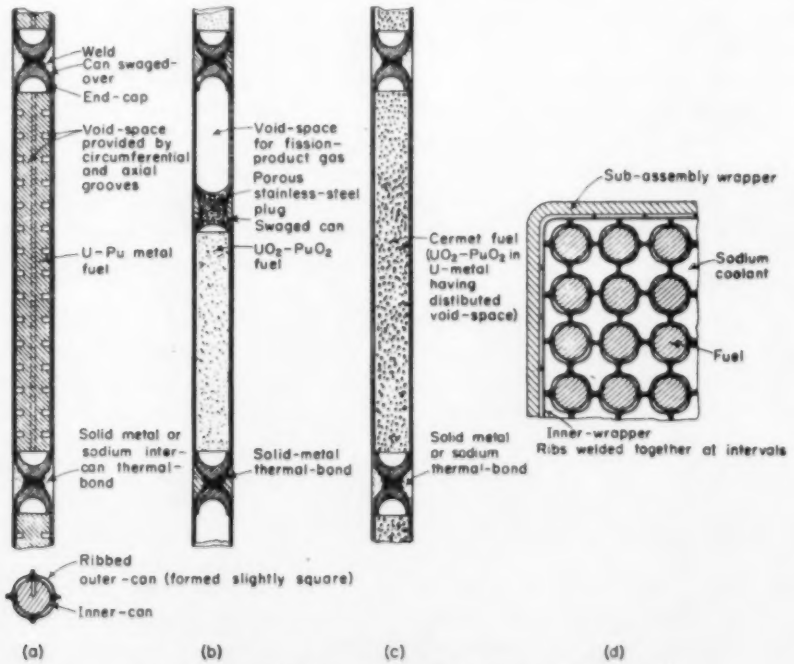

FIG. 9 (a–d).—Application of the strong can/weak-fuel plus void-space principle to the design of fast reactor fuel-elements for three types of fuel: (a) unalloyed uranium or uranium-plutonium alloy; (b) uranium or uranium-plutonium oxide fuel; and (c) $PuO_2 - UO_2$ cermet in unalloyed uranium. (d) shows a portion of a sub-assembly. In each case the fuel is about 0·2 in. dia. and shown doubly-canned to guard against defects in the can, though this may not be necessary.

TABLE 7.—ESTIMATED PERFORMANCE OF THREE POSSIBLE FAST REACTOR FUELS UNDER PRACTICAL OPERATING CONDITIONS

Property	Sym-bol	Unit	Uranium metal with 38% void		Uranium oxide with 50% void		Cermet (UO_2/U metal with void)	
Fuel element description. See Fig.			9(a)		9(b)		9(c)	
					upper void:			
Composition by volume: U-metal		%	72·5		excluded	included	69·0	
Composition by volume: UO_2		%	none		88·9	66·7	13·3	
Composition by volume: void		%	27·5		11·1	33·3	17·7	
vol. void/vol. U + UO_2	v_0	%	38		12·5	50	20	
Thermal conductivity (average): metal fuel	k_m	w/°C in.	0·54				0·60	
Thermal conductivity (average): oxide fuel	k_0	w/°C in.	—		0·05		0·07	
Thermal conductivity (average): canning mat.	k_c	w/°C in.			0·50			
Canning material					Nimonic 80			
Can creep stress (normal)	c	klb/in.²			50			
(at 150% power)		klb/in.²			40			
Operating conditions								
Specific power:– per in³ of U + UO_2 + void	H	kw/in.³	40·6		40·6	30·4	40·6	
Specific power:– per g of U + UO_2	s	w/g	182		253		172	
Fuel-surface heat-flux	h	kw/in.²	1·79		1·79		1·79	
Temperatures—at % power:—		%	100	150	100	150	100	150
Coolant (at max. fuel temp. posn.)		°C	440	510	440	510	440	510
Outer can—average		°C	474	560	474	560	474	560
Inner can—average		°C	542	663	542	663	542	663
Fuel—average		°C	645	818	1400	1950	640	810
—centre		°C	720	930	2200	melting	710(3)	910(3)
							750(3)	970(3)
Burn-up predictions								
Bursting pressure:— inner can	p	klb/in.²	6·4	5·1	6·4	5·1	6·4	5·1
Bursting pressure:— both cans	p_f	klb/in²	12	9·5	12	9·5	12	9·5
Max. burn-up at 2% outer-can strain and pressure p_f	b_f	%	13	10	29	23	>9(4)	>7
Maximum operational can pressure	p_m	klb/in.²	4·2	5	4·2	5	4·2	5
Maximum operational burn-up(1)	b_m	%	5·5		13		>3·5(4)	
MW days/in³ (fuel + void) at b_m		MW days	12		13		>8	
Days in reactor at full power		days	300		440		>200	

(1) Percentage of total U atoms, (2) of U matrix, (3) of UO_2 central island (250 μ dia.), (4) figures estimated assuming 100 per cent gas release from UO_2.

Figure 9 (a–d) shows a fast reactor sub-assembly based on double-canning and Table 7 summarizes the chief design features. The outer-can has axial ribs and is formed slightly square-shaped, to positively locate the capsules with some flexibility incorporated, to avoid unnecessarily close dimensional tolerances and to permit at least 5 per cent diametric strain of the inner-can before the outer can is stressed.

The maximum operating burn-up (b_m) of an 182 W/g fuel element is predicted to be 4 per cent. The bursting pressure of the fuel element at 50 per cent power overload is 8000 lb/in.², the predicted pressure at b_m is 4000 lb/in.² giving the required factor of safety of 2. The can pressure at maximum burn-up at normal operating conditions is 3000 lb/in.², whereas under these conditions 12,000 lb/in.² could be withstood, even assuming a creep stress of 50,000 lb/in.² whereas most elements should have a creep stress of 100,000 lb/in.² Provided these assumptions can be realized, therefore, there would seem good reason to believe that metal fuel is capable of achieving both the necessary high burn-up for competitive nuclear power and at the same time achieving the necessary high safety standards. With plutonium fuel, however, it

may be necessary for the inner can, at least, to be a high creep-strength refractory-metal or to have a substantial refractory-metal inner-lining.

Oxide fuels in fast reactors

Lack of data makes accurate design of an oxide fuel-element for a fast reactor virtually impossible at this stage. The most important data necessary is fission-product gas-release as a function of burn-up, oxide-density and also with time, to determine gas release on overloads. Although there is some fission gas release data at low burn-up, (~1 per cent) there is very little at high ratings and burn-ups of 4 to 10 per cent, necessary for economic power in fast reactors. Much theoretical work has been done on this subject but at the moment fission-product gas-release cannot be predicted even within a factor of $x \div 10$, due to inaccurate knowledge of the diffusion constant and particularly its dependence on oxide temperature and density.

Oxide fuel in fast reactors will have considerable safety difficulties to face. As in water-cooled thermal reactors (LEWIS, 1959), a leaky can will lead to ingress of sodium and, as the centre temperatures necessary in fast reactors will be at least 1200°C, the sodium will undoubtedly boil and rupture the can. In this instance, therefore, some secondary can seal will be necessary; this could be a doubly-sealed can or possibly the inner can could be uranium metal.

Another possible difficulty with oxide fuel is that autocatalytic (positive feedback) conditions could arise leading to sudden fission-product gas-release and a sudden rise in can pressure. For example, the development of a crack could lead to higher fuel temperatures, the release of more gas, further cracking and so on. Moreover, the pressures involved with oxide can be 2 to 3 times higher than with metal fuel due to the higher operating temperature.

If the design basis of oxide fuel elements in a fast reactor is that fission product gas release must be kept low (say less than 5 per cent), then an extremely conservative design philosophy would have to be adopted. Centre temperature will have to be kept low (1000–1400°C at normal full power) but even then the 50 per cent overload condition may give trouble. In addition, the low thermal conductivity and high ratings makes the oxide pin size very small (of the order of 0·1 in.) and the oxide should be of high density, which in turn implies that, if for some accidental reason there is a significant fission gas release, the void space to accommodate this is small, so can pressures tend to be high and autocatalytic conditions as described above could be initiated.

It would appear at this stage dangerous to design a fuel element for operation at 4 per cent burn-up on any other basis than a possible 100 per cent fission product gas release; moreover this release must pessimistically be assumed to occur at overload so that the gas is at fuel temperature—a further serious disadvantage. To ease the design problems which this philosophy engenders, it now becomes desirable to use low density fuel so that space is provided for the gas, despite the fact that doing this causes increased gas release. If the can must now act as a pressure vessel then, as with the metal fuel, security must be provided against defects in the can which necessitates double-canning, which is also desirable to avoid ingress of sodium at shut-down. The low fuel density, the high fission-gas temperatures due to the high fuel temperature and the high proportion of canning material, leads to significant worsening of the economic situation which can only be offset by high power-densities and high centre temperature, which in turn virtually guarantees that the 100 per cent gas release assumed is in fact realized.

It appears, therefore, that the main advantage of oxide fuel over metal of good dimensional stability under irradiation cannot be relied upon under highly rated, high burn-up conditions in a fast reactor and that if oxide fuel has to be designed for 100 per cent gas release, then it will suffer seriously in economic comparison with metal fuel. However, this does not mean that oxide fuel can be dismissed as a potential power fast reactor fuel. As can be seen above, the designer is virtually forced to a highly rated design and to assume 100 per cent fission gas release. If this gas release could be guaranteed, then the virtue of oxide over metal could be that it releases its gas, not that it retains it. The design approach under these conditions would then be to operate at high temperature and specific power, to encourage continuous gas release under normal operating conditions either to the coolant or to a reservoir outside the fuel and at coolant temperature.

To put this another way, fission-gas release in oxide is likely to be highly variable: it is extremely temperature-dependent, present data indicating a variation in fission gas release of 0·1 per cent to 100 per cent from about 800°C to near the melting point; it is also likely to be strongly density-dependent. This wide variation, probably over a range of 0·01 per cent to 100 per cent, permits great flexibility in design; in thermal reactors, the low temperature, high density and moderate burn-up design requirements encourage operation under low fission-gas release conditions. With fast reactors, the high-rating, high-temperature, high burn-up requirements essential to economic

VOL.
14
196

power, encourage operation at 100 per cent release conditions. Two additional factors encourage this latter approach: the large temperature-gradient under fast reactor conditions should assist fission-gas release from the colder surface-fuel; moreover, it is likely that above 2000°C infra-red radiation effect will raise the fuel thermal conductivity and help to stabilize centre temperature below the melting point. A design based on this approach is indicated in Fig. 9(b) and summarized in Table 7.

As already mentioned, insufficient data is available to make any accurate assessment of the safe maximum operating burn-up of oxide fuel, but Table 7 suggests that the doubly-canned, highly-rated, high burn-up oxide fuel design is unlikely to be a great improvement over the metal design and may well be inferior. As figures stand, oxide fuel would appear to be capable of the same power density in the fuel itself but the need to provide void space above the fuel within the capsule, reduces the core power density from 40·6 to 30·4 kW/in.^{3} making the oxide core larger and increasing is pumping losses in the design shown. To obtain the same energy output from a capsule its burn-up (per cent U + Pu atoms fissioned) must be raised to 12 per cent compared with 5·5 per cent for the metal fuel. However, the approximate analysis indicates that with 50 per cent void as provided, this should be achievable with the same factor of safety as the metal. This presumes, however, continuous release of gas to the upper void space and that other fission products with boiling points below 2600°C (Rb, Sr, Te, Ta, I, Cs, Ba, La, Ce, Sn) do not contribute greatly to the fission product gas pressure by condensing on the capsule wall. If they do not do this, their presence could raise the pressure 4 times. Another difficulty is the behaviour of the UO_2 itself over long periods at high temperature and particularly of PUO_2–UO_2 in which Pu and U segregation may take place. The fuel reprocessing and refabrication cost is unlikely to differ appreciably between the two fuels but the oxide core will suffer with an increased fuel inventory and a reduced breeding gain. The use of void space adjacent to the fuel, within the can but at coolant temperature, appears a practical design at this stage. Continuous gas release to the coolant outside the can is somewhat more speculative but is not ruled out; it offers rewards of very high burn-up.

Cermet fuels

Cermet fuels, that is ceramic fuel dispersed in a metal matrix such as UO_2 in stainless-steel of 10w/o Mo-U, differ from the oxide fuel element design in that the ceramic islands will run cooler and possibly retain its fission product gas. The excellent irradiation stability of UO_2 in stainless-steel cermet would appear to result from this and from the good strength of the matrix. Most irradiation tests have been with a UO_2 content of only 15 per cent but this would be unacceptably low in a fast reactor as it leads to a breeding ratio of less than unity and the large expense of a continuous fissile-fuel feed during reactor operation. In a fast reactor, economic requirements force development in the direction of a high (UO_2 + PuO_2) content of about 50 per cent by volume; at this volume ratio no reliance can be placed on the strength of the matrix; the strength must therefore be provided by the can. The desirable matrix properties therefore become high thermal conductivity, good can compatibility, low fabrication and reprocessing cost and, if possible, a high uranium content for good breeding. If uranium itself is used in the matrix, the PuO_2/UO_2 ratio becomes a design variable: if UO_2 is dispensed with altogether, the burn-up in the PuO_2 could be unnecessarily limiting though the effective matrix conductivity and breeding gain are high; if too much UO_2 is provided, the design tends towards the 50 per cent oxide content with its problems of manufacture, interconnexion of grains, poor effective thermal conductivity and poor breeding. Optimization of the various factors can only be approximate but this suggests an optimum PuO_2–UO_2 volume ratio of about 20 per cent. At 50 per cent burn-up in the oxide, the burn-up in the matrix would be nearly 3 per cent of uranium atoms, (and 7 per cent of all Pu and U atoms (in UO_2 + U matrix)). A matrix burn-up of 3 per cent is very high and the arguments of Section 4 become relevant which suggest that to achieve this, 25 per cent void in the fuel is desirable and a strong can must be employed.

The question is, therefore: does the PuO_2–UO_2 islands in the matrix retain its fission product gas under all operating and overload conditions? If it does, there is no doubt that the overall burn-up is higher than in the metal core (with void replacing oxygen). If 100 per cent fission gas is released, then the cermet is inferior to metal with correspondingly increased void-space. Irradiation tests to date look encouraging, however, and suggest that a marriage of oxide and uranium metal in the form of a cermet could be beneficial to both: the oxide could contribute reduced gas release and the retention of plutonium in the more inert oxide phase, so that the can/fuel compatibility is improved and enables Nimonic cans to be used if can temperature is kept below about 700°C; the metal contribution is that it seals off the oxide so that ingress of sodium from a leaky can no longer

presents a safety problem; at the same time the metal contributes its higher thermal conductivity to reducing oxide temperature to a level below about 900°C where danger of gas release is smaller. To reduce gas escape by recoil from the oxide and possibly excessive matrix damage by fission fragments, the oxide particle size must be fairly large; a value greater than 250 microns (0·010 in.) diameter would appear desirable. A fuel element based on these principles is illustrated in Fig. 9 (c).

It is not proposed to examine the implications of other fuels in the fast reactor, such as carbides, liquid fuels and pastes, as the information on them is inadequate at this stage.

6. SUMMARY AND CONCLUSIONS

It is suggested that under fast-reactor irradiation-conditions, fission product gas accumulation in pores within the fuel is chiefly responsible for irradiation swelling of metal fuel. A theory is proposed relating swelling with burn-up, fuel-temperature, fuel and can tensile-strength and size of can (equations (3.7)–(3.10)) and this is used to predict fuel-element behaviour under a number of conditions, good agreement with known behaviour being obtained. It is concluded that if metal fuel is contained in a strong can with space provided within the can for fuel to expand and to accommodate the fission-product gas, a high burn-up of about 4 per cent average under fast reactor conditions should be achievable, which is very much higher than the present limits of about 0·1 per cent burn-up in unalloyed uranium and 0·5 per cent in 10w/o Mo-U; moreover, centre fuel temperature can be raised from about 600°C to 700°C or even higher.

The design problems of fuel elements in fast reactors are discussed with particular reference to the metal-fuel pin as proposed earlier in the paper, and also when oxide is dispersed in it; a design for a straight oxide fuel pin is also proposed, (see Fig. 9). If designed on the basis of retaining fission gas, it seems unlikely that a satisfactory oxide pin is practicable, capable of the high burn-up necessary for economic power and at the same time presenting negligible safety hazard. A preferable method would appear to be to design for and to encourage 100 per cent gas release by operating at high-ratings, high-temperature and by providing appreciable void-space for the fission gas; even under these conditions, it would appear unlikely that oxide fuel will be better than metal. A cermet fuel of UO_2–PuO_2 dispersed in uranium metal, again in a strong can and using weakened unalloyed uranium with void space, appears a suitable way of combining the good properties of both fuels and could result in an excellent high burn-up fuel for fast reactors. Economic electrical power should be possible in U.K. from a large-power fast reactor with any of the three fuel elements proposed, if the predicted burn-up is achieved.

REFERENCES

BURRIS L. JR. and DILLON I. G. (1957) *Estimation of Fission Product Spectra in Discharged Fuel from Fast Reactors.* ANL-5742.

CHURCHMAN A. T., BARNES R. S. and COTTRELL A. H. (1958) *Effects of Heat and Pressure on the Swelling of Irradiated Uranium.* A.E.R.E. M/R 2510.

DIETRICH J. R. and ZINN W. H. (1958) *Solid Fuel Reactors* p. 511, Addison-Wesley-IDO-2021-Rev. 1, March 1958. Original data U.S.A.E.C. Report.

ENDERBY J. A. (1956) *Plastic Flow and the Swelling of Gas Bubbles in Uranium.* IGR-R/R-198.

Enrico Fermi Atomic Power Plant (1959) Atomic Power Development Associates, Inc. Pub. APDA-124.

FOREMAN A. J. E. (1956) *Calculations on the Rate of Swelling of Gas Bubbles in Uranium.* A.E.R.E. T/M 134.

JENS W. H. *et al.* (1958) *Recommendation for a New Core Development Programme.* A.P.D.A. Tech. Memo. F–10.

JORGENSON S. M. (1960) *Trans. ASME J. Engng. Industr.* **5**, 103.

LEESER D. O., ROUGH F. A. and BAUER A. A. (1958) *Proceedings of the Second International Conference on the Peaceful Uses of Atomic Energy, Geneva,* A/Conf. 15/P/622. United Nations, N.Y.

LEWIS W. B. (1959) *J. Inst. Mech. Engrs.* **6**, No. 8.

Reactor Core Materials (1959) Tech. Progr. Rev. prepared by Batelle Memorial Inst., Vol. 2, No. 1, p. 5. (Original data LEESER *et al.* (1958)).

DE MASTRY J. A. SHOBER F. R. and DICKERSON R. F. (1960) *Development of High-strength Niobium-Alloys for Elevated Temperature Applications.* BMI-1417.

SYKES E. C., HADDRELL V. J. and PFEIL P. C. L. (1956) *Metallographic Examination of Three Irradiated Uranium Alloy Specimens.* A.E.R.E. M/R 2002.

WAGNER R. K. and KLINE H. E. (1959) *High-Strength Zirconium Alloys* 41st Annual Convention of Amer. Soc. Metals, Chicago.

WYATT L. M. (1955) *The Behaviour of Fissile Material Under Irradiation at Elevated Temperatures.* A.E.R.E. M/R 1750.

VOL 14 196

Reactor Science and Technology (J.N.E. Parts A/B), 1961, Vol. 14, pp. 49 to 54. Pergamon Press Ltd. Printed in Northern Ireland

LETTERS TO THE EDITORS

Dosage au moyen de la spectrométrie alpha du ^{239}Pu dans un échantillon d'uranium naturel irradié

(*Received* 2 *September* 1960)

En vue de mesurer le facteur de conversion initial du réacteur BR1 de Mol, nous avons mis au point une technique de détection par spectrométrie alpha du ^{239}Pu formé. De même que pour la mesure du facteur antitrappe ρ, les conditions expérimentales doivent si possible satisfaire aux exigences suivantes:

1. Le milieu ne doit pas être perturbé.
2. La mesure doit être faite dans les conditions réelles de fonctionnement du réacteur notamment au point de vue température.

Ces deux conditions sont nécessaires, étant donné la sensibilité du taux de production du ^{239}Pu vis à vis de la distribution spectrale des neutrons.

3. La mesure doit présenter les meilleures garanties au point de vue précision.

Les deux méthodes utilisées jusqu'ici (Campbell et Carter, 1958) l'activation de détecteurs en ^{238}U et l'évaluation par spectrométrie gamma du ^{239}Np formé dans des détecteurs d'uranium naturel ne nous semblaient pas remplir de façon satisfaisante les conditions énumérés ci-dessus.

La méthode de dosage du ^{239}Pu par spectrométrie de masse (Hurst *et al.*, 1957) nécessite une irradiation prolongée et ne peut donc s'appliquer à une mesure du taux de formation initial.

Par contre, une mesure par spectrométrie alpha semble répondre aux conditions demandées, notamment en ce qui concerne la condition (2). Etant donné les temps de vie relatifs de ^{238}U, ^{239}U et ^{239}Pu, la mesure exige un flux intégré de l'ordre de 10^{19} *nvt*, ce qui, dans les cas usuels, permet de faire l'irradiation dans les conditions réelles de puissance du réacteur, tout en n'atteignant pas en fin d'irradiation, une activité excessive due aux produits de fission. Dans le cas de BR1, par exemple, dont le flux central vaut $2{\cdot}5 \times 10^{13}$ n/cm^3 sec on peut adopter une irradiation de $\simeq$9 jours correspondant à un cycle de fonctionnement du réacteur; l'uranium irradié peut ensuite être manipulé sans précautions excessives après 1 à 2 mois de refroidissement.

La méthode que nous avons suivie comprend la mise en solution de l'échantillon d'uranium à analyser, la préparation d'un dépôt mince et enfin la mesure de son spectre alpha avec une résolution d'au moins 2 per cent. Les pics alpha de ^{238}U et ^{234}U constituent des références internes très commodes.

La validité de cette méthode repose essentiellement sur l'absence d'effet discriminateur entre Pu et U, tout au long des opérations. Ceci exclut notamment la préparation des dépôts minces par voie électrolytique.

Nous avons finalement adopté le procédé suivant:

1. Dissolution de l'échantillon métallique dans HNO_3 en excès.

2. Addition de tétra-éthylène glycol, à raison de 20 cm^3 de TEG environ par cm^3 de solution (le pH de la solution finale est voisin de 4.)

3. Pipetage de la solution, qui est étendue sur un support uni en acier inoxydable poli mécaniquement et nettoyé au CCl_4.

4. Séchage du dépôt à la lampe I.R. ou à l'étuve à 80°C environ.

5. Calcination du dépôt à 500°C pendant 5 à 10 minutes.

La méthode adoptée est inspirée de celle décrite dans la littérature (Miscellaneous Physical and Chemical Techniques of the Los Alamos Project). Pour une densité d'émetteur alpha de 0·1 mg/cm^2, le spectre alpha, mesuré avec une chambre à grille type Tracerlab (mélange Argon-CH_4) suivie d'un analyseur de hauteur d'impulsions à 256 chenaux de marque RCL, présente une résolution <2 %. Afin d'éviter toute possibilité de discrimination U–Pu nous effectuons toutes les opérations énumérées ci-dessus sur le support même de la source. La Fig. 1 montre un spectre alpha uranium-plutonium obtenu par ce procédé.

Avec la chambre utilisée, le rapport des activités de ^{239}Pu et U naturel peut être évalué avec une précision de 2 à 3 % lorsqu'il est compris entre 0·05 et 0·5 environ (soit un rapport des pics ^{239}Pu et ^{234}U de 0·1 à 1·0). D'autre part, les essais effectués indiquent qu'il est possible de déceler la présence de 10^{-10} g de ^{239}Pu dans une quantité totale de U naturel de 4×10^{-6} g.

La linéarité de la méthode a été vérifiée et est excellente entre les limites indiquées ci-dessus. Pour des activités ^{239}Pu comprises environ entre 0·5 et 10 fois l'activité de l'uranium naturel, la forme dissymétrique du pic ^{239}Pu entraine un écart graduel dont la correction est difficile à apprécier. Pour des activités ^{239}Pu encore plus élevées, on peut utiliser la méthode adoptée à Chalk River (Hurst *et al.*, 1957) consistant à compter globalement tous les alphas émis par les échantillons; mais l'activité beta et gamma de ceux-ci, due aux produits de fission, pose notamment de sérieux problèmes de manipulations.

D'autre part, la comparaison des spectres de différents dépôts préparés à partir d'une même solution initiale indique que la reproductibilité est de l'ordre de 4 per cent. Le fait que cette dispersion est plus grande que l'erreur statistique des mesures d'un même dépôt peut être attribué à la différence entre les états de surface des dépôts; si la distribution des émetteurs alpha n'est pas identique, on peut s'attendre à une variation de la forme des pics alpha, spécialement du côté des basses énergies.

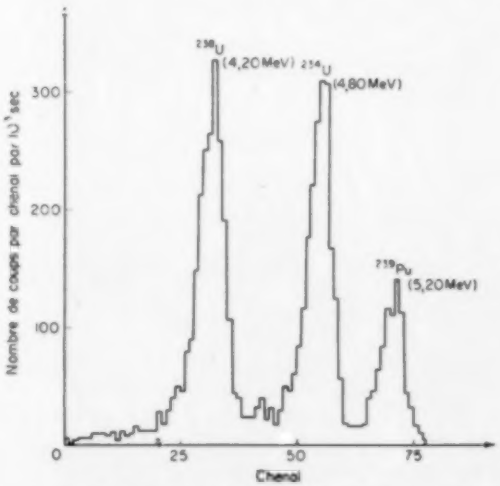

Fig 1.—Spectre alpha d'un échantillon d'uranium métallique irradié (flux intégré env. 10^{19} *nvt*.)

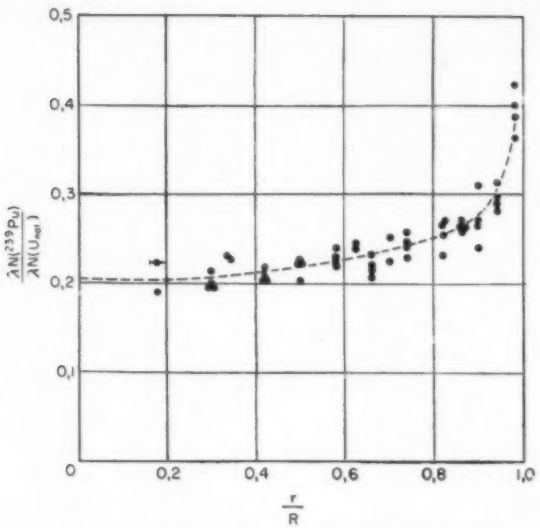

FIG. 2.—Distribution du ^{239}Pu dans un barreau type BR1 (U naturel métal, densité 18·7, rayon $R = 12{\cdot}5$ mm) irradié dans un flux intégré de $1{\cdot}9 \times 10^{18}$ *nvt*. La barre d'erreur horizontale représente l'épaisseur des échantillons examinés.

Ce défaut peut être minimisé en collimatant les alpha dans la mesure où l'intensité de la source le permet.

A titre d'application de la méthode nous indiquons sur la Fig. 2, les résultats obtenus à partir d'un barreau d'uranium type BR1 (barreau d'uranium naturel métallique de forme cylindrique, $\phi = 25$ mm, poids spécifique 18·7 gm/cm³, ayant subi une irradiation intégrée de $1{\cdot}9 \times 10^{18}$ neutrons par cm²). La courbe reliant les points expérimentaux a été tracée arbitrairement et n'est pas une courbe théorique.

Remerciement—L'auteur remercie M. NÈVE DE MÉVERGNIES pour l'aide et les conseils apportés à ce travail.

R. BERTRAND

Centre d'Etudes Nucléaires,
Mol, Belgium

REFERENCES

CAMPBELL C. G. et CARTER M. D. (1958) *The Experimental Determination of Conversion Factors and Fast Fission Factors.* AERE R/R 2397.

HURST D. G., BOOTH A. H., LOUNSBURY M. et HANNA G. C. (1957) *NRX Rod* 683. *Analysis of Irradiated Uranium and Estimation of Effective Cross-Section.* AECL 447.

Miscellaneous Physical and Chemical Techniques of the Los Alamos Project, National Nuclear Energy Series, Div. V, (1952), Vol. 3, pp. 8, 12. McGraw-Hill.

The specific alpha activity and half-life of ^{233}U

(*Received* 1 *November* 1960)

THE half-life of ^{233}U has been measured by several workers. HYDE *et al.* (1945) obtained the value of $(1{\cdot}62 \pm 0{\cdot}01) \times 10^5$ years and this was confirmed by HYDE (1957) using two further samples of ^{233}U. A recent determination by DOKUCHAEV and OSIPOV (1960) gave the value $(1{\cdot}626 \pm 0{\cdot}008) \times 10^5$ years. ^{233}U is frequently employed as a 'spike' in the mass spectrometric assay of small amounts of uranium by the isotope dilution method, the spike solution normally being standardized by alpha-counting. For such work an accurate value for the half-life of ^{233}U is essential and it was therefore decided to carry out an independent determination. This has been done by determining the specific activity of purified ^{233}U using a low-geometry alpha-counter. The isotopic composition was determined by mass spectrometry and alpha pulse analysis.

TABLE I

Nuclide	Nuclide/^{238}U by atoms
^{233}U	5·17 ± 0·03
^{234}U	0·00496 ± 0·00011
^{235}U	0·0073 ± 0·00015
^{236}U	0·000023

The ^{233}U was already in a state of high chemical purity, but was further purified as follows. The uranium was adsorbed from solution in 6M-hydrochloric acid on to CG400 anion exchange resin. After washing the column with 6M-hydrochloric acid, the uranium was eluted with 0·5M-hydrochloric acid. After conversion to nitrate the uranium was then extracted by ether from an aqueous solution 0·5M in nitric acid and saturated with ammonium nitrate. The ethereal uranyl nitrate solution was evaporated to dryness in a current of air and heated in a furnace for two hours at 750°C to convert the uranium to U_3O_8 (DUVAL, 1953).

A sample of the ^{233}U was analysed mass spectrometrically. The isotopic composition obtained is given in Table 1.

From these results it is calculated that the mean atomic weight of the uranium is 233·9 with negligible error and the percentage by weight of ^{233}U in the oxide is 70·48 ± 0·07.

Alpha pulse analysis was carried out using a gridded ion chamber. The alpha activity under the 5·31 MeV peak, due to ^{233}U, was (0·08 ± 0·01) per cent of the total, all the other activity being attributable to ^{233}U and ^{234}U (4·71 to 4·82 MeV).

From Table 1 the proportion of ^{234}U activity is 0·06 per cent with negligible error. Hence the alpha activity due to ^{233}U is (99·86 ± 0·01) per cent of the total.

Three portions of the U_3O_8 were weighed out accurately to 0·01 mg, dissolved in nitric acid, diluted to 5–7 g and the solutions weighed. Each solution was then diluted further, all measurements again being by weight.

Several sources were prepared by evaporating weighed portions of each solution on 1 in. diameter stainless steel disks. A drop of a 2 per cent aqueous solution of tetra-ethylene glycol was added to the solution on each disk to help spreading. The dry sources were heated quickly in a flame and then alpha counted.

To determine absolutely the disintegration rates of the alpha-sources, a low geometry counter with a collimated beam was used. The counter was of identical type to that designed by HURST, HALL and GLOVER (1951). HURST *et al.* discuss the errors involved in measuring the geometry factor, with particular reference to the vertical and lateral displacement of the source with respect to the collimators. Taking all factors into consideration they conclude that the coefficient of variation in the geometry factor is 0·53 per cent.

The maximum thickness of uranium on any source was 30 μg/cm². The figures in Table 2 show that the source strength, and hence the thickness, varied over an eleven-fold range, with no regular variation of the specific activity. This indicates that there were no significant counting losses due to self-absorption

VOL 14 196

TABLE 2

Series	1		2		3	
Wt. of U_3O_8 (mg)	35·12		53·77		70·19	
Wt. of main solution (g)	6·4029		5·8334		6·6678	
Wt. of portion taken for further dilution (g)	1·1481		0·4394		0·8852	
Wt. of dilute solution (g)	51·279		25·399		28·114	
	A	B	A	B	A	B
Wt. of dilute solution taken for source (column A) and alpha activity in counts/min (column B)	0·3154 0·3099 0·2470	818·2 795·8 640·9	0·4382 0·3734 0·3204 0·08270 0·05306	1,461 1,251 1,075 277·3 177·6	0·2858 0·2424 0·1920 0·1720 0·07370	1,987 1,689 1,338 1,193 511·5
Specific count rate of U_3O_8 (counts/min/mg)	21,125 20,911 21,130		20,908 21,010 21,040 21,027 20,990		20,976 21,023 21,026 20,927 20,940	

Mean specific count rate of U_3O_8 = 21,000 ± 70 counts/min/ mg.
Percentage ^{233}U by weight in U_3O_8 = 70·48 ± 0·07.
Percentage of total alpha-particles due to ^{233}U = 99·86 ± 0·01.
Geometry factor of counter = 708·7 ± 3·8.
Therefore, specific activity of ^{233}U = (2·109 ± 0·012) × 10^7 dis/min/mg.
Half-life of ^{233}U = (1·615 ± 0·009) × 10^5 years.
(This value agrees within experimental error with those of HYDE (1957) and of DOKUCHAEV and OSIPOV (1960).)

in the source. Sufficient counts were recorded so that the random error was always less than 0·3 per cent and in many cases less than 0·1 per cent.

The errors involved in weighing out U_3O_8 and the various solutions were negligible compared with other operations. Consequently in determining the mean specific count rate of U_3O_8 each of the 13 sources has been given equal weight, and the standard deviation of the mean calculated in the usual way. The uncertainty in the final value for ^{233}U half-life is almost entirely due to that in the geometry factor of the low geometry counter.

Acknowledgements—The author's thanks are due to MR. D. FARRINGTON for performing the mass-spectrometric analysis, to MR. M. MORGAN for counting the alpha-sources, and to DR. R. G. MONK for his interest in the work.

D. S. POPPLEWELL
Atomic Weapons Research Establishment
Aldermaston, Berks.

REFERENCES

DOKUCHAEV IA. P. and OSIPOV I. S. (1960) *J. Nucl. Energy* **11**, 194.
DUVAL C. (1953) *Inorganic Thermogravimetric Analysis* p. 502 *et seq.*, Elsevier, Amsterdam.
HURST R., HALL G. R. and GLOVER K. M. (1951) A.E.R.E. Report C/R 647.
HYDE E. K. (1957) U.S.A.E.C. Report TID–5223.
HYDE E. K., HAGEMANN F. and KATZIN L. I. (1945) U.S.A.E.C. Report CC–2636.

X-ray diffraction studies of fission fragment damage in uranium carbide and nitride

(*Received* 24 *October* 1960)

A RELEASE of approximately 190 MeV of energy is associated with every fission event and about 85 per cent of this energy is carried by a pair of heavy, highly-ionized atoms which move through matter and lose their energy by collisions with electrons and atoms. When the fission fragments pass through a solid, a large number of atoms are knocked out from their positions in the crystal. The configuration produced by the passage of the fast particle will not be frozen in but some rearrangement will take place while the disturbed region of the crystal remains agitated, furthermore those defects which are mobile at the irradiation temperature will anneal out. The residual damage in the crystal will consist of interstitial atoms and vacancies either single or grouped and in materials containing more than one type of atom disordering or replacement of atoms is possible.

TEWORDT (1958) showed theoretically that in copper, single interstitial atoms have a marked effect upon the unit cell size and it is probably reasonable to assume that in general an expansion of the unit cell of an irradiated crystal will reflect the concentration of single and possibly small groups of interstitial atoms and the disordering of the structure if this is possible. If a given crystal can contain only a certain concentration of defects of a given type at least until it becomes heavily damaged, the number of atoms affected by a single damage producing event can be deduced from the measurements of unit cell expansion.

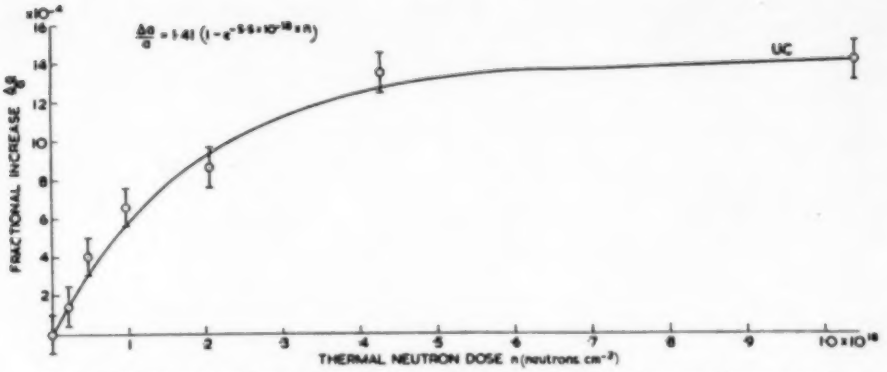

FIG. 1.—Fractional increase in unit cell size for irradiated uranium carbide as a function of dose.

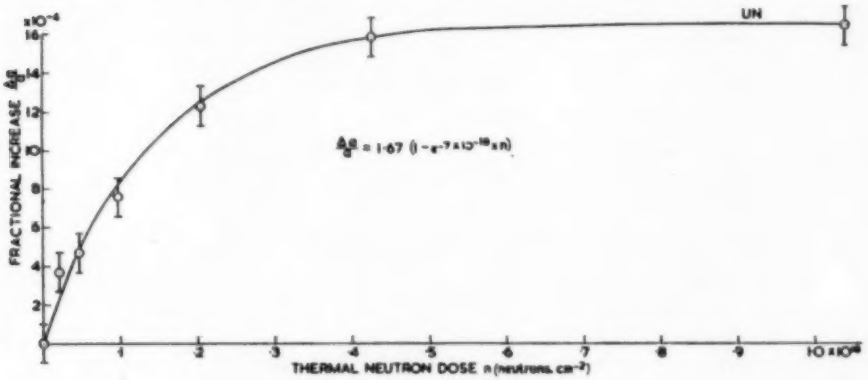

FIG. 2.—Fractional increase in unit cell size for irradiated uranium nitride as a function of dose.

TABLE 1.—ESTIMATES OF THE NUMBER OF ATOMS AFFECTED BY A FISSION EVENT

Material	Property measured	Number of atoms affected	Reference
U metal	Electrical resistance	$\sim 10^7$	QUERE and NAKACHE (1959)
U-Mo alloy	Electrical resistance	$\sim 3 \times 10^6$	KONOBEEVSKII *et al.* (1959)
U-Mo alloy	Diffusion	$\sim 1 \times 10^6$	KONOBEEVSKII *et al.* (1959)
$(ZrU)O_2$	Phase transformation	$\sim 10^6$	WITTELS and SHERILL (1959)
U_3O_8	Stored energy	$\sim 3{\cdot}4 \times 10^7$	CHILDS and MCGURN (1959)
UC	Cell expansion	$\sim 2{\cdot}8 \times 10^6$	Present work
UN	Cell expansion	$\sim 3{\cdot}5 \times 10^6$	Present work

Measurements of changes in unit cell size were conducted on UC and UN powders made from natural uranium and irradiated for various periods of time in BEPO reactor in a flux of approximately 10^{12} neutrons cm^{-2} sec^{-1} at pile ambient temperature (about 60°C). Specimens for X-ray examination were prepared before irradiation by pressing UC and UN powders into annealed high-purity aluminium disks. These disks were then irradiated together with cobalt neutron dose monitors in evacuated and cold-welded aluminium cans.

Since X-ray detectors are sensitive to radiations emitted by radioactive materials standard X-ray diffraction techniques cannot be used for the examination of irradiated samples. A diffractometer used in this work constructed at A.E.R.E., Harwell (ADAM, 1958) employs the principle of monochromatisation of the diffracted beam (CUMMINGS, KAULTIZ and SANDERSON, 1955). This experimental arrangement with a proportional counter as a detector and a single channel analyser reduces the background due to the sample activity and fluorescence to negligible proportions. Satisfactory reproducibility in unit cell size determinations was obtained from the measurements of positions of diffraction line peaks, using tungsten L-α radiation. The separation of L-α doublets is reasonably large and the weak α_2-component can be easily eliminated by careful adjustment of slits placed in front of the counter.

Figures 1 and 2 show fractional changes in unit cell size in neutron irradiated UC and UN as functions of neutron dose. Within the accuracy of experiment the changes follow $[1 - \exp(-\gamma n)]$ law where n is the neutron dose and γ is constant for a given material.

The damage in neutron irradiated materials containing fissile atoms is mainly caused by fission fragments. Assuming that the rate at which the fraction of affected atoms Y in the crystal

VOL 14 196

increases with dose n is proportional to the fraction of atoms in the crystal which have not been affected, we have

$$\frac{dY}{dn} = \gamma(1 - Y)$$

and therefore $$Y = 1 - e^{-\gamma n}.$$

If the fractional change in the unit cell size is proportional to the fraction of atoms affected by the passage of fission fragments, we have

$$\frac{\Delta a}{a} = A(1 - e^{-\gamma n}).$$

The number of fission events per atom of material irradiated to a neutron dose n is equal to $\sigma_f n$ where σ_f is the fission cross-section. We can write thus

$$\gamma n = k\sigma_f n$$

where $k = \gamma/\sigma_f$ is the number of atoms affected by a single fission event. Experimental curves obtained for UC and UN show saturation effects at high neutron doses and values for k obtained from these curves are $2{\cdot}8 \times 10^6$ atoms per fission event for UC and $3{\cdot}5 \times 10^6$ atoms per fission event for UN. The fraction of uranium atoms which were destroyed by fission at the highest neutron doses in this investigation was approximately 4×10^{-6}, this corresponds to a burn-up of the order of 3·5 MWD/Te.

Table 1 summarizes the available estimates of the number of atoms affected by a fission event. Although none of these estimates can be regarded as highly accurate the differences between certain materials are large and undoubtedly significant. Further studies are required to relate the numbers of atoms affected by a fission event to the properties of materials and their irradiation behaviour.

J. Adam
M. D. Rogers

Atomic Energy Research Establishment
Harwell, Didcot, Berks.

REFERENCES

Adam J. (1958) A.E.R.E. M and C/R 2751.
Childs B. G. and McGurn J. (1959) Canadian Report, CRMet-868.
Cummings W. V. *et al.* (1955) *Rev. Sci. Instrum.* **26**, 5.
Konobeevskii S. T. *et al.* (1959) *J. Nucl. Energy* **9**, 75.
Quere Y. and Nakache F. (1959) *J. Nucl. Mat.* **1**, 203.
Tewordt L. (1958) *Phys. Rev.* **109**, 61.
Wittels M. C. and Sherrill F. A. (1959) *Phys. Rev. (Letters)* **3**, 176.

Measurements of some resonance activation integrals

(*Received* 31 *January* 1961)

The resonance integrals of sodium, manganese, cobalt, ^{63}Cu, ^{65}Cu and of ^{98}Mo have been determined from cadmium ratio measurements in a neutron beam. The method was the same as the one used earlier by Jirlow and Johansson (1960), so only a brief outline is given here.

The cadmium ratio of the actual substance and of a 1/v absorber (a thin BF_3 counter) were measured in a neutron beam from the reactor R1. The neutron spectrum in the beam was accurately known from measurements with a fast chopper, as described by Johansson *et al.* (1960). Corrections could thus be made for the deviation of the flux from $1/E$ dependence. Also the effective cut-off energy to be used for the 1·1 mm thick cadmium could be measured directly.

The results of the measurements are given in Table 1. The lower limit of the resonance integral has been fixed at 0·5 eV and the 1/v part is not included.

The factor k shows the corrections which have been made in the resonance integrals for scattering and self-absorption of neutrons in the foils. Multiple scattering as well as energy changes in the collisions have been taken into account. The errors given in k arise only from the calculation methods. The uncertainties caused by incomplete knowledge of resonance parameters and by effect of Doppler broadening have been included in the final values for the resonance integrals.

The 0·0253 eV cross-sections given in Table 1 with the exception of that for ^{98}Mo have been taken from Hughes and Schwartz (1958) and from Hughes *et al.* (1960). The thermal cross-section of ^{98}Mo given there appeared too high so it was determined in a separate measurement. Gold and molybdenum foils were irradiated in the thermal column of the reactor R1 and the photo peaks at 0·411 and 0·740 MeV were compared using a scintillation counter. The cross-section obtained is only about one third of that given in the cited references. Probably

Table 1.—Results from the measurements

Substance	σ (0·0253) (barns)	Foil thickness (cm $\times 10^{-4}$)	k	Resonance integral (barns)
Na	0·520 ± 0·010	30	0·983 ± 0·015	0·07 ± 0·01
Mn	13·3 ± 0·2	1·53	0·974 ± 0·022	8·15 ± 0·60
Co	38·0 ± 0·7	2·27	0·950 ± 0·033	55·2 ± 4·5
^{63}Cu	4·50 ± 0·15	20	1·04 ± 0·01	3·09 ± 0·15
^{65}Cu	2·0 ± 0·3	100	1·015 ± 0·010	1·38 ± 0·23
^{98}Mo	0·18 ± 0·02	100	1·13 ± 0·01	10·7 ± 2·5

earlier measurements have been made in broad reactor spectra with no corrections for epithermal effects.

We have not found any values for the resonance integrals of sodium and ^{98}Mo in the literature. Our value for manganese is within the limits of error of the result 9·5 ± 5·0 barns found by TATTERSALL *et al.* (1960) and it is in very good agreement with the value 7·8 ± 0·8 given by WALKER *et al.* (1960).

The measurements on cobalt were made on the isomer cobalt-60^{m} whose half-life is 10·4 min. In the evaluation we have assumed that the cross-section ratios for the production of the 10·4 min and 5·25 year states are the same for thermal and resonance neutrons and have thus obtained the total activation integral of 55·2 ± 4·5 barns given in Table 1. If we include the 1/v part, 0·45 × 38·0 = 17·1 barns we get 72·3 ± 5·0 barns. This value compares well with the result 75 ± 5 by JOHNSTON *et al.* (1960) and with the result 73 ± 5 by EASTWOOD and WERNER (1959). The result by JOHNSTON *et al.* has been obtained from cadmium ratio measurements using the value 37·0 barns for the thermal cross-section of cobalt and 1565 barns (incl. 1/v) for the resonance integral of gold which was chosen as a standard.

EASTWOOD and WERNER on the other hand have measured the absolute epithermal activities of cobalt and gold. The resonance integral of cobalt has been obtained from the value 1558 barns for gold.

The resonance activation integral of natural copper is calculated to be 2·56 ± 0·15 barns from the values in the Table 1. This is significantly higher than the recent result 1·2 ± 0·5 barns obtained for the resonance absorption integral by TATTERSALL *et al.* (1960).

R. DAHLBERG
A B Atomenergi K. JIRLOW
Stockholm E. JOHANSSON
Sweden

REFERENCES

EASTWOOD T. A. and WERNER R. D. (1959) Chalk River Report CI-207. Unpublished.

HUGHES D. J. and SCHWARTZ R. B. (1958) *Neutron Cross Sections*, 2nd edn., U.S. Atomic Energy Commission, BNL-325.

HUGHES D. J., MAGURNO B. A. and BRUSSEL M. K. (1960) *Neutron Cross-Sections*, 2nd edn., Suppl. No. 1. U.S. Atomic Energy Commission, BNL-325.

JIRLOW K. and JOHANSSON E. (1960) *J. Nucl. Energy* Part A: *Reactor Science*, **11**, 101.

JOHANSSON E., LAMPA E. and SJÖSTRAND N. G. (1960) *Ark. Fys.* **18**, 513.

JOHNSTON F. J., HALPERIN J. and STOUGHTON R. W. (1960) *J. Nucl. Energy*, Part A: *Reactor Science* **11**, 95.

TATTERSALL R. B., ROSE H., PATTENDEN S. K. and JOWITT D. (1960) *J. Nucl. Energy*, Part A: *Reactor Science* **12**, 32.

WALKER W. H., WESTCOTT C. H. and ALEXANDER T. K. (1960) *Canad. J. Phys.* **38**, 57.

VOL.
14
196

Reactor Science and Technology (J.N.E. Parts A/B), 1961, Vol. 14, pp. 55 to 58. Pergamon Press Ltd. Printed in Northern Ireland

PULSED OPERATION OF A FAST REACTOR*†

I. I. BONDARENKO and YU. YA. STAVISSKII

Abstract—Formulae are given for the duration of the power pulses and for the variation of power with time. Possible parameters are given for a pulsed fast reactor that could be used for nuclear physics research.

FOR many physical experiments using nuclear reactors the deciding factor is not the mean reactor power over long time intervals but the power during the short interval of time necessary for the experiment. In such cases pulsed operation of the reactor proves to be most advantageous, i.e. operation in which the power of the reactor increases by a large factor during a short interval of time. The advantage of pulsed operation shows itself most clearly in a fast reactor because in it the lifetime of the neutrons is very small compared to that in reactors of other types.

A pulsed reactor can be used as follows:

(1) In experiments using a time-of-flight neutron velocity selector;

(2) In the study of short-lived activities (delayed neutrons,[1,2] short-lived isomers, etc.);

(3) In various investigations in which the main difficulty is due to background not connected with the operation of the reactor.

In 1955 Blokhintsev proposed a pulsed reactor in which the power pulse arises from the motion of a part of the core which is fixed on a rotating disk. In such an arrangement the reactor remains sub-critical over a prolonged period and becomes super-critical only during short intervals of time, namely, when the moving part of the core passes through the main fixed section of the core.

The variation of reactor power with time during a pulse can be expressed with sufficient accuracy by the following equation:

$$dw(t) = \left(\frac{w(t)\varepsilon(t)}{\tau} + \frac{S}{\tau\nu}\right) dt. \qquad (1)$$

Here $w(t)$ is the instantaneous value of the reactor power (the number of fissions per sec), τ is the mean lifetime of the prompt neutrons‡, ν is the number of secondary neutrons, S is the strength of the external neutron source and $\varepsilon(t)$ is the excess multiplication coefficient (super-criticality) of the prompt neutrons in the reactor. In this equation the influence of delayed neutrons has not been taken into account since their lifetime in the case considered is much greater than the duration of the power excursion.

In order to obtain a short power burst one must make $\varepsilon(t)$ positive over short time. We take as the origin of time ($t = 0$) the moment when $\varepsilon(t)$ has its maximum value (see Fig. 1). We shall assume that the function $\varepsilon(t)$ is symmetric with respect to the point $t = 0$. This condition is evidently always satisfied if the variation in the reactivity is effected by a uniform displacement of a moveable part of the core.

At an instant of time far removed from the beginning of the pulse $\varepsilon(t)$ has a constant negative value equal to ε_1. During this period the power of the reactor is also constant:

$$W_1 = -\frac{S}{\varepsilon_1 \nu}. \qquad (2)$$

Subsequently $\varepsilon(t)$ begins to increase. As long as the

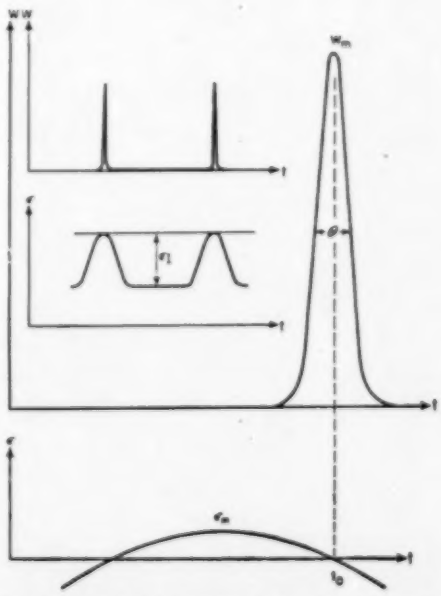

FIG. 1.—Schematic development of the power pulses in the pulsed operation of a fast reactor.

* Translated by N. KEMMER from *Atomnaya Energiya* **7**, 417 (1959).

† This article reports on work performed in 1956. Some of the data presented in it were also obtained by T. N. ZUBAREV.

‡ For a determination of the mean lifetime of prompt neutrons see the paper by USACHEV.[3]

rate of increase of $\varepsilon(t)$ is sufficiently small and its value still remains sufficiently far from zero, the process has a quasi-static character. During this period of time the reactor power at any instant is near its equilibrium value

$$w(t) = -\frac{S}{\varepsilon(t)\nu}. \tag{3}$$

This state of affairs persists as long as the condition

$$\frac{dw(t)}{w(t)} \ll \varepsilon(t)\frac{dt}{\tau} \tag{4}$$

is satisfied. Subsequently the power begins to increase more slowly than would follow from equation (3). Calculations show that as $\varepsilon(t)$ becomes zero the reactor power reaches the value

$$w(-t_0) \approx \frac{1{\cdot}25\,S}{\nu\sqrt{\tau\gamma}}, \tag{5}$$

where $\gamma = \left.\dfrac{d\varepsilon(t)}{dt}\right|_{t=-t_0}$. After this $\varepsilon(t)$ becomes positive and the required increase of power begins. In describing the variation of power in this period the second term of the r.h.s. of equation (1) can be neglected. This does not lead to significant errors if one is dealing with pulses during which the reactor power increases by a large factor, which is the case of interest here.

Then

$$\frac{dw(t)}{w(t)} = \frac{\varepsilon(t)\,dt}{\tau}. \tag{6}$$

The maximum value of the power, w_m, reached at the instant $t = t_0$ (when $\varepsilon(t)$ again takes the value 0), is

$$\begin{aligned} w_m &= w(-t_0)\exp\left[\int_{-t_0}^{t_0}\frac{\varepsilon(t)\,dt}{\tau}\right] \\ &= \frac{1{\cdot}25\,S}{\nu\sqrt{\tau\gamma}}\exp\left[\int_{-t_0}^{t_0}\frac{\varepsilon(t)\,dt}{\tau}\right]. \end{aligned} \tag{7}$$

Let us examine the shape of the pulse near the maximum. At times t near to t_0 the dependence of $\varepsilon(t)$ can be represented as follows:

$$\varepsilon(t) = -\gamma(t - t_0). \tag{8}$$

We then obtain from equation (6)

$$w(t) = w_m \exp\left[-\frac{(t-t_0)^2\gamma}{2\tau}\right].$$

Thus near the maximum the pulse has a Gaussian form with a half-width θ given by

$$\theta \simeq 2{\cdot}35\sqrt{\frac{\tau}{\gamma}}. \tag{9}$$

Further away from the maximum the shape of the pulse differs from the Gaussian form. Its increase is somewhat slower and its drop more rapid. However, numerical calculations from equation (1) show that for large power pulses significant deviations from Gaussian form are observed only at the edges of the pulse and contribute only slightly to the total energy of the pulse.

In reactors the maximum value of $\varepsilon(t)$, namely ε_m, is always small compared to unity. Therefore the dependence of ε on the position, x, of the moveable part of the core may be given approximately in parabolic form

$$\varepsilon(x) = \varepsilon_m - \alpha x^2, \tag{10}$$

where α is a quantity depending on the parameters of the moving part of the core and of the reactor. This constant characterizes the steepness of the variation of the activity with displacement of the moving part of the core. The dependence of ε on time is expressed in terms of the magnitude of α and the speed v of the motion of the moving part of the core as follows:

$$\varepsilon = \varepsilon_m - \alpha v^2 t^2.$$

Using (7) and (10) we obtain an expression for the total number of fissions during a pulse

$$\begin{aligned} E &= \frac{S}{\nu}K(\varepsilon_m); \\ K(\varepsilon_m) &= \frac{1{\cdot}25}{v\alpha^{\frac{1}{2}}\varepsilon_m^{\frac{1}{2}}}\exp\left(\frac{1{\cdot}33\,\varepsilon_m^{3/2}}{v\tau\alpha^{\frac{1}{2}}}\right). \end{aligned} \tag{11}$$

It is also of interest to know the dependence of the duration of the pulse on the basic quantities characterizing the reactor (τ, α, v). From the relations given above one can obtain the following expression:

$$\theta = 1{\cdot}74\frac{\tau^{\frac{1}{2}}}{\alpha^{\frac{1}{2}}v^{\frac{1}{2}}}A. \tag{12}$$

Thus the duration of the pulse decreases with decreasing τ and with increasing α and v. The duration depends also on the energy of the pulse (more precisely on the ratio of the pulse energy to the strength of the extraneous neutron sources). However, over a wide range of pulse energies this dependence is very

VOL
14
196

weak. In equation (12) the dependence is contained in the coefficient A:

$$A \simeq \left[\ln \frac{8E}{S} \nu_T^{1/3} \chi^{2/3} t^{4/3}\right]^{-(1/6)}.$$

Until now we have investigated single power pulses. We now consider the case when the reactor operates periodically, giving n pulses in one second. Under such conditions sources of delayed neutrons will accumulate in the reactor. If the reactor power is at all appreciable, then the sources of delayed neutrons accumulated during the previous impulses,

$$S = \sum_i c_i \lambda_i, \tag{13}$$

will be significant extraneous sources relative to the pulse. Here c_i is the concentration of the predecessors of the delayed neutrons in the i-th group and λ_i is the corresponding decay constant. If the interval between pulses is small compared to the lifetime of the delayed neutrons the mean power of the reactor $W(t)$ can be expressed as

$$W(t) = E(t)n + E(t)n \frac{\beta}{\varepsilon_I}. \tag{14}$$

Here the second term represents the power generated during the interval between pulses. In the cases of greatest interest, practically the whole power must be generated during the pulses. For this to be so it is necessary that

$$\frac{\beta}{\varepsilon_I} \ll 1.$$

We shall consider that this condition does hold in what follows.

Taking into account the accumulation and decay of the delayed neutrons we obtain from equation (11) the following equation describing the variation of the mean power:

$$W(t) = \frac{\sum_i c_i(t)\lambda_i}{\nu} K(\varepsilon_m)n; \tag{15a}$$

$$\frac{dc_i(t)}{dt} = -\lambda_i c_i(t) + W(t)\nu\beta_i. \tag{15b}$$

Here β_i is the yield of delayed neutrons of the i-th group, $\sum_i \beta_i = \beta$. From these equations it is easy to obtain a condition for quasi-stationary reactor operation (pulse amplitude independent of time):

$$K(\varepsilon_m)n\beta = 1. \tag{16}$$

Let us denote the ε_m which satisfies equation (16) by ε_0. Thus when the reactor operates with $\varepsilon_m = \varepsilon_0$ a self-sustaining chain reaction is realized, which corresponds to the operation of an ordinary reactor under stationary conditions with $K_{\text{eff}} = 1$. For $\varepsilon_m > \varepsilon_0$ the chain reaction dies away. It is interesting to note that the time-dependence of the mean power of a pulsed reactor after a small perturbation (for ε_m near to ε_0) is similar to the time-dependence of the power in ordinary fast reactors.

To show this let us write the equations for ordinary reactors as follows:

$$W(t) = \frac{\sum_i \lambda_i c_i(t)}{\nu} \frac{1}{\beta - \varepsilon(t)}; \tag{17a}$$

$$\frac{dc_i}{dt} = -\lambda_i c_i(t) + W(t)\nu\beta_i. \tag{17b}$$

It is here assumed that the lifetime of the prompt neutrons is zero. For reactors with a short life-time of prompt neutrons (fast reactors) this assumption is always justified. In conditions of delayed criticality it is easy to show that, in the case of small perturbations, the system of equations (15) describing a pulsed reactor coincides with the system (17) if one denotes

$$\frac{K(\varepsilon_0)}{\left.\frac{dK(\varepsilon_m)}{d\varepsilon_m}\right|_{\varepsilon_m=\varepsilon_0}} \quad \text{by } \beta^*.$$

Thus the time-dependence of the mean power of a pulsed reactor proves to be the same as for an ordinary reactor, for a certain effective fraction of delayed neutrons. Thus a pulsed reactor may be controlled using the same type of regulating system as for ordinary reactors. Here the displacement of the controlling mechanism leads to a change of ε_m.

For large perturbations the kinetics of a pulsed reactor differ from those of ordinary reactors. This difference shows itself for instance in the fact that for ordinary reactors, as distinct from pulsed reactors, the regulating influence of delayed neutrons disappears for $\varepsilon > \beta$, and this essentially changes the reactor kinetics.

As an example let us state the result of calculations for one variant of a fast reactor with pulsed operation. In this case the core contains plutonium and the moving part of the core is ^{235}U. The value of the basic reactor parameters determining its operation

under pulsed conditions is $\alpha = 7{\cdot}5 \times 10^{-3}$ cm^2, $\tau = 10^{-8}$ sec and $\varepsilon_I = 0{\cdot}2$. At a velocity of motion of the moving core section of 300 m/sec and a pulse frequency of 10 per second, the duration of a pulse will be 13×10^{-6} sec at an equilibrium value of the instantaneous critical excess $\varepsilon_0 = 2{\cdot}6 \times 10^{-3}$. The effective proportion of delayed neutrons in these conditions is $2{\cdot}4 \times 10^{-4}$. At a mean reactor power of 10 kilowatts the power in pulsed operation reaches $\sim 10^5$ kilowatts.

Acknowledgements—In conclusion the authors wish to express their deep indebtedness to D. I. BLOKHINTSEV, A. I. LEIPUNSKII and O. D. KAZACHKOVKY for constant attention and advice and also to F. I. and F. V. KRUSNARYOV for valuable discussion.

REFERENCES

1. HOFFMANN F. DE, FELD B. T. and STEIN P. R., *Phys. Rev.* **74**, 1330, (1948).
2. PAXTON H. C., *Nucleonics* **13**, No. 10, 48 (1955).
3. USACHEV L. N., *Reactor Construction and Theory of Reactors*, Moscow, Acad. Sci. U.S.S.R. (1955).

VOL
14
196

Reactor Science and Technology (J.N.E. Parts A/B), 1961, Vol. 14, pp. 59 to 66. Pergamon Press Ltd. Printed in Northern Ireland

LETTERS TO THE EDITORS

Fall-out of ^{90}Sr in the Leningrad region*

(*Received* 23 *April* 1959)

MEASUREMENTS of the ^{90}Sr in the atmospheric fall-out have been carried out since 1954 in the Leningrad region. We have previously discussed observations on the fall-out of accumulating products of nuclear explosions[1] made during 1954–55, our calculations being based on HUNTER and BALLOU's data.[2]

In 1956 a large number of fall-out samples were analysed specifically for ^{90}Sr. It was suggested that the mean percentage of ^{90}Sr in these samples was the same as that in the total annual fall-out, the amount of which was already known.[1] From this the quantity of ^{90}Sr in the fall-out for 1956 was calculated.

TABLE 1.—FALL-OUT OF ^{90}Sr

	Annual fall-out (mc km^{-2})	Residual fall-out on 1 Jan. 1957 (mc km^{-2})
1954–55	1·1	1
1956	2·6	2·5
1957	3·4	3·4
Total on 1 Jan. 1958	7·1	6·9

In 1957 complete radio-chemical analyses were performed on the fall-out products collected in a high-walled vessel containing a small quantity of acidified water. Strontium and cerium were separated, and the amounts of ^{90}Sr and ^{144}Ce were determined. The quantity of the latter in the fall-out for 1957 was 55·7 mc km^{-2}. The results for ^{90}Sr are given in Table 1.

V. P. SHVEDOV
M. I. ZHILKINA
V. K. ZINOV'EVA
L. M. IVANOVA
T. P. MAKAROVA
N. A. PAVLOVA

REFERENCES

1. SHVEDOV V. P., BLINOV V. A., GEDEONOV L. I. and ANKUDINOV E. V., *J. Nucl. Energy* **11**, 48 (1959).
2. HUNTER H. and BALLOU N., *Nucleonics* **9**, 5, C–2 (1951).

The dose of external gamma-radiation from the fall-out of certain fission products†

(*Received* 30 *May*, 1959)

DURING 1958 the radioactive fall-out in the town of Zelenogorsk was collected every month in pans 1 square metre in area. The contents of the pans were dried, reduced to ash and then monitored with a single-channel gamma-ray scintillation spectrometer, embodying a large CsI crystal.

In the γ-spectra of the radioactive fall-out lines of energies 150, 500 and 700 keV were detected, whose intensities diminished with half-lives of 30, 40 and 70 days. This made it possible to ascribe the corresponding γ-lines to ^{141}Ce, ^{103}Ru and $^{95}(Zr + Nb)$. To relate the area of each photo-peak to the absolute β-activity of the corresponding isotope, a calibration of the γ-spectrometer was performed with the aid of a 4π counter. The isotopes to be determined were separated radio-chemically from a series of samples and their β-activities were measured subsequently in calibrated toroidal β-counters. The comparison of the spectrometric and radio-chemical methods showed that the error in the determination of the absolute activity of γ-radiation by spectrometric means was no greater than 10 per cent. The absolute ^{137}Cs activity contained in the fall-out was determined by radio-chemical methods.

The absolute activity of any isotope (A_{tot}) deposited per month over 1 square metre of the earth's surface can be represented in the form of a geometric progression

$$A_{tot} = A_0 + A_0 e^{-\lambda} + A_0 e^{-2\lambda} + \ldots + A_0 e^{-t\lambda},$$

where A_0 is the mean activity of the isotope deposited per square metre per day, λ is the decay constant of the isotope (day^{-1}) and t is the period of collection in days. Hence

$$A_{tot} = \frac{A_0(1 - e^{-\lambda t})}{1 - e^{-\lambda}}.$$

Thus one can determine the mean activity (A_0) of the isotope and therefore also the number of active atoms of this isotope deposited per day. Knowledge of the relationship between the activity of the isotope and the number of subsequent decays of its disintegration products enables one to calculate the dose due to all subsequent γ-radiation from it.

The dose of γ-radiation from the radioactive fall-out was calculated for a point one metre above the earth's surface, without taking into account the absorption of the γ-radiation. The dose was calculated by integrating the γ-radiation over an infinite plane surface,[1] taking into account secondary rays according to the formula of HIRSCHFELDER.[2,3] The calculated doses are given in the Table. The strength of the 30-year dose from ^{95}Zr, ^{103}Ru, or ^{141}Ce is equal to the total annual dose. Thus if the annual dose from the γ-radiation of ^{137}Cs is equal to 1 mr/year, the dose from ^{95}Zr, ^{103}Ru and ^{141}Ce is 7·5 mr, i.e. as a

TABLE 1.—30-YEAR DOSE FROM RADIOACTIVE FALL-OUT IN 1958

Isotope	Dose (mr)
$^{95}(Zr + Nb)$	6·5
^{103}Ru	0·9
^{141}Ce	0·1
^{137}Cs	32·6
Total	40·1

* Translated by G. RYBACK from *Atomnaya Energiya* 7, 5, 479 (1959).
† Translated by N. KEMMER from *Atomnaya Energiya* 7, 6 (1959).

result of continuing tests of atomic weapons the short-lived isotopes contribute a substantial part of the dose from external radiation. The strength of the dose from radioactive fall-out in 1958 is already one-third of the world average dose from cosmic radiation (28 mr). The 30-year dose from radioactive fall-out from 1954–1956 inclusive previously calculated by us is 16 mr[4] and that due to radioactive fall-out in 1957 is 18 mr. The sharp increase of the dose indicates the growing danger from tests of atomic weapons.

V. P. Shvedov
G. V. Yakovleva
M. I. Shilkina
T. P. Makarova

REFERENCES

1. Gorshkov G. V., *The Gamma Radiation of Radioactive Bodies*, Leningrad (1956).
2. Hirschfelder J. and Adams E. A., *Phys. Rev.* **73**, 863 (1948).
3. Hirschfelder J., Magee J. and Hall M., *Phys. Rev.* **73**, 853 (1948).
4. Gedeonov L. I., Shvedov V. P. and Yaklovleva G. V. This issue, p. 64.

A new graphical method of calculating the dose field of extended sources*

(*Received* 4 *March* 1959)

When designing high-intensity γ-ray installations for irradiating samples or when working out radiation shielding problems it is often necessary to know the dose field due to the source. Such sources are of various shapes and some of the shapes may be quite complex. Where the problem involves an extended source,[1,2] an exact solution is possible only when the shape of the source is very simple and it often happens that such simple cases are of no practical interest. For certain other cases which are of practical interest, nomograms have been constructed or auxiliary coefficients have been determined using numerical methods to integrate the dose-rate equations.[3-5] Up to the present there has been no general method of calculating the dose field due to an extended source which applies to any case (in a homogeneous medium or in the absence of such a medium) and which provides a known degree of accuracy.

The method of calculating the dose field proposed here avoids the use of numerical integration and yields approximate expressions in terms of elementary or tabulated functions having a specified degree of accuracy. We will apply this method to some examples where the shape of the source is of practical interest and for which, at present, no general solution exists.

1. AN INFINITELY THIN RECTANGULAR SOURCE OF FINITE AREA

For the purpose of calculating the dose rate at any point p above a plane rectangular source (represented in Fig. 1 by the broken line) it is sufficient to find the dose rate from the rectangular portion of the source *Oabc*, where the sides of the rectangle are L and S and the ratio between them can be any value.

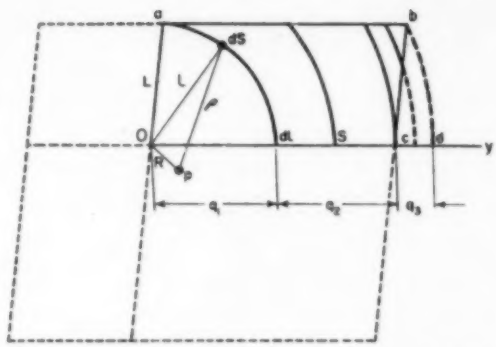

Fig. 1.—Transition from a rectangular plane source LS with constant specific surface activity q to a fictitious linear source $Od = J$ with a specific linear activity which is different in different regions: $Oy_1 \leqslant L \ldots q_1$; $L \leqslant y_2 \leqslant S \ldots q_2$; $S \leqslant y_3 \leqslant \sqrt{(L^2 + S^2)} \ldots q_3$.

Let the perpendicular distance from the radiating plane to the point p be R, the specific surface activity be q and let the width of the rectangle *Oabc* be $S = nL (n \geqslant 1)$. All those elements in *Oabc* which lie at the same distance ρ from the point p contribute equal dose rates at this point. These elements (dS) may therefore be replaced by a source dl which lies at the same distance ρ and which has an activity equal to the sum of the activities of the elements dS. From this it follows that the dose rate produced at point p by the portion of the source *Oabc* will be produced also by a linear source *Od* with a length J and an activity which will vary along its length according to a definite distribution law (see Fig. 2). At the same time, the total activity of this linear source J must equal the total activity of the rectangle *Oabc*. We will now find how this activity is distributed along this fictitious source J.

The elements of the plane which are at equal distances from the point p lie on the arc of the circle having centre O and radius r (Fig. 1). The linear specific activity at each point of source J is proportional to the length of the corresponding arc which lies within the rectangle *Oabc*.

At first, over that portion of the linear source where $0 \leqslant y \leqslant L$, the linear specific activity increases in accordance with the law:

$$q_1 = q \frac{\pi}{2} y. \tag{1}$$

Then, over the portion where $L \leqslant y \leqslant S$, the specific activity falls according to the law:

$$q_2 = qy \arctan L \frac{L}{\sqrt{y^2 - L^2}}. \tag{2}$$

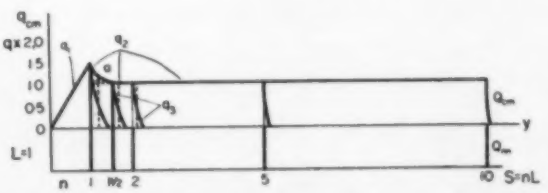

Fig. 2.—Specific linear activity distribution along the fictitious linear source for different side ratios $S/L = n$ of the rectangular source which the linear source replaces.

* Translated by D. L. Allan from *Atomnaya Energiya* **7**, 281 (1959).

Finally, from $y = S$ to $y = \sqrt{S^2 + L^2} = J$ the linear specific activity decreases to zero according to the law:

$$q_3 = qy\left[\arctan\frac{L}{\sqrt{y^2 - L^2}} - \arctan\frac{\sqrt{y^2 - S^2}}{S}\right]. \quad (3)$$

Figure 2 shows the linear specific activity distribution along the fictitious linear source which has the same effect at point p as the portion *Oabc* of the plane source. The figure shows how the activity distribution varies as the side ratio $n = S/L$ is increased.

For q_2 and q_3 we can take a linear distribution law and we then obtain

$$q_1 = q\frac{\pi}{2}y = ay, \quad \text{for} \quad 0 < y < L.$$

In place of q_2 and q_3, we will take

$$q_3' = q\frac{S + \sqrt{L^2 + S^2}}{2} \times \arctan\frac{L}{\sqrt{\left(\frac{S + \sqrt{L^2 + S^2}}{2}\right)^2 - L^2}} = qc \quad (4)$$

for

$$L < y < \frac{S + \sqrt{L^2 + S^2}}{2}.$$

A mean error of 2–5 per cent in relation to source parameters and geometry is introduced by the linear approximation made in equation (4).

In air, the dose rate from the portion *Oabc* of the plane finite source will be

$$P = K_\gamma q\left\{\frac{\pi}{4}\ln\frac{L^2 + R^2}{R^2} + \frac{C}{R}\left[\arctan\frac{S + \sqrt{L^2 + S^2}}{2R} - \arctan\frac{L}{R}\right]\right\}. \quad (5)$$

Equation (5) was tested by comparing it with a nomogram generalizing the results obtained by numerical integration for

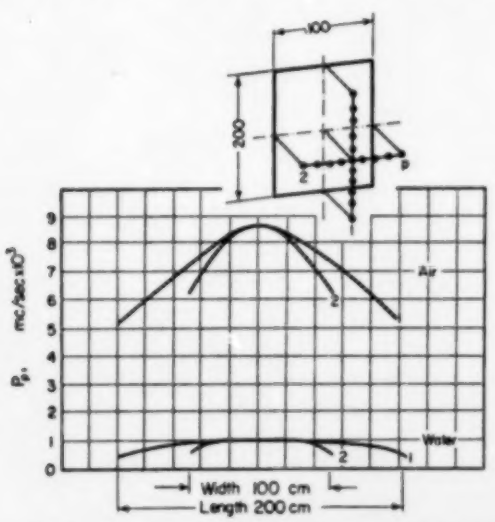

FIG. 3.—Dose rate distribution above a plane rectangular ^{60}Co source in air and in an absorbing medium.

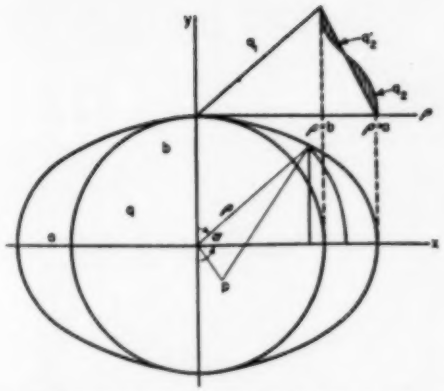

FIG. 4.—Transition from a plane elliptical source with a constant specific activity to a fictitious linear source with an activity distribution which varies along its length.

certain values of the side ratio of the rectangle *Oabc*.[3] The two methods agreed to within the accuracy with which the quantities could be determined from the nomogram for all values of R/S and L/S for which the nomogram had been plotted.

If the plane source lies in an absorbing medium then, after allowing for multiple scattering, the dose rate from the portion *Oabc* is given by

$$P = K_\gamma q\left\{-\frac{\pi}{2}\left(A_1\left[E_1(-b_1) - E_i\left(-b_1\sec\arctan\frac{L}{R}\right)\right] + A_2 \times \left[E_i(-b_2) - E_i\left(-b_2\sec\arctan\frac{L}{R}\right)\right]\right) + \frac{C}{R}\left[A_1\int_0^{\arctan\frac{S+\sqrt{L^2+S^2}}{2}} e^{-b_1\sec\varphi}\,d\varphi + A_2\int_0^{\arctan\frac{S+\sqrt{L^2+S^2}}{2}} e^{-b_2\sec\varphi}\,d\varphi - A_1\int_0^{\arctan\frac{L}{R}} e^{-b_1\sec\varphi}\,d\varphi - A_2\int_0^{\arctan\frac{L}{R}} e^{-b_2\sec\varphi}\,d\varphi\right]\right\}. \quad (6)$$

Figure 3 shows how the dose varies along the axes of a 200 × 100 cm plane rectangular source at a distance $R = 50$ cm above it. The surface specific activity is $q = 1$ mg equiv. cm^{-2} and the curves are for air and for an absorbing medium (water). It will be seen that the presence of the absorbing and scattering medium not only reduces the dose rate but also smooths out the dose field above a plane source.

2. A PLANE SOURCE OF ELLIPTICAL SHAPE

GORSHKOV[2] has calculated the dose rate both in air and in an absorbing medium from a disk-shaped source of radiation at a point above the centre of the disk. We shall now derive an expression for the more general case where the source has an elliptical shape with arbitrary eccentricity. Let the major and minor axes of the ellipse be a and b respectively (Fig. 4). For

the interval $0 \leqslant \rho \leqslant b$, the activity distribution of the corresponding fictitious linear source will be

$$q_1 = 2\pi q\rho \tag{7}$$

where q is the specific activity per unit area of the ellipse. For the interval, $b \leqslant \rho \leqslant a$, we have

$$q_2 = 4\rho\alpha q$$

where

$$\alpha = \arctan\frac{y}{x} = \arctan\left[\frac{b}{a}\sqrt{\frac{a^2-\rho^2}{\rho^2-b^2}}\right]$$

and

$$q_2 = 4\rho q \arctan\left[\frac{b}{a}\sqrt{\frac{a^2-\rho^2}{\rho^2-b^2}}\right]. \tag{8}$$

Figure 5 shows the activity distribution along the fictitious linear source whose length a is normalized to 1, for three cases: $a = b$, $a = 2b$ and $a = 10b$. When $a \neq b$, one can apply the linear approximation:

$$q_2' = \frac{a-\rho}{a-b}\,2\pi bq. \tag{9}$$

With this approximation the total activity of the linear source is still equal to the total activity of the ellipse but the activity distribution over the more remote regions of the source is changed very slightly. Using equations (7) and (9) we obtain the following results; for a source in air

$$P = \pi K_\gamma q\left\{\ln\frac{R^2+b^2}{R^2} + \frac{2b}{a-b} \times \left[\frac{a}{R}\left(\arctan\frac{a}{R} - \arctan\frac{b}{R}\right) - \frac{1}{2}\ln\frac{a^2+R^2}{b^2+R^2}\right]\right\} \tag{10}$$

and for a source in an absorbing medium

$$\begin{aligned} P = {} & -2\pi qK_\gamma\left\{A_1\left[E_i(-b_1) - E_i\left(-b_1\sec\arctan\frac{b}{R}\right)\right]\right. \\ & \left. + A_2\left[E_i(-b_2) - E_i\left(-b_2\sec\arctan\frac{b}{R}\right)\right]\right\} \\ & + 2\pi qK_\gamma\frac{b}{a-b}\left\{\frac{a}{R}\left[A_1\int_{\arctan\frac{b}{R}}^{\arctan\frac{a}{R}} e^{-b_1\sec\varphi}\,d\varphi\right.\right. \\ & \left.\left. + A_2\int_{\arctan\frac{b}{R}}^{\arctan\frac{a}{R}} e^{-b_2\sec\varphi}\,d\varphi\right]\right. \\ & + A_1\left[E_i\left(-b_1\sec\arctan\frac{b}{R}\right)\right. \\ & \left. - E_i\left(-b_1\sec\arctan\frac{a}{R}\right)\right] \\ & + A_2\left[E_i\left(-b_2\sec\arctan\frac{b}{R}\right)\right. \\ & \left.\left. - E_i\left(-b_2\sec\arctan\frac{a}{R}\right)\right]\right\}. \end{aligned} \tag{11}$$

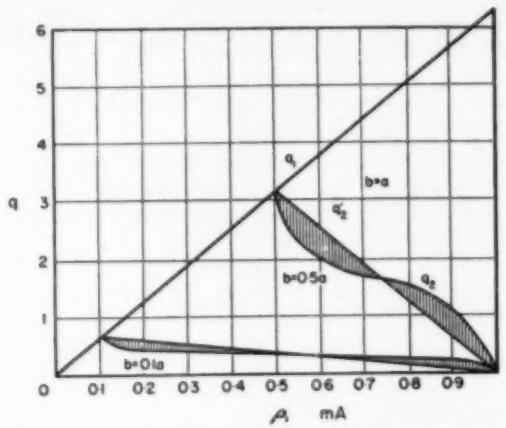

FIG. 5.—Specific linear activity distribution along a fictitious linear source for different values of the ratio $b/a = m(m < 1)$.

3. LINEAR SOURCES

The proposed method can be used to find equivalent sources which occupy different positions with respect to the point of measurement. Suppose we have a linear source L with a specific activity q which is constant throughout its length. We will find a linear source l perpendicular to this source which produces the same dose rate at point p as source L (see Fig. 6 (a and b)). The specific linear activity q_1 of the new source varies along its length.

From Fig. 6, we have

$$d\rho = dx = dy\sin\varphi = \frac{\sqrt{(x+R)^2 - R^2}}{x+R}\,dx$$

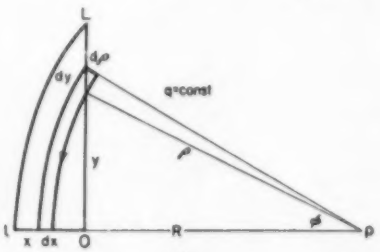

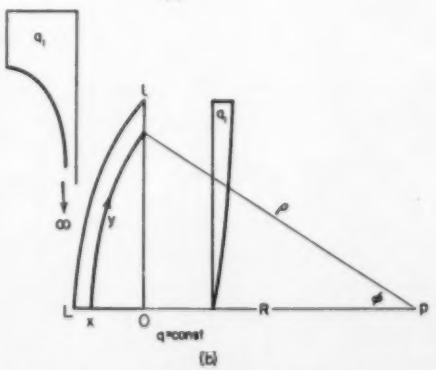

FIG. 6(a,b).—Transition from a linear source with a uniform activity distribution to a linear source with a non-uniform activity distribution and at right angles to the first. (a) Transition from source lying along x-axis to source along y-axis. (b) Transition from source lying along y-axis to source along x-axis.

and since

$$q\,dy = q_1\,dx,$$

we have

$$q_1 = q\,\frac{x+R}{\sqrt{(x+R)^2 - R^2}}. \qquad (12)$$

Equation (12) gives the activity distribution along the source l.

Now let there be a linear source of length L lying along the x-axis and having a uniform activity distribution. A source of length l lying along the y-axis and equivalent to L will have a specific linear activity distribution given by

$$q_1 = q\,\frac{y}{\sqrt{R^2 + y^2}}. \qquad (13)$$

CONCLUSION

The proposed method yields approximate expressions for the dose rate from plane sources of various shapes in terms of variously disposed linear sources giving the same dose rate at the given point. An extension of the method to include volume sources would be very interesting.

A. A. Bibergal

REFERENCES

1. Rockwell T., *Reactor Shielding Design Manual*, McGraw–Hill, New York (1956).
2. Gorshkov G. V., *Gamma Radiation from Radioactive Materials*, Leningrad State University (1956).
3. Kovalev E. E., Popov V. I. and Smirennii L. N., *J. Nucl. Energy* **5**, 424 (1957).
4. Kalinin I. A. and Vertebnii P. Ia., *Zh. fiz. khim.* **32**, No. 9, 2192 (1958).
5. Kovalev E. E., *Atomnaya Energiya*, 2, 538 (1957).

Fall-out after the cessation of nuclear weapon tests*

(*Received* 25 *May* 1959)

Since 1956 the Physics Panel of the Faculty of Medicine in Hradec Kralové, Czechoslovakia, has been carrying out measurements of the radioactivity of rainwater, initially in conjunction with the Geophysical Institute (Meteorological Department) in Hradec Kralové. Since nuclear weapon tests ceased we have continued to collect radioactive fall-out, at present at 2–3 day intervals, using the methods described by Shvedov *et al.*[1] The bottom of a high-walled plastic basin ~1 m² in area is covered with a thin uniform layer of water, and the collected material is treated as previously described.[1] The ash, while still moist, is transferred to an aluminium dish of area 3 cm² and is dried under a lamp, after which the β-activity is measured with conventional equipment. The γ-activity of some samples was also measured, using a scintillation counter. The decay of the more active samples was followed for several months using an automatic recording counter apparatus constructed by our assistant G. Macku.

Since samples collected from an area of 1 m² are relatively thick (usually tens of mg cm⁻²), it was necessary to make careful corrections for the self-absorption of the β-radiation using the largest possible number of samples. Good results were obtained by the following method. Part of the ash obtained from one sample was placed on an aluminium dish, the surface density being gradually raised from about 3 mg cm⁻² (self-absorption negligible) to >100 mg cm⁻². A curve showing the counting rate per mg of sample as a function of its surface density enabled the self-absorption correction to be found for each sample. Observations on the absorption in aluminium of the β-emission from the samples gave an approximate value for the β-radiation energy. Basically there are two β-groups with energies of 0·6 and 2·1 MeV respectively. In heavy samples (i.e. the majority of those studied) the weaker radiation is almost completely absorbed. The γ-radiations were counted with a scintillation detector. Their energies determined approximately from their absorption in copper and lead plates were 0·2 and 0·8 MeV. The absolute β-activity of the samples was obtained by comparison with a ^{90}Sr standard provided by the Dosimetry Department of the Institute of Nuclear Studies, Prague.

The indices representing the mean activity of fall-out for the period from 1 January–15 May 1959 are approximately four times the mean values for 1958 and three times those for the second half of 1958. The highest activity ($10{\cdot}1 \times 10^{-9}$ c l⁻¹) was observed for rain which fell on 6 April 1959. Some data on fall-out activity are given in Table 1. The fall-out was measured after several days had elapsed and results of the measurements of further samples were added to obtain the total monthly fall-out activity. The total activity for the six months was 327 mc km⁻², and the mean daily radioactive fall-out was 1·8 mc km⁻². The low values recorded for November 1958 are in part due to the low rainfall during that month.

Table 1.—Radioactive fall-out from 1 November 1958 to 31 May 1959

	Mean intensity per month (mc km⁻²)	Mean intensity per day (mc km⁻²)
1958, November	8·1	0·27
December	104·7	3·4
1959, January	62·1	2·0
February	75·1	2·7
March	31·5	1·0
April	45·8	1·5
May	41·6	1·3

In the three months from 1 November 1958 to 30 (*sic*) January 1959 the total fall-out was 175 mc km⁻², in the three months from 1 February to 30 April 1959 152 mc km⁻². It is more correct, however, to consider the cumulative fall-out density instead of the summed activity.[1] Using graphical methods, we have found that up to 3–4 months after collection a mean index $n = 1{\cdot}13$ is valid; for older samples the index is $n = 1{\cdot}64$. For this reason we used the equation

$$A = A_1 t^{-1{\cdot}64} = A_1 (T - T_0)^{-1{\cdot}64}$$

(where A_1 = activity after the elapse of the unit of time and $t = T - T_0$ = age of sample) for calculating the cumulative activity of samples more than 100 days old.

The date T_0 of a nuclear weapon test could be approximately

* Translated by G. Ryback from *Atomnaya Energiya* **7**, 480 (1959).

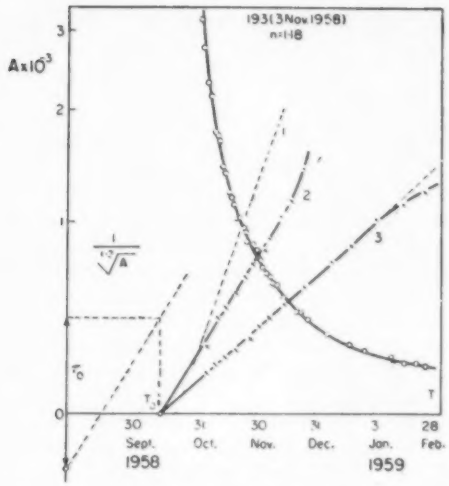

FIG. 1.—Radioactive decay of a fall-out sample from 3 November 1958.
The activity A (counts. min^{-1}) is shown as a function of time. The date of origin of the radioactivity (approx. 11 October 1958) has been determined and confirmed graphically by means of curves 2 and 3. Curve 1 would correspond to $n = 1{\cdot}0$; in fact $n = 1{\cdot}18$, as determined by means of the triangle on the left. Curve 3 is the result of the difference in dates τ corresponding to activities A and $A/2$, respectively. The deviation of curves 2 and 3 from their initial linearity is due to a small additional activity from earlier nuclear weapon tests.

determined by a graphical method (see Figs. 1 and 2). The activity of initially strong samples was continuously measured, so that the true values were employed in the summation. For the less active samples the methods of SHVEDOV *et al.*[1] were used.

From 1 November 1958 to 31 January 1959 the cumulative radioactive fall-out density was 90 mc km^{-2}; from 1 February to 30 April 1959 the density was 88 mc km^{-2}. Since in three months the activity decreased from 90 to 33 mc km^{-2}, the cumulative radioactive fall-out density six months after the cessation of the nuclear tests was 121 mc km^{-2}. In the graphical

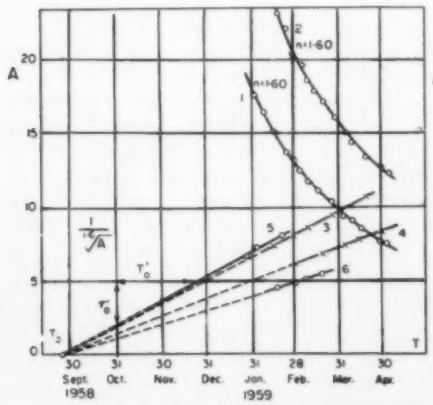

FIG. 2.—Radioactive decay of two fall-out samples, with the value $n = 1{\cdot}60$ determined graphically.
Samples (curves 1 and 2) collected 23 January and 16 February 1959, respectively. Graphically determined date of origin of radioactivity, approx. 25 September 1958 (curves 5 and 6); control curves, 3 and 4.

determination of T_0 and n it is convenient to assume that the points whose ordinates are determined by the difference in dates corresponding to the arbitrarily chosen activities A and A/k define a straight line intersecting the time axis at T_0, the slope of which depends on k and n. It has been shown[2] that after 100 days the activity of radioactive fission fragments is given by the expression

$$A = A_1 t^{-1{\cdot}60},$$

Using the latest data, a decay curve for β-active fragments has been constructed[3] which gives $n = 1{\cdot}5$ to $1{\cdot}7$ for fragments 3–4 months old. Our decay curves (for 18 'strong' samples) gives $n = 1{\cdot}64$ for fragments older than 3 months. Only in a few cases was an abnormally rapid decay with $n = 3$ to 4 observed (e.g. for samples collected on 23 January 1959, the activity of which initially fell very rapidly.) In March 1959 the decay index became constant at $n = 1{\cdot}6$. GEDEONOV[4] points out that rapid decay may be due to the presence of products formed by the action of neutrons. The activity of these would fall more rapidly than that of fission fragments.

For some time after the cessation of nuclear weapon tests one continues to find sufficient active samples having a definite age. Even some months later most samples of radioactive fall-out are in such a form that they can be considered as isolated clouds of fission fragments. SITTKUS[5] has pointed out that the mixing of atomic clouds is relatively insignificant. The decay curves for most of our samples may be taken as decay curves for fission fragments with some additional activity, which is negligible at first, but becomes significant after several months (see Fig. 1).

W. SANTHOLZER

REFERENCES

1. SHVEDOV V. P., BLINOV V. A., GEDEONOV L. I. and ANKUDINOV E. P., *J. Nucl. Energy* **11**, 1, 48 (1959).
2. HUNTER H. and BALLOU N., *Nucleonics* **9**, 5, C–2 (1951).
3. MALÝ J., KUTZENDÖRFER J., MACHÁČEK V., KOURIM V. and JEŘÁBEK V., *Czech. Phys. J.* **6**, 661 (1956).
4. GEDEONOV L. I., *Atomnaya Energiya* **2**, 260 (1957).
5. SITTKUS A., *Zeit. Phys. Atmos.* **30**, 200 (1958).

Calculation of the dose of external γ-radiation from the fall-out of radioactive fission products*

(*Received* 18 *July* 1959)

IN connexion with past tests of atomic weapons and the fall-out of radioactive fission products on the earth's surface estimates of the dose of external γ-radiation are made in many places, based on data from continuous observation of radioactive fall-out. The direct measurement of the γ-ray dose of the radioactive fall-out at great distances from the point of explosion is not possible because the natural γ-background is much greater than the γ-radiation of fission product fall-out. The only possible method of determining the dose is calculation.

In the present paper we estimate the γ-radiation dose from fission fragments that have fallen out on the territory of the Leningrad region from the beginning of atomic weapon testing up to 1 January 1957.

* Translated by N. KEMMER from *Atomnaya Energiya* **75**, 45 (1959).

The dose was calculated for a point at 1 metre above the earth's surface. In the calculation it was assumed that all the active substances in the fall-out remain in the uppermost, infinitely thin and flat layer of the earth's surface. Factors tending to decrease the activity, such as the washing out of the soil, evaporation and screening by irregularities of the surface, were not taken into account. Only the natural decay of the active substances in the fall-out was taken into account. The dose of γ-radiation was calculated from the moment of fall-out until the fragments decayed completely (up to $t = \infty$). Such a calculation allows one to estimate only the upper limit of the dose.

The calculation was performed according to the formula

$$D = kQ,$$

where D is the dose in roentgens, i.e. the amount of energy generated by the γ-radiation in 1 cm³ of air and Q is the total number of β-rays emitted after the instant of fall-out from the fission fragments deposited on each cm² of the earth's surface. k is the coefficient which gives the magnitude of the dose at a height of one metre above the earth if there is one decay per cm² of the earth's surface.

The number of decays after deposition from fragments with ages greater than 60 days was calculated according to the formula[1]

$$Q = 3515\, at \qquad (1)$$

where a is the activity (decay/min) of the fall-out particles on each cm² of the earth's surface and t is their age in days. The number of decays to be expected for deposits with ages less than 60 days was found according to the formula

$$Q = a\phi(t) \qquad (2)$$

where $\phi(t)$ was found from the curve given by BLINOV and GEDEONOV.[1] The activity of the fission fragments falling out on 1 cm² of the earth's surface was measured daily from 6 March 1954 onwards according to the method described by SHVEDOV, BLINOV, GEDEONOV and ANKUDINOV.[2] The fission fragments were assumed to have been produced in the middle of the series of tests most closely preceding the time of fall-out. The calculated numbers of decays to be expected are given in Table 1.

Taking into account the comparatively small power of the weapon tests performed before 1954 one can assume that the activity of all material deposited before 1954 does not exceed the activity of the deposits for the year 1954. The number of decays to be expected over 1 cm² of the earth's surface from all tests can then be estimated to be $Q = 4{\cdot}3 \times 10^7$ decays/cm².

TABLE 1.—NUMBER OF FUTURE DECAYS OVER 1 CM² OF THE EARTH'S SURFACE

Year of fall-out	No. of future decays over 1 cm² of earth's surface
1945	$8{\cdot}88 \times 10^6$
1955	$14{\cdot}7 \times 10^6$
1956	$10{\cdot}9 \times 10^6$
1954–1956	$34{\cdot}5 \times 10^6$

The evaluation of the coefficient k was performed in three stages: (1) calculation of the number of gamma quanta per expected β-decay in the mixture of fission fragments; (2) calculation of the flux of gamma-ray quanta from an infinite surface through a surface element of area 1 cm² at a height of one metre above the earth; (3) calculation of the γ-radiation dose in roentgens.

The number of γ-quanta per expected β-decay depends on the age of the fragments at the moment of fall-out, which for simplicity of calculation was taken to be 75 days.

The β-active fragments which still remain in a mixture whose age exceeds 75 days are given in Table 2, if their amount exceeds 0·2 per cent of the whole content.

Table 2 allows for the fact that in the equilibrium chain ^{106}Ru–^{106}Rh only one β-decay registers, since the energies of the β-particles of ^{106}Ru are so insignificant that they are not registered in the measurement in a thick source. For the same reason ^{147}Pn and ^{151}Sn are absent from the Table.

The mean number of γ-quanta per decay is found from the formula

$$\nu = \frac{\sum_{i=1}^{11} a_i b_i}{\sum_{i=1} a_i}. \qquad (3)$$

The mean energy of the γ-quanta emitted can be found from the formula

$$E_{\text{av.}} = \frac{\sum_{1}^{11} a_i b_i c_i}{\sum_{i=1}^{11} a_i b_i}. \qquad (4)$$

TABLE 2.—RELATIVE NUMBERS OF FUTURE DECAYS IN A MIXTURE 75 DAYS OLD

Isotope	Decay period	Yield at moment of formation	Fraction of total number of future decays *a*	Number of γ-quanta per β-decay *b*	Mean γ-quanta energy *c*
^{89}Sr	54 days	5	0·058	0	0
^{90}Sr	27 years	5	0·150	0	0
^{91}Y	61 days	5	0·060	0	0
^{95}Zr–^{95}Nb	65 days	6	0·160	1	0·72
^{95}Nb	35 days	0	0·054	1	0·75
^{103}Ru	42 days	3	0·032	1	0·5
^{106}Ru–^{106}Rh	1 year	2·5	0·066	0·2	0·8
^{137}Cs	33 years	5	0·150	0·92	0·68
^{141}Ce	33 days	6	0·44	0·7	0·15
^{144}Ce	290 days	5	0·113	0·5	0·08
^{144}Pr	—	5	0·133	0·01	—

The fission fragment mixture at an age of 75 days has $\nu = 0{\cdot}45$ quanta per expected β-decay and $E_{av.} = 0{\cdot}60$ MeV.

The flux of γ-quanta emitted from an infinite plane contaminated by fission fragments passing through a surface element of area 1 cm² at a height of one metre above the plane, neglecting secondary radiation, is determined by equation (5) given by GORSHKOV[3]

$$N = -\frac{Q_i}{2} E_i(-100\,\mu) \tag{5}$$

where N is the required γ-quantum flux, Q the number of β-decays per cm² of earth's surface, v is the number of γ-quanta per β-decay, $E_i(-100\,\mu)$ is the function E_i for the value $(-100\,\mu)$ of the argument; μ is the attenuation coefficient of the rays in air in cm^{-1} (for $E_{av.} = 0{\cdot}60$ MeV) and is equal to $10{\cdot}8 \times 10^{-5}$ cm^{-1}.

The energy losses of γ-rays in air if the true absorption coefficient $\tau + \sigma_\beta$ is small are given by

$$\Delta I = I_0 - I = I_0\{1 - \exp[-(\tau + \sigma_\beta)x]\} = I_0(\tau + \sigma_\beta)x \tag{6}$$

where $I_0 = NE_{av.}$, x is the path of the γ-rays in air (cm) and $(\tau + \sigma_\beta)$ is the coefficient of true absorption arising from the Compton and photoeffects; $\tau + \sigma_\beta = 3{\cdot}8 \times 10^{-5}$ cm^{-1}.

Gamma rays passing through 1 cm of air released an energy

$$\Delta W = I(\tau + \sigma_\beta) = NE_{av.}(\tau + \sigma_\beta)\ \text{MeV} \tag{7}$$

and the dose in roentgens[3] is

$$D = 1{\cdot}45 \times 10^{-5} NE_{av.}(\tau + \sigma_\beta). \tag{8}$$

Inserting expression (5) into equation (8) we obtain

$$D = -1{\cdot}45 \times 10^{-5} \frac{Qv(\tau + \sigma_\beta)E_{av.}}{2} E_i(-100\,\mu)\text{r}. \tag{9}$$

Putting in the numerical values for $v, \tau + \sigma_\beta, E_{av.}$ and $E_i(-100\,\mu)$ we get

$$D = 3{\cdot}7 \times 10^{-10} Q\ \text{r}. \tag{10}$$

The quantity $3{\cdot}7 \times 10^{-10}$ gives the dose one metre above the earth if there is 1 decay per cm² of the earth's surface. The estimates of this quantity according to the data available in the literature give the following values (r/decay): $8{\cdot}2 \times 10^{-10}$,[4] $4{\cdot}6 \times 10^{-10}$,[5] 16×10^{-10},[6] $3{\cdot}4 \times 10^{-10}$.[7] The first of the values given must be assumed to be too large because in its calculation it was assumed that there is one γ-quantum emitted for every β-decay. If one assumes that in one decay 0·45 γ-quanta are radiated the first value becomes $3{\cdot}7 \times 10^{-10}$ r/decay. EISENBUD and HARLEY[6] note that they give only an order of magnitude estimate.

Taking these statements into account, the different estimates of the strength of the dose per single fission process agree well with the value found in the present paper. If one inserts into expression (10) for D the previously calculated $Q = 4{\cdot}3 \times 10^7$ decays/cm² one obtains

$$D = 0{\cdot}016\ \text{r in 30 years}.$$

For England the value of the dose has been estimated as 0·55 r.[8] For the U.S.A. the magnitude of the dose calculated under the assumptions accepted in this paper, fluctuates according to the distance from the test areas between the limits 0·006 to 0·160 r.[9] The dose to which a person is exposed over 30 years from cosmic rays and from the natural activity of the soil lies within the limits 4·3–5·5 r.[10,11] From a comparison of the data given here one sees that the γ-radiation doses obtained for various countries are close to each other in magnitude and are much smaller than the doses from natural γ-rays. Although it follows from these data that the external γ-radiation of radioactive deposits does not represent a direct danger nevertheless the presence of additional radiation can be the cause of undesirable genetical consequences. In addition a considerable part of the fall-out activity is due to ^{90}Sr, which presents a danger if ingested into the human body.

Acknowledgement—The authors wish to express their gratitude to PROF. K. K. AGLINTSEV for his valuable advice in the performance of this work.

L. I. GEDEONOV
V. P. SHVEDOV
G. V. YAKOVLEVA

REFERENCES

1. BLINOV V. A. and GEDEONOV L. I., *The Physics and Thermal Technology of Reactors*, Suppl. I to *Atomnaya Energiya* 96 (1958).
2. SHVEDOV V. P., BLINOV V. A., GEDEONOV L. I. and ANKUDINOV E. P., *Atomnaya Energiya* **5**, 577 (1958).
3. GORSHKOV G. V., *The Gamma Radiation of Radioactive Bodies*, Leningrad (1956).
4. *The Effects of Atomic Weapons*, U.S. Govt. Print. Office, Washington (1950).
5. LAPP E., *Bull. Atom. Sci.* **11**, No. 2, 45 (1955).
6. EISENBUD M. and HARLEY J., *Science* **121**, 677 (1955).
7. BLIFFORD I. and ROSENSTOCK H., *Science* **123**, 619 (1955).
8. COCKROFT J., *Nature, Lond.* **175**, 873 (1955).
9. EISENBUD M. and HARLEY J., *Science* **124**, 251 (1955).
10. LAPP E., *Bull. Atom. Sci.* **11**, No. 6, 216 (1955).
11. *Science* **123**, 1157 (1956).

VOL
14
196

Reactor Science and Technology (J.N.E Parts A/B), 1961, Vol. 14, pp. 67 to 68. Pergamon Press Ltd. Printed in Northern Ireland

ABSTRACTS AND TITLES OF FUTURE PAPERS

Atomnaya Energiya

Vol. 9, No. 5

Use of (α,n) reactions in quantitative assays of dressing products for beryllium, boron and fluorine: I. N. PLAKSIN, V. N. SMIRNOV and L. P. STARCHIK.

A rapid method based on (α,n) reactions is described for use in assaying dressed products for Be, B, and F. The α-ray source is 250 μ of ^{210}Po; the neutrons are recorded by a neutron counter. The dressed products examined in this way are fluorite and ores of boron and beryllium, or ores rich in B and F, the error of measurement being 1·5–2%. Any one element can be assayed provided that the content of any other element having a high (α,n) cross section is constant.

Replacement of a block in a two-dimensional rectangular array: L. TRLIFAY and J. ROČEK.

The results are given from a study of the effects of modifying one block in an infinite uniform two-dimensional square array. The solution obtained for an inactive medium is analogous to one given elsewhere; that for a medium producing neutron multiplication is obtained by means of a modified form of a method used in the quantum theory of fields. The case of a critical infinite array is considered as the limit of the two preceding cases. The results obtained (subject to homogenization conditions) correspond to those found for the analogous homogeneous case.

Tests for the instability resulting from temperature changes occurring during transient modes of operation of a reactor: R. JANE and R. DESAY.

A discussion is given of the kinetics of a Calder Hall type uranium-graphite reactor; allowance is made for the temperature coefficient of reactivity and for the reactivity changes resulting from burn-up. It is found that the minimum positive period is not less than 170 sec for levels of burn-up up to 3000 MW-days/ton.

Isothermal irradiation of non-fissile materials in a reactor by means of calorimetric devices: N. F. PRAVDYUK, V. N. KUZNETSOV and N. I. LALETIN.

A discussion is given of the heat generated in irradiated inactive materials by the gamma rays produced in the core of a reactor. The mass absorption coefficient is calculated as a function of Z for an RFT spectrum. A description is given of a steady-state method developed on the RFT for calculating the heat q released in unit mass of an inactive material irradiated within a fuel-rod assembly. The results for aluminium, steel 30, tin, and lead range from 2·2 to 3·7 W/g for cylinders 13·5 and 10 mm in diameter used in a 10 MW reactor. It is found that q varies as a function of the height of a channel passing through the core according to a cosine law. A method is described that has been used in isothermal irradiations of specimens and cans at temperatures in excess of the temperature of the coolant.

Uranium monocarbide: G. A. MEERSON, R. G. KOTEL'NIKOV and S. N. BASHLYKOV.

Uranium monocarbide is of interest as a material for fuel rods and for nuclear thermoelectric generators. A study of the relation of composition to synthesis conditions has resulted in a scheme for the best method of making carbide of stoichiometric composition. It is possible to make specimens of porosity about 5% as a result of the sintering and hot-pressing studies that have been made on UC and mixtures of UC with U. The density of UC powder (pyknometer) is 12·97 ± 0·60 g/cm³; UC has a microhardness of 923 ± 56 kg/mm², and its thermal conductivity varies from 0·028 to 0·04 cal cm^{-1} sec^{-1} C^{-1} in the range from 100 to 700°C; the mean linear expansion coefficient for the range from 20 to 1500°C is 11·6 × 10^{-6}. Specimens of UC have been cycled 500 times between 200 and 1000°C without rupture; specimens of UC + U have withstood more than 1000 such cycles.

The increase in internal friction associated with temperature changes in uranium: YU. N. SOKURSKII and YU. V. BOBKOV.

An internal-friction mechanism described previously for heated uranium has been used to derive a semi-quantitative estimate of the increase in internal friction as a function of the rate of heating and of the frequency and amplitude of the oscillations. The results agree satisfactorily with those found from experiment. A study is made of the effects of the initial state of the material on the increase in the internal friction during the initial stages of the heating.

Letters to the Editor

The fission cross-sections of ^{232}Th, ^{235}U, ^{237}Np, and ^{238}U for neutrons of energies ranging from 10 to 22 MeV: V. M. PANKRATOV, N. A. VLASOV and B. V. RYBAKOV.

Measurement of radiative-capture cross sections for fast neutrons: YU. YA. STAVISSKII and V. A. TOLSTIKOV.

The gamma rays produced when neutrons of energy 3 MeV are scattered inelastically: A. L. ANDROSENKO, D. L. BRODER and A. I. LASHUK.

Production of thin layers of thorium, uranium, neptunium, plutonium and americium: G. I. KHLEBNIKOV and E. P. DERGUNOV.

A device for examining the effects of gamma rays on semiconductor materials: B. M. KONOVALENKO, S. M. RYVKIN, I. D. YAROSHETSKII and L. P. BOGOMAZOV.

Measurement of the speed of ultrasound in molten alkali metals: YU. S. TRELIN, I. N. VASIL'ev and V. V. ROSHCHUPKIN.

Radiation-induced chlorination of benzene: L. A. KRASNOUSOV, P. V. ZIMAKOV and E. V. VOLKOVA.

Thermodynamics of the reduction of KF and NaF by metallic calcium and magnesium: I. M. DUBROVIN and A. K. EVSEEV.

News of Science and Technology—Bibliography

Vol. 9, No. 6

Spectra of neutrons emitted in the fission of ^{235}U at angles of 0, 45, and 90° to the line of flight of the fragments: YU. A. VASIL'EV, YU.S. ZAMYATNIN, E. I. SIROTININ and E. F. FOMUSHKIN.

The spectra of the neutrons emitted at angles of 0, 45, and 90° to the line of flight of the heavy fragments emitted from ^{235}U bombarded by neutrons of energy 14·3 MeV have been measured; the fluxes N are found to be such that

$$N(0°):N(45°):N(90°) = (3{\cdot}23 \pm 0{\cdot}12):(1{\cdot}75 \pm 0{\cdot}07):1{\cdot}00.$$

Calculations are presented to show that the results cannot be explained in terms of an isotropic Maxwellian distribution in a system based on a fragment.

Coherent radiation from the electrons in a synchrotron: YU. M. ADO and V. V. ELYAN.

Experiments were carried out with the 280 MeV synchrotron (with betatron initiation) at the Institute of Physics, Academy of Sciences of the USSR. For various electron distributions within the accelerator system the coherent radiation has been examined at a wavelength of 10 cm, which corresponds to the 50th harmonic of the circulation frequency. The theory of coherent radiation is confirmed for the most part, but discrepancies are found when the electron distribution is almost uniform. The emission has been used to measure the frequency and adiabatic damping of the phase oscillations.

Heat transfer between mercury and water flowing in a closely packed assembly of rods: V. I. SUBBOTIN, P. A. USHAKOV, B. N. GABRIANOVICH and A. V. ZHUKOV.

Results are presented from an experimental study of heat transfer to mercury and water in a close-packed assembly of rods. Thermal models of the rods are considered. Measurements are reported for the temperature distribution at the heat-transfer surfaces. Descriptions are given of the apparatus, the techniques, and the method of evaluating the results. An approximate calculation method is presented for one array of close-packed rods.

Effects of a partly inserted absorbing rod on a neutron flux density distribution: J. CHERMAK and L. TRLIFAY.

A method is presented for calculating the effect of a cylindrical absorbing rod partly inserted into a reactor having no reflector. The perturbation in the flux density near the rod can be estimated in relatively simple fashion. The one-group equation $\phi + B^2\phi = 0$ is used, subject to special boundary conditions at the surface of the rod. The B^2 and ϕ are calculated for several positions of the rod.

Isotopic composition of uranium from rare-earth minerals: YU. A. SURKOV, A. A. VOROB'EV, V. A. KOROLEV and V. D. VILENSKII.

In an attempt to detect ^{247}Cm, which may occur in nature, uranium from rare-earth minerals (orthite, xenotime, and gadolinite) has been examined by means of an ionization chamber to a multichannel pulse-height analyser. The results are discussed. A method is presented which enables one to calculate exactly the distortion introduced into the α-ray spectrum by an ionization chamber having electron collimation. It is shown that small specimens (0·2 – 1 mg U) may be assayed for $^{235}U/^{238}U$ ratio with an error of about 1% by means of the α-ray spectrometer.

Methods of directional recording for gamma rays: V. P. BOVIN.

An analysis is given of the main characteristics and parameters of directional radiation detectors. Special attention is given to coincidence-type directional scintillation detectors and it is demonstrated that such detectors are very much better than the corresponding gas-discharge devices in performance. Various coincidence systems are described suitable for a variety of purposes in detecting and assaying radioelements.

Letters to the Editor

Crosssection of the $^6Li(n,\alpha)^3H$ reaction at 2·15 MeV: V. P. PERELYGIN and K. D. TOLSTOV.

Generation of beams of fast neutrons: V. S. BARASHENKOV and HSIEN TING-CH'ANG.

Model of a ring phasotron: V. A. PETUKHOV, I. GABANETS, A. A. ZHURAVLEV, M. KARMASIN, V. I. KOTOV, E. A. MYAE, YU. L. OBUKHOV, V. SOKHOR, YU. TSIRAK, F. BENDA, I. DOBIASH. M. MAREK, T. FUKATKO and L. V. SVETOV.

Similitude methods applied to generalizing experimental results on critical heat fluxes for boiling liquids: S. S. KUTATELADZE and G. I. BOBROVICH.

Heat transfer to an Na-K alloy in an annulus: E. M. KHABAKHPASHEVA and YU. M. IL'IN.

The thermal resistance of a contact: YU. P. SHLYKOV and E. A. GANIN.

Effects of nuclear radiation on the dielectric parameters of insulating materials: K. A. VODOP'YANOV, B. I. VOROZHTSOV, M. D. LAVROV, E. S. NESMEYANOVA and G. I. POTAKHOVA.

Isotopic composition of ruthenium: K. G. ORDZHONIKIDZE and O. S. AKIRTAVA.

Heat of formation of $PuBe^{13}$: V. V. AKHACHINSKII and L. M. KOPYTIN.

Measurement of the absolute concentration of thoron in the air of industrial buildings: YU. N. BURMISTENKO.

The shape of the absorption curve for beta rays in aluminium: N. E. TSVETAEVA.

News of Science and Technology—Bibliography

VOL. 14 196

Reactor Science and Technology (Journal of Nuclear Energy, Parts A & B), 1961, Vol. 14, pp. 69 to 75. Pergamon Press Ltd. Printed in Northern Ireland

CROSS-SECTIONS FOR THE $(n, 2n)$ REACTIONS OF ^{232}Th, ^{238}U AND ^{237}Np WITH 14 MeV NEUTRONS

J. L. PERKIN and R. F. COLEMAN
Atomic Weapons Research Establishment, Aldermaston, Berks.

(*Received* 22 *June* 1960)

Abstract—Cross-sections for the reactions ^{232}Th$(n, 2n)^{231}$Th, ^{238}U$(n, 2n)^{237}$U and ^{237}Np$(n, 2n)^{236}$Np with 14 MeV neutrons were found by activation methods.

^{231}Th and ^{237}U were detected by observing their γ-rays with a sodium iodide scintillation spectrometer. ^{236}Np was estimated by counting the α-particle activity of its daughter ^{236}Pu.

The cross-sections found were as follows:

Target nuclide	$(n, 2n)$ cross-section (barns)	Neutron energy (MeV)
^{232}Th	1·20 ± 0·05	14·1 ± 0·3
^{238}U	0·69 ± 0·04	14·5 ± 0·4
^{237}Np	0·39 ± 0·07	14·5 ± 0·4.

INTRODUCTION

CROSS-SECTIONS for the $(n, 2n)$ reactions of ^{232}Th, ^{238}U and ^{237}Np with 14 MeV neutrons have been measured using activation methods. This work formed part of a more general programme concerned with the interaction of fast neutrons with some of the heavy elements, extending over several years.

The cross-section of the ^{232}Th$(n, 2n)^{231}$Th reaction at 15 MeV has been previously reported by PHILLIPS (1956) who detected the 25·6 keV γ-ray from the decay of ^{231}Th produced in this reaction with a proportional counter filled with krypton. The counter was calibrated absolutely in terms of ^{231}Th activity by observing this same γ-ray from a weighed quantity of ^{235}U which contained an equilibrium amount of its daughter ^{231}Th. A value of 1·1 ± 0·1 barns was found.

In the experiments reported here a sodium iodide γ-ray scintillation spectrometer was used to detect the ^{231}Th activity produced. The calibration of this counter in terms of absolute ^{231}Th activity was similar to the method used by PHILLIPS. In this case, however, the 58·5 and 85 keV γ-rays from the decay of ^{231}Th were used and the standardized source of ^{231}Th was chemically separated before calibration to eliminate the γ-ray spectrum from ^{235}U.

Since this work was completed the excitation function of this reaction has been measured by TEWES *et al.* (1959). Cross-sections of 1·327 and 1·148 barns were found for neutron energies of 14·0 and 14·47 MeV respectively.

Several measurements of the ^{238}U$(n, 2n)^{237}$U reaction cross-section have been published. A value of 0·4 ± 0·3 barns for neutrons of 14 MeV was obtained by GRAVES (ca. 1951). More recently POOLE (1954) published a value of 0·65 ± 0·05 barns for neutrons of the same energy.

POOLE used a xenon-filled proportional counter to detect the 59 keV ^{237}Np γ-ray emitted in the decay of ^{237}U. The efficiency of the proportional counter for 59 keV γ-rays was found by calibrating with a source of ^{241}Am which decays by α-emission to ^{237}Np. BELING, NEWTON and ROSE (1952) report a yield of 0·40 ± 0·015 59 keV γ-rays per α-particle for this decay. POOLE assumed this same figure for the yield of 59 keV γ-rays per ^{237}U disintegration. PHILLIPS (1956) using the same technique obtained a value in agreement with POOLE. However, the states of ^{237}Np fed by the decay of ^{237}U are at a higher excitation than those fed by the decay of ^{241}Am. Thus the yield of 59 keV γ-rays per disintegration could differ in the two cases. In the present experiments this difficulty was overcome by calibrating the detector with a thin source of ^{237}U, prepared by α-decay of ^{241}Pu and standardized by β-counting in a 4π proportional counter.

Since this work was completed two further papers have been published describing ^{238}U$(n, 2n)^{237}$U cross-section determinations. One by KNIGHT, SMITH and WARREN (1958) refers to some unpublished work by GRAVES *et al.* concerning the variation of this cross-section in the neutron energy range 13 to 15 MeV. The 14·5 MeV value is quoted as 0·7 barns. In the other paper by ANTROPOV *et al.* (1958) the $(n, 2n)$ cross-section was measured relative to the fission cross-section of ^{238}U. A small quantity of uranium was irradiated, the fission products were separated and analysed and the ^{237}U activity was counted

directly in a 4π proportional counter. Their result for 15 MeV neutrons is 0·9 ± 0·15 barns.

There are no published data on the $^{237}Np(n, 2n)^{236}Np$ reaction. The method used in the present work to find the cross-section was to allow the ^{236}Np (22 hr) produced to decay and to count the α-particle activity of its daughter ^{236}Pu (2·7 yr) using a gridded ionization chamber.

MEASUREMENT OF THE NEUTRON FLUX

Fast neutrons were obtained by bombarding a tritiated zirconium target with 160 keV (or in one case 500 keV) deuterons. The neutron flux was monitored by counting the associated α-particles from the D–T reaction in a known geometry and at an angle of 135° to the beam. As the angular distribution of neutrons from this reaction with low energy deuterons is isotropic in the centre of mass system (BAME and PERRY, 1957), the neutron flux can be calculated in any direction. In these experiments, however, the samples had to be irradiated very close to the source to obtain sufficient activity. Under these conditions it was not possible to make an accurate estimate of the flux through the sample. This difficulty was overcome by monitoring the neutron flux in the sample position with the activity produced by the $^{27}Al(n, \alpha)^{24}Na$ reaction in an aluminium disk placed in contact with the sample.

The β-activity from this reaction was measured with an end-window Geiger counter and compared with the activity produced in similar disks irradiated in positions of well defined geometry. Two such positions were chosen at right angles to the deuteron beam direction on opposite sides of the tritium target and at equal distances from it. In this way errors due to the finite size of the source were minimized. The flux through the samples could then be calculated to ±3 per cent, the main error arising from the calculation of the flux in the positions of well defined geometry.

In the case of the uranium experiments, copper disks were used instead of aluminium ones and a sodium iodide scintillation spectrometer was used to detect the positron annihilation quanta from the ^{64}Cu produced in the $^{65}Cu(n, 2n)^{64}Cu$ reaction.

EXPERIMENTAL DETAILS OF THE $^{232}Th(n, 2n)^{231}Th$ CROSS-SECTION MEASUREMENT

Preparation of the thorium samples

For ease of handling and in order to obtain uniformly thin layers, the thorium used in these experiments was in the form of oxide between two layers of Sellotape. The oxide, ground to a fine powder, was dusted over circular areas of the sticky surface of the tape and the excess was brushed off.

Two such areas were placed face to face giving a layer of thorium oxide of about 15 mg covering an area of 2 cm^2. Before putting together, an aluminium disk of the same diameter for monitoring the neutron flux was inserted. As the thickness of the whole sandwich so formed was only about 5×10^{-3} cm, the aluminium disk gave a correct indication of the mean neutron flux throughout the thorium.

The weight of oxide in a sample was measured at the end of the experiment by ashing the sample, and weighing the residue.

Preparation of thorium samples containing ^{231}Th used for calibration

Samples were prepared using thorium oxide which contained ^{231}Th produced by α-decay of ^{235}U. About 100 mg of uranium metal (^{235}U containing ^{231}Th in equilibrium) and 20 mg of thorium nitrate were dissolved in aqua regia, evaporated to dryness and the residue dissolved in 6-M hydrochloric acid. The solution was passed through an anion exchanger (De-acidite, FF, particle size less than 50 μ) and the column washed with more 6-M hydrochloric acid to elute the thorium. The effluent was evaporated to small bulk and neutralized with ammonia. The hydroxide was filtered off and then ignited to the dioxide. The chemical yield of the separation was 100 per cent. The ^{235}U metal used consisted of 93 ± 1 per cent ^{235}U, about 5·5 per cent of ^{238}U and about 1 per cent ^{234}U.

After mounting in Sellotape, as already described, the sample was placed close to a γ-ray scintillation spectrometer employing a sodium iodide crystal 2¼ in. in diameter and 2¼ in. long. The γ-ray spectrum observed was similar to those shown in Fig. 1(a) or (b). The main features were in accord with the more detailed work of GHIORSO (1951), BELL *et al.* (1952), JOHNSON (1956) and FREEDMAN *et al.* (1953) on the decay of ^{231}Th. A comparison of this spectrum with that of ^{235}U showed that less than 0·5 per cent of ^{235}U remained in the sample.

The decay of the 85 keV and partly resolved 58·5 keV peak from the decay of ^{231}Th in this spectrum was measured using a γ-ray energy counting channel of 40 to 120 keV.

The chemical processing already described removed all the natural decay products of thorium other than ^{228}Th (1·9 year radio-thorium). The growth of daughters from the decay of ^{232}Th can be neglected since the half-life of the first member of the decay chain ^{228}Ra is 6·7 years. However, the longest lived member of the

VOL 14 196

seven isotopes in the chain below ^{228}Th is ^{224}Ra (the first) with a half-life of 3·64 days. A correction for this amounting to about 3 per cent was obtained by observing in a separate experiment the growth of the γ-ray activity of ^{224}Ra and its daughters with a thorium oxide sample processed as described but without the addition of ^{231}Th.

A very small long-lived residual activity which remained after applying this correction was almost certainly due to ^{234}Th (24·1 days) and its daughter ^{234}Pa (1·18 min) which are derived from the ^{238}U content of the ^{235}U sample. Subtraction of this activity gives a half-life of 26 hours for ^{231}Th decay which agrees within experimental error with the value of 25·6 hours found by JAFFEY *et al.* (1951).

The decay curve was extrapolated back to the time of separation of ^{231}Th from its parent ^{235}U. The counting rate at this time was compared with the absolute activity as calculated from the weight of ^{235}U used and the half-life of ^{235}U as measured by FLEMING *et al.* (1952). A value of 4·1 per cent was obtained for the efficiency of the counter for detecting ^{231}Th in the particular γ-ray counting channel used.

Determination of the ^{232}Th$(n, 2n)^{231}$Th *cross-section*

A sample of thorium oxide of weight 16·7 mg was irradiated for 5·5 hours in a neutron flux of $3{\cdot}5 \times 10^8$ sec^{-1} cm^{-2}. Before irradiation the sample had been stripped of the natural daughters of thorium as described in the last section.

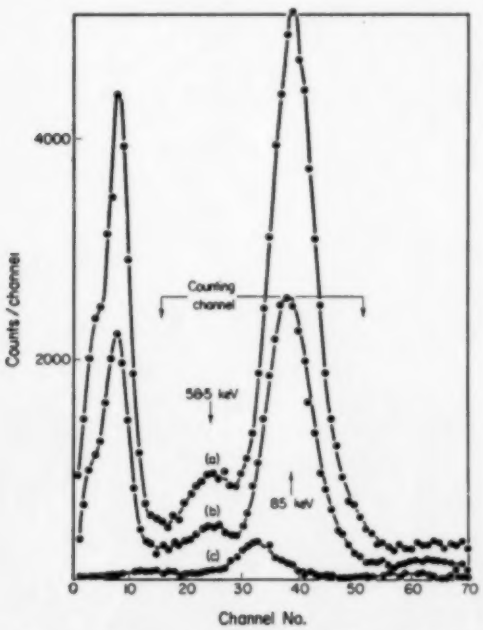

FIG. 1.—The gamma-energy spectrum of a sample of thorium after irradiation with 14 MeV neutrons.
Spectrum observed (a) 0·76 days, (b) 2·01 days and (c) 14·0 days after the end of the irradiation.

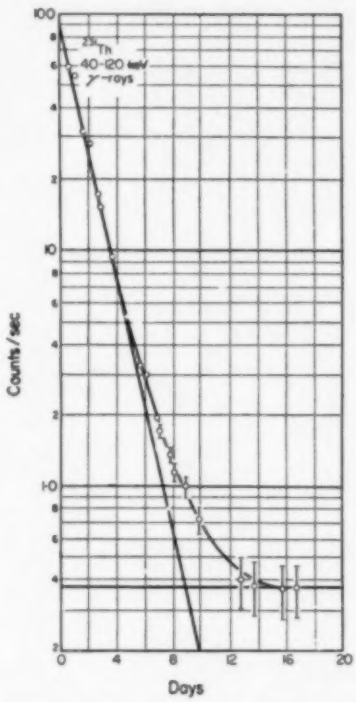

FIG. 2.—Decay of ^{231}Th produced by irradiation of thorium with 14 MeV neutrons.

In Fig. 1, the γ-ray spectrum of the irradiated sample is shown. It was identical with that of the calibration sources of ^{231}Th. The residual spectrum two weeks after the irradiation is due mainly to the growth of the natural activity arising from thorium. In Fig. 2, the decay of the γ-ray activity in the region 40–120 keV is plotted. The relatively small natural growth of activity of thorium has been subtracted. The very small residual activity is due presumably to long-lived fission products. Subtracting this activity gives a straight logarithmic plot. The half-life for this decay was found to be 26 hours and confirms the identification of the activity as being due to that of ^{231}Th.

The cross-section for the $(n, 2n)$ reaction was calculated from the usual formula $\sigma = C/Nn$ where C is the activity observed corrected for the efficiency of the counter, the chemical yield, and the finite time of irradiation; n is the mean neutron flux through the target material and N is the number of target nuclei. The result is,

$$\sigma(n, 2n) = 1{\cdot}20 \pm 0{\cdot}05 \text{ barns.}$$

The various errors which go to make up the estimated error are those involved in the estimation of the

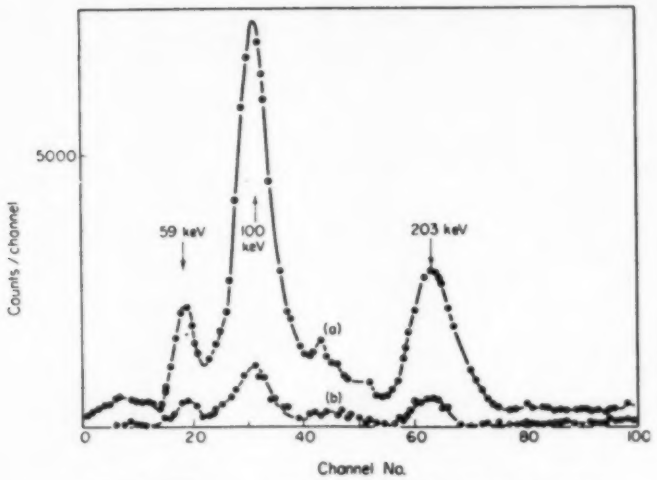

FIG. 3.—The gamma-energy spectrum of a sample of uranium after irradiation with 14·5 MeV neutrons. Spectrum observed (a) 7 days and (b) 27 days after the end of the irradiation.

neutron flux, the weight of thorium, the counting statistics and the efficiency of the counter. These amount to 3 per cent, 1 per cent, 1 per cent, and 3 per cent, respectively.

The cross-section found refers to neutrons in the energy range 13·8 to 14·4 MeV. The uncertainty in neutron energy is due to the variation of the neutron energy with angle of emission from the D-T reaction and the proximity of the irradiated thorium sample to the neutron source.

EXPERIMENTAL DETAILS OF THE $^{238}U(n, 2n)^{237}U$ CROSS-SECTION MEASUREMENT

Detection of the ^{237}U activity produced

Some 275 mg of uranium oxide was irradiated for 3 hours in a neutron flux of $2{\cdot}16 \times 10^8$ sec^{-1} cm^{-2}. After irradiation the sample was placed close to a sodium iodide scintillation spectrometer similar to that used for the thorium $(n, 2n)$ cross-section determination. No chemical separation of fission products was attempted as this was found to be unnecessary.

Two γ-ray spectra taken at different times after the end of the irradiation are shown in Fig. 3. The spectrum obtained from an identical sample of unirradiated uranium oxide has been subtracted in each case. The observed spectra are the same as that of the calibrated source of ^{237}U described in the next section. The three peaks observed are the 59 keV and 203 keV γ-rays of ^{237}Np from the decay of ^{237}U and the 100 keV X-ray from the internal conversion of the 203 keV γ-ray.

The decay of the numbers of counts in each peak over a period of about one month were measured and are shown in Fig. 4. The statistical accuracy of the

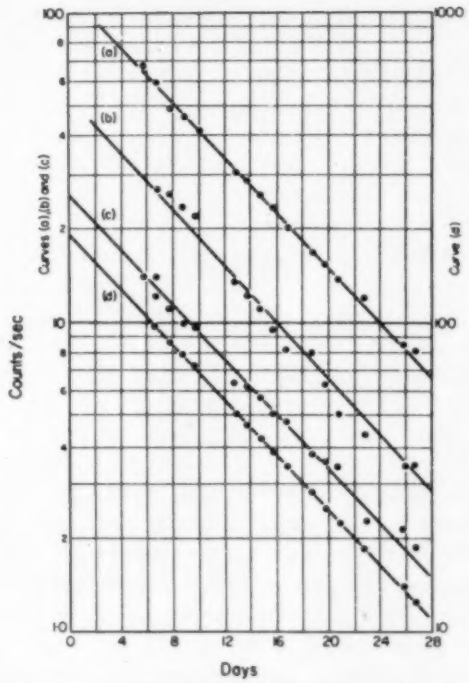

FIG. 4.—Decay of ^{237}U produced by irradiation of uranium with 14·5 MeV neutrons. Decay of the 100 keV peak (a), 203 keV peak (b), 59 keV peak (c), and sum total of these peaks (d).

data for the 100 keV peak and for the sum of all three peaks was sufficiently good to fix the half-life for the decay as $6{\cdot}75 \pm 0{\cdot}1$ days, which agrees with the value found by POOLE (1954) for ^{237}U. The decay curves show no evidence of significant amounts of fission product γ-ray activity in this energy region.

Calibration of the spectrometer and the thick source correction

A stock solution of ^{237}U was prepared from the α-decay of ^{241}Pu. This solution was standardized by evaporating a known aliquot on a 20 μg cm^{-2} plastic film and counting in a 4π proportional counter. The overall efficiency of the counter was estimated to be 98 ± 2 per cent from other work (PATE and YAFFE, 1955) with a similar counter and very thin β-particle sources of comparable energy to the β-particles and conversion electrons emitted from ^{237}U (WAGNER *et al.*, 1953).

Another known aliquot from the stock solution of ^{237}U was evaporated on a thick backing covering an area the same as the irradiated uranium oxide. It was then counted using the same three channels selected for the irradiated uranium oxide. Measurements were made at distances from the sodium iodide crystal

VOL 14 196

TABLE 1

Gamma ray peak energy (keV)	59	100	203
Observed ^{237}U activity extrapolated back to the end of the irradiation (c/s)	26	116	54
The thick source attenuation correction factor, A, for 275 mg (103 mg cm^{-2}) of U_3O_8	1·43	1·16	1·08
Efficiency of the counter E, using the standard source of ^{237}U. Counts per ^{237}U disintegration	0·0345	0·130	0·0505
$\frac{\textit{Observed activity} \times A}{E}$	1080	1035	1155

corresponding to the two surfaces of the thick irradiated uranium oxide source when in position for counting. The difference between these counting rates amounted to about 10 per cent and a mean value was taken to compare with that of the irradiated sample.

Apart from this geometrical correction for the thickness of the irradiated sample, a correction was also required for the attenuation of the various γ-rays in the uranium oxide. To estimate this the counting rate of the ^{237}U source was measured with various thicknesses of uranium oxide between it and the sodium iodide crystal. The natural counting rate of the uranium oxide was subtracted from the combined spectrum in each measurement. The conditions for the back scattering of γ-rays were arranged to be the same throughout the measurements. The logarithm of the attenuation of the 59 and 203 keV γ-rays and of the attenuation of the 100 keV X-ray was found to depend linearly on the thickness of uranium oxide. The observed thick target activity can therefore be taken as $\frac{I}{\lambda x}(1 - e^{-\lambda x}) = \frac{I}{A}$ (say) where I is half the total activity of the source, x its thickness and λ its absorption coefficient for γ-rays of a particular energy.

The results obtained are shown in Table 1. It can be seen that the calculated absolute ^{237}U activity of the irradiated sample is independent (to within ± 5 per cent) of the particular γ-ray measured. This confirms the validity of the attenuation corrections made.

Result for the $^{238}U(n, 2n)^{237}U$ cross-section

The following result for neutrons of 14·5 $\pm$ 0·4 MeV was obtained

$$\sigma(n, 2n) = 0{\cdot}69 \pm 0{\cdot}04 \text{ barns.}$$

The various errors which go to make up the estimated error are those involved in the measurement of the neutron flux, the thick source correction, the weight of uranium, and the 4π calibration of the standard ^{237}U source. These amounted to 5 per cent, 2 per cent, 1 per cent and 2 per cent, respectively.

EXPERIMENTAL DETAILS OF THE $^{237}Np(n, 2n)^{236}Np$ CROSS-SECTION MEASUREMENT

Preliminary purification of neptunium

The neptunium dioxide available for these experiments contained about 0·05 per cent ^{239}Pu by weight and it was necessary (see following section) to reduce this contamination to a very low level before irradiating with neutrons. A separation scheme was devised based on an anion exchange separation of Pu^{3+} and Np^{4+} chloride complexes.

Neptunium dioxide was dissolved in 16-M nitric acid and sodium bromate. The solution was reduced to a small bulk, diluted to 1 to 2-M nitric acid and excess hydrazine nitrate added. The solution was boiled and then allowed to stand overnight. The hydrazine reduced plutonium to the trivalent state and neptunium to the pentavalent and quadravalent states. The solution was made ammoniacal with gaseous ammonia and the precipitated neptunium and plutonium spun off. After washing with a little dilute ammonia the precipitate was dissolved in 11-M hydrochloric acid containing 5 per cent hydriodic acid. This solution was passed through an ion exchange column (10 cm long, 0·4 cm diameter) containing Amberlite XE 199. The column was washed with 20 ml of the hydrochloric-hydriodic acid mixture and then with 5 ml of concentrated hydrochloric acid. The neptunium was then washed off the column with 4-M hydrochloric acid. The solution was evaporated to dryness, the residue taken up in concentrated nitric acid and again evaporated to dryness. The nitric acid treatment was repeated three times. Finally the residue was dissolved in 6-M nitric acid and transferred to a platinum crucible containing sufficient cellulose powder to absorb the solution. The powder was carefully dried and then

ignited at 800°C to leave finally divided neptunium dioxide.

Separation and purification of plutonium from irradiated neptunium

Some 72 mg of purified neptunium dioxide was irradiated for 4 hours in a neutron flux of $2{\cdot}57 \times 10^9$ sec^{-1} cm^{-2} and set aside for one week to allow the ^{236}Np to decay to ^{236}Pu. This plutonium was then chemically separated and its α-particle activity measured.

As the separation and purification scheme were not quantitative it was necessary to add a known quantity of plutonium tracer which could then be redetermined at the end of the scheme and so correct the final activity observed for the portion lost.

The only plutonium isotope available was ^{239}Pu and it was necessary, therefore, to take into account the effect of the traces of ^{239}Pu remaining in the neptunium on the chemical yield determination. This was done by dividing the irradiated neptunium sample into two fractions. To the larger of these fractions was added a known amount of ^{239}Pu tracer. Plutonium was then separated from both fractions using the methods described later.

The α-particle energy spectra from these two fractions were analysed using a gridded ionization chamber to find the ratio of ^{239}Pu to ^{236}Pu present. The ratio was smaller of course for the fraction without added ^{239}Pu tracer. In order to obtain the chemical yield of the fraction with added tracer the ^{239}Pu activity observed was corrected for contamination using the $^{239}Pu/^{236}Pu$ ratio measured for the fraction without added tracer. In the present experiment the ^{239}Pu contamination represented only 20·5 per cent of the added ^{239}Pu tracer after separation.

Details of the separation

The irradiated neptunium was dissolved and the hydroxides of neptunium and plutonium were separated as previously described. The precipitate was dissolved in 16-M nitric acid and evaporated to dryness. The residue was taken up in 11-M hydrochloric acid and transferred to an ion exchange column (10 cm × 0·4 cm diam.) containing Amberlite XE 119. The solution was forced through the column at a rate of about 6 drops/minute and then washed with 5 ml of 11-M hydrochloric acid. The plutonium was eluted by washing with 20 ml of 11-M hydrochloric acid containing 5 per cent hydriodic acid. After the first 5 ml had passed through the column the solution was allowed to drip through under gravity for one hour giving time for the hydriodic acid to reduce the plutonium to the trivalent state. The remaining 15 ml were passed through more quickly (10 drops/minute).

The effluent containing plutonium was evaporated to dryness and then evaporated twice more with 11-M hydrochloric acid and finally twice with 16-M nitric acid. The residue was dissolved in 6-M hydrochloric acid, 0·5 mg of neodymium carrier added, and the hydroxides precipitated with gaseous ammonia. The hydroxides were dissolved in 0·3 ml of 11-M hydrochloric acid and transferred to an Amberlite XE 119 column (5 cm long × 0·2 cm diam). The column was washed with 3 ml of 11-M hydrochloric acid and the effluent rejected. Plutonium was then eluted by 5 ml of 11-M hydrochloric acid–1 per cent hydriodic acid. The effluent was evaporated to dryness twice with 11-M hydrochloric acid and then with 16-M nitric acid. The residue was taken up in 2 drops of 16-M nitric acid diluted with 8 drops of 10-M ammonium nitrate and extracted with 2 × 0·5 ml of hexone. The hexone solution was washed with the ammonium nitrate-nitric acid mixture and then evaporated on to a stainless steel disk for α-counting. The chemical yield was 24·6 ± 0·25 per cent.

Alpha particle assay of the separated plutonium

An α-particle pulse analysis spectrum of the separated plutonium fraction is shown in Fig. 5. Three peaks

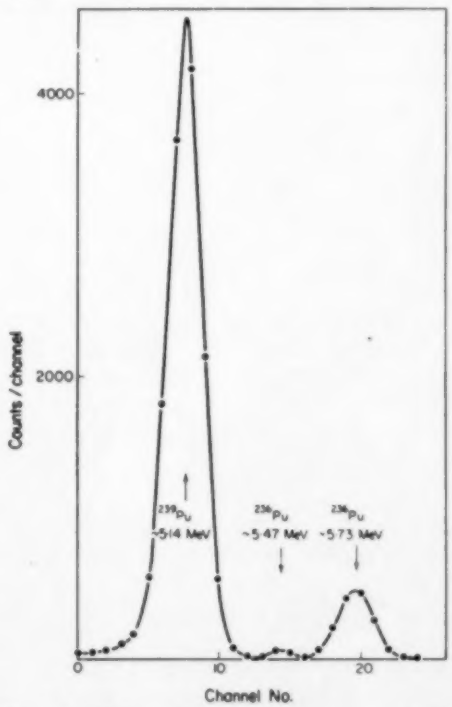

FIG. 5.—Alpha-particle energy spectrum of plutonium separated from neptunium after irradiation with 14·5 MeV neutrons.

due to ^{239}Pu, ^{238}Pu and ^{236}Pu are well resolved. The ^{238}Pu present is associated with the ^{239}Pu contamination in the original sample. The ^{239}Pu peak is due mainly to the ^{239}Pu added for chemical yield measurements as discussed previously. The counting rate of the ^{236}Pu produced was found to be $1{\cdot}150 \pm 0{\cdot}029$ per second.

The counting efficiency of the gridded ionization chamber was found to be 50 per cent using ^{239}Pu sources made from a stock solution which had been standardized with a 4π proportional counter.

Result for the ^{237}Np$(n, 2n)^{236}$Np *cross-section*

The result obtained for neutrons of $14{\cdot}5 \pm 0{\cdot}4$ MeV is

$$\sigma(n, 2n) = 0{\cdot}39 \pm 0{\cdot}06 \text{ barns.}$$

In computing this cross-section from the experimental data it was assumed that the half-life of ^{236}Pu was $2{\cdot}7 \pm 0{\cdot}3$ yr (JAMES *et al.*, 1949) and that the β-particle/electron capture branching ratio of ^{236}Np decay to ^{236}Pu and to ^{236}U is $0{\cdot}96 \pm 0{\cdot}16$ (GINDLER, 1959). The errors quoted for the half-life and branching ratio are included in that of the cross-section result.

It should be noted that the observed cross-section does not include that part of the $(n, 2n)$ reaction which leads to the long lived (5000 yr) isomer of ^{236}Np reported by STUDIER *et al.* (1955) and GINDLER *et al.* (1958). This part must however be small for the following reason.

The total inelastic neutron cross-section of ^{237}Np for neutrons of 14·5 MeV, inferred from the measured values for other heavy nuclides (MCGREGOR, BALL and BOOTH, 1957) is $2{\cdot}9 \pm 0{\cdot}1$ barns. This cross-section is composed of the (n, n'), $(n, 2n)$ $(n, 3n)$ and fission cross-sections. The fission cross-section is $2{\cdot}5 \pm 0{\cdot}07$ barns (MOAT, 1960). The total $(n, 2n)$ cross-section must therefore be $\leqslant 0{\cdot}4 \pm 0{\cdot}15$ barn.

It also follows that the sum of the (n, n') and $(n, 3n)$ cross-sections is $\leqslant 0{\cdot}2$ barn. From the summary by COON (1958) of inelastic neutron scattering experiments with heavy elements it can be deduced that the (n, n') cross-section should be about this value. It is not possible to predict a value for the $(n, 3n)$ cross-section because of the absence of experimentally determined excitation functions for this type of reaction. It will however be relatively small because the threshold for this reaction, calculated from the mass tables of CAMERON (1957), is high (12·4 MeV).

Acknowledgment—We would like to thank DR. J. W. WEALE for supplying sources of ^{237}U and ^{241}Am.

REFERENCES

ANTROPOV G. P., ZISIN IU. A., KOVRIZHNIKH A. A. and LBOV A. A. (1958) *Atomnaya Energiya* **5**, 456.

BAME S. J. and PERRY J. E. (1957) *Phys. Rev.* **107**, 1616.

BELING J. K., NEWTON O. J. and ROSE B. (1952) *Phys. Rev.* **86**, 797.

BELL P. R., DAVIS R. C., FRANCIS J. E. and CASSIDY M. (1952) Oak Ridge National Lab. Report ORNL-1164, p. 3, U.S. Atomic Energy Commission.

CAMERON A. G. W. (1957) *A Revised Semi-Empirical Atomic Mass Formula.* Atomic Energy of Canada Ltd. Report CRP-690.

COON J. H. (1958) *Proceedings of the Second International Conference on the Peaceful Uses of Atomic Energy, Geneva,* Paper A/Conf 15/P/666, p. 5. United Nations, N.Y.

FLEMING E. H. JR., GHIORSO A. and CUNNINGHAM B. B. (1952) *Phys. Rev.* **88**, 642.

FREEDMAN M. S., JAFFEY A. H., WAGNER F. JR. and MAY J. (1953) *Phys. Rev.* **89**, 302.

GHIORSO A. (1951) *Phys. Rev.* **82**, 979.

GINDLER J. E., HUIZENGA J. R. and ENGELKEMEIR D. W. (1958) *Phys. Rev.* **109**, 1263.

GINDLER J. E. and SJOBLOM R. K. (1959) *J. Inorg. Nucl. Chem.* **12**, 8.

GRAVES E. R. (1951) *The Reactor Handbook*, Vol. 1, AECD 3645. U.S. Atomic Energy Commission.

JAFFEY A. H., LERNER J. and WARSHAW S. (1951) *Phys. Rev.* **82**, 498.

JAMES R. A., FLORIN A. E., HOPKINS H. H. JR. and GHIORSO A. (1949) *Products of Helium–Ion and Deuteron Bombardment of* ^{235}U *and* ^{238}U. National Nuclear Energy Series **14B**, 1604. McGraw-Hill.

JOHANSSON S. A. E. (1956) *Ark. Fys.* **10**, 97.

KNIGHT J. D., SMITH R. K. and WARREN B. (1956) *Phys. Rev.* **112**, 259.

MCGREGOR M., BALL W. P. and BOOTH R. (1957) *Phys. Rev.* **108**, 726.

MOAT A. (1961) To be published.

PATE P. D. and YAFFE L. (1955) *Canad. J. Chem.* **33**, 15, 610, 929, 1626; *ibid.* **34**, 265.

PHILLIPS J. A. (1956) Private communication.

POOLE M. J. (1954) Private communication.

STUDIER M. H., GRINDLER J. E. and STEVENS C. M. (1955) *Phys. Rev.* **97**, 88.

TEWES H. A., CARETTO, A. A. and MILLER A. E. (1959) *Buli. Amer. Phys. Soc.* II, **4**, (8) 445; Private communication.

WAGNER F. JR., FREEDMAN M. S., ENGELKEMEIR D. W. and HUIZENGA J. R. (1953) *Phys. Rev.* **89**, 502.

Reactor Science and Technology (Journal of Nuclear Energy, Parts A and B), 1961, Vol. 14, pp. 76 to 84. Pergamon Press Ltd. Printed in Northern Ireland

MEASUREMENTS OF THE ENERGY DEPENDENCE OF THE CROSS-SECTION OF THE Cl(n,γ) REACTION

N. T. KASHUKEEV, YU. P. POPOV and F. L. SHAPIRO
Lebedev Physical Institute of the Academy of Sciences of the U.S.S.R., Moscow

(*Received* 15 *June* 1960)

Abstract—The energy dependence of the cross-section for the reaction (n,γ) in natural chlorine in the energy range from several eV to ~20 keV was measured with the aid of a slowing-down-time neutron spectrometer employing lead. For the energy of the negative level of chlorine the value $E_0 = -210 \pm 10$ eV was obtained. The parameters of the 405 eV level were determined $\sigma_0\Gamma_\gamma = 90 \pm 8$ BeV, $g\Gamma_n = (2{\cdot}4 \div 4{\cdot}0) \times 10^{-3}$ eV depending on the assumed compound nucleus spin. A resonance was noted in the measurements at $E_0 = 4{\cdot}3 \pm 0{\cdot}5$ keV with the strength $\sigma_0\Gamma_\gamma = 60 \pm 20$ BeV.

1. INTRODUCTION

THE interaction of slow neutrons with chlorine has been studied by various authors (HIBDON and MUELHAUSE, 1950; TOLLER *et al.*, 1955; BRUGGER *et al.*, 1957); however, they measured only the total cross-sections. In HIBDON and MUELHAUSE (1950) total cross-sections were obtained for three values of neutron energy (120, 345 and 2700 eV). The results of the measurements together with the known capture and scattering cross-sections of thermal neutrons are well described by the Breit-Wigner formula for a single level with resonance energy $E_0 = -75$ eV. This negative resonance was attributed to isotope ^{35}Cl, since in the first place the capture cross-section for thermal neutrons of ^{35}Cl is two orders of magnitude greater than the capture cross-section of ^{37}Cl. And in the second place near the binding energy of the neutron the density of the nuclear levels of ^{36}Cl (binding energy 8·6 MeV (ENDT and BRAAMS, 1957)) should be considerably greater than the density of the nuclear levels of ^{38}Cl (binding energy 6·1 MeV (ENDT and BRAAMS, 1957)). In TOLLER *et al.* (1955) total neutron cross-sections of ^{35}Cl and ^{37}Cl were measured in the energy range from 2 to 200 keV. In the region $E < 20$ keV a resonance was noted in ^{37}Cl with an energy $E_0 = 8{\cdot}8$ keV and the width $\Gamma = 0{\cdot}09$ keV. In BRUGGER *et al.* (1957) comprising the energy range 0·03 eV to 15 keV the existence of a resonance at 8·8 keV and a negative resonance for ^{35}Cl was corroborated, for the latter the value $E_0 = -140$ eV was obtained. In addition a very narrow resonance at $E_0 = 405$ eV was seen which was stronger in the sample enriched with the isotope ^{35}Cl. For the parameters of the 405 eV resonance the estimates given are $\Gamma < 0{\cdot}6$ eV, $\sigma_0 > 580$ barns.

The measurements of the energy dependence of neutron capture cross-sections are obviously of interest in defining more precisely the parameters of resonance levels of chlorine. In effect, in the region affected by the negative level, the total cross-section is defined by 5 parameters (E_0, Γ_γ, Γ_n, σ_{pot} and radius of the channel R (BLATT and WEISKOPF, 1954)) whereas the capture cross-sections depends only on three parameters (E_0, Γ_γ and Γ_n) which makes the analysis much easier. Weak resonances are easily noticeable in the measurements of the capture cross-sections insofar as the source of the background i.e. potential scattering, which is unavoidable in the measurements of total cross-sections, is absent in this case.

In the present paper the measurements of the energy dependence of the cross-section for neutron capture by chlorine in the energy range 10 eV to 20 keV are given which were carried out with a slowing-down-time neutron spectrometer employing lead (LAZAREVA *et al.*, 1955; BERGMAN *et al.*, 1955, 1957a and 1957b). Preliminary results of this work were given elsewhere (BERGMAN *et al.*, 1957b).

2. METHOD OF MEASURING

The principle of the slowing-down-time neutron spectrometer can be briefly described as follows. In the centre of a large lead cube, 0·5–1 microsecond pulses of fast neutrons are generated 625 times per second. At time t after the pulse the neutrons are slowed down to a mean energy determined by the following equation (BERGMAN *et al.*, 1957a):

$$E = \frac{183}{(t + 0{\cdot}3)^2}\ \text{keV} \qquad (1)$$

where t is the slowing down time in microseconds. Mean square scattering of neutron energies around the mean value is ~15 per cent at $E < 1$ keV and ~35 per cent at $E = 10$ keV (BERGMAN *et al.*, 1957a).

In measuring the energy dependence of the capture cross-section a γ-ray detector and the sample studied

were placed inside the cube. The intensity of capture γ-rays from the sample $J_\gamma(t)$ is determined as a function of slowing-down-time. $J_\gamma(t)$ is obtained by subtracting from the measurements the background, measured without the sample, and introducing a small correction which takes into account the effect of the neutrons from preceding pulses. At the same point of the cube with the aid of a detector with an efficiency proportional to $1/v$ (a proportional counter with a thin layer of ^{6}LiF), the neutron density is measured:

$$J_{\mathrm{Li}}(t) \sim \int n(E, t)\, dE, \tag{2}$$

where $n(E, t)\, dE$ is the density of the neutrons with an energy range E, $E + dE$, at the moment of time t.

In the case of a thin sample

$$J_\gamma(t) \sim \int n(E, t) v\sigma_\gamma(E)\, dE, \tag{3}$$

where v is the velocity of the neutron, σ_γ (E) is the capture cross-section. Let us designate $Q(E, t) \equiv n(E, t) \int n(E, t)_{dE}\, n(E, t)\, dE = \varphi(E, t)$ normalized for unit neutron spectrum at a given point of the cube.

It can be shown that

$$\int_0^\infty \varphi(E, t)\, dt = \frac{1}{\xi \Sigma_s v E} \tag{4}$$

where $\xi \simeq \frac{2}{M}$, M is the mass number of lead, Σ_s is the macroscopic cross-section of the scattering of lead.

In order to prove this we will substitute the integral (4) with the sum

$$\int_0^\infty \varphi(E, t)\, dt = \Delta t \sum_{i=0}^{\infty} \varphi(E, t_i), \qquad (t_i = \Delta t \,.\, i). \tag{4a}$$

The sum $\sum_{i=0}^{\infty} \varphi(E, t_i)$ may be considered as neutron density at energy E, generated by a continuous source emitting $1/\Delta t$ neutrons per sec. Thus when $E \gg kT$ (T is the absolute temperature of lead) it is the Fermi spectrum (see for example AKHIEZER and POMERANCHUK (1950)) and (4a) transforms into (4). In reasoning thus, we disregarded the effect of neutron diffusion on the rate of slowing down. This is permissible owing to the fact that, for example, the measured dependence (1) of average neutron energy in the cube on the slowing down time coincides very accurately with the one expected for an unlimited medium.

From (2) and (3) we have

$$\frac{J_\gamma}{J_{\mathrm{Li}}}(t) = k \int \varphi(E, t) v\sigma_\gamma(E)\, dE = k \langle v\sigma_\gamma \rangle, \tag{5}$$

where $\langle v\sigma_\gamma \rangle$ is the value $v\sigma_\gamma(E)$ averaged over the neutron spectrum in the cube at the time t, i.e. corresponding to the average neutron energy determined by the expression (1); k is a scaling factor. The area under the curve $\frac{J_\gamma}{J_{\mathrm{Li}}}(t)$ is proportional to the resonance absorption integral R_γ

$$\int_{t_1}^{t_2} \frac{\tau_\gamma}{\tau_{\mathrm{Li}}}(t)\, dt = \frac{k}{\xi \Sigma_s} \int_{E_2}^{E_1} \sigma_\gamma(E) \frac{dE}{E} = \frac{k}{\xi \Sigma_s} R_\gamma. \tag{6}$$

Equation (6) can be easily proved for an isolated narrow ($\Gamma \ll E$) resonance. In this case it may be considered that integration of time extends from 0 to ∞ and (6) is obtained by integration (5) of time with the use of equation (4). In a general case formula (6) is an approximation useful when $E_2 \gg kT$.

In the case of a thick sample the resonance integral R_γ in (6) must be substituted with an effective resonance integral $R_{\gamma\mathrm{eff}}$ which for an isolated resonance is equal to

$$R_{\gamma\mathrm{eff}} = \frac{\overline{A(l)}}{N\bar{l}} \frac{\Gamma_\gamma}{\Gamma E_0}, \tag{7}$$

where

$$A(l) = \int_{\mathrm{res}} (1 - e^{-Nl\sigma(E)})\, dE, \tag{8}$$

$$\overline{A(l)} = \int f(l)\, A(l)\, dl, \tag{9}$$

$f(l)\, dl$ is the probability that the length of the path of a neutron through the material of the sample is within the limits l and $l + dl$, $\bar{l} = \int l f(l)\, dl$ is the average length of the path, N is the number of nuclei per cm^3 of the sample.

Expression (7) does not take into account the absorption which takes place after the scattering of the neutrons in the sample and, therefore, can be used when $\Gamma_n \ll \Gamma_\gamma$ or when the energy lost by the neutron during the scattering in the sample is much greater than the width of the absorption band (i.e. $\xi E_0 \gg \Gamma$ for a thin sample and $\xi E_0 \gg \sqrt{(Nl\sigma_0)}\Gamma$ for a thick sample). The taking into account of scattering is discussed in MELKONIAN (1955).

Graphs connecting $A(l)$ and $\sigma_0\Gamma$ are given in HUGHES (1955). It is known that when $Nl\sigma_0 \ll 1$ (σ_0 is the total cross-section at the maximum of the resonance peak) $A(l) \sim l$ and $\overline{A(l)} = A(\bar{l})$; when $Nl\sigma_0 \gg 1$ then $A(l) \sim \sqrt{l}$ and $\overline{A(l)} = A((\overline{\sqrt{l}})^2)$. For the usual configurations of the samples the difference between $\overline{\sqrt{l}}$ and $\sqrt{\bar{l}}$ is small ($\sqrt{\bar{l}}/\overline{\sqrt{l}} = 1{\cdot}06$ for the plate and $1{\cdot}02$ for the sphere); therefore, in calculating, $\overline{A(l)}$ was substituted by $A(\bar{l})$. In the case of isotropic irradiation of a sample the average path $\bar{l}$ is obtained by the following simple geometrical equation

$$\bar{l} = \frac{4V}{S} \tag{10}$$

where V is the volume of the sample, S is the area of a closed surface laid out in such a manner that every straight line intersecting the surface passes through the sample and every straight line passing through the sample intersects the surface only twice.*

Using equation (5) in the energy region in which the capture cross-section is known (for example thermal energies) or applying (6) to the resonance with known parameters, one can determine the scaling factor k. After this (5) and (6) can be used in determining the capture cross-sections and resonance integrals.

In using the calibration method described above, it is assumed that the detection efficiency of the capture γ-rays remains constant even when the energy of the captured neutrons varies.

In using a detector with an efficiency proportional to the energy of the γ-quantum, the probability of recording the absorption of a slow neutron is proportional to the binding energy of the neutron. In this case the condition for constant efficiency will be fulfilled for a mono-isotopic substance or for a mixture of isotopes in which the binding energies do not differ to any great extent.

3. MEASUREMENTS

The simplest detector of γ-rays with an efficiency proportional to the energy of a γ-quantum, is a Geiger counter with walls thicker than the range of the secondary electron of maximum energy (BRANDT *et al.*, 1946; FOULER *et al.*, 1948). However, inasmuch as the dead time of such counters is quite long they could not be used in the present work. A proportional counter has satisfactory time characteristics and its efficiency is nearly linear (Fig. 2) (OKOROKOV, 1958); for this reason it was used in these measurements. The counter (glass with an aquadag cathode) was filled with the mixture A (500 mm), He (40 mm) and CO_2 (25 mm); the diameter of the counter was 14 mm, the diameter of the wire was 0·2 mm. To prevent any variation in the efficiency of detection of the γ-ray background from lead in placing the sample on the counter (transition effect), the latter was surrounded by sheet lead (1–3 mm).

In addition to the proportional counter a scintillation counter was used with a fluorite crystal 25 mm in diameter and 10 mm thick. In order to eliminate the transition effect the crystal was covered with a hood made out of bismuth 2 mm thick (Fig. 1). The curve showing the dependence of the efficiency on the energy of γ-quantum differs markedly from the corresponding curve obtained by proportional counters (Fig. 2); the difference increases with the increase of the bias level of the scintillation counter (the curve 1 was taken at the minimum bias level).

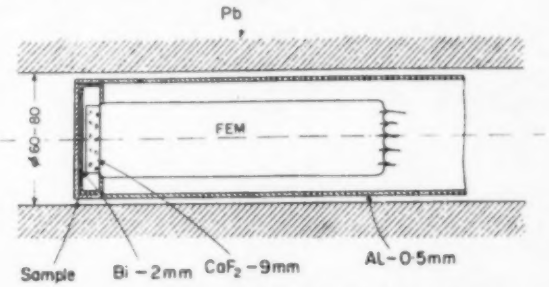

FIG. 1.—The arrangement of the sample and the scintillation detector of γ-rays in the channel of the lead cube.

Fluorite was selected as a scintillator since crystals containing iodine produce a considerable background from the capture of neutrons by iodine, and in large organic scintillators the neutron spectrum is distorted because of the hydrogen content, thereby decreasing the resolution of the spectrometer. In order to increase the sensitivity of the photomultiplier to the ultraviolet radiation of fluorite ($\lambda_{max} \sim 2500$ Å), in the present work we used specially made photomultipliers PhEM–19 with quartz windows.

Due to the fact that during a neutron pulse the counting rate of fast neutrons and γ-rays is so high that it causes counting losses in the channels of the time analyser coming after the neutron pulse, the photomultiplier was cut-off during the neutron pulse. For this purpose simultaneously with the neutron burst the second and sixth dynodes were fed with a square-wave of approximately 50 V. With suitable selection of total voltage, the distribution of voltage on the dynodes of PhEM and the width of the square-wave, the photomultiplier completely recovers its efficiency about 1 or 2 microseconds after the neutron burst (VOLKOV *et al.*, 1960).

In almost all the measurements the counts were recorded simultaneously on a 50-channel time analyser with the channel width 0·476 microseconds in the slowing down range t = 0–20 microseconds and on a 100-channel time analyser with a channel width of 1 microsecond or 5 microseconds for $T \geq 20$ microseconds. The first analyser was designed and

* For samples shaped in the form of a cylinder closed at one end, in which the bottom and the walls are hollow,

$$\bar{l} = \frac{2}{R}\frac{R^3H - r^2h}{R + H}$$

where R and H are respectively the outer radius and the height of the cylinder, and r and h are the radius and height of the inner cavity. For cylindrical samples with hollow walls the formula is strictly speaking not applicable insofar as it does not take into account that the neutrons travelling axially inside the tube do not pass through the sample. However, in the case of the samples used in this work the error is not more than 1 per cent.

VOL
14
196

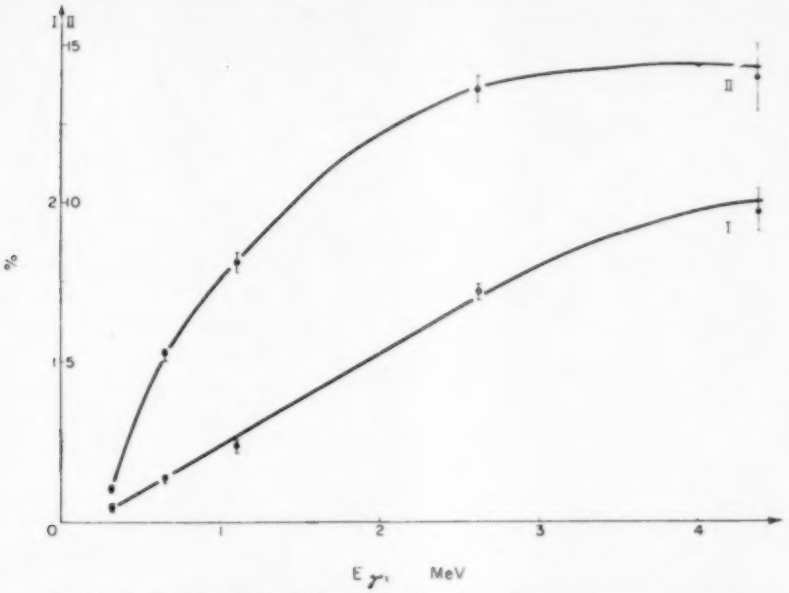

FIG. 2.—Dependence of the efficiency of used up detectors on the energy of gamma rays.
(I) Proportional counter with walls consisting of 1 mm of duralumin and 3 mm of lead.
(II) Scintillation counter with a crystal of fluorite 10 mm thick, diam. 25 mm and a Bi hood (2 mm).

built by I. V. Shtranikh and the second by L. A. Matalin and I. V. Shtranikh.

The samples used in the measurements were either $PlCl_2$ (powder) or CCl_4 (liquid). The dimensions and shape of the containers for the samples were as follows:

(a) with the proportional counter the inner diameter of the duralumin tube having a hollow wall was 40 mm and the length was ~330 mm.

(b) with the scintillation counter the inner diameter of the cup with hollow walls and bottom was 42 mm and the depth was 15 mm.

The outer dimensions of the containers depended on the thickness of the layer of $PbCl_2$ or CCl_4. In the thinnest and thickest samples used the thickness of the layer corresponded to the mean path of the neutron through the sample $l = 0{\cdot}42$ and $l = 3{\cdot}63$ g/cm² of chlorine. The thickness of the duralumin walls of the containers was 0·5 mm.

Similar containers were used for measuring the background; they contained the same quantity of lead or carbon (the same number of nuclei per cm²) as the sample. The effect and the background were measured alternately until sufficient statistics had been obtained. Two proportional α-counters which registered α-particles liberated simultaneously with the neutrons in the reaction $^3H(d, n)^4He$ were used as monitors.

4. RESULTS OF MEASUREMENTS

1. *Capture cross-section.* In Fig. 3 the curve $\frac{J_\gamma}{J_{Li}}(t)$ is given as an example. The solid curve refers to the sample in which $l = 1{\cdot}98$ g/cm² of chlorine, and to the same scale the dotted curve is the background.

With the aid of equations (5) and (1) from this curve we obtained the curve $\sigma_\gamma(E)$. The scaling factor k was determined from the value of the capture cross-section at neutron energy $E = 20$ eV. The latter was calculated from the known capture cross-section of chlorine for thermal neutrons ($\sigma_\gamma = 33{\cdot}6 \pm 1{\cdot}1$) with a slight correction for deviation from the law $1/v$, caused by the negative level $E_0 = -210$ eV (see below). Direct calibration in the thermal region was inconvenient owing to the fact that in this region the samples were rather thick.

The resulting curve $\sigma_\gamma(E)$ obtained by averaging 15 series of measurements with different samples and detectors is given in Fig. 4. The points on the peak $E_0 = 405$ eV were obtained from the measurements of samples ≃0·5 g/cm² Cl thick. The curve shows a resonance peak at $E_0 = 4{\cdot}3 \pm 0{\cdot}5$ keV, which was not observed in previous papers (TOLLER *et al.*, 1955; BRUGGER *et al.*, 1957). On the other hand the peak at $E_0 = 8{\cdot}8$ keV (TOLLER *et al.*, 1955; BRUGGER *et al.*, 1957), was not observed in our measurements; this is not surprising since the resonance at 8·8 keV is caused by a less common isotope, the efficiency of recording γ-rays of ^{38}Cl is less (insofar as in ^{38}Cl the neutron binding energy is smaller) the resolving power of the spectrometer at this energy is several times less than at $E = 4$ keV.

In processing the results of the measurements the absorption of background γ-rays by the sample was

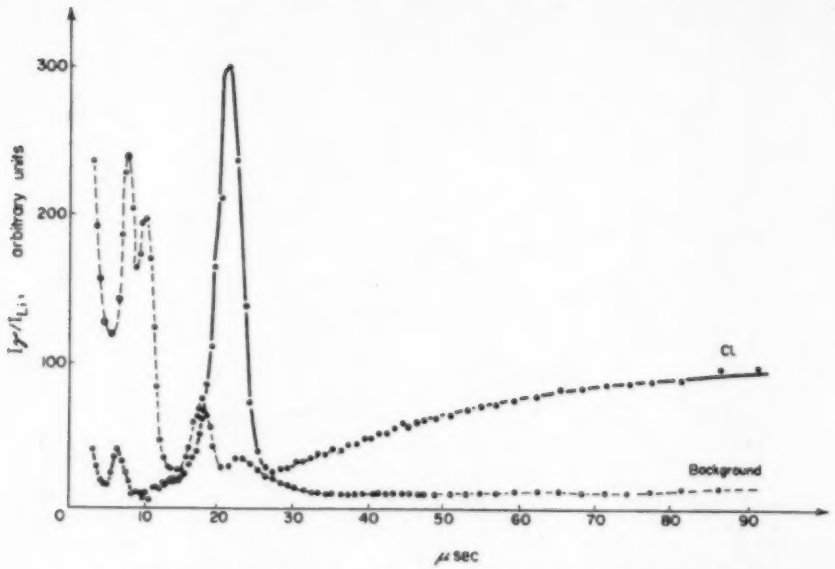

FIG. 3.—Graphs $J_\gamma/J_{Li}(t)$ and J of the background $J_{Li}(t)$ plotted to the same scale.

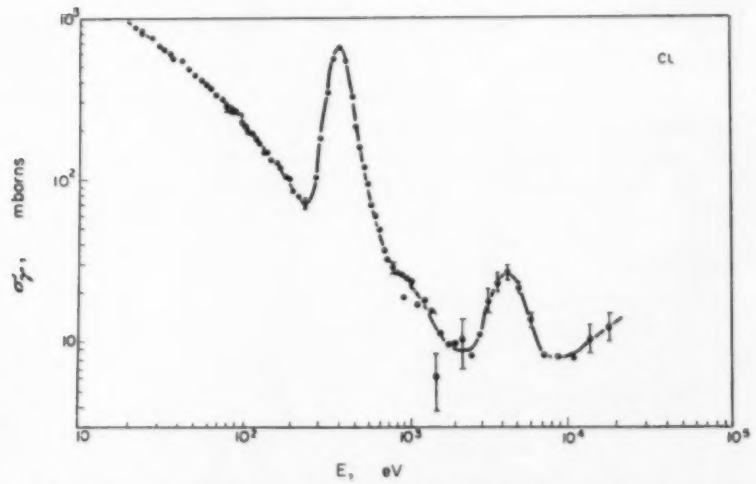

FIG. 4.—Dependence of the neutron capture cross-section in natural chlorine on neutron energy. The curve is normalized to the thermal neutron capture cross-section $\sigma_\gamma = 31{\cdot}6$ barns (HUGHES and HARVEY, 1955). If we take $\sigma_\gamma = 33{\cdot}6$ barns (HUGHES and SCHWARTZ, 1958) the ordinates of the curve must be increased by 6 per cent.

not taken into account. Using a special set-up producing the same spectrum of background gamma rays this effect was estimated experimentally (OKOROKOV, 1958). These measurements showed that even in the region of the worst relationship of the effect to the background, the absorption of background γ-rays will introduce a difference in the final results not exceeding 5 per cent.

In principle a sample with mass number less than the mass number of lead affects the spectrum of the slowing down neutrons. As a result of this the outline of the peaks on the background curve (Fig. 3) changes in the presence of the sample, which might lead to inaccuracies in subtracting the background effect. Control measurements were carried out with a thick sample of sulphur, which in its slowing down properties is close to chlorine, but has no resonances in the region studied. Measurements have shown the absence of an appreciable neutron slowing down effect in the sample.

In Fig. 4 root-mean-square errors are given calculated from scatter of individual measurements. These errors are greater than the statistical errors of measurements especially in the region 1–3 keV and greater than 15 keV, since we have here the worst relationship of the effect to the background (see

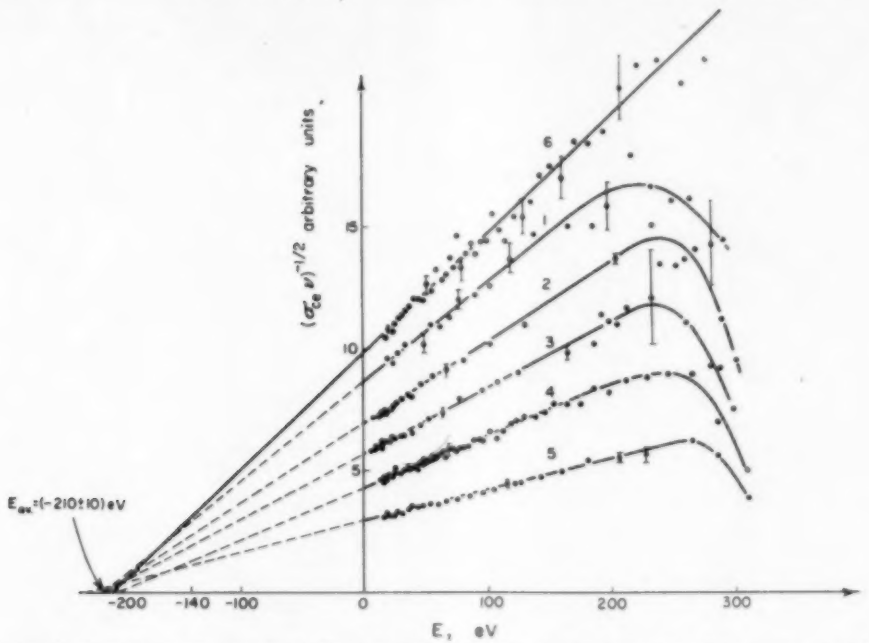

FIG. 5.—Showing the dependence of curves $(\sigma_\gamma v)^{-1/2}$ on neutron energy for the determination of the energy of the negative level. Curves 1–5 taken with a scintillation counter, curve 6 taken with a proportional counter. Samples:
1 and 3: Pb Cl_2 0·63 g/cm²
2 and 5: CCl_4 1·89 g/cm²
4: Pb Cl_2 1·38 g/cm²
6: Pb Cl_2 0·42 g/cm².

Fig. 3). To these one must add the calibration error (±3 per cent) and the error caused by the difference in detecting efficiency of neutron capture of the two isotopes of chlorine. However, extrapolating according to the law $1/v$, the capture cross-section of ^{37}Cl in the studied energy range is 5 to 50 times less than the measured capture cross-section; the contribution of the peak 8·8 keV is several times less than the cross-section measured in that energy range. In view of this the second of these errors is small: it is negligibly small below the 405 eV peak and <10 per cent above this peak.

The measurements gave the values of the resonance integral in the range 0·49 to 2×10^4 eV $R_\gamma = 14{\cdot}0 \pm 0{\cdot}7$ barns. If we take into account that the resonance integral for $E > 2 \times 10^4$ eV in our estimates is of the order of 0·03 then the value $14{\cdot}0 \pm 0{\cdot}7$ barns is in good agreement with the values 12 barns (MACKLIN and POMERANCE, 1955) and $12{\cdot}7 \pm 1{\cdot}7$ barns (KLEMENT'EV and GRYAZEV, 1957), obtained for the total resonance integral in measurements in reactors. The main contribution to the resonance integral is by the negative chlorine level. The contribution of the level $E_0 = 405$ eV is $R_\gamma = \dfrac{\pi\sigma_0\Gamma_\gamma}{2E_0} = 0{\cdot}39 \pm 0{\cdot}04$ and the contribution of the level 4·3 keV is $R_\gamma = (2{\cdot}1 \pm 0{\cdot}7) \times 10^{-2}$ barns. The contribution of separate parts of the spectrum in the resonance integral is distributed as follows: $0{\cdot}49 < E < 250$ eV, $R_\gamma = 13{\cdot}5$ barns; 250 eV $< E < 2$ keV, $R_\gamma = 0{\cdot}4 \pm 10$ per cent and $E < 2$ keV, $R_\gamma = 6 \times 10^{-2}$ barns ± 50 per cent.

2. *The negative level of chlorine.* For a narrow single level ($\Gamma \ll E_0$), from Breit-Wigner's formula it is easy to obtain the following equation

$$(\sigma_\gamma v)^{-1/2} = \text{Const}\,(E - E_0). \qquad (11)$$

Figure 5 shows the graphs $(\sigma_\gamma v)^{-1/2} = f(E)$, which were obtained from our data. For convenience the curves 1 to 6 are plotted on a different scale. When $E > 200$ eV the 405 eV level appears on the curve. When $E < 200$ eV the linear dependence (11) is satisfied with the value $E_0 = -210 \pm 10$ eV. This value differs markedly from the value $E_0 = 140 \pm 5$ eV, obtained in BRUGGER *et al.* (1957) by a more indirect method, namely by fitting a Breit-Wigner curve to the experimental data for the total cross-section*. An attempt was made to fit the Breit-Wigner curve with total cross-section (BRUGGER *et al.*, 1957; HUGHES and SCHWARTZ, 1958) assuming that $E_0 = -210$ eV.

* *Note added in proof:* This difference may be almost removed if one assumes that the capture cross-section contains a $1/v$ component, which is equal to ~10 per cent at thermal energy. This component may be due to either distant levels or direct capture (see LANE and LYNN, 1960). More accurate measurements are needed to fix the point.

TABLE 1.—PARAMETERS OF THE NEGATIVE LEVEL OF ^{36}Cl WHICH BEST DESCRIBE THE COURSE OF TOTAL CROSS-SECTIONS OF CHLORINE

Authors	E_0 (eV)	g	Γ_n^0 (eV)	Γ_γ (eV)	σ_{pot} (barn)	R (Fermi)	Calculated for energy $E = 0.025$ eV	
							σ_γ (barns)	$\sigma_{incoherent}$ (barns)
Present work	Independent measurement -210 ± 10	5/8	1·38 ±0·02	0·50 ±0·01	1·2 ±0·2	1·0 ±0·5	Assumed 33·0	7·7 ± 0·5
BRUGGER *et al.* (1957)	-140 ± 5	5/8	0·72 ±0·05	0·48 ±0·02	1·13 ±0·10	Assumed 4·74	34·5 ± 3·4	7·8 ± 0·7

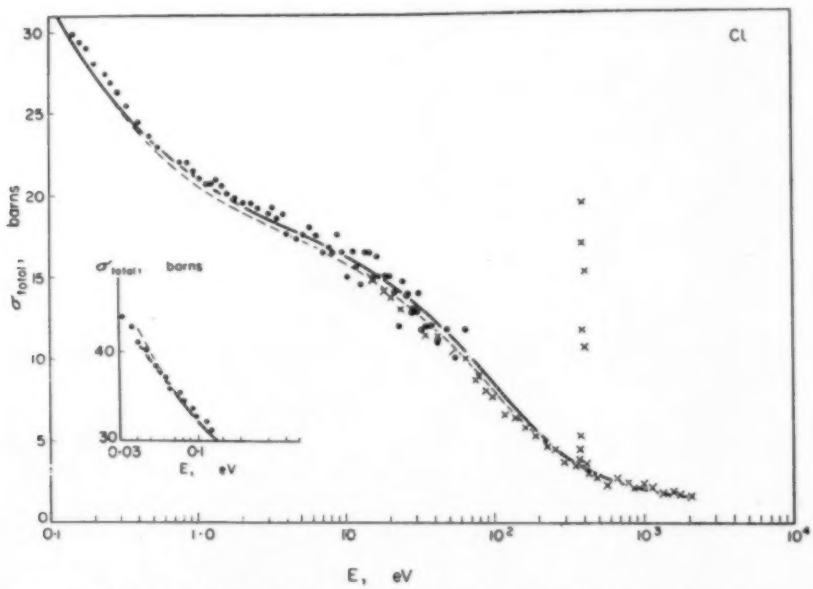

FIG. 6.—Results of fitting of the Breit-Wigner formula with the experimental values of total cross-sections (HUGHES and SCHWARTZ, 1958):
· – points obtained on a crystal spectrometer;
× – points obtained on a fast chopper;
– – – curve plotted from parameters of the level from BRUGGER *et al.* (1957);
—— curve plotted from parameters of the level from the present work.

A set of parameters of the negative level, giving the best fit is given in Table 1. It is assumed that the statistical weight g equals 5/8; when $g = 3/8$ we were unable to obtain a better fit; however, the cross-section of incoherent scattering is much greater than if $g = 5/8$ which in turn is greater than the experimental value $\sigma_{incoherent} = (3{\cdot}9 \pm 3{\cdot}1)$ barns (HUGHES and SCHWARTZ 1958).

A curve plotted for the set of parameters mentioned above, is in somewhat better agreement with the experimental data in the region of small energies than the curve given in BRUGGER *et al.* (1957), but it is definitely higher in the region of 100 eV (Fig. 6). The radius of interference R and the cross-section of potential scattering σ_{pot} were much smaller than the radius of the chlorine nucleus ($R_0 = r_0 A^{1/3} = 4{\cdot}74 \times 10^{-13}$ cm) and the value $4\pi R_0^2 = 2{\cdot}83$ barns respectively. The difference is probably due to the influence of other S-levels besides the $E_0 = -210$ eV level. However, owing to the fact that the fit of the curve in Fig. 6 with the experimental points is not very good, a more detailed discussion of this problem seems to be premature, especially since the experimental data (BRUGGER *et al.*, 1957) which were used, are not entirely satisfactory. Namely, the points obtained on a crystal spectrometer and on the time of flight

spectrometer do not coincide in the overlapping region (15 ÷ 75 eV); in the region higher than 6 keV the values of the total cross-sections given in BRUGGER *et al.* (1957) are somewhat less than those given in TOLLER *et al.* (1955).

3. *Parameters of the* 405 eV *and* 4·3 keV *levels.* The parameters of the 405 eV level were determined from the areas under the curves $\frac{J_\gamma}{J_{Li}}(t)$ for samples of different thickness. From these areas one must subtract the 'base' caused by the $E_0 = -210$ eV level, which is ~10 per cent of the entire area. The 'base' was calculated theoretically on the basis of the parameters of the negative level which are indicated above. The 'base' of the peak determined graphically, was always somewhat greater. This might have been due to the effect of other unknown levels (a level is probably present with $E_0 \simeq 1{\cdot}1$ keV (POPOV and SHAPIRO)). Therefore, from the area of the peak, we substracted the half sum of the areas of the bases determined by calculation and graphically, and their half-difference was added to the experimental error. The resulting area was used in determining the value $A(\bar{l})\frac{\Gamma_\gamma}{\Gamma}$ according to formulas (6) and (7).

The results of measurements of the area under the capture curve for the peak at 405 eV by means of proportional counters and a scintillation counter at different bias level (up to 3 MeV of gamma-ray energy) coincided, in spite of the fact that the curves showing the dependence of ε on E are markedly different. This indicates that the spectra of the capture-gamma rays for the level, responsible for the thermal cross-section and the $E_0 = 405$ eV level are not very different. Similar measurements were not carried out at higher energies owing to limited statistics.

Defining the values Γ_γ and Γ_n, we find the values of $A(\bar{l})$ and with the aid of graphs $A/\Delta = f(Nl\sigma_0\Gamma/\Delta)$ given in HUGHES (1955), we determine $\sigma_0\Gamma$ (Δ is the Doppler width). The curve $\sigma_0\Gamma = f(\Gamma_n)$ was plotted for the given value Γ_γ; the point of intersection of this curve with the theoretical straight line

$$\sigma_0\Gamma = 4\pi p\lambda_0^2 g\Gamma_n \qquad (12)$$

(p is the isotopic content) gives the value $\sigma_0\Gamma$ for the given values of g and Γ_γ and for the given thickness of the sample.* The intersection point of the curves $\sigma_0\Gamma = f(\Gamma_\gamma)$ of two samples of different thickness gives the values $\sigma_0\Gamma$ and Γ_γ. Inasmuch as none of the five samples used were of sufficient thickness such procedure made it possible only to reach the conclusion that within the errors of the measurements the radiation width of the level is in the range of 0·15 eV $< \Gamma_\gamma <$ 0·6 eV. The values of $\sigma_0\Gamma$ and Γ_n proved to be only slightly dependent on Γ_γ, insofar as $\Gamma_n \ll \Gamma_\gamma$ and that in the case of a thin sample the experiment gives directly the value of $\sigma_0\Gamma_\gamma$ (equation (6)). Assuming the same radiation width as in the case of the negative level ($\Gamma_\gamma = 0{\cdot}5$ eV) we obtain the following possible sets of parameters for the 405 eV level (Table 2). Owing to the small neutron width of the

TABLE 2.—PARAMETERS OF THE RESONANCE OF ^{35}Cl AT $E_0 = 405$ eV
(Assumed $\Gamma_\gamma = 0{\cdot}5$ eV; $\Gamma_p = 70 \times 10^{-3}$ eV
POPOV and SHAPIRO)

g	$\Gamma_n \times 10^3$ (eV)	$\Gamma_n^0 \times 10^3$ (eV)	$\sigma_0\Gamma$ BeV	σ_0 (barns)
1/8	32 ± 5	16 ± 2	190 ± 30	208 ± 30
3/8	6·8 ± 0·5	3·4 ± 0·2	122 ± 15	182 ± 20
5/8	3·8 ± 0·3	1·9 ± 0·1	115 ± 10	180 ± 15
7/8	2·7 ± 0·2	1·4 ± 0·1	113 ± 10	178 ± 15

level it might be a P-level with the possible values of the statistics factor $g = \frac{1}{8}, \frac{3}{8}, \frac{5}{8}$ and $\frac{7}{8}$. The value of $\sigma_0 \simeq$ 180 barns is not in agreement with the estimate $\sigma_0 > 580$ obtained in BRUGGER *et al.* (1957). The reason for this difference is not clear; it diminishes if the radiation width of the 405 eV level is considerably less than the radiation width of the −210 eV level and is close to the lowest possible value of 0·15 eV.

In the case of the previously unknown $E_0 = 4{\cdot}3 \pm$ 0·5 keV level, owing to the unsatisfactory relationship of the effect and background the statistics obtained were obviously inadequate for the analysis of this level by means of samples of different thickness. Therefore, calculations similar to those for the 405 eV level, were made for a curve averaged over all the samples. Table 3 gives the values of $\sigma_{para}\Gamma_\gamma$ for the 4·3 keV resonance

TABLE 3.—PARAMETERS OF THE RESONANCE ^{35}Cl
AT $E_0 = 4{\cdot}3 \pm 0{\cdot}5$ keV
(Assumed $\Gamma_\gamma = 0{\cdot}5$ eV; $\Gamma_p = 35 \times 10^{-3}$ eV,
POPOV and SHAPIRO)

g	$\Gamma_n \times 10^3$ (eV)	$\Gamma_n^0 \times 10^3$ (eV)	$\sigma_0\Gamma$ (eV)	σ_0 (barns)
3/8	>70	>11	>136	~100
5/8	41 ± 15	6·3	118 ± 30	123 ± 30
7/8	25 ± 6	3·8	98 ± 25	122 ± 30

obtained on the assumption that this resonance is from isotope ^{35}Cl (POPOV and SHAPIRO) with the value of $\Gamma_\gamma = 0{\cdot}5$ eV. The error in the results of Table 3 is

* In the present article the cross-sections and the values of $\sigma_0\Gamma$ in every case are given for the natural mixture of isotopes of chlorine.

mostly caused by the uncertainty in the subtraction of the 'base.'

It is known (BLATT and WEISKOPF, 1954) that the ratio of the reduced widths $\Gamma_n^0 = \Gamma_n E^{-1/2}$ of the S and P-levels is of the order of magnitude of $(R/\lambda)^2$. In the case of chlorine the value $(R/\lambda)^2$ is $\sim 0{\cdot}4 \times 10^{-3}$ at $E_0 = 405$ eV and $\sim 5{\cdot}10^{-3}$ at $E_0 = 4{\cdot}3$ keV. The data in Tables 1–3 show that the ratios of the reduced widths of 405 eV and 4·3 keV levels and of the reduced width of the −210 eV level which is an S-level, equal $(1{\cdot}0 \div 11) \times 10^{-3}$ and $(2{\cdot}5 \div 7) \times 10^{-3}$ respectively. Thus, it is quite probable that the 405 eV and 4·3 keV levels are actually P-levels.

Acknowledgments—The authors are grateful to I. M. FRANK for his interest in the work, to YU. A. BEREZIN who participated in the first stage of the work, to A. A. BERGMAN and A. I. ISAKOV for assistance in measuring and to I. V. SHTRANIKH and A. M. KLABUKOV for adjusting the electronics.

REFERENCES

AKHIEZER A. and POMERANCHUK I. (1950) *Certain Problems of Nuclear Theory*, Moscow-Leningrad.

BERGMAN A. A., ISAKOV A. I., MURIN I. D., SHAPIRO F. L., SHTRANIKH I. V. and KAZARNOVSKII M. V. (1955) *Proceedings of the First International Conference on the Peaceful Uses of Atomic Energy, Geneva*, P/642. United Nations, N.Y.

BERGMAN A. A., ISAKOV A. I., POPOV YU. P. and SHAPIRO F. L. (1957a) *Zh. eksp. teor. fiz.* **33**, 9.

BERGMAN A. A., ISAKOV A. I., POPOV YU. P. and SHAPIRO F. L. (1957b) *Proceedings of the All-union (Moscow) Conference on Nuclear Reactions*, p. 140.

BLATT J. and WEISKOPF V. (1954) *Theoretical Nuclear Physics* (Russian translation). Foreign Literature Publishing House, Moscow.

BRANDT H., GUGELOT P. G., HUBER O., MEDICUS H., PREISWERK P. and SCHERER P. (1946) *H.P.A.* **19**, 77; FOWLER W. A., LAURITSEN C. C. and LAURITSEN T. (1948) *R.M.F.* **20**, 265.

BRUGGER R. M., EVANS T. E., JOKI E. G. and SHANKLAND K. S. (1957) *Phys. Rev.* **104**, 1054.

ENDT P. M. and BRAAMS C. M. (1957) *R.M.F.* **29**, 727.

HIBDON C. T. and MUEHLHAUSE C. O. (1950) *Phys. Rev.* **79**, 44.

HUGHES D. J. (1955) *J. Nucl. Energy.* **1**, 237.

HUGHES D. J. and HARVEY J. A. (1955) BNL-325.

HUGHES D. J. and SCHWARTZ R. B. (1958) (2nd Ed.) BNL-325.

KLEMENT'EV V. B. and GRYAZEV V. M. (1957) *Atomnaya Energiya* **3**, 507.

LANE A. M. and LYMM J. E. (1960) *Nucl. Phys.* **17**, 563.

LAZAREVA L. E., FEINBERG E. L. and SHAPIRO F. L. (1955) *Zh. eksp. teor. fiz.* **29**, 381.

MACKLIN R. L. and POMERANCE H. S. (1955) *Proceedings of the First International Conference on the Peaceful Uses of Atomic Energy, Geneva*, P/833. United Nations, N.Y.

MELKONIAN E. (1955) *Proceedings of the First International Conference on the Peaceful Uses of Atomic Energy, Geneva*, Vol. 4, P/583. United Nations, N.Y.

OKOROKOV A. I. (1958) (Thesis) Institute of Physics, USSR Academy of Sciences.

POPOV YU. P. and SHAPIRO F. L. *Zh. eksp. teor. fiz.* To be published.

TOLLER L. A., PATTERSON J. R. and H. W. NEWSON (1955) *Phys. Rev.* **99**, 620.

VOLKOV A. N., KLABUKOV A. M. and POPOV YU. P. (1960) *Prib. tekh. eksp.* **2**, 68.

Note added in proof: Slow neutrons can induce the reaction (n,p) in one of the chlorine isotopes—^{35}Cl. After the completion of this work (1958) the reaction Cl(n,p) in the energy interval $E < 20$ keV was studied (POPOV and SHAPIRO *Zh. eksp. teor. fiz.*). To be published.

In the (n,p) cross-section curve resonances at $E_0 = 0{\cdot}405$ and 4·3 keV appeared, that shows that they indeed belong to the isotope ^{35}Cl. A hump at ~1 keV is even more pronounced in the (n,p) compared to the (n,γ) curve. This can possibly be accounted for by a resonance with E_0 1·1 ± 0·2 keV.

The resonance parameters given in this paper were recalculated taking into account the data on (n,p) reaction.

Reactor Science and Technology (Journal of Nuclear Energy, Parts A & B), 1961, Vol. 14, pp. 85 to 90. Pergamon Press Ltd. Printed in Northern Ireland

THE ENERGY DEPENDENCE OF THE FISSION CROSS-SECTIONS OF ^{238}U, ^{235}U AND ^{239}Pu FOR NEUTRONS IN THE ENERGY RANGE 12·6 TO 20 MeV

B. ADAMS, R. BATCHELOR and T. S. GREEN
Atomic Weapons Research Establishment, Aldermaston, Berks.

(*Received* 21 *June* 1960)

Abstract—Measurements of the variations of the fission cross-sections of ^{238}U, ^{235}U and ^{239}Pu have been made in the energy region 12·6 to 20 MeV. Relative measurements on ^{238}U were made using a multiplate fission counter and these were normalized to a known value at 14 MeV. Ratio measurements were then used to obtain the cross-sections of ^{235}U and ^{239}Pu.

VOL. 14 1961

1. INTRODUCTION

A CONSIDERABLE number of measurements have been made of the cross-sections for fission by neutrons and their dependence upon energy up to 10 MeV. Most of this work has been summarized by ALLEN and HENKEL (1957) and HEMMENDINGER (1958). One of the interesting features of the results is the rise in the cross-sections to a second plateau in the region of 6 MeV due to the onset of the $(n, n'f)$ reaction. At a higher energy, when the $(n, 2nf)$ process becomes energetically possible, a further increase in the cross-section is expected and, as pointed out by JACKSON (1956) this should be particularly noticeable for a relatively poor fissile nucleus such as ^{238}U. Absolute measurements at 14 MeV, reported by MOAT (1958) and UTTLEY and PHILLIPS (1956), are higher than the cross-sections in the region of the second plateau, and indicate that such an increase takes place.

The work reported here, which concerns the measurement of the variation of the fission cross-sections of ^{238}U, ^{235}U and ^{239}Pu in the energy range 12·6 to 20 MeV, was carried out prior to the review by HEMMENDINGER (1958). In this review some Los Alamos results on ^{238}U in the range up to 22 MeV are presented and the presence of the third plateau is clearly demonstrated. These results have been discussed by LEACHMAN (1958) and HALPERN (1959) but as yet no experimental details have been published.

Neutrons in the required energy range were produced by bombarding tritium with deuterons accelerated by the Aldermaston 6 MV Van de Graaff. The highest deuteron energy used was about 3·7 MeV, the threshold for the break-up of the deuteron into a proton and a neutron, and hence the limit at which monoenergetic neutrons are produced.

First the variation in the ^{238}U cross-section was investigated by measuring the number of fission events in a multiplate fission counter placed in a measured flux of neutrons, as a function of energy. The determination of the neutron flux was made with a proton recoil spectrometer. Absolute values have been deduced by normalizing the relative values to the 14 MeV value obtained by MOAT (1958).

The relative variation of the ratios

$$\frac{\sigma_f(^{235}U)}{\sigma_f(^{238}U)} \quad \text{and} \quad \frac{\sigma_f(^{239}Pu)}{\sigma_f(^{238}U)}$$

were then measured and by combining these results with the previous measurements on ^{238}U, the variations of $\sigma_f(^{235}U)$ and $\sigma_f(^{239}Pu)$ have been obtained.

2. EXPERIMENTAL TECHNIQUE

A schematic diagram of the experimental arrangement is shown in Fig. 1. For the ^{238}U measurements, the ^{238}U fission counter and the proton telescope were placed in fixed positions on two arms which could be rotated between 140° left and 140° right in the horizontal plane about the centre of a tritium gas target. The counters were normally placed on opposite sides of, but at equal angles to the direction of the incident deuteron beam. Different neutron energies were selected by choosing appropriate values of the incident deuteron energy and the angle of observation. For the ratio measurements the proton telescope was replaced by either a ^{235}U or a ^{239}Pu loaded counter. The amount of material used for supporting the counter was reduced to the minimum consistent with rigidity. A long counter was placed in the forward direction to monitor the neutron production and the beam current was monitored with a current integrator.

The gas target cell is shown in detail in Fig. 2. The beam enters the cell through a nickel window, 0·0002 in. thick, covering an aperture of ¼ in. diameter. With a gas pressure of 1 atmosphere this window could withstand a beam of about

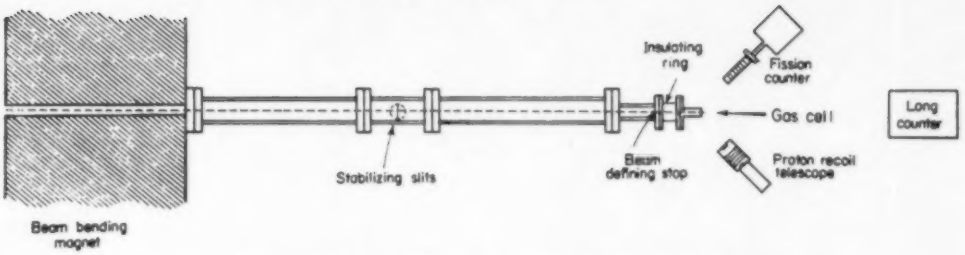

FIG. 1.—Schematic diagram of experimental arrangement.

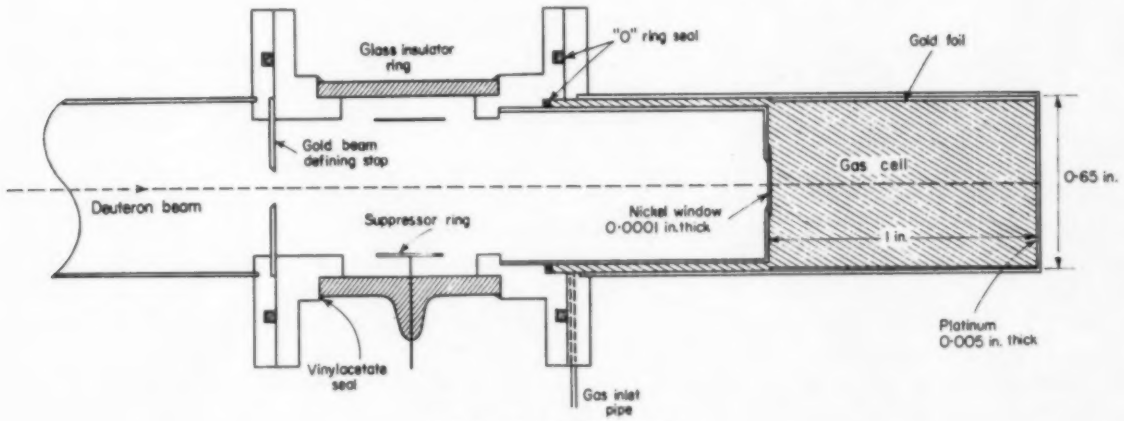

FIG. 2.—Gas target assembly.

1 μA for several days without the leak rate through it becoming excessive. To reduce background the beam was defined by a gold stop of aperture slightly less than the window, the cell was lined with gold foil and the end plate in which the beam stopped was made of platinum.

The gas cell was normally run at 1 atmosphere pressure. At low deuteron energies, however, the pressure was reduced to $\frac{1}{2}$ atmosphere to keep the effective centre of the neutron source approximately at the physical centre of the cell. Deuterons of 1 MeV incident on the cell window lose about 400 keV in the window and 400 keV in the gas (at 1 atmosphere). Because of the rapid increase of the (d, T) cross-section with decreasing deuteron energy in this range, the neutron production increases along the length of the cell and the effective source centre is displaced by about 3 mm. The effect is reduced by reducing the gas pressure and is not important at high energies.

The system for filling the cell was similar to that described by JOHNSON and BANTA (1956), the tritium being stored in a furnace containing pyrophoric uranium. Because of the small but finite leak rate of tritium through the window when under bombardment, and the danger of window fracture, the accelerator pumps were backed by a recovery system.

The design of the multiplate fission counter was similar to that described by ALLEN and FERGUSON (1955). The fissile material was coated on platinum backings to a thickness of 1·5 mg/cm² by a technique of painting on successive thin films of the nitrate suspended in an organic liquid and then firing after each application to produce the oxide. The amounts of material loaded into the counters and the isotopic purities are shown in Table 1.

Reasonable bias curves, suitable for relative measurements, were obtained in all cases, although, not surprisingly the performance of the uranium counters was much better than the plutonium counter. The bias voltage used for each counter was kept constant throughout the experiments. The possible effects of variations of kinetic energy distributions and fragment angular distributions with variation of incident neutron energy have been neglected.

TABLE 1

Counter No.	Material	Loading of counter mg of metal	Isotopic content
1	^{238}U	53	Natural U
2	^{235}U	80	93·3% ^{235}U 5·5% ^{238}U 1·2% ^{234}U
3	^{239}Pu	20	97·9% ^{239}Pu 2·1% ^{240}Pu

The proton recoil telescope was similar to that described by JOHNSON and TRAIL (1956). Protons emitted from a thin polythene foil within a small angle to the forward direction are counted by a CsI scintillator, the pulse height out from this being proportional to the energy of the neutron which ejected the proton. To reduce background the protons are made to pass through two proportional counters between the foil and the CsI, and only those pulses in the CsI which are in coincidence with those in the proportional counters are accepted. A typical pulse height spectrum obtained with 14 MeV neutrons is shown in Fig. 3, together with a background run obtained with the foil removed. The pulses due to the incidence of neutrons on the foil are obtained by subtraction of the background and it is seen that these lie entirely in the peak. The absolute neutron flux can be obtained from the counting rate in this peak, the hydrogen

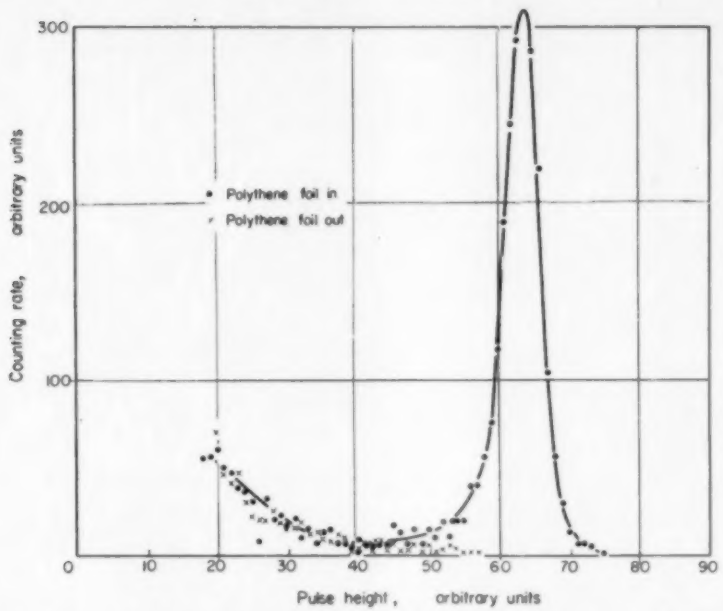

FIG. 3.—Pulse height spectrum obtained with the proton telescope for incident 14 MeV neutrons.

content of the foil, the effective angular acceptance for counting proton recoils and the differential (n, p) cross-section at $0°(\sigma_{n,p}(0°))$. In this experiment only relative measurements are required and hence the measured counting rates only need to be corrected for variation of $\sigma_{n,p}(0°)$ with energy. The latter was taken from the curve published by FOWLER and BROLLEY (1956).

3. PROCEDURE

Before the actual runs were started several preliminary measurements were made to check that the neutrons giving rise to counts in the various counters came directly from the target. The counting rates were measured as a function of distance from the centre of the cell. It was found that up to 25 cm the inverse square law was obeyed to within 1 or 2 per cent. As a further check the ^{238}U and ^{239}Pu counters were shielded with cadmium to see whether any thermalized neutrons were contributing to the counts: the effect was found to be negligible. It was also found that the scattering of neutrons by one counter into any other was negligible.

In the main part of the experiment the aim was to obtain consistent sets of data. For this reason a set of measurements at three or four different neutron energies was sandwiched between measurements made at 14 MeV. Neutrons of this energy could be obtained with the counters placed at 100° to the beam and with deuterons of energies up to 1·7 MeV incident on the foil. As a check, measurements were actually made at three different deuteron energies and each gave the same result.

Two procedures were adopted in making the measurements. In the first, sets of data were taken at various angles of observation with the incident deuteron energy fixed at 1·0, 1·32 and 1·96 MeV respectively; in the second the angle was fixed at 40° and the energy varied. Measurements were also made with the counters interchanged to cancel out any effects due to slight misalignments. This was particularly important at high energies and forward angles since the angular distributions are peaked forward. A good check on the consistency of the results came from the fact that for certain neutron energies,

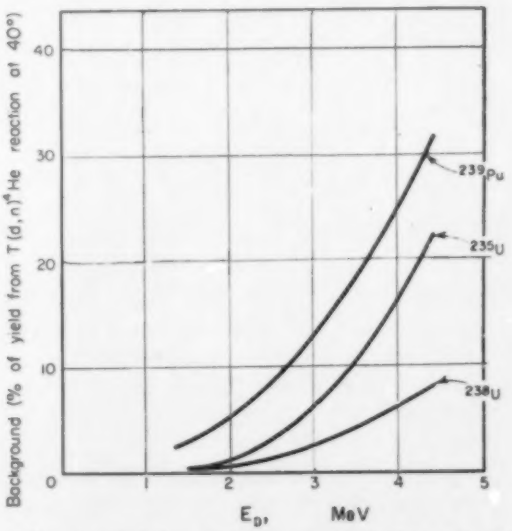

FIG. 4.—Variation of fission counter backgrounds with incident deuteron energy.

TABLE 2.—VALUES OF $\sigma_f(^{238}U)$, $\sigma_f(^{235}U)/\sigma_f(^{238}U)$ AND $\sigma_f(^{239}Pu)/\sigma_f(^{238}U)$, EACH NORMALIZED TO UNITY AT 14 MEV

E_n (MeV)	$\sigma_f{}^{238}U$	E_n (MeV)	$\sigma_f(^{235}U)/\sigma_f(^{238}U)$	E_n (MeV)	$\sigma_f(^{239}Pu/\sigma_f(^{238}U))$
12·7	0·89 ± 0·03	13·2	0·99 ± 0·02	13·4	1·01 ± 0·02
13·0	0·91 ± 0·03	13·5	0·99 ± 0·01	14·0	1·00 ± 0·01
13·5	0·93 ± 0·02	14·0	1·00 ± 0·01	14·4	0·97 ± 0·02
14·0	1·00 ± 0·02	14·4	0·93 ± 0·03	14·9	0·91 ± 0·02
14·5	1·04 ± 0·02	15·3	0·93 ± 0·01	15·3	0·92 ± 0·02
15·0	1·11 ± 0·02	16·0	0·92 ± 0·01	16·0	0·86 ± 0·02
15·4	1·11 ± 0·02	16·5	0·85 ± 0·02	16·5	0·84 ± 0·02
16·0	1·13 ± 0·03	16·9	0·86 ± 0·03	16·9	0·83 ± 0·02
16·4	1·19 ± 0·03	17·4	0·83 ± 0·03	17·5	0·82 ± 0·03
17·0	1·15 ± 0·03	18·0	0·86 ± 0·02	18·0	0·79 ± 0·03
17·5	1·18 ± 0·03	18·4	0·88 ± 0·03	18·4	0·79 ± 0·03
18·4	1·20 ± 0·03	19·0	0·88 ± 0·03	19·0	0·76 ± 0·03
18·9	1·30 ± 0·04	19·4	0·87 ± 0·03	19·4	0·76 ± 0·03
19·4	1·31 ± 0·05				

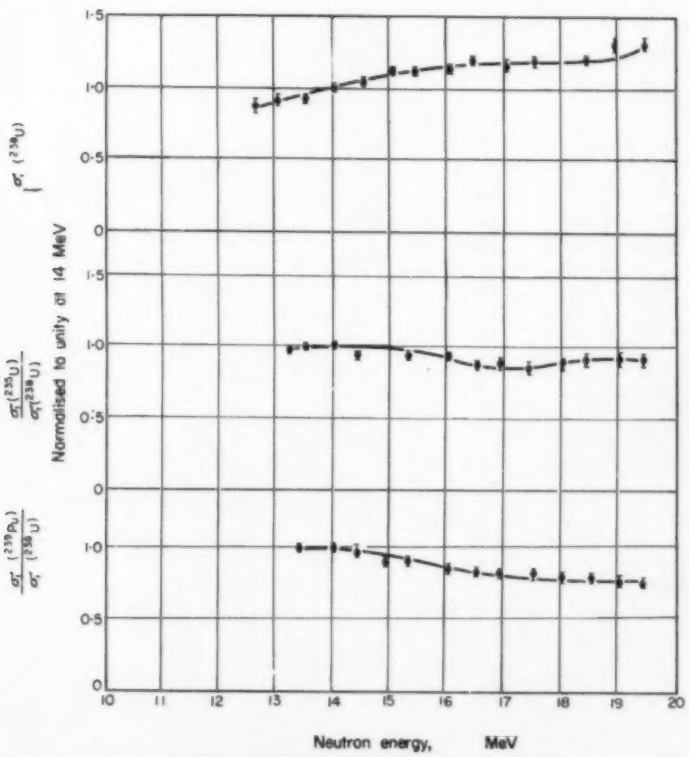

FIG. 5.—Variations of $\sigma_f(^{238}U)$, $\sigma_f(^{235}U)/\sigma_f(^{238}U)$ and $\sigma_f(^{239}Pu)/\sigma_f(^{238}U)$ with neutron energy.

data obtained under different conditions were the same. Furthermore, the angular distributions of the emitted neutrons at incident deuteron energies of 1·00, 1·32 and 1·96 MeV as measured by the proton telescope agreed with data reported by BAME and PERRY (1957).

Background measurements were made by removing the gas from the cell. The trend of the backgrounds expressed as a percentage of the true counts is shown in Fig. 4. The high relative background of the plutonium counter at low deuteron energies is due to α-particle build-up.

4. RESULTS

The experimental results for the variation of the ^{238}U cross-section and the ratios

$$\frac{\sigma_f(^{235}U)}{\sigma_f(^{238}U)} \quad \text{and} \quad \frac{\sigma_f(^{239}Pu)}{\sigma_f(^{238}U)}$$

are shown in Table 2 and Fig. 5.

TABLE 3.—VALUES OF σ_f FOR ^{238}U, ^{235}U AND ^{239}Pu

E_n (MeV)	$\sigma_f(^{238}U)$(barns)	E_n (MeV)	$\sigma_f(^{235}U)$ (barns)	E_n (MeV)	$\sigma_f(^{239}Pu)$ (barns)
12·7	1·01 ± 0·04	13·2	1·90 ± 0·10	13·4	2·48 ± 0·10
13·0	1·03 ± 0·04	13·5	1·98 ± 0·10	14·0	2·61 ± 0·08
13·5	1·05 ± 0·03	14·0	2·13 ± 0·09	14·4	2·64 ± 0·10
14·0	1·13 ± 0·02	14·4	2·06 ± 0·10	14·9	2·58 ± 0·11
14·5	1·18 ± 0·03	15·3	2·21 ± 0·10	15·3	2·66 ± 0·11
15·0	1·25 ± 0·03	16·0	2·22 ± 0·10	16·0	2·54 ± 0·11
15·4	1·25 ± 0·03	16·5	2·07 ± 0·10	16·5	2·52 ± 0·11
16·0	1·28 ± 0·04	16·9	2·11 ± 0·10	16·9	2·50 ± 0·11
16·4	1·34 ± 0·04	17·4	2·05 ± 0·10	17·5	2·51 ± 0·13
17·0	1·30 ± 0·04	18·0	2·17 ± 0·10	18·0	2·45 ± 0·13
17·5	1·33 ± 0·04	18·4	2·27 ± 0·10	18·4	2·50 ± 0·13
18·4	1·36 ± 0·04	19·0	2·32 ± 0·10	19·0	2·48 ± 0·13
18·9	1·47 ± 0·05	19·4	2·43 ± 0·10	19·4	2·61 ± 0·15
19·4	1·48 ± 0·06				

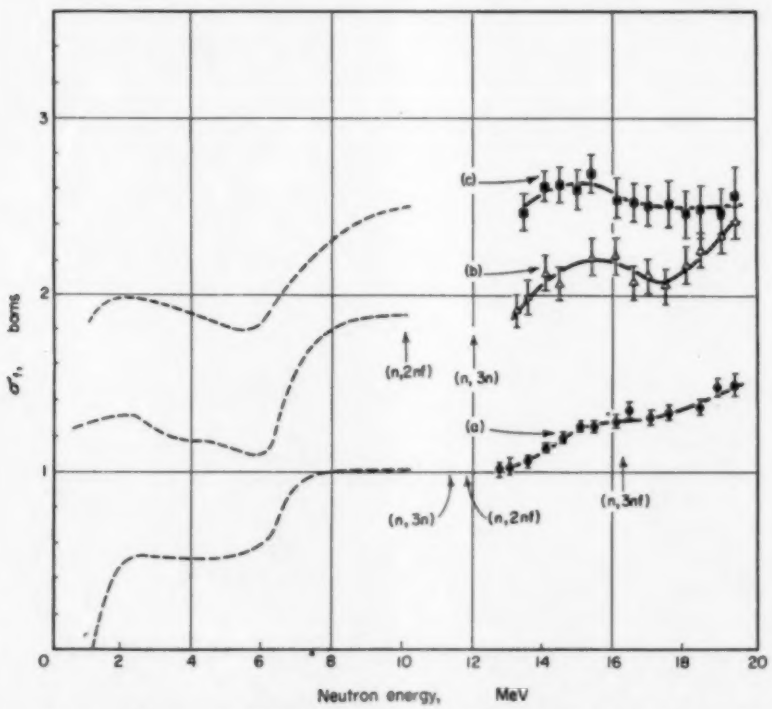

FIG. 6.—Fission cross-sections of ^{238}U, curve (a), ^{235}U, curve (b) and ^{239}Pu, curve (c). Dotted curve represents previous results (HEMMENDINGER 1958).

The ^{235}U data have been corrected for the ^{238}U impurity: a similar correction to the ^{239}Pu data for the ^{240}Pu impurity is not possible since the cross-section of the latter is not known.

The errors shown are statistical and are represented as standard deviations. The statistics on the ^{238}U data are primarily determined by the low efficiency of the proton telescope. The energy resolution varies over the energy range but on the average is about 400 keV. This spread arises mainly from geometrical effects and the energy loss of the deuterons in the gas cell. The former is important at high energy and the latter at low energy.

In Table 3 and Fig. 6, the deduced cross-sections for the three nuclei are shown. These are based upon the values at 14 MeV quoted by MOAT (1958). The data for ^{235}U and ^{239}Pu are obtained by combining the ratio data with the smooth curve drawn through the ^{238}U results.

5. DISCUSSION

The results on ^{238}U reported here are in very good agreement with those obtained at Los Alamos. The

second and third steps in the curve correspond to the onset of the $(n, n'f)$ and $(n, 2nf)$ reactions, respectively.

Theoretical predictions of the value of the cross-section on the third plateau have been made by JACKSON (1956) and HENKEL (see LEACHMAN 1958). In these calculations it is assumed that a compound nucleus is formed which decays by either neutron emission or fission. Each neutron emission leads to a new compound nucleus. Values, which are independent of energy, are assumed for the fissionability of

$$\left(\frac{\Gamma_f}{\Gamma_f + \Gamma_n}\right)$$

the relevant nuclei, ^{239}U, ^{238}U and ^{237}U. Taking a value of 2·6 barns for the total reaction cross-section, σ_R, at all energies, JACKSON obtained a value of 1·6 barns for the fission cross-section of ^{238}U on the third plateau. HENKEL found a value of 1·5 barns having first calculated σ_R on the basis of the optical model. Both of these values are higher than the experimental value of 1·3 barns.

As suggested by HALPERN (1959) the theoretical values are expected to be in error because of the neglect of direct interactions, uncertainties in the value of σ_R and the assumption that the fissionability is energy independent. Lack of quantitative data on these effects makes it difficult to improve the comparison of theoretical and experimental results.

The step at about 14 MeV in the ^{235}U curve occurs at a higher energy than the expected threshold for the $(n, 2nf)$ at 10·6 MeV. This figure is the sum of the fission threshold of ^{234}U, 5·2 MeV, measured by the ^{233}U(d, pf) reaction (NORTHROP, STOKES and BOYER, 1959), and the neutron binding energy, obtained from CAMERON's mass tables (1957). Although fission thresholds measured by (d, pf) reactions are likely to be less than those measured by (n, f) reactions, due to possible confusion of the bumps on the threshold curves (HALPERN, 1959), it is difficult to believe that this accounts for the discrepancy observed here. More measurements in the region 10–13 MeV would be of interest. The observed decrease after 14 MeV may be due to the fall in Γ_f/Γ_n for the compound nucleus ^{236}U. For this nucleus the neutron binding energy (B_n) is greater than the fission barrier (B_f). In such a case HALPERN (1959) points out Γ_f/Γ_n falls with excitation energy according to the formula

$$\frac{\Gamma_f}{\Gamma_n} = N \exp\left(\frac{B_n - B_f}{T}\right)$$

where N is a factor which depends slightly on energy and T is the nuclear temperature.

The ^{239}Pu cross-section reaches the total inelastic cross-section at 10 MeV and is therefore not expected to show further steps.

Acknowledgments—We are indebted to DR. P. GREGORY, for preparing the fission foils and to MR. G. CHAPLIN who constructed the gas target and assisted with some of the measurements. We also wish to thank the operating crew of the Van de Graaff for their co-operation.

REFERENCES

ALLEN W. D. and FERGUSON A. T. G. (1955) *J. Nucl. Energy* **2**, 38.

ALLEN W. D. and HENKEL R. L. (1957) *Fast Neutron Data on the Isotopes of Thorium, Uranium and Plutonium.* Progress in Nuclear Energy, Series I, Vol. 2.

BAME S. J. and PERRY J. E. (1957) *Phys. Rev.* **107**, 1616.

CAMERON A. G. W. (1957) *A Revised Semi-Empirical Atomic Mass Formula*, A.E.C.L., Chalk River Report No. CRP 690.

CRANBERG L., ARMSTRONG A. H. and HENKEL R. L. (1956) *Phys. Rev.* **104**, 1639.

FOWLER J. L. and BROLLEY J. E. (1956) *Rev. Mod. Phys.* **28**, 103.

HALPERN I. (1959) *Ann. Rev. Nucl. Sci.* **9**, 245.

HEMMENDINGER A. (1958) *Proceedings of the Second International Conference on the Peaceful Uses of Atomic Energy, Geneva*, Paper A/Conf. 15/P/663. United Nations, N.Y.

JACKSON J. D. (1956) *Fission by MeV Neutrons*, Chalk River Report No. CRP-642-A, 125.

JOHNSON C. H. and BANTA H. E. (1956) *Rev. Sci. Instrum.* **27**, 132.

JOHNSON C. H. and TRAIL C. C. (1956) *Rev. Sci. Instrum.* **27**, 468.

LEACHMAN R. B. (1959) *The Fission Process—Mechanisms and Data.* Progress in Nuclear Energy, Series I, Vol. 3, 144.

MOAT A. (1958) Private communication.

NORTHROP J. A., STOKES R. N. and BOYER K. (1959) *Phys. Rev.* **115**, 1277.

UTTLEY C. A. and PHILLIPS. J. A. (1956) Private communication.

VOL
14
196

Reactor Science and Technology (Journal of Nuclear Energy, Parts A and B), 1961, Vol. 14, pp. 91 to 99. Pergamon Press Ltd. Printed in Northern Ireland

MEASUREMENTS OF THE REACTION RATE DISTRIBUTION PRODUCED BY A SOURCE OF 14 MeV NEUTRONS AT THE CENTRE OF A URANIUM METAL PILE

J. W. WEALE, H. GOODFELLOW, M. H. MCTAGGART and M. L. MULLENDER
Atomic Weapons Research Establishment, Aldermaston, Berks.

(*Received* 23 *August* 1960)

Abstract—Measurements have been made of the 14 MeV flux, the total neutron leakage and the reaction rate distributions for $^{235}U(n,f)$, $^{238}U(n,f)$, $^{238}U(n,\gamma)$ and $^{239}Pu(n,f)$ in uranium piles of density 16·3 g/cm³ and total weight up to 20 tons.

1. INTRODUCTION

IN a recent paper (ALLEN *et al.*, 1960) subsequently referred to as (I), measurements of 14 MeV neutron reactions in natural uranium shells of thickness up to 11·3 cm are described. The neutrons were produced at a target at the centre of the shell and measurements were made of the total neutron flux escaping from the shell. These measurements were aimed primarily at the determination of the $(n,3n)$ reaction cross-section at 14 MeV. The present experiments have extended this work to assemblies large enough to absorb virtually all the 14 MeV neutrons and to establish a flux of secondary neutrons with an approximately equilibrium energy spectrum. Measurements were made of the neutron leakage, total fissions, 14 MeV and secondary neutron fluxes, and total ^{239}Pu production resulting from a 14 MeV neutron source at the centre of a cylindrical uranium pile 42 inches high and 39 inches in diameter. The flux distributions were also measured for a series of smaller cylinders of height 42 inches and diameter 28, 24, 20 and 16 inches and for these the other reaction rates were derived from the flux distributions by comparison with the large cylinder results. The integrated reaction rates were thus obtained as a function of the thickness of uranium surrounding a point 14 MeV neutron source. The results should provide a useful reference for checking fast neutron data in the fission energy region and may be of value in the design of blankets for thermonuclear reactors using DT fusion.

2. DESCRIPTION OF THE PILE ASSEMBLIES

In order to provide experimental flexibility the assemblies were constructed of metal rods. The rods were 42 inches long and 1·150 inches in diameter, of magnesium–reduced metal as used in Calder Hall reactors. A total weight of 19·3 tons of metal was available for the experiments. The rods were mounted vertically with their ends located in accurately drilled holes in a steel base plate so as to form a close-packed hexagonal lattice. The standard rod spacing is shown in Fig. 1, which also shows the outlines of the various sizes of cylinder used. Figure 2 shows the general appearance of the pile. The average density of the arrangement was 0·87 times that of the metal rods, i.e. 16·3 g/cm³. The top ends of the rods were separated by steel spacing pins and the whole pile was held together by aluminium plates mounted on a steel framework. Removal of its six spacing pins enabled any rod to be removed to provide a counter channel without disturbing the rest of the pile. The source of neutrons was a 'thick' Zr–T target bombarded by 200 kilo-volt deuterons from a Cockcroft-Walton accelerator. Access for the thin-walled brass drift-tube was provided by a channel $2\frac{3}{4}$ in. deep and $\frac{7}{8}$ in. wide as shown in Fig. 3 and the source was thus located in the central rod position with its centre 22 in. from the top surface of the pile. The source was 6 ft above the concrete floor of the laboratory and, apart from the steel framework, there was no other reflecting or moderating material within 8 ft in any direction.

A steady DT source strength of up to 5×10^9 neutrons per second was used and the content of DD neutrons from absorbed gas was estimated as not more than 2 per cent. The target assembly was water cooled. An extra tube was provided leading from the target to an α-counter at an angle of 177° to the deuteron beam. The absolute strength of the neutron source was determined from the α-count rate and the measured solid angle using the method described by BENVENISTE and ZENGER (1954).

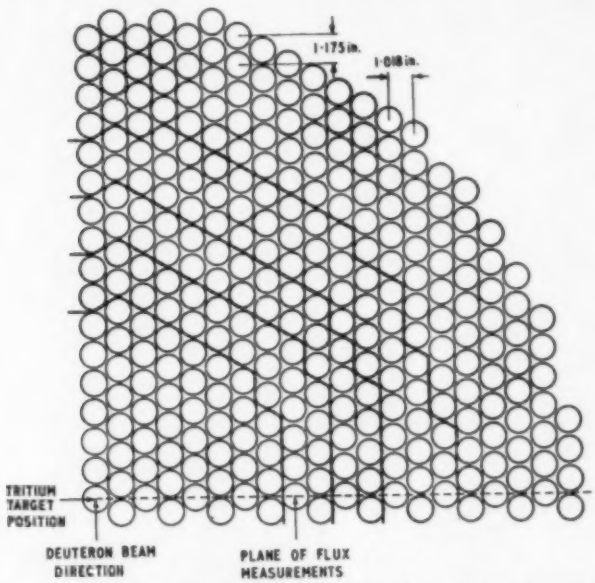

FIG. 1.—Plan of the lattice showing the rod spacing and the pile outlines.

3. MEASUREMENTS OF 14 MeV FLUX

The flux of 14 MeV neutrons was measured by a method similar to that described in (I), using the $(n,2n)$ reaction in ^{63}Cu, (threshold 11·5 MeV). Copper cylinders 1¼ inch long and ¼ inch in diameter were irradiated for 20 minutes in the pile and the 9·9 minute ^{62}Cu positron activity was counted in a NaI(Tl) well-crystal with a pulse-height-analyser set on the 0·51 MeV annihilation—γ-peak. Calibration was achieved by irradiating the slugs in a 14 MeV flux of known intensity. Half-life checks were made and a small correction for the content of 12·8 hour ^{64}Cu was found necessary. This varied with the position in the pile and was measured separately for each irradiation.

Voids were made in the required positions in the pile by removing a complete rod and inserting a 22 inch long uranium sleeve containing two copper cylinders located by spacers of thin brass tube. One cylinder used as a reference was placed in the horizontal source plane and the other at the required vertical distance above it. Rods of uranium 2 inches long were placed above and below the copper cylinders so that they were completely surrounded by uranium. The presence of a small void was shown to make no difference to the measured copper activation. The reproducibility of the measurements was ±2 per cent in the central region but was about ±4 per cent at the pile edge because of the low count rate and higher proportion of background and ^{64}Cu counts.

Results for the large cylindrical pile are shown in Fig. 4 as a graph of 14 MeV flux multiplied by R^2, where R is the distance from the target centre to the centre of the copper cylinder. Out to 40 cm the horizontal distribution is closely fitted by the straight line

$$\phi R^2 = 0{\cdot}101 \exp(-0{\cdot}117R). \qquad (1)$$

The vertical distribution at a horizontal distance of 5·2 cm has approximately the same slope but is displaced outwards by about 4 cm. This is attributed to the extra length of the source cavity in the vertical direction.

4. FISSION CHAMBER MEASUREMENTS

The fission rates in ^{239}Pu, ^{235}U and ^{238}U were measured using cylindrical fission chambers of standard Harwell design (ABSON *et al.*, 1958; AVES *et al.*, 1954). The dimensions and fillings are listed in Table 1.

TABLE 1

Counter filling	Effective weight of main constituent (mg)	Outer diam. (cm)	Active length (cm)
^{239}Pu 98%, ^{240}Pu 2%	0·82	0·62	2·0
^{235}U 93%, ^{238}U 5·2%, ^{234}U 1·8%	91·1	2·98	6·05
^{238}U 99·98%, ^{235}U 0·02%	104·1	2·98	6·05

The effective weights appropriate to the counting conditions were determined by irradiating the counters at a known distance from a point source of 14 MeV neutrons whose strength was determined by counting the associated α-particles. The same counting conditions were used for the flux measurements. The 14 MeV cross-sections used in this calibration are listed in Table 3. The errors in the effective weights are equal to the combined errors (standard deviations) of the cross-sections and the uncertainties in determination of neutron flux from the α-count, but, since the same α-counter assembly was used in the actual experiments, the measured results of fissions per gramme include only the cross-section errors.

Flux measurements in the pile were made by removing a complete rod and locating the counter at the required vertical position in the empty channel. Checks made at various positions showed that within the accuracy of the measurements there was no difference between results obtained with a void below the counter and those obtained when that void was filled with uranium. In the case of the small diameter ^{239}Pu fission chamber

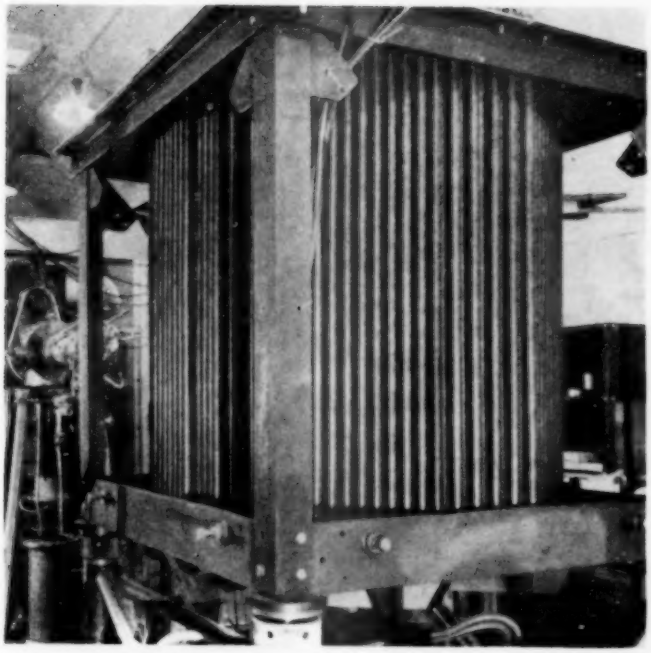

FIG. 2.—General view of the assembly showing the 39 inch diameter pile.

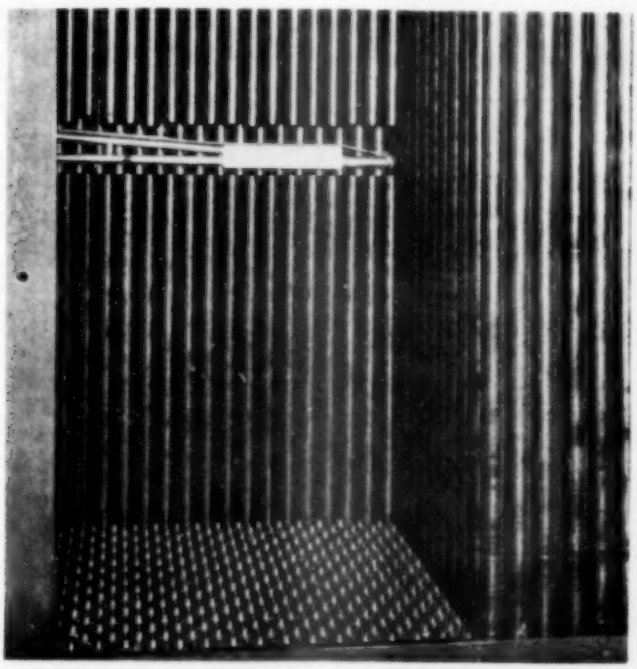

FIG. 3.—The 39 inch diameter pile with one-quarter of the rods removed to show the accelerator drift tube and the target arrangement.

VOL.
14
196

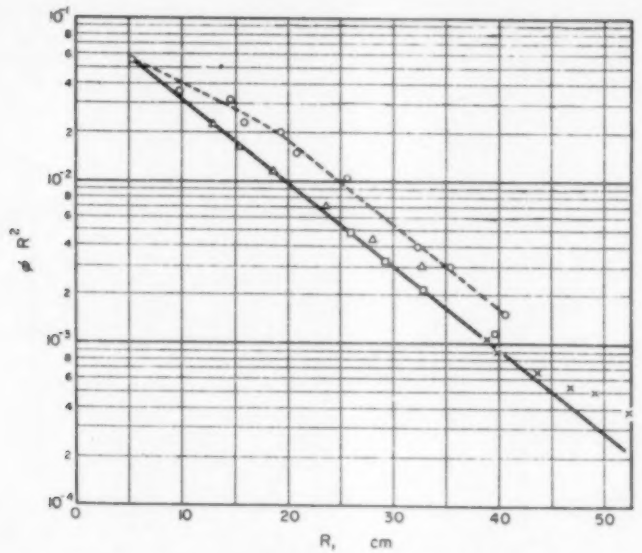

FIG. 4.—Distribution of 14 MeV neutron flux as measured by Cu cylinder irradiations. Four vertical distributions were measured at horizontal distances of 5·2, 13·0, 26·0 and 39·0 cm respectively and each distribution is given a separate symbol. The first position in each group is in the horizontal mid-plane. The unbroken straight line is that given by equation (1).

the gap between the counter and the surrounding rods was filled by a 22 inch long sleeve of uranium (internal and external diameters 0·56 and 1·15 inches) and the counter itself was surrounded by a 0·012 inch thick Cd sheath. After preliminary surveys had established the symmetry of the flux distributions in the horizontal plane all measurements were made in a vertical plane through the target perpendicular to the direction of the deuteron beam. The statistical accuracy of the counting was better than ±1 per cent for all measurements but slight variations in counter positioning and performance increased the probable error to ±3 per cent for each point (in addition to any error in 14 MeV cross-section values).

The resulting reaction rate distributions separated into 14 MeV and secondary neutron components are shown in Figs. 5, 6, 7 and 8. The separation was

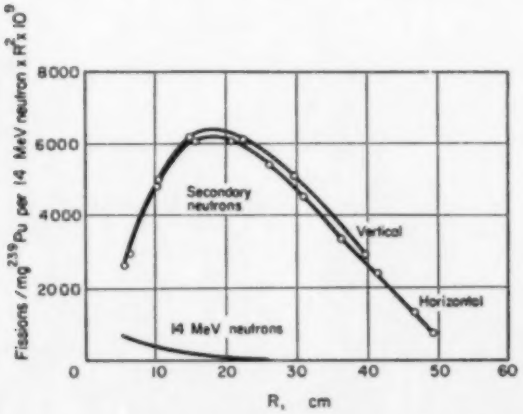

FIG. 5.—Distribution of ^{239}Pu fission rate in the 39 inch diameter pile. The vertical scan is at a horizontal distance of 5·3 cm from the centre.

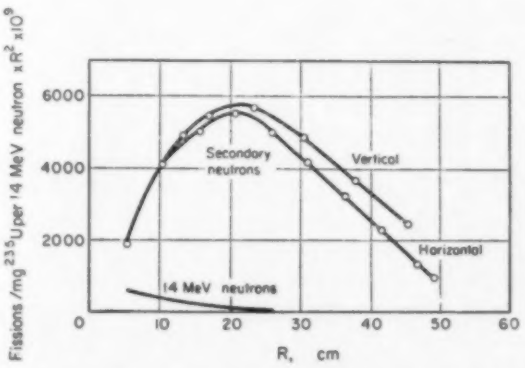

FIG. 6.—Distribution of ^{235}U fission rate in the 39 inch diameter pile. The vertical scan is at a horizontal distance of 10·5 cm from the centre.

achieved by subtracting from the total the 14 MeV reactions rates calculated from the measured 14 MeV flux. The ordinate 'Flux × R^2' was used because it indicates the relative contributions to the integrated reaction rate from different regions of the pile. In the case of ^{235}U and ^{239}Pu fission the contribution from 14 MeV neutrons is negligible beyond 20 cm from the target. The contribution from the secondary neutrons rises to a peak at about 20 cm—corresponding to the increase in secondary neutron flux as the 14 MeV neutrons are degraded in energy—and then falls approximately linearly as the secondary neutrons are themselves absorbed or lost by leakage. In the case of ^{238}U fissions the contribution from the 14 MeV

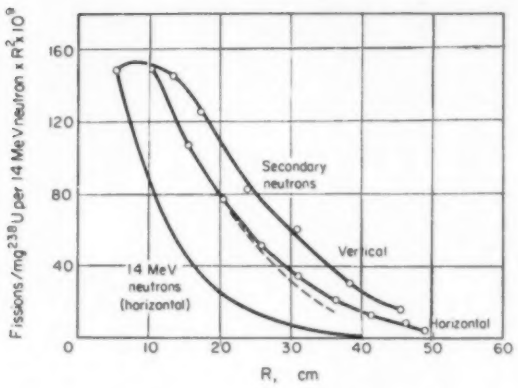

FIG. 7.—Distribution of ^{238}U fission rate in the 39 inch and 28 inch diameter piles. The vertical scan is at a horizontal distance of 10·5 cm from the centre and is for the 39 inch pile only. The horizontal distribution for the 28 inch pile is indicated by the broken line.

neutrons is much more important and the peak contribution from the secondaries is nearer to the pile centre because only the higher energy secondaries are above the fission threshold. The difference between the vertical and horizontal distributions is attributed partly to the extra length of the source cavity in the vertical direction and partly to the effect of streaming in a vertical direction between the uranium rods. The flux distribution in the horizontal direction is taken to be that corresponding to a homogeneous pile of the average uranium density. The variation of the distributions which is produced by reducing the pile radius is shown by the graphs in Fig. 8 of the ^{239}Pu fission rate distributions for the five different cylinders. For the higher energy neutrons this variation is less marked as is shown by the comparison of 39 inch and 28 inch cylinder results for the ^{238}U fission rate in Fig. 7.

5. MEASUREMENTS OF THE ^{238}U(n,γ) REACTION

Because the low cross-section and the low flux in the outer parts of the assembly required the use of large samples to obtain reasonable count rate, measurements were made of ^{239}Np rather than ^{239}U. Chemical separation of ^{239}Np eliminated the difficulties of thick sample correction and of fission product backgrounds. A disadvantage of the method is the need for a long irradiation in order to approach the equilibrium activity of ^{239}Np. A 24-hour irradiation at an average source strength of 2×10^9 neutrons/sec was necessary for accurate results at the outermost parts of the large pile.

Samples of natural uranium metal weighing about 1 gramme were mounted in thin brass tubes and placed in the gaps between the uranium rods at various positions in the pile in a plane perpendicular to the deuteron beam. After irradiation the uranium metal was dissolved in aqua regia together with a quantity of ^{237}Np tracer and the solution was evaporated to dryness to ensure exchange between the neptunium isotopes. After dissolving the residue in dilute sulphuric acid, the neptunium was reduced to neptunium^{IV} with hydrazine and then coprecipitated with neodymium fluoride. The neptunium was extracted from 1-M hydrochloric acid into a benzene solution of T.T.A. and back extracted into 6-M nitric acid. Finally the neptunium was absorbed on an anion exchange column from concentrated hydrochloric acid and then eluted using 2-M hydrochloric acid solution. Sources were mounted on stainless steel disks and the ^{239}Np β-activity was counted in an end-window proportional counter which was standardized by reference to ^{241}Am (CRIPPS and WEALE, 1958). The chemical yield was determined by α-counting the ^{237}Np tracer. The combined error of the chemistry and the counting was estimated at ± 4 per cent except for the extreme edge measurement where the error rises to ± 7 per cent.

Results for the large pile are shown in Fig. 9. These are total reaction rates but the contribution from 14 MeV neutrons is negligibly small. The distribution follows the same general shape as that for ^{235}U fission.

6. MEASUREMENTS OF NEUTRON LEAKAGE

For the large cylindrical pile, measurements of the total neutron leakage were made using a 'long' counter. The leakage energy spectrum is a degraded fission spectrum with no 14 MeV or thermal content and the long counter efficiency is approximately energy independent over this range (e.g. MCTAGGART, 1959). The counter efficiency was determined by counting a mock fission source which had itself been calibrated by comparison with a standard source in a manganese bath. Before applying this result to the pile measurements a correction of -3 per cent was made to allow for the increased angular spread of the pile as compared with the calibrating source. Because of the lack of spherical symmetry in the assemblies it was necessary to

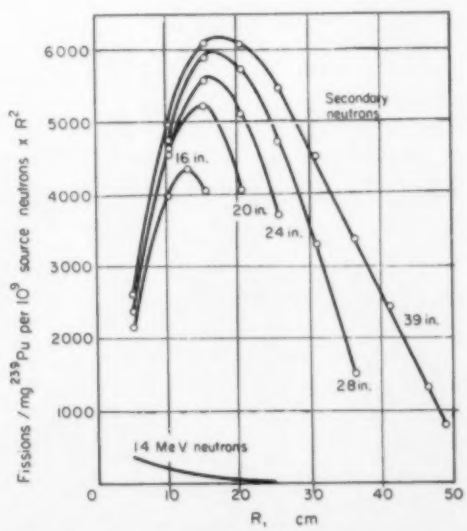

FIG. 8.—Horizontal distribution of ^{239}Pu fission rate for each of the piles studied.

measure the leakage at a number of positions. The counter was pointed at the pile centre with its front face at a distance of 200 cm from the target and measurements were made for representative values of 'latitude' and 'longitude.' Graphs of leakage versus the pile thickness in the direction of measurement were constructed, thus enabling the leakage in any direction to be determined by interpolation. These results were then integrated over all directions to derive the total neutron leakage per 14 MeV source neutron. Results for the 39 inch cylinder are listed in Table 2.

The probable error in the determination of the counter efficiency was estimated as ±3 per cent and that of the numerical integration of the results over a spherical surface as ±3 per cent giving an overall probable error of ±4 per cent.

7. NEUTRON BALANCE IN THE LARGE CYLINDRICAL PILE

In order to check the self-consistency of the results a neutron balance sheet was drawn up for the large cylindrical pile. The total fissions and captures were integrated numerically for the whole pile volume. The 14 MeV fission contributions and the $(n,2n)$ and $(n,3n)$ integrals were derived from the measured flux and the data listed in Table 3. Since virtually all the 14 MeV neutrons undergo non-elastic collisions, (see Fig. 4), the 14 MeV reaction integrals, including inelastic scatter, were balanced to unity. It was assumed that secondary neutrons make no significant contributions to the $(n,3n)$ reaction but an allowance for their contribution to the $(n,2n)$ reaction was included. The complete neutron balance sheet is shown in Table 4.

The net neutron gain, which should be zero, is

$$(4{\cdot}90 \pm 0{\cdot}19) - (4{\cdot}49 \pm 0{\cdot}24) = 0{\cdot}41 \pm 0{\cdot}31.$$

The balance is most sensitive to the ^{238}U fission and capture terms and there is an indication that the fission term may be too high and the capture term too low. A change of one standard deviation in each would make the balance exact.

8. THE SECONDARY NEUTRON 'EQUILIBRIUM' SPECTRUM

The secondary neutrons produced by the 14 MeV $(n,3n)$, $(n,2n)$ and (n,f) reactions are expected to have

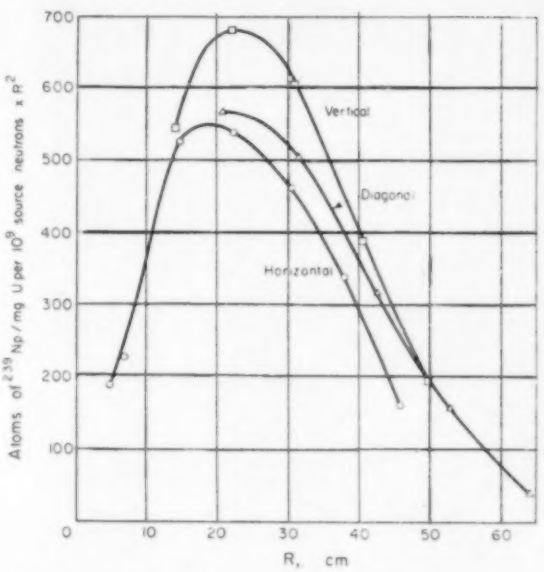

FIG. 9.—Distribution of ^{238}U neutron capture rate for the 39 inch diameter pile. The vertical scan is at a horizontal distance of 6·9 cm from the centre.

an energy distribution approximating to a somewhat degraded fission spectrum (VASIL'EV *et al.*, 1957; ZAMYATNIN *et al.*, 1959) and the average number of secondaries produced per 14 MeV source neutron is 3·3 (1). Few 14 MeV neutrons remain at 20 cm from the target and beyond this distance the neutron flux is due to the diffusion and further multiplication or absorption of the secondary neutrons. The average energy of these neutrons is expected to decline until an equilibrium is set up between those processes which tend to harden the spectrum (fission at all energies and preferential capture of slow neutrons) and those which tend to soften the spectrum (inelastic collisions and preferential leakage of fast neutrons). Such an equilibrium spectrum was observed in the uranium blanket surrounding the Zephyr core and in other uranium assemblies (see review by CODD *et al.*, 1956). The existence of a similar spectrum in the outer parts of the large pile in the present series of experiments is demonstrated in Fig. 10 by the graphs showing the

TABLE 2.—NEUTRON LEAKAGE PER 4π SOLID ANGLE PER SOURCE NEUTRON (39 INCH CYLINDER)

Angle to beam \ Angle of elevation	0 (Horizontal)	22½	45	60	90	Integrated leakage
0	0·553	0·477	—	—	0·306	
30	0·549	0·451	—	—	0·306	0·408
60	0·603	0·450	—	—	0·306	
90	0·607	0·490	0·294	0·292	0·306	

TABLE 3.—NUCLEAR DATA
(The ν values are listed for ^{238}U at 1·5 MeV and for ^{235}U at 0·5 MeV, these being the estimated mean energies of fission for the secondary neutrons)

$\sigma(n,f)$	14·2 MeV	^{235}U ^{238}U ^{239}Pu	2·13 ± 0·09 barns 1·13 ± 0·02 barns 2·61 ± 0·08 barns	MOAT, unpublished
$\sigma(ne)$	14·2 MeV	^{238}U	2·89 ± 0·05 barn	COHEN, 1960
$\sigma(n,2n)$	14·5 MeV	^{238}U	0·69 ± 0·04 barn	PERKIN and COLEMAN, 1960
$\sigma(n,3n)$	13·4 to 14·8 MeV	^{238}U	0·95 ± 0·15 barn	ALLEN *et al.*, 1960
ν	14·2 MeV	^{238}U ^{235}U	4·44 ± 0·12 4·28 ± 0·08	MOAT *et al.*, 1960
ν	1·5 MeV	^{238}U	2·55 ± 0·09	as derived in (I)
	0·5 MeV	^{235}U	2·43 ± 0·05	MOAT *et al.*, 1960 (interpolation)

TABLE 4.—NEUTRON BALANCE SHEET FOR THE LARGE CYLINDER

Reaction	Reaction rate per source neutron R	Neutron gain per source neutron		Analysis of errors
$^{238}U(n,f)$ Total 14 MeV Non-14 MeV	1·18 ± 0·06 0·39 0·79	$R(\nu - 1)$	2·56 ± 0·16 1·34 1·22	$(\nu - 1)$ errors are 4%, σ errors are 2%, counting and integration errors are 3% each. Combined error = 6%
$^{235}U(n,f)$ Total 14 MeV Non-14 MeV	0·281 ± 0·017 0·006 0·275	$R(\nu - 1)$	0·413 ± 0·025 0·020 0·393	As for ^{238}U Combined error = 6%
$^{238}U(n,3n)$ Total	0·327 ± 0·052	$2R$	0·65 ± 0·10	σ has 15% error. (There is a corresponding uncertainty in $\sigma(n,n')$)
$^{238}U(n,2n)$ Total 14 MeV Non-14 MeV	0·277 ± 0·008 0·237 ± 0·007 0·040 ± 0·004	R	0·277 ± 0·008	σ_{14} has 3% error. Non-14 MeV contribution has 10% error
$^{238}U(n,\gamma)$ Total	4·08 ± 0·24	$-R$	−4·08 ± 0·24	Absolute ^{239}Np determination 4%. Neutron source strength 3%. Integration 3%
Leakage Total	0·41 ± 0·02	$-R$	−0·41 ± 0·02	Counter efficiency 3% Integration 3%
Production at source	1·0	R	1·0	No error, by definition

VOL 14 196

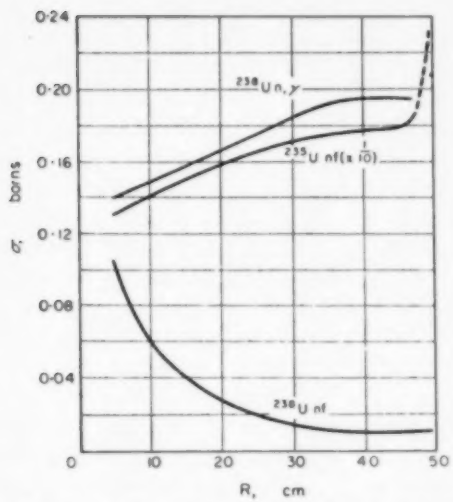

FIG. 10.—Effective reaction cross-sections in the secondary neutron flux as a function of horizontal radius in the 39 inch pile. The values are based on a constant ^{239}Pu fission cross-section of 1·81 barns. Without including any error in this value, the estimated errors in the effective cross-sections are 5 per cent for $^{238}U(n,f)$ 7 per cent for $^{235}U(n,f)$ and 8 per cent for $^{238}U(n,\gamma)$.

spatial variation of the effective reaction cross-sections. The neutron flux used in determining these cross-sections was derived from the ^{239}Pu fission rate by assuming a constant cross-section of 1·81 barns for this reaction in the secondary neutron spectrum. This is a good approximation over the expected neutron energy range (c.f. HUGHES and SCHWARTZ, 1958). The secondary neutron reaction rates were used for $^{235}U(n,f)$ and $^{238}U(n,f)$ and the total reaction rate was used for $^{238}U(n,\gamma)$ since the 14 MeV contribution is negligible in this case. The cross-section curves indicate a rapid degradation of secondary neutron energy in the inner part of the pile, followed by a much slower degradation beyond 20 cm from the target. For distances greater than 35 cm the cross-sections are approximately constant, showing that in this outer region the spectrum is in equilibrium. The sharp rise in the $^{235}U(n,f)$ cross-section at the pile edge is attributed to room-scattered low energy neutrons.

In the region of the equilibrium spectrum the neutron flux should be capable of representation by one group diffusion theory as though derived from a spherically symmetric central source. In this case the flux would be given by

$$\phi(r) = \frac{A}{r}\sinh\left(\frac{r_0 - r}{L}\right) \qquad (2)$$

where r_0 is the extrapolated radius of the pile, A is a constant and L is the diffusion length of the neutrons. Since the ^{239}Pu fission cross-section is approximately constant for the secondary neutrons, the non-14 MeV ^{239}Pu fission rate can be used as a measure of the secondary neutron flux and should be represented by equation (2). For the region beyond 30 cm a good representation is obtained using the values $L = 12{\cdot}6 \pm 1{\cdot}0$ cm and $r_0 = 55 \pm 2$ cm. Allowing for the uranium density the equivalent diffusion length for solid uranium would be $11{\cdot}0 \pm 1{\cdot}0$ cm which compares with the values of 12·5 cm in EBR I and Topsy, 11·9 cm in the Zephyr blanket and 10·0 cm in the ANL measurement (CODD *et al.*, 1956). Using the relation

$$L^2 = \tfrac{1}{3}\lambda_a\lambda_{tr}$$

and taking the absorption mean free path, λ_a, as that due to (n,γ) processes only, the transport mean free path, λ_{tr}, is 3·8 cm for the experimental system (density = 16·3 g/cm^3).

A useful measure of the hardness of the equilibrium spectrum is the ratio of ^{235}U/^{238}U fissions per atom. In the present experiments this ratio is 175 ± 12 which is close to the value of 180 ± 30 observed in the Zephyr blanket, although rather lower than other experimental values (CODD *et al.*, 1956).

9. EQUIVALENT SPHERICAL SYSTEMS

The way in which the reaction integrals vary with uranium thickness is most readily demonstrated by using the cylindrical pile results to derive reaction integrals for spherical systems of corresponding size. This was done by assuming that the reaction rate distributions measured in the horizontal plane of a cylinder are the same as those which would be observed in a sphere of the same radius as the cylinder. The reaction rate ratios $^{235}U(n,f)/^{239}Pu(n,f)$, $^{238}U(n,\gamma)/^{239}Pu(n,f)$ and $^{238}U(n,f)/^{239}Pu(n,f)$ for the secondary neutron flux were obtained as a function of radius from the 19·5 in. cylinder results and were used to determine the distributions for $^{235}U(n,f)$, $^{238}U(n,\gamma)$ and $^{238}U(n,f)$ in the smaller cylinders from their measured $^{239}Pu(n,f)$ distributions. The contributions from the 14 MeV flux were calculated from the flux distribution of equation (1) and the known cross-sections. Integration over a sphere of radius equal to the cylinder radius then gave the total reaction rates, and the construction of a neutron balance as in Table 4 enabled the total neutron leakage to be derived for each equivalent sphere. The results corrected to full density uranium are shown graphically in Fig. 11 together with the results of (1) for small spherical shells. There is thus established a complete representation of the reaction rate integrals and the leakage as a function of uranium thickness around a point source

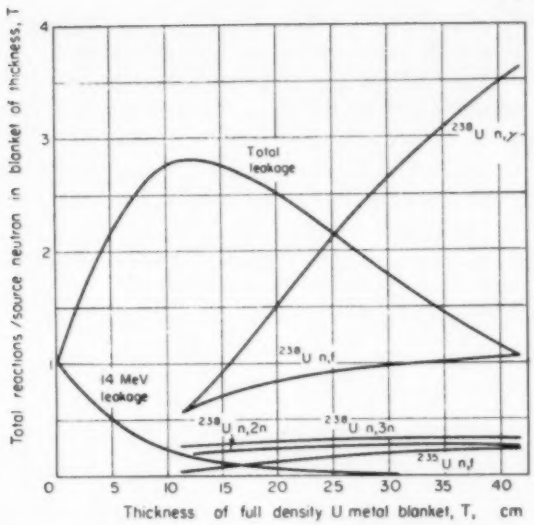

FIG. 11.—Total integrated neutron reactions and leakage per source neutron as a function of uranium blanket thickness. (Point 14 MeV central source and spherical geometry.) The curves for uranium thickness up to 11·3 cm are derived from (1).

of 14 MeV neutrons for thicknesses up to 42 cm. Neutron leakage rises at first as a result of multiplication by $(n,2n)$, $(n,3n)$ and fission processes, a peak is reached at about 12 cm and the leakage then steadily declines as the addition of more uranium absorbs the secondary neutrons. There is a corresponding steady rise in ^{239}Pu production. The $(n,2n)$ and $(n,3n)$ integrals do not increase much for uranium thicknesses greater than 10 cm. The ^{235}U fission integral rises steadily but is a relatively small contribution even for a 42 cm thickness.

The integrated 14 MeV neutron reactions are independent of the size of the source cavity within the sphere provided the source is located at the centre of the cavity and the actual uranium thickness is kept constant. To a first approximation this is also true of the integrated secondary neutron reactions. The above results can therefore be applied to make a preliminary assessment of the utilization of uranium in the design of blankets for thermonuclear DT reactors and this is discussed in the next section.

10. APPLICATION TO THE DESIGN OF A BLANKET FOR A THERMONUCLEAR REACTOR

It is well known that the DT reaction requires a lower temperature than the DD reaction for the useful production of thermonuclear power (POST, 1956). Therefore, although the DD system is the more attractive because of fuel availability, it is likely that the first fusion systems to yield useful energy will use the DT reaction. Since tritium is radioactive with a half-life of 12 years, it does not occur in nature to a significant extent. Thus a reactor operating on the DT reaction must regenerate its fuel from the 14 MeV neutrons produced in the fusion reactions themselves. This can conveniently be done by allowing the 14 MeV neutrons to interact with a suitable neutron multiplier such as uranium or beryllium, followed by absorption of the secondary neutrons in lithium. Although beryllium has the advantage of multiplication without the production of radioactivity, uranium has the advantage that in the process of multiplication there is a very large gain of energy due to fission. The present results show (Fig. 11) that, even for a fairly thin blanket of uranium, the fission energy released per 14 MeV neutron is many times larger than that derived from the original fusion reaction. A blanket thickness of 15 cm, for example, would generate 150 MeV of fission energy, release 2·8 secondary neutrons and produce 0·9 atoms of fission reactor fuel, ^{239}Pu, for each 14 MeV neutron produced in fusion. Allowing for losses in coolant and structural materials, at least 2 secondary neutrons could be absorbed in an outer blanket of lithium to produce tritium. A thicker uranium blanket, say 30 cm, would increase the fission energy to about 220 MeV, increase the ^{239}Pu production by a factor of 3 and reduce the leakage to 1·8. Since each 14 MeV source neutron represents an energy release in the fusion plasma of only 3·5 MeV, any uranium-blanketed fusion reactor would produce considerably more energy from ^{238}U fission than from DT fusion and the fusion reactor would act as a very high intensity neutron source driving a sub-critical fission system. If fusion technology were sufficiently advanced, such a fusion-fission system might compete with the fast fission reactor as a self-sufficient power generator burning ^{238}U and lithium, its most important advantage being the simplicity of design made possible by the absence of criticality hazards and reactivity balance requirements.

The fusion-fission system may provide a useful intermediate stage in the development of economic power from fusion alone since the efficiency required from the fusion generator for overall economy in this mixed system would not have to be so high. The fusion reactor might even be accepted as a nett absorber of energy, running at a temperature below the break-even temperature but being maintained, by energy feed-back from the blanket, at a sufficiently high temperature to act as a high efficiency neutron source. Taking the break-even temperature as 4 keV (POST, 1956), the system could, for example, be operated steadily at 2 keV if 16·5 MeV electrical energy per

VOL. 14 196

fusion reaction was fed back to the plasma from the blanket. The ratio of fission to fusion power in the system could be increased by moderating the neutrons in the outer region of the uranium so as to increase the ^{235}U fission rate at the expense of ^{239}Pu production. If these quantities were made equal for a system still yielding about 2 leakage neutrons, the fission power in the blanket would be doubled, and moderation of the leakage neutrons would also minimize the thickness of the outer lithium layer required for tritium production. Further experiments are now being carried out to study these combined systems.

Acknowledgments—This work was initiated by DR. K. W. ALLEN and MR. J. J. MCENHILL. Valuable assistance in the experimental work has been given by MRS. M. A. DUNCAN and MR. J. GRAY, and by members of the Radiochemistry Group who undertook the chemical separation and counting of ^{239}Np.

REFERENCES

ABSON W., SALMON P. G. and PYRAH S. (1958) The Design, Performance and Use of Fission Counters. *J. Brit. Nucl. Energy Conf.* 210.

ALLEN K. W., BOMYER P. and PERKIN J. L. (1961). This issue p. 100.

AVES R., BARNES D. and MACKENZIE R. B. (1954) *Fission Chambers for Neutron Detection.* AERE RP/R 1330 *J. Nucl. Energy* **1**, 110 (1954).

BENVENISTE J. and ZENGER J. (1954) *Information on the Neutrons Produced in the* $^3H(d,n)^4$ He *Reaction.* UCRL–4266.

CODD J., SHEPHERD L. R. and TAIT J. H. (1956) *The Physics of Fast Reactors.* Progress in Nuclear Energy, Series I, Vol. I.

COHEN A. V. (1961) *Total Inelastic Cross-Sections of Uranium in the Energy Range* 13 *to* 19 MeV *and Beryllium at* 14 MeV. To be published.

CRIPPS F. H. and WEALE J. W. (1958) *J. Inorg. Nucl. Chem.* **7**, 229.

HUGHES D. J. and SCHWARTZ R. B. (1958) *Neutron Cross-Sections* BNL–325, (2nd Ed.).

MCTAGGART M. H. (1959) Unpublished information.

MOAT A., MATHER D. and MCTAGGART M. H. (1961) *Some Experimental Determinations of the Number of Prompt Neutrons from Fission.* To be published.

PERKIN J. L. and COLEMAN R. F. (1961). This issue, p. 69.

POST R. F. (1956) *Rev. Mod. Phys.* **28**, 3, 338.

VASIL'EV I. A., ZAMYATNIN I. S., TOROPOV P. V. and FORMUSHKIN E. F. (1957) *Sov. J. Atomic Energy* **3**, 1430.

ZAMYATNIN Y. S., IVANOVA N. I. and SAFINA I. N. (1959) *J. Nucl. Energy* **9**, 194.

OL.
14
961

Reactor Science and Technology (Journal of Nuclear Energy, Parts A & B), 1961, Vol. 14, pp. 100 to 106. Pergamon Press Ltd. Printed in Northern Ireland

THE INTERACTION OF 14 MeV NEUTRONS WITH URANIUM

K. W. ALLEN, P. BOMYER and J. L. PERKIN
Atomic Weapons Research Establishment, Aldermaston, Berks.

(*Received* 5 *September* 1960)

Abstract—The multiplication of 14 MeV neutrons in uranium shells has been studied. The measurements lead to a value of η, the average number of neutrons produced per inelastic collision of a 14 MeV neutron, of $3{\cdot}30 \pm 0{\cdot}15$. Neutron interactions in a thick uranium shell have also been investigated and effective cross-sections for the reactions $^{238}U(n,f)$, $^{235}U(n,f)$ and $^{238}U(n,\gamma)$ have been obtained for the inelastic neutron spectrum in the shell.

The value of η, combined with other nuclear data, leads to the following cross-section data for ^{238}U for neutrons in the energy range 13·4 to 14·8 MeV.

$$1{\cdot}1 > \sigma_{n,3n} > 0{\cdot}8 \text{ barn}$$
$$0 < \sigma_{n,n'} < 0{\cdot}3 \text{ barn.}$$

1. INTRODUCTION

IN addition to elastic scattering, the interaction of 14 MeV neutrons with uranium can lead to fission, to the emission of two or three neutrons, or to re-emission of a single neutron with reduced energy. The radiative capture cross-section has been shown to be $\sim 3 \times 10^{-27}$ cm² (PERKIN, O'CONNOR and COLEMAN, 1958) and cross-sections for the emission of protons and α-particles will be greatly reduced by the potential barrier. Even in a direct interaction process (AUSTERN, BUTLER and MCMANUS, 1953) the cross-section for emission of a charged particle is unlikely to be greater than 10^{-25} cm². Thus for 14 MeV neutrons incident on uranium, fission and neutron emission are the most probable processes, and it is convenient to define a quantity η equal to the average number of neutrons released per inelastic collision of a 14 MeV neutron in uranium. It may easily be shown that

$$\eta = 1 + \frac{(\bar{\nu} - 1)\sigma_f + \sigma_{n,2n} + 2\sigma_{n,3n}}{\sigma_i} \qquad (1)$$

with $$\sigma_i = \sigma_f + \sigma_{n,n'} + \sigma_{n,2n} + \sigma_{n,3n}. \qquad (2)$$

If we surround a point source of 14 MeV neutrons with a thin shell of uranium then clearly

$$M = T + \eta(1 - T) \qquad (3)$$

where the neutron multiplication M is defined as the number of neutrons emerging from the shell per incident 14 MeV neutron and the transmission T is the fraction of neutrons emerging from the shell without having suffered an *inelastic* collision. The transmission of uranium shells has been measured with good accuracy by ALMQVIST and CLARKE (private communication), KIRKBRIDE and PAGE (private communication) and COHEN (1960). It is therefore possible to determine η directly by measuring M and T experimentally, and from the value of η it is possible to *deduce* the value of $\sigma_{n,n'}$ and $\sigma_{n,3n}$ using equations (1) and (2), since the other quantities have been determined experimentally.

Measurements of 14 MeV neutron cross-sections by this method were first reported by GRAVES and DAVIS (1955) for a number of non-fissile elements. Similar measurements for uranium have also been reported recently by LEBEDEV *et al.* (1959). Multiplication measurements with uranium shells were begun at Harwell in 1954 (POOLE, private communication) and are in fair agreement with the measurements reported in this paper.

In addition to multiplication measurements with uranium shells of various sizes and thickness, we have carried out a detailed study of the neutron processes taking place within a thick shell of uranium in which 83 per cent of the 14 MeV neutrons emerging from a central source suffered inelastic collisions. By combining these measurements with the neutron multiplication of the shell, it was possible to write down a neutron balance equation in which η was the only unknown quantity. The value of η obtained in this way agreed within experimental error with the value obtained from the thin shell experiments and indicates a large cross-section for the $^{238}U(n, 3n)^{236}U$ reaction at 14 MeV.

2. MEASUREMENT OF MULTIPLICATION

2.1. *Target assembly*

14 MeV neutrons were produced by bombarding a thick zirconium tritide target with 160 keV deuterons.

VOL
14
196

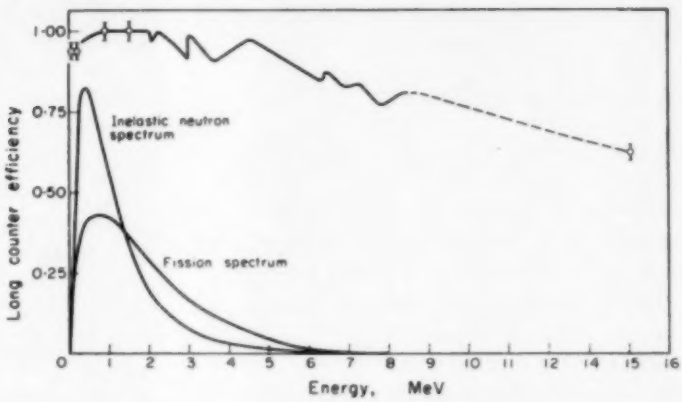

FIG. 1.—Long counter efficiency as a function of neutron energy. The inelastic neutron spectrum is taken from VASIL'EV *et al.* (1957) and ZAMYATNIN *et al.* (1959) and the fission spectrum from CRANBERG *et al.* (1956).

The neutron yield was determined absolutely by counting the associated α-particles with a proportional counter at 135° to the direction of the deuteron beam. The target assembly was constructed from thin walled brass tubes to minimize neutron scattering and the target was air cooled. Small corrections (~2 per cent) were necessary for the interaction of the 14 MeV neutrons with the 0·020 in. tungsten target backing and with the brass target assembly. The target was 6 ft above the concrete floor of the laboratory with at least 9 ft clearance in all other directions.

2.2. *Counters*

Neutrons were counted with a long counter assembly similar to that of HANSON and MCKIBBEN (1947). In their multiplication experiments with 14 MeV neutrons, GRAVES and DAVIS (1955) used a long counter which has been modified so that the sensitivity for 14 MeV neutrons was the same as for fission neutrons. This was achieved by withdrawing the BF_3 counter further back into the paraffin wax, and necessarily involved some loss in sensitivity for low energy neutrons. As it is known for heavy elements in general (GRAVES and ROSEN, 1953) and for uranium in particular (VASIL'EV *et al.*, 1957; ZAMYATNIN *et al.*, 1959) that the majority of the inelastic neutrons have energies less than ~4 MeV, it was decided to use unmodified counters in the present experiments because of their more uniform response to the lower energy neutrons. A correction was made for the reduced sensitivity to 14 MeV neutrons. For a *thin* shell we can therefore write

$$M_a = T + \eta k(1 - T) \qquad (4)$$

where M_a is the *apparent* multiplication and k is the ratio of the sensitivity of the counter for the inelastic neutrons relative to its sensitivity for 14 MeV neutrons.

The long counter used in the present experiments is that described by MCTAGGART (1959) and its relative response to neutrons of different energies is shown in Fig. 1 and Table 1. In Fig. 1, the solid line in the energy range 1·2 to 9 MeV was taken from the work of HADDAN, PERRY and SMITH at Los Alamos, who obtained the relative response of a long counter for monokinetic neutrons by standardization against a proton recoil counter. The Los Alamos counter was very similar to the Aldermaston counter, and used a 1 in. diameter BF_3 tube. The Los Alamos curve was normalized to unity and to the Aldermaston calibration points in the neighbourhood of 1 MeV.

In order to determine the constant k, it was necessary to measure the ratio of the sensitivity for 14 MeV neutrons to that for the inelastic neutrons from uranium. The sensitivity of the long counter for this spectrum, relative to a fission spectrum, was computed to be 0·998 ± 0·002 from the response curve of Fig. 1. The absolute sensitivity of the counter to fission neutrons was found by means of a mock fission source which had been compared directly with the A.E.R.E. standard fission neutron source (RICHMOND, 1958). The absolute sensitivity at 14 MeV was found in the usual way by counting the associated α-particles from the D + T reaction.

2.3. *Experimental procedure*

The dimensions of the uranium shells used are recorded in Table 2. All the shells were fabricated in the form of interlocking hemispherical pairs and were held in position by a light tubular support. For a long counter 100 cm from the target assembly, the effective scattering by the support was found to be about 2·5 per cent for 14 MeV neutrons and 3 per cent for fission neutrons.

The bombardment of any solid material by deuterons always results in the production of D + D neutrons from collisions between the deuterons in the beam and deuterium atoms held in the material and arising from the beam itself. By careful design of the

TABLE 1.—RELATIVE ENERGY SENSITIVITY OF THE LONG COUNTER

Energy	24 keV	220 keV	830 keV	Mock fission	14 MeV
Relative response	0·944 ± 0·025	0·940 ± 0·025	1·00 ± 0·025	1·00	0·63 ± 0·025

target assembly, the correction due to D + D neutrons was less than 0·5 per cent for the thin shell measurements, but amounted to 3·4 per cent for the thick shell. The D + D neutrons were produced where the beam struck defining apertures some distance from the target and did not multiply significantly in the shell. An early design of target assembly was used for the thick shell measurements; a better design would have reduced the correction for D + D neutrons.

A series of multiplications runs were carried out for each shell. A typical run included three measurements:

(a) neutron count with the bare target,
(b) neutron count with the shell in position,
(c) neutron count with a standardized mock fission source very close to the zirconium tritide target.

(a) and (b) were carried out with 14 MeV neutrons and (a) served to standardize the counter for these neutrons; (c) served as a calibration *in situ* for fission neutrons. Measurements were carried out with counters at various distances from the target and at angles of 0°, 45°, 90° and 135° to the beam direction. The experimental multiplication M_e was calculated from the expression

$$M_e = T + \frac{R(0) - T}{k} \cdot \frac{c_0(\theta)}{\bar{c}_0} .$$

T is the transmission of the shell, assumed independent of energy and calculated as described below; $R(\theta)$ is the ratio of the normalized counting rate with the shell in position to the normalized counting rate without the shell; k is the ratio of the counter sensitivity to fission neutrons to that for 14 MeV neutrons (as shown in Section 2.2, the sensitivity of the counter to inelastic neutrons from uranium is not significantly different from its sensitivity to fission neutrons); $c_0(\theta)/\bar{c}_0$ is a factor to take account of the angular distribution of 14 MeV neutrons and is approximately the ratio of the 14 MeV neutron intensity at an angle θ to the intensity at 90°. The angular distribution of the neutrons is isotropic in the centre of mass system and therefore slightly anisotropic in the laboratory system at the bombarding energy of 160 keV used in these experiments.

TABLE 2.—DIMENSIONS OF URANIUM SHELLS USED IN THE MULTIPLICATION EXPERIMENTS

Shell No.	Inner radius (cm)	Outer radius (cm)	Thickness (cm)
1	11·93	12·70	0·77
2	5·85	7·88	2·03
3	5·85	9·91	4·06
4	4·44	15·75	11·31

TABLE 3(a).—THE EXPERIMENTAL MULTIPLICATION AS A FUNCTION OF THE ANGULAR POSITION OF THE LONG COUNTER WITH RESPECT TO THE DEUTERON BEAM

$\theta°$	0	45	90	135
M_e	1·570	1·566	1·585	1·553

TABLE 3(b).—THE EXPERIMENTAL MULTIPLICATION AS A FUNCTION OF THE DISTANCE OF THE LONG COUNTER FROM THE NEUTRON SOURCE FOR A FIXED ANGULAR POSITION

Distance (cm)	65·2	93·1	103·2	132·1
M_e	1·542	1·561	1·566	1·566

The transmissions of the shells were calculated from the measured densities and the values of σ_i and σ_{el}, the elastic transport cross-section, using the procedure of BETHE, BEYSTER and CARTER (1956). σ_{el} was estimated to be 0·51 barn from an optical model calculation. The total inelastic cross-section of uranium, σ_i, was taken to be 2·89 ± 0·05 barns (COHEN, 1960).

A typical set of results for one shell are recorded in Table 3, and a summary of all the multiplication measurements is presented in Table 4. In order to show the degree of internal consistency, the measurements are quoted to more significant figures than the absolute accuracy of the counter calibration justifies.

Also recorded in Table 4 are the values of $\eta_e = (M_e - T)/(1 - T)$. The quantity η_e only becomes equal to η for very thin shells, and the very weak dependence of η on T must mean that over quite a range of shell thicknesses, the net number of neutrons produced by interactions of the *inelastic* neutrons must be zero. The measurements reported on Sections 3.1 and 3.4 show that the cross-sections for fission and capture in ^{238}U by the inelastic neutrons are about 50 mb and about 150 mb respectively. The corresponding mean free path for an inelastic interaction is therefore about 100 cm, so that the probability of a collision resulting in capture or fission is quite small, even allowing for the large transport cross-section of the inelastic neutrons. Since the two effects act in opposite

TABLE 4.—SUMMARY OF MULTIPLICATION RESULTS

Shell No.	Thickness (cm)	T	M_e	η_e
1	0·77	0·905	1·224	3·36
2	2·03	0·752	1·568	3·29
3	4·06	0·557	1·990	3·24
4	11·31	0·171	2·809	3·18

directions, the overall change in the neutron multiplication is very small.

The value of η_e obtained from the thin shells must therefore be very close to the value of η, and allowing for uncertainties in M and T we find, using the three thinner shells,

$$\eta = 3{\cdot}29 \pm 0{\cdot}15. \qquad (5)$$

Finally, a small correction (about 1 per cent) is necessary for the ^{235}U content of the uranium but has not been made to the results quoted here. A value of η from the thick shell measurements is reported in Section 3.5.

3. NEUTRON INTERACTIONS IN THE THICK SHELL

In order to investigate directly the secondary neutron processes occurring in uranium, a probe channel 0·25 inch in diameter was cut through the thick shell. A section through the shell is shown in Fig. 4.

In describing the processes which occur within the shell, it is convenient to divide the neutrons into a 14 MeV group and an inelastic group. This is a reasonable assumption because it is known that there are very few inelastic neutrons with energies greater than about 4 MeV. Quantities referring to 14 MeV neutrons will bear the subscript 0 and those referring to inelastic neutrons the subscript i. We may then express the neutron multiplication of the shell as follows:

$$M = 1 + F_0^{238}(\bar{\nu}_0^{238} - 1) + F_0^{235}(\bar{\nu}_0^{235} - 1) + P_0^{238} + 2Q_0^{238} + F_i(\bar{\nu}_i^{238} - 1) + F_i^{235}(\bar{\nu}_i^{235} - 1) + P_i^{238} - C_i^{238}$$

F, P, Q and C refer respectively to the number of reactions of type (n,f), $(n,2n)$, $(n,3n)$ and (n,γ) occurring in the shell per 14 MeV neutron emitted from the central source. In the above equation, $(n,2n)$ and $(n,3n)$ processes in ^{235}U have been ignored. This is justified within the experimental error of the measurements.

We may also write

$$M = M_0 + F_i^{238}(\bar{\nu}_i^{238} - 1) + F_i^{235}(\bar{\nu}_i^{235} - 1) + P_i^{238} - C_i^{238} \qquad (6)$$

where M_0 is the equivalent thin shell multiplication, i.e. the multiplication that would be measured if all the secondary neutrons escaped without interacting. η is then related to M_0 by the equation

$$\eta = \frac{M_0 - T}{1 - T} \qquad \text{as before.} \qquad (7)$$

With the exception of M_0, all the quantities in (5) are either known constants or can be measured experimentally. Thus M_0 and η may be calculated.

3.1. *Measurement of fission yields*

To measure the fission yields, small fission chambers containing ^{235}U, ^{239}Pu and natural uranium were introduced into the probe channel. The chambers were similar to those developed for measurements with the zero energy fast reactor Zephyr at A.E.R.E. (AVES *et al.*, 1954). Their external diameter was 0·25 in. and the active lengths varied between 0·4 in. and 0·8 in. The fission rates were referred to the 14 MeV neutron source strength by counting the associated α-particles from the D + T reaction in the usual way.

The effective mass of fissile material in the chambers was measured by irradiating the chambers in a known 14 MeV neutron flux and counting fission pulses above a fixed bias. The same bias was used when counting fissions in the uranium shell and, as the 14 MeV fission cross-sections are known accurately for the materials used, (MOAT, unpublished) it was possible to determine fission yields in the shell per unit mass of material in the chamber.

Fig. 2 shows the fission yield in ^{238}U, normalized as described above, as a function of distance from the centre of the shell. Curve (a) is the total fission yield. Curve (b) is the fission yield due to 14 MeV neutrons. It was calculated from the 14 MeV neutron flux in the shell measured with a calibrated copper threshold detector as described in Section 3.2 and assuming a 14 MeV fission cross-section of 1·13 ± 0·02 barns (MOAT, unpublished). Curve (c) is the difference between curve (a) and curve (b) and is therefore the fission yield in ^{238}U due to the inelastic neutrons. Similar curves were obtained with the ^{235}U and ^{239}Pu fission chambers.

TABLE 5

	^{238}U	^{235}U
14 MeV fissions per source neutron	0·324	0·0043
Inelastic neutron fissions per source neutron	0·249	0·0349
Totals	0·573	0·0392

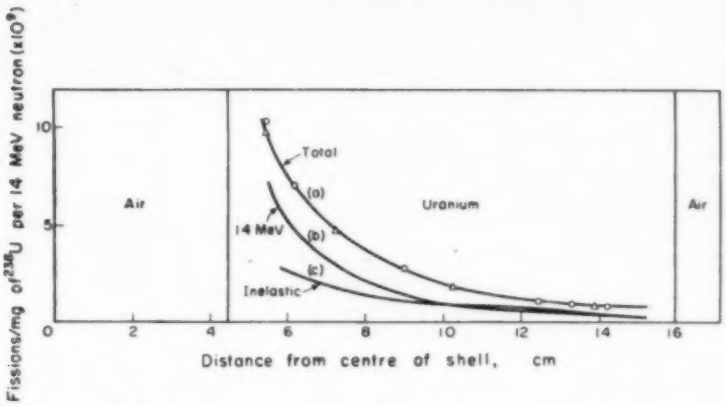

FIG. 2.—Fission yields in the thick uranium shell. The upper curve (a) is the total fission yield, curve (b) is that due to 14 MeV neutrons and curve (c), obtained by difference, is the fission yield due to the inelastic neutrons.

The yields of 14 MeV fissions and inelastic neutron fissions of ^{238}U and ^{235}U can be found by integration of the fission vs. radius curves and the results are exhibited in Table 5. It is seen that most of the fissions in ^{235}U are due to inelastic neutrons, whereas in ^{238}U there are about equal numbers of inelastic and 14 MeV fissions. Although natural uranium contains only 0·7 per cent of ^{235}U, 7 per cent of the total fissions occurred in that isotope.

The fast fission cross-section of ^{239}Pu is fairly energy independent in the energy region 0·1 to 5 MeV (HUGHES and HARVEY, 1955). If we assume the average cross-section in this region is 1·81 barns (obtaining by averaging over the inelastic neutron spectrum), we can calculate the effective fission cross-sections of ^{238}U and ^{235}U for the inelastic neutron spectrum in different parts of the shell. These cross-sections are plotted in Fig. 3, and it is seen that their variation with position in the shell is quite small. The maximum value of σ_f for ^{238}U, 74 mb, is considerably less than the value of 0·305 $\pm$ 0·005 barn obtained for an unmoderated fission spectrum (LEACHMAN and SCHMITT, 1957).

Using Zephyr data (HOLMES *et al.*, 1956), values of the effective ^{238}U$(n, \gamma)^{239}$U cross-section can be obtained corresponding to the values of σ_f for ^{238}U. Integration throughout the shell using these values leads to a yield of 0·58 $\pm$ 0·15 atom of ^{239}U per 14 MeV neutron, and this is the value used in the calculation of η from the thick shell measurements (Section 3.4.).

3.2. *Measurement of the fast neutron flux in the shell*

The ^{63}Cu$(n, 2n)^{62}$Cu reaction with a threshold of 11·1 MeV was used to measure the variation of the 14 MeV component of the neutron flux, in the shell. Copper cylinders 1 cm long and 0·25 inch in diameter were placed at various points along the length of the probe hole in the thick shell and natural uranium cylinders were used as spacers.

After a 10 min irradiation, the copper cylinders were removed and placed in turn in a sodium iodide crystal scintillation counter. The 0·51 MeV annihilation quanta originating from the positron decay of ^{62}Cu (half-life 9·9 min) were counted with a single channel pulse height analyser and a scaler. The

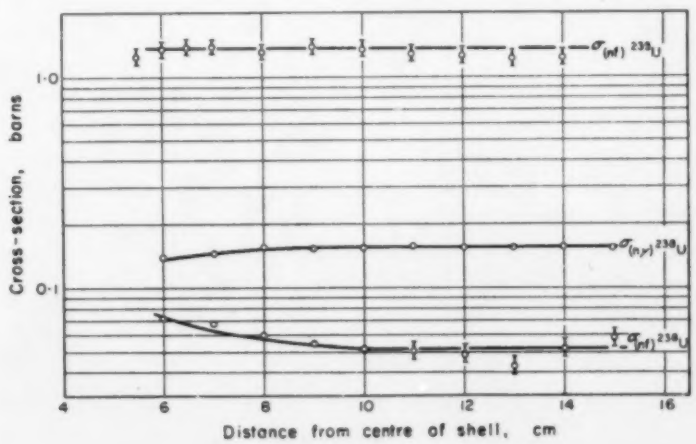

FIG. 3.—Effective cross-sections for fission and capture derived for the inelastic spectrum in the thick shell.

cylinders were counted in sequence and the counting rates for each cylinder were extrapolated back to a time corresponding to the end of the irradiation. Corrections were made for background and for counts due to positrons originating from the $^{65}Cu(n, 2n)^{64}Cu$ reaction (half-life 12·8 hours).

The result of such an irradiation is shown in Fig. 4. The points are normalized to the central position in the probe channel, i.e. at the point closest to the D + T neutron source. The asymmetry of the activation curve is due to the higher neutron yield and energy in the forward hemisphere. Using the Los Alamos results (FOWLER and SLYE, 1950; BROLLEY, FOWLER and SCHLACKS, 1952) for the variation of the cross-section of the $^{63}Cu(n, 2n)^{62}Cu$ reaction with neutron energy, and correcting for the variation of the neutron yield and energy with angle, all the results were normalized to the yield and energy of the neutrons at 45°. The validity of these corrections is evident in Fig. 4 where points from both ends of the probe channel are satisfied by a common curve (dashed curve in Fig. 4).

To obtain the absolute neutron flux, a copper cylinder was irradiated at the normalizing position in the absence of the uranium shell. The activity measured was related to the neutron flux at that point by noting the distance between the cylinder and the target, and by measuring the neutron output in the usual way by counting the associated α-particles from the D + T reaction.

3.3. *Yield of* ^{237}U

The yield of ^{237}U from the reaction $^{238}U(n, 2n)^{237}U$, which has a threshold of 5·99 MeV, arises principally from the 14 MeV neutron component in the shell. Taking a value of 0·69 ± 0·04 barn for $\sigma_{n,2n}$ for neutrons of energy 14·5 MeV, the energy for which the copper detector results were normalized, the yield of ^{237}U from the fast neutron component was found to be 0·19 ± 0·01 atom per 14 MeV neutron emitted from the central source.

A small contribution to the ^{237}U yield, estimated to be about 0·02, came from the tail of the inelastic neutron spectrum in the shell. Thus the total yield of ^{237}U per 14 MeV neutron emitted from the source was

$$P = P_0 + P_i = 0{\cdot}19 + 0{\cdot}02 = 0{\cdot}21 \pm 0{\cdot}01.$$

3.4. *Value of* η *from the thick shell*

From equation (6)

$$M = M_0 + F_i(\bar{\nu}^{238} - 1) + F_i^{235}(\bar{\nu}_i^{235} - 1) + P_i^{238} - C_i.$$

Taking $\bar{\nu}_i^{238} = 2{\cdot}57 \pm 0{\cdot}09$ (TERRELL, 1957* for 1·5 MeV neutrons) and $\bar{\nu}_i^{235} = 2{\cdot}39 \pm 0{\cdot}05$ (MOAT *et al.*, 1960 for 75 keV neutrons), we find $M_0 = 2{\cdot}93$.

Using (7), this leads to $\eta = 3{\cdot}33 \pm 0{\cdot}18$.

4. DISCUSSION

The values of η obtained from the thin shells and the thick shell agree very closely and we take the best value to be

$$\eta = 3{\cdot}30 \pm 0{\cdot}15.$$

Using equation (1) with $\sigma_{n,2n} = 0{\cdot}69 \pm 0{\cdot}04$ (PERKIN *et al.*, 1960), $\sigma_i = 2{\cdot}89 \pm 0{\cdot}05$ (COHEN, 1960), $\bar{\nu}$ (14 MeV) = 4·44 ± 0·12, (MOAT *et al.*, 1960) and $\sigma_f = 1{\cdot}13 \pm 0{\cdot}02$ (MOAT, unpublished) we have

$$3{\cdot}30 \pm 0{\cdot}15 = 1 + \frac{(3{\cdot}44 \pm 0{\cdot}12) \times (1{\cdot}13 \pm 0{\cdot}02) + 0{\cdot}69 \pm 0{\cdot}04 + 2\sigma_{n,3n}}{2{\cdot}89 \pm 0{\cdot}05}$$

which leads to $\sigma_{n,3n} = 1{\cdot}03 \pm 0{\cdot}25$ barns.
Taking account of equation (2), we find

$$1{\cdot}1 \geqslant \sigma_{n,3n} \geqslant 0{\cdot}8 \text{ barn}$$

$$0 \leqslant \sigma_{n,n'} \leqslant 0{\cdot}3 \text{ barn}.$$

* TERRELL quotes $\bar{\nu} = 2{\cdot}65 \pm 0{\cdot}09$ relative to $\bar{\nu}(^{235}U) = 2{\cdot}47 \pm 0{\cdot}03$. For consistency we have taken $\nu = 2{\cdot}57$ corresponding to $(\bar{\nu}^{235}U) = 2{\cdot}39$.

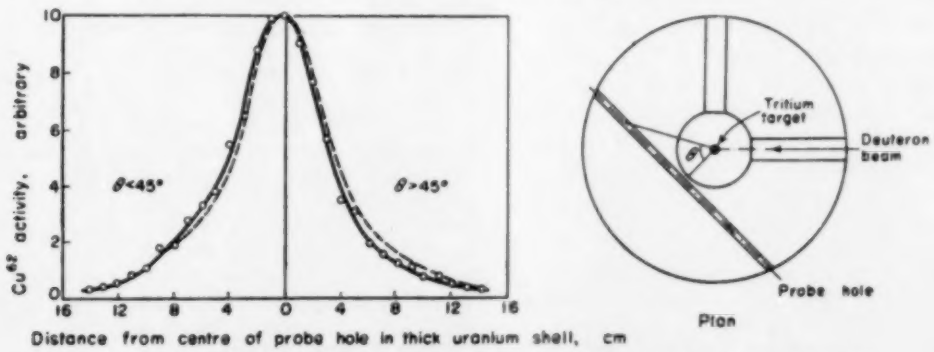

FIG. 4.—The ^{62}Cu activity from a small irradiated Cu cylinder at various distances from the centre of the probe canal. After correction for variation of neutron energy and intensity with angle, the dashed curve is obtained. The experimental arrangement is also shown.

It must be remembered that the value deduced here for $\sigma_{n,3n}$ represents an average over the neutron energy range 13·4 to 14·8 MeV. This is the energy spread in the D + T neutrons from a thick target bombarded by 160 keV deuterons. The $(n, 2n)$ and $(n, 3n)$ cross-sections are expected to vary rapidly with energy in this range, although their sum should be approximately constant.

The value of η reported here is rather higher than the value of $2{\cdot}8 \pm 0{\cdot}25$ reported by LEBEDEV *et al.* (1959). Part of the discrepancy may be due to the fact that the Russian workers made a 6 per cent correction for interactions of secondary neutrons in their uranium shell. According to the measurements reported here with shells of different thicknesses, this correction seems to be rather large.

In the interpretation of our multiplication measurements, we have taken a total inelastic cross-section of $2{\cdot}89 \pm 0{\cdot}05$ barns (COHEN, 1960). This value agrees well with unpublished Chalk River work (ALMQVIST and CLARKE, private communication) and with the result of LEBEDEV *et al.* (1959), but is rather higher than a Los Alamos value of $2{\cdot}74 \pm 0{\cdot}04$ barns quoted by COON *et al.* (1958). Use of this lower value for σ_i would not significantly change the range of values within which $\sigma_{n,n'}$ must lie, but it would lower $\sigma_{n,3n}$.

Since the binding energy of a neutron in ^{238}U is 5·99 MeV, neutrons resulting from the (n, n') process alone must have energies in excess of 8 MeV. Many of these would have been detected in the Los Alamos measurements (see GRAVES and DAVIS (1955) for an account of the experimental technique), so that the value of $2{\cdot}74 \pm 0{\cdot}04$ barns is probably more nearly representative of $\sigma_i - \sigma_{n,n'}$ than of σ_i. A value of $\sigma_{n,n'}$ in the range 0·15 to 0·2 barn would be in agreement with data on this process for other heavy elements (COON *et al.*, 1958; ROSEN and STEWART, 1957) and also with a calculation based on the direct interaction theory of BROWN and MUIRHEAD (1957), which gives a value of 0·14 barn for $\sigma_{n,n'}$ at 14 MeV.

Thus the interpretation of the multiplication measurements would appear to be in general accord with all known data on the interaction of 14 MeV neutrons with uranium. Further detailed studies of the neutron economy involving the use of larger quantities of uranium are reported in the accompanying paper by WEALE *et al.* (1960).

Acknowledgments—It is a pleasure to acknowledge our indebtedness to many of our colleagues for much helpful discussion. In particular we should like to thank MR. J. J. MCENHILL for much assistance in the early stages of this work, MR. M. H. MCTAGGART (Aldermaston) DR. R. A. NOBLES (Los Alamos), DR. W. D. ALLEN and DR. A. T. G. FERGUSON (Harwell) for communication and discussion in advance of publication of their work on the long counter, and MR. A. MOAT and DR. A. V. COHEN for allowing us to use some of their unpublished data. We are also grateful to DR. M. J. POOLE for making available the results obtained by his group at Harwell, and to DRS. ALMQVIST and CLARKE of Chalk River for information on relevant Canadian experiments. We also wish to thank DR. S. C. CURRAN, F.R.S., for his support and interest in these experiments and for many helpful discussions.

The co-operation and technical assistance of MR. D. AKERS and MR. J. PROSSER have been invaluable to us throughout the course of this work.

REFERENCES

ALMQVIST E. and CLARKE L. R. (1958) Private communication.
AUSTERN N.; BUTLER S. T. and MCMANUS H. (1953) *Phys. Rev.* **92,** 3 50.
AVES R., BARNES D. and MCKENZIE R. B. (1954) *J. Nucl. Energy* **1,** 110.
BETHE H. A., BEYSTER J. R. and CARTER R. E. (1956) *J. Nucl. Energy* **3,** 273.
BROLLEY J. E., FOWLER J. L. and SCHLACKS L. K (1952) *Phys. Rev.* **88,** 618.
BROWN G. E. and MUIRHEAD H. (1957) *Phil. Mag.* (8th series) **2,** 473.
COON J. H., DAVIS R. W., FELTHAUSER H. E. and NICODEMUS D. B. (1958) *Phys. Rev.* **111,** 250.
CRANBERG L., FRYE G., NERESON N. and ROSEN L. (1956) *Phys. Rev.* **103,** 662.
COHEN A. V. (1961) Total Inelastic Cross-sections of Uranium in the Energy Range 13 to 19 MeV and Beryllium at 14 MeV. *J. Nucl. Energy*. To be published.
FOWLER J. L. and SLYE J. M. (1950). *Phys. Rev.* **7,** 787.
GRAVES E. R. and DAVIS R. W. (1955) *Phys. Rev.* **97,** 1205.
GRAVES E. R. and ROSEN L. (1953). *Phys. Rev.* **89,** 343.
HANSON A. O. and MCKIBBEN J. L. (1947) *Phys. Rev.* **72,** 673.
HOLMES J. E. R., CURRY M. U. and WALDEGRAVE M. (1956) *Neutron Distribution in the Air-Spaced Core Assembly of Zephyr* A.E.R.E. R/R 1949.
KIRKBRIDE J. and PAGE D. I. (1956) Private communication.
LEACHMAN R. B. and SCHMITT H. W. (1957). *J. Nucl. Energy* **4,** 38.
LEBEDEV P. P., ZISIN IU. A., KLINTSON IU. S. and STSIBORSKII B. D. (1959) *J. Nucl. Energy* Part A: *Reactor Science* **11,** 39.
MCTAGGART M. H. (1959). *A Study of the Neutron Long Counter.* A.W.R.E. Report NR/A–1/59.
MOAT A. *Fission Cross-Section for* 14 MeV *Neutrons.* To be published. (Privately circulated).
MOAT A., MATHER D. and MCTAGGART M. H. (1960). Some Experimental Determinations of the Number of Prompt Neutrons from Fission. *J. Nucl. Energy*. To be published.
PERKIN J. L., O'CONNOR L. P. and COLEMAN R. F. (1958) *Proc. Phys. Soc. Lond.* **A 72,** 505.
POOLE M. J. (1956) Private communication.
RICHMOND R. (1958) *The Standardization of Neutron Sources.* Progress in Nuclear Energy, Series I. Physics and Mathematics, p. 165.
ROSEN L. and STEWART L. (1957) *Phys. Rev.* **107, 824.**
TERRELL J. (1957) *Phys. Rev.* **108,** 783.
VASIL'EV I. A., ZAMYATNIN Y. S., TOROPOV P. V. and FOMUSHKIN E. F. (1957) *Sov. J. Atomic Energy* **3,** 1430.
WEALE J. W., GOODFELLOW H., MCTAGGART M. H. and MULLENDER M. (1961) This issue, p. 91.
ZAMYATNIN Y. S., IVANOVA N. I. and SAFINA I. N. (1959) *J. Nucl. Energy* **9,** 194.

VOL. 14 196

Reactor Science and Technology (Journal of Nuclear Energy, Parts A & B), 1961, Vol. 14, pp. 107 to 116. Pergamon Press Ltd. Printed in Northern Ireland

THE EFFECT OF INTERNAL STRESSES DUE TO IRRADIATION GROWTH AND THERMAL CYCLING ON THE CREEP OF URANIUM, IN THE CASES OF BOTH ELASTIC AND PLASTIC BEHAVIOUR

W. S. BLACKBURN
C. A. Parsons and Co. Ltd., Fossway, Newcastle-upon-Tyne

(*Received* 3 *October* 1960)

Abstract—Theories are developed to derive differential equations from which the effect of irradiation growth and uniform continuous thermal cycling on the creep of uranium under applied uniaxial stress may be determined when the material remains elastic. Two alternative assumptions are made of uniform deformation and of uniform internal stress in the uranium crystals.

Solutions are obtained in several cases and an approximate method is presented which applies over a large range if primary creep effects are neglected. Over this range, tables are deduced from which it may be seen how the internal stress at any temperature increases with the irradiation growth and the mean temperature deviation of the cycle, while remaining independent of its period. The way is shown in which the logarithm of the creep acceleration factor varies as the logarithm of the ratio of internal to applied stress decreases, decreasing initially linearly and subsequently more slowly.

The creep rate under a uniaxial load has also been deduced when the material has become plastic due to irradiation growth or to a constant rate of change of temperature and, also, if the applied stress is small, when it is plastic due to thermal cycling and irradiation growth acting simultaneously.

Satisfactory agreement with experiment is found for the results in both the elastic and plastic ranges.

VOL. 14 961

1. INTRODUCTION

PREVIOUS work by the present author has dealt with the separate effects of internal stresses caused by uniform continuous thermal cycling and irradiation growth on the creep of uranium under a uniaxial load when the material does not become plastic. This theory is summarized and extended in Section 2. Equations, figures and tables are quoted from BLACKBURN (1960) and BLACKBURN, HARNBY and STOBO (1960) but are given new numbers for this report, the source being indicated. Equations have the original number and report reference in brackets after the new number.

Theories to be applied when the internal stresses in uranium are sufficiently high to cause plastic flow, have been presented by ANDERSON and BISHOP (1957); YOUNG, GARDINER and ROTSEY (1960). That of ANDERSON and BISHOP (1957) is extended in Section 3. It is assumed throughout that the yield point is sharp with no work hardening, and that both the yield point and Young's modulus may be treated as independent of the temperature. It is further assumed that the material is either completely elastic or completely plastic at any time.

2. THEORY WHEN INTERNAL STRESS IS IN THE ELASTIC RANGE

To calculate the deformation of an aggregate of non-isotropic crystals from their individual properties, assumptions must be made unless the orientation and location of each crystal is known. For simplicity we assume each crystal to undergo a homogeneous deformation. In general this prohibits the continuity of both stresses and displacements between the crystals. We require however, for static equilibrium, that the mean components of stress and displacement over the crystal orientations should equal the corresponding components of any applied stress and displacement. Another assumption is also necessary. The simplest is that the stress is uniform (i.e. the same throughout all crystals); this however leads to the conclusion that the creep rate is the same under temperature variations as it would be if the temperature were maintained at its instantaneous value, in contradiction to the experimental evidence. An alternative assumption is that the deformation is uniform, while yet another possibility is that the stress components are the sum of those of the applied stress and of an internal stress which is independent of the applied stress and uniform with respect to the crystal axes. Both of these assumptions are developed below. The former is probably more realistic and leads to results in better agreement with experiment, but the latter can be developed further and leads to simpler computations, in particular when irradiation growth is important.

We consider the equation relating the strain rate of an elementary particle under a homogeneous deformation to the stress, stress rate, rate of irradiation

growth, change of thermal expansion, and stress rate history. The following equation is assumed:

$$\frac{d\epsilon_{ij}}{dt} = \frac{d(\alpha_{ij}T)}{dt} + \frac{d}{dt}\left\{F\left(\tau_{ij} - \frac{\nu\sum_k \tau_{kk}\delta_{ij}}{1+\nu}\right)\right\} + \left[\frac{3}{2}\right]^{(n+1)/2} \times Ce^{-B/T}\cdot\sigma_{ij}J^{n-1} + \gamma_{ij} + \int_0^t Ke^{\kappa(\tau-t)}\frac{d\sigma_{ij}}{d\tau}\,d\tau \quad (1)$$

[(1), BLACKBURN, HARNBY and STOBO (1960)].

The second term denotes the derivative of a stress/strain relationship in which Poisson's ratio is constant but Young's modulus is stress-dependent. The third term is conventionally used to approximate secondary creep. The final term, representing a delayed elastic response under varying stress, is the simplest of the appropriate form but may be generalized if necessary to fit experimental data.

By adding the three equations for the normal strain rates, we obtain separate equations for the rate of change of volume and hence for the rates of change of strain deviation in terms of the rates of change of stress deviation and its derivatives. It is found that under continuous thermal cycling, neither this cycling nor any irradiation growth occurring with it make an appreciable net change in volume for randomly orientated aggregates not near the yield stress. Hence we are primarily interested in the rate of strain deviation along the axis of the load. By symmetry, the other rates of normal strain deviation equal $-\frac{1}{2}$ of this.

2.1 *Assumption of uniform deformation due to thermal cycling and irradiation growth*

If uniform deformation is assumed and the initial conditions are known, we require only one equation in addition to

$$\frac{d(F\sigma_{33})}{dt} = \frac{d\epsilon}{dt} - \int_0^t Ke^{\kappa(\tau-t)}\frac{d\sigma_{33}}{d\tau}\,d\tau - \left[\frac{3}{2}\right]^{(n+1)/2} \times Ce^{-B/T}\cdot\sigma_{33}J^{n-1} + \frac{d}{dt}\left\{T(\alpha^*_{bb}\sin^2\theta + \alpha^*_{aa}\cos^2\theta\cos^2\psi + \alpha^*_{cc}\cos^2\theta\sin^2\psi)\right\} + \gamma(\cos^2\psi\cos^2\theta - \sin^2\theta),$$

$$\frac{d(F\sigma_{11})}{dt} = \frac{d}{dt}\left\{T(\alpha^*_{bb}\cos^2\theta + \alpha^*_{aa}\cos^2\psi\sin^2\theta + \alpha^*_{cc}\sin^2\psi\sin^2\theta)\right\} - \frac{1}{2}\frac{d\epsilon}{dt} - \int_0^t Ke^{\kappa(\tau-t)}\frac{d\sigma_{11}}{d\tau}\,d\tau - \left[\frac{3}{2}\right]^{(n+1)/2} \times Ce^{-B/T}\cdot\sigma_{11}J^{n-1} + \gamma(\cos^2\psi\sin^2\theta - \cos^2\theta),$$

$$\frac{d(F\sigma_{13})}{dt} = \frac{d}{dt}\left\{T(\alpha^*_{bb} - \alpha^*_{aa}\cos^2\psi - \alpha^*_{cc}\sin^2\psi)\right\} \times \cos\theta\sin\theta - \int_0^t Ke^{\kappa(\tau-t)}\frac{d\sigma_{13}}{d\tau}\,d\tau - \left[\frac{3}{2}\right]^{(n+1)/2}\cdot Ce^{-B/T}\cdot\sigma_{13}J^{n-1} - \gamma(1+\cos^2\psi)\cos\theta\sin\theta,$$

$$\frac{d(F_{23})}{dt} = \left[\frac{d}{dt}\left\{T(\alpha^*_{cc} - \alpha^*_{aa})\right\} - \gamma\right]\cos\theta\sin\psi\cos\psi - \int_0^t Ke^{\kappa(\tau-t)}\frac{d\sigma_{23}}{d\tau}\,d\tau - \left[\frac{3}{2}\right]^{(n+1)/2} \times Ce^{-B/T}\cdot\sigma_{23}J^{n-1},$$

$$\frac{d(F\sigma_{12})}{dt} = \left[\frac{d}{dt}\left\{T(\alpha^*_{aa} - \alpha^*_{cc})\right\} + \gamma\right]\sin\theta\cos\psi\sin\psi - \int_0^t Ke^{\kappa(\tau-t)}\frac{d\sigma_{12}}{d\tau} - \left[\frac{3}{2}\right]^{(n+1)/2} \times Ce^{-B/T}\cdot\sigma_{12}J^{n-1}, \quad (2)$$

taken for all orientations. In practice only a small number of orientations is assumed. If irradiation growth is absent and the difference in coefficients of thermal expansion along the a and c-axes is neglected, we are free to choose the a, b, x and z-axes to be coplanar, thus reducing the number of orientations required for accuracy and the number of non-degenerate equations per orientation.

The additional equation may be obtained by writing $d\sigma_{33}/dt$ in terms of the other variables for each orientation and equating its mean value to zero since it is the derivative of the constant applied stress. This equation,

$$\sum_{(k)(h)}\frac{S_{(k,h)}\sigma_{33(k,h)}}{F_{(k,h)}}\cdot\frac{dF_{(k,h)}}{dt} = \frac{d\epsilon}{dt}\sum_{(k,h)}\frac{S_{(k,h)}}{F_{(k,h)}} + \gamma\sum_{(k,h)}\frac{S_{(k,h)}}{F_{(k,h)}}(\cos^2\psi_{(h)}\cos^2\theta_{(k)} - \sin^2\theta_{(k)}) + \frac{d}{dt}\left\{T\sum_{(k,h)}\frac{S_{(k,h)}}{F_{(k,h)}}(\alpha^*_{bb}\sin^2\theta_{(k)} + \alpha^*_{aa}\cos^2\theta_{(k)}\cos^2\psi_{(h)} + \alpha^*_{cc}\cos^2\theta_{(k)}\sin^2\psi_{(h)})\right\} - \left[\frac{3}{2}\right]^{(n+1)/2}\cdot Ce^{-B/T}\cdot\sum_{(k,h)}\frac{S_{(k,h)}J^{n-1}_{(k,h)}}{F_{(k,h)}}\sigma_{33(k,h)} - \sum_{(k,h)}\int_0^t\frac{S_{(k,h)}K_{(k,h)}}{F_{(k,h)}}e^{\kappa(\tau-t)}\frac{d\sigma_{33(k,h)}}{d\tau}\,d\tau \quad (3)$$

simplifies to

$$\frac{d\epsilon}{dt}\sum_{(k)}S_{(k)} = \left[\frac{3}{2}\right]^{(n+1)/2}\cdot Ce^{-B/T}\cdot\sum_{(k)}S_{(k)}\sigma_{33(k)}J^{n-1}_{(k)} \quad (4)$$

[(6), BLACKBURN, HARNBY and STOBO (1960)]

VOL 14 196

TABLE 1.—CREEP ACCELERATION FACTORS (BLACKBURN, HARNBY and STOBO, 1960)

Expression for the ratio of accelerated creep rate / unaccelerated creep rate	$\frac{w}{I}$ 0·25	0·50	0·75	1·00	1·50	2·50	5·00
$\left[\frac{3}{2}\right]^{(n+1)/2}\cdot\left[\frac{I}{w}\right]^{n}\cdot\int_0^1\left\{\frac{2w}{3I}+\frac{3x^2-1}{\sqrt{6}}\right\}\left[\frac{2w^2}{3I^2}+\frac{2w(3x^2-1)}{I\sqrt{6}}+1\right]^{(n-1)/2}dx$	14·8	5·48	3·23	2·33	1·59	1·23	1·06

Equation (10) [(18), BLACKBURN, HARNBY and STOBO (1960)] where $x = \sin\theta$

for linear stress/strain relationships and linear primary creep, in the case of random orientation.

2.2 *Assumption of uniform internal stress due to uniform continuous thermal cycling*

From the alternative assumption of the stress being the sum of the applied stress and an internal stress independent of the applied stress and uniform with respect to the crystal axes, we may derive

$$\frac{d(FI)}{dt}=\sqrt{\frac{3}{2}}\frac{d(\alpha T)}{dt}-\int_0^t Ke^{\kappa(\tau-t)}\frac{dI}{d\tau}\,d\tau-\left[\frac{3}{2}\right]^{(n+1)/2}\cdot Ce^{-B/T}\cdot I|I|^{n-1} \quad (5)$$

[(9), BLACKBURN, HARNBY and STOBO (1960)]

for I when it is due to thermal cycling and

$$\frac{d\epsilon}{dt}=\frac{1}{4\pi}\int_0^{2\pi}\int_{-\pi/2}^{\pi/2}\cos\theta\left\{\frac{d[F(s_{33}+2w/3)}{dt}+\int_0^t Ke^{\kappa(\tau-t)}\frac{ds_{33}}{d\tau}\,d\tau+\left[\frac{3}{2}\right]^{(n+1)/2}\cdot Ce^{-B/T}\times\right.$$
$$\left.\times(s_{33}+2w/3)(I^2+2ws_{33}+2w^2/3)^{(n-1)/2}\right\}d\theta\,d\psi \quad (6)$$

[(12), BLACKBURN, HARNBY and STOBO (1960)]

for the rate of change of strain deviation in the direction of an applied uniaxial load. For a linear stress/strain relation and primary creep this reduces to

$$\frac{d\epsilon}{dt}=\frac{1}{2\pi}\left[\frac{3}{2}\right]^{(n+1)/2}\cdot Ce^{-B/T}\int_0^{2\pi}\int_0^{\pi/2}\cos\theta\,(s_{33}+2w/3)\times(I^2+2ws_{33}+2w^2/3)^{(n-1)/2}\,d\theta\,d\psi \quad (7)$$

[(13), BLACKBURN, HARNBY and STOBO (1960)]

and for small applied stress it simplifies further to

$$\frac{d\epsilon}{dt}=\left[\frac{3}{2}\right]^{(n+1)/2}\frac{Cw(4n+16)}{30}I^{n-1}e^{-B/T}. \quad (8)$$

[(15), BLACKBURN, HARNBY and STOBO (1960)].

The instantaneous creep acceleration factor has been evaluated from

$$\frac{d\epsilon}{dt}=\left[\frac{3}{2}\right]^{(n+1)/2}\cdot Ce^{-B/T}\cdot I^n\times\int_0^{\pi/2}\cos\theta\left[\frac{2w}{3I}+\frac{3\sin^2\theta-1}{\sqrt{6}}\right]\times\left\{1+\frac{2w(3\sin^2\theta-1)}{I\sqrt{6}}+\frac{2w^2}{3I^2}\right\}^{(n-1)/2}d\theta \quad (9)$$

[(17), BLACKBURN, HARNBY and STOBO (1960)]

the result being

$$\frac{\text{cycled creep rate}}{\text{uncycled creep rate}}=\left[\frac{3}{2}\right]^{(n+1)/2}\cdot\left\{\frac{I}{w}\right\}^n\times\int_0^1\left\{\frac{2w}{3I}+\frac{3x^2-1}{\sqrt{6}}\right\}\times\left[\frac{2w^2}{3I^2}+\frac{2(3x^2-1)w}{I\sqrt{6}}+1\right]^{(n-1)/2}dx \quad (10)$$

[(18), BLACKBURN, HARNBY and STOBO (1960)]

and is presented in Table 1 and Fig. 1. It may be seen to resemble a straight line until $3w > I$ when plotted as a function of w/I with logarithmic scales.

Rather than integrate the simultaneous non-linear differential equations, various simplifications may be made, e.g. the internal stress may be treated as unaffected by creep, or the internal stress may be replaced by its mean value. Results obtained using the latter assumption of constant uniform internal stress for the case when the material is subjected to the cycles described in Fig. 2, together with more accurate results obtained for the same cycles by integrating the differential equations neglecting primary creep are presented in Table 2. Adequate agreement is obtained with the more accurate calculations and the experimental results (Table 2).

The mean value of the internal stress for small short cycles may be obtained if primary creep is neglected,

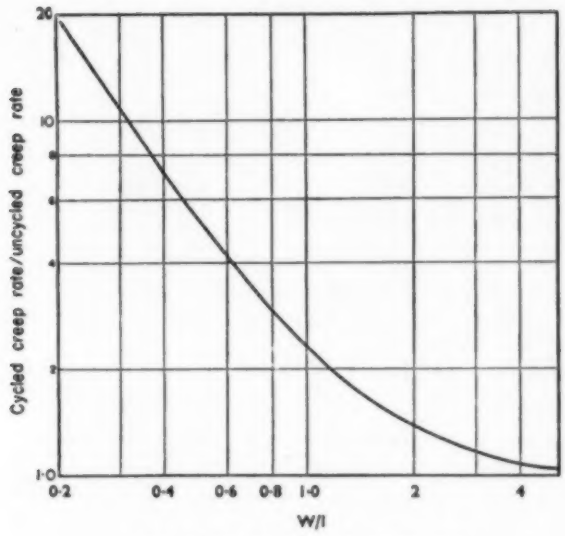

FIG. 1.—Graph of function in Table 1.

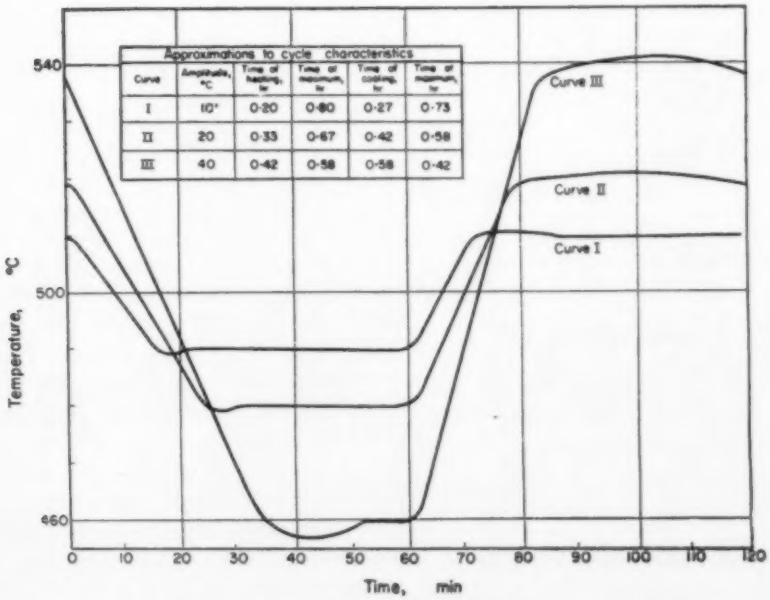

FIG. 2.—Temperature cycling curves.

TABLE 2.—CREEP RATES FOR URANIUM UNDER 2 HOUR PERIOD THERMAL CYCLING AT 500°C

Cycle (Fig. 2)		Applied stress (t.s.i.)	Experimental values of creep rate ($hr^{-1} \times 10^6$)	Theoretical values of creep rate with various assumptions		
Amplitude (°C)	Mean temp. devn.(°C)			Uniform deformation ($hr^{-1} \times 10^6$)	Uniform internal stress ($hr^{-1} \times 10^6$)	Constant uniform internal stress ($hr^{-1} \times 10^6$)
10	8·8	½	5,6,10,12,13,17	16	16	15
20	16·2	½	17,17,25,30,39,45	37	41	46
20	16·2	1	43,50,63,72,83	79	89	93

TABLE 3
(From Table 2, BLACKBURN, HARNBY and STOBO (1960))

Cycling conditions	500° ± 10°C (0·5 t.s.i.)	500° ± 20°C (1·0 t.s.i.)	500° ± 20°C (0·5 t.s.i.)	500° ± 40°C (0·5 t.s.i.)
Mean Internal Stress / Maximum internal stress in absence of creep	0·88	0·83	0·83	0·69
Mean temp. deviation / Amplitude of cycle	0·88	0·81	0·81	0·69

TABLE 4
(β : quantity such that secondary creep effects on internal stress are unimportant if $\beta m^2 \Delta^{2(n-1)}$ is small)

Temperature (°C)	Estimate of Young's modulus (p.s.i. × 10^{-6})	Estimate of $\sqrt{1{\cdot}5}\, E\alpha/(1+\nu)$ (p.s.i./°C)	β ($hr^{-2}\,°C^{-3\cdot 64}$)	Time for applied stress of 8 t.s.i. to relax to 2 t.s.i.(hr)
450	12	500	$0{\cdot}644 \times 10^{-7}$	20
500	8	250	$0{\cdot}322 \times 10^{-6}$	3·1
550	6	125	$0{\cdot}117 \times 10^{-5}$	0·57
600	4	100	$0{\cdot}896 \times 10^{-5}$	0·15

since as is shown in Table 3, the ratio of the mean internal stress to the maximum internal stress in the absence of relaxation is approximately equal to the ratio of the mean to the maximum temperature deviations, and these latter three quantities are readily obtainable for a given cycle. This result implies that the mean temperature deviation is more important than the amplitude and that secondary creep and the shape of the cycle are unimportant as far as the creep acceleration factor is concerned except for long or large cycles. To estimate at what amplitude and period of cycle this approximation breaks down, we consider the case of instantaneous temperature changes and relaxation under secondary creep. Then neglecting the cube of the period we find that the mean internal stress is given by

$$\sqrt{\frac{3}{2}}\frac{\alpha\Delta E}{1+\nu}\{1-(n-1)\beta m^2\Delta^{2(n-1)}+\cdots\}$$

where

$$\beta=\left[\frac{3}{2}\right]^{2n}\frac{n}{48(n-1)}\left[\frac{CEe^{-B/T}}{1+\nu}\right]^2\left[\frac{\alpha E}{1+\nu}\right]^{2(n-1)} \quad (11)$$

Thus the approximation applies when $\beta m^2\,\Delta^{2(n-1)}$ is small. For various temperatures, β is given in Table 4 using values of $[\sqrt{1{\cdot}5}\alpha E(1+\nu)]$ suggested by ANDERSON (1959) and values of B, C and n taken from GARDINER, JOHNSON and WARD (1959). Using the same values of Young's modulus, the times calculated for an applied stress of 8 t.s.i. to relax at these temperatures under secondary creep are included in the Table. Good correspondence with experiment is obtained.

2.3 *Uniform internal stress due to irradiation growth*

When the internal stress is due to irradiation growth

equation (8) is unaltered but equations (9) and (5) are replaced by

$$\frac{d\epsilon}{dt} = \frac{1}{\pi}\left[\frac{3}{2}\right]^{(n+1)/2} \cdot e^{-B/T} \cdot CI^n \int_0^{\pi}\int_0^1 \left[\frac{2w}{3I} + \frac{\cos^2\psi\,(1-x^2) - x^2}{\sqrt{2}}\right] \times \left\{1 + \frac{\sqrt{2}\,w[\cos^2\psi\,(1-x^2) - x^2]}{I} + \frac{2w^2}{3I^2}\right\}^{(n-1)/2} dx\,d\psi \tag{12}$$

[(9) BLACKBURN (1960)]

and $$\frac{dI}{dt} = \frac{E}{1+\nu}\left\{\sqrt{2}\gamma - \left[\tfrac{3}{2}\right]^{(n+1)/2} \cdot Ce^{-B/T} I|I|^{n-1}\right\}, \tag{13}$$

[(6) BLACKBURN (1960)]

neglecting primary creep and the stress-dependence of the stress/strain relation. The creep acceleration factor evaluated from equation (12) is presented in Table 5 and is found to agree closely with Table 1 for the case of thermal cycling. For an irradiation growth rate γ, the solution of equation (13) tends asymptotically to

$$\sqrt{\frac{2}{3}}\left[\frac{2\gamma}{\sqrt{3}Ce^{-B/T}}\right]^{1/n}. \tag{14}$$

TABLE 5.—EFFECT OF IRRADIATION ON CREEP RATE
(Table 3, BLACKBURN (1960))

w/I	Creep rate with irradiation / Creep rate without irradiation	Linearized approximation
0·25	14·9	14·6
0·5	5·5	5·08
0·75	3·25	2·74
1·0	2·34	1·77
1·5	1·63	0·955
2·5	1·23	0·44
5·0	1·06	0·153

TABLE 6.—ASYMPTOTIC VALUES OF INTERNAL STRESS
(Table 2, BLACKBURN (1960))

T(°C)	γ(yr^{-1})	I(p.s.i.)
270	0·18	549,000
305	0·14	162,000
380	0·068	16,600
400	0·046	8,980
403	0·04	7,950
450	0·01	1,750

Values of this expression at various temperatures are presented in Table 6 and the speed of approach to the asymptotic value in a particular case is presented in Table 7.

TABLE 7.—TIME FOR INTERNAL STRESS TO APPROACH ASYMPTOTIC VALUE AT 403°C IN A FLUX OF 3×10^{12} NEUTRONS CM^{-2} SEC^{-1}
(Table 1, BLACKBURN (1960))

t(hr)	I(p.s.i.)
43·65	4000
74·54	6000
101·44	7000
127·37	7500
154·41	7750
186·25	7875
∞	7950

2.4 *Uniform internal stress due to simultaneous thermal cycling and irradiation growth*

When both effects occur, equation (5) is replaced by

$$\frac{ds_{aa}}{dt} = \frac{E}{1+\nu}\left\{\gamma - \frac{1}{2}\frac{d(\alpha T)}{dt} - Ce^{-B/T}\left[\frac{3}{2}\right]^{(n+1)/2} s_{aa}I^{n-1}\right\},$$

$$\frac{ds_{cc}}{dt} = -\frac{E}{1+\nu}\left\{\frac{1}{2}\frac{d(\alpha T)}{dt} + Ce^{-B/T}\left[\frac{3}{2}\right]^{(n+1)/2} s_{cc}I^{n-1}\right\} \tag{15}$$

These equations can be integrated numerically, starting with s_{cc} zero and $\sqrt{2}s_{aa}$ as the asymptotic value taken by the internal stress in the absence of thermal cycling. Since we have shown the proportionate increases in creep rate under a uniaxial load, due to thermal cycling and to irradiation growth acting individually to be similar, the corresponding increase when both act simultaneously may be determined approximately by using Table 1 or Fig. 1 when the internal stress is known.

Equations (15) were integrated through 18 successive thermal cycles at 400°C, the mean internal stresses due to thermal cycling and irradiation being in the ratio 4 : 3. No significant variation in mean internal stress was found after the second cycle. It was therefore decided to integrate equations (15) through two

VOL 14 196

TABLE 8

Mean internal stress due to thermal cycling alone / Mean internal stress due to irradiation alone	0	0·1	0·2	0·35	0·48	0·555	1·0	2·0	3·0	∞
Mean internal stress due to both effects / Mean internal stress due to each, added	1	0·9	0·84	0·74	0·69	0·67	0·65	0·72	0·77	1

cycles, for various ratios of the mean internal stresses due to thermal cycling and irradiation growth acting individually, to determine the ratio of the mean internal stress (during the second cycle) when the effects act together, to the sum of the mean internal stresses when they act separately. The cycles considered were of two hour period at 450°C, the periods of heating and cooling each lasting for half the cycle. The relationship between the ratios is presented in Table 8. That these results are not critically dependent on the temperature and shape of cycle was checked by considering another cycle at 400°C where the heating and cooling each last for 20 per cent of the period. For both cycles, for a given ratio of internal stress from thermal cycling to internal stress from irradiation growth of 0·555, a value of 0·67 was derived for the ratio of the total internal stress I due to both effects to the sum of the internal stresses I due to each.

3. THEORY WHEN INTERNAL STRESS IS IN THE PLASTIC RANGE

3.1 *Internal stress due to irradiation growth or constant rate of change of temperature*

Each crystal is assumed to undergo the same deformation and become plastic due to a constant applied rate of strain deviation β_{ij} (due to thermal expansion or irradiation growth). We assume the rate of strain deviation is the sum of the rates of strain deviation due to temperature changes, irradiation growth, elastic deformation, plastic flow and creep. Then when the stresses have approached their asymptotic values, the rate of strain deviation η_{ij} is given by

$$\eta_{ij} = \beta_{ij} + \sigma_{ij}\{[\tfrac{3}{2}]^{(n+1)/2} Ce^{-B/T} J^{n-1} + 1/\lambda\} \quad (16)$$

where λ is a constant to be determined from the yield condition $J^2 = \frac{2}{3} Y^2$ and Y is the yield stress. Hence we have:

$$\sum_{i,j} (\eta_{ij} - \beta_{ij})(\eta_{ij} - \beta_{ij}) = \tfrac{2}{3} Y^2(1/\lambda + \tfrac{3}{2} Ce^{-B/T} Y^{n-1})^2. \quad (17)$$

Equating the components of the mean stress deviations to those of the applied stress deviations w_{ij} gives:

$$w_{ij} = \frac{Y}{\sqrt{24}\pi} \int_S \frac{(\eta_{ij} - \beta_{ij})\, dS}{\sqrt{\sum_{i,j}(\eta_{ij} - \beta_{ij})(\eta_{ij} - \beta_{ij})}} \quad (18)$$

where the integration is taken over all orientations.

This equation may be solved for the strain rates η_{ij}. If the crystals are randomly orientated, equation (18) simplifies to:

$$\tfrac{2}{3} w = \frac{Y}{4\pi\sqrt{1{\cdot}5}} \times \int_S \frac{(d\epsilon/dt - \beta_{33})\, dS}{\sqrt{\left[\sum_{i,j} \beta_{ij}\beta_{ij} - 3\beta_{33}\frac{d\epsilon}{dt} + 1{\cdot}5\left(\frac{d\epsilon}{dt}\right)^2\right]}} \quad (19)$$

when w is a uniaxial stress acting along the z-axis.

There are three particular cases of interest. In the first, deduced by ANDERSON and BISHOP (1957) β_{ij} is due to irradiation growth and:

$$\frac{2}{3} w = \frac{2Y}{3\pi} \int_0^{\pi} \int_0^1 \frac{\left\{\frac{d\epsilon}{dt} + \frac{1}{2}\sqrt{\tfrac{1}{2}\beta_{ij}\beta_{ij}[(1 + \cos^2\psi)\, x^2 - \cos^2\psi]}\right\} dx\, d\psi}{\sqrt{\left[\left(\frac{d\epsilon}{dt}\right)^2 + \sqrt{\tfrac{1}{2}\beta_{ij}\beta_{ij}[(1 + \cos^2\psi)x^2 - \cos^2\psi]}\,\frac{d\epsilon}{dt} + \tfrac{2}{3}\beta_{ij}\beta_{ij}\right]}}. \quad (20)$$

In the second, β_{ij} is due to differential thermal expansion:

$$\frac{2w}{3} = \frac{2Y}{3} \int_0^1 \frac{\left\{\frac{d\epsilon}{dt} + \frac{1}{2}(3x^2 - 1)\sqrt{\tfrac{2}{3}\Sigma\beta_{ij}\beta_{ij}}\right\} dx}{\sqrt{\left[\left(\frac{d\epsilon}{dt}\right)^2 + (3x^2 - 1)\sqrt{\tfrac{2}{3}\Sigma\beta_{ij}\beta_{ij}}\,\frac{d\epsilon}{dt} + \tfrac{2}{3}\Sigma\beta_{ij}\beta_{ij}\right]}}. \quad (21)$$

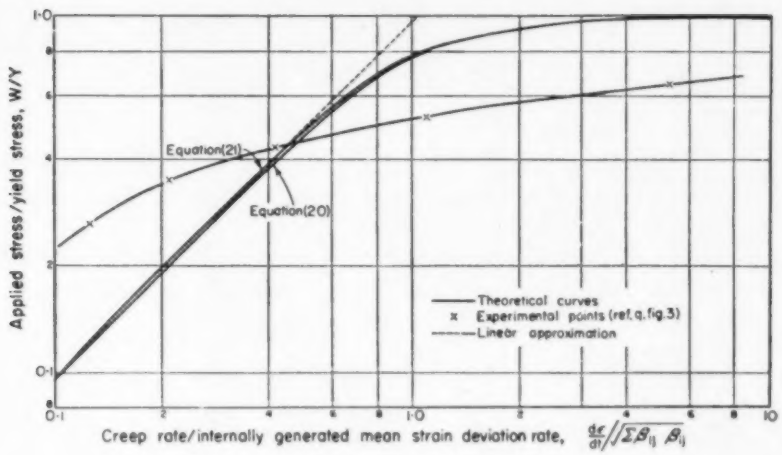

FIG. 3.—The relationship between w/y and $\frac{d\epsilon}{dt}\Big/\sqrt{(\Sigma\beta_{ij}\beta_{ij})}$.

From equations (20) and (21) w/Y, the ratio of applied to yield stress has been obtained as a function of

$$\frac{d\epsilon/dt}{\sqrt{\Sigma\beta_{ij}\beta_{ij}}}.$$

The results which are given in Table 9 and Fig. 3 show their satisfactory agreement with experimental values of YOUNG, GARDINER and ROTSEY (1960).

3.2 *Small applied stress*

Whatever the form of β_{ij}, if $d\epsilon/dt$ is small compared with it, equation (19) reduces to:

$$\frac{2}{3}w = \frac{4\sqrt{2}\,Y}{5\sqrt{3\Sigma\beta_{ij}\beta_{ij}}}\frac{d\epsilon}{dt}. \qquad (22)$$

If the applied stress is small compared with the yield stress, the rates of change of stress will be small and equation (16) may be expected to apply if β_{ij} varies with time while retaining the same principal axes. Although the principal directions in fact change when thermal cycling and irradiation growth act simultaneously, the case where β_{ij} varies in magnitude without changing its axes may be considered to be a reasonable approximation.

Let

$$\sqrt{\Sigma\beta_{ij}\beta_{ij}} = g + f \qquad (23)$$

where g is proportional to the rate of irradiation growth and f is proportional to the rate of temperature change. Assume the cycling to have a period m and not more than one maximum in its derivative per cycle. The cycle is treated as beginning when f becomes negative.

Further development depends on the behaviour of $f+g$. If it does not change sign the material remains plastic with instantaneous creep rate (from equation (22)) given by:

$$\frac{d\epsilon}{dt} = \frac{5\sqrt{6}\,w}{12Y}(f+g). \qquad (24)$$

Thus the mean creep rate $\overline{\frac{d\epsilon}{dt}} = \frac{5\sqrt{6}w}{12Y}g. \qquad (25)$

When $f+g$ changes sign, the material ceases to be plastic and we may assume it to undergo normal secondary creep under a small applied stress w and large internal stress, I. Neglecting primary creep and assuming linear elasticity, the mean effect of secondary

TABLE 9.—RATIO OF CREEP RATE UNDER AN EXTERNAL LOAD TO INTERNALLY-GENERATED STRAIN RATE DEVIATION WHEN THE INTERNAL STRESS EQUALS THE YIELD STRESS

Creep rate / Internally generated, mean strain deviation rate i.e. $\frac{d\epsilon}{dt}\Big/\sqrt{\Sigma\beta_{ij}\beta_{ij}}$	Applied stress / Yield stress $\left(\frac{w}{Y}\right)$	
	Thermal cycling case	Irradiation growth case
0·001	0·00098	0·00098
0·002	0·00196	0·00196
0·005	0·0049	0·0049
0·01	0·0098	0·0098
0·02	0·0196	0·0196
0·05	0·0493	0·049
0·1	0·099	0·098
0·2	0·199	0·194
0·5	0·479	0·465
0·75	0·654	0·647
2·0	0·933	0·936
5·0	0·989	0·989
10·0	0·997	0·997

creep on the internal stress is also negligible for a fast cycle. The creep rate has been shown by HODGKINS (1960) to be

$$\frac{d\epsilon}{dt} = \frac{10wn}{3(4n+1)}\left[\frac{3}{2}\right]^{(n+1)/2} \cdot Ce^{-B/T} I^{n-1} \qquad (26)$$

The material remains non-plastic from time t_1 to time t_2 when

$$\int_{t_1}^{t_2}(f+g)\,dt = 0 \qquad (27a)$$

or

$$= \frac{2\sqrt{2}(1+\nu)Y}{\sqrt{3}\,E}. \qquad (27b)$$

If this integral becomes zero first, the material remains plastic for the rest of the cycle. Otherwise the material becomes non-plastic between times t_3 and t_4 where t_3 is the time when $f+g$ is again zero and t_4 is such that,

$$\int_{t_3}^{t_4}(f+g)dt = \frac{2\sqrt{2}(1+\nu)Y}{\sqrt{3}E}. \qquad (28)$$

For (27a) and (27b) the mean creep rates are given by:

$$\frac{\overline{d\epsilon}}{dt} = \frac{5w}{4Ym}\sqrt{\frac{2}{3}}\left\{\int_0^{t_1}|f+g|dt + \int_{t_2}^{m}|f+g|dt\right\} + \frac{10wn}{3m(4n+1)}\left[\frac{3}{2}\right]^{(n+1)/2} C \times \int_{t_1}^{t_2}\left\{\sqrt{\frac{2}{3}}\,Y + \frac{E}{1+\nu}\int_{t_1}^{t}(f+g)dt\right\}^{n-1} e^{-B/T}\,dt, \qquad (29)$$

and

$$\frac{\overline{d\epsilon}}{dt} = \frac{5w}{4Ym}\sqrt{\frac{2}{3}}\left\{\int_0^{t_1}|f+g|dt + \int_{t_2}^{t_3}|f+g|dt + \int_{t_4}^{m}|f+g|dt\right\} + \frac{10wn}{3m(4n+1)} \times \left[\frac{3}{2}\right]^{(n+1)/2} C\left[\int_{t_1}^{t_2}\left\{\sqrt{\frac{2}{3}}\,Y + \frac{E}{1+\nu} \times \int_{t_1}^{t}(f+g)dt\right\}^{n-1} e^{-B/T}\,dt + \int_{t_3}^{t_4}\left\{\sqrt{\frac{2}{3}}\,Y + \frac{E}{1+\nu}\int_{t_3}^{t}(f+g)\,dt\right\}^{n-1} e^{-B/T}\,dt. \qquad (30)$$

Consider the particular case of a saw-tooth temperature cycle, when f is a square wave, and assume for simplicity that $Ce^{-B/T}$ may be replaced by its mean value. If $g > |f|$, $g+f$ never changes sign and equation (25) applies. If $g < |f|$, $t_1 = 0$ and equations (27a) and (27b) are replaced by:

$$(f-g)\frac{Em}{2(1+\nu)} < 2\sqrt{\tfrac{2}{3}}\,Y \qquad (31a)$$

and

$$(f-g)\frac{Em}{2(1+\nu)} > 2\sqrt{\tfrac{2}{3}}\,Y. \qquad (31b)$$

If (31a) occurs first, $t_2 = \dfrac{mf}{f+g}$ and the mean creep rate is:

$$\frac{\overline{d\epsilon}}{dt} = \frac{5w}{4Y}\sqrt{\frac{2}{3}}\,g + \frac{20(1{\cdot}5)^{(n+1)/2}Ce^{-B/T}wf(1+\nu)}{3(4n+1)mE(f^2-g^2)} \times \left\{[\sqrt{\tfrac{2}{3}}\,Y]^n - \left|\sqrt{\tfrac{2}{3}}\,Y - \frac{Em(f-g)}{2(1+\nu)}\right|^{n-1} \times \left[\sqrt{\tfrac{2}{3}}\,Y - \frac{Em(f-g)}{2(1+\nu)}\right]\right\}. \qquad (32)$$

If (31b) occurs first: $t_2 = \dfrac{2\sqrt{2}(1+\nu)Y}{\sqrt{3}E(f-g)}$,

$$t_3 = \tfrac{1}{2}\,m,$$

$$t_4 = \tfrac{1}{2}m + \frac{2\sqrt{2}(1+\nu)Y}{\sqrt{3}\,E(f+g)},$$

and the mean creep rate is:

$$\frac{\overline{d\epsilon}}{dt} = \frac{5w}{4Y}\sqrt{\frac{2}{3}}\left[f - \frac{4\sqrt{2}(1+\nu)Y}{\sqrt{3}mE}\right] + \frac{40\,Ce^{-B/T}wf(1+\nu)Y^n}{\sqrt{6}(4n+1)mE(f^2-g^2)}. \qquad (33)$$

When g is zero we have the case of continuous thermal cycling in the absence of irradiation. We note that depending on the form and starting point of the cycle, the initial cycle may give rise to either a smaller or a greater creep rate than the subsequent ones, and in particular it may give rise to plasticity when the subsequent ones do not if

$$2\sqrt{2}\,Y/(\sqrt{3}Em) < f < 4\sqrt{2}\,Y/(\sqrt{3}Em).$$

4. CONCLUSIONS

The creep rate of randomly orientated uranium under a uniaxial load when the material is plastic due to irradiation growth or a constant rate of change of temperature, may be obtained from Table 9 or Fig. 3. For small applied stress it approximately equals the ratio of the applied stress to the yield stress multiplied by the internally generated mean strain deviation rate.

When large thermal cycling and irradiation growth occur together, and the applied stress is small there are three distinct cases for which the mean creep rates are

given by equations (26) (29) and (30) respectively. For a saw-tooth thermal cycle, the criteria of division are:

$$\text{(a)} \qquad (f-g) < 0;$$

$$\text{(b)} \quad 0 < (f-g) < \frac{4\sqrt{6}Y}{3Em};$$

and

$$\text{(c)} \qquad (f-g) > \frac{4\sqrt{6}Y}{3\,Em}.$$

In the first case the mean creep rate is unaltered from that due to the irradiation growth; in the second case there is an additional accelerated secondary creep term and in the final case the mean creep rate is that due to the thermal cycling together with the secondary creep term. These creep rates would be diminished if relaxation of the internal stress were allowed for. This effect will be most important for slow cycles, when the thermal cycling effect is slightly greater than the irradiation effect.

The following procedures may be used to estimate the creep acceleration factor of a specimen of uranium under uniform continuous thermal cycling and irradiation when the material remains elastic.

If maximum accuracy is required equations (2) should be integrated. A quicker procedure is to integrate equations (15) and (9) simultaneously. Unless the cycling has a large amplitude or period, there is also available the following process which does not involve the solution of differential equations, provided it is assumed that primary creep effects are negligible.

The instantaneous creep acceleration factor may be obtained from Table 1 (or Fig. 1), using throughout the cycle the same value of I taken from Table 8 where the internal stress due to irradiation growth alone is calculated from (14), while the mean internal stress due to thermal cycling alone is determined by multiplying the mean temperature deviation of the cycle by $\sqrt{1{\cdot}5}\,E\alpha/(1+\nu)$. The last step is justified if $\beta\Delta^3 m^2$ is small where β is given in Table 4, m is the period and Δ is the mean temperature deviation.

In using these processes, B, C and n should take the values suggested by CHAMBERLAIN and BABIK (1960) while values of $\sqrt{1{\cdot}5}\,E\alpha/(1+\nu)$ should be chosen to be less than the values obtained by determining the constants individually, to agree with the values derived by UKAEA from analysis of the results of thermal cycling experiments. Interim values of UKAEA results have been given by ANDERSON (1959) (repeated in Table 4).

Acknowledgments—The writer is grateful to MR. D. CLARKSON and MR. D. R. NEALEY for assistance in the computations and to C. A. Parsons and Co., Ltd. for permission to publish.

NOMENCLATURE

E Young's modulus

f rate of internal strain deviation $\sqrt{\Sigma\beta_{ij}\beta_{ij}}$ produced by thermal cycling

g rate of internal strain deviation $\sqrt{\Sigma\beta_{ij}\beta_{ij}}$ produced by irradiation growth

g_{ij} metric tensor

I internal stress, $\sqrt{\Sigma s_{ij}s_{ij}}$

J $\sqrt{\Sigma\sigma_{ij}\sigma_{ij}}$

K, F experimentally determined functions of both J and T

m period of temperature cycle

n, B, C, experimentally determined constants

s_{ij} internal stress deviation

$S_{(k)}$ $S_{(k,k)}$ frequency distributions

t present time

T absolute temperature

w applied uniaxial stress acting along z-axis

w_{ij} applied stress deviations

Y yield stress

α_{ij} coefficient of thermal expansion

$\alpha_{ij}^* = \alpha_{ij} - \frac{1}{3}g_{ij}\sum_k \alpha_{kk}$

$\alpha = \frac{1}{3}\sum_k \alpha_{kk} - \alpha_{kk}$

β_{ij} rate of internal strain deviation

γ_{ij} rate of irradiation growth

ν Poisson's ratio

Δ mean temperature deviation of cycle

$\frac{d\epsilon_{ij}}{dt}$ rate of strain

$\frac{d\epsilon}{dt}$ instantaneous creep rate of uranium

$\frac{d\epsilon}{dt}$ mean creep rate

λ constant

σ_{ij} stress deviation

τ_{ij} stress components

τ past time

(x, y, z) axes in space such that the uniaxial stress acts along the z-axis

(a, b, c) axes of crystal

$\frac{1}{2}\pi$-θ angle between b and z-axes

$\frac{1}{2}\pi$-ϕ angle between x-axis and normal to (b, z) plane.

$\frac{1}{2}\pi$-ψ angle between a-axis and normal to (b, z) plane.

REFERENCES

ANDERSON R. G. (1959) Private communication.

ANDERSON R. G. and BISHOP J. F. W. (1957) *The Effect of Neutron Irradiation and Thermal Cycling on the Permanent Deformation of Uranium.* To be published.

BLACKBURN W. S. (1961) *The Effect of Irradiation Growth on the Creep of Uranium under a Uniaxial Load. Phil. Mag.* To be published.

BLACKBURN W. S., HARNBY G. and STOBO J. J. (1960) *J. Nucl. Energy* Part A: *Reactor Science* **12**, 162.

CHAMBERLAIN J. and BABIK S. (1960) Private communication.

GARDINER K. M., JOHNSON M. P. and WARD D. A. (1959) Private communication.

HODGKINS W. R. (1960) Private communication.

YOUNG A. G., GARDINER K. M. and ROTSEY W. B. (1960) *J. Nucl. Mat.* **2**, 234.

Reactor Science and Technology (Journal of Nuclear Energy, Parts A & B), 1961, Vol. 14, p. 117. Pergamon Press Ltd. Printed in Northern Ireland

BOOK REVIEW

Nuclear Reactor Stability, A. HITCHCOCK (Nucl. Engng. Monograph). Temple Press, 1960, x + 61 pp., 12*s.* 6*d.*

TWELVE titles in this series have now appeared and further are in preparation, which indicates the range of specialist subjects included in the complex of nuclear engineering. This monograph is concerned with the stability about equilibrium of the spatial distribution of power density and temperature within a reactor whose neutron balance is subject to small arbitrary fluctuations. This topic is now of considerable practical importance as well as of academic interest. On the one hand it confronts the engineer engaged currently in the design and operation of large nuclear power reactors, whilst on the other hand it is an absorbing and advanced field of study for the applied mathematician.

Chapter 1—an introduction to the dynamics of power reactors—defines the coefficients of reactivity and indicates the magnitudes of the time constants of the associated reactor quantities. Possible sources of instability are given as moderator temperature, xenon–135 and voidage. Spatial instability is distinguished from a purely time-dependent process and the necessity for its control is emphasized when restrictions exist on local excursions in reactor variables.

Chapter 2 outlines the analysis of stability of the system on the assumption that the partial differential equations which describe transport processes can be resolved into a set of coupled ordinary differential equations in time. This resolution is made generally in terms of spatial modes or finite differences.

Chapters 3, 4 and 5 refer to the effects of temperature, xenon–135 and voidage respectively, when control is treated as a constraint. A more detailed analysis is shown to be required for the axial direction when this is associated with coolant flow and control rod action. Chapter 6 introduces control rods explicitly but in an idealized form. Two appendices deal with properties of 'flattened' reactors.

It is inevitable in a text of such wide scope which is compressed into a short monograph that a number of points should invite comment. On p. 13 what is termed modal analysis might be considered to be harmonic analysis; on p. 15 the physical significance of neglected cross-coupling terms is not discussed; the boundary condition on p. 25 is inconsistent with that on p. 55; Fig. 5 on p. 40 is somewhat confusing; and the statement on p. 53 regarding stability analysis of a controlled reactor gives necessary rather than sufficient criteria. None of these comments is intended to detract from the merits of this valuable work.

The monograph is to be welcomed as a most useful and comprehensive addition to this series. It provides working rules, illustrated by numerical examples, for stability analysis as an integral part of reactor design calculations. It will undoubtedly stimulate further progress in this field particularly, one hopes, in the design of operational control units.

A. FONDA

OL.
14
961

Reactor Science and Technology (Journal of Nuclear Energy, Parts A and B), 1961, Vol. 14, pp. 118 to 123. Pergamon Press Ltd. Printed in Northern Ireland

$M1$ TRANSITIONS FROM HIGHLY-EXCITED STATES*

L. V. GROSHEV and A. M. DEMIDOV

(*Received* 15 *May* 1959)

Abstract—$M1$ transition probabilities from states formed by the capture of thermal neutrons are discussed for even-odd and odd-odd target nuclei with $A = 20$–60. According to the single-particle model this type of transition is l–forbidden. A comparison with $E1$ transition probabilities shows that for the even-odd nuclei the forbidden $M1$ transition probabilities which we observed are not very different from the l–allowed $M1$ transition probabilities for the lighter nuclei. In the case of odd-odd nuclei, certain $M1$ transitions are characterized by a large number of quanta per neutron captured and by a high value of $|M|^2_{M1}/(|M|^2_{s1})_{max}$.

DURING the past few years a number of authors[1–4] have made attempts to analyse thermal neutron nuclear capture processes and the subsequent transitions to low-lying states of the final nucleus in terms of the single-particle model. This model has provided an explanation of some of the regularities observed in the spectra of γ-rays emitted in (n,γ) reactions. In particular, for nuclei with mass numbers $A = 20$–60, the model readily explains the correlation observed between the intensities of $E1$ transitions from the initial neutron capture state and the reduced widths of the final levels.[4] We therefore thought it would be interesting to make a single particle model analysis of the probabilities for $M1$ transitions from the initial capture state for a group of nuclei having comparable mass numbers.

FORBIDDENNESS OF $M1$ TRANSITIONS ACCORDING TO THE SINGLE-PARTICLE MODEL

Let us first restrict our analysis to the consideration of $M1$ transitions in even-odd nuclei formed in (n,γ) reactions. For nuclei in the range $A = 20$–60, $M1$ transitions occur in the following nuclei: ^{25}Mg, ^{29}Si, ^{33}S and ^{41}Ca. In the cases we are considering, the thermal neutrons are captured by even-even nuclei and therefore the $M1$ transitions from the capture states must go to $1/2^+$ or $3/2^+$ levels. Measurements of the angular distributions of the protons emitted in (d,p) reactions show that the majority of levels of this type are formed by the capture of $l_n = 0$ or $l_n = 2$ neutrons. In nuclei with A between 20 and 40, the $2s_{1/2}$ and $1d_{3/2}$ neutrons states are only weakly excited and this affects the chance of observing $M1$ transitions in these nuclei. If the $M1$ transitions are due to transitions of the captured neutrons then they must be of the type $(ns_{1/2} \rightarrow 2s_{1/2})$ or $(ns_{1/2} \rightarrow 1d_{3/2})$ where $n > 2$. The matrix element for both types of neutron transition is strictly zero according to the single particle model.

ORDER OF FORBIDDENNESS OF $M1$ TRANSITIONS

To find the order of forbiddenness of these $M1$ transitions we must compare their probabilities with the probabilities for allowed transitions calculated from the single-particle formulae. That is, we must find the quantity

$$|M|^2 = \frac{\Gamma_{exp}}{\Gamma_B D/D_0} \tag{1}$$

where D is the observed density of neutron s-resonances with a given angular momentum and D_0 is the single-particle level density at low excitation energies (for the given angular momentum and parity).

In our case Γ_{exp} can be found from the formula $\Gamma_{exp} = \Gamma_\gamma I_\gamma$, where Γ_γ is the total radiation width and I_γ is the number of γ-quanta per neutron captured for a given transition. We shall suppose that the total radiation width of the neutron resonance for which the width Γ_γ was found is exactly the same as the radiation width of the state formed by thermal neutron capture. The quantity Γ_B in equation (1) determines the neutron transition probability calculated from the formulae of the single-particle model.[5] For the neutron transition we will adopt the following expressions, which allow for the motion of the nuclear core.

$$\Gamma_B(E1) = 0{\cdot}021\, A^{2/3}\, E_\gamma^3 \text{ eV} \tag{2}$$

$$\Gamma_B(M1) = 0{\cdot}015\, E_\gamma^3 \text{ eV} \tag{3}$$

where E_γ is expressed in MeV. It should be stressed that the magnitude of D_0 is very uncertain.

* Translated by D. L. ALLAN from *Atomnaya Energiya* 7, 321 (1959).

Table 1 gives the values of Γ_γ and D for nuclei with $A = 20$–40. These values are very inaccurate and some of them may be quite wrong. However, from the values of Γ_γ and D given for ^{29}Si and ^{33}S, and taking $D_0 = 1$ MeV, we can make a very crude estimate of the magnitude of $|M|^2$ for these nuclei. For $E1$ transitions $|M|^2$ is, on the average, about 1·3

TABLE 1.—RADIATION WIDTHS AND DENSITY OF NEUTRON s-RESONANCES FOR NUCLEI WITH $A = 20$–40

Nucleus	^{24}Na	^{28}Al	^{29}Si	^{33}S	^{36}Cl
E_{res}, keV	2·9	—	190	111	−0·14
Γ_γ, eV	0·4[6]	0·24?	9[6]	25[6]	0·48[7]
D, keV	400[6]	50[6]	500[6]	200[6]	40[6]

and for $M1$ transitions it is about 0·2. The observed values of $|M|^2$ for $M1$ transitions are given in Table 2.

The order of forbiddenness of $M1$ transitions can also be found indirectly by comparing their probabilities with the $E1$ transition probabilities in a given nucleus.

The data on $M1$ transitions from the initial capture levels of even-odd nuclei have been gathered together in Table 2. The table also gives the properties of the initial and final states* and the values of the quantity $|M|^2_{M1}/(|M|^2_{E1})_{max}$. Here, the subscript "max" indicates that the value taken for $|M|^2_{E1}$ applies to the most probable $E1$ transition out of all the $E1$ transitions from the capture state of a particular nucleus.

In Table 2 the $M1$ transitions have been divided into two major groups according to the orbital angular momentum change which accompanies the neutron transition. A separate place has been given to the $M1$ transition in ^{29}Si, which goes to a level corresponding to a proton group in the (d,p) reaction having an isotropic angular distribution. The last column but one of Table 2 gives the values of $|M|^2_{M1}$ deduced from Γ_γ and D with $D_0 = 1$ MeV.

From the values given in the last column of Table 2 it follows that if, for a given nucleus one equates the probability of the most intense $E1$ transition with the single particle transition probability then, on the average, $|M|^2_{M1}$ will be ~0·1. At the same time $|M|^2_{M1}$ is roughly the same for all three of the groups in Table 2 if one excludes the transitions to states in ^{41}Ca with $l_n = 0$, which it is known are not pure single particle $2s_{1/2}$ states.

WILKINSON[11] has examined the ratio of the probabilities of $M1$ and $E1$ transitions for light nuclei ($A < 20$). In this region of mass number, $M1$ transitions occur mainly between p-levels and so they may be considered to be l-allowed transitions. It is unfortunate that in the case of light nuclei it is not possible to compare the $E1$ and $M1$ transition probabilities for the decay of the same state as we did for states excited by thermal neutron capture. This is because either the γ-ray spectra are not sufficiently well-known or because the low lying levels in the light nuclei have the same parity. We must therefore

* We will assume that the $1/2^+ \to 3/2^+$ transitions are pure $M1$ transitions, since an $E2$ admixture is to be expected only when the $M1$ transitions are highly forbidden or where the $E2$ transition probability is greatly enhanced by collective effects. From our analysis it is apparent that the $M1$ transitions are not highly forbidden and the observed $E2$ transition probabilities correspond to their single particle values.[10]

TABLE 2.—$M1$ TRANSITIONS FROM INITIAL STATES OF EVEN-ODD NUCLEI

Type of transition	Nucleus	J^π of initial state	Properties of final state			E_γ (MeV)	I_γ(%)	$\lvert M\rvert^2_{M1}$	$\lvert M\rvert^2_{M1}$ / $(\lvert M\rvert^2_{E1})_{max}$
			E(MeV)	J^π	l_n				
$\Delta l_n = 0$	^{25}Mg	$1/2^+$	0·58	$1/2^+$	0	6·74	2·6	—	0·1
	^{25}Mg	$1/2^+$	2·56	$1/2^+$	0	4·77	1·3	—	0·12
	^{29}Si	$1/2^+$	g.s.*	$1/2^+$	0	8·47	2	0·04	0·025
	^{33}S	$1/2^+$	0·84	$1/2^+$	0	7·80	2·6	0·47	0·15
$(s_{1/2} - s_{1/2})$	^{41}Ca	$1/2^+$	2·68	$1/2^+$	0	5·70	1·4	—	1
	^{41}Ca	$1/2^+$	3·40	$1/2^+$	0	4·94	3	—	1·5
$\Delta l_n = 2$	^{25}Mg	$1/2^+$	0·98	$3/2^+$	2	6·36	4·3	—	0·2
	^{25}Mg	$1/2^+$	2·81	$3/2^+$	2	4·52†	<2†	—	<0·25
$(s_{1/2} - d_{3/2})$	^{29}Si	$1/2^+$	1·28	$3/2^+$	2	7·22	7·5	0·24	0·15
	^{33}S	$1/2^+$	g.s.*	$3/2^+$	2	8·64	1·8	0·24	0·08
$1/2^+ \to 3/2^+$	^{29}Si	$1/2^+$	2·43	$3/2^+$	Isotropic	6·04	1·2	0·07	0·04

* g.s. Ground state of nucleus.
† Existence uncertain, intensity is only an estimate.

compare the $E1$ and $M1$ transition probabilities for different states of the light nuclei.*

Following WILKINSON,[11] taking into account the motion of the nuclear core and putting $D = D_0$, we obtain the average values

$$|M|^2_{E1} = 0{\cdot}15 \qquad \text{and} \qquad |M|^2_{M1} = 0{\cdot}15$$

and

$$|M|^2_{M1}/|M|^2_{E1} \simeq 1.$$

If we can assume that the $E1$ matrix elements for $A < 20$ are not very different from those for $A = 20$–40, and if we then compare $|M|^2_{M1}$ with the maximum value of $|M|^2_{E1}$, we obtain the qualitative result that the probabilities of the forbidden $M1$ transitions which we observed are not very different from the l-allowed transition probabilities.

CAUSES OF RELAXATION IN SELECTION RULE

A large number of forbidden $M1$ transitions with $\Delta l = 2$ are observed between the low-lying levels of odd mass heavy nuclei. More detailed information about these levels is given in the Appendix.

Several authors[12–18] have studied some of the possible reasons why the forbiddenness of such $M1$ transitions is relaxed. In particular the following factors have been investigated: (1) charge-exchange and spin-exchange interactions between the two nucleons, (2) spin-orbit coupling, (3) coupling between the nucleons and nuclear surface oscillations, (4) admixture of other nucleon configurations with the given single-particle state.

It has been shown that factors 1, 2, 3 could not substantially increase the probability of those $M1$ transitions which follow (n,γ) reactions. We will not give the arguments which have led to this conclusion here since they are very similar to those given, for example, by DE-WAARD and GERHOLM.[13] The most obvious explanation for the observed $M1$ transition probabilities is that they are due to the mixing of nucleon configurations in the initial and possibly also the final states. It should be borne in mind that the mixing will be such as to change the state of only one particle in the corresponding transition or such that the coupling of only one momentum with respect to another is changed. In addition the mixing will occur between states lying close together and having the same parity; thus the most probable mixing of the $s_{1/2}$ and $d_{3/2}$ states will be with $s_{1/2}$, $d_{3/2}$ and $d_{5/2}$ states. For example, the $M1$ transitions in ^{29}Si can correspond to the following changes in the neutron configurations.

For $1/2^+ \to 3/2^+$ transitions with mixing in the initial state

$$[(d_{5/2}\, d_{3/2})_{J=2}\, d_{3/2}]_{1/2^+} \to [(d^6_{5/2})_{J=0}\, d_{3/2}]_{3/2^+}$$

and, where there is mixing in the final state:

$$[(d^6_{5/2})_{J=0} s_{1/2}]_{1/2^+} \to [(d^5_{5/2}\, d_{3/2})_{J=2} s_{1/2}]_{3/2^+}$$

and for $1/2^+ \to 1/2^+$ transitions

$$[(d^5_{5/2}\, d_{3/2})_{J=1} s_{1/2}]_{1/2^+} \rightleftarrows [(d^6_{5/2})_{J=0} s_{1/2}]_{1/2^+}.$$

The direction of the transition in the last example depends on whether the mixing is in the initial or final states.

Mixed nucleon configurations can arise in the initial state when a compound nucleus is formed because then the nuclear excitation energy can be concentrated upon a complete range of possible nucleon configurations. However, the notion of compound nucleus formation is not in accord with the $E1$ transition data—in particular, the correlation between the $E1$ transition matrices and the reduced widths of the levels to which the transitions go.[4]

The data on $E1$ and $M1$ transitions from thermal neutron capture states can be shown to be mutually consistent without bringing in the supposition that a compound nucleus is formed. It is sufficient to suppose that only a small number of nucleon configurations are excited in the initial state when a nucleus captures a neutron, for example, the ^{29}Si configurations given above. The probability of a direct transition of the captured neutron must be several times greater than the probability of exciting such configurations. This is not inconsistent with the data on the size of $|M|^2_{M1}$, since for the nuclei ^{25}Mg, ^{29}Si and ^{33}S it is known that in every case this quantity is smaller than $(|M|^2_{E1})_{max}$.

$M1$ TRANSITIONS IN ODD-ODD NUCLEI

Information on $M1$ transitions in ^{24}Na, ^{28}Al, ^{32}P and ^{36}Cl has been collected together in Table 3. As in Table 2, the transitions have been divided into groups according to the angular momentum change Δl_n. A separate position in the table has been given to the transition in ^{24}Na which goes to the 0·47 MeV level. It seems that this transition corresponds to a change in the state of the last neutron $s_{1/2} \to d_{5/2}$, for this would explain the low probability of this transition. As a result of the different possible mutual orientations of the angular momenta of the odd

* WILKINSON[11] did not consider nuclei with different Z and N parity separately because he failed to appreciate the large variation of $|M|^2$ for the different nuclear categories. It is clear that the $M1$ as well as the $E1$ transitions which were systematized by WILKINSON may include different kinds of forbiddenness. Here, however, we will consider only l-forbiddenness.

VOL 14 196

TABLE 3.—$M1$ TRANSITIONS FROM INITIAL STATES OF ODD-ODD NUCLEI

Type of transition	Nucleus	J^π of initial state	Properties of final state			E_γ(MeV)	I_γ(%)	$\lvert M\rvert^2_{M1}$	$\lvert M\rvert^2_{M1}$ / $(\lvert M\rvert^2_{E1})_{max}$
			E(MeV)	J^π	l_n				
	^{24}Na	$1^+, 2^+$	0·56	2^+	0	6·40	22	0·059	1·2
	^{24}Na	$1^+, 2^+$	1·34	1^+	0	5·61	4·5	0·023	0·6
	^{24}Na	$1^+, 2^+$	1·84	$1^+, 2^+$	0	5·12	0·8	0·004	0·1
	^{28}Al	$2^+, 3^+$	g.s.	3^+	0	7·72	24	0·17	1·5
$\Delta l_n = 0$	^{28}Al	$2^+, 3^+$	0·03	2^+	0	(7·70)	<5	—	<0·3
	^{28}Al	$2^+, 3^+$	0·97	2^+	0	6·76	1·7	0·017	0·2
	^{28}Al	$2^+, 3^+$	2·14	$2^+, 3^+$	0	5·60	1·2	0·022	0·2
$(s_{1/2} - s_{1/2})$	^{28}Al	$2^+, 3^+$	2·49	$2^+, 3^+$	0	4·73	<8	—	—
	^{28}Al	$2^+, 3^+$	3·29	$2^+, 3^+$	0	4·42	1	0·037	0·4
	^{28}Al	$2^+, 3^+$	3·35	$2^+, 3^+$	0	(4·38)	<0·3	—	<0·12
	^{28}Al	$2^+, 3^+$	3·67	$2^+, 3^+$	0	4·06	2	0·094	1
	^{28}Al	$2^+, 3^+$	3·70	$2^+, 3^+$	0	(4·03)	<0·5	—	<0·25
	^{28}Al	$2^+, 3^+$	4·24	$2^+, 3^+$	0	2·98	<8	—	—
	^{32}P	$0^+, 1^+$	0·51	$0^+, 1^+$	0	7·42	4	—	0·6
	^{32}P	$0^+, 1^+$	1·15	$0^+, 1^+$	0	6·76	10	—	2
	^{36}Cl	$1^+, 2^+$	1·16	$1^+, 2^+$	0	7·41	10	0·19	7
	^{36}Cl	$1^+, 2^+$	1·60	$1^+, 2^+$	0	6·96	1·9	0·05	2
$\Delta l_n = 2$	^{28}Al	$2^+, 3^+$	1·63	—	2	6·13	3	—	0·5
	^{32}P	$0^+, 1^+$	g.s.	1^+	2	7·94	0·3	—	0·03
	^{32}P	$0^+, 1^+$	0·08	2^+	2	7·85	0·9	—	0·1
$(s_{1/2} - d_{3/2})$	^{36}Cl	$1^+, 2^+$	g.s.	2^+	2	8·56	2·8	0·035	1·5
	^{36}Cl	$1^+, 2^+$	0·79	—	2	7·78	7·8	—	5
$\Delta l_n = 2$ $(s_{1/2} - d_{5/2})$	^{24}Na	$1^+, 2^+$	0·47	1^+	2	(6·49)	<0·1	—	<0·03

Notes: (1) g.s.—ground state; (2) values in brackets indicate energies of γ-rays which could not be detected, estimates of their intensities are given; (3) as a rule, only l_n is known for the excited levels of odd-odd nuclei. However, in spite of the uncertainty in the value of J we can say that transitions to $l_n = 0$ levels are $M1$ transitions. $(\lvert M\rvert^2_{E1})_{max}$ refers to the most probable transition of all transitions which go to $l_n = 1$ levels.

neutron and proton, the odd-odd nuclei contain $j - j$ multiplets. This leads to a considerable increase in the number of $M1$ transitions and so also to more $l_n = 0$ and $l_n = 2$ levels in odd-odd than in even-odd nuclei.[3]

From the data given in Tables 2 and 3 it follows that the quantity $\lvert M\rvert^2_{M1}/(\lvert M\rvert^2_{E1})_{max}$ is appreciably larger for odd-odd nuclei than for the corresponding even-odd nuclei. However, one cannot say for certain whether the increase in the value of this ratio is due to an increase in the $M1$ transition probability or to a decrease in the $E1$ transition probability. There is no reason to suppose that $(\lvert M\rvert^2_{E1})_{max}$ remains unchanged as one goes from odd-odd to even-odd nuclei. Crude estimates of $(\lvert M\rvert^2_{E1})_{max}$, based upon the values of Γ_γ and D given in Table 1 and with $D_0 = 1$ MeV, are given in Table 4. It will be seen that $(\lvert M\rvert^2_{E1})_{max}$ decreases on the average by a factor of 30 as one goes

TABLE 4.—ESTIMATES OF $(\lvert M\rvert^2_{E1})_{max}$

Z and N odd or even	Nucleus	E_γ(MeV)	I_γ(%)	Properties of states			$(\lvert M\rvert^2_{E1})_{max}$
				Initial J^π	Final		
					J^π	l_n	
Even-odd nuclei	^{29}Si	2·10	16	$1/2^+$	$1/2^-$	1	1·66
	^{33}S	2·97	13	$1/2^+$	$1/2^-$	1	2·95
Odd-odd nuclei	^{24}Na	2·41	10·5	$1^+, 2^+$	—	1	0·04
	^{28}Al	2·28	5·1	$2^+, 3^+$	—	1	0·11
	^{36}Cl	4·98	6	$1^+, 2^+$	—	1	0·025

from even-odd to odd-odd nuclei, whereas $|M^2_{M1}|$ (see Tables 2 and 3) falls by a factor of about 3 only. It must be remembered that this comparison is not very reliable because of the very inaccurate values used for Γ_γ and D.

On the other hand one might expect the $M1$ transition probabilities to increase on the grounds that such transitions are favoured by the coupling between the odd neutron and the odd proton. For example, GRECHUKHIN[19] has shown that for certain $\Delta l_n = 0$ transitions the $M1$ transition probability can be increased by virtue of a re-orientation of the neutron angular momentum with respect to the angular momentum of the odd proton. Such transitions are rather similar to the $^1s_0 \rightarrow {}^3s_1$ transition in the deuteron, or to transitions between the members of a $j - j$ multiplet, which are also dependent upon the different mutual orientation of the angular momenta of the odd neutron and proton. As is well known, the matrix elements for this type of transition are large.[20–23]

It immediately becomes apparent from Table 3 that some of the $\Delta l_n = 0$ transitions (in particular, the 6·40 MeV transition in ^{24}Na, the 7·72 MeV transition in ^{28}Al, the 6·76 MeV transition in ^{32}P and the 7·41 MeV transition in ^{36}Cl) do in fact lead to a large number of quanta per neutron captured (0·1–0·7) and to large values of the quantity $|M|^2_{M1}/(|M|^2_{E1})_{max}$ (on the average $\sim$1·5).

REFERENCES

1. SHUT'KO A. V. and ZARETSKII D. F., *Zh. eksp. teor. fiz.* **29,** 866 (1955).
2. LANE A. and LYNN J., *Proceedings of the Second International Conference on the Peaceful Uses of Atomic Energy, Geneva,* Vol. 15, p. 38. United Nations, New York (1958); LYNN J., *Proceedings of the International Conference on the Neutron Interactions with the Nucleus,* New York (1957).
3. GROSHEV L. V. and DEMIDOV A. M., *J. Nucl. Energy* **8,** 103 (1958–59).
4. GROSHEV L. V., DEMIDOV A. M., LUTSENKO V. N. and PELEKHOV V. I., *Proceedings of the Second International Conference on the Peaceful Uses of Atomic Energy, Geneva,* Vol. 15, p. 138. United Nations, New York (1958).
5. MOSKOWSKI S., *Phys. Rev.* **89,** 474 (1953).
6. LEVIN L. and HUGHES D., *Phys. Rev.* **101,** 1328 (1956).
7. BRUGGER R., EVANS J., IOKI E. and SHANKLAND R., *Phys. Rev.* **104,** 1054 (1956).
8. HIBDON C., *Proceedings of the Second International Conference on the Peaceful Uses of Atomic Energy, Geneva,* Vol. 15, p. 72. United Nations, New York (1958).
9. HUGHES D. and SCHWARTZ R., *Neutron Cross-Sections,* U.S.A.E.C. Report BNL-325 (1958).
10. BARTHOLOMEW G., CAMPION R., KNOWLES J. and MANNING G., *Proceedings of the International Conference on the Neutron Interactions with the Nucleus,* New York (1957).
11. WILKINSON D., *Phil. Mag.* **1,** 127 (1956).
12. GRAHAM R. and BELL R., *Canad. J. Phys.* **31,** 377 (1953).
13. DE-WAARD H. and GERHOLM T., *Nucl., Phys.* **1,** 281 (1956).
14. SACHS R. and ROSS M., *Phys. Rev.* **84,** 379 (1951).
15. RUSSEK A., *Phys. Rev.* **99,** 834 (1955).
16. FEINBERG E., *Shell Theory of Nuclei,* p. 211, Princeton (1955); GOLDHAMMER P., *Phys. Rev.* **101,** 1375 (1956).
17. VOLKOV A., *Phys. Rev.* **94,** 1664 (1954).
18. ARIMA A., HORIE H. and SANO M., *Progr. theor. phys.* **17,** 567 (1957).
19. GRECHUKHIN D. P., *Zh. eksp. teor. fiz.* **33,** 183 (1957).
20. BLATT J. and WEISSKOPF V. F., *Theoretical Nuclear Physics,* John Wiley, New York (1952).
21. SEVERINS J. and HANNA S., *Phys. Rev.* **100,** 1254 (1955).
22. DE SHALIT A., *Phys. Rev.* **105,** 1537 (1957).
23. GOLDHABER M. and WENESER I., *Ann. Rev. Nucl. Sci.* **5,** 1 (1955).
24. ALVÄGER T., JOHANSSON B. and ZUK W. *Ark. Fys.* **14,** 4, 373 (1958).
25. LINDQVIST T. and MARKLUND I., *Nucl. Phys.* **1,** 281 (1956).
26. WAY K., KUNDU D. N., MCGINNIS C. L. and VAN LIESHOUT R., *Ann. Rev. Nucl. Sci.* **6,** 129.
27. MCGOWAN F. and STELSON P., *Phys. Rev.* **109,** 901 (1958).
28. STROMINGER D., HOLLANDER J. and SEABORG G. *Rev. Mod. Phys.* **30,** 585 (1958).

APPENDIX

M1 *transitions between weakly excited states of heavy nuclei*

There is a fairly large amount of information in the literature on the probabilities of $M1$ transitions between the low lying states of odd mass heavy nuclei. As a result of contributions by a number of authors[12,13,24,25] it has been known for some time now that forbidden $M1$ transitions with $\Delta l_n = 2$ have the regular feature that: (1) the spread in the values of the matrix elements is small not only for odd proton nuclei but for odd neutron nuclei as well; (2) in addition, the matrix elements for odd proton nuclei are 300 times smaller and for odd neutron nuclei they are 60 times smaller than the corresponding single particle allowed $M1$ transition matrices. This behaviour is illustrated in Fig. 1 which gives the reduced lifetimes $\tau_\gamma E^3$ for $M1$ transitions with $\Delta l = 2$. These lifetimes are plotted separately for nuclei with an odd number of neutrons (left-hand part) and an odd number of protons (right-hand part). τ_γ was obtained from the formula

$$\tau_\gamma = 1{\cdot}44(1 + \alpha_{total})\left(1 + \frac{E2}{M1}\right)T_{1/2} \qquad (4)$$

where the term $E2/M1$ allows for an admixture of $E2$ in the transition. Most of the results presented in Fig. 1 have been taken from previously published work.[12,13,24] Exceptions are our own point for ^{203}Tl, ($E_\gamma = 0{\cdot}279$ MeV) which now lies considerably higher in this plot due to the adoption of a new value of τ_γ, and the addition of two new points in the left-hand part of the plot: ^{111}Cd ($E_\gamma = 0{\cdot}432$ MeV) and ^{113}Cd ($E_\gamma = 0{\cdot}300$ MeV), which have been reliably computed from Coulomb excitation data.

The small spread in the values of the matrix elements may be due to the fact that at the boundaries of each group of odd nuclei the transitions we are considering belong to one and the same type. In the case of the odd neutron nuclei we are concerned with $2d_{3/2} - 3s_{1/2}$ transitions and in the case of odd proton nuclei with $1g_{7/2} - 2d_{5/2}$ transitions, apart from ^{197}Au,

^{203}Tl and ^{205}Tl where the transitions belong to the type $2d_{3/2} - 3s_{1/2}$. In all probability, the relaxation of the forbiddenness in $M1$ transitions with $\Delta l = 2$ and $\Delta j = 1$ is due to configuration mixing[18] and this mixing will, of course, be different in transitions of different types. This explains the different orders of forbiddenness of $M1$ transitions in odd neutron and odd proton nuclei.

It is to be expected that the spin-orbit interaction plays some part in reducing the forbiddenness of $M1$ transitions in odd proton nuclei. To find the extent to which configuration mixing affects the probability of $M1$ transitions one ought really to make a rather better estimate of the spin-orbit interaction contribution than that made by DE-WAARD and GERHOLM.[13]

In addition to the l-forbidden $M1$ transitions we considered also other reasonably well-established $M1$ transitions in heavy odd nuceli ($A > 90$) for which τ_γ has been measured. The reduced lifetimes of these transitions are given in Fig. 2. The values of $\tau_\gamma E_\gamma^3$ appearing on the left-hand side of this figure were calculated from the data given in a recent detailed article by MCGOWAN and STELSON[27] on Coulomb excitation. The reduced $M1$ transition probabilities given in this article are mainly for odd proton nuclei. The values of $\tau_\gamma E_\gamma^3$ for $M1$ transitions for the odd neutron nuclei plotted on the right-hand side of Fig. 2 were calculated from the data given by STROMINGER *et al.*[28]

Before we start to discuss the results given in Fig. 2 we must say a few words about the division of the $M1$ transition data between Figs. 1 and 2. If we can assume that Fig. 1 contains the well-established transitions with $\Delta l = 2$, then Fig. 2

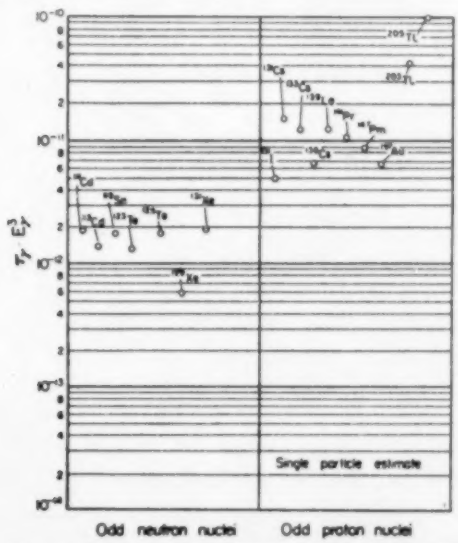

FIG. 1.—Reduced lifetimes of l-forbidden $M1$ transitions.

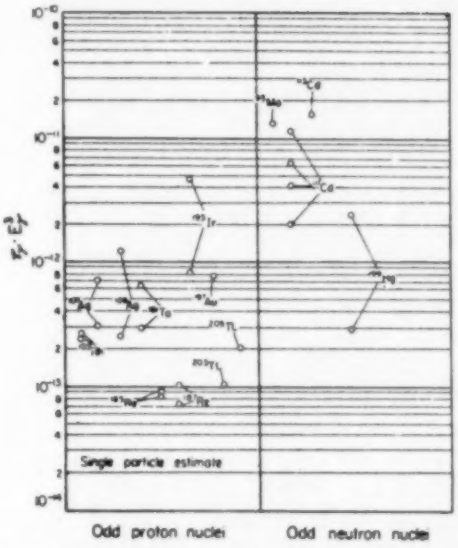

FIG. 2.—Reduced lifetimes of $M1$ transitions which are not attributed to l-forbidden transitions.

contains all the remaining transitions; that is not only those which are forbidden for other reasons but also the allowed transitions. In particular, a few $\Delta l = 2$ transitions may find their way into Fig. 2. It will be remembered that according to the single-particle model the only allowed transitions are those of the type $nd_{3/2} - nd_{5/2}$, $ng_{7/2} - ng_{9/2}$ etc.

If we now look at the left-hand side of Fig. 2 we notice that most of the transitions in the odd proton nuclei are considerably more probable than the transitions in the right-hand side of Fig. 1. It is significant also that the $M1$ transitions in ^{203}Tl (0·400 MeV) and ^{205}Tl (0·410 MeV), which according to the single-particle model are allowed transitions, have matrix elements which are close to the single particle estimates, whereas the $M1$ transitions with $\Delta l = 2$ in ^{203}Tl (0·279 MeV) and ^{205}Tl (0·205) are forbidden to an appreciably greater extent than is the case for other odd proton nuclei (see right-hand side of Fig. 1).

As regards the $M1$ transitions for odd neutron nuclei (right-hand side of Fig. 2), the available data are rather sparse and there is almost no information on mixed $M1 + E2$ transitions. We would stress that the effect of making an allowance for an $E2$ admixture is to raise the points in our diagram. For these nuclei most of the $M1$ transitions have very small matrix elements. The reason why these matrix elements are not closer to the single-particle estimates for odd neutron nuclei is still not understood. It may be that this class of nuclei has not been properly examined, or the discrepancy may be due to some other cause.

Reactor Science and Technology (Journal of Nuclear Energy, Parts A & B), 1961, Vol. 14, pp. 124 to 126. Pergamon Press Ltd. Printed in Northern Ireland

STABILITY OF THE HEAT OUTPUT FROM A PULSED REACTOR*

T. N. ZUBAREV

(*Received* 19 *December* 1958)

Abstract—The stability conditions for linear and cosine laws of reactivity change during a neutron pulse are considered and formulae are deduced for the heat produced.

IN a previous paper[1] the author has investigated the operating conditions of a pulsed reactor in which the duration of the neutron burst automatically decreases or increases following an increase or decrease of the maximum reactivity of the reactor during the burst. This ensures stability of the heat output. We now consider the dependence of the heat output in a pulsed reactor on various factors characterizing the intensity of the neutron bursts, under the following conditions:

$$T \ll \frac{1}{\omega} \ll \bar{T}_d, \tag{1}$$

$$\frac{\Delta k_0}{\omega T} > 1, \tag{2}$$

$$|\Delta k(t)| \ll 1. \tag{3}$$

Here T is the lifetime of the neutrons in the reactor, $\bar{T}_d$ the mean half-life of the fission fragments emitting delayed neutrons; $\omega = 2\pi/T_n$ (where T_n is the period of a single neutron burst); $\Delta k(t) = k_{ett}(t) - 1$, $\Delta k_0 = (k_{ett})_{max} - 1$ where $k_{ett}(t)$ and $(k_{ett})_{max}$ are the effective neutron multiplication coefficients in the reactor (not taking into account the delayed neutrons) at the instant t and at the instant of maximum reactivity during the neutron burst, respectively.

If the conditions (1), (3) and $\Delta k(t) < 0$ are satisfied the dependence on time of the number of neutrons in the reactor pulse is given by $N(t)$, which satisfies the equation

$$dN = \frac{N}{T}\,\Delta k(t)\,dt + \frac{N_d}{T}\,dt, \tag{4}$$

where N_d, the equilibrium number of delayed neutrons in the reactor, is determined by the mean reactor power. If the heat output between neutron bursts is substantially less than the heat output during the burst, we have

$$N_d \simeq \frac{Q\nu\beta T}{q_0 T_p}, \tag{5}$$

where Q and q_0 are the quantities of heat generated in the reactor during a single neutron burst and in the fission of one uranium nucleus respectively, β is the proportion of delayed neutrons, ν is the total number of neutrons produced in the fission of a uranium nucleus and T_p is the time between two consecutive neutron bursts.

The relation (5) is valid in the case of a constant heat output during the neutron bursts ignoring the fission fragments in the core. If the heat output changes gradually from one burst to the next, one must in relation (5) replace Q by the quantity

$$\bar{Q} \simeq \frac{T_p \sum_i Q_i}{\bar{T}_d}, \tag{6}$$

where Q_i is the heat output during the i-th neutron burst and the summation is over the bursts which preceded the one considered within a time $\bar{T}_d$.

For $\Delta k(t) > 0$ the sources of delayed neutrons may be neglected and equation (4) assumes the form

$$dN = \frac{N}{T}\,\Delta k(t)\,dt. \tag{7}$$

The quantity of heat generated in the reactor during a neutron burst is

$$Q = q\int \frac{N(t)}{T}\,dt \simeq \frac{q}{T}\int N(t)\,dt, \tag{8}$$

where q is the quantity of heat generated by the absorption of one neutron.

Let the reactivity change during a neutron burst according to the law

$$\Delta k(t) = \Delta k_0 \frac{2}{\pi}\,\omega t \quad \text{for} \quad t < \frac{\pi}{2\omega}, \tag{9}$$

$$\Delta k(t) = \Delta k_0 \left(1 - \frac{2}{\pi}\,\omega t\right) \quad \text{for} \quad t > \frac{\pi}{2\omega}, \tag{10}$$

while initially ($t = t_1$) we have

$$\Delta k(t_1) = -\Delta k_1, \left|\frac{\Delta k_1}{\Delta k_0}\right| > 1. \tag{11}$$

* Translated by N. KEMMER from *Atomnaya Energiya* 7, 421 (1959).

Using the relation (9) and integrating equation (4) between the limits $t = 0$ and $t_1 = -\pi\Delta k_1/2\omega\,\Delta k_0$ we obtain the value $N(t)$ for $\Delta k(t) = 0$:

$$N_0 = \frac{N_d}{\Delta k_1}\exp\left[-\left(\frac{\Delta k_1}{\Delta k_0}a\right)^2\right] \times\left\{1 + 2\frac{\Delta k_1}{\Delta k_0}a\exp\left[-\left(\frac{\Delta k_1}{\Delta k_0}a\right)^2\right] \times\int_{-\frac{\Delta k_1}{\Delta k_0}a}^{0}\exp(-z^2)\,dz\right\}, \tag{12}$$

where

$$a = \frac{\sqrt{\pi}}{2}\sqrt{\frac{\Delta k_0}{\omega T}}.$$

If the conditions (1), (2) and (11) are satisfied we find from relations (12)

$$N_0 \simeq \frac{\pi}{2\sqrt{\Delta k_0\omega T}}N_d. \tag{13}$$

We denote the quantity of heat generated when $\Delta k(t)$ changes between the limits 0 to Δk_0, Δk_0 to 0, 0 to $(-\Delta k_1)$, by Q_1, Q_2 and Q_3 respectively. If then $\Delta k(t)$ varies according to (9) and (10) we obtain from (7), (8) and (13)

$$Q_1 \simeq \frac{(\pi)^{3/2}}{2}\frac{qN_d}{\Delta k_0\omega T}\int_0^a\exp(z^2)\,dz, \tag{14}$$

$$Q_2 \simeq \frac{(\pi)^{3/2}}{2}\frac{qN_d}{\Delta k_0\omega T}\exp(2a^2)\int_0^a\exp(-z^2)\,dz, \tag{15}$$

$$Q_3 \simeq \frac{(\pi)^{3/2}}{2}\frac{qN_d}{\Delta k_0\omega T}\exp(2a^2)\int_0^{\frac{\Delta k_1}{\Delta k_0}a}\exp(-z^2)\,dz. \tag{16}$$

Taking into account that

$$\int_0^x\exp(z^2)\,dz = \frac{\exp(x^2)}{2x}\left\{1 - \frac{M(-\tfrac{1}{2}, \tfrac{1}{2}, x^2)}{\exp(x^2)}\right\},$$

where $M(-\frac{1}{2}, \frac{1}{2}, x^2)$ is the confluent hypergeometric function[2] we find from (14) to (16) subject to condition (2) the total heat output during a neutron burst if $\Delta k(t)$ varies according to the linear law

$$Q_{1\text{in}} = Q_1 + Q_2 + Q_3 \simeq 2q\left(\frac{\pi}{2}\right)^2\frac{N_d}{\Delta k_0\omega T}\exp\left(\frac{\pi}{2}\frac{\Delta K_0}{\omega T}\right). \tag{17}$$

The greater part of the heat is generated as $\Delta k(t)$ decreases ($Q_1 \ll Q_2$) from Δk_0 to 0, and an approximately equal amount of heat is generated during the decay of the chain reaction ($Q_2 \simeq Q_3$). The greatest value of the neutron flux in the reactor is attained as $\Delta k(t)$ falls through the value zero $\Delta k(t) = 0$.

We have assumed that $\Delta k(t)$ varies linearly, but in certain pulsed reactor systems $\Delta k(t)$ may vary smoothly about its maximum value. The corresponding correction in the magnitude of the heat output proves to be considerable, but may be found easily.

Assume that $\Delta k(t)$ varies according to the law

$$\Delta k(t) = \Delta k_0\cos\omega t. \tag{18}$$

Then, using equation (7), relations (8) and (13) and condition (2), we obtain

$$Q_{\cos} \simeq 2\pi\frac{qN_0}{\omega T}\exp\left(\frac{\Delta k_0}{\omega T}\right)I_0\left(\frac{\Delta k_0}{\omega T}\right) \simeq \left(\frac{\pi}{2}\right)^{3/2}\frac{2qN_d}{\Delta k_0\omega T}\exp\frac{2\,\Delta k_0}{\omega T}, \tag{19}$$

where $I_0(\Delta k_0/(\omega t))$ is the zero-order Bessel function with imaginary argument.

Using the relations obtained we shall discuss the stability conditions for the heat output in a pulsed reactor. We denote by K the ratio of the quantity of heat generated during the given neutron burst to the mean quantity of heat generated during previous bursts, during a time of the order of $\bar{T}_d$. By comparing equations (17), (19), (5) and (6) we obtain

$$K = \nu\beta\theta\frac{T}{T_p}f(\Delta k_0, \omega T), \tag{20}$$

where θ is the probability of neutron capture by a uranium nucleus and $f(\Delta k_0, \omega T)$ is a certain function of the parameters of the neutron burst. The form of the function $f(\Delta k_0, \omega T)$ is determined by the variation of the reactivity during a neutron burst. In the variation of reactivity according to equations (9) and (10), we have

$$f_{1\text{in}}(\Delta k_0, \omega T) \simeq 2\left(\frac{\pi}{2}\right)^2\frac{\exp\left(\frac{\pi}{2}\frac{\Delta k_0}{\omega T}\right)}{\Delta k_0\omega T}, \tag{21}$$

while for a variation according to equation (18), we have

$$f_{\cos}(\Delta k_0, \omega T) \simeq 2\left(\frac{\pi}{2}\right)^{3/2}\frac{\exp\left(\frac{2\Delta k_0}{\omega T}\right)}{\Delta k_0\omega T}. \tag{22}$$

The condition $K = 1$ can be called the condition of stability of heat output, for if it is satisfied the heat output during a neutron burst (if there are no external neutron sources) remains unchanged from one burst to the next.

In all cases of practical interest $\Delta k_0 > 0{\cdot}01$, $\theta \leqslant 1$, $\nu > 2$, $\beta \simeq 0{\cdot}008$. In such a case we obtain from

equations (20) to (22) that for $K = 1$ condition (2) is satisfied if

$$\frac{T_p}{T_n} > 10.$$

Equations (17) and (19) also allow one to obtain the relation between the relative variations of heat output during a neutron burst and the variations of the other parameters characterizing the burst:

$$\frac{\Delta Q}{Q} \simeq \frac{\Delta N_d}{N_d} + \alpha \frac{\Delta k_0}{\omega T} \left(\frac{\Delta(\Delta k_0)}{\Delta k_0} - \frac{\Delta(\omega t)}{\omega T} \right). \quad (23)$$

Here the coefficient α is equal to $\frac{1}{2}\pi$ and 2 for linear and cosine variations of $\Delta k(t)$ respectively.

By considering relation (23) we see that the maintenance of stable heat output during the bursts ($\Delta Q/Q = 0$) is possible for small variations in Δk_0 and ωT if the condition

$$\frac{\Delta(\Delta k_0)}{\Delta k_0} = \frac{\Delta(\omega T)}{\omega T} \quad (24)$$

is fulfilled.

Acknowledgments—The author wishes to thank YU. N. ZANKOV and A. K. SOKOLOV for discussion of the results of the present paper.

REFERENCES

1. ZUBAREV T. N., *Atomnaya Energiya* **5**, 605 (1958).
2. JAHNKE E. and EMDE F., *Tables of Functions*, Dover Publns. (1943).

VOL
14
196

Reactor Science and Technology (Journal of Nuclear Energy, Parts A and B), 1961, Vol. 14, pp. 127 to 131. Pergamon Press Ltd. Printed in Northern Ireland

ELECTROLYTIC SEPARATION OF SMALL QUANTITIES OF URANIUM, NEPTUNIUM, PLUTONIUM AND AMERICIUM*

A. G. SAMARTSEVA

(*Received* 4 *September* 1958)

Abstract—When studying the nuclear properties of elements or investigating isotopic compositions it is necessary to produce thin uniform coatings; in the analytical chemistry of the transuranium elements quantitative separation of these elements is important, and they may be present in tracer quantities. The present paper describes an original electrolytic method for the quantitative separation of traces of uranium neptunium, plutonium and americium from acid solutions. It is shown that the yield of elements in the electrolysis does not depend on the anion of the electrolyte, but is determined primarily by the pH of the solution. Conditions for the quantitative electrolytic separation of plutonium in the presence of various metal impurities are specified; the influence of iron was eliminated by introducing oxalic acid into the electrolyte.

VOL. 14 1961

THE electrolytic separation of the transuranium elements from aqueous solutions is an excellent method of producing thin uniform coatings for studying the nuclear properties or the isotopic composition of these radioelements. This method can also be used with success in the analytical chemistry of the transuranium elements, since it enables them to be separated quantitatively and without carriers even when they are present in solution in tracer quantities.

We have previously devised a method for the quantitative separation of uranium[1] and also of the transuranium elements[2] from solutions of mineral acids. The present paper is a continuation of those investigations.

Uranium, neptunium, plutonium and americium were separated in an ordinary electrolytic cell consisting of a small platinum cup (the anode) and an elongated platinum petal with a working area of 1 cm^2 (the cathode). In a cell of this kind it is possible to work with an electrolyte at any pH value without significant losses of radioelements through adsorption on the walls, such as is observed when a glass or plexiglas electrolyser is used. The solution was stirred by the cathode, which rotated at a speed of 60–80 rev/min. Electrolytic separation of the radioelement took place on both sides of the petal cathode simultaneously; the α-activity on this electrode was measured in a special chamber.[3]

The isotopes ^{233}U, ^{237}Np, ^{239}Pu, ^{241}Am were used in the work. By means of an ionization chamber and a multichannel amplitude analyser it was shown that ^{239}Pu contains 0·7–0·9 per cent of mixed ^{241}Am and ^{238}Pu, and that ^{237}Np contains ~2·0 per cent ^{239}Pu. No impurities were discovered in the isotope ^{241}Am; the ^{233}U was not analysed. Weighable quantities of the hydroxides of the elements were dissolved in the acids used as electrolytes. Studies of the valency states of the elements in the initial solutions showed that ^{233}U was in the hexavalent state; ^{237}Np consisted of Np^{VI}—10·2 per cent, Np^{V}— ~90 per cent, Np^{IV}— <1 per cent; ^{239}Pu consisted of Pu^{VI}— 14·3 per cent, Pu^{IV}—56·1 per cent, Pu^{III}—28·9 per cent); ^{241}Am was in the trivalent state.

The electrolytes used were nitric, hydrochloric, perchloric, sulphuric and oxalic acids at a hydrogen ion concentration of 10^{-1} to 10^{-4} M and buffer solutions at a hydrogen ion concentration of 10^{-5} to 10^{-9} M. The investigation was carried out with the following molar concentrations of the radioisotopes in the electrolyte: ^{233}U—$1{\cdot}3 \times 10^{-8}$; ^{237}Np—$(0{\cdot}2$–$1{\cdot}2)10^{-6}$; ^{239}Pu—$4{\cdot}1 \times 10^{-9}$; ^{241}Am—$1{\cdot}4 \times 10^{-10}$.

The experimental data presented here in the form of Tables and curves are in all cases the means of from three to five individual measurements.

ELECTROLYTIC SEPARATION OF URANIUM, NEPTUNIUM, PLUTONIUM AND AMERICIUM FROM WEAKLY ACID SOLUTIONS

Experimental data on yields as a function of the pH of the nitric acid solutions, current density and plating time are presented in Figs. 1–3 respectively.

It can be seen from Fig. 1 that the maximum yield for uranium is observed at a pH of 2·5 and for neptunium and plutonium at a pH of 2·0. The sudden

* Translated by R. D. M. HEGARTY from *Atomnaya Energiya* **8**, 324 (1960).

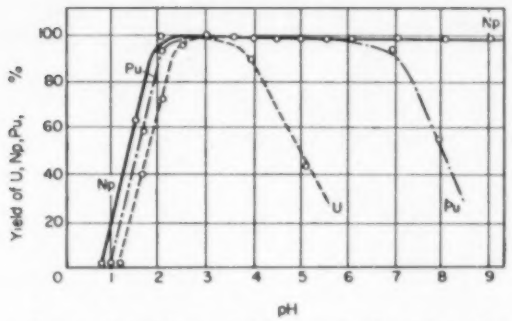

FIG. 1.—Dependence of yields on pH of solution. Current density at the cathode 100 mA/cm², electrolysis time 2 hr.

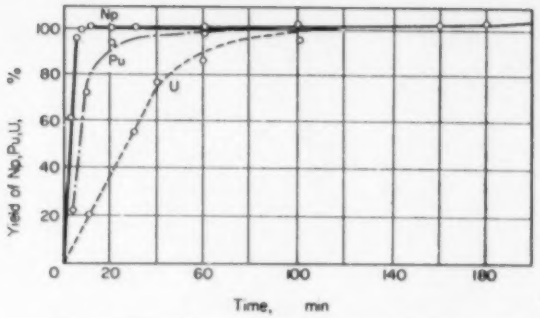

FIG. 3.—Dependence of yields on electrolysis time. pH = 3, current density 100 mA/cm².

fall in uranium yield for pH > 4 apparently indicates that the degree of hydrolysis is greater for uranium than for neptunium and plutonium. The last two elements are probably in the pentavalent state under these conditions and therefore do not hydrolyse up to a pH of 7–8.[4]

The very large differences between the rates of electrolytic separation of uranium, neptunium and plutonium can be seen from Fig. 3. This is explained, apparently, partly by the fact that the mechanism of electrolytic reduction is different for each element, but also by the different stability of the pentavalent ions, which are intermediate products of the first stage of reduction in the cathode region. According to Reference[5] near a mercury-drop cathode at a pH of 2·5 uranium first reduces to the pentavalent state:

$$UO_2^{++} + e^- \rightarrow UO_2^+,$$

which then undergoes the reaction:

$$2U^V \rightarrow U^{IV} + U^{VI}.$$

As a result of repeated oxidation-reduction reactions the rate of separation of uranium at the cathode becomes less. Neptunium, on the other hand, which in the initial solution is in the stable pentavalent state, immediately reduces to the tetravalent state at the cathode itself. The rate of electrolytic separation is mainly determined by the mobility of the ions; it is twenty times greater than the rate of separation of uranium (see Fig. 3).

In view of the fact that in the initial solution plutonium was mainly in a tri- or tetravalent state, it first oxidized to the pentavalent state and then, at the instant of separation at the cathode, again reduced to the tetravalent state. It can be seen from Fig. 1 that plutonium does in fact oxidize to Pu^V as it does not hydrolyse in solutions from pH = 7, i.e. in these conditions it behaves like Np^V.

The results obtained enabled the optimum conditions for quantitative electrolytic separation of thorium, uranium, neptunium, plutonium and americium to be selected separately (Table 1).

Tracer quantities of thorium, uranium, neptunium, plutonium and americium are deposited quantitatively on the platinum cathode under approximately the same conditions.

Table 2 presents experimental data on the electrolytic separation of transuranium elements from solutions of various mineral acids.

As can be seen from the table, the transuranium elements separate quantitatively from the solutions studied, so that the yield of these elements does not depend on the character of the electrolyte anion,

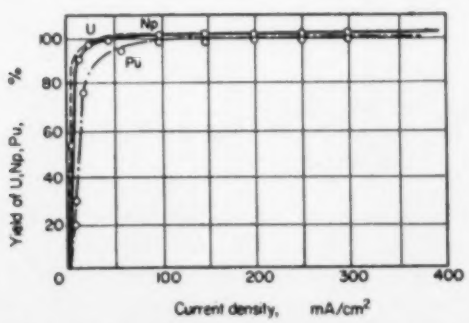

FIG. 2.—Dependence of yields on current density. pH = 3, electrolysis time 2 hr.

TABLE 1.—OPTIMUM CONDITIONS FOR ELECTROLYTIC SEPARATION OF THORIUM, URANIUM, NEPTUNIUM, PLUTONIUM AND AMERICIUM FROM A NITRIC ACID SOLUTION

Element	Volume of solution (ml)	pH	Current density (mA/cm²)	Duration of electrolysis (min)	Yield (%)
Th (Io)	20	2·5	100	120	99·8
U	20	2·5	100	120	100·1
Np	80	3	250	10	100·4
Pu	20	3	100	120	100·0
Am	20	3	100	5	99·7

TABLE 2.—ELECTROLYTIC SEPARATION OF URANIUM, NEPTUNIUM, PLUTONIUM AND AMERICIUM FROM SOLUTIONS OF VARIOUS ACIDS
(pH equal to 2–3, current density 100 mA/cm²)

Number of experiments	Acid	Yield of element (%)			
		U	Np	Pu	Am
5	H_2SO_4	100·1	99·8	97·8	99·2
13	HCl	100·0	100·0	98·9	98·9
7	$HClO_4$	100·6	100·2	100·1	99·7
50	HNO_3	100·0	100·2	100·6	100·2
28	$H_2C_2O_4$	100·2	98·9	99·7	98·7

but is strongly dependent on the hydrogen ion concentration.

Fig. 4 presents data on the kinetics of the electrolytic separation of plutonium from hydrochloric and perchloric acids. It is best to use nitric acid as the electrolyte, and not hydrochloric or perchloric.

ELECTROLYTIC SEPARATION OF URANIUM, NEPTUNIUM AND PLUTONIUM FROM AN 0·1 M SOLUTION OF NITRIC ACID

As it is not always convenient in practice to work with low (0·01 to 0·001 M) concentrations of acids, we endeavoured to find conditions for the electrolytic separation of the transuranium elements from more acid solutions. It was noticed earlier that as the hydrogen ion concentration increases, the current density must also be increased. However the first experiments in this direction proved unsuccessful, since over a wide range of current densities (400–3000 mA/cm²) only a very slight electrolytic separation of neptunium and plutonium was observed; under these conditions uranium separates quantitatively at a current density of 700–1000 mA/cm².

We found that if the initial plutonium solution was evaporated to dryness three or four times with a small amount of concentrated nitric acid (i.e. converted to the tetravalent state) and the residue then

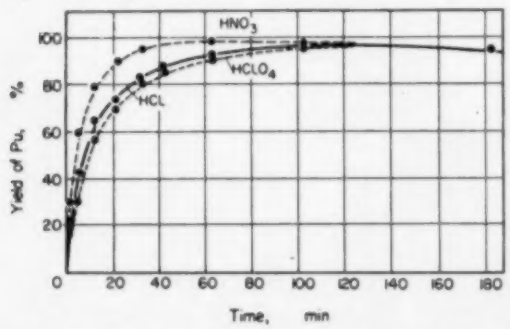

FIG. 4.—Dependence of yield of plutonium on duration of experiment.
pH = 3, current density 100 mA/cm².

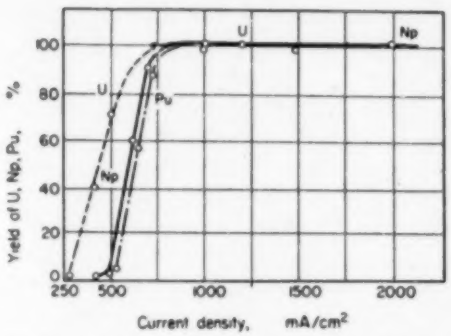

FIG. 5.—Dependence of yields on current density. 0·1 M solution of nitric acid, electrolysis time 2 hr.

dissolved in 20 ml of 0·1 M nitric acid, then the plutonium was deposited quantitatively from this solution by electrolysis. Experimental data on the yields of uranium, plutonium and neptunium from 0·1 M nitric acid as functions of current density and time of electrolysis are presented in Figs. 5 and 6 respectively.

The differences between the rates of electrolytic separation for uranium, neptunium and plutonium are probably explained by the different valencies of the elements in the initial solution and, consequently, by the different mechanisms of electrolytic reduction.

On the basis of the data obtained, the following optimum conditions were selected for the electrolytic separation of uranium, neptunium and plutonium from 0·1 M solutions of nitric acid: (1) current density at the cathode 750–1000 mA/cm²; (2) electrolysis time 2–3 hours; (3) volume of solution 20–40 ml. We used these conditions later during the electrolytic separation of transuranium elements in the presence of impurity ions.

ELECTROLYTIC SEPARATION OF PLUTONIUM IN THE PRESENCE OF IMPURITY IONS

All the existing methods for the electrolytic separation of transuranium elements from alkaline, weak

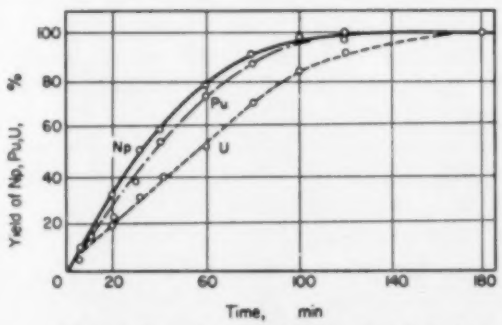

FIG. 6.—Dependence of yields on electrolysis time.
0·1 M solution of nitric acid, current density 1000 mA/cm².

acid and especially from alcohol-acetone-water solutions are applicable only to very pure solutions. In practice, however, it is very often necessary to deal with solutions containing a large quantity of foreign elements. Electrolysis of plutonium from such solutions proceeds in a non-quantitative manner or is not observed at all. In electrolysis from alkaline solutions precipitates of iron and aluminium hydroxides separate out, carrying with them the radioactive element. In weak acid solutions hydrolysis of the foreign elements begins in the electrolysis process with the separation of precipitates, and in alcohol-acetone-water solutions the plutonium itself hydrolyses and also passes into the precipitate.

We endeavoured to find conditions for the quantitative electrolytic separation of plutonium directly

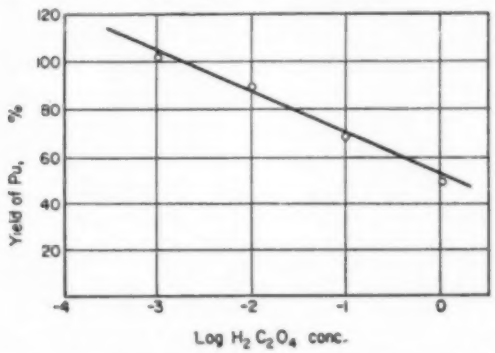

FIG. 7.—Dependence of plutonium yield on oxalic acid concentration.
0·1 M solution of nitric acid, current density 1000 mA/cm², duration of electrolysis 2 hr.

from an initial solution containing up to 10 mg (*in toto*) of iron, aluminium, lanthanum, barium, chromium, manganese, potassium and sodium. Of all the elements enumerated, the greatest hindrance in the electrolysis of plutonium is iron. Oxalic acid was used to convert the iron to a complex, and a solution of this acid is also a good electrolyte for plutonium. To increase the hydrogen ion concentration of the electrolyte the experiments were performed in an 0·1 N solution of nitric acid.

In order to find the optimum conditions for electrolytic separation of plutonium from a mixture of oxalic and nitric acids in the presence of impurity ions, it is of prime importance to examine how a change in oxalic acid concentration affects the plutonium yield. The results obtained are presented in Fig. 7.

It is interesting to notice that the quantitative yield of plutonium from a mixture of the two acids is observed at the same oxalic acid concentration as in the absence of nitric acid. It may therefore be supposed that nitric acid does not take part directly in the

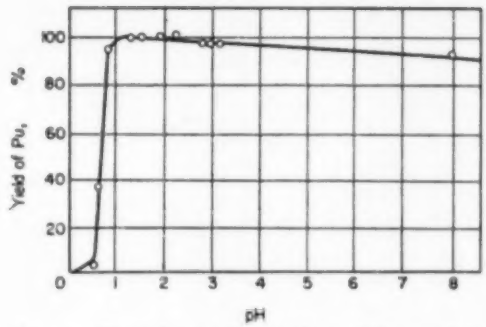

FIG. 8.—Dependence of plutonium yield on nitric acid concentration.
0·002 M solution of oxalic acid, current density 1000 mA/cm², duration of electrolysis 2 hr.

mechanism of electrolytic separation of plutonium at the cathode. Reference[6] also confirms that under these experimental conditions plutonium must exist as the positively charged ion complex $PuC_2O_4^{++}$.

The dependence of the plutonium yield on the nitric acid concentration in the system was next investigated. The results are presented in Fig. 8. They show that quantitative electrolytic separation of plutonium from a mixture of the two acids is achieved over a very wide range of pH values. The best results are observed at a pH of 1·2–1·4. The sharp jump in plutonium yield at pH 0·8 on Fig. 8 shows that for quantitative electrolysis of plutonium under these conditions a nitric acid concentration over 0·25 M is not to be recommended.

The dependence of plutonium yield on cathode current density was also studied. The results are presented in Fig. 9, from which it can be seen that under these conditions a quantitative plutonium yield is observed at a current density of 1000–2000 mA/cm².

The plutonium yield as a function of the time of electrolysis is shown in Fig. 10, from which it can be seen that under the conditions selected the electrolytic separation of plutonium is completed within 1·5–2 hours.

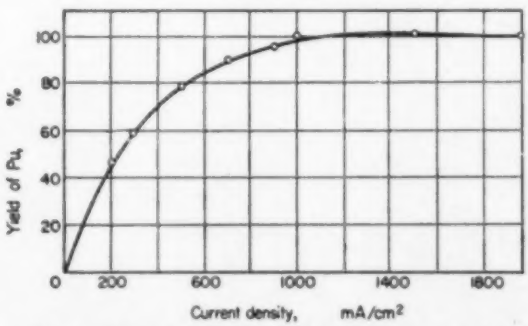

FIG. 9.—Dependence of plutonium yield on current density.
Solution 0·1 M for nitric acid and 0·002 M for oxalic acid; pH = 1·3; duration of electrolysis 2 hr.

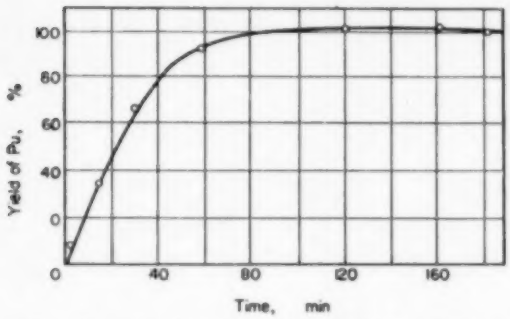

FIG. 10.—Dependence of plutonium yield on duration of electrolysis.
Solution 0·1 M for nitric acid and 0·002 M for oxalic acid; pH = 1·3; current density 1000 mA/cm².

The above investigation of the electrolytic separation of plutonium from a mixture of oxalic and nitric acids leads to the following optimum conditions for this separation: (1) oxalic acid concentration 0·002 M; (2) nitric acid concentration 0·125 M; (3) solution pH 1·3; (4) cathode current density 1000 mA/cm²; (5) volume of solution 20–40 ml; (6) duration of electrolysis 1·5–2 hours.

The experiments are performed in the following manner. An aliquot part of the original solution 0·1–5 ml in volume is placed in a platinum cup and the solution evaporated to dryness on a water bath. The residue is treated two or three times with concentrated nitric acid. Then 0·1 ml of a 1 M solution of oxalic acid and 10 ml of 0·5 M nitric acid is added and left on the water bath under a watch glass for 10–15 min (in order to dissolve the dry residue completely). After this 30 ml of distilled water are added to the cup and electrolysis carried out in the manner described.

When all the above conditions are fulfilled, quantitative electrolytic separation of plutonium is observed, as Table 3 shows. The results presented show that the reproducibility of the experiments on the electrolytic separation of plutonium in the presence of impurity ions is completely satisfactory. This method may therefore be used in the analytical chemistry of plutonium, as it enables plutonium to be determined in solution more accurately and considerably more quickly than the chemical method would. Under these conditions uranium and neptunium are also electroprecipitated quantitatively. All impurity ions remain in solution.

TABLE 3.—ELECTROLYTIC SEPARATION OF PLUTONIUM FROM A MIXTURE OF OXALIC AND NITRIC ACIDS IN THE PRESENCE OF IMPURITY IONS

$H_2C_2O_4$ (M)	pH	Pu	
		Taken (imp/min)	Yield (%)
0·002	1·3	2020	98·9
0·002	1·3	2020	99·2
0·002	1·3	2020	99·0
0·002	1·3	2020	100·0
0·002	1·3	2020	99·4
0·002	1·3	2020	100·6
0·002	1·3	2020	100·2
		Mean	99·9 ± 0·7%

The following conclusions may be drawn from the foregoing:

1. A quantitative method has been devised for the electrolytic separation of uranium, neptunium, plutonium and americium from solutions of sulphuric, hydrochloric, perchloric and oxalic acids at a hydrogen ion concentration of 10^{-3} M.

2. It has been shown that the controlling factor in the quantitative electrolytic separation of uranium, neptunium, plutonium and americium is not the character of the electrolyte anion but the hydrogen ion concentration.

3. The kinetics of the electrolytic separation of uranium, neptunium and plutonium from a nitric acid solution have been studied at hydrogen ion concentrations of 10^{-3} M and 10^{-1} M.

4. The kinetics of the electrolytic separation of plutonium from solutions of hydrochloric and perchloric acids have been studied at a hydrogen ion concentration of 10^{-3} M.

5. The dependence of the yield of uranium, neptunium and plutonium on the cathode current density and also on the electrolyte pH has been investigated.

6. An analytical method has been proposed, consisting of the electrolytic separation of plutonium in the presence of impurity ions, which enables tracer quantities of plutonium to be determined quantitatively and without a carrier directly from the original solution.

7. The method given for the electrolytic separation of the transuranium elements may be used both in the analytical chemistry of these elements and for the preparation of standards and targets.

REFERENCES

1. SAMARTSEVA A. G., *Trans. Radium Inst.* **7**, 137 (1956).
2. SAMARTSEVA A. G., *Symposium on Isotopes and Radiations in Chemistry*, Moscow, Izd-vo AN SSSR, p. 318 (1958).
3. BUGORKOV S. S., MALKIN L. Z., PETRZHAK K. A., YAKOVLEV V. A. and YAKUNIN M. I., *Trans. Radium Inst.* **9**, 214 (1958).
4. GEVANTMAN L. H. and KRAUS K. A., *The Transuranium Elements*, Div. IV, Vol. 14B, Part I. New York, p. 500 (1949).
5. KRAUS K. A., NELSON F. and JOHNSON G. L., *J. Amer. Chem. Soc.* **71**, No. 7, 2510 (1947).
6. REAS W., *The Transuranium Elements*, Div. IV, Vol. 14B, Part I. New York, p. 423 (1949).

Reactor Science and Technology (Journal of Nuclear Energy, Parts A & B), 1961, Vol. 14, pp. 132 to 141. Pergamon Press Ltd. Printed in Northern Ireland

LETTERS TO THE EDITORS

The mechanism of distribution of liquids in a plate extractor*

(*Received* 31 *March* 1959)

EXTRACTION plants with perforated (gauze) plates are widely used, since they are simple in construction, are relatively cheap and are not greatly affected by the presence of solid particles in the liquids being treated.

The efficiency of extractors of this and other types depends primarily upon the surface area of the phase boundary, and it is therefore important to understand the mechanism of boundary formation during the countercurrent flow of the liquids. This is assisted by investigating both the processes occurring in plate extractors and ways of accelerating them.

The surface area of the phase boundaries depends largely on the degree of dispersion of the liquids, which in turn depends on the forces which act on the drops during their continuous motion through the column. The drop size is determined by the balance between the forces of inertia and of surface tension; the former causes subdivision of drops during collisions with other drops or with the plates, while the latter characterized by the the size of the surface tension favours coalescence of drops. The balance of forces which controls the rate at which liquid is renewed in the plate apertures determines the nature of the boundaries between the phases, since generation of phase boundaries takes place in a thin layer of liquid in direct contact with the apertures.

The efficiency of conventional extraction columns with perforated plates is inadequate because the surface forces considerably exceed the forces of inertia, which are determined simply by the difference between the specific gravities of the two liquids. On the other hand similar columns are used with good results for vapour–liquid systems, e.g. in fractionation. The high efficiency of plate fractionation columns is due to the fact that inertial forces, which are proportional to the difference between the specific gravities are considerably greater for a vapour and a liquid than for two liquids.

A comparison between the performance of liquid–liquid and vapour–liquid plate columns suggests that it might be possible to increase the flow energy in the column by introducing a stream of gas, and thus to use the forces acting in vapour–liquid fractionation columns. Because it does not call for more complicated design and does not give rise to additional difficulties in use, this method of improving the extraction efficiency is superior to other known methods (involving e.g. stirrers, pulsators, etc.) for introducing additional energy into liquid systems. Such a system has not previously been considered and published data on the subject are lacking.

The suggestion made above has been fully confirmed by experiments, and has led to the design of a plate column with air-stream mixing shown in Fig. 1. This column differs from conventional types only in that air is introduced into the column at the lower end, near the entry of the lighter phase. The column

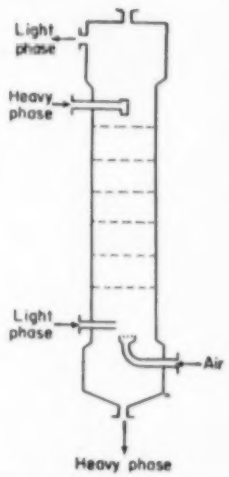

FIG. 1.—Plate column with air-stream mixing, diagrammatic.

has no transfer tubes, and all flow takes place through the apertures of the sieve-type plates. The operating conditions are stable when the air speed is below 0·03 m sec^{-1}. If more air is introduced, air bubbles which form between the liquid drops reduce the effective area of the phase boundary and lower the extraction efficiency of the column. Moreover, at air speeds exceeding 0·1 m sec^{-1}, which begins to exceed the speed at which free air bubbles can rise to the surface, the normal operation of the extractor is disturbed by the appearance of cellular foam on the plates.

The air speed adopted in our experiments ensured a relatively large through-put of liquids. It is interesting to note that the upper limiting air speed for a liquid–liquid extractor with air-stream mixing is the lower limiting air speed for vapour–liquid

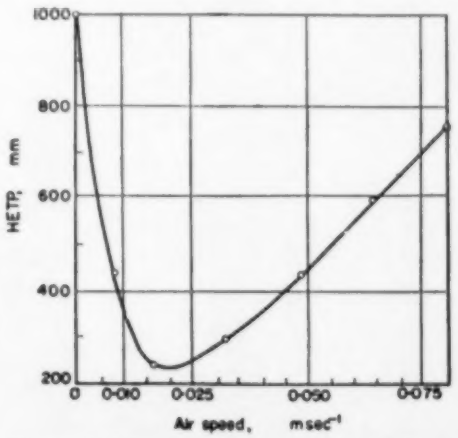

FIG. 2.—Relationship between extraction efficiency and air speed. The column height equivalent to one theoretical plate (HETP) is taken as 1000 mm for a column without air-mixing.

* Translated by G. RYBACK from *Atomnaya Energiya* 7, 159 (1959).

plate columns, since normal working conditions in an extractor depend on the presence of air bubbles.

Plate columns with air-stream mixing were used for the system water–nitric acid–uranyl nitrate–tributyl phosphate in paraffin oil. The extraction efficiency was found to be nearly three times that of conventional filled columns. The total capacity was ~30 $m^3 m^{-2} hr^{-1}$ of liquid with the optimum air mixing. By studying the relationship between the extraction efficiency and the speed of the air stream it was shown that the optimum speed was 0·01–0·03 m sec^{-1} (Fig. 2). Losses of extracting agent from the column due to the air current were negligible.

The experiments demonstrate that extraction columns with air-stream mixing are highly efficient and have a high output, and that further study of them would undoubtedly be interesting.

N. P. Galkin N. E. Goriainov
V. B. Tikhomirov V. D. Fedorov

The density of heavy water*†

(*Received* 19 *December* 1958)

The density of heavy water at temperatures up to 300° and pressures up to 100 kg cm^{-2} has been measured by means of a constant-volume piezometer. The piezometer was filled with heavy water at a temperature and pressure at which the density is known to an accuracy of ~0·003 per cent;[1] the known volume of the piezometer and the density of the liquid gave the initial quantity of the latter. The piezometer was then placed in a thermostatted high-pressure vessel, the liquid being confined by a mercury thread moving in a thin capillary tube. As the liquid was heated it expanded, and the mercury was adjusted to its original level by first raising the pressure to the required value and then releasing liquid from the piezometer. The liquid released from the piezometer was weighed, and the density was calculated, making corrections for the change in the volume of the piezometer and in the amount of liquid in the capillary dead-space outside the thermostat.

Fig. 1 represents the experimental arrangement. The piezometer, a cylindrical stainless steel vessel having two stainless steel capillary tubes (i.d. 0·3 mm) soldered into the bottom, is placed in a pressure vessel consisting of a lower block (1) and an upper, flanged, thick-walled cylinder (2). One of the capillaries is connected through a valve (5) with the heavy water supply system, and through another valve (7) with the bleed tube. The other capillary is connected (via graded seals) with a glass capillary tube dipping into a reservoir of mercury. Platinum contacts sealed into the glass capillary record the level of the mercury. Since this part of the apparatus is outside the thermostat, all the mercury is approximately at room temperature.

The heavy water in the piezometer is compressed by nitrogen introduced into the pressure vessel from a thermal pressure booster (cylinders *M* and *B*), using a valve (8) and a bubbler (16) for observing the flow of nitrogen. By expelling mercury from the reservoir the nitrogen compresses the liquid to the required pressure. The piezometer walls are therefore not subject to pressure on the outside only.

The thermostat enveloping the upper part of the pressure vessel consists of a main copper block (10) and two end-blocks

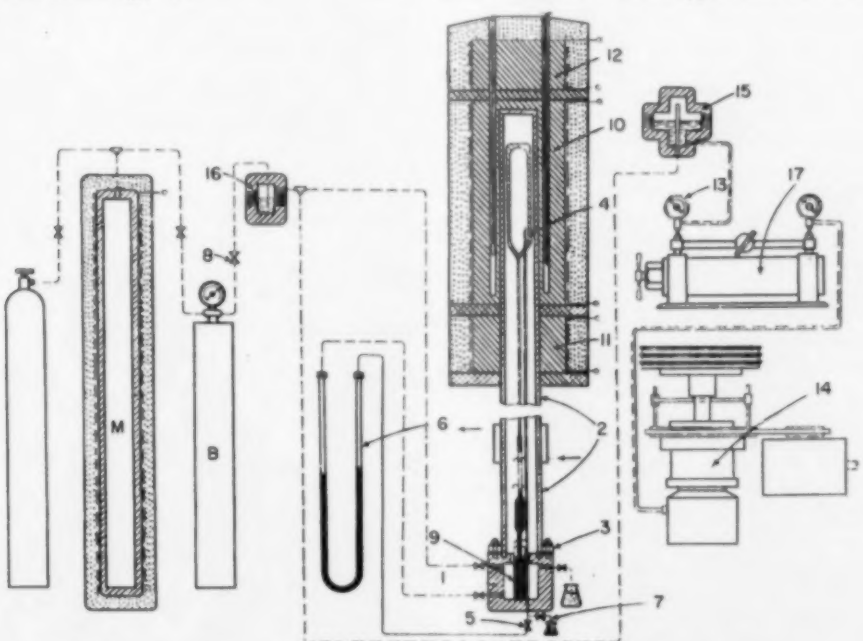

Fig. 1.—Apparatus: (1) lower block of pressure vessel; (2) upper cylinder of pressure vessel; (3) flange joint; (4) piezometer; (5) valve; (6) heavy water supply system; (7) bleed tube; (8) nitrogen inlet valve; (9) mercury reservoir; (10) main thermostat block; (11) lower thermostat block; (12) upper thermostat block; (13) Bourdon gauge; (14) free piston manometer; (15) separator; (16) bubbler; (17) oil press; *M* and *B*, cylinders of the thermal pressure booster.

* Translated by G. Ryback from *Atomnaya Energiya* 7, 457 (1959).

† Read at the Scientific and Technical Conference of the All-Union Institute of Heat Technology, 1957.

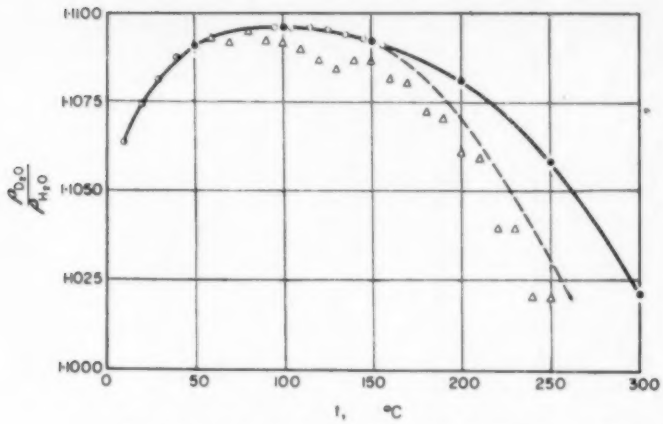

FIG. 2.—Relationship between the ratio of densities of D_2O and H_2O and temperature.
● Present work;
◑ KIRSCHENBAUM,[1] for $\rho_{D_2O} = 1{\cdot}10448$ g cm^{-3} at 25°C;
○ GROSSMAN-DOERTH;[4]
△ HEIKS *et al.*;[5]
– – – – – extrapolation of data from WHALLEY.[6]

(11, 12), all three provided with heating coils connected to a stabilized voltage source.

The volume of piezometer I at 20°C was 118·160 ± 0·005 cm³ (mean of 12 independent measurements). Piezometer II, used in some of the experiments, had a volume of 104·448 ± 0·005 cm³.

The liquid filling the dead-space outside the thermostat made up ~0·12 per cent of the working volume, and was for the most part at room temperature. Moreover, changes in the quantity of liquid in the dead-space did not exceed 1 per cent under any of the conditions encountered in the experiments. Thus the error introduced by ignoring such changes did not exceed 0·001 per cent. The dead-space intermediate in temperature between the thermostat and the room was only 0·02 per cent of the piezometer volume, and could be estimated with sufficient precision.

The temperature of the liquid was taken as equal to that of the thermostat, which was measured by means of a platinum resistance thermometer (accuracy ±0·01°). The pressure was measured with a class 0·2 standard Bourdon gauge and a free piston manometer (14) connected through an oil press (17) and a separator (15) to the pressure vessel.

In preliminary experiments we tested the apparatus by measuring the density of ordinary water at 100°C, The results agreed within 0·01 per cent with the known value. The density of heavy water was then measured along isotherms at approximately 50°, 100°, 150°, 200°, 250° and 300°C, at pressures up to 100 kg cm^{-2}. Within the pressure range of our experiments the density isotherms are straight lines, as in the case of ordinary water. Within that range, and within the limits of accuracy of the experiments, the effects of pressure on the densities of D_2O and H_2O are identical, i.e. the ratio ρ_{D_2O}/ρ_{H_2O} is independent of pressure.

The ratio ρ_{D_2O}/ρ_{H_2O} at different temperatures is given in Fig. 2 and Table 1, the values of ρ_{H_2O} being taken from KEYES[2] and SMITH[3]. The maximum error in ρ_{D_2O}, calculated from the probable errors, is 0·01–0·03 per cent (the latter value refers to the 300°C isotherm). The scatter of experimental points relative to the smooth isothermal curves is less than 0·005 per cent; this indicates good reproducibility of measurements and small random errors.

Figure 2 also compares our results with those of GROSSMAN-DOERTH[4] for temperatures from 95°–160°C and HEIKS *et al.*[5] for 35°–250°C. Our results agree within 0·01 per cent with those of the first author, but differ considerably from the results of HEIKS *et al.*; the difference increases at higher temperatures, reaching 0·35 per cent at 250°C. The disparity is due to the low accuracy of measurements by HEIKS *et al.*, who themselves estimate the probable error to be ±0·2 per cent at room temperature and ±0·6 per cent at high temperatures. WHALLEY[6] also comments on the unreliability of these authors' data, and considers that ρ_{D_2O}/ρ_{H_2O} ratios obtained by extrapolation of GROSSMAN-DOERTH's data[4] are more correct. In WHALLEY's extrapolation the curve was drawn parallel to the smooth curve through the experimental points of HEIKS *et al.*, and Fig. 2 shows that the values given by this extrapolation are closer to our results than are the experimental values of HEIKS *et al.* But since there remains a discrepancy of 0·25 per cent at 250°C, we cannot confirm WHALLEY's values. The experimental data of CHANG and TUNG[7] and of SCHRODER and WIRTZ[8] at about 100°C (not shown in Fig. 2) are in very good agreement with our results.

TABLE 1.—RATIO OF DENSITIES OF D_2O AND H_2O AT DIFFERENT TEMPERATURES

t(°C)	ρ_{D_2O}/ρ_{H_2O}	t(°C)	ρ_{D_2O}/ρ_{H_2O}
50	1·10904	180	1·10862
60	1·10930	190	1·10834
70	1·10944	200	1·10802
80	1·10950	210	1·10772
90	1·10953	220	1·10740
100	1·10955	230	1·10704
110	1·10955	240	1·10660
120	1·10951	250	1·10610
130	1·10943	260	1·10552
140	1·10933	270	1·10484
150	1·10920	280	1·10405
160	1·10905	290	1·10315
170	1·10855	300	1·10210

VOL
14
196

Figure 2 and Table 1 are recommended for determining the density of D_2O at temperatures up to 300°C and pressures up to 100 kg cm^{-2} using density tables for H_2O.

S. L. Rivkin

REFERENCES

1. Kirschenbaum I., *Physical Properties and Analysis of Heavy Water*, McGraw-Hill (1951).
2. Keyes F., *Proc. Amer. Acad. Arts. Sci.* **68**, 505 (1933).
3. Smith L., *Proc. Amer. Acad. Arts. Sci.* **69**, 137 (1934).
4. Grossman-Doerth U., *Z. Naturf.* **A10**, 799 (1955).
5. Heiks J., Barnett M., Jones L. and Orban E., *J. Phys. Chem.* **58**, 488 (1954).
6. Whalley E., *The Thermodynamic and Transport Properties of Heavy Water. Joint Conference on Thermodynamic and Transport Properties of Fluids* (1957).
7. Chang T. and Tung L., *Nature, Lond.* **163**, 737 (1949).
8. Schroder R. and Wirtz K., *Z. Naturf.* **A6**, 220 (1951).

The viscosity of heavy water*

(*Received* 2 *July* 1959)

The viscosity of heavy water has been studied by very few authors. Heiks *et al.*[1] cover the widest temperature range, using Lawaczeck's method, but their results are not particularly reliable. More reliable data have been obtained for relatively narrow temperature range up to 125°C by Hardy and Cottington,[2] using the capillary method. In the present investigation we have used a method developed by Timrot and previously employed for measuring the viscosity of ordinary water.[3,4] The viscosity was measured by a capillary method in which the pressure difference at the ends of the capillary was produced and measured by means of a ring balance, which also served to measure the volume of liquid passing through the capillary.

The apparatus is shown in Fig. 1. The ring balance consists of a tube (2) of diameter 30 mm, bent in an arc of radius 40 cm. The arms of the arc are attached by two smaller tubes (3) to a cylindrical hub (8) joined by flanges to a central tube (4) which contains the capillary (1). The capillary, like the other main components of the apparatus, is of stainless steel, and has the following dimensions: length, 329·5 mm; i.d. 0·546 mm; o.d. 2 mm. To prevent sagging it is placed in a thick-walled stainless steel tube, o.d. 6 mm.

That part of the central tube (4) which encloses the capillary is surrounded by a copper cylinder to equalize its temperature. The cylinder carries three nichrome heating coils fed from a stabilized a.c. source, a main coil covering the whole cylinder and two guard-coils to compensate for the heat loss at the ends. Using five thermocouples measuring to ±0·1°C, the temperature over the working section was maintained uniform and constant with time to ±0·2°C for temperatures up to 100°C, and to ±0·5°C for higher temperatures.

Prior to the measurements, the ring balance was adjusted so that the centre of gravity of the balance coincided with the axis of rotation of the system, using for this purpose special correcting weights. To determine the magnitude of the correcting weights (<5 per cent of the main weights) the experiment was carried out with two different loadings at the same temperature and pressure.

The apparatus was next calibrated to determine the pressure difference produced by the applied weights, and the amount of liquid passing through the capillary. The correction (<0·5 per cent) for the resistance of the connecting tubes was measured separately in experiments without the capillary. The applied weight (60–400 g) was chosen to maintain laminar flow in the capillary.

The coefficient of viscosity was calculated from Poiseuille's equation, using the Hagenbach-Couette correction for kinetic energy (<1·5 per cent of the coefficient). The following additional corrections were applied: x_1 for the movement due to the

* Translated by G. Ryback from *Atomnaya Energiya* **7**, 459 (1959).

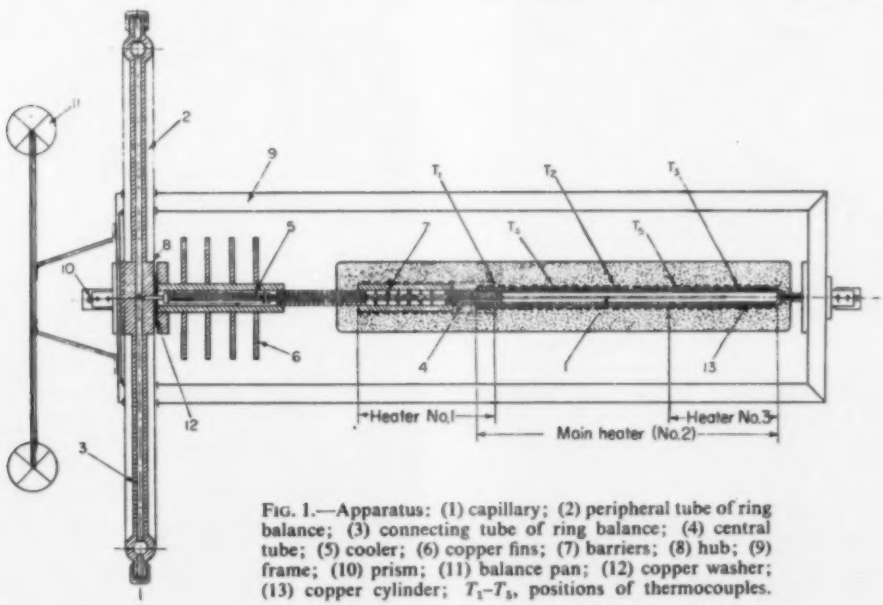

Fig. 1.—Apparatus: (1) capillary; (2) peripheral tube of ring balance; (3) connecting tube of ring balance; (4) central tube; (5) cooler; (6) copper fins; (7) barriers; (8) hub; (9) frame; (10) prism; (11) balance pan; (12) copper washer; (13) copper cylinder; T_1–T_5, positions of thermocouples.

TABLE 1.—MEASURED VALUES OF THE VISCOSITY OF D_2O

t(°C)	p (kg cm^{-2})	p (kg sec^2 m^{-4})	G_1(g)	τ_1 (sec mm^{-1})	G_2*(g)	τ_2 (sec mm^{-1})	$\nu \times 10^6$ (m^2 sec^{-1})	$\mu_{D_2O} \times 10^6$ (kg sec m^{-2})	$\mu_{H_2O} \times 10^6$, (kg sec m^{-2})	$\frac{\mu_{D_2O}}{\mu_{H_2O}}$
15·2	46·0	113·0	400	8·84	200	17·94	130	147	117	1·256
16·0	47·5	113·0	100	36·88	50	80·00	128	144	114	1·263
16·5	47·9	113·0	400	8·50	200	17·52	123	139	113	1·230
18·1	97·2	113·2	200	15·68	100	30·27	122	138	109	1·266
18·3	97·5	113·2	400	7·78	200	15·46	117	132	107	1·234
18·3	97·5	113·2	200	15·48	100	30·32	118	134	107	1·252
18·8	99·0	113·2	200	15·32	100	29·86	118	134	106	1·264
19·1	55·0	113·0	400	7·88	200	16·18	115	130	105	1·238
19·2	51·5	113·1	400	7·62	200	15·17	114	130	105	1·238
20·6	57·0	113·0	400	7·38	200	14·70	110	125	101	1·238
47·4	70·8	113·1	200	8·45	100	16·92	62·4	70·6	59·0	1·197
56·0	75·8	112·0	200	7·69	100	15·97	54·9	61·5	51·3	1·199
68·3	89·7	111·2	200	5·95	100	11·43	45·5	50·6	42·7	1·185
96·9	100·0	109·2	100	8·34	50	16·26	31·4	34·3	30·0	1·143
98·7	103·1	109·1	100	8·51	50	17·11	31·0	33·8	29·4	1·150
101·0	120·0	109·0	100	8·75	50	18·23	30·9	33·7	28·7	1·174
109·2	100·0	108·2	150	4·92	75	9·16	29·0	31·4	26·9	1·167
148·7	86·0	104·3	80	7·10	40	13·53	21·5	22·4	19·4	1·155
201·2	111·2	98·3	80	5·38	40	10·10	16·0	15·7	14·0	1·121
205·3	242·0	99·8	80	6·14	40	13·20	16·1	15·9	14·1	1·128
206·4	53·6	97·1	80	6·00	40	12·94	15·6	15·2	13·6	1·118
246·7	321·8	93·7	80	5·44	40	11·30	14·4	13·5	12·1	1·116
247·2	325·0	93·6	80	5·43	40	11·30	14·4	13·5	12·1	1·116
288·0	111·5	84·7	60	5·85	30	10·71	13·2	11·2	10·1	1·109

* Experiments with a second load G_2 served only to find the correction x_1.

balance itself; x_2 for the resistance in the connecting tubes; and x_3 for the expansion of the capillary when heated. The term x_3 was calculated from the expression

$$L_t = L_0\{1 + (0{\cdot}151 \times 10^{-4})t + (0{\cdot}95 \times 10^{-6})t^2 - (0{\cdot}5 \times 10^{-11})t^3\}.$$

The final expression, which includes the corrections and the quantities obtained by calibration, becomes

$$\nu = 0{\cdot}03769\,[G_1 + (x_1 - x_2)]\frac{\tau_1}{\alpha} - 467{\cdot}8\,\frac{\alpha}{\rho\tau_1} - x_3,$$

where ν is the kinetic coefficient of viscosity in m^2 sec^{-1}; G_1 the load in g; τ the reciprocal flow rate of the liquid in the capillary, in sec mm^{-1}; and ρ the density of the liquid in kg sec^{-2} m^{-4}. $\alpha = \gamma_p/\gamma_0$ is a term expressing the compressibility of the liquid, γ_p and γ_0 being the densities at 20°C of D_2O measured at the pressure of the experiment and at 1 atm (the pressure at which calibration was carried out), respectively. The values of ρ_{D_2O} are those of RIVKIN.[5]

The viscosity of pure D_2O was measured at 45–325 kg cm^{-2} and at temperatures between room temperature and 283°C. It was shown that within the pressure and temperature range of the experiments, the viscosity of D_2O varies with pressure in the same way as that of H_2O.

Table 1 gives our results for D_2O, and Table 2 the smoothed values at the saturation pressures. The maximum estimated error is ±2 per cent. The ratio μ_{D_2O}/μ_{H_2O} can be seen to decrease with rising temperature (Fig. 2), e.g. from 1·24 at 20°C to 1·11 at 280°C. The values of μ_{H_2O} were taken from tables.[6]

TABLE 2.—SMOOTHED VALUES OF THE VISCOSITY OF D_2O AT THE SATURATION PRESSURES

t(°C)	$\mu_{D_2O} \times 10^6$ (kg sec m^{-2})	$\frac{\mu_{D_2O}}{\mu_{H_2O}}$	t(°C)	$\mu_{D_2O} \times 10^6$ (kg sec m^{-2})	$\frac{\mu_{D_2O}}{\mu_{H_2O}}$
15	140·5	1·258	150	21·6	1·137
20	127·7	1·247	160	20·0	1·133
30	103·3	1·228	170	18·8	1·130
40	80·7	1·212	180	17·6	1·128
50	67·1	1·199	190	16·5	1·125
60	56·9	1·188	200	15·6	1·123
70	48·8	1·179	210	14·9	1·122
80	42·4	1·172	220	14·2	1·119
90	37·4	1·165	230	13·6	1·118
100	33·4	1·159	240	13·1	1·117
110	30·4	1·153	250	12·5	1·115
120	27·8	1·148	260	12·0	1·113
130	25·4	1·143	270	11·5	1·110
140	23·4	1·139	280	11·1	1·109

Figure 2 also compares our data with those of other authors. The ratios μ_{D_2O}/μ_{H_2O} obtained by HARDY and COTTINGTON[8] agree within 1 per cent with our values. Those of HEIKS *et al.*[11] are an average 2 per cent lower than our values, the difference increasing with rising temperature. Figure 2 also includes the results of LEWIS and MACDONALD.[7]

D. L. TIMROT
K. F. SHUISKAIA

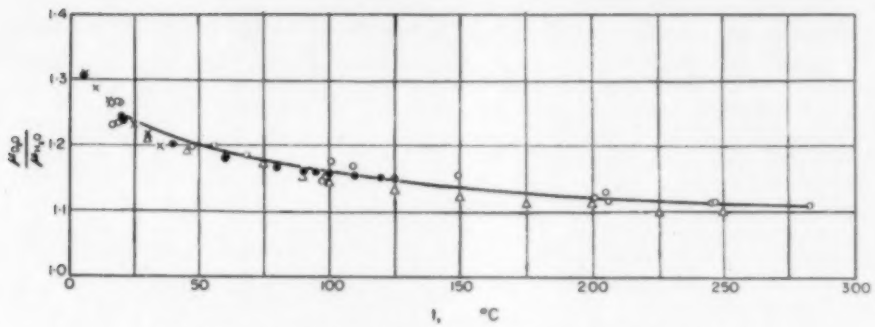

FIG. 2.—Comparison of experimental data on the viscosity of D_2O.
○ Present work;
● HARDY and COTTINGTON;[2]
△ HEIKS *et al.*,[1]
× LEWIS and MACDONALD.[7]

REFERENCES

1. HEIKS J., BARNETT M., JONES L. and ORBAN E., *J. Phys. Chem.* **58**, 488 (1954).
2. HARDY R. and COTTINGTON R., *J. Chem. Phys.* **17**, 509 (1949).
3. TIMROT D. L., *Bull. All-Union Inst. Heat Technol.* No. 3 (1940).
4. KHLOPKINA A., Dissertation, Moscow Power Inst. (1954).
5. RIVKIN S. L., *Atomnaya Energiya* **7**, 457 (1959).
6. *Tables of Thermodynamic Properties of Water and Water-Vapour*, Gosenergoizdat, Moscow (1958).
7. LEWIS N. and MACDONALD T., *J. Amer. Chem. Soc.* **55**, 4730 (1933).

The specific heat of heavy water*†

(*Received* 19 *December* 1958)

WE have measured the specific heat of heavy water by means of a closed-circuit adiabatic flow calorimeter (Fig. 1). While the method has previously been used at the All-Union Institute of Heat Technology to study the specific heat of ordinary water

* Translated by G. RYBACK from *Atomnaya Energiya* **7**, 462 (1959).
† Read at the Scientific and Technical Conference of the All-Union Institute of Heat Technology, 1957.

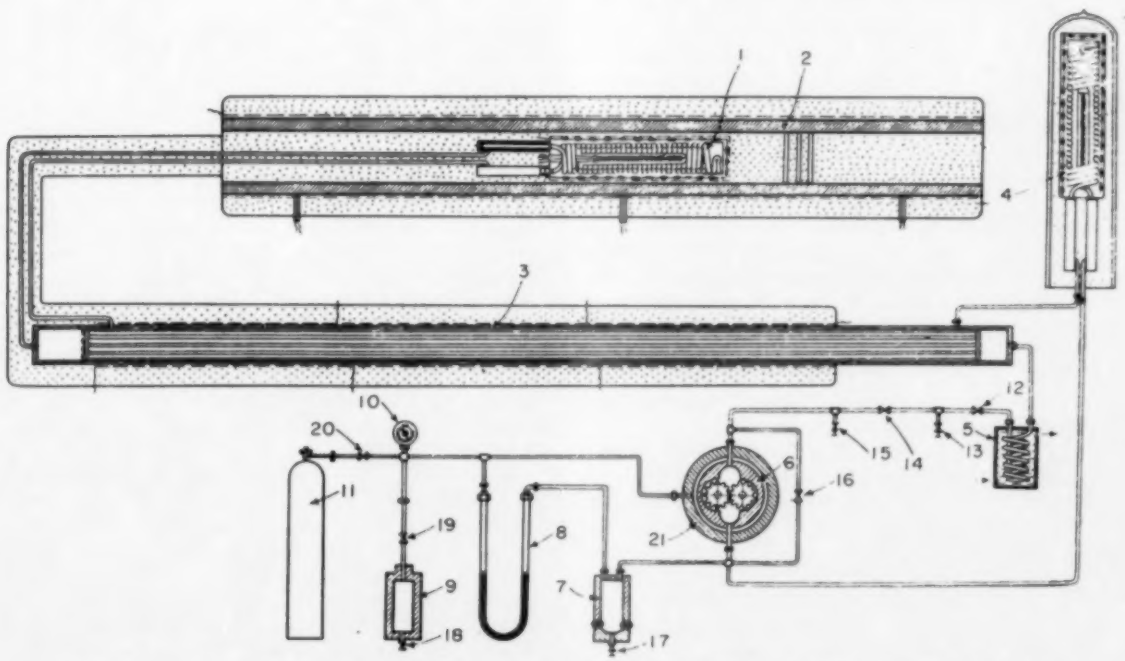

FIG. 1.—Apparatus: (1) adiabatic calorimeter; (2) thermostat; (3) heat exchanger; (4) flow-meter; (5) cooling unit; (6) gear-pump; (7) mercury trap; (8) U-tube; (9) gas cylinder; (10) standard Bourdon gauge; (11) nitrogen cylinder (12); control valve; (13–20) high pressure valves; (21) high-pressure vessel.

and water vapour at high temperatures and pressures,[1,2] the earlier apparatus differs substantially from ours.

A gear-pump delivers heavy water to a special flow-meter (4), and thence via the heat-exchanger (3) where the liquid is heated to a predetermined temperature, to the thermostatted calorimeter. From the calorimeter the liquid returns through the tubes of the heat exchanger where it is partly cooled by the incoming liquid, passes through a cooling unit (5) and then returns to the circulating pump.

The system is pressurized by nitrogen cylinder. The aim of the mercury-filled U-tube is to obtain equal pressure of the liquid in the system and of the gas in the high-pressure vessel (21) surrounding the pump and its drive (an asynchronous motor) have been equalized; this eliminates one-sided pressure on the pump. The use of a circulating pump driven by an asynchronous motor has enabled us to maintain a constant flow of D_2O (variation 0·1–0·2 per cent) without recourse to special flow regulators.

The measuring calorimeter is constructed in the form of a double coil, to the ends of which are welded sleeves containing the thermocouples. A nichrome heater, mounted on a quartz former and fed from a high capacity accumulator battery, is placed inside the coil, and two cylindrical copper jackets envelop the coil to smooth out the temperature distribution. A multi-junction differential thermocouple covering the whole surface of the coil is placed in the gap between the two copper cylinders, so that the thermocouple reading corresponds to the total exchange of heat between the calorimeter and the surroundings. Adiabatic conditions are achieved by adjusting the thermostat until the thermocouple reads zero or almost zero. The thermocouple also measures the uncompensated heat flow through the jacket of the calorimeter, which is usually very small. The temperature rise in the D_2O flowing through the calorimeter is measured by the differential chromel-alumel thermocouple in the sleeves on the ends of the coil, the same thermocouple being also used for measuring the temperature of the D_2O entering the calorimeter.

A calorimetric method is used for determining the rate of flow of D_2O. It consists essentially of measuring the amount of heat supplied to a second adiabatic calorimeter (4) in the circuit, and the subsequent rise in temperature of the D_2O. Since the liquid enters this calorimeter at approximately room temperature, the flow rate can be calculated from the specific heat, which at this temperature is known with sufficient accuracy; the pressure dependence of the specific heat is small and can be allowed for. The flow-meter is constructed in the same way as the measuring calorimeter, but is coated with an insulating layer and placed in a dewar vessel. The temperature rise is measured with a five-junction chromel-alumel thermocouple. We used COCKETT and FERGUSON's values[3] for the specific heat of D_2O at 10–50°C. The effect of pressure (0·4 per cent at 20°C and 100 kg cm^{-2}) was calculated from the data for H_2O, the pressure being measured with a class 0·2 standard Bourdon gauge.

Prior to the main measurements, the differential thermocouples in the flow-meter and in the measuring calorimeter were calibrated against a standard platinum resistance thermometer. The apparatus was adjusted and tested using ordinary water, the physical properties of which are known with high accuracy over a wide range of temperatures and pressures. Our measurements of the specific heat of H_2O at temperatures between 60° and 250°C and at pressures up to 50 kg cm^{-2} agree within 0·2–0·3 per cent with KOCH's data.[4]

The specific heat of D_2O was measured along isobars at 50 and 100 kg cm^{-2} for temperatures ranging from 50°C to just below the saturation temperature at the corresponding pressure. The temperature of the D_2O entering the measuring calorimeter was maintained constant within 0·01°–0·02°C. The temperature rise on passing through the calorimeter was 4°–8°C, the amount of heat supplied by the heater in the measuring calorimeter was 40–70 kcal hr^{-1}, and the correction for the heat exchange between the calorimeter and the surroundings was 0·01–0·1 kcal hr^{-1}. D_2O flowed through the calorimeter at a rate ~8 kg hr^{-1}.

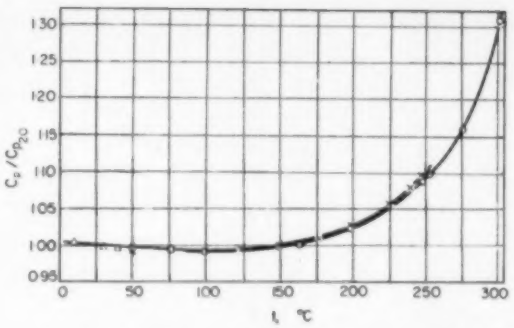

FIG. 2.—Experimental values of the specific heat of D_2O.
× 50 kg cm^{-2} (present work);
○ 100 kg cm^{-2} (present work);
△ 1 kg cm^{-2} (COCKETT and FERGUSON[3]).

We calculated the ratio of the specific heats of D_2O at the mean temperature of the measuring calorimeter and of the flow-meter respectively, at similar pressures:

$$\frac{(C_p)_{p,t}}{(C_p)_{p,t_f}} = \frac{(Q_m + q_m)\,\Delta t_f}{(Q_f + q_f)\,\Delta t_m}.$$

Here subscript m refers to the measuring calorimeter and subscript f to the flow-meter, Q is the amount of heat supplied by the heaters, q is the correction for the heat loss from the calorimeters to the surroundings (as measured by the multi-junction differential thermocouples), and Δt is the temperature difference between the D_2O entering and leaving the calorimeters. The specific heat was finally referred to the value at 20°C by introducing a correction (less than 0·2 per cent) for the actual mean temperature in the flow-meter, using the data of COCKETT and FERGUSON.[3] The results are given in Fig. 2, which shows that the scatter of the points is less than 0·2 per cent.

Using the results of COCKETT and FERGUSON[3] and assuming that at 20°C changes of pressure affect the specific heats of D_2O and H_2O equally (0·2 per cent for 50 kg cm^{-2}), we have calculated the true specific heat of D_2O (Table 1). We also determined the ratio of the specific heats of D_2O and H_2O as a function of temperature for two pressures, 50 and 100 kg cm^{-2} (Fig. 3).

The ratio C_{pD_2O}/C_{pH_2O} was found to be independent of pressure (within the range of our experiments). It decreases with rising temperature from 1·006 at 20°C to 0·956 at 250°C; near the latter temperature may reach a minimum, since it remains almost constant up to 300°C. Fig. 3 may be used for determining the specific heat of D_2O from data for H_2O. The maximum error has been shown to be less than 0·8 per cent.

Figure 2 compares the results of our studies with those of COCKETT and FERGUSON[3] for temperatures in the range 10°–50°C. The diagram shows that the temperature dependence of C_{pD_2O} determined by these authors agrees closely with that found by us. On the other hand the values obtained by

TABLE 1.—THE RATIO C_pD_2O/C_pH_2O AND THE TRUE SPECIFIC HEAT OF D_2O

t(°C)	$\frac{C_pD_2O}{C_pH_2O}$	C_pD_2O at 50 kg cm^{-2}	C_pD_2O at 100 kg cm^{-2}
20	1·006	1·002	1·000
40	1·004	0·998	0·996
60	1·002	0·996	0·993
80	0·997	0·996	0·995
100	0·992	0·995	0·992
120	0·986	0·996	0·992
140	0·980	0·998	0·994
160	0·972	1·004	1·000
180	0·966	1·014	1·008
200	0·962	1·030	1·023
220	0·958	1·051	1·043
240	0·957	1·083	1·073
260	0·957	1·130	1·116
280	0·957	—	1·178
300	0·958	—	1·294

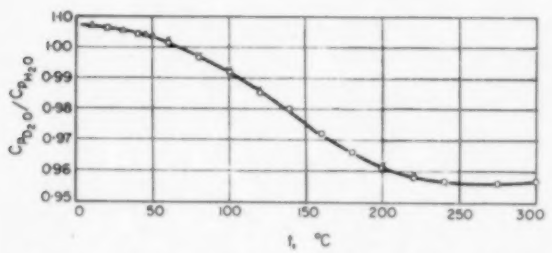

FIG. 3.—Ratio of specific heats of D_2O and H_2O as a function of temperature.

EUCKEN[5] for the range 10°–125°C are lower than ours, the difference being as great as 1–1·2 per cent.

S. L. RIVKIN
B. N. EGOROV

REFERENCES

1. TIMROT D. L., VARGAFTIK N. B. and RIVKIN S. L., *Bull. All-Union Inst. Heat Technol.* **4**, 1 (1948).
2. SIROTA A. M. and TIMROT D. L., *Teploenergetika* **7**, 16 (1956).
3. COCKETT A. H. and FERGUSON A., *Phil. Mag.* **29**, 185 (1940).
4. KOCH W., *Forsch. Geb. Ingenieurwesens* **A5**, 138 (1934).
5. EUCKEN A., *Aktuelle Probleme der Physikalische Chemie*, Akademie-Verlag, Berlin (1953).

A possible method of increasing the yields of nuclear reactions in thin targets*

(*Received* 13 *February* 1959)

IT is well-known that for incident charged particles having identical energies E_0, the yield of nuclear reaction products from a thin target is always less than that from a thick target. For example, in the case of the reaction $^{63}Cu(d, 2n)^{63}Zn$ at an incident energy $E_0 = 10$ MeV, the ratio of the yields from thin and thick targets $\Delta Y/Y \simeq 0{\cdot}05$, when the energy loss in the thin target is $\Delta E_0 = 0{\cdot}1$ MeV. Whether the target is thick or thin the loss of particles due to the actual nuclear reactions is quite negligible ($10^{-6} - 10^{-4}$); the main cause of the decreased efficiency of a thick target arises from the ionization energy loss which slows down and ultimately completely stops the charged particles within the target material. On the other hand, the particles pass completely through a thin target and lose only part of their energy. Provided these particles have not expended too much of their energy in the target, it is possible to apply a magnetic field in such a way that the particles are re-directed on to the same target. The effectiveness of these particles is diminished for the reasons given above but the induced specific activity undergoes a sharp increase in comparison with the thick target specific activity. If the particles are given additional energy ΔE_0 after each passage through the target then one can arrange that the nuclear reaction takes place at a fixed incident energy given by $E_0 = 4{\cdot}8 \times 10^5 (HR)^2 \times \frac{Z_a^2}{a}$. If this is done we have in effect a resonance between the energy loss in the material and the imparted energy increment. Such conditions can be produced in a cyclic accelerator by arranging that the energy loss in a target thickness Δl_r is matched by the energy gain per revolution: i.e. $\Delta E_0 = 2Z_a V_0 \cos\varphi$ (φ is the phase of the accelerating field at radius R and V_0 is the accelerating voltage in MeV). A better scheme is to take two targets of thickness $\Delta l_r/2$, each of which is symmetrically placed with respect to the centre of the accelerator. From the relation for the specific energy losses we find that

$$\Delta l_r \simeq 7 \times 10^{-3} \frac{AE_0}{aZ_aZ} \frac{2V_0 \cos\varphi}{\ln \frac{200E_0}{aZ}} \text{ g cm}^{-2}. \qquad (1)$$

In order to maintain this condition when the targets are extremely thin and the accelerating slit is very narrow compared with the circumference of the stable orbit, the particles may have to make many traversals (ν) of the target. However, in actual practice Δl_r is never very small because the particles are multiply scattered within the targets. This broadens the beam and may cause the particles to strike the walls of the vacuum chamber if the focusing action of the magnetic field is not sufficiently strong. We estimated this effect and the focusing properties of the magnetic field using the results of CASSELS *et al.*[1] in conjunction with equation (1). We obtained a lower limit for the effective number of traversals and thus for the total yield $Y_{eff} = \frac{\sigma N_0}{A} \nu_{eff} \Delta l_r$.

We have

$$\nu_{eff} \simeq (3\text{–}4) \times 10^3 n \left(\frac{d}{R}\right)^2 \frac{aE_0}{ZZ_a 2V_0 \cos\varphi} \frac{\ln \frac{200E_0}{aZ}}{\ln 183Z^{1/2}} \qquad (2)$$

$$\nu_{eff} \simeq (6\text{–}8) \times 10^{-4} \frac{(Hd)^2 E_0 n(E_0) \sigma(E_0)}{aZ^2 \ln 183Z^{-1/3}}. \qquad (3)$$

Here $\sigma(E_0)$ is the cross-section of the reaction in barns, H is the magnetic field in kilo-oersteds; $n(E_0)$ is the exponent characterizing the magnetic field shape and d is the half-height

* Translated by D. L. ALLAN from *Atomnaya Energiya* **7**, 472 (1959).

of the dees in cm. It follows from this relation that the total yield depends on the incident particle energy through the factor $E_0 n(E_0)\sigma(E_0)$ and that therefore it is advantageous to operate the accelerator so that the particles are accelerated in an orbit where this product has a maximum value. It is also clear that making the magnetic field more non-uniform and increasing the height of the dees in the stable orbit region both lead to an increase in ν_{ett} and so also to an increase in the total yield.

From equation (1) it follows that at a given orbit the resonance thickness of the target depends on the phase and this, in turn, depends on the resonance conditions of the accelerator. Consequently, provided we choose $\Delta l_e < (\Delta l_e)_{\varphi=0}$, condition (1) can be satisfied by making a suitable adjustment of the magnetic field (the adjustment can be effected by observing the neutron radiation).

It should be noted that although the energy loss in a thin target is smaller than in a thick target it is more difficult to remove the heat. It is therefore necessary to have properly designed targets if high currents are to be used. Rough calculation of the size of the currents which can be used gives

$$\nu_{ett} j \simeq \left\{ \frac{6}{V_0 \cos\varphi} \left(\frac{T}{1000} \right)^4 + \frac{2\lambda(T - T_0)}{S\rho} \right\}, \qquad (4)$$

where the first term represents radiation loss and the second represents the heat transfer. T is the absolute temperature of the target, λ is the thermal conductivity in 10^{11} MeV cm^{-1} sec^{-1}, ρ is the density in g cm^{-3}, S is the beam cross-sectional area and j is the initial current.

For a cyclotron with $H = 15{\cdot}5$ kilo-oersted, $V_0 = 0{\cdot}1$ MeV, $n = 0{\cdot}25$, $\varphi = 60°$[2] and a copper target we have $\Delta l_e = 2{\cdot}2$ mg cm^{-2}, $\nu_{ett} = 24$, $\nu_{ett} \times j = 200 - 300$ μa and $Y_{ett}/Y \simeq 1$–2. That is, the thin target yield is a little greater than the thick target yield and the thin target specific activity is as much as 100 times greater.

The thin target yield of a nuclear reaction can be increased without using a magnetic field if the targets are placed one behind the other and the energy loss in each target is compensated by a suitable resonance method. In this case the effects due to scattering are less important and the thermal load is negligible.

The proposed method would be particularly useful when accelerating low energy particles; for example, when producing neutrons by the D-D and D-T reactions. In these cases the energy of the incident particles is rather low ($\leqslant 0{\cdot}5$ MeV) and, since $\Delta Y/Y \simeq 1$ at low energies, an increase in the number of traversals (or in the number of targets, in the scheme not employing a magnetic field) would result in a net gain in yield if the foregoing conditions were maintained.

Acknowledgments—The author thanks A. A. Pliutto, N. I. Leont'ev and P. P. Dmitriev for helpful discussion.

M. Z. Maksimov

REFERENCES

1. Cassels J., Dickson J. and Howlett J., *Proc. Phys. Soc.* 64B, No. 540, 719 (1951).
2. Dmitriev P. P., Krasnov N. N. and Khaprov E. N., *Atomnaya Energiya* **3**, 45 (1957).

The spectra of neutrons scattered by oxygen, antimony and chromium*

(*Received* 23 *February* 1959)

In spite of the large amount of work which has been devoted to the study of the interaction of neutrons with nuclei, there are still very few experiments in which the spectra of scattered neutrons have been measured. Such neutron spectra provide a means of determining the energies and partial excitation cross-sections of nuclear levels uniquely, whereas the interpretation of γ-ray spectra is complicated by the existence of γ-cascade processes.

We report here the results of some measurements on the spectra of neutrons scattered elastically and inelastically by antimony and chromium nuclei and elastically by oxygen nuclei. The D(d, n)^{3}He reaction was used as the source of neutrons, 150 keV deuterons being accelerated on to a target of heavy ice. The scatterers were placed at an angle of 13° with respect to the deuteron beam direction, corresponding to a neutron energy of 2·9 ± 0·1 MeV. A ring-shaped geometry was used: the scatterers were toroids with a circular cross-section and were made of materials having the natural isotopic composition. The chromium scatterer consisted of a thin-walled toroidal container filled with chromium oxide.

The measurements were made in four stages: first the intensity of the direct beam was measured, secondly the background intensity, thirdly the scattered neutron intensity and finally the background again. The stability of the counting equipment was checked during the measurements by recording α-particle pulses. In all cases the scattering angle was 90°.

The neutron spectrometer was a spherical ionization chamber used in conjunction with a linear amplifier and a 50 channel pulse height analyser.[2] In contrast to the work reported by Nemets and Pasechnik[2], the chamber used by Vertebnii[3] was filled with methane which increased the efficiency but reduced the energy resolution of the equipment. For the purpose of working out the elastic and inelastic scattering cross-sections we used the same method as that given by Nemets and Pasechnik.[2]

The spectra of neutrons scattered from antimony and chromium are shown in Fig. 1. Curve (a) is the spectrum of the neutrons in the direct beam, the broken line being the same spectrum after wall effect[3] corrections have been applied. Curve (b) is the spectrum of neutrons scattered from antimony, (c) is the spectrum obtained for chromium oxide and (d) is this same spectrum corrected for the wall effect.

It can be seen from curve (b) that three excited levels in antimony are observed at 0·85, 1·33 and 1·68 MeV. The excitation cross-sections of these levels are 22 ± 2, 80 ± 9 and 11 ± 1 mb ster^{-1}, respectively. The elastic scattering cross-section is 147 ± 16 mb ster^{-1}.

For chromium (curves (c) and (d)), in addition to the 1·45 MeV level found by Freeman[5] we found a further level at 1·82 MeV. The differential inelastic scattering cross-sections are 59 ± 6 and 24 ± 3 mb ster^{-1}, respectively, and the elastic scattering cross-section is 208 ± 28 mb ster^{-1}.

* Translated by D. L. Allan from *Atomnaya Energiya* **7**, 477 (1959).

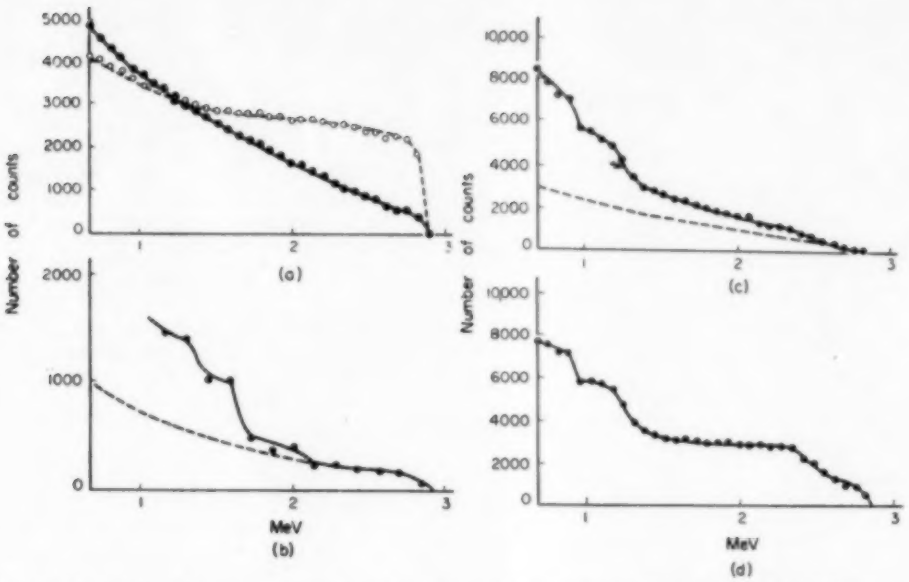

FIG. 1(a–d).—Neutron spectra. (a) Direct beam, (b) scattered from antimony, (c) and (d) scattered from chromium oxide.

Finally, we found that the elastic scattering cross-section for 2·9 MeV neutrons on oxygen was 47 ± 5 mb ster^{-1}.

IU. V. GOFMAN
O. F. NEMETS
V. V. TOKAREVSKII

REFERENCES

1. NEMETS O. F., Thesis, Institute of Physics, Ukr.S.S.R. Academy of Sciences, Kiev (1954).
2. NEMETS O. F. and PASECHNIK M. V., *Proceedings of the U.S.S.R. Academy of Sciences Conference on the Peaceful Uses of Atomic Energy, Kiev*, p. 86 (1958).
3. VERTEBNII V. P., Thesis, Institute of Physics, Ukr.S.S.R. Academy of Sciences, Kiev (1955).
4. NEMETS O. F., *Ukr. fiz. zh.* **2**, 101 (1957).
5. FREEMAN J., *Progr. Nucl. Phys.* **5**, 37 (1956).

The dose field of a line source*

(*Received* 4 *May* 1959)

IN certain types of industrial and experimental application it is convenient to use rod sources. Sources of this shape are particularly useful in transportable γ-applicators and so an approximate though reasonably accurate calculation of a dose field due to a line source should be of interest.

It is known that the dose rate P_A at a point A at depth h inside an object irradiated by a source of length L (Fig. 1) is given by formula:

$$P_A = \frac{k_\gamma m}{H}\int_0^{\varphi_0} Be^{\mu h \sec\varphi}\, d\varphi, \qquad (1)$$

where $\varphi_0 = \arctan\frac{L}{H}$; H is the distance of point A from the source; k_γ is the isotope constant; m is the linear source activity in millicuries cm^{-1} (if m is expressed in mg Ra equiv., then $k_\gamma = 8{\cdot}4$ r. hr^{-1} = 0·14 r. min^{-1}); B is the dose build-up factor of FANO,[1,2] which allows for the effect of multiple scattering on the absorption of radiation passing through matter; μ is the linear absorption coefficient for a narrow beam of γ-rays.

Using the analytical expression for the build-up factor B:

$$B = A_1 e^{-\alpha_1 \mu h} + A_2 e^{-\alpha_2 \mu h}, \qquad (2)$$

the dose rate P_A can be given in terms of a sum of tabulated integrals (SIEVERT[3]):

$$P_A = \frac{k_\gamma m}{H}\left[A_1\int_0^{\varphi_0} e^{-\mu h(\alpha_1+1)\sec\varphi}\, d\varphi + A_2\int_0^{\varphi_0} e^{-\mu h(\alpha_2+1)\sec\varphi}\, d\varphi\right], \qquad (3)$$

where $A_2 = 1 - A_1$; α_1 and α_2 are constants given in References[4,5] for various absorbers and radiations. Formula (3) holds strictly for infinite geometry and when applied to problems involving finite bodies it yields results accurate to about 10 per cent.

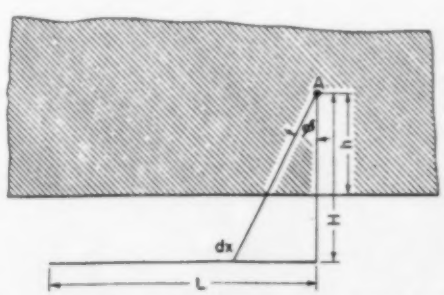

FIG. 1.—Explanatory diagram for the calculation of dose rates due to a line source.

Calculations of the dose field have been performed for ^{60}Co, which is widely used at present for irradiation purposes. Water

* Translated by J. ADAM from *Atomnaya Energiya* **8**, 154 (1960).

was taken as the absorbing medium and following values have been assumed for the required constants: the absorption coefficient for a narrow beam of ^{60}Co radiation in water $\mu = 0{\cdot}063\ \text{cm}^{-1}$; $\alpha_1 = -0{\cdot}095$; $\alpha_2 = 0{\cdot}060$; $A_1 = 8{\cdot}88$; $A_2 = 1 - A_1 = -7{\cdot}88$.

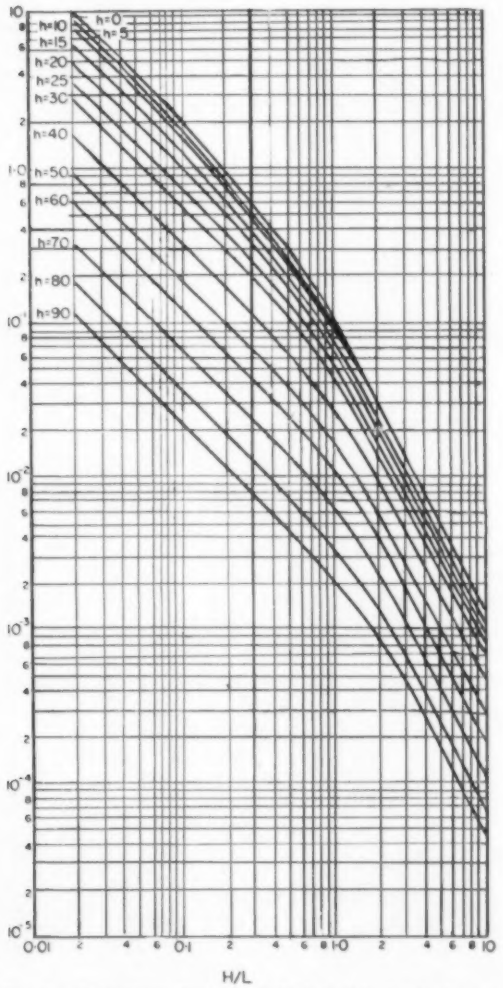

FIG. 2.—Nomogram for the calculation of dose rates in water due to a line source.

Figure 2 shows a series of curves to be used in calculating the dose rate in r. min^{-1} at various distances H from a line source and for various depths h in the irradiated object, of density $\rho = 1\ \text{g cm}^{-3}$. The curves give ε in terms of the ratio H/L, where ε is defined by:

$$\varepsilon = \frac{k_\gamma L}{H}\left[A_1\int_0^{\varphi_0} e^{-\mu h(\alpha_1+1)\sec\varphi}\,d\varphi + A_2\int_0^{\varphi_0} e^{-\mu h(\alpha_2+1)\sec\varphi}\,d\varphi\right]. \quad (4)$$

Thus

$$P_A = \frac{m}{L}\varepsilon. \quad (5)$$

The dose rate in air P_0 at a point A for given H/L can be obtained using curve $h = 0$ (Fig. 2). It appears, from the analysis of curves which show the changes in the relative values of dose rates P_h/P_0 in a medium for various values of H/L, that the dose rate in water may be expressed with an accuracy of 10–15 per cent by an empirical formula:

$$P_A = P_0\eta e^{-0{\cdot}05(h-\Delta)}, \quad (6)$$

where P_0 is the dose in air at the given point and η and Δ are constants which depend on the relative distance H/L. The above formula is valid for $h > 10$ cm if $H/L < 0{\cdot}1$; for $h > 15$ cm if $0{\cdot}6 > H/L > 0{\cdot}2$ and for $h > 20$ cm if $10 > H/L > 0{\cdot}7$. For smaller values of h

$$P_A = P_0[1 - 2\,.\,10^{-3}(h - \sigma)]. \quad (7)$$

Constants required in equations (6) and (7) are given in Table 1.

TABLE 1.—CONSTANTS REQUIRED IN FORMULAE (6) AND (7)

Range of H/L	η	Δ	σ	Formula (7) must be used if h is:
0·01 – 0·1	$(1 - 2 \times 10^{-3}h)$	5	0	<10 cm
0·2 – 0·6	1	8	3	<15 cm
0·7 – 1·0	1	12	3	<20 cm
2·0 – 10·0	$(1 + 4 \times 10^{-3}h)$	15	5	<20 cm

If the density of the irradiated body is ρ the dose rate can be determined using curves in Fig. 2 or formulae (6) or (7) for a given H/L and depth in the medium h' if h is taken equal to $h'\rho$.

Thus doses from linear ^{60}Co sources in water or in air equivalent media can be calculated simply and with reasonable accuracy by using curves or empirical formulae given in this paper. The same curves and formulae can be used when dealing with sources of other shapes which can be treated as compounds of linear sources.

V. S. GRAMMATIKATI
U. YA. MARGULIS
V. G. KHRUSHCHEV

REFERENCES

1. SPENCER L. and FANO U., *J. Res. Nat. Bur. Stand.* **46**, 446 (1951).
2. FANO U., *Nucleonics* **2**, No. 8, 1 (1953).
3. SIEVERT R., *Eine Methode zur Messung von Röntgen-Radium und Ultrastrahlen Nebst Einige Untersuchungen über die Anwendbarkeit derSelben in der Physik und der Medizin.* Stockholm (1932).
4. GOLDSTEIN. H., *Calculation of the Penetration of Gamma-Rays*, USAEC Report NDA-NYO 3075 (1954).
5. ROCKWELL T. (Ed.), *Reactor Shielding Manual* USAEC T.I.D.-7004 (1956).

Reactor Science and Technology (Journal of Nuclear Energy Parts A & B), 1961, Vol. 14, p. 143, Pergamon Press Ltd. Printed in Northern Ireland

ERRATA

HILLIER M. J. *Thermal Stresses in Reactor Shells due to γ-Irradiation, J. Nucl. Energy*, **8**, 33.

IT has been pointed out by DR. LECH. SZYMENDERA of the Institute of Nuclear Research, Warsaw, that there are a number of algebraic errors in the original paper under the above title. The purpose of this note is to correct these errors. The opportunity has been taken to rewrite equations (21), (22), (25) and (26), which were originally written incorrectly, in a more convenient form; otherwise the corrections are due to DR. SZYMENDERA.

The graphs presented in the original paper remain essentially unaltered except that the vertical ordinates in Fig. 6 should be multiplied by a factor of 4. The corrections are as follows (the prefixed numbers in brackets refer to the original formulae):

Corrections

(2) For $H = \frac{1}{2}H_0E_2[\mu x]$,
read $H = 2H_0E_2[\mu x]$

(the last equation of the Appendix, p. 47, *should read*

$$H = 2J\mu_s E_\gamma E_2[\mu x])$$

(23, 24) For $\frac{\theta_0}{6}$ *read* $\frac{2}{3}\theta_0$

Equation (21)

$$\theta = \theta_0[1 - e^{-\mu x} - (1 - e^{-\mu T})\cdot x/T] + \theta_{s1} + (\theta_{s2} - \theta_{s1})\cdot x/T.$$

Equation (22)

(a) $$\theta_{s1} = \left\{\frac{Q}{U_1}\frac{1}{1+q}[q(1+p_2)+p_2] + \theta_1(1+p_2) + \theta_2 p_1\right\}(1+p_1+p_2)^{-1}$$

(b) $$\theta_{s2} - \theta_{s1} = \left\{\frac{Q}{U_1}\frac{1}{1+q}(p_2/p_1 - q) + \theta_2 - \theta_1\right\} \times (1+p_1+p_2)^{-1}$$

(c) $$q = \frac{(1-\mu T) - e^{-\mu T}}{e^{-\mu T}(1+\mu T) - 1}$$

(d) $$\frac{Q}{U_1} = \theta_0\mu T\cdot p_1(1 - e^{-\mu T}).$$

Equation (25)

$$\theta = \frac{2\theta_0}{3}\{1 - 3E_4[\mu x] + [3E_4[\mu T] - 1]x/T\} + \theta_{s1} + (\theta_{s2} - \theta_{s1})\cdot x/T.$$

Equation (26)

(a) $$\theta_{s1} = \left\{\frac{Q}{U_1}\frac{1}{1+q}[q(1+p_2)+p_2] + \theta_1(1+p_2) + \theta_2 p_1\right\}(1+p_1+p_2)^{-1}$$

(b) $$\theta_{s2} - \theta_{s1} = \left\{\frac{Q}{U_1}\frac{1}{1+q}(p_2/p_1 - q) + \theta_2 - \theta_1\right\} \times (1+p_1+p_2)^{-1}$$

(c) $$q = \frac{3\mu T + 6E_4[\mu T] - 2}{2 - 6\mu T\cdot E_3[\mu T] - 6E_4[\mu T]}$$

(d) $$\frac{Q}{U_1} = \tfrac{1}{2}\theta_0\cdot\mu T\cdot p_1[1 - 2E_3[\mu T]].$$

Equation (30)

$$\theta_{s1} = [\theta_1(p_2 + \ln b/a) + \theta_2 p_1](\ln b/a + p_1 + p_2)^{-1} + \frac{Q}{U_1}\frac{(q + b/a)\cdot p_2 + q\cdot\ln b/a}{(q + b/a)(\ln b/a + p_1 + p_2)}.$$

Equation (31)

$$\theta_{s2} = [\theta_1 p_2 + \theta_2(p_1 + \ln b/a)](\ln b/a + p_1 + p_2)^{-1} + \frac{Q}{U_1}\frac{p_2(q + b/a) + b/a\cdot p_2/p_1\cdot\ln b/a}{(q + b/a)(\ln b/a + p_1 + p_2)}$$

Equation (32)

$$\theta_{s1} - \theta_{s2} = \left\{(\theta_1 - \theta_2)\ln b/a + \frac{Q}{U_1}\frac{[q - b/a\cdot p_2/p_1]\ln b/a}{q + b/a}\right\} \times (\ln b/a + p_1 + p_2)^{-1}.$$

Equation (36)

$$\theta = \theta_0\cdot\frac{a\cdot e^a}{\rho}[\rho E_2[a] + a\cdot E_2[\rho] - B(\rho - a)].$$

Equation (40)

$$\sigma_y = \sigma_z = \frac{\sigma_0}{2\mu T}[(2+\mu T)e^{-\mu T} - (2 - \mu T)].$$

Equation (41)

$$\sigma_y = \sigma_z = \frac{\sigma_0}{2\mu T}[(2+\mu T)e^{-\mu T} - (2 - \mu T)] \mp \frac{\alpha E(\theta_1 - \theta_2)}{2(1-\nu)(1+p_1+p_2)} \mp \frac{\alpha E}{2(1-\nu)}\cdot\frac{Q}{U_1}\cdot\frac{(q - p_2/p_1)}{(1+q)(1+p_1+p_2)}.$$

Equation (42)

$$q = \frac{\mu T - (1 - e^{-\mu T})}{1 - e^{-\mu T}(1+\mu T)}.$$

Equation (45)

$$\sigma_y = \sigma_z = \frac{\sigma_0}{6\mu T}\{2\mu T[2 - 3\mu T\cdot E_3[\mu T]] - 3[1 - 4E_3[\mu T]]\}.$$

Equation (46)

$$\sigma_y = \sigma_z = \frac{\sigma_0}{6\mu T}\{2\mu T[1 + 3E_4[\mu T]] - 3[1 - 4E_3[\mu T]]\}.$$

Equation (47)

$$\sigma_y = \sigma_z = \frac{\sigma_0}{6\mu T}\{2\mu T[1 + 3E_4[\mu T]] - 3[1 - 4E_3[\mu T]]\} \mp \frac{\alpha E(\theta_1 - \theta_2)}{2(1-\nu)(1+p_1+p_2)} \mp \frac{\alpha E}{2(1-\nu)}\cdot\frac{Q}{U_1}\cdot\frac{(q - p_2/p_1)}{(1+q)(1+p_1+p_2)}.$$

Equation (48)

$$q = \frac{3\mu T + 6E_4[\mu T] - 2}{2 - 6\mu T\cdot E_3[\mu T] - 6E_4[\mu T]}.$$

Equation (51)

$$\sigma_z = \sigma_t = \frac{\sigma_0 a e^a}{2(b^2 - a^2)\ln b/a}\{(b^2 - a^2)[E_1[a] - E_1[b]] + 2\ln b/a[(1+b)e^{-b} - (1+a)e^{-a}]\}.$$

VOL
14
196

Reactor Science and Technology (J.N.E. Parts A/B), 1961, Vol. 14, pp. 145 to 154. Pergamon Press Ltd. Printed in Northern Ireland

STUDIES IN THE METABOLISM OF CARRIER-FREE RADIORUTHENIUM—II

THE UPTAKE OF NITROSYL-RUTHENIUM COMPLEXES FROM THE GASTROINTESTINAL TRACT

R. S. BRUCE and T. E. F. CARR
Medical Research Council Radiobiological Research Unit, Harwell, Berks.

(*Received* 4 *November* 1960)

Abstract—Carrier-free radioruthenium, as the nitrosyl-trinitrate, has been administered orally to rabbits and rats, both as a single dose and as repeated doses for a prolonged period. The amount of ruthenium absorbed and the distribution within the tissues have been estimated. Rabbits absorbed 13 per cent of a single dose and rats absorbed about 3 per cent, while after 7 days the amounts retained in the tissues were 1 per cent and 0·4 per cent respectively. The half-time for elimination of ruthenium by the rabbit during the first 10 days was 1·6 days and thereafter increased to at least 7 weeks.

After 50 weeks, during which ruthenium was administered twice weekly to a rabbit, only 3·8 per cent of the average weekly dose was retained in the animal 18 days after the last dose. It is concluded that the retention from each of the serial doses was less than that from a single dose. The amount of ruthenium retained by rats receiving ruthenium twice weekly, did not increase between 41 and 58 weeks and averaged 3 per cent of the weekly dose.

No single tissue exhibited a particularly high concentration of ruthenium after either single or multiple doses. It would appear that some part of the nitrosyl-ruthenium combines with the tissues and that the rate of loss of ruthenium from a tissue may be governed by its catabolic rate.

VOL. 14 1961

AMONG the longer-lived isotopes resulting from nuclear fission are those of ruthenium, one of which, ^{106}Ru, has a physical half-life of 1 year. Studies in the biological behaviour of this element by other workers have been almost entirely concerned with ruthenium administered as the chloride. Preliminary investigations in this laboratory (BRUCE and CARR, 1960) however, showed that derivatives of nitrosyl-ruthenium were absorbed from the gastrointestinal tract to a much greater extent than the chloride; an average of 13 per cent of the nitrosyl form was absorbed by rabbits compared with 3 per cent of the chloride. No other information is available on the metabolism of nitrosyl-ruthenium and because this form predominates in radioactive effluent, the high uptake observed in the preliminary experiments called for further study.

The preliminary investigations were confined to determining the distribution of ruthenium in laboratory animals during the first week after a single oral dose. The work has now been extended to measure retention by animals over a longer period after a single dose and to discover whether repeated dosage leads to progressive accumulation of ruthenium in any organ.

SOME ASPECTS OF RUTHENIUM CHEMISTRY

The chemistry of ruthenium in nitric acid solutions and of nitrosyl-ruthenium, $(RuNO)^{III}$, derivatives has been described (FLETCHER *et al.*, 1955; BROWN *et al.*, 1958) and only a brief account is appropriate here. When irradiated reactor fuel is dissolved in nitric acid for processing, three main ruthenium species may be formed, (i) Ru^{IV} nitrate, (ii) RuNO nitrato complexes and (iii) RuNO nitro complexes. The nitrate is readily converted to nitrosyl-ruthenium by traces of nitrous acid which are normally present in nitric acid solutions. The relative proportions of the nitrato and nitro complexes depend on the ratio of the nitric acid and nitrous acid concentrations in the solution. These complexes are of the type $[RuNO(NO_3)_3(H_2O)_2]$ and $[RuNO(NO_2)_2(H_2O)_2OH]$ but their exact composition depends on the concentration of nitric acid present.

In aqueous solution the trinitrato complex hydrolyses rapidly to a dinitrato and then more slowly to a mononitrato complex and finally to a trihydroxy complex. Depending on the conditions, any two or more of these forms may be in equilibrium with one another.

$$RuNO(NO_3)_3\,(H_2O)_2 \rightarrow RuNO(NO_3)_2\,OH\,(H_2O)_2$$
$$\downarrow$$
$$RuNO(NO_3)\,(OH)_2\,(H_2O)_2$$
$$\downarrow$$
$$RuNO(OH)3\,(H_2O)_2.$$

The nitrosyl-ruthenium radical under appropriate conditions will also form complexes of differing

strength with many other ligands, e.g. ClO_4^-, F^-, $<NO_3^-$, $<Cl^-$, $<NO_2^-$. The ligands OH^-, SO_4^{--} and $C_2O_4^{--}$ give complexes comparable with Cl^-.

While the composition of the complexes changes according to the conditions, the RuNO group itself is very stable. When strongly alkaline solutions of the nitrato complexes are heated with Devarda's alloy the nitrosyl group is completely reduced to ammonia. Heating with strong oxidizing agents in acid solution slowly oxidizes the ruthenium to the tetroxide and fusing with alkali/nitrate mixtures also eliminates the nitrosyl group.

Brown *et al.* (1958) conclude that the complexity of ruthenium chemistry arises not so much from the number of oxidation states that are possible for this element but rather, in the case of nitrosyl-ruthenium, the diversity of compounds containing ruthenium in a common valency state. Consequently it is difficult to offer any prediction of the chemical nature of the complexes formed by nitrosyl-ruthenium in biological systems. However it seems likely that the RuNO group will persist since drastic treatment is required to decompose it.

MATERIALS AND METHODS

At the outset of these investigations the only well characterized derivative of nitrosyl-ruthenium was the trinitrato complex (Martin, 1953) which is obtained as a rose-red deliquescent solid by slow evaporation of a nitric acid solution in a vacuum desiccator over solid caustic soda. This complex was therefore chosen for metabolic study and was prepared under similar conditions by evaporation of nitric acid solutions of carrier-free nitrosyl-ruthenium.* The evaporation was carried out in the presence of kieselguhr which is chemically inert but allowed the ruthenium to be handled conveniently.

The details of experimental procedure have already been given (Bruce and Carr, 1960). Both sandylop and Dutch rabbits have been used and also albino rats from an inbred Wistar strain. The animals were fed on standard diets and kept in metabolism cages which allowed separation of faeces and urine. The ruthenium was administered orally on kieselguhr either in a gelatine capsule, or as a moist pellet from a tube and plunger, and intragastrically as a solution.

In most experiments ruthenium was assayed by dissolving the sample in nitric acid and counting in a halogen quenched Veall type liquid counter in conjunction with standard counting equipment. Ruthenium-106 itself is a soft β-emitter (maximum energy 0·04 MeV) but the daughter, rhodium-106 (half-life 30 seconds), is a hard β-emitter (maximum energy 3·5 MeV) and is readily counted. Corrections were made for radioactive decay whenever appropriate.

RESULTS

A. *Metabolism of nitrosyl-ruthenium following a single oral dose*

1. *Rabbits.* Two Dutch rabbits were fed nitrosyl-ruthenium and sacrificed after four days. Blood samples were taken by venipuncture at intervals during the experiment and faeces and urine were collected daily. The gross distribution of the ruthenium and the distribution in the gastrointestinal tract were determined at sacrifice and the results are shown in Tables 1(a) and (b). Table 1(c) gives the percentage of the dose excreted daily in the faeces and urine. Relatively little of the ruthenium administered, or even of that absorbed,† was retained in the tissues after four days. A better comparison of the distribution of ruthenium in the tissues of the two animals can be made if variations due to differences in absorption are eliminated by expressing the data as a percentage of the total retained (Table 2), when it will be seen that the results for the two animals are very similar. The concentration of ruthenium was highest in the kidney and liver with the mean bone concentration next. It is evident however that the ruthenium was not distributed evenly through the bone but was more concentrated in the ends, probably in the region of bone growth at the time of feeding. The concentration of ruthenium in the other tissues assayed was lower than that in the blood at the time of sacrifice and the concentration in the brain was particularly low.

Although the proportion of nitrosyl-ruthenium retained by the rabbit was less than 2 per cent of the dose after four days, it was considered desirable to discover the rate of disappearance from the various tissues. To this end, five sandylop rabbits were fed nitrosyl-ruthenium and sacrificed after 7, 14, 21, 28 and 42 days respectively. Faeces and urine were collected separately, blood samples were taken during the course of the experiment and the ruthenium in the tissues was assayed when the animals were killed.

The distribution of the ruthenium at the time of death is summarized in Table 3. It will be seen that after 7 days, 3 per cent of the administered ruthenium remained in the gastrointestinal tract but that most had been cleared by the fourteenth day. Retention in the rest of the body was low and did not change significantly between 14 and 42 days. The pelt and

* These solutions were supplied by the Radiochemical Centre, Amersham, Bucks.

† No account has been taken of ruthenium absorbed from the gastrointestinal tract and subsequently re-excreted into it.

VOL 14 196

TABLE 1.—THE DISTRIBUTION OF NITROSYL-RUTHENIUM 4 DAYS AFTER ADMINISTRATION TO TWO RABBITS

(a) Overall distribution

	% of dose	
	R465	R467
Tissues excluding gut	1·83	0·75
Gut walls	0·47	0·46
Gut contents	11·7	11·4
Faeces	75·2	79·5
Urine	10·7	7·8

(b) Distribution in the gastrointestinal tract

	% of dose		% of dose/g × 10^3
	R465	R467	R467
Stomach	0·02	0·01	2·5
Small intestine	0·20	0·28	9·7
Caecum	0·18	0·12	7·1
Colon	0·04	0·04	5·6
Rectum	0·03	0·01	2·0
Stomach contents	0·08	2·49	42
Small intestine contents	0·55	0·75	42
Caecum contents	8·52	6·75	155
Colon contents	0·88	0·72	200
Rectum contents	1·68	0·69	230

(c) Rate of excretion as percentage of the dose per day

Day	Faeces		Urine	
	R465	R467	R465	R467
1	33·1	37·1	7·1	4·0
2	28·9	25·4	1·9	2·1
3	7·3	9·5	1·1	1·1
4	5·9	7·5	0·7	0·6

residual carcass (mainly bone and muscle) accounted for most of the retained activity, the liver and kidneys being the only other major contributors. The proportion of ruthenium absorbed did not differ greatly between animals and was comparable with other experiments.

Figure 1 shows the typical pattern of the cumulative total excretion in urine and faeces. The total remaining in the rabbit and the daily excretion in the urine decreased rapidly for the first few days. The half-time for the retention during the first 10 days was approximately 1·6 days and thereafter increased to at least 7 weeks.

The relationship between the concentration of ruthenium in the blood and the time from feeding is shown in Fig. 2. The level in the blood rose very rapidly after feeding (Fig. 2(a)) and reached a

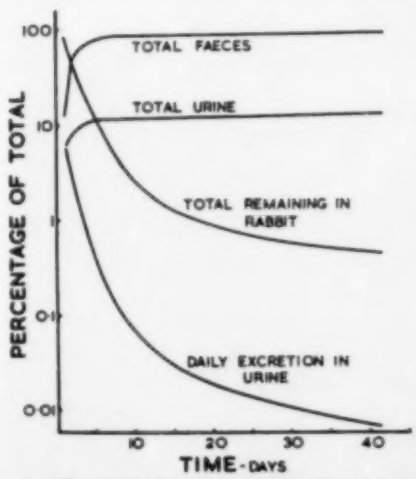

FIG. 1.—The retention and excretion of ruthenium by the rabbit after a single oral dose of nitrosyl-ruthenium.

TABLE 2.—THE DISTRIBUTION OF NITROSYL-RUTHENIUM RETAINED BY TWO RABBITS FOUR DAYS AFTER ADMINISTRATION

	% of retained ruthenium		% retained/g	
	R465	R467	R465	R467
Kidneys	12·3	12·2	1·35	1·30
Liver	23·4	16·5	0·66	0·34
Blood	–	—	0·13	0·14
Testes	0·17	0·20	0·12	0·08
Spleen	0·02	0·04	0·10	0·13
Pelt	16·0	20·0	0·10	0·12
Lungs	0·62	0·45	0·08	0·07
Heart	0·27	0·23	0·08	0·06
Adrenals	0·02	0·02	0·07	0·10
Gall bladder	0·06	0·04	0·05	0·05
Thymus	0·12	0·08	0·04	0·05
Pancreas	0·19	0·04	0·25	0·03
Muscle	—	—	0·02	0·03
Brain	0·03	0·01	0·003	0·001
Femur ends			0·43	0·28
Femur shaft			0·17	0·14
Femur marrow			0·10	0·09
Tibia & fibula			0·22	0·21
Humerus & scapula			0·19	0·23
Bone—mean value	27·5*	28·7*	0·23	0·22

* Estimates derived from the concentrations in the bones sampled assuming that the skeletal weight in the Dutch rabbit is 10 per cent of the total weight.

TABLE 3.—THE EFFECT OF TIME FROM FEEDING ON THE DISTRIBUTION OF NITROSYL-RUTHENIUM IN RABBITS

	Percentage of total administered				
Time from feeding (days) Animal number	7 R15	14 R16	21 R17	28 R18	42 R19
Stomach + contents	0·46	0·012	0·008	0·004	0·005
S. intestine + contents	0·20	0·017	0·008	0·006	0·005
Caecum + contents	1·76	0·084	0·017	0·007	0·011
Colon + contents	0·48	0·029	0·006	0·003	0·003
Rectum + contents	0·52	0·050	0·004	0·002	0·003
Total retained in the gut	3·41	0·192	0·043	0·022	0·027
Liver	0·17	0·081	0·063	0·059	0·078
Kidneys	0·12	0·037	0·021	—	0·015
Spleen	0·001	<0·001	<0·001	<0·001	<0·001
Heart	0·005	0·002	0·001	0·001	0·001
Lungs	0·006	0·002	0·001	0·001	0·002
Testes	0·003	0·001	<0·001	0·001	—
Pelt	0·23	0·14	0·14	0·22	0·25
Carcass (residual)	0·60	0·36	0·24	0·31	0·35
Total retained in tissues excluding the gut	1·14	0·63	0·47	0·60	0·69
Urine	13·4	10·8	10·3	12·5	12·4
Faeces	82·1	88·4	89·1	86·9	86·9

VOL 14 196

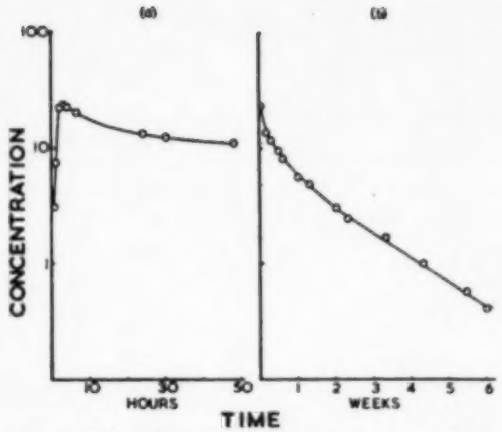

FIG. 2.—The relationship between the concentration of ruthenium in the blood and the time after administration of a single oral dose of nitrosyl-ruthenium to a rabbit.

maximum in two to three hours. On an extended time scale (Fig. 2(b)) the concentration decreased rapidly during the first few days and then after about 2 weeks the decrease was logarithmic, corresponding to a half-time of about 10 days. At least 90 per cent of the ruthenium in the blood was found in the plasma.

The concentration of ruthenium in the tissues has been expressed in terms of a standard amount absorbed to allow for differences in the uptake by individual animals (Table 4). For all the tissues except blood, the change in concentration with time followed the general pattern of retention shown in Fig. 1. The values for the blood concentrations of the individual animals lie on a curve similar in shape to that given in Fig. 2.

2. *Rats.* The distribution of nitrosyl-ruthenium in rats after a single oral dose for a period of up to seven days from feeding has already been described (BRUCE and CARR, 1960). In connexion with a further experiment, in which there was repeated administration of ruthenium (*vide infra*), it was desirable to know the rate of disappearance of ruthenium from the rat over a longer period of time. A solution of nitrosyl-ruthenium was administered by stomach tube to four rats from each of five litters. One rat from each litter was sacrificed after 7, 14, 21, and 28 days and the ruthenium in the tissues was assayed. The urine and faeces of the rats sacrificed at 7 and 14 days were assayed separately for the first 7 days. For the remainder, the urine and faeces were combined for assay.

Table 5 shows that the amount remaining in the gut was negligible even at 7 days and that once again there was considerable variation in the amount of ruthenium absorbed by different rats, which was reflected in the amount retained. The variability of the retention by individual rats sacrificed at any one time was such that differences in retention with time cannot be shown. The concentration of ruthenium in the tissues, apart from the kidneys, does not appear to decrease after the first seven days (Table 6). If the concentrations are adjusted for the amount retained, differences between animals sacrificed at one time become relatively small, indicating that while uptake varied, the distribution of the retained ruthenium did not (cf. Table 2 giving similarly adjusted values for rabbits).

B. *Uptake and metabolism of nitrosyl-ruthenium following repeated oral administration*

The experiments described so far have all been concerned with the fate of single doses of ruthenium

TABLE 4.—THE RELATIVE CONCENTRATIONS OF RUTHENIUM IN THE TISSUES OF RABBITS AT DIFFERENT TIMES AFTER FEEDING NITROSYL-RUTHENIUM

	Percentage of dose absorbed per g × 10^3					
Time from feeding (days)	4	7	14	21	28	42
Rabbit number	*	R15	R16	R17	R18	R19
Liver	62·7	14·3	10·8	6·14	5·81	7·28
Kidney	154	31·1	19·6	7·94	—	5·16
Spleen	13·3	5·60	2·50	2·43	2·99	0·92
Heart	8·1	2·65	2·00	0·93	0·92	0·94
Lungs	9·1	2·52	2·02	0·91	1·15	1·04
Testes	12·3	2·35	1·70	0·80	0·81	—
Muscle	2·5	0·63	0·73	0·54	0·66	0·74
Pelt	12·2	4·65	3·27	2·81	3·96	—
Tibiae and fibulae	25·3	4·09	5·39	3·05	3·65	2·59
Femur shaft	18·5	3·79	4·12	2·53	3·84	1·93
Femur ends	43·8	6·19	4·19	3·99	4·91	3·51
Femur marrow	10·7	3·33	3·37	2·39	2·10	2·63
Blood	15·9	4·06	2·16	0·83	0·70	0·42

* Mean value for tissues from Dutch rabbits Nos. 465 and 467.

Table 5.—The retention of nitrosyl-ruthenium by rats at various times after feeding

Time from feeding	Rat number	Percentage of dose			
		Retained in gut	Retained in carcass excluding gut	In urine during first 7 days	Absorbed*
7 days	39	0·017	0·34	2·1	2·4
	40	0·220	0·93	3·7	4·6
	41	0·018	0·20	1·8	2·1
	42	0·016	0·24	1·5	1·7
	43	0·014	0·22	2·1	2·3
	Mean	0·056	0·39	2·2	2·6
14 days	44	0·006	0·24	1·4	1·7
	45	0·004	0·19	1·1	1·3
	46	0·003	0·10	1·7	1·8
	47	0·011	0·42	2·1	2·5
	48	0·040	1·52	6·9	8·4
	Mean	0·013	0·49	2·6	3·1
21 days	49	0·007	0·15		
	50	0·004	0·05		
	51	0·022	0·50		
	52	0·004	0·08		
	53	0·004	0·07		
	Mean	0·008	0·17		
28 days	54	0·015	0·58		
	55	0·016	0·37		
	56	0·014	0·40		
	57	0·004	0·11		
	58	0·001	0·07		
	Mean	0·010	0·30		

* The fraction absorbed is taken as that appearing in the urine together with that remaining in the carcass excluding the gut.

Table 6.—Distribution of nitrosyl-ruthenium in rats at various intervals after feeding

Time from feeding (days)	Percentage of dose/g × 10^3 (mean values from 5 animals)						
	Kidney	Liver	Muscle	Pelt	Carcass	Femora	Gut
7	23·0	1·4	0·6	1·6	1·2	2·6	1·5
14	15·3	1·2	0·7	1·9	2·0	1·4	0·4
21	5·4	0·7	0·3	0·9	0·4	1·7	0·2
28	4·1	0·6	0·9	1·8	0·8	3·3	0·2

to animals. As there was evidence that ruthenium absorbed by bone was only slowly liberated, it was decided to investigate whether repeated doses of ruthenium could lead to an accumulation in bone or in any other tissue. Exploratory experiments were therefore carried out in which one rabbit and sixteen rats were fed with repeated small doses of nitrosyl-ruthenium over prolonged periods.

1. *Rabbit experiment.* Nitrosyl-ruthenium on kieselguhr was fed in a gelatine capsule to a sandylop rabbit twice weekly for fifty weeks. The animal was seven months old when the experiment began and its weight, which did not change appreciably, was 3 kg. The average weekly dose was 6 microcuries and the total fed amounted to 300 microcuries. The faeces were collected twice a week when the ruthenium was

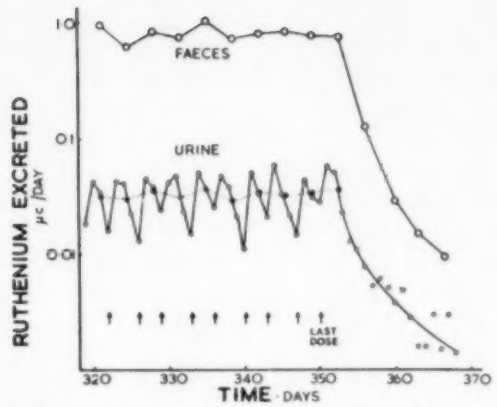

FIG. 3.—The pattern of faecal and urinary excretion when nitrosyl-ruthenium was fed twice weekly to a rabbit and when administration was discontinued.
(The small arrows indicate times when ruthenium was administered. The dotted line shows the mean urinary excretion per day for each dose of ruthenium.)

fed and the urine was collected daily. Blood samples were taken at intervals during the experiment just before administering the ruthenium. The rabbit was sacrificed 18 days after the last dose so that the rapidly eliminated fraction would be excreted and the long-term components of retention could be observed.

The pattern of faecal and urinary excretion of ruthenium for the last weeks of the experiment is illustrated by Fig. 3. The amount of ruthenium excreted per day in the urine was greatest in the day following the dose and decreased on successive days, increasing abruptly again after the next dose. This pattern remained fairly constant up to the last dose after which the rate fell sharply. The mean urinary excretion of ruthenium for each dose over the whole period of the experiment was 5·43 ± 0·13 per cent; only during the period following the initial dose and before the second dose was the proportion of ruthenium in the urine comparable with that found for rabbits receiving a single feed (approximately 10 per cent). The mean concentration of ruthenium in the blood did not change greatly over the experimental period.

TABLE 7.—THE GROSS DISTRIBUTION OF RUTHENIUM ADMINISTERED TWICE WEEKLY TO A RABBIT FOR 50 WEEKS

	μc	% of total dose
Total in animal at death	0·23	0·077
Total in urine	16·9	5·7
Total in faeces	280	94

The gross distribution of the ruthenium at the time of sacrifice is summarized in Table 7 from which it will be seen that only a very small percentage of the total was retained 18 days after the last dose. The distribution of the retained ruthenium in the rabbit is given in Table 8 and the results show that the pelt, bone and muscle accounted for a very large proportion of the total. The concentration of ruthenium in the tissues,

TABLE 8.—DISTRIBUTION OF RUTHENIUM IN A RABBIT 18 DAYS AFTER DISCONTINUING TWICE WEEKLY FEEDING OF NITROSYL-RUTHENIUM

	% of total retained at death	Concentration (μc/g × 10⁴)	
Stomach and contents	1·28	0·24	
Small intestine and contents	0·63	0·20	
Caecum and contents	6·45	1·28	
Colon and contents	1·77	1·23	
Rectum and contents	1·64	1·23	
Liver	4·33	1·46	
Kidneys	1·28	1·54	
Spleen	0·05	0·72	
Heart	0·17	0·39	
Lungs	0·27	0·46	
Testes	0·17	0·36	
Pelt	34·6	1·68	
Blood		0·06	
Muscle		0·33	
Tibiae and fibulae		1·22	Mean value for bone 1·06
Femur shaft		0·66	
Femur ends		1·11	
Femur marrow		0·36	
Total Bone*	24·9		
Total Muscle*	23·5		

* Calculated from the sample concentrations assuming that the ratio of the wet weight of muscle to bone is 3:1 in the carcass.

apart from blood, was relatively uniform differing only by a factor of five throughout.

2. *Rat experiment.* Sixteen rats were fed nitrosyl-ruthenium twice a week with an average dose of 0·75 microcuries per week to each animal. The ruthenium, on kieselguhr, was administered as a paste into the oesophagus of the rat by means of a tube and plunger. As it was not possible to measure the precise dose administered each time, the results have been based on the amount of ruthenium recovered. It will be seen from Table 9 however, that the average weekly dose for all the rats was uniform.

The rats were kept in pairs and the combined urine and faeces from each pair were collected twice weekly immediately prior to the administration of ruthenium. The excreta were homogenized with water and the ruthenium assayed by counting samples of the homogenate. After different periods of dosage the administration of ruthenium was discontinued to pairs of animals which were sacrificed 14 days after the last dose.

The results are summarized in Tables 9 and 10. It will be seen that apart from the first four animals, the amount of ruthenium retained per animal did not differ greatly and did not increase significantly with the period of dosage. As with the rabbit, there is no evidence that any tissue had an exceptionally high concentration nor was there any long term retention of ruthenium in the gastrointestinal tract.

The first four rats (2/1 and 1/2) were litter-mates and proved to be abnormal. They were found to be suffering from a chronic renal disease for which no satisfactory explanation can be offered at present though a hereditary factor may be involved. None of the other litters showed any abnormality and there is no reason for supposing that this condition was due to radiation damage. It will be observed that the abnormal litter showed a higher retention of ruthenium. This may have been due to impaired kidney function or to low food intake reducing the dilution with food in the gastrointestinal tract and so increasing uptake.

DISCUSSION

The present investigation confirms the findings reported previously (BRUCE and CARR, 1960) with regard to the high proportion of ruthenium absorbed following oral administration as a nitrosyl complex and its distribution within the animal. Although more tissues have been assayed, there is no evidence that ruthenium is accumulated selectively in any tissue to the same extent as many elements (e.g. bone seeking elements). The highest concentrations occur in the kidney, liver, pelt and bone.

The slope of the curve for total retention by the rabbit (Fig. 1) changes progressively with time from feeding, rapidly during the first few days but more slowly thereafter. An estimate of the slope of the latter part of the curve indicates a minimum half-life of 7 weeks for the retained ruthenium after 40 days. The concentrations in the individual tissues also decrease as though more than one half-life was involved and not as a single exponential. This may be due to uneven distribution within the tissue leading to differential retention in the various zones. For instance, a rough separation of the femur into marrow, shaft and ends showed that the concentration was not uniform and was highest in the ends. This disparity may be associated with a better blood supply to the ends and possibly with deposition in the zone of bone growth. Some evidence for this occurs in the data of THOMPSON *et al.* (1958) who found that deposition of ruthenium is greater in the bone of young growing rats than in older animals.

It has already been seen (Fig. 2) that after an initial rapid decrease, the ruthenium concentration in the blood decreased exponentially with a half-life of about 10 days. This is comparable with the half-life of rabbit plasma proteins (COHEN *et al.*, 1956) which suggests that ruthenium was attached to the proteins and that the slower disappearance from blood was associated with protein breakdown. Similarly in other tissues, the longer-term retention may be due to combination of ruthenium with protein in the tissue and the disappearance of the ruthenium governed by the rate of breakdown of this protein. The initial rapid decrease in ruthenium concentration in all the tissues probably represents the loss of a labile form of ruthenium into the blood followed by rapid removal by the kidneys.

The slow rate of loss of ruthenium from the tissues after the first 14 days following a single dose suggests that repeated doses would result in a progressive increase in ruthenium concentration until equilibrium was established. After 50 weeks of serial dosage and 18 days after the final dose, the rabbit retained 0·23 μc of ruthenium equivalent to 3·8 per cent of the average weekly dose while at a similar time after a single dose the retention was about 0·5 per cent (Table 3). If the retention of each serial dose was also 0·5 per cent, the half-life of the longer term component would have to be about 5 weeks in order to give an equilibrium retention of 3·8 per cent of the weekly dose. However, as was seen from Fig. 1, the half-life after 40 days was at least 7 weeks and the slope of the curve was still changing. Consequently it must be concluded that the retention from each of the serial doses was less than

VOL
14
196

TABLE 9.—THE RETENTION OF NITROSYL-RUTHENIUM IN RATS AFTER REPEATED SMALL DOSES

Rat	No. of days from first to last feed	Total dose (μc)	Average weekly dose (μc)	Total retention (μc × 100)	Retention as percentage of weekly dose
1/2 *A*	206	20·1	0·69	7·03	10·2
1/2 *B*	245	25·8	0·74	6·26	8·5
2/1 *A*	206	22·1	0·76	—	—
2/1 *B*	245	26·0	0·74	6·89	9·3
2/0 *A*	287	30·0	0·73	2·12	2·9
2/0 *B*				1·66	2·3
0/2 *A*		30·6	0·75	2·27	3·0
0/2 *B*				2·16	2·9
Mean		30·3		2·05	2·8
1/0 *A*	367	39·2	0·75	2·90	3·9
1/0 *B*				2·36	3·1
0/1 *A*		38·6	0·74	2·52	3·4
0/1 *B*				2·45	3·3
Mean		38·9		2·56	3·4
0/0 *A*	406	45·7	0·79	2·62	3·3
0/0 *B*				2·21	2·8
1/1 *A*		43·7	0·75	2·29	3·0
1/1 *B*				2·45	3·3
Mean		44·7		2·39	3·1

TABLE 10.—THE CONCENTRATION OF RUTHENIUM IN SELECTED TISSUES OF RATS FED REPEATED SMALL DOSES OF NITROSYL-RUTHENIUM FOR PROLONGED PERIODS

No. of days from first to last feeding	287	367
Mean weekly dose (μc) per rat	0·74	0·75
	Concentration (μc/g × 10^4)*	
Liver	0·37	0·26
Kidneys	1·03	0·86
Spleen	0·76	0·31
Testes	0·26	0·11
Lungs	0·38	0·32
Heart	0·26	0·22
Muscle	0·31	0·40
Pelt	1·17	1·16
Femora	0·84	0·91

* Mean value from 4 rats.

VOL. 14 1961

that observed from a single dose; otherwise, with a longer half-life than five weeks, the retention would have been greater than that observed. Further evidence for lower retention from the serial doses lies in the reduced urinary excretion compared with that following a single dose (5·4 per cent compared with 11 per cent).

THOMPSON *et al.* (1958) also found inconsistencies in the proportion of ruthenium chloride retained by rats as a result of serial feeding compared with that forecast from a single dose. In the present experiment with rats which were fed serial doses of nitrosyl-ruthenium for 1 year, about 3 per cent of the weekly dose was retained. This value does not differ greatly from the result for the rabbit but no comparison can be made between the retention after single and serial dosage because of the high variability of the data from individual rats fed single doses. These differences between individual rats occurred despite care taken to follow a uniform procedure for administration. The results from rats fed serial doses varied much less, probably because differences in uptake from individual doses cancelled out over a period of time. The method of administration may also influence absorption since in the present experiments rats absorbed about 3 per cent of a single dose administered by stomach tube, whereas in previous experiments (BRUCE and CARR, 1960) there was a mean uptake of 8 per cent when the ruthenium was given in paste pellets.

It is evident that even though a high proportion of nitrosyl-ruthenium may be absorbed from the gut, there is no appreciable long-term retention in any organ even after repeated dosage. Apart from the gastrointestinal tract, the tissue which is subjected to the highest concentration of ruthenium is the kidney.

Acknowledgment—The authors wish to acknowledge the helpful discussions on the chemistry of ruthenium which they have had with members of the Chemistry Division, A.E.R.E., Harwell.

REFERENCES

BROWN P. G. M., FLETCHER J. M., HARDY C. J., KENNEDY J., SCARGILL D., WAIN A. G. and WOODHEAD J. L. (1958) *Proceedings of the Second International Conference on the Peaceful Uses of Atomic Energy, Geneva*, P/31, **17**, 118. United Nations, N.Y.

BRUCE R. S. and CARR T. E. F. (1961) *Reactor Sci. Technol. (Journal of Nuclear Energy* Parts A/B) **14**, 9.

COHEN S., HOLLOWAY R. C., MATTHEWS C. and MCFARLANE A. S. (1956) *Biochem. J.* **62**, 143.

FLETCHER J. M., JENKINS I. L., LEVER F. M., MARTIN F. S., POWELL A. R. and TODD R. (1955) *J. Inorg. Nucl. Chem.* **1**, 378.

MARTIN F. S. (1953) *Chem. Industr.* 824.

THOMPSON R. C., WEEKS M. H., HOLLIS O. L., BALLOU J. E. and OAKLEY W. D. (1958) *Amer. J. Roentgenol.* **79**, 1026.

VOL
14
196

Reactor Science and Technology (J.N.E. Parts A/B), 1961, Vol. 14, pp. 155 to 167. Pergamon Press Ltd. Printed in Northern Ireland.

ENVIRONMENTAL MONITORING AFTER ACCIDENTAL DEPOSITION OF RADIOACTIVITY

A. C. CHAMBERLAIN, R. J. GARNER and D. WILLIAMS
Atomic Energy Research Establishment, Harwell, Berks.

(*Received* 6 *October* 1960)

Abstract—In Part I the entry of accidentally dispersed activity into milk is considered. From experimental data on the transfer of radioiodine, radiostrontium and radiocaesium from grass to milk by the cow, the emergency permissible deposition of these substances on grass is calculated and compared with the relative abundance of the nuclides on various assumptions. It is concluded that iodine-131 will nearly always be the limiting factor, though only marginally so if fission products are deposited in the proportions found in the reactor.

In Part II the assessment of deposition of iodine-131 by measurement of gamma dose rate is considered. The dose rates at 3 and 500 feet above ground and the corresponding responses of gamma scintillator instruments are calculated. If iodine-131 is the only activity deposited, the increase in dose rate above background corresponding to the emergency permissible deposition (0·4 μc/m^2) is 3·3 μr/hr at 3 feet and about 0·3 μr/hr at 500 feet. The problems of measuring these dose rates by car-borne or aerial survey are discussed and illustrated by results obtained after the Windscale accident of October, 1957.

VOL. 14 1961

PART I: ENTRY OF ACTIVITY INTO MILK

1. *Definition of problems*

IF there is an accident to a reactor, critical assembly or chemical plant, it will be necessary to determine the areas in which food and drink and, in particular, milk are liable to be seriously contaminated. To a large extent this will be done by direct measurement of the activity in the milk or other foodstuff, but there will also be a need to determine the fall-out pattern by measurements of dose rate and the activity in grass and soil in the environment.

Methods for measuring the activity of fission products in milk and grass have been given by BRYANT, MORGAN and SPICER (1959), BOOKER (1958) and COX and MORGAN (1959). The organization necessary to make measurements in an emergency has been described by DUNSTER, MCLEAN, HOWELLS and TEMPLETON (1958). The time taken to make a measurement depends on the nature of the activity looked for and the extent to which it is masked by other activities. It is sometimes possible to determine the activity of gamma-emitting nuclides such as iodine-131, caesium-137, and barium-140 by gamma spectrometry of samples of grass or milk without any previous chemical separation. The method is then very quick if a multichannel gamma kicksorter is used. If several nuclides are present, however, it may not be possible to sort out the gamma spectrum, and the peaks from the biologically important nuclides may be difficult to distinguish. Radiochemical separation must then be done, and this is also nearly always necessary for determination of the beta-emitters, in particular strontium-89 and 90.

Much time will be saved if the fall-out pattern and the area in which serious contamination has occurred, can be determined by measurements of gamma dose-rate in the environment, using portable instruments.

Suppose, for example, that an emission of activity took place at 1500 hours on a day in late autumn in Northern England, just as the cows were coming in for the afternoon milking. Suppose the weather was such that the cows were kept in during the night but sent out to graze in the morning. No appreciable activity would appear in the milk till the afternoon of the day following the emission, so that a period of at least 24 hours would elapse before milk samples could be usefully analysed. During that time the nature of the activity emitted and the isopleths of deposition would have to be determined and a preliminary decision taken on the area over which milk would be unfit for consumption. It might well be that in the circumstances a ban on the consumption of milk would be applied over a larger area than eventually proved necessary. The restrictions would be lifted as the results of measurements in milk became available, but at least the first decision would have to be made on the results of gamma surveys, supported by a limited number of physical and chemical analyses of grass.

The present paper is concerned with the sort of measurements that would be made and the deduction

that could be drawn from them, during the first 24 hours after the release, within which time the decision whether or not a milk ban was needed, and if so over what area, would have to be taken.

Experience gained during the Windscale accident of October 1957, is valuable at many points, but it must not be assumed that circumstances would be the same on any future occasion. For example, the problem of appreciation at Windscale was simplified by the nature of the activity released. It had previously been assumed (e.g. by MARLEY and FRY, 1955) that the various fission products would be emitted and deposited in the proportions found in the pile. At Windscale, the release was almost confined to isotopes of the noble gases and the volatile elements tellurium, iodine and caesium. However, laboratory experiments (MEGAW *et al.*, 1960) show that the release of oxide particles containing mixed fission products is at least as likely as that of iodine vapour. During the Windscale accident, the temperature was high enough to cause sintering of oxide, but not high enough to vaporize the fuel or the bulk of the fission products. Also the air velocity in the pile was relatively low, consequently the oxide particles remained in the hot channels. Conditions might be different on any future occasion, and at least four possibilities must be considered.

(a) *Instantaneous fission products.* A criticality accident or emission from a previously zero energy reactor creates fission product activity in a very short time. This activity is dispersed by the violent boiling of a solution or the vaporization of a fuel element.

(b) '*Reactor*' *fission products.* Activity is released from fuel in substantially the proportions present after long irradiation, for example by the emission of oxide particles. All but the very long-lived fission products are in radiative equilibrium and have activity proportional to their fission cross sections.

(c) *Volatile fission products.* The noble gases and the elements tellurium, iodine and caesium are liberated in the proportions present in long-irradiated fuel.

(d) *Iodine-131 only.* A release of iodine-131 takes place, for example, by a mishap to a chemical separation plant.

It will be assumed that the nuclides are deposited on grass in the same relative amounts as they are emitted, except that the noble gases are not deposited. This was approximately the case at Windscale (CHAMBERLAIN and DUNSTER, 1958), at least in the area within about 30 miles of the pile where intensive surveying was done.

2. *Activity in milk*

The emergency permissible daily intakes of iodine-131, strontium-89 and 90 and caesium-137 at various ages by persons in the environment of a nuclear energy establishment have been set by the Medical Research Council (1959). Emergency permissible levels in milk are derived from them, the critical case being that of the six-month-old infant assumed to drink 0·9 litres of cow's milk daily. Considerably higher levels would be permissible if the use of fresh cow's milk by infants was in some way discontinued for the period following the accident.

The extent to which fission products deposited upon grazing land will enter milk may vary greatly depending upon many factors. The assumptions made in order to obtain some estimate of the maximum levels of contamination in milk likely to be encountered under field conditions from the experimental data available on the transfer of fission products from diet to milk in cows have been summarized by GARNER (1960). Figure 1 has been constructed from the data given by GARNER and shows the change in activity with time for each nuclide following a deposition on herbage of 1 $\mu c/m^2$ over a short period of time.

Even under constant experimental conditions, there are considerable variations between individual animals. Further, the assumptions made are considered to represent the worst case likely to occur under conditions of British agriculture. There are many factors which, in normal circumstances, would probably reduce the quantity of fission products transferred to milk. Figure 1, therefore, presents the most pessimistic picture.

The time which elapses after the deposition before the activity in milk reaches its peak varies from one nuclide to another, depending on the radioactive half-life and the metabolism of that element in the cow. Thus, when one day has elapsed, the activity of ^{131}I in milk is 77 per cent of the eventual peak, but that of ^{89}Sr only 22 per cent. After about 6 days, the slope of the lines in Fig. 1 is a function of the radioactive half-life, and for the long-lived nuclides the peak is not reached theoretically until the grazing cycle is complete at 21 days, but in practice this will be modified to some degree by leaching of activity from the grass.

Neglecting effects associated with the radioactive half-lives, the secretion of the elements iodine and caesium in the milk as a fraction of the cow's intake is similar, and much greater than that of the alkaline earths or tellurium.

The results in Fig. 1 for ^{131}I can be compared with the findings after the Windscale accident of October 10th and 11th, 1957. The accident occurred at a time of year when the growth of grass in the fields had nearly stopped. During the first few days, the cattle were probably receiving a high proportion of their food

VOL
14
196

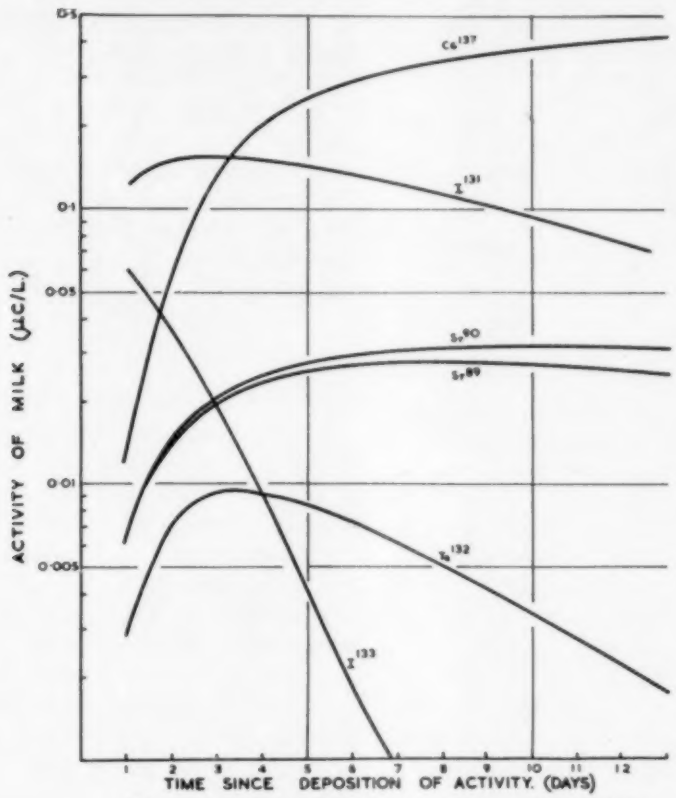

FIG. 1.—Activity in milk following deposition of 1μc/m^2 of various nuclides. (Free grazing conditions in summer.)

from free grazing, but this proportion declined after a week or so had passed.

The effects of the reduced availability of grass were reflected in the way in which the activity of milk varied with time. The peak activity in milk from local farms occurred at about the expected time, but from the fourth day onwards the activity declined more rapidly than can be accounted for by radioactive decay alone. At Seascale, Sellafield and Corney in West Cumberland, the effective half-life was about five days (BOOKER, 1958) and further away in the Leeds district it was about 3 to 5 days (BURCH, 1959). The reason for attributing these facts to reduced availability of grass rather than to leaching is that the ^{131}I activity per unit weight of grass did not decay at a rate faster than the radioactive decay.

The activity of milk at or near the peak is compared with the theoretical prediction in Table 1. The total initial fall-out of iodine-131, as at 0001 hours on October 11th, at each locality, given in the second column, has been derived by a consideration of all the available evidence (CHAMBERLAIN, 1959a).

The agreement between the results found at Windscale and those predicted from experimental work is fairly good, but must be considered to some extent fortuitous.

The results for strontium in Fig. 1 can be checked by reference to data on the fall-out of strontium-90 from distant tests of nuclear weapons. It can be deduced from GARNER's results that a steady deposition of 1 μc/m^2 day should result in an activity of 0·58 μc/l in milk

TABLE 1.—COMPARISON OF WINDSCALE RESULTS WITH THEORETICAL PREDICTIONS

Locality	Fall-out of ^{131}I on 11/10/57 (μc/m^2)	^{131}I in milk (μc/l)			Ratio *a*/*b*
		Date	(a) as found	(b) derived from Fig. 1	
Seascale (Acrelands)	19	13/10	1·4	2·6	0·54
Corney (Foldgate)	10	13/10	0·94	1·5	0·62
Bootle (Stub Place)	2·2	13/10	0·36	0·34	1·06
Pennington	4·8	13/10	0·6	0·73	0·82
Leeds District	0·16	16/10	0·018	0·021	0·86
				Mean	0·78

TABLE 2.—EMERGENCY PERMISSIBLE LEVELS FOLLOWING SINGLE DEPOSITION

Nuclide	^{131}I	^{133}I	^{89}Sr	^{90}Sr	^{137}Cs
Daily intake—adult (μc)	1·3		0·2	0·002	1·15
Daily intake—infant (μc)	0·06		0·2	0·002	0·15
Emergency permissible peak activity of milk ($\mu c/l$)	0·065	1·6	0·22	0·0022	0·17
Initial deposition ($\mu c/m^2$)	0·4	30	8	0·08	0·4

during the grazing season. (The calculation is equivalent to extrapolating the ^{90}Sr curve in Fig. 1 to the end of the grazing cycle at 21 days and then taking the area under it). During 1955 and 1956, there was a fairly constant rate of fall-out of strontium-90 of 2·5 mc/km^2 year, or 6·8 $\mu\mu c/m^2$ day, in regions of S.W. Britain where the annual rainfall was 40 inches. It follows that an activity of $0{\cdot}58 \times 6{\cdot}8 = 4{\cdot}0$ $\mu\mu c/l$ in milk would be expected from Fig. 1. The activity measured in dried milk from Somerset during 1955 and 1956 averaged 4·2 $\mu\mu c$ ^{90}Sr per g Ca, (BRYANT *et al.*, 1957) equivalent to about 4·8 $\mu\mu c/l$ in liquid milk. The measured activity is thus very close to the expected value, assuming that foliar contamination of the herbage is the chief mode of uptake of strontium-90 by grass growing on normal soils (BRYANT *et al.*, 1956, 1957; RUSSELL, 1958; MORGAN, 1959).

The results of Fig. 1 can be combined with the emergency permissible levels in milk (Medical Research Council, 1959) to derive the corresponding deposition of each activity.

The emergency permissible deposition of each nuclide separately is calculated to lead to the emergency permissible dose in the appropriate organ of the body. The figure for ^{133}I has been derived from that for ^{131}I by allowing for (a) the total activities of the two isotopes secreted in milk per unit deposition and (b) the doses to the thyroid per unit activity ingested. When two nuclides which irradiate the same organ are present, the permissible levels must be adjusted accordingly.

3. *Fission product activities*

In Table 3 is shown the relative amounts of the nuclides of biological importance, and of some others, in mixed fission products after 24 hours decay from the moment of release. The fission data of BLOMEKE (1955) have been used in the calculation. The types (a) to (d) of possible release set out in Section 1 are considered. For 'instantaneous' and 'reactor' fission products it is assumed that the nuclides are released and deposited in the proportions present in the reactor or other source, except that the noble gases are assumed not to be deposited. This is a reasonable assumption if the disseminated activity consists of particles of uranium oxide, or an aerosol produced by sudden severe boiling of a solution or slurry containing fissionable material.

A decay period of 24 hours from the time of the accident to the time of measurement is assumed, this being approximately the period before significant activity will appear in milk.

The first 5 rows of Table 3 are concerned with the nuclides which may be transferred in dangerous

TABLE 3.—ACTIVITY OF NUCLIDES, RELATIVE TO ^{131}I, AFTER 24 HOURS DECAY

Nuclide	Half-life	Relative activity (a) Instantaneous fission products	(b) Reactor fission products (300 days irradiation)	(c) Volatile fission products (300 days irradiation)	Relative permissible levels in grass
^{131}I	8·0 d	1·00	1·00	1·00	1·00
^{133}I	21 hr	8·2	0·8	0·8	70
^{89}Sr	50·5 d	0·3	1·8	—	20
^{90}Sr	28 yr	0·002	0·05	—	0·2
^{137}Cs	27 yr	0·002	0·04	0·04	1·0
^{132}Te	3·2 d	2·9	1·3	1·3	
^{140}Ba	12·8 d	1·4	2·2	—	
^{103}Ru	40 d	0·2	1·1	—	
^{95}Zr	65 d	0·3	2·5	—	
Total f.p.		100	30	~3	

amounts in milk,* and in the right-hand column is shown the relative permissible levels of these nuclides in grass.

It appears that in any of the three mixtures (a), (b) and (c), ^{131}I is the most dangerous activity. Comparing ^{89}Sr for example with ^{131}I, the relative activities are 0·3 in case (a), or 1·8 in case (b), whereas the permissible level in grass is 20 times greater for ^{89}Sr. Comparing ^{90}Sr with ^{131}I, the margin is not so great, and if the relative activities were in some way altered by a factor of 4 in favour of ^{90}Sr, this nuclide would become the critical hazard in case (b). This might occur for either of the following reasons:

(i) *Reduced emission of* ^{131}I. The relative activities of 'reactor' fission products in Table 4 are calculated assuming that a reactor is continuously under power up to the time of the accident. If the fuel has been well irradiated but there have been lengthy shut down periods during the two or three weeks previous to the accident, the ^{131}I activity will be reduced relative to that of longer-lived nuclides.

(ii) *Reduced deposition of* ^{131}I. Circumstances can be imagined in which ^{131}I is emitted as a gas or adsorbed on small particles but other fission products are emitted as larger oxide particles, with high rate of fall in air. Experimental work shows that this is unlikely, and indeed the converse is more probable, namely that the rate of deposition of iodine (as a vapour) and its retention on herbage would be higher than for particulate fission products.

In any accident in which fuel reaches a high temperature, as at Windscale, it is likely that there will be preferential release of iodine, which is then much the most important hazard. Nevertheless, determination of the deposition of strontium-90 on grass is an obvious urgent requirement and this can only be done by radiochemical analysis.

PART II: ASSESSMENT OF DEPOSITION OF IODINE-131 BY MEASUREMENTS OF GAMMA DOSE-RATE

4. *Gamma dose-rate from deposited activity*

The gamma dose-rate in the environment must be measured immediately there is any suspicion of an accidental emission having taken place so as to determine whether there is a hazard from external radiation. This was done promptly in the immediate environment at Windscale by the Health Physics staff (PENNEY, 1957). A survey for this purpose presents considerable problems of organization, but technically the measurements are not difficult.

The problem considered in this paper is whether measurements of gamma dose-rate, either on the ground or by aerial survey, can be used to delineate the area where milk restrictions will have to be made.

In Fig. 2 is shown the dose rate at heights of 3 feet and 500 feet above a plane surface uniformly contaminated with nuclides emitting gamma rays of various energies. The calculations (STEWART, 1958; CHAMBERLAIN, 1959b) take into account the build-up of the intensity of the scattered gamma rays by using the build-up factors of GOLDSTEIN and WILKINS (1954).

There are difficulties in obtaining direct experimental checks of the results in Fig. 2, and in estimating to what extent the dose rate is reduced by penetration of activity into the ground and absorption of the gamma rays in herbage or soil. An indirect check has been made by comparing the deposition of activity near Windscale, as deduced from the gamma dose-rate, with measurements of the activity in grass and soil (CHAMBERLAIN, 1958), and it appears that the theoretical calculations are fairly well verified.

From Fig. 2 it can be deduced that the dose rate at 3 feet above a plane surface contamination with 1 c/m² of iodine-131 is 8·2 r/hr. It follows that the emergency permissible deposition of 0·4 μc/m² of iodine-131 (Table 2) would give a dose rate of 3·3 μr/hr.

It is possible that there might be an emission consisting of iodine-131 and nothing else, but it is more probable that other nuclides would be emitted and deposited simultaneously. In Fig. 3 is shown the dose rates in μr/hr, at 3 ft above ground as a function of time since the deposition took place, assuming a deposition of 0·4 μc/m² of iodine-131 with other fission products. The four possibilities set out in Section 1 are considered, namely, that the fall-out consists of

(a) mixed fission products in the 'instantaneous' proportions,†
(b) mixed fission products in the proportions found in fuel irradiated for 300 days,
(c) volatile fission products (I, Te, Cs) in the proportions found in fuel irradiated for 300 days,
(d) iodine-131 only.

Figure 3 shows that the dose rate associated with a deposition of 0·4 μc/m² of iodine-131, measured one day afterwards, may be anything between 400 and 3 μr/hr, depending on which type of release has occurred. Moreover a release could be intermediate in nature

* ^{132}Te may be present in milk, but it can be shown that the hazard from that nuclide, and its daughter product ^{132}I (half-life 2·3 hr) is always small in comparison with the hazard from ^{131}I. The same is true of ^{140}Ba in comparison with ^{89}Sr.

† Most of the iodine-131 in fission products is not formed directly at fission but by the decay of tellurium-131 (half-life 25 m). The activity of iodine-131 in grass after a release of instantaneous fission products would be small initially but would build up as the deposited tellurium-131 decayed.

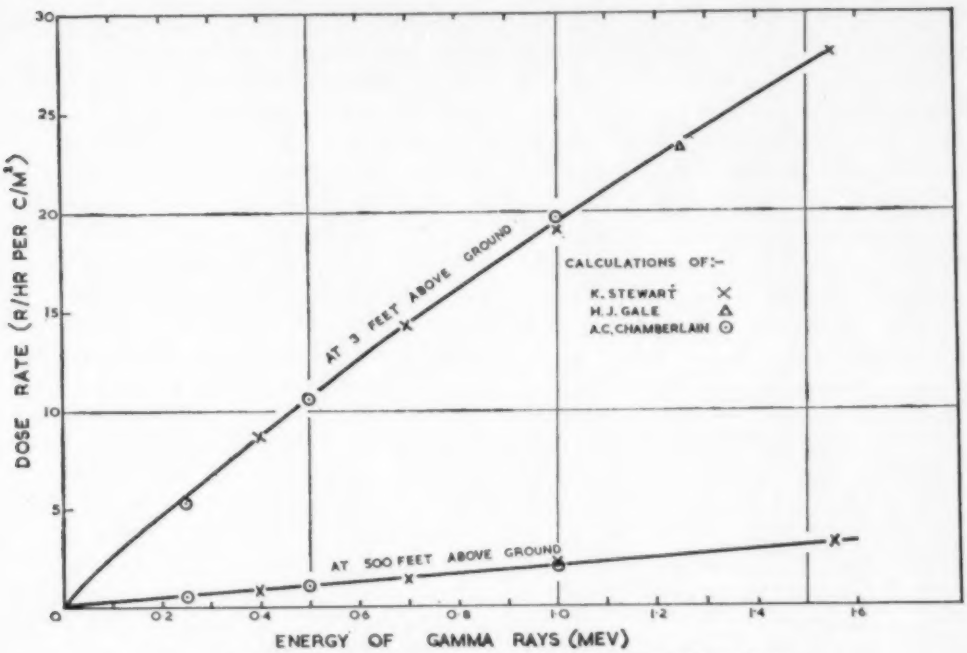

FIG. 2.—Dose rate in air above infinite plane source of γ-emitters.

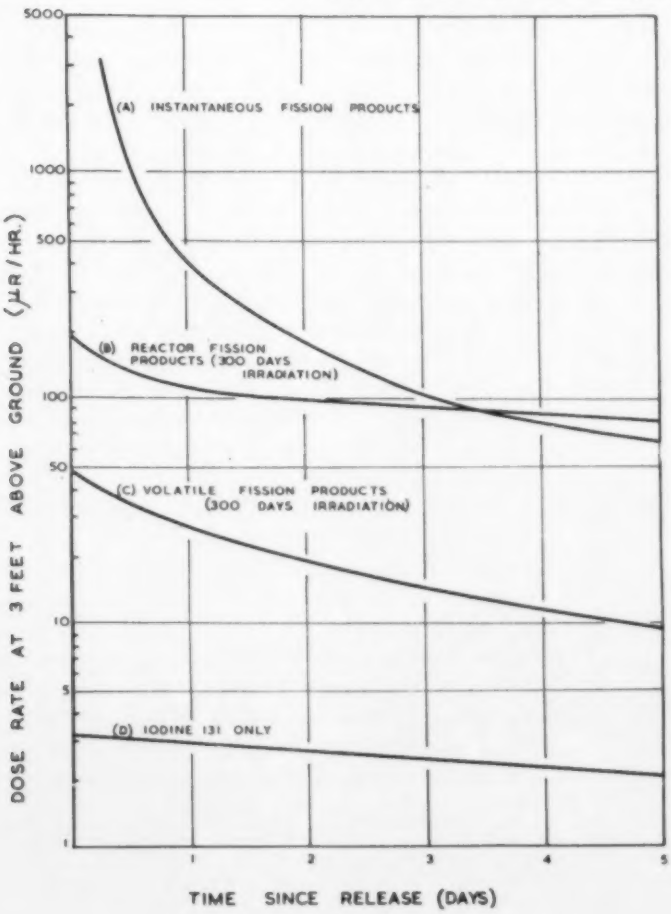
DOSE RATE AT 3 FEET ABOVE GROUND (μR/HR.)
TIME SINCE RELEASE (DAYS)
(A) INSTANTANEOUS FISSION PRODUCTS
(B) REACTOR FISSION PRODUCTS (300 DAYS IRRADIATION)
(C) VOLATILE FISSION PRODUCTS (300 DAYS IRRADIATION)
(D) IODINE 131 ONLY

FIG. 3.—Gamma dose rates from fission products associated with 0·4 μc/m² of iodine-131 on the ground.

between two of the cases (a) to (d), for example the fuel might have had some previous burn-up and then a large irradiation in a short time.

Two conclusions can be drawn from Fig. 3.

(i) The gamma dose-rate corresponding to that deposition of iodine-131 which will create a milk hazard can vary by a factor of about 100 depending on the circumstances of the release. The dose rate may fall considerably during the first few hours.

(ii) The external dose rate is nevertheless not a serious hazard, even in condition (a) above, at the level where a milk hazard exists. The milk restriction area is always larger than the evacuation area.

The dose rates shown in Fig. 3 must be considered with relation to the background gamma dose-rate above which any increase must be measured. Natural background, caused by cosmic rays and the natural activity in the soil and air, typically varies from about 6 to 15 μr/hr at 1 metre above ground, according to location (SPIERS, 1956). The variations are mainly caused by differences in the uranium, thorium and potassium content of rocks, and can be allowed for if background gamma surveys are made.

During and immediately following the intensive testing of nuclear weapons, the world-wide fall-out of fission products (especially zirconium-95 and niobium-95) caused increases in gamma background. In Britain during 1959 the contribution from this source varied from 1 to 10 μr/hr (SPIERS, 1959; PEIRSON and SALMON, 1959; VENNART, 1960), depending on rainfall and on whether the ground had been recently cultivated. With the recent cessation of tests, the difficulties of distinguishing weapon fall-out from other contamination have been greatly reduced.

5. *Gamma survey instruments*

The dose rates in Figs. 2 and 3 are in terms of roentgens per hour, a unit of rate of ionization in air. If the gamma absorption characteristics of a radiation detector are made similar to those of air (e.g. an ionization chamber or organic scintillator) measurements of the rate of ionization or energy absorption in the detector material can be expressed in roentgens per hour. However, where the mean atomic number of the detector material differs from that of air, such measurements no longer indicate true dose-rate and an even more marked divergence occurs if the radiation flux is measured in place of the rate of energy absorption. Inorganic scintillators (e.g. thallium-activated sodium iodide crystals) have advantages in survey work since their high gamma detection efficiency permits the design of sensitive compact instruments. Furthermore, their sensitivity to cosmic radiation is decreased and their gamma sensitivity accordingly increased by employing flux measurements rather than energy-absorption measurement, since all detected quanta then contribute equally, irrespective of energy, to the instrument indication. Thus, the most convenient survey instrument for gamma-radiation measurements is one which is also markedly energy-dependent in terms of dose rate and has a greater response per roentgen per hour for low rather than high-energy gammas (WILLIAMS, 1958). This is an advantage in measuring iodine-131, of which the principal gamma ray has energy 0·364 MeV, in the presence of natural background radiation.

The portable scintillation ratemeter type 1413A, which was originally designed for geological survey, has been found very suitable for environmental monitoring. It is normally used for measurements at fixed stations, but may also be employed as car-borne survey instrument. The characteristics of the 1413, and of two other similar instruments, i.e. 1444 and 1531, used for car-borne and aerial surveys respectively, are summarized in Table 4.*

One version of the aerial survey instrument (type 1531A) is shown in Fig. 4. The three scintillation detector heads are in the background, and the ratemeter control unit and twin channel recorder are in the foreground. When mounted in the aircraft, the detector heads are near the tail, remote from the luminous instruments in the crew compartment.

The calibrations of the instruments for the gammas from radium and iodine-131 were obtained by exposing known sources at various distances (WILLIAMS, 1958; BOOKER and CAMBRAY, 1960). Some variation in sensitivity was found depending on the orientation of the crystal with respect of the source. The results quoted in Table 4 were obtained with normal incidence of the gamma-rays to the crystal. In the field, most of the unscattered gamma rays strike the crystal normally, since the flux is mostly horizontal near the ground but mostly vertical at 500 feet. This is not necessarily the case with the scattered rays, which contribute significantly to the total response especially in the airborne application.

6. *Use of scintillation instruments for survey*

WILLIAMS, CAMBRAY and MASKELL (1958), PALMER (1958), WILLIAMS and CAMBRAY (1960) and WILLIAMS *et al.* (1960) have described the methods of using scintillation instruments for environmental survey. Useful experience was gained during the period following the Windscale accident of October 1957.

* Details of these instruments are given in BISAY *et al.* (1958) and PICKUP (1960).

TABLE 4.—GAMMA SCINTILLATION SURVEY INSTRUMENTS

Type	1413	1444	1531
Method of carriage	Hand or car	Car	Aircraft
Crystal diameter (in.)	1½	4½	4½ } 3 in parallel
Crystal thickness	1	1	1 }
Orientation of crystal axis	Horizontal	Horizontal	Vertical
Ratemeter display	Meter or chart	chart	chart
Ratemeter units	mr/hr	c/s	c/s
Calibration: c/s per μr/hr from Ra gammas	7	58	173
Factor of overestimation for ^{131}I gammas*	3·1	2·6	2·6

* Factor of overestimation =

$$\frac{\text{Response to } ^{131}\text{I source}}{\text{Response to Ra source}} \times \frac{\text{Dose rate } (\mu\text{r/hr}) \text{ from Ra source}}{\text{Dose rate } (\mu\text{r/hr}) \text{ from } ^{131}\text{I source}}.$$

Hand, car-borne and airborne instruments were all used, and found to have complementary advantages.

(i) *Portable instruments* (*Type* 1413). Since the dose rate corresponding to a deposition of 0·4 μc/m^2 of iodine-131 is 3·3 μr/hr, and the 1413 instrument has a factor of overestimation for iodine-131 gammas of 3·1, the indicated dose rate at the 0·4 μc/m^2 level is 10 μr/hr, assuming that no other isotope besides iodine-131 is present. This is detectable above background and the sensitivity is therefore adequate.

In practice the actual dose rate will differ from the theoretical since:

(a) other isotopes will usually be present

(b) penetration of activity into the ground and foliage cover will reduce the dose rate.

In the Windscale accident, the only isotopes, in addition to iodine-131, which contributed materially to the dose rate were the 77 hr half-life tellurium-132 and its 2·3 hr daughter product iodine-132. (The circumstances of the accident were such that only volatile fission products such as iodine, tellurium and caesium were emitted to any significant degree, and moreover the reactor had been shut down for 4 days previous to the accident. The conditions were, therefore, intermediate between (c) and (d) of Section 4.) The dose rate from tellurium-132 + iodine-132 was initially about 160 per cent of that from iodine-131 and fell to 75 per cent after 6 days, (CHAMBERLAIN, 1958). When allowance was made for this, reasonable agreement was found between estimates of the deposition of iodine-131 by the gamma survey and by analysis of grass and soil (BOOKER, 1958; CHAMBERLAIN, 1958, 1959a).

In using the portable instrument for environmental monitoring, the following procedures should be adopted.

(a) Measurements should be made at a standard height (3 feet) over short grass and at least 50 feet away from buildings, roads, hedges, vehicles, etc. Where possible, locations should be chosen where the natural background has previously been measured.

(b) Precautions should be taken against contamination of the instrument. The best way of checking the datum level (cosmic background + inherent count rate of instrument) is to read the instrument over a stretch of water.

(c) Representative samples of grass and soil, from measured areas of ground, should be taken at reference stations where repeated gamma readings are made.

(d) Comparisons should be made between the reading of the scintillation instrument and the dose rate measured by an ionization chamber or Geiger-Müller counter. These instruments are less energy-dependent than scintillation counters (WILLIAMS, 1958; GALE, CHISHOLM and PEAPLE, 1959).

(ii) *Car-borne instrument.* If an instrument is mounted in a car and its output is connected to a chart recorder, a rapid and continuous survey can be made and the results recorded for future reference. The disadvantages are that the vehicle may become contaminated and that the dose rate over the road will not be the same as over pasture. Measurements at Windscale showed that the dose rate over roads was only 60 per cent of that over pasture, a difference which may be attributable to reduced deposition on smooth surfaces (MEGAW, 1958). In addition, there are anomalies in the background gamma dose-rate over roads and near buildings, caused by the use of granite and similar materials.

These difficulties may be reduced by mounting the instrument on a pole extending above or to one side of the vehicle, so that the detector receives a greater proportion of gamma rays from activity on the adjacent fields, (WILLIAMS *et al.*, 1960).

VOL.
14
1961

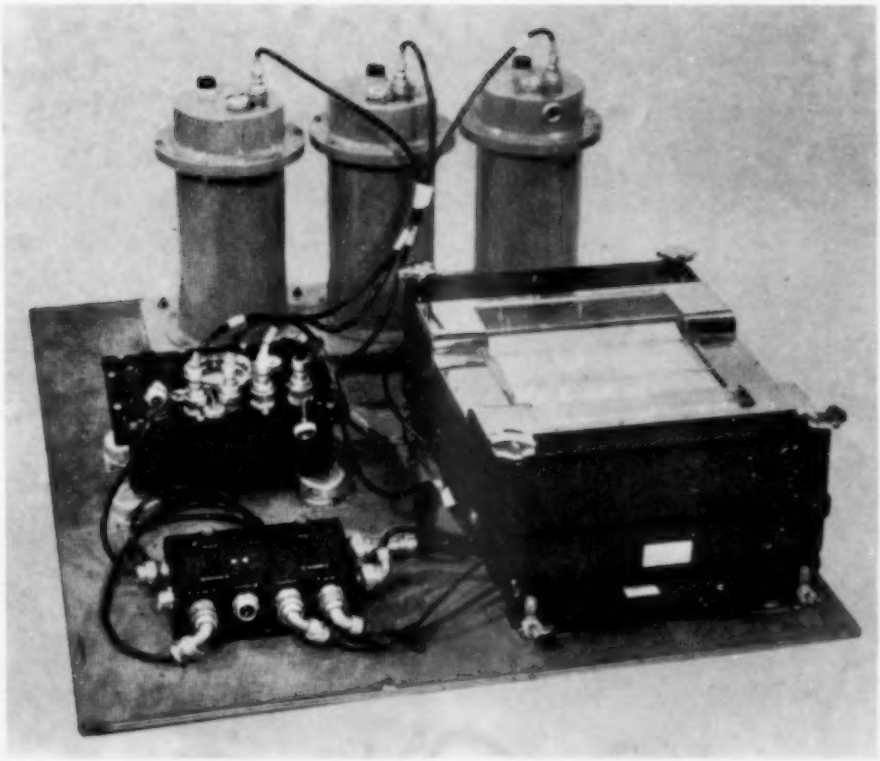

FIG. 4.—Aerial survey instrument, type 1531A.

VOL
14
196

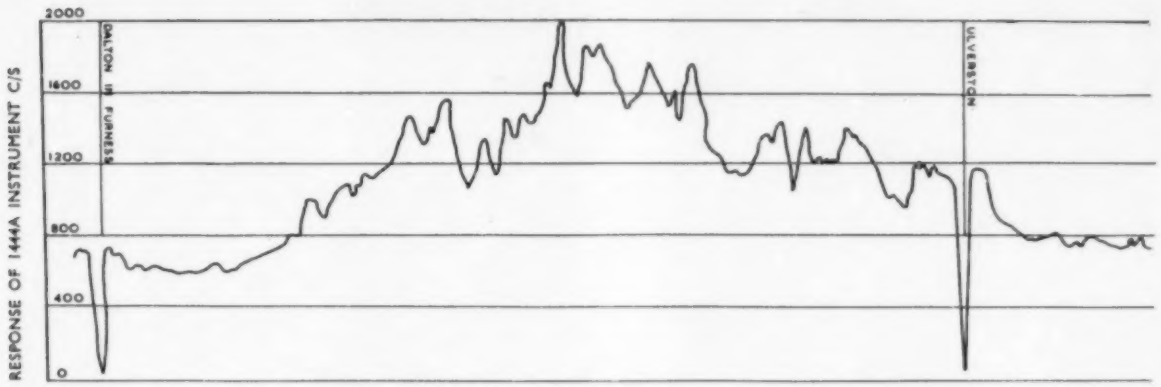

FIG. 5.—Part of trace of car-borne recorder made on 17 October, 1957.

It is of interest to examine whether the results of a car-borne survey could be used to predict the area in which the emergency permissible level of iodine-131 in milk would be exceeded.

A chart record was obtained with a car-borne 1444 instrument travelling to Windscale on 17th October, 1957, six days after the accident. The first well-defined increase in the response was observed as the car travelled from Ulverston to Dalton-in-Furness in Cumberland, between which places the main plume of iodine-131 had passed, and this part of the record is shown in Fig. 5. A map of the district is shown in Fig. 6, and the route taken on 17.10.57 is shown by a line which is marked with cross lines in those parts of the journey where the record shows a reading of greater than 1160 c/s and which is plain in the other parts. The figure of 1160 c/s is derived from

$$\text{count rate} = c(d_1 f_1 + d_2 f_2)$$

where c = calibration factor for 1444 in terms of radium gammas
= 58 c/s per μr/hr
f_1 = response factor for ^{131}I gammas = 2·6
f_2 = response factor for background = 1
d_1 = dose rate from ^{131}I activity of 0·4 μc/m^2
= 3·3 μr/hr
d_2 = dose rate from background = 11·5 μr/hr (as measured 8 months later).

(This assessment ignores the contribution to dose rate from gammas of ^{132}Te + ^{132}I, and also the reduction of dose rates over roads as compared with pasture, but it is estimated that these two factors approximately cancelled one another.)

The parts of the route shown as a crossed line in Fig. 6 should, therefore, correspond to the areas in which the iodine-131 activity was in excess of 0·4 μc/m^2 on 17th October, 1957.

Measurements of the iodine-131 activity in milk were made as part of the survey of biological materials in the district (DUNSTER *et al.*, 1958; BOOKER, 1958). The area in which the milk activity on October 20th exceeded the emergency permissible level of 65 mμc/l is shown by hatching on Fig. 6. The date, October

Route of car on 17 10 57
Part of route where 1444 A reading exceeded 1190 cts/sec
Area in which activity of milk on 20 10 57 exceeded 65mμc/ℓ
WINDSCALE
N
0 5
SCALE OF MILES
ULVERSTON
DALTON IN FURNESS

FIG. 6.—Car-borne survey in Windscale area.

TABLE 5.—RATIO OF DOSE RATES AT 3 FEET AND 500 FEET

Method	Gamma energy (MeV)	Ratio of dose rates 3 ft/500 ft	Reference
(a) Activity on surface			
Theoretical	0·4 0·7 1·0 1·55	10·5 10·2 10·8 11·2	STEWART (1958)
Experimental—Bomb fall-out	0·7 (?)	9·4	GLASSTONE (1957)
(b) Activity in soil or sea			
Experimental—Natural activity U, Th series and ^{40}K	0–2·6 range	3·3	BOWIE *et al.* (1958)
		2·9	WILLIAMS and CAMBRAY (1960)
		3	DAVIS and REINHARDT (1957)
Fall-out in sea	0·7 (?)	3·1	GLASSTONE (1957)

20th, has been chosen because it can be shown from Fig. 1 that the activity of iodine-131 in milk on that day should bear the same relation to the gamma activity of iodine-131 on October 17th, as the peak activity in milk on October 13th bears to the gamma activity on October 11th, immediately after the accident. It can be seen that the parts of the car survey route where the count rate exceeded 1160 c/s correspond fairly well to the area of hatching. The problem of vehicle contamination was avoided in this instance since the survey vehicle came from outside the area and did not enter the highly contaminated zone until the survey was complete.

The conclusion from Fig. 6 is that a car-borne survey is capable of delineating with fair accuracy the milk restriction area in an incident in which iodine-131 is deposited, provided that the instrument readings can be related to iodine-131 activity in grass and milk. This relation can be obtained by calculation if iodine-131 is the only nuclide to contribute a significant proportion of the dose rate. If other nuclides are present, the gamma intensity detected by the survey instrument will be increased relative to the background radiation as shown in Fig. 3, but the readings must then be related to analytical measurements of nuclides in grass and milk.

7. *Aerial survey*

An aerial survey is a rapid method of establishing the pattern of fall-out. The advantages and disadvantages compared with ground survey methods have been summarized by WILLIAMS, CAMBRAY and MASKELL (1958) and PALMER, (1959). An aerial survey of the Windscale district after the accident of October, 1957, was carried out (WILLIAMS *et al.*, 1958) and despite its hurried inception and the lack of a pre-incident survey, gave a clear indication of the main areas of contamination.

Aerial surveys are usually carried out at a nominal height of 500 ft but in practice the ground clearance varies between 450 and 600 ft, the greatest variations occurring over hilly ground.

Table 5 shows the ratio of dose rates at 3 feet and 500 feet above ground,

(i) when activity is deposited on the ground surface and

(ii) when it is uniformly mixed in the ground or sea to a considerable depth.

For activity on the ground surface, the true dose rate at 500 ft is about a tenth of that at 3 ft. By theoretical calculation, using build-up factors for the contribution of scattered dose, this factor is approximately independent of the initial gamma energy in the range 0·4–1·5 MeV.

The response of the aerial survey equipment to activity on the ground depends on the energy spectrum and the spatial distribution of the flux at the instrument, both of which are a function of the height above

ground. The response of the 1531 instrument to a uniform contamination of 1 $\mu c/m^2$ of iodine-131 on the ground can be derived in three ways:

(a) *Experimental.* WILLIAMS and CAMBRAY (1960) carried out experiments at Harwell. The 1531 instrument was suspended at a height of 60 feet on a wooden tower and an iodine-131 source was positioned on the ground at various distances between 100 and 1200 ft from the tower base. The count rate above background was observed and from the results it was deduced that

1 $\mu c/m^2$ of iodine-131 on ground

$\rightarrow$ 290 c/s on 1531 at 500 feet.

(b) *Theoretical.* From Fig. 2, the dose rate at 500 feet from 1 $\mu c/m^2$ of iodine-131 is 0·78 $\mu r/hr$. Since the radium calibration of the 1531 is 173 c/s per $\mu r/hr$, and the factor of overestimation for iodine-131 gammas is 2·6, it follows that

1 $\mu c/m^2$ of iodine-131 on ground

$\rightarrow 0{\cdot}78 \times 173 \times 2{\cdot}6$

$= 350$ c/s on 1531 at 500 feet.

(c) *Windscale correlation.* From the airborne and ground level measurements in the environment after the Windscale accident, CHAMBERLAIN (1958) deduced the empirical correlation

72 μ/hr indicated dose rate on 1413 at ground level

$\rightarrow$ 1000 c/s on 1531 on 500 feet.

From Fig. 2 and Table 4:

1 $\mu c/m^2$ on ground

$\rightarrow 8{\cdot}2 \times 3{\cdot}1$

$= 25{\cdot}4\ \mu r/hr$ on 1413.

Therefore 1 $\mu c/m^2$ of iodine-131 on ground

$$\rightarrow \frac{1000 \times 25{\cdot}4}{72}$$

$= 350$ c/s on 1531 at 500 feet.

The three methods, therefore, agree reasonably well and show that if there were a deposition of 0·4 $\mu c/m^2$ of iodine-131 (equivalent to the emergency permissible level in Table 2), and no other isotopes were present, the corresponding count rate on the 1531 aerial survey instrument at 500 feet would be about 130 c/s. This must be compared with the count rate due to the inherent radioactivity of the instrument, cosmic rays and the natural activity in the air and on the ground. The total contribution from the instrument, cosmic rays and natural activity in air was determined by WILLIAMS and CAMBRAY (1960) by making flights over estuaries and other large stretches of water, and was found to be 180–190 c/s. This remained fairly constant with time and with position. The contribution to the count rate at 500 ft from natural activity in the ground was found to vary from about 250 c/s over chalk to 670 over granite. This response is also dependent on the height of the aircraft above ground.

It follows that the count rate due to 0·4 $\mu c/m^2$ of iodine-131 would be of the same order as the variation associated with different geological strata. If background surveys are made among known flight lines in the district of a reactor, and the same flight lines are followed in any subsequent operational survey, it should be possible to detect the presence of 0·4 $\mu c/m^2$ of iodine-131 with reasonable accuracy.

If other fission products besides iodine-131 are deposited, the count rates will be increased relative to background and the sensitivity thereby increased. Calibration of the aerial survey measurements must then be performed by flying over selected areas where grass and milk samples can be taken. The areas must be selected so that:

(i) the fall-out is reasonably uniform over an area of about 1 km^2,

(ii) the activity per unit area was such as to give an adequate indication on the aerial instrument.

Figure 7 shows the trace obtained in the first aerial survey made over the Windscale area on 19th October, 1957, by WILLIAMS, CAMBRAY and MASKELL (1958). The flight track is in the lower part of the figure and the hatched area represents the region in which 0·65 $\mu c/l$ or more of iodine-131 in milk was measured on 20th October.

The datum level (inherent instrument background + cosmic rays) has been subtracted from the reading before plotting in Fig. 7. The contribution from natural activity in soil can be estimated from results obtained over parts of Cumberland not affected by deposition of iodine-131, and was about 300 ± 100 c/s. The count from iodine-131 at the 0·4 $\mu c/m^2$ level is estimated above at 130 c/s, and smaller contributions from tellurium-131 plus iodine-132 would increase this to about 200 c/s. It follows that the total count rate equivalent to the emergency permissible activity in milk should have been 500 ± 100 c/s. Examination of Fig. 7 indicates that the count rate corresponding to the boundaries of the hatched areas was about 800 c/s. This can be regarded as reasonable agreement, particularly as the grazing of the cattle was becoming very restricted with the onset of autumn.

Figure 7 illustrates also the advantage of the aerial

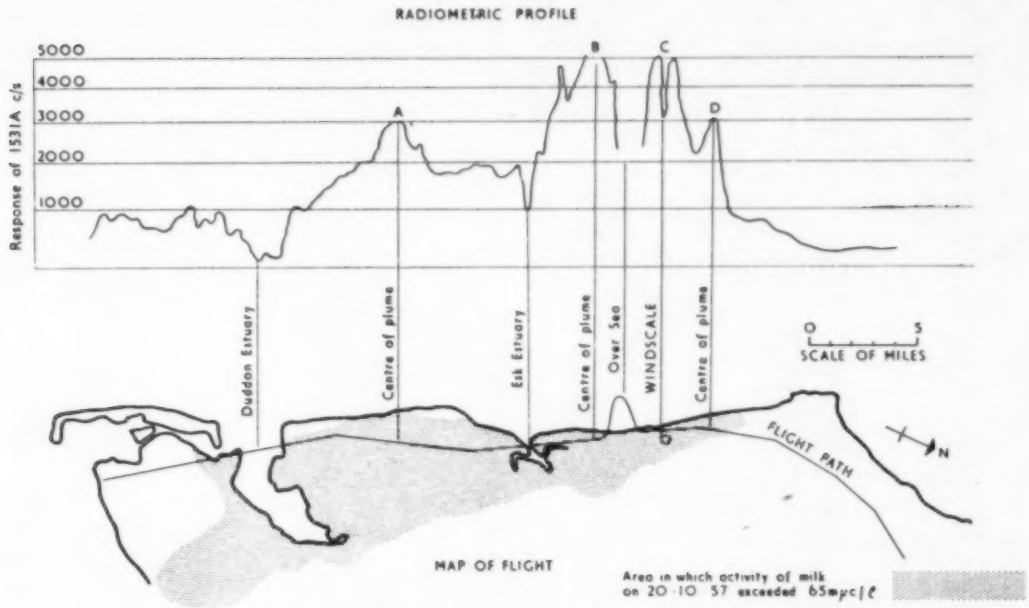

FIG. 7.—Aerial survey in Windscale area.

survey in covering the ground irrespective of roads. The peaks on the trace marked *A*, *B*, *C* can be identified as follows:

A, *B*: aircraft over main plume of deposition S.E. of Windscale.

C: aircraft over factory and within 600 yd of pile filters (which held many curies of activity).

The quite well defined peak *D* is of interest because it shows the existence of a plume of deposition to the N.W. of the Windscale pile. This plume was quite narrow and the half-value width can be shown from Fig. 7 to have been only about 300 yds at a distance of 2 miles from Windscale. The existence of a plume in this direction was revealed also by relatively high milk activities found at two farms N.E. of Windscale, but had the sampling of milk undertaken by the Windscale staff been less thorough, it might well have been missed.

The deviation out to sea as the aircraft approached Windscale was occasioned by the recorder going off scale. The sharp dip in the middle of peak *C* may be a saturation effect. The 1531A instrument used for this survey is known to saturate at high-gamma dose rates with the result that the recorder indication falls back from full-scale; this effect was of no importance in the geological survey application for which the equipment was designed. A later instrument, Type 1531B, however, was arranged to be free from this defect.

The aerial survey method has the advantages that it is very rapid (once the aircraft is airborne), and that the countryside can be covered irrespective of surface communications; for example, offshore islands present no difficulty. The disadvantages are reduced availability in bad weather and the fact that the dose rate from surface contamination falls off with height more rapidly than the dose rate from activity in the ground.

3. *Summary and conclusion*

If there is fall-out of radioactivity in the neighbourhood after an accident to a reactor, critical assembly or chemical plant, an estimate of the possible hazard to milk supplies must be made. The greatest hazard will usually be that of iodine-131.

Using data on the transfer of iodine from grass to milk by the cow, an estimate can be made of the deposition of iodine-131 which will cause milk to be dangerously contaminated. This deposition can be measured by surveys of gamma dose rate in the environment. If iodine-131 only is deposited, the increment to be measured in the gamma dose rate is less than the natural background in most locations. Gamma scintillator instruments amplify this increment because they are more sensitive to low than to high gamma energies. Experience gained at Windscale shows that the measurement is feasible.

If other fission products are deposited together with iodine-131, the gamma dose rate corresponding to a potential hazard to milk is increased, but the gamma readings must then be interpreted by reference to measurements of iodine-131 and strontium-89 and 90 in grass and milk.

VOL. 14 196

REFERENCES

Bisby H., Williams D., and Hale F. H. (1958) *Proceedings of the Second International Conference on the Peaceful Uses of Atomic Energy, Geneva*, **3**, 60. United Nations, N.Y.

Blomeke J. O. (1955) ORNL 1783.

Booker D. V. (1958) A.E.R.E. HP/R 2607.

Booker D. V. and Cambray R. S. (1960) Unpublished.

Bowie S. H. U., Muller J. M., Pickup J. and Williams D. (1958) *Proceedings of the Second International Conference on the Peaceful Uses of Atomic Energy, Geneva*, **2**, 787. United Nations, N.Y.

Bryant F. J., Chamberlain A. C., Morgan A. and Spicer G. S. (1956) A.E.R.E. HP/R 2056.

Bryant F. J., Chamberlain A. C., Morgan A. and Spicer G. S. (1957) *J. Nucl. Energy* **6**, 22.

Bryant F. J., Morgan A. and Spicer G. S. (1959) A.E.R.E.-R3030.

Burch P. R. J. (1959) *Nature, Lond.* **183**, 515.

Chamberlain A. C. (1958) A.E.R.E. HP/R 2606.

Chamberlain A. C. (1959a) *Quart. J. Roy. Met. Soc.* **85**, 350.

Chamberlain A. C. (1959b) Unpublished.

Chamberlain A. C. and Dunster H. J. (1958) *Nature, Lond.* **182**, 627.

Cox G. W. and Morgan A. (1959) AERE-M431.

Davis F. J. and Reinhardt P. W. (1957) *Nucl. Sci. Engng.* **2**, 713.

Dunster H. J., McLean A. S., Howells H. and Templeton W. L. (1958) *Proceedings of the Second International Conference on the Peaceful Uses of Atomic Energy, Geneva*, **18**, 296. United Nations, N.Y.

Gale H. J., Chisholm J. M. and Peaple L. H. J. (1959) A.E.R.E. HP/R 2701.

Garner R. J. (1960) *Nature, Lond.* **186**, 1063.

Glasstone S. (Ed.) (1957) *Effects of Nuclear Weapons.* U.S.A.E.C., Washington D.C.

Goldstein H. and Wilkins J. E. (1954) NYO 3075, U.S.A.E.C., Washington D.C.

Marley W. G. and Fry T. M. (1955) *Proceedings of the First International Conference on the Peaceful Uses of Atomic Energy, Geneva*, **13**, 102. United Nations, New York.

Medical Research Council (1959) *Brit. med. J.* **i**, 967.

Megaw W. J. (1958) Private communication.

Megaw W. J., Chadwick R. C., Wells A. C. and Bridges J. E. (1960) A.E.R.E.-R 3435.

Morgan A. (1959) *J. Nucl. Energy* Part A: *Reactor Sci.* **11**, 8.

Palmer G. H. (1958) A.E.R.E. HP/R 2742.

Peirson D. H. and Salmon L. (1959) *Nature, Lond.* **184**, 1678.

Penney, Sir W. (Chairman of Committee of Inquiry) (1957) *Accident at Windscale No. 1 Pile on 10th October*, 1957. Cmnd. 302, H.M.S.O.

Pickup J. (1960) A.E.R.E.-R 2953.

Spiers F. W. (1956) *Brit. J. Radiol.* **29**, 409.

Spiers F. W. (1959) *Nature, Lond.* **184**, 1680.

Stewart K. (1958) Private communication.

Vennart J. (1960) *Nature, Lond.* **185**, 722.

Williams D. (1959) A.E.R.E. EL/M 102.

Williams D., Cambray R. S. and Maskell S. C. (1958) A.E.R.E EL/R 2438.

Williams D. and Cambray R. S. (1960) A.E.R.E.-R 2954.

Williams D., Pickup J., Cambray R. S. and Wilkins J. (1960) A.E.R.E.-R 3478.

OL.
14
961

Reactor Science and Technology (J.N.E. Parts A/B), 1961, Vol. 14, pp. 168 to 179. Pergamon Press Ltd. Printed in Northern Ireland

METHOD FOR ANALYSING LOW-ENRICHMENT, LIGHT-WATER CORES

R. W. DEUTSCH
General Nuclear Engineering Corporation, Dunedin, Fla., U.S.A.

(*Received* 25 *July* 1960)

Abstract—A three-group method is developed for analysing light-water UO_2 cores of low enrichment. The method is composed of a series of sub-routines that are consolidated to produce a set of self-consistent multigroup parameters. The thermal cross-sections are determined by averaging the cross-section over a 'hardened' or shifted Maxwellian spectrum, the amount of hardening being a function of the macroscopic absorption-to-slowing-down ratio. The disadvantage factor is calculated using diffusion theory for the moderator and a transport condition at the surface of the rod, the accuracy of the calculation being comparable to a P-3 calculation. The epithermal capture cross-section of ^{238}U is based on the measurement of Hellstrand including a 1·1 barn $1/v$ absorption, and ignores epithermal self-shielding effects even for very close-packed lattices. The fast-fission factor is calculated relative to the experimental measurements for UO_2. The diffusion coefficients are found by averaging the measured cross-sections over the appropriate neutron flux in each neutron energy group. The slowing-down cross-section is defined as the diffusion coefficient divided by the neutron age, the age being determined by calculating equivalent transport and slowing-down factors relative to light-water measurements.

Utilizing the two-dimensional IBM-704 PDQ digital computer code, a comparison is made with the available experimental information using oxide fuel. These experiments, which contain rod-type fuel elements, cover a wide range of ^{235}U enrichment and water-to-uranium ratio. The reactivity and power distribution predictions are very good. The reactivity calculations check to within 2 per cent Δk for all cases, most cases being within 1 per cent Δk.

VOL
14
196

1. INTRODUCTION

THE physics information desired by the reactor designer consists mainly of the gross operating characteristics of the reactor, such as reactivity, reactivity coefficients and power distributions. In order to obtain this information for power reactors possessing hydrogenous moderators, the physics analysis is usually based on multigroup equations whose solution requires the utilization of large digital computer machines. Although the machine and its accompanying nuclear codes has removed many of the geometrical uncertainties that were formerly associated with nuclear core design, the basic accuracy of the theoretical analysis has not been greatly increased. The fact that most light-water power reactors that are scheduled for construction today require prototype critical experiments or extreme conservatism in the nuclear design is indicative of the reliability attributed to theoretical analysis. Unfortunately, further improvement in computer machines will not remedy the situation. The machine is only a tool that will do the bidding of its master. If the multigroup equations with the appropriate multigroup coefficients do not describe adequately the physical system, the answers will be wrong regardless of the size of the machine.

In recent years, there has been a large accumulation of both theoretical and experimental information associated with neutron interaction in fission reactors. Therefore, it may seem surprising that the calculation of input data has not been able to keep pace with the rapid growth of the capability of digital computers. However, a closer examination of the available physics information reveals that most of the information cannot be used directly in core analysis, but usually requires a considerable amount of interpretation. For example, most of the critical experiments usually are affected by several variables whose effects are automatically lumped together in a critical fuel loading measurement. At the other extreme, individual microscopic quantities (lattice parameters) are measured, which contribute to the understanding of physical processes, but do not yield quantities which can be used directly in a practical calculation. Therefore, although there is a wealth of information available, the amount that can be used to predict the behaviour of a core design that deviates from present designs is comparatively small.

In the development of a few-group method based on present experimental information, one must necessarily make many arbitrary assumptions. These assumptions not only include the averaging of cross-sections and the determination of lattice parameters but also involve the choice of multigroup equations;

the number of groups, the energy interval for each group, and possible simplifications—such as the neglect of specific epithermal phenomena—are often made arbitrarily. The choice of a geometric model for the core is affected by the definition of the fuel element boundaries and by the method of treating the structural regions and water channels. In order to support a valid and systematical procedure, a comparison should be made with several critical experiments. The results of this comparison could determine directly some parameters; or they could be fed back into the analysis to change the averaging process, the definition of equations, or the definition of geometric model. In this manner, one arrives at a complete analytical 'package' in which all components are interrelated. To be worthwhile, this 'package' should then be capable of calculating any similar configuration under any prescribed conditions to a known degree of accuracy without introducing any further changes in the 'package'.

In a previous paper, a 'package' method is described for determining three-group constants for homogeneous, hydrogenous, fully enriched reactors (DEUTSCH, 1957). The method, although comparatively simple, has been quite successful in predicting the nuclear characteristics of this reactor type. This paper extends the method, with some modifications, to determine three-group constants for low ^{235}U enrichment, light-water, UO_2 cores. The method of analysis is composed of a series of sub-routines that are consolidated to produce a self-consistent set of multigroup parameters. These methods can be applied in a straightforward fashion to the usual complex engineering core designs and are in good agreement with present experimental information.

2. DESCRIPTION OF METHOD

A. *Three-group equations*

The three-group method that is used to calculate reactivity and power distributions assumes that only thermal fissions occur in ^{235}U and that fast fissions and epithermal absorptions occur only in ^{238}U. The three-group equations are the following:

$$\begin{aligned} -D_1\nabla^2\phi_1 + \Sigma_{s1_1}\phi_1 &= \epsilon\nu\Sigma_{f_3}\phi_3 \\ -D_2\nabla^2\phi_2 + (\Sigma_{a_2} + \Sigma_{s1_2})\phi_2 &= \Sigma_{s1_1}\phi_1 \\ -D_3\nabla^2\phi_3 + \Sigma_{a_3}\phi_3 &= \Sigma_{s1_2}\phi_2 \end{aligned} \qquad (1)$$

where D is the diffusion coefficient, Σ_{s1} is the slowing-down or removal cross-section, Σ_a is the absorption cross-section, Σ_f is the fission cross-section, ϵ is the fast-fission factor, ν is the number of neutrons released per fission and the subscripts are designations of the neutron energy groups.

The three neutron energy groups can be defined as the fast, epithermal and thermal groups. The energy interval for the first group is from 10 MeV to 180 keV; for the epithermal group, the energy interval is from 180 keV to a thermal cut-off; for the thermal group, the energy interval is from the thermal cut-off to zero energy.

The number of groups and their energy intervals have been chosen arbitrarily. It appears that it is necessary to have at least two groups other than the thermal group to describe adequately neutron losses in hydrogenous reactors. One of these, the high-energy group, describes fast-neutron leakage; the other, the epithermal group, describes resonance capture in ^{238}U and control rods. For very large reactors the fast leakage becomes small and there appears the possibility that two groups might be adequate. However, it still may be necessary to perform small reactor analysis upon sections of the core that are used in critical experiments. Thus, it is preferred to use three groups and to have a method that is independent of reactor size.

The energy interval for the first group, 10 MeV to 180 keV, is wide enough to permit the assumption that all prompt neutrons are born within this group. The second group extends from 180 keV to a thermal cut-off energy. This cut-off energy is lower than the cadmium cut-off energy for all systems that are considered. This definition, which is an analytical convenience, makes it difficult to compare directly thermal flux measurements with analysis. However, the important quantity is power distribution and, here, a direct comparison is possible.

The assumption that there are no epithermal fissions and captures in ^{235}U requires some explanation. Although experiments have been performed using almost pure ^{235}U samples, no experiments have been reported that measure the epithermal absorption of ^{235}U in the presence of 25 to 75 times greater concentrations of ^{238}U. It is difficult to evolve an analytical expression for epithermal capture and fission in ^{235}U in the presence of ^{238}U. It was originally intended to use some critical measurements to determine this parameter. However, it has turned out that the agreement with critical experiments in both reactivity and power distribution is achieved without inclusion of epithermal fission. These results seem to indicate that the epithermal neutron capture of ^{235}U in low-enrichment lattices is relatively small and, for this particular method, is compensated by the methods used in calculating the other parameters.

B. *Thermal cross-sections*

1. *Neutron temperature.* In order to determine the thermal cross-sections, the microscopic cross-sections must be averaged over the proper thermal neutron spectrum. The procedure that has been adopted is to assume a 'hardened' or shifted Maxwellian spectrum whose most probable energy, T_n, is determined by the following expression:

$$T_n = T\left(1 + 0{\cdot}75\,\frac{\Sigma_a}{\xi\Sigma_s}\right)^2 \tag{2}$$

where T is the physical temperature in electron volts and $\frac{\Sigma_a}{\xi\Sigma_s}$ is the ratio of the absorption cross-section at temperature T to the slowing-down cross-section just above thermal energies. The shifted Maxwellian spectrum has a thermal cut-off at $4T_n$. Equation (2) with the 0·75 factor multiplying $\frac{\Sigma_a}{\xi\Sigma_s}$ has been determined by a comparison with analysis using the Wigner-Wilkins thermal neutron spectrum (ZWEIFEL and PETRIE, 1956) for $\frac{\Sigma_a}{\xi\Sigma_s} \leq 0{\cdot}5$. This expression will yield essentially the same average thermal cross-sections for ^{235}U and for a $1/v$ absorber as the comparable Wigner-Wilkins spectrum.

A neutron temperature, T_n, is chosen for every fuel and water channel region within the reactor. For a structural region that is adjacent to a water channel, the neutron temperature of the water channel is used.

The method of spectrum hardening has a very significant effect on the disadvantage factor calculations and, consequently, on the thermal utilization. This is particularly evident in cores utilizing stainless steel cladding and containing a relatively high ^{235}U enrichment.

2. *Microscopic absorption cross-sections.* The microscopic cross-sections for $1/v$ absorbers at a neutron velocity of 2200 m/sec are the following (HUGHES and SCHWARTZ, 1958):

	σ_{2200} (barns)
Al	0·23
H	0·332
Cr	3·10
Fe	2·53
Ni	4·8
Mn	13·2
^{235}U	2·71
Zr	0·18

The average thermal cross-sections are found by averaging over the Maxwellian spectrum determined by equation (2) in the interval from 0 to $4T_n$. For the $1/v$ absorbers, numerical factors can be simply calculated to convert from the value at 2200 m/sec.

$$\bar{\sigma}_{\frac{1}{v}} = 0{\cdot}93\left(\frac{0{\cdot}0253}{T_n}\right)^{1/2}\bar{\sigma}_{2200}. \tag{3}$$

For the non-$1/v$ absorbers, a numerical average of the cross-sections is required. For ^{235}U, the following average absorption microscopic cross-sections have been computed:

T(eV)	$\bar{\sigma}_{^{235}U}$(barns)
0·025	633
0·040	484
0·060	387
0·080	338
0·100	303

The value of ν, neutrons released per thermal fission, for ^{235}U is 2·46. The value of α, ratio of resonance-to-fission capture for thermal neutrons, is assumed to be 0·184 for ^{235}U independent of neutron energy.

3. *Microscopic thermal transport cross-sections.* The transport cross-section, σ_{tr}, of an atom is defined in the usual manner for isotropic scattering:

$$\sigma_{tr} = \sigma_s\left(1 - \frac{2}{3A}\right) \tag{4}$$

where σ_s is the scattering cross-section and A is the atomic mass. The hydrogen transport cross-section is assumed to have a $1/v$ dependence and is averaged in a similar manner to the $1/v$ absorber. For all other elements, the transport cross-section is assumed to be independent of temperature and spectrum.

	$\sigma_s\left(1 - \frac{2}{3A}\right)$(barns)
Al	1·4
H	$36{\cdot}8\left(\frac{1}{v}\right)$
Cr	3·0
Fe	11·0
Ni	17·5
Mn	2·3
O	4·0
^{238}U	8·3
Zr	8·0

4. *Macroscopic cross-sections.* The macroscopic thermal cross-section for a fuel region within the core is:

$$\Sigma_{a_3} = \frac{v_F\Sigma_F + \frac{\phi_M}{\phi_F}v_M\Sigma_M + \frac{\phi_{Cl}}{\phi_F}v_{Cl}\Sigma_{Cl} + \frac{\phi_{St}}{\phi_F}v_{St}\Sigma_{St}}{(1 - v_M - v_{Cl} - v_{St}) + \frac{\phi_M}{\phi_F}v_M + \frac{\phi_{Cl}}{\phi_F}v_{Cl} + \frac{\phi_{St}}{\phi_F}v_{St}} \tag{5}$$

VOL 14 196

where F, M, Cl, and St refer to the fuel, moderator, cladding, and structure, respectively; v is the volume fraction; $\frac{\phi_M}{\phi_F}$, $\frac{\phi_{Cl}}{\phi_F}$ and $\frac{\phi_{St}}{\phi_F}$ refer to the disadvantage factors for the respective regions.

Σ_{tr_3} is similarly defined. The total transport cross-section $\Sigma_{tr_{tot}}$ is the sum of Σ_{tr_3} and Σ_{a_3}. The thermal diffusion coefficient D_3 for the region is:

$$D_3 = \frac{1}{3\Sigma_{tr_{tot}}} = \frac{1}{3(\Sigma_{tr_3} + \Sigma_{a_3})}. \tag{6}$$

5. *Thermal constants for water channel regions.* The average absorption and transport cross-sections for water channel regions are calculated based on the neutron temperature determined by equation (2). In addition, a correction is made to account for the discontinuity in neutron temperature between the water channel region and the fuel region. The water in the fuel region adjacent to the water channel should be slightly less hardened or have a slightly higher absorption than the remainder of the fuel region. The following formula, which assumes the linear channel dimension to be increased by two transport mean free paths, is applied to the absorption cross-section in the water channel region to account for this increased absorption:

$$\Sigma'_{a_3} = \Sigma_{a_3}\left(\frac{1 + \frac{2\lambda}{t}}{1 + \frac{2\lambda}{t}\sqrt{\frac{T_C}{T_F}}}\right) \tag{7}$$

where λ is the transport mean free path in the water channel, t is the channel width and T_C and T_F are the neutron temperatures of the channel and fuel respectively.

C. *Disadvantage factors*

The disadvantage factor can be evaluated by a P–3 calculation in which the hardened cross-section prescription that has been previously described is used to calculate the input data. However, for rod-shaped elements, an analytical expression was developed which agrees almost identically with the P–3 calculation. In this formulation, the disadvantage factor is calculated using diffusion theory in the moderator and a transport condition at the surface of the rod. The clad is treated as a void region to calculate $\frac{\phi_M}{\phi_F}$, the relative flux in the water to that in the fuel. The disadvantage factor of the clad is then taken as

$$1 + \frac{\phi_M}{\phi_F}/2.$$

$$\frac{\phi_M}{\phi_F} = \frac{3}{2}\frac{\Sigma R_0}{k\lambda}\left\{kd + \frac{I_0(kR_1)K_1(kR_2) + I_1(kR_2)k_0(kR_1)}{I_1(kR_2)K_1(kR_1) - I_1(kR_1)K_1(kR_2)} - \frac{2kR_1}{k^2R_2^2 - k^2R_1^2}\right\} \tag{8}$$

d is the reciprocal of the logarithmic derivative of the flux at the surface of the rod and is defined, as follows:

$$d = \Delta\left(\frac{R_0}{\lambda}\right) + \frac{4}{3}\lambda\left(\frac{1 - 2f\Sigma R_0}{2f\Sigma R_0}\right) \tag{9}$$

R_0 = radius of fuel pellet;
R_1 = outer radius of fuel element cladding;
R_2 = outer radius of unit cylindricalized cell;
λ = neutron transport mean free path in the moderator;
k = inverse neutron thermal diffusion length;
Σ = microscopic absorption cross-section of fuel;
f = self-shielding factor for a cylinder and is shown in Fig. 1 and described in STORM *et al.*, 1952;

$\Delta\left(\frac{R_0}{\lambda}\right)$ = geometrical function and is shown in Fig. 2 and described in DAVISON, 1951.

D. *Epithermal capture in* ^{238}U

The macroscopic epithermal capture cross-section for ^{238}U within a region at room temperature is, as follows:

$$\Sigma_{a_1} = \frac{v_F N_F \sigma_0}{\Delta u} \tag{10}$$

where v_F is the volume fraction of the fuel, N_F is the number of fuel atoms/cm^3, σ_0 is the resonance integral, and Δu is the lethargy of the epithermal group.

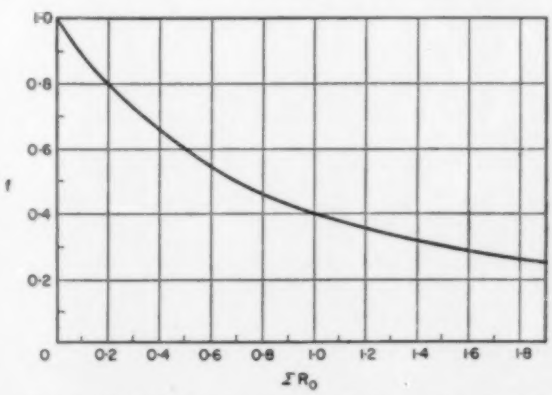

FIG. 1.—Self-shielding factor for a cylinder as a function of the product of macroscopic cross-section and radius (DAITCH *et al.*, 1959).

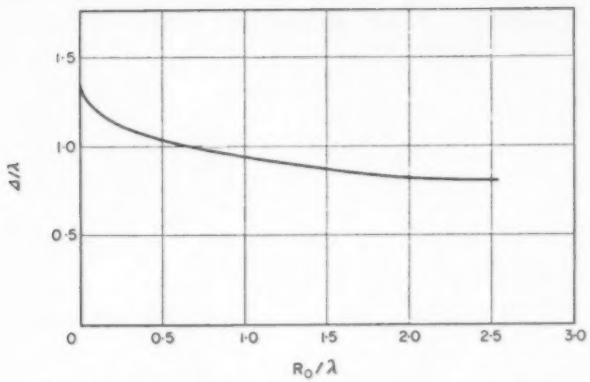

FIG. 2.—Δ (R_0/λ) for a cylinder (DANNELS and EICH, 1959).

The resonance integral that is used in equation (10) is:

$$\sigma_0 = 5{\cdot}25 + 26{\cdot}6\sqrt{\frac{S}{M}} \qquad (11)$$

where S/M is the surface-to-mass ratio of the fuel. This value is based on the single rod measurements of HELLSTRAND (1957), and includes 1·1 barn $1/v$ absorption. This cross-section is applied without any correction for epithermal self-shielding, such as the Dancoff correction. It is not clear why this simple definition should apply for very tight lattices. However, another aspect of equation (11) is: it is the resonance integral that is consistent with the entire calculation procedure and that happens to coincide with HELLSTRAND's measurements.

The resonance escape probability, p, which is not explicitly used in the analysis, can be defined:

$$p = \frac{\Sigma_{sl_2}}{\Sigma_{sl_2} + \Sigma_{a_2}} . \qquad (12)$$

This is the quantity that will be compared to the experimental measurement.

E. *Fast fission in* ^{238}U

The fast fission factor, ϵ, is calculated relative to the experimental measurements for UO_2 (KLEIN *et al.*, 1957). It is assumed that ϵ, which is a measure of the number of fast fissions occurring in ^{238}U relative to the number occurring in ^{235}U, can be calculated as though the entire fuel region were homogeneous. The calculated fast-fission factor, ϵ', for a light-water lattice relative to an experimental measurement, ϵ_1', is:

$$\epsilon - 1 = (\epsilon' - 1)\frac{N_0}{N_0'} \times \frac{(v'_{H_2O}\Sigma'_{H_2O} + v'_{^{238}U}\Sigma'_{^{238}U} + v'_{St}\Sigma'_{St})}{(v_{H_2O}\Sigma_{HO_2} + v_{^{238}U}\Sigma_{^{238}U} + v_{St}\Sigma_{St})} \qquad (13)$$

v is the volume fraction of each material; N_0 is the number of ^{238}U atoms per cubic centimetre; Σ is the total slowing-down cross-section; the subscript, St, refers to the structural and cladding material; the prime refers to the experimental measurement.

In using the homogeneous approximation to calculate ϵ, it is necessary to include all regions within the fuel zone to compute the composition. If the fuel element and water channels are treated as separate regions within the fuel zone, the composition used for the determination of ϵ must include both the fuel element and water channel as though they were a homogeneous mixture.

The microscopic cross-sections used in equation (13) are the following:

	σ(barns)
Al	0·38
H_2O	5·20
Stainless steel (18% Cr; 8% Ni)	1·04
UO_2	3·70
Zr	1·16

F. *Diffusion coefficients*

The diffusion coefficients for the first and second groups are defined in a manner similar to that used for the thermal diffusion coefficients—with the exception that the absorption, which is relatively small, is neglected. The microscopic transport cross-sections are found by averaging the measured values over appropriate neutron fluxes. The first group flux is assumed to be the flux determined by the infinite Boltzmann equation for a fission source in pure water. The second group is assumed to have a $1/E$ energy dependence. The resulting microscopic transport cross-sections are the following for each group:

	σ_{tr_1}(barns)	σ_{tr_2}(barns)
Al	3·08	1·78
H_2O	6·03	16·44
Stainless steel (18% Cr; 8% Ni)	3·09	9·02
UO_2	14·18	21·28
Zr	6·27	7·08

The total macroscopic transport cross-section, Σ_{tr}, is the sum of the volume-weighted individual macroscopic cross-sections and

$$D = \frac{1}{3\Sigma_{tr}} .$$

G. *Slowing-down cross-sections and the neutron age*

The slowing-down or removal cross-section, Σ_{sl}, for each group, is defined as the ratio of the diffusion coefficient to the neutron age for a non-absorbing medium.

VOL
14
196

The neutron age is determined for the fast and epithermal groups by calculating the equivalent transport and slowing-down factors of the materials relative to those of pure water, neglecting absorption occurring within the group. The displacement of water by other materials perturbs the experimentally measured water age. The experimental age in pure water has been selected as 30·5 cm² to indium resonance (1·46 eV) (HILL *et al.*, 1955 and GOLDSTEIN *et al.*, 1958). Although there is a published measurement of a smaller age value (LOMBARD and BLANCHARD, 1960), for this particular method of analysis, the 30·5 cm² value is best able to predict both the results of migration area measurements and the reactivity of small oxide fueled cores in which the neutron leakage is quite high. The age is divided such that 25 cm² of the total is associated with the first group and the remainder with the second group. In addition, the age in the second group must be extended to the thermal cut-off. For the first group:

$$\tau_1 = \frac{25\left(1 + \sum_{i=1}^{N} v_i\right)^2}{\left(\mathscr{D}_{H_2O} + \sum_i^N v_i X_i\right)\left(\mathscr{D}_{H_2O} + \sum_i^N v_i Y_i\right)} \quad (14)$$

where v_i is the volume ratio of ith material to water, X_i and Y_i are the transport and slowing down equivalence of the ith material to water; and $\mathscr{D}$ is the density of water.

For the second group:

$$\tau_2 = \frac{5{\cdot}5\dfrac{\Delta u}{11{\cdot}75}\left(1 + \sum_i v_i\right)^2}{\left(\mathscr{D}_{H_2O} + \sum_i^N v_i X_i\right)\left(\mathscr{D}_{H_2O} + \sum_i^N v_i Y_i\right)} \quad (15)$$

where v, X and Y are defined the same as for the first group, and Δu is the lethargy interval of the epithermal group. The equivalence factors are the following for each group:

	X_1	X_2	Y_1	Y_2
Al	0·922	0·195	0·103	0·006
Stainless steel [$\rho = 7{\cdot}85$ g/cm³; 18% Cr; 8% Ni]	1·30	1·39	0·189	0·021
UO_2 (10·25 g/cm³)	1·61	0·885	0·445	0·019
Zr	1·33	0·547	0·107	0·005

This total age, τ, for any region, corrected for the absorption in the epithermal group is:

$$\tau = \tau_1 + \frac{\Sigma_{s_{l_2}}}{\Sigma_{s_{l_2}} + \Sigma_{a_2}} \tau_2 \quad (16)$$

the migration area, M^2, is the sum of the total age and the square of the thermal diffusion length.

H. *Reflector savings and hand calculations*

The reflector savings of the water reflector is a function of the leakage of neutrons from the core. An expression for the reflector savings, δ, which appears to be consistent with both machine calculations and experimental measurement is:

$$\delta(\text{cm}) = 7{\cdot}2 + 0{\cdot}10(M^2 - 40{\cdot}0) \quad (17)$$

where M^2 is the migration area.

This expression may be used to calculate the geometric bucklings that enter into multigroup problems.

For uniform lattices whose outer boundaries approach simple geometric shapes, one can use the reflector savings to calculate an overall geometric buckling, B^2. This buckling can then be inserted into equation (1) to yield a simple reactivity expression that will approximate the comparable machine calculation. Setting $\nabla^2\phi = -B^2\phi$ in equation (1) yields:

$$k = \frac{\dfrac{\epsilon v \Sigma_{f_2}}{\Sigma_{a_2}}}{(1 + B^2\tau_1)\left(1 + B^2\tau_2 + \dfrac{\Sigma_{a_1}}{\Sigma_{s_{l_2}}}\right)(1 + B^2L^2)} \quad (18)$$

For a cylindrical geometry:

$$B^2 = \left(\frac{2{\cdot}405}{R + \delta}\right)^2 + \left(\frac{\pi}{H + 2\delta}\right)^2 \quad (19)$$

where δ is determined by equation (17).

I. *Control rod calculations*

For core analysis in which it is desirable to treat highly absorbing materials (such as control rods) as discrete regions, it is necessary to use a transport condition at the surface of the region. This transport condition is a function of the transmission probability (WACHSPRESS, 1958 and DEUTSCH, 1958). The assumption is made that it is only necessary to consider the absorption in the thermal and epithermal groups. Since the rods are normally thermally black, the thermal transmission probability is very close to zero. On the other hand, the epithermal transmission probability will tend to be closer to unity since the rods are normally epithermally grey. The epithermal transmission probability cannot be calculated directly with any degree of certainty because of the uncertainties in both the epithermal flux and cross-sections. It is best to determine this value directly from experiment. Presently, critical experiments are being planned in which the epithermal transmission probability consistent with the entire calculational procedure will be

measured for cadmium and borated stainless steel rods.*

For applications to core analysis in which it is desirable to homogenize the control rod region with the fuel region, the area absorption method can be used (DEUTSCH, 1958 and PEARLSTEIN, 1958). The area absorption method utilizes the thermal and epithermal transmission probabilities to reduce the source strength for epithermal and thermal neutron groups. In this manner, the rod absorption can be considered without treating the rods as discrete regions.

J. *Adjoint calculations*

For perturbation and reactivity coefficient calculations, it is necessary to calculate the adjoint fluxes. Because no epithermal fission capture is assumed in the formulation, it is possible to transform the real flux equations into the adjoint equations by simply inserting artificial cross-sections which are a linear combination of the real flux input data. In this manner one computer code can perform both real and adjoint calculations.

If the following substitutions are made in equation (1) which formally contain a first-group absorption term, Σ_{a_1}, although it is zero for all real flux calculations, the adjoint equations shown below are produced.

$$\phi_1 = \Psi_3,\ D_1 = D_3,\ \epsilon\nu\Sigma_{f_3} = \epsilon\nu\Sigma_{f_2},\ \Sigma_{a_1} = \Sigma_{a_3} - \Sigma_{sl_2}$$

$$\phi_2 = \Psi_2,\ D_2 = D_2,\ \Sigma_{sl_1} = \Sigma_{sl_2},\ \Sigma_{a_2} = \Sigma_{a_2} + \Sigma_{sl_2} - \Sigma_{sl_1}$$

$$\phi_3 = \Psi_1,\ D_3 = D_1,\ \Sigma_{sl_2} = \Sigma_{sl_1},\ \Sigma_{a_3} = \Sigma_{sl_1}$$

$$-D_1\nabla^2\Psi_1 + \Sigma_{sl_1}\Psi_1 = \Sigma_{sl_1}\Psi_2$$

$$-D_2\nabla^2\Psi_2 + (\Sigma_{a_2} + \Sigma_{sl_2})\Psi_2 = \Sigma_{sl_2}\Psi_3$$

$$-D_3\nabla^2\Psi_3 + \Sigma_{a_3}\Psi_3 = \epsilon\nu\Sigma_{f_3}\Psi_1. \qquad (20)$$

3. ANALYSIS OF CRITICAL EXPERIMENTS

The sole justification of the method is the ability to predict reactivity and power distributions. Both of these quantities are readily measurable and furnish a direct comparison with theory. At the same time, it is desirable that the individual sub-routines that calculate reactor parameters agree with the measured values in order for the method to be valid for temperature and isotopic changes. However, a comparison between theory and experiment in regard to lattice parameters is much more difficult to interpret, since the lattice parameters may not be calculated under the conditions for which they are measured. Further, the measurements themselves may require a large amount of analysis to reduce them to simple parameters. In making the present comparison between theory and experiment, only a surface inspection has been made of the experimental quantities in order to ascertain how they are related to the corresponding analytical quantities. For example, the disadvantage factor is defined as the ratio of the thermal flux in the moderator to that in the fuel. However, the definition of the experimental thermal flux is not quite the same as that used in the theoretical analysis. Also, these definitions may vary from experiment to experiment. The theory values listed in the analysis of the critical experiments are calculated analytic values; when comparison is made with experiment, the most closely related experimental quantities are quoted.

Three critical experiments have been analysed. These experiments represent the presently available experimental information for cores consisting of low enrichment oxide fuel, moderated with light water. These experiments are: the Westinghouse TRX Critical Experiments (KLEIN *et al.*, 1957; KOUTZ *et al.*, 1958), the Westinghouse Yankee Critical Experiments (DAVISON *et al.*, 1959), and the Babcock and Wilcox N.S. Savannah Critical Experiments (BALL *et al.*, 1958). All of these experiments used rod-type fuel elements, and covered a wide range of water-to-fuel ratios. The TRX experiment included a 1·3 per cent ^{235}U enrichment, and utilized aluminium clad rods. The Yankee experiment included a 2·7 per cent ^{235}U enrichment, and utilized stainless steel clad rods. The N.S. Savannah experiment included a 4 per cent ^{235}U enrichment, and utilized both stainless steel clad rods and an aluminium and stainless steel box structure.

The analysis consists of calculating the individual parameters by the previously described methods, these calculations effectively homogenizing each of the fuel regions in the core. These parameters are then inserted in equation (1). For complex geometries, the equations are solved numerically by the IBM-704 PDQ Two-Dimensional Code (BILODEAU *et al.*, 1957).

It should be recognized that the computational codes and their applications introduce other uncertainties into the analysis. Two different codes seemingly solving the same equations with precisely the same input data may give slightly different answers because of the differences in mathematical methods used to solve the equations. Also, the same code analysing the same problem can give slightly different answers, depending on the choice of mesh spacing used to

* These measurements are part of the Nuclear Superheat Experimental Programme being performed by Combustion Engineering, Inc., Windsor, Connecticut.

VOL 14 196

describe the problem and depending upon the convergence criterion. For all experiments that have been analysed in this report, fairly coarse mesh spacings have been used in order to minimize the cost of each problem. The standard that has been adopted is to use one mesh space in any direction for each fuel rod and two mesh spaces for a pure water channel. The convergence criterion that is used for the PDQ code to terminate the iteration cycle is: epsilon = 0·05. In determining the detailed power distribution, rod by rod, the resulting power distribution is averaged over each mesh space.

A. *TRX critical experiments* (KLEIN *et al.*, 1957; KOUTZ *et al.*, 1958)

Measurements of lattice parameters and critical configurations have been made for both slightly enriched uranium metal and uranium oxide fueled lattices. Three measurements were made using high-density (10·53 g/cm³) UO_2 rods enriched with 1·311 wt per cent ^{235}U. Each rod was made up of 0·383 in. diameter pellets. These pellets were inserted into aluminium tubes of 0·028 in. wall thickness to form rods 48 inches in length. There is a 0·005 in. radial gap between the fuel and the aluminium. Three different lattice spacings were measured with a water-to-uranium-metal ratio of 2·9, 3·6 and 4·9. The comparisons between the measurements and calculations are as follows (see Table 1 below).

Based on the measured critical bucklings, the calculated reactivity using equation (18) is:

	Reactivity	
W/U	Theory	Experiment
2·9	0·9961	1·0000
3·6	0·9982	1·0000
4·9	0·9999	1·0000

B. *Yankee critical experiments** (DAVISON *et al.*, 1959)

Measurement of lattice parameters, critical configurations, and power distributions were made for uranium oxide lattices with a ^{235}U enrichment of 2·70 wt per cent and a density of 10·2 g/cm³. Each fuel rod was made up of 0·3 in. diameter pellets clad with stainless steel tubing of 0·0161 in. wall thickness. There was a 0·0031 in. radial gap between the pellets and the tubing. The length of the fuel rod was 48·0 inches. Three different configurations were measured. The water-to-uranium ratios for these measurements were 2·2, 2·9 and 3·9. The lattice parameter measurements have not been reported as yet. The following table lists the calculated parameters:

W/U	p	ϵ	$\frac{\phi_M}{\phi_T}$	M^2
2·2	0·7204	1·0576	1·1182	41·93
2·9	0·7748	1·0473	1·1311	40·05
3·9	0·8186	1·0387	1·1447	38·67

The disadvantage factor of 1·127 ± 0·01 has been reported for the 3·9 *W/U* experiment.

The radial and axial reflector savings have been measured, utilizing activation techniques. The following is a comparison of the theory with the experimental results for the activity induced in individual fuel rods:

W/U	Radial Savings	Axial Savings
2·2 (Theory)	7·39	14·78
(Experiment, Fuel Rods)	8·19 ± 0·18	13·84 ± 0·66
2·9 (Theory)	7·24	14·48
(Experiment, Fuel Rods)	7·04 ± 0·37	13·58 ± 0·83
3·9 (Theory)	7·07	14·14
(Experiment, Fuel Rods)	7·32 ± 0·10	13·72 ± 0·84

The critical configurations and power distributions have been calculated for the three lattices with control rod followers in the core. For this calculation, the PDQ two-dimensional code was used. The following reactivities were calculated:

W/U	Theory	Experiment
2·2	0·9835	1·0007
2·9	0·9904	1·0006
3·9	0·9925	1·0002

The calculated power distributions along a 45-degree traverse for these calculations are shown in Figs. 3, 4 and 5.

* The author is indebted to P. W. DAVISON for having data made available that are more detailed than data presented in related reports.

TABLE 1

W/U	p	ϵ	$\frac{\phi_M}{\phi_T}$	M^2	δ_{radial}	δ_{axial}
2·9 Theory	0·7865	1·0500	1·1086	45·07	7·72	15·44
Experiment	0·775 ± 0·004	1·046 ± 0·002	1·10 ± 0·01	45·8	7·86 ± 0·12	15·27 ± 0·41
3·6 Theory	0·8216	1·0422	1·1172	43·25	7·54	15·08
Experiment	0·815 ± 0·004	1·042 ± 0·002	1·13 ± 0·01	44·3	7·41 ± 0·13	14·69 ± 0·43
4·9 Theory	0·8609	1·0333	1·1301	41·32	7·33	14·66
Experiment	0·850 ± 0·004	1·034 ± 0·002	1·13 ± 0·01	40·6	7·10 ± 0·10	14·52 ± 17

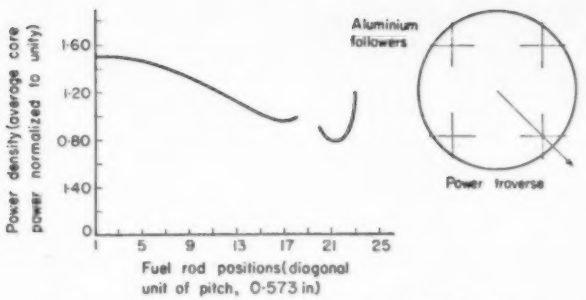

FIG. 3.—Radial power distribution for 2·2/1 *W/U* Yankee experiment, with 3,017 fuel rods and four control-rod followers in core.

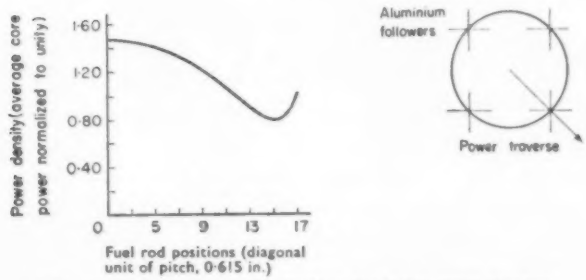

FIG. 4.—Radial power distribution for 2·9/1 *W/U* Yankee experiment, with 1,833 fuel rods and four control-rod followers in core.

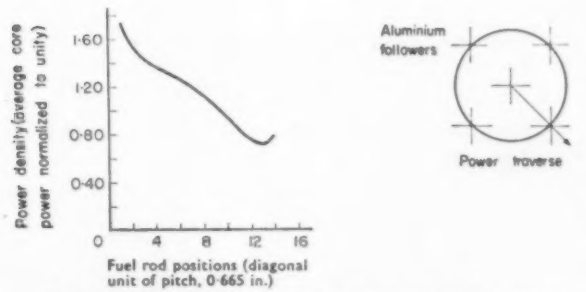

FIG. 5.—Radial power distribution for 3·9/1 *W/U* Yankee experiment, with 1,332 fuel rods and five control-rod followers in core.

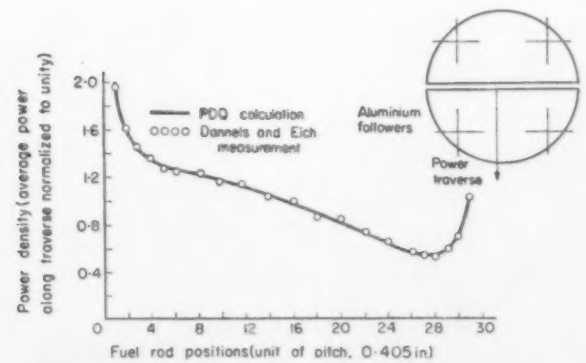

FIG. 6.—Comparison of calculated and experimental radial power density of 0·405 in. water channel bisecting core of 2·2/1 *W/U* Yankee experiment, with 2,874 fuel rods and four control-rod followers in core.

An additional experiment has been performed with the 2·2 *W/U* lattice to investigate water channel peaking (DANNELS and EICH, 1959). For this experiment, the central row of elements was removed from the core and power traverses were made perpendicular to the water channel. Figure 6 describes the core configuration, and shows the comparison of the experimental measurement with the theoretical results. The channel peaking factor—defined as the ratio of the power in the rod adjacent to the channel with the channel present, to the power in the rod without the channel present—is calculated to be 1·50, as compared to a measured value of 1·47.

Another set of measurements of the lattice parameters using 4·4 wt per cent enriched fuel—in a lattice otherwise similar to the 3·9 *W/U* lattice—has been reported (GROB *et al.*, 1959). For this lattice, the comparison between theory and measurement is:

	p	ϵ	$\frac{\phi_M}{\overline{F\phi}}$
Theory	0·8160	1·0392	1·2001
Experiment	0·805 ± 0·015	1·039 ± 0·003	1·25 ± 0·02

C. *N.S. Savannah critical experiments** (BALL *et al.*, 1958)

Measurements of critical configurations and power distributions have been performed with 4·02 wt per cent ^{235}U enriched fuel. The swaged stainless steel clad fuel rods had an o.d. of 0·500 in. including a stainless steel jacket of 0·0283 in. wall thickness. The active length of fuel rod was 66·5 in. The density of the UO_2 was 9·45 g/cm^3. Two lattice spacings have been investigated, one having a *W/U* ratio of 2·7, the other a *W/U* ratio of 3·6.

The disadvantage factors for moderator and cladding have been measured for these lattices. In addition to the hand calculation method, equation (8), a P–3 calculation using the CEPTR code (DAITCH *et al.*, 1959) with cross-sections hardened by equation (2) has been carried out for the 3·6 *W/U* lattice.

W/U	$\frac{\phi_M}{\phi_F}$	$\frac{\phi_{cl}}{\phi_F}$
2·7 Theory	1·2170	1·1085
Experiment	1·29 ± 0·06	1·19 ± 0·06
3·6 Theory	1·2578	1·1299
Theory (P–3)	1·2656	1·1125
Experiment	1·40 ± 0·03	1·09 ± 0·03

For the 2·7 *W/U* lattice, two different critical measurements were performed. One core, designated

* The author is indebted to R. M. BALL and A. M. MACKINNEY for having data made available that are more detailed than data presented in related reports.

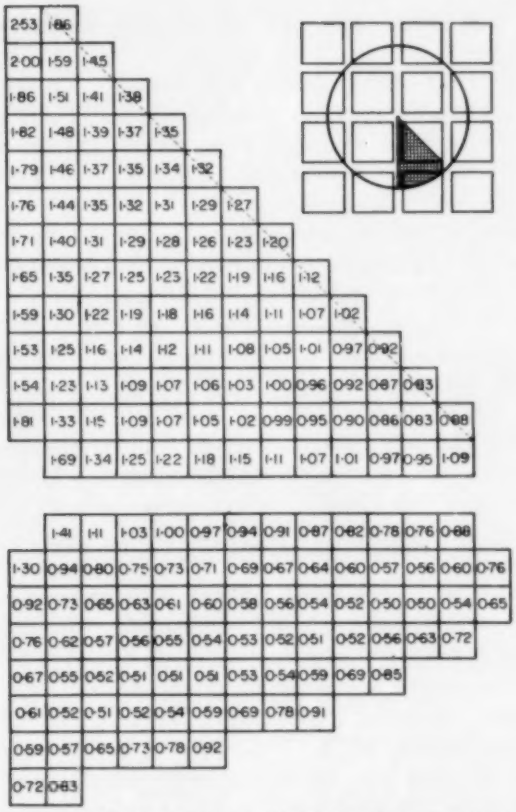

FIG. 7.—Two-dimensional rod-by-rod radial power distribution for 2·7/1 *W/U* N.S. Savannah experiment, having average core power normalized to unity; with 1,416 fuel rods, 0·83 in. water channels, and 0·156 in. stainless steel box walls in core.

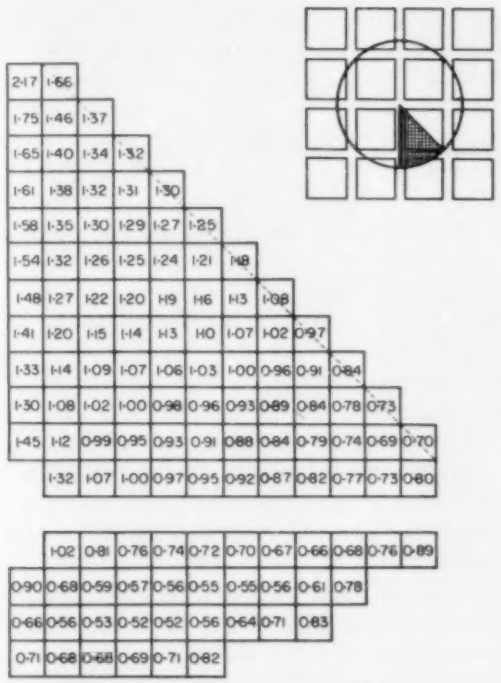

FIG. 8.—Two-dimensional rod-by-rod radial power distribution for 3·6/1 *W/U* N.S. Savannah experiment, having average core power normalized to unity; with 948 fuel rods, 0·83 in. water channels, and 0·156 in. stainless steel box walls in core.

Core II, contained 0·83 in. water channels and 0·156 in. stainless steel walls. The other core, designated Core III, had 0·83 in. water channels and 0·130 in. aluminium walls. There are 192 fuel rod positions within a box, 14 × 14 lattice, with the four corner rods missing. The comparison of the calculated reactivity with experiment is the following:

	Reactivity	
	Theory	Experiment
Core II	1·0010	1·0006
Core III	0·9985	1·0017

The calculated rod-by-rod power distribution in Core II is given in Fig. 7. The water channel peaking factor—equal to the ratio: power in the corner rod with the channels, to power in the rod without channels—is 1·81. There is no published measured power distribution for this core. However, for the same lattice in a larger core, a channel peaking factor of 1·77 can be inferred from the measurements (*Nuclear Merchant Ship Reactor Project, Quarterly Technical Report*).

For the 3·6 *W/U* lattice, three different critical measurements were performed. One core, designated Core IV, contained 0·83 in. water channels and 0·130 in. aluminium walls. The second core, designated Core V, contained no fuel assembly walls or water channels. The third core, designated Core VI, contained 0·83 in. water channels and 0·156 in. stainless steel walls. There were 165 fuel rod positions within a box, 13 × 13 lattice, with the four corner rods missing.

The comparison of the calculated reactivity with experiment is:

	Reactivity	
	Theory	Experiment
Core IV	0·9981	1·0011
Core V	0·9950	1·0012
Core VI	0·9979	1·0013

The calculated rod-by-rod power distribution in Core VI is given in Fig. 8. The water channel peaking factor is 1·59. There is no published measured power distribution for this core; however, for the same lattice in a larger core, a channel peaking factor of 1·57 can be inferred from the measurements (*Nuclear Merchant Ship Reactor Project, Quarterly Technical Report*).

4. DISCUSSION OF RESULTS

Although experimental critical configurations can

be determined to a very high degree of accuracy, there always exists an uncertainty as to the detailed composition of the core. The mechanical tolerances on fuel pellets, fuel cladding and structural material as well as uncertainties in the purity of materials introduce uncertainties of the order of 0·5 per cent Δk in any composition. Therefore, one should not expect an analytical method to duplicate criticality measurements to better than about 0·5 per cent Δk. The 'package' method described here gives a good correlation for the existing experimental information; all cases check to within 2 per cent Δk, most cases to within 1 per cent Δk.

What is usually desired in core analysis is the prediction both of the lower limit of reactivity in the hot operating condition with no control elements present and of the upper limit of the reactivity in the cold clean condition with all control elements present. These two conditions determine the reactivity lifetime and the shutdown safety margin. The comparison of the calculational method with cold clean experiments without control rods does not directly evaluate the accuracy of the method for either of these conditions. However, the initial cold clean condition with control rods present does not appear to furnish too much difficulty. It is practical to determine directly the epithermal transmission probability for the rod directly from critical experiments (see Section 2, I—*Control rod calculations*). In this manner, the cold control rod calculations should be of the same order of accuracy as the cold, no-control-rod calculation. On the other hand, the accuracy of the reactivity calculation for the initial hot operating condition cannot be extrapolated from the cold calculations. Nevertheless, since both the cold experiments and the analysis have been carried out over a wide range of enrichment, water-to-uranium-fuel ratio, and geometry, it is expected that the same degree of accuracy will be maintained. Furthermore, it should be noted that in almost all comparisons with experiment the analysis underestimates the reactivity, the system being more reactive than calculated. Therefore, this systematic deviation acts as a small safety factor in predicting the minimum reactivity in the hot condition.

The agreement of the power distributions with experiment indicates that this method is capable of calculating the rod-by-rod power distributions, although more detailed comparisons with experiments are required to estimate the accuracy. It should be noted that the initial assumption neglecting epithermal fissions has a tendency to overestimate the local peaking factors, since the epithermal diffusion length is much longer than that which occurs at thermal energies.

For burn-up calculations, it is necessary to provide cross-sections for the plutonium isotopes—^{239}Pu, ^{240}Pu and ^{241}Pu. Each of these isotopes has its own peculiarities and each requires special attention. It would appear that the thermal and epithermal effects of plutonium can be handled by calculating equivalent thermal cross-sections for the isotopes, using the entire method as previously described. This approach is presently being employed. However, experimental confirmation is required, especially for high burn-ups, where plutonium content is a major fraction of the fuel concentration.

Finally, some remark should be made in regard to how changes are to be made in the entire calculational procedure. Obviously, it will prove necessary to devise—for grossly different reactor configurations, such as those which involve annular fuel elements—new subroutines to calculate lattice parameters. Also, future experimental information at elevated temperatures and with high plutonium concentrations may indicate that it is desirable to make changes in the overall analytical 'package.' However, changes cannot be made arbitrarily to satisfy a new condition. Any change or addition must be made in such manner as to maintain the internal consistency of the method and to agree with previous experiments.

REFERENCES

BALL R. M., MACKINNEY A. L., MORTENSON J. H., ROSS D. A. and WILLIAMS D. V. (1958) *Trans. Amer. Nucl. Soc.* **1**, No. 2, 107.

BILODEAU G. G., CADWELL W. R., DORSEY J. P., FAIREY J. G. and VARGA R. S. (1957) *PDQ—An IBM-704 Code to Solve the Two-Dimensional, Few-Group Neutron Diffusion Equations.* WAPD-TM-70.

DAITCH P. B., MCGOVERN B. J. and SCHILDER M. (1959) *CEPTR, An IBM-704 Code to Solve the P-3 Approximation to the One-Velocity Transport Equation in Cylindrical Geometry.* MPC-20.

DANNELS R. A. and EICH W. J. (1959) *Neutron Flux Peaking and Power Shapes*, YAEC-151.

DAVISON B. (1951) *Proc. Phys. Soc., Lond.* **A64**, 881.

DAVISON P. W., BERG S. S., BERGMANN W. H., HANLEN O. F., JENNINGS B. and LEAMER R. D. (1959) *Yankee Critical Experiments.* YAEC-94.

DEUTSCH R. W. (1957) *Nucleonics* **15**, No. 1, 47.

DEUTSCH R. W. (1958) *Nucl. Sci. Engng.* **4**, 322.

GOLDSTEIN H., ZWEIFEL P. F. and FOSTER D. G. (1958) *Proceedings of the Second International Conference on the Peaceful Uses of Atomic Energy, Geneva*, Vol. 16, 379. United Nations, N.Y.

GROB V., RITZ H. and SANTANDREA H. (1959) *Measurements of Parameters Leading to p, f and ϵ in Water-Moderated, 4·4 per cent Enriched UO_2 Lattice.* WCAP-1175.

HELLSTRAND E. (1957) *J. appl. Phys.* **28**, 1943.

HILL J. E., ROBERTS L. D. and FITCH J. E. (1955) *J. appl. Phys.* **26,** 1013.

HUGHES D. J. and SCHWARTZ R. B. (1958). *Neutron Cross Sections.* 2nd Edn. BNL-325,

KLEIN D., KRANZ A. Z., SMITH G. G., BAER W. and JUREN J. DE (1957) *Nucl. Sci. Engng.* **3,** 403.

KOUTZ H., SCHER R., BROWN J. R., KLEIN D., STEIN S., HELLENS R. L., ARNOLD H., BALL R. M. and DAVISON P. W. (1958) *Proceedings of the Second International Conference on the Peaceful Uses of Atomic Energy, Geneva,* Vol. 12, p. 446. United Nations, N.Y.

LOMBARD D. B. and BLANCHARD C. H. (1960) *Nucl. Sci. Engng.* **7,** 448.

Nuclear Merchant Ship Reactor Project (1958) Quarterly Technical Report, April—June 1958. BAW-1118.

PEARLSTEIN S. (1958) *Nucl. Sci. Engng.* **4,** 322.

STORM M. L., HURWITZ H. and ROE G. M. (1952) *Gamma Ray Absorption Distributions for Plane, Spherical and Cylindrical Geometries.* KAPL-783.

WACHSPRESS E. L. (1958) *Nucl. Sci. Engng.* **3,** 186.

ZWEIFEL P. F. and PETRIE C. D. (1956) *Averages for Thermal Cross Sections for Hydrogen-Moderated Assemblies.* KAPL-1469.

OL.
14
961

Reactor Science and Technology (J.N.E. Parts A/B), 1961, Vol. 14, pp. 180 to 185. Pergamon Press Ltd. Printed in Northern Ireland

THE NON-ELASTIC NEUTRON CROSS-SECTION FOR URANIUM AT 13–19 MeV AND BERYLLIUM AT 14 MeV

A. V. COHEN
Atomic Weapons Research Establishment, Aldermaston, Berks.

(*Received* 25 *July* 1960)

Abstract—The non-elastic cross-sections of uranium and beryllium have been measured for neutrons of 14·08 MeV using a sphere absorption technique. The results are:

U $2{\cdot}89 \pm 0{\cdot}05$ barns

Be $0{\cdot}50 \pm 0{\cdot}035$ barns.

The cross-section for inelastic scatter to the Be level at 2·43 MeV is $0{\cdot}20 \pm 0{\cdot}045$ barns.

The variation with energy of the non-elastic cross-section of uranium has also been investigated, using neutrons from 13·35 MeV to 18·54 MeV.

1. INTRODUCTION

THE non-elastic neutron cross-section (that is, the total cross section less the elastic cross-section) can conveniently be measured by the sphere transmission technique (e.g. GRAVES and DAVIES, 1955). The most obvious approach is to surround the neutron source with a sphere of the absorbing material, but if this is done, then the source must be isotropic and the neutron energy independent of angle of emission.

BETHE, BEYSTER and CARTER (1956 and 1957) have shown in a series of papers that these restrictions no longer apply if the sphere surrounds a small isotropic counter. This technique has been much exploited, using threshold detectors, e.g. by PHILLIPS *et al.* (1952), or biassed scintillation counters, e.g. by TAYLOR *et al.* (1955). Since a relatively narrow angular pencil of neutrons may thus be selected, one may measure the excitation function of a non-elastic neutron cross-section, as in the work of BALL *et al.* (1958).

In this paper such methods have been applied to measure the variation of the non-elastic neutron cross-section for uranium between energies of 13·35 and 18·54 MeV, and for beryllium at an energy of 14·08 MeV.

2. EXPERIMENTAL TECHNIQUES

2.1 *Neutron detectors*

The neutrons were detected in a ¾ in. diameter sphere of plastic scintillator, attached by a 9 in. length of 1 in. diameter light-pipe to a Dumont 6292 photomultiplier. Neutrons elastically scattered in the hydrogen of the plastic produce a continuum of recoil protons of energy ranging up to the maximum neutron energy, and the scintillations from these are detected in the photomultiplier, amplified and recorded on a pulse-height analyser; to keep the correction for the overall dead-time of 0·8 msec below 2 per cent, the counting rate was kept in the range 25 to 60 per second. The behaviour of such counters has been described e.g. by TAYLOR *et al.* (1956).

The expected continuum due to neutrons of a given energy is not quite flat, partly because of escaping protons, partly because of the anisotropy of (n,p) scattering at 14 MeV, and partly because the scintillation pulse-height is not linearly dependent on proton energy. This last effect is discussed generally by BIRKS (1954) and by SWARTZ and OWEN (1956) and specifically for plastic scintillators by NESZMELYI and PALLA (1958). Corrections for this effect were applied where necessary. Electrons give a larger pulse-size than do protons of the same energy, so that gamma rays of energy 7·5 MeV would give rise to a continuum whose maximum nearly coincides with that of 14 MeV neutrons.

A typical spectrum using 14 MeV neutrons obtained as described in Section 2.2 is shown in Fig. 1(a), together with neutron energy scale (Fig. 1c). We arbitrarily select as 14 MeV the point at which the unabsorbed neutron spectrum is reduced to 90 per cent of the plateau counting rate, and scale the other energy points according to the references above; thus the energy scale is only approximate. The background, which begins to be noticeable in the region of 9 MeV neutron energies, was investigated by placing a 4 ft copper shadow bar, 2 in. in diameter, between source and counter, and observing the pulse height spectrum, the effect on this background of the uranium sphere

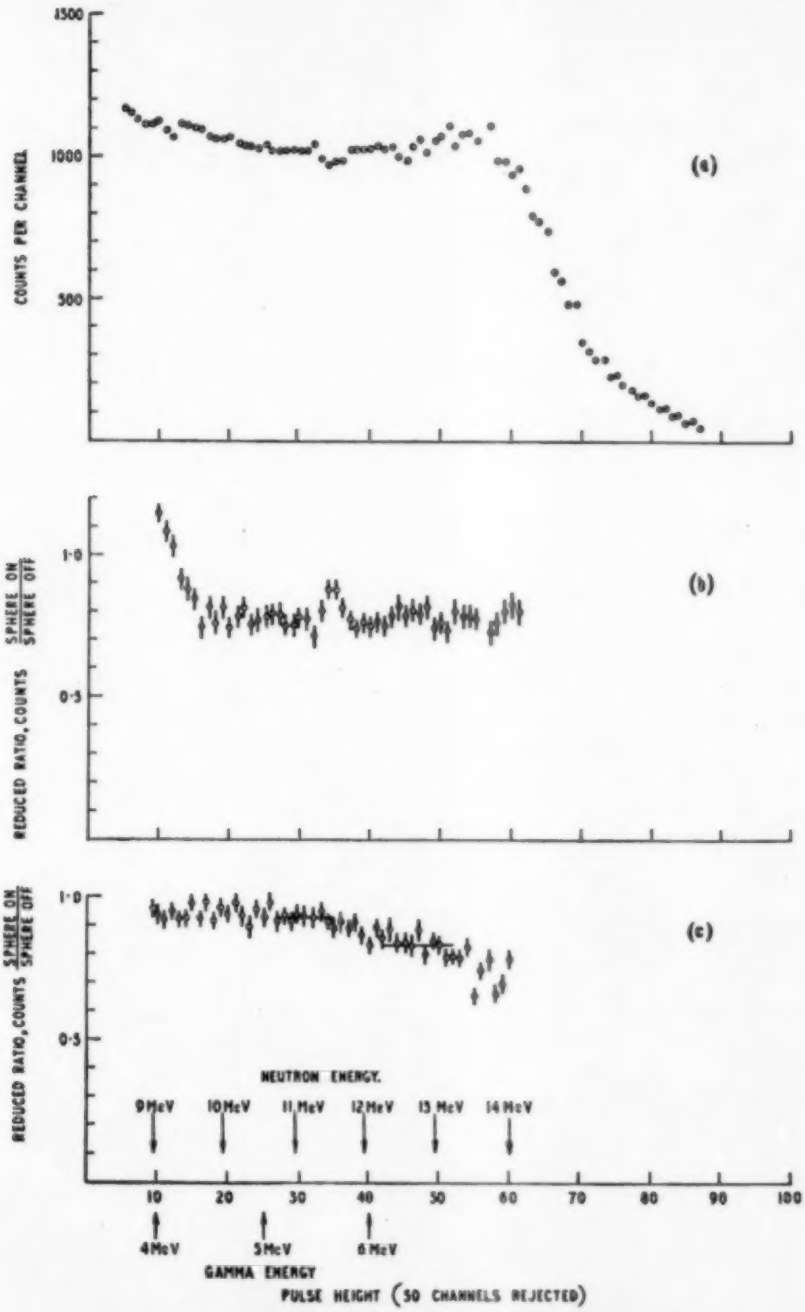

FIG. 1.—Typical data as a function of pulse-height. An approximate energy scale is noted at the bottom of the diagram. (a) Pulse-height spectrum for 14 MeV neutrons. (b) 'Reduced ratio' for uranium, that is, counts with uranium sphere on, divided by the corresponding figure without the sphere, and normalized. Note the flatness of the curve between 9·5 and 14 MeV. (c) 'Reduced ratio' for beryllium. Note the two plateaux, whose significance is discussed in the text. The lines represent the regions from which transmission data were extracted. The region in which the step occurs corresponds to the 2·43 MeV level in ^{9}Be.

was also investigated. In the neutron energy range 13–14 MeV, the background was about 1 per cent, and the absorption observed when the counter was surrounded by the uranium sphere suggested that this was mainly due to partially degraded neutrons, while below 8 MeV neutron energy the background was clearly due mainly to gamma radiation, whose maximum energy would accordingly be about 3·5–4 MeV. In the intermediate region, corresponding to 9–13 MeV neutron energy, the mean background amounted to some 8 per cent. It is assumed to be mixed (50 ± 25 per cent gamma radiation) for the purposes of the estimate made in Section 3.1.

In an auxiliary experiment, in which the angle between the line joining counter to source and the light pipe was varied from the normal 180° to as little as 45°, it was shown that the counter was isotropic in the neutron energy range 9–14 MeV, to within better than 2 per cent.

2.2 14 *MeV*

A beam of several microamperes of 500 keV deuterons from the A.W.R.E. high-tension accelerator were directed onto a copper target, coated with 200 $\mu g/cm^2$ zirconium impregnated with tritium, forming a neutron source of approximately 2×10^8 n/sec. The neutrons were observed at 90° to the incident beam (at which angle their energy is 14·08 ± 0·04 MeV) at a distance of 3·5 meters from the target; the source strength was monitored by observing the associated α-particles emitted at 135°. The whole experiment was carried out on a light weight floor, so that source and detector were at least 10 ft from any substantial source of scattering.

The pulse-height spectrum in the scintillation counter described above was observed successively, with and without a pair of uranium hemispheres surrounding the counter, and the reduced ratio (counts with sphere on divided by counts with sphere off, normalized by the alpha monitor) was calculated for each channel; a typical reduced ratio curve is shown in Fig. 1(b). In the range 9·5–14 MeV this is substantially flat; the mean height of the lower half of the plateau differed from the upper half by ±0·3 per cent averaging over all the runs performed.

Two pairs of uranium hemispheres were used. One had an internal diameter of approximately 4·6 in. and an external diameter of approximately 6·2 in. while the corresponding figures for the larger pair were 6·2 in. and 7·8 in. A 1¼ in. hole at the equator allowed the entrance of the light pipe.

An exactly similar technique was used to investigate beryllium at 14 MeV. The beryllium sphere had approximate internal and external diameters of 3·9 in. and 6·2 in. respectively, and was covered with a protective paint of negligible thickness.

2.3 13·35–18·54 *MeV*

A 5 μA beam of deuterons from the A.W.R.E. 3 MeV Electrostatic Generator, at nominal energies of 1·5 MeV and 2·2 MeV, was directed on a similar zirconium tritide target. Since at these energies, the T(d,n) neutron yield was much lower, the neutron source strength was now only some 5×10^6 n/sec, and the counter was therefore placed at selected angles at a distance of 1 m from the target. To minimize angular spread, only the smaller uranium sphere was used.

As before, the experiment was conducted on a light-weight floor. The gamma background was however, now much larger relative to the neutron yield, because of the higher beam energy and the diminished neutron yield. It was found impracticable to observe at deuteron energies greater than 2·2 MeV, or at angles greater than 120°.

The machine energy was accurately calibrated against the threshold of the $^7Li(p,n)$ reaction.

3. RESULTS

3.1 *Uranium at* 14 *MeV*

The transmission was deduced from that part of the pulse-height spectrum corresponding to the neutron energy range 13–14 MeV, to minimize the effect of background. Corrections were applied (in order of importance) for pulse-height analyser dead-time, increased counting rate per channel due to slight energy degradation following on neutron scattering in uranium, background, and finite geometrical effects. This last effect was estimated as about 0·1 per cent using the methods described by BETHE *et al.* (1956 and 1957). The effect of non-linear response in the scintillator was negligible. The transmission was 0·752 ± 0·0045 for the smaller sphere (mean of 3 runs) and 0·743 ± ·006 for the larger sphere (mean of 2 runs).

From this, the non-elastic cross-section for 14·08 MeV neutrons of uranium was calculated, applying the methods of BETHE *et al.* (1956 and 1957). These authors give several forms of correction for the increase of effective sphere thickness due to multiple neutron scatter. The correction used here is the fullest one given, which allows for the variation of scattered neutron escape probability with the number of scatters. An elastic transport cross-section of 0·51 ± 0·07 barns, as indicated by optical model calculations, was used and the correction to transmission due to this effect is 1·008 ± 0·003.

VOL 14 196

The weighted mean of all results is then 2·89 ± 0·05 barns.

Were the background negligible, the flatness of the ratio curve in the neutron energy range 9·5–14 MeV would suggest that the cross-section for inelastic scatter of neutrons into this energy range was less than 30 mbarn. This would still be true if the background were wholly due to partially degraded neutrons, since the non-elastic cross-section for neutrons in uranium is not strongly dependent on energy (see Section 3.3). However, below neutron energies of 9 MeV the background is mostly due to gamma-radiation of 4 MeV or less, and we have assumed that in the 9·5–14 MeV region, the background is some 50 per cent ± 25 per cent gamma radiation. If no neutrons were scattered into this energy region, the reduced ratio curve should therefore have sloped downwards somewhat with decreasing energy. As this is not so, it is probable that some inelastic scatter of neutrons to this energy range does indeed occur, the two effects fortuitously cancelling. Allowing for non-linearity of scintillator response, we may infer that the cross-section required for this process is 130 ± 80 mbarn, much of the estimated error arising from uncertainty as to the nature of the background and the amount of gamma-rays produced by inelastic neutron scatter in the uranium, the effect of which is apparent at lower energies.

Some confirmation of this estimated cross-section may be obtained by extrapolation of the results of ZAMIATNIN *et al.* (1959), which suggests that this cross-section is probably less than 300 mbarn, while BALL *et al.* (1958) have measured the corresponding figure for lead, as 161 ± 45 mbarn. The present estimate is thus in reasonable agreement with previous work.

This comparatively low figure arises because uranium has many accessible levels of high excitation, so that emission of relatively low energy neutrons is favoured. Rough calculations using direct interaction models (AUSTERN *et al.*, 1953; BROWN and MUIRHEAD, 1957) predict cross-sections of about 150 mbarn for inelastic scattering into the 9·5–14 MeV region.

3.2 *Beryllium at* 14 *MeV*

A typical 'ratio curve' is shown in Fig. 1(c). Elastic scattering in a light element degrades the neutrons far more than in uranium. This has two effects: the plateau is much less well-defined, and the correction to counting rate per channel due to elastic degradation is more important.

The accessible levels of ^{9}Be are few (1·8 MeV, 2·43 MeV, 3·1 MeV, 4·8 MeV, 6·8 MeV, 7·9 MeV and 11·3 MeV) and it is indeed problematic if the 1·8 MeV level exists. It might therefore be expected that inelastic scattering to the individual low-lying levels is of much greater importance than in the case of uranium, where the level density increases much more rapidly with excitation. For this reason despite the effect of moderation in rounding the edge of the plateau, it is nevertheless observed that the plateau has a step corresponding to inelastic scattering to the 2·43 MeV level in beryllium.

The transmission of the sphere may be measured from the high-energy end of the plateau as 0·818 ± ·012 (mean of three runs). From the lower energy part of the plateau one may deduce a transmission (0·893 ± ·013) which includes neutrons scattered to the 2·43 MeV level. For this estimate, the corrections due to increase in channel counts due to inelastic degradation, ($\leqslant$2 per cent) and to non-linearity of scintillator response (0·6 per cent) were found to be significant.

Using the fuller method of BETHE *et al.*, to allow for the lengthening of effective sphere thickness by multiple scattering, and an assumed elastic transport cross-section of 0·36 ± 0·17 barns, one finds that the effect on transmission is about 1·006 ± 0·004 and one obtains for the cross-sections:

non-elastic cross-section 0·497 ± 0·035 barns

cross-section for inelastic scatter to 2·43 MeV level 0·196 ± 0·045 barns.

3.3 *Uranium* 13·35–18·54 *MeV*

Because of the much larger background, the ratio-curve plateau is in this case not as well-defined as for 14 MeV neutrons. The correction due to this effect, and the associated errors due to uncertainty as to the nature of the background, predominate over other errors. Results are indicated in Table 1, where for completeness the 14 MeV point is also included, and the results are displayed in Fig. 2.

The spread in the neutron energies indicated in the Table arises from target thickness, and finite size of sphere.

4. DISCUSSION

4.1 *Uranium*

COON *et al.* (1958) quote an unpublished result of GRAVES and DAVIS as low as 2·73 ± 0·04 barns. If GRAVES and DAVIS biassed their counter in this work, as in their published work in 1955 on other elements, to reject neutrons of energy less than 9 MeV, then this discrepancy of 0·16 ± 0·06 barns may be accounted for by neutrons inelastically scattered into the 9–14 MeV energy range, which we have estimated to be of this order. This explanation is confirmed by the work of MACGREGOR *et al.* (1957) who measure non-elastic cross-sections for various elements at 14 MeV at a

TABLE 1

Neutron energy (MeV)	No. of runs	Fully corrected transmission	Assumed transport cross-section (barns)	Non-elastic cross-section (barns)
13·35 ± 0·14	5	0·722 ± 0·022	0·53	3·25 ± 0·25
14·08 ± 0·04	3	0·752 ± 0·0045	0·51	2·89 ± 0·05*
15·04 ± 0·20	3	0·726 ± 0·019	0·50	3·21 ± 0·23
15·94 ± 0·20	3	0·751 ± 0·025	0·48	2·87 ± 0·28
16·72 ± 0·15	4	0·755 ± 0·018	0·47	2·82 ± 0·22
17·45 ± 0·10	5	0·741 ± 0·025	0·46	3·02 ± 0·25
18·54 ± 0·20	6	0·788 ± 0·028	0·45	2·42 ± 0·30

* This cross-section includes the results of using the larger sphere.

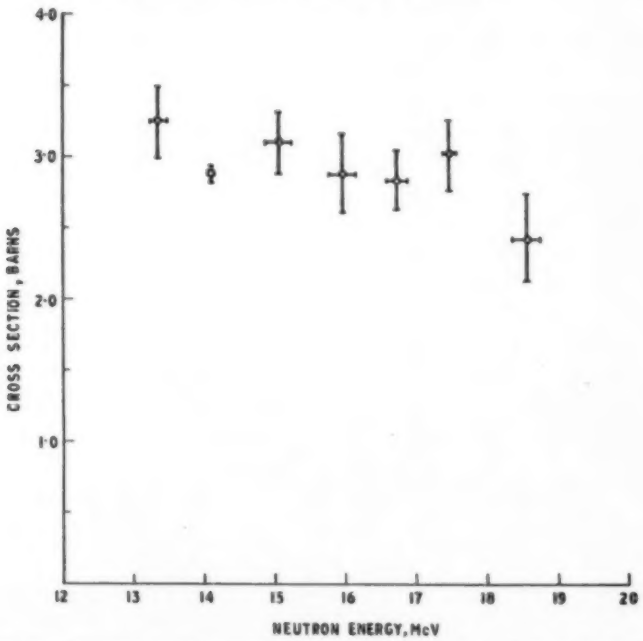

FIG. 2.—Uranium non-elastic neutron cross-section as a function of neutron energy.

series of biases. Taking their measurements of heavy elements in the corresponding neutron energy range we have a difference that is always of the order 100–130 mbarn.

It is of interest to take the cross-sections of MACGREGOR *et al.* at 13·1 MeV bias, which should be roughly comparable with the present result, and divide the values by $\pi(R + \lambda)^2$

Pb	0·852 ± 0·007	(MACGREGOR)
Bi	0·842 ± 0·010	(MACGREGOR)
U	0·875 ± 0·015	(present work)

Thus the present value is in reasonable agreement with the observed cross-sections in this region. Further remarks on MACGREGORS's technique are made below (Section 4.2).

In going from 13·35 to 18·54 MeV it is possible to discern a downward trend of perhaps as much as 10 per cent, in the non-elastic cross-section. The total cross-section actually rises from 5·87 barns at 14 MeV (COON *et al.*, 1952) to 6·05 barns at 19 MeV (HENKEL *et al.*, 1954), so in this energy region, the elastic cross-section must actually rise with energy. The work of BONNER *et al.* (1959) shows that a very similar situation holds for lead and bismuth.

4.2 *Beryllium*

The present value for the non-elastic cross-section may be compared with previous work:

TAYLOR *et al.* (1955)	0·37 ± 0·08 barns
FLEROV and TALYZIN (1957)	0·64 ± 0·02 barns
MACGREGOR *et al.* (1957)	0·49 ± 0·02 barns
Present work	0·50 ± 0·035 barns

The comparatively low value of TAYLOR *et al.* may well be accounted for by the rather low bias they chose (11·2 and 11·9 MeV) so that the transmission might include some of the neutrons scattered to the first excited state, thus lowering the apparent non-elastic cross-section. The Russian value is high, and this may be because they seem to have underestimated the BETHE correction.

The results of MACGREGOR *et al.* for the non-elastic cross-section seem to agree well with that of the present work. However, they publish a series of cross-sections corresponding to several biases, and there is no trace of a significant change in the cross-section corresponding to the 2·43 MeV level. Their measurements do not seem to support our value of 0·196 ± 0·045 barns for inelastic scattering to this level, which we feel is reasonably well established, and which moreover compares well with the value of 0·17 ± 0·03 barns obtained by the time of flight technique by ANDERSON *et al.* (1958).

The reason for this discrepancy may lie in the fact that MACGREGOR *et al.* observed cross-sections at a limited number of biases. The BETHE correction is large, and if somewhat overestimated may mask a change in the cross-section. In such circumstances it is probably best to consider a curve such as that in Fig. 1(c) which effectively displays many biases at once and will be more likely to reveal a change in transmission which is noticeable as a trend, but which might not be considered significant from isolated bias values.

5. CONCLUSIONS

The non-elastic neutron cross-section has been measured for uranium at 14 MeV with small error, and in the neutron energy range 13·35 MeV–18·54 MeV with larger errors.

Reasons for preferring the present 14 MeV value to some previously reported work are given: the present results are not dissimilar to those obtained by previous workers with lead and bismuth.

For beryllium, the cross-sections for non-elastic processes, and for inelastic scatter to the excited state at 2·43 MeV have been measured, and the reasons for the discrepancy between the present value of the non-elastic cross-sections and that of previous workers have been discussed. The present technique of observing the sphere transmission as a function of pulse-height spectrum has been shown to be particularly valuable in tracing small steps due to inelastic scatter to individual levels, or to determining the portion of the inelastic cross-section depending on neutron emission into a given energy range.

Acknowledgements—Grateful thanks are due to DR. K. W. ALLEN for initially suggesting this problem, and for much advice and encouragement during the course of the work, as well as his kindness in discussing his work on the neutron multiplication in uranium (ALLEN *et al.*, 1960) which was unpublished at the time this paper was written.

The technical assistance of MR. A. J. COLE and MR. J. COUPLAND is gratefully acknowledged.

REFERENCES

ALLEN K. W., BOMYER P. and PERKIN J. L. (1961) *Reactor Sci. Technol. (Journal of Nuclear Energy* Parts A/B) **14**, 100.

ANDERSON J. D., GARDNER C. C., MCCLURE J. W., NAKADA M. P. and WONG C. (1958) *Phys. Rev.* **111**, 572.

AUSTERN N., BUTLER S. T. and MCMANUS H. (1953) *Phys. Rev.* **92**, 350.

BALL W. P., MACGREGOR M. H. and BOOTH R. (1958) *Phys. Rev.* **110**, 1392.

BETHE H. A., BEYSTER J. R. and CARTER R. E. (1956) *J. Nucl. Energy* **3**, 207.

BETHE H. A., BEYSTER J. R. and CARTER R. E. (1956) *J. Nucl. Energy* **3**, 273.

BETHE H. A., BEYSTER J. R. and CARTER R. E. (1957) *J. Nucl. Energy* **4**, 3.

BETHE H. A., BEYSTER J. R. and CARTER R. E. (1957) *J. Nucl. Energy* **4**, 147.

BIRKS J. B. (1954) *Scintillation Counters*, Pergamon Press, London.

BONNER T. W. and SLATTERLY J. C. (1959) *Phys. Rev.* **113**, 1088.

BROWN G. and MUIRHEAD H. (1957) *Phil. Mag.* **2**, [8] 473.

COON J. H., DAVIS R. W., FELTHAUSER H. E. and NICODEMUS D. B. (1958) *Phys. Rev.* **111**, 250.

COON J. H., GRAVES E. R. and BARSCHALL H. H. (1952) *Phys. Rev.* **88**, 562.

FLEROV N. N. and TALYZIN V. M. (1957) *J. Nucl. Energy*, **4**, 529.

GRAVES E. R. and DAVIS R. W. (1955) *Phys. Rev.* **97**, 1205.

HENKEL R. L., CRANBERG L., JARVIS G. A., NOBLES R. and PERRY J. E. (1954) *Phys. Rev.* **94**, 141.

MACGREGOR M. H., BALL W. P. and BOOTH R. (1957) *Phys. Rev.* **108**, 726.

NESZMELYI A. and PALLA G. (1958) *A Magyar Tudomanyos Akad. Kasponte Fis. Kutato Intezetuk* **6**, (3) 138.

PHILLIPS D. D., DAVIS R. W. and GRAVES E. R. (1952) *Phys. Rev.* **88**, 600.

SWARTZ C. D. and OWEN G. E. (1960) *Fast Neutron Physics* Vol. I, pp. 211–246. Interscience, New York.

TAYLOR H. L., LÖNSJÖ O. and BONNER T. W. (1955) *Phys. Rev.* **100**, 174.

ZAMIATNIN Y. S., SAFINA I. N., GUTNIKOVA E. K. and IVANOVA N. I. (1959) *J. Nucl. Energy* **9**, 194.

Reactor Science and Technology (J.N.E. Parts A/B), 1961, Vol. 14, pp. 186 to 188. Pergamon Press Ltd. Printed in Northern Ireland

THE DIFFUSION LENGTH OF THERMAL NEUTRONS IN POISONED WATER

M. REIER

Westinghouse Electric Corporation, Bettis Atomic Power Laboratory, Pittsburgh, Pa., U.S.A.

(*Received* 15 *August* 1960)

Abstract—The diffusion length of thermal neutrons has been measured in water poisoned with boron in amounts such that $\Sigma_{aB} = 0{\cdot}5$, $1{\cdot}0$, and $1{\cdot}5\,\Sigma_{aH}$. The data indicate that $1/L^2$ is a linear function of Σ_a for pure water and the two weaker poisons. For the maximum poison used, however, $1/L^2$ departs from the straight line, revealing the presence of a spectral hardening effect. The value of the diffusion constant, $D_0 = Dv$, calculated from the data, equals 37618 ± 205 cm²/sec. Assuming that $\sigma_{aB} = 755 \pm 2b$, σ_{aH} is calculated to be $0{\cdot}328 \pm 0{\cdot}006b$. In addition, the case of a non $1/v$ absorber, cadmium is treated.

INTRODUCTION

As a continuation of our measurements on the diffusion length, L, of thermal neutrons in water at various temperatures (REIER and DE JUREN, 1960), we have measured L in water at 23°C at boron concentrations as a B_2O_3 solution such that $\Sigma_{aB} = 0{\cdot}5$, $1{\cdot}0$ and $1{\cdot}5\,\Sigma_H$ and at one cadmium concentration as a $CdSO_4$ solution. Since $L = (\lambda_{1T}\lambda_a/3)^{1/2}$, L in pure water poisoned by a $1/v$ absorber should be directly calculable from the unpoisoned case, unless the additional absorption changes the spectrum sufficiently to cause a measurable change in λ_{1T}. A plot of $1/L^2$ vs. Σ_a for varying amounts of $1/v$ absorber is a sensitive test of this effect.

EXPERIMENTAL ARRANGEMENTS

The experimental arrangement and all corrections which have to be applied to the data are similar to those described by REIER and DE JUREN (1960). Because of the smaller values of L encountered in the poisoned cases compared with pure water, the data were taken from 13 cm from the source to only about 20 cm.

The amount of poison which can be added is limited by the technique used in this experiment as the solution of the diffusion equation with source term becomes invalid if L is less than b, the relaxation length of the source neutrons (1·58 cm for Sb–Be neutrons in water). This may be seen by examining the steady-state diffusion equation (equation (1)) and its general solution (equation (2)):

$$D_0\nabla^2 n - nv\,\Sigma_a + q = 0. \qquad (1)$$

$D_0 = v\lambda_{1T}/3$ and q, the source term, is assumed to vary as $Ke^{-r/b}/r^2$ at large distances from the source. The general solution of equation (1) is (DE JUREN and ROSENWASSER, 1953):

$$n = \frac{KL}{2D_0}\frac{e^{-r/L}}{r}\left[C - \int_{\alpha_I r}^{\infty}\frac{e^{-x}}{x}\,dx + e^{2r/L}\int_{\alpha_{II} r}^{\infty}\frac{e^{-x}}{x}\,dx\right], \qquad (2)$$

where

$\int_{\alpha_I r}^{\infty}\frac{e^{-x}dx}{x}$ is the exponential integral $E_1(\alpha r)$,

and $\alpha_I = 1/b - 1/L$,

$\alpha_{II} = 1/b + 1/L$.

The integral, $E_1(\alpha_I r)$ diverges if $\alpha_I \leq 0$.

RESULTS

The correction for the fast neutron source term, which was only 0·8 per cent for the case of pure water (REIER and DE JUREN, 1960), rises to a value of 7·9 per cent for the largest boron concentration used. A calculation using a few-thermal-group, spatially dependent diffusion code (CANTWELL, Private communication) shows that the spectrum has reached equilibrium in a region of measurement for the maximum boron concentration in this experiment. If the value of the fast neutron relaxation length, b, is continually changing and is 10 per cent less in the region of 13 to 20 cm than where it was measured (from 12 to 15 cm), the value of L for that concentration is about one per cent too low. The random error in b (about one per cent) has a negligible effect on the overall error of the experiment.

Although addition of boron to the water may cause a change in the thermal neutron spectrum, this does not affect the relative absorption of boron to hydrogen since they are both $1/v$ absorbers. Such is not the case with cadmium. Accordingly, the cadmium and boron

TABLE 1

E (eV)	$N(E)$ Water	$N(E)$ Boron	$N(E)$ Cadmium
0·0010	0·1500	0·1470	0·1483
0·0100	0·3341	0·3290	0·3310
0·0200	0·3203	0·3171	0·3180
0·0300	0·2661	0·2649	0·2648
0·0400	0·2085	0·2089	0·2081
0·0500	0·1582	0·1597	0·1585
0·0700	0·0865	0·0889	0·0875
0·1000	0·0328	0·0351	0·0341
0·2000	0·00148	0·00243	0·00229
0·2500	0·00055	0·00120	0·00117

cross-sections were averaged over the resulting flux-weighted Wigner-Wilkins spectrums using the Sofocate Code (AMSTER and SUAREZ, 1957) for an amount of poison such that $\Sigma_{aB} = \Sigma_{aCd} = 1{\cdot}5\ \Sigma_{aH}$. The spectrum resulting from the boron poison case was only slightly more energetic than that from the cadmium, which in turn was more energetic than the pure water case.

Table 1 shows a comparison of the neutron density $N(E)$ for the three cases at several energies.

These spectra were averaged over all space and do not give a detailed picture as a function of distance from the source. The above Wigner-Wilkins spectra do not apply since the neutron density in the region of interest results from thermal diffusion with no slowing down contributions. The calculation was made to indicate the extent of the spectral difference between the boron and cadmium case. The amount of poison added, even in the extreme cases, does not cause a marked change in the shape of the neutron spectra which remain essentially Maxwellian. Accordingly, the cadmium cross-section was averaged over the Maxwellian flux and a value of 2968b was obtained at 23°C. The source term correction for the cadmium case may not be precise as can be seen in equation (12) of REIER and DE JUREN (1960). Since it involves the ratio of the cross-section of the poisoned to unpoisoned water, its accuracy depends upon the validity of the cross-section averaging process described above. The data is shown in Table 2.

Figure 1 is a plot of $1/L^2$ vs. Σ_a/Σ_{aH} for the boron poisoning. The departure from linearity is clearly seen in the value corresponding to $\Sigma_{aB} = 1{\cdot}5\ \Sigma_{aH}$, which may be explained in terms of spectral hardening decreasing the scattering cross-section and making the scattering more forward. Both effects tend to increase the diffusion constant. The value of $D_0 = Dv$ obtained from $L^2\Sigma_a$ for pure water is 37,651 $\pm$ 290 cm²/sec. The value obtained from a weighted average for all measurements except $\Sigma_{aB} = 1{\cdot}5\ \Sigma_{aH}$ is

TABLE 2

Poison cross-section	L	Source term corr. (per cent)	Per cent over-correction if $b = 1{\cdot}42$ instead of 1·58 cm
$\Sigma_{aB} = 0$	2·779 $\pm$ 0·007	0·8	0·2
$\Sigma_{aB} = 0{\cdot}5\ \Sigma_{aH}$	2·275 $\pm$ 0·011	4·3	0·61
$\Sigma_{aB} = 1{\cdot}0\ \Sigma_{aH}$	1·955 $\pm$ 0·011	6·1	0·78
$\Sigma_{aB} = 1{\cdot}5\ \Sigma_{aH}$	1·810 $\pm$ 0·006	7·9	1·02
$\Sigma_{aCd} = 1{\cdot}5\ \Sigma_{aH}$	1·766 $\pm$ 0·004	9·4	2·50

37,618 $\pm$ 205 cm²/sec. The boron cross-section was assumed to be 755 $\pm$ 2b at 2·2 $\times$ 10⁵ cm²/sec. This value of D_0 is about 3·5 per cent higher than VON DARDEL's value of 36,340 $\pm$ 750 (VON DARDEL and SJÖSTRAND, 1954) using a pulsed source of neutrons. They pointed out, however, that L measured with a steady state source should be about one per cent higher than L measured with a pulsed source in pure water. With a difference of two per cent accounted for in this way, the results are in substantial agreement.

An alternative approach might be used in treating the data. By making use of the three measured values of $1/L^2$ on the linear region of Fig. 1, it is possible to get the ratio σ_{aB}/σ_{aH} for the two poisoned cases in terms

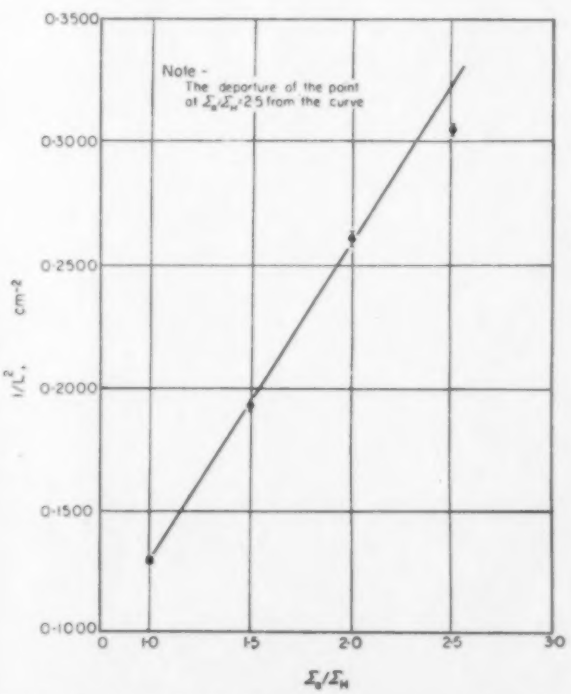

FIG. 1.—Variation of $1/L^2$ with neutron capture cross-section with boron poisoning. (The effect of the experimental change on the diffusion length is clearly shown.)

of the ratio of the unpoisoned to the poisoned L^2. This is shown in equations (3) and (4).

$$L_1^2 \pm \epsilon_1 = D/\Sigma_{aH}, L_2^2 \pm \epsilon_2 = D/(\Sigma_{aH} + \Sigma_{aB}),$$
$$L_3^2 \pm \epsilon_3 = D/(\Sigma_{aH} + 2\Sigma_{aB}) \quad (3)$$

where Σ_{aB} is the cross-section of boron in medium 2 and $2\Sigma_{aB}$ is the corresponding cross-section in medium 3.

$$\Sigma_{aB}/\Sigma_{aH} = (L_1^2/L_2^2 \pm \epsilon_{12}) - 1,$$
$$2\Sigma_{aB}/\Sigma_{aH} = (L_1^2/L_3^2 \pm \epsilon_{13}) - 1. \quad (4)$$

This method of getting the ratio of the cross-sections is inherently inaccurate as may be seen by examining equation (4). The weighted average of the two ratios is $\Sigma_{aB}/\Sigma_{aH} = 0{\cdot}506 \pm 0{\cdot}009$. Again, if σ_{aB} is taken to be $755 \pm 2b$, we get $\sigma_{aH} = 0{\cdot}328 \pm 0{\cdot}006b$, in agreement with the present world average of $0{\cdot}332 \pm 0{\cdot}002b$.

Acknowledgments—I would like to express my gratitude to DR. J. A. DE JUREN for many helpful discussions during the course of this experiment and to W. D. OGLETHORPE for his assistance in taking data.

REFERENCES

AMSTER H. and SUAREZ R. (1957) WAPD-TM-39.
CANTWELL R. M. Private communication.
DARDEL G. F. VON and SJOSTRAND N. G. (1954) *Phys. Rev.* **96**, 1245.
JUREN J. A. DE and ROSENWASSER H. (1953) *J. Res. nat. Bur. Standards* **51**, 203.
REIER M. and DEJUREN J. A. (1960) WAPD-T-1082.

VOL
14
196

Reactor Science and Technology (J.N.E. Parts A/B), 1961, Vol. 14, pp. 189 to 199. Pergamon Press Ltd. Printed in Northern Ireland

NUCLEAR SAFETY OF UO_2–ThO_2–H_2O SYSTEMS

D. B. WEHMEYER and K. E. ROACH
The Babcock & Wilcox Company, Atomic Energy Division, Lynchburg, Virginia, U.S.A.

(*First received* 31 *August* 1960 *and in revised form* 21 *November* 1960)

Abstract—A large number of clean critical assemblies with H_2O moderator and reflector have been correlated with a modified two-group theoretical model. Agreement of theory and experiment is good over a wide range of moderation, geometry and material composition. Within the range of correlation, the model can be used to determine mass and geometry limits for processing fissionable material. This method is used to determine minimum critical conditions of UO_2–ThO_2–H_2O systems. Appropriate safety factors are derived and safe processing limits are determined.

INTRODUCTION

IN order to process fissionable material safely and economically, it is important to have accurate determinations of critical conditions for a chain reaction. Since the fissionable material can be subjected to a wide variety of conditions during processing, it is impractical to measure the multiplication of every possible situation. However, as many experimental determinations as possible of the various critical conditions should be made, and a good theoretical model is needed to interpolate between experiments and to extrapolate outside the range of the experiments. For interpolation between widely differing experiments, and for extrapolation, a tneoretical model is needed that not only fits the critical experiments well, but also one which uses basic data and which is founded on the basic principles of reactor theory. A modified two-group model (EDLUND *et al.*, 1958) describes the principal features of water moderated reactors and is easy to use to cover a variety of nuclear safety conditions. This model correlates with good accuracy all clean critical experiments on water moderated and reflected systems and should thus be a good one for general nuclear safety use. Although the model should give a good qualitative representation of all simple geometry thermal reactor systems, a number of quantitative data are used to fit the experimental assemblies, so that quantitative nuclear safety calculations are only valid within the region verified by experiment.

THEORETICAL MODEL

The modified two-group model (EDLUND *et al.*, 1958) used in this analysis calculates the K_{eff} of a clean reactor by

$$K_{eff} = \frac{\eta^{th}\epsilon f P_{25} P_f P_{el}}{(1 + L^2B^2)(1 + \tau B^2)} + \frac{\eta^{r}\epsilon P_f (1 - P_{25})}{1 + \tau B^2} \quad (1)$$

Simple formulas based on experimental data have been obtained for the calculation of each of the nuclear parameters that appear in equation (1). These formulas are given below.

$$\eta^{th} = 2{\cdot}07 \text{ for } {}^{235}U \quad (2)$$

$$\eta^{r} = 1{\cdot}62 \text{ for } {}^{235}U \quad (3)$$

obtained by numerical integration of the cross-section curves and resonance parameters (HUGHES and SCHWARTZ, 1958) above cadmium cut-off.

$$\epsilon_{28} = 1{\cdot}004 + 0{\cdot}137\left(\frac{N_H}{Nu}\right)^{-0{\cdot}764} \text{ for } {}^{238}U \text{ systems.} \quad (4)$$

The experimental data (KLEIN *et al.*, 1958) were fitted well by this curve.

$$\epsilon_{02} = 1{\cdot}0007 + 0{\cdot}0249\left(\frac{N_H}{N_{25} + N_{02}}\right)^{-0{\cdot}764} \text{ for } {}^{232}Th. \quad (5)$$

Experimental data of ϵ is not available for thorium. However, the fast fission rate in a thorium system should be approximately that of a similar uranium system multiplied by the ratio of the fission cross-sections. Based on this approximation, the fast effect in a thorium lattice can be related to that in a uranium one by

$$\frac{\epsilon_{02} - 1}{\epsilon_{28} - 1} = \frac{\sigma_{02}^{F}[\nu_{02} - (1 + \alpha_{02})]}{\sigma_{28}^{F}[\nu_{28} - (1 + \alpha_{28})]}.$$

Numerical values chosen for these quantities are

$$\sigma_{02}^{F} = 0{\cdot}135b \qquad \nu_{02} = 2{\cdot}4 \qquad \alpha_{02} = 0{\cdot}2$$

$$\sigma_{28}^{F} = 0{\cdot}575b \qquad \nu_{28} = 2{\cdot}65 \qquad \alpha_{28} = 0{\cdot}1.$$

The thermal utilization f is given by

$$f = \left[1 + \frac{\Sigma_{fertile}^{A}}{\Sigma_{25}^{A}} + \frac{\Sigma_{clad}^{A}}{\Sigma_{25}^{A}} \cdot \frac{\phi_{el}}{\phi_{25}} + \frac{\Sigma_{water}^{A}}{\Sigma_{25}^{A}} \cdot \frac{\phi_w}{\phi_{25}}\right]^{-1} \quad (6)$$

All of the cross-sections that appear in equation (6) are homogenized over the lattice cell and are averaged over a Maxwell Boltzmann distribution. A formula for the flux ratio $\frac{\phi_w}{\phi_{25}}$ in heterogeneous lattices has been developed by M. M. Levine based on a simplified Dancoff treatment (BELL, 1959) in a two-region problem. The expression for the two-region thermal utilization f_1 in terms of collision and escape probabilities is

$$f_1 = \frac{(1 - S_F)(1 - P_M)}{(1 - S_M P_M)(1 - S_F P_F) - S_M S_F (1 - P_M)(1 - P_F)}$$

where $S = \frac{\Sigma_S}{\Sigma_{\text{total}}}$ in either the fuel lump (F) or the moderator (M) and P is the probability that a neutron in a region will make its next collision in that region. Expressions for P_M and P_F in terms of cross-sections and geometry are

$$1 - P_F = \frac{\tau}{\Sigma_F + \tau}, \qquad \tau = \frac{\frac{S}{4V_F}}{1 + \frac{S}{4V_M \Sigma_M}}$$

$$(1 - P_M)\Sigma_M V_M = (1 - P_F)\Sigma_F V_F$$

where Σ_F is the total cross-section in the fuel, Σ_M is the total cross-section in the moderator and V_F and V_M are the respective volumes of fuel and moderator. The ordinary expression for thermal utilization in a two region problem is

$$f_2 = \frac{\Sigma_A^{\text{fuel}} \phi_{\text{fuel}} V_F}{\Sigma_A^{\text{fuel}} \phi_{\text{fuel}} V_F + \Sigma_A^{\text{mod.}} \phi_{\text{mod.}} V_M}.$$

Equating f_1 and f_2 and solving for $\frac{\phi_w}{\phi_{\text{fuel}}}$ yields

$$\frac{\phi_w}{\phi_{25}} = 1 + \frac{\Sigma_A^{\text{fuel}}}{\frac{S}{4V_{\text{fuel}}}}. \tag{7}$$

The ratio $\frac{\phi_{\text{cl}}}{\phi_{25}}$ is assumed to be half-way between unity and $\frac{\phi_w}{\phi_{25}}$, i.e.

$$\frac{\phi_{\text{cl}}}{\phi_{25}} = \frac{1}{2}\left(1 + \frac{\phi_w}{\phi_{25}}\right). \tag{8}$$

The resonance escape probabilities (P_{25}, P_f, P_{cl}) that appear in equation (1) are computed by

$$P = \exp - \frac{NR_{\text{eff}}}{\xi\Sigma_s}. \tag{9}$$

N is the number of absorber atoms per cubic centimetre of core, R_{eff} is the effective resonance integral of the absorber and $\xi\Sigma_s$ is the slowing down power homogenized over the core. The effective resonance integrals used in the analysis of critical experiments were:

$R_{25} = 487b$ for ^{235}U obtained from numerical integration of the cross-section curves and resonance parameters (HUGHES and SCHWARTZ, 1958).

$R_{\text{cl}} = 2{\cdot}75b$ for stainless steel
$= 0{\cdot}2b$ for aluminium

$R_{28} = 5{\cdot}25 + 26{\cdot}6\sqrt{\frac{\gamma S}{M_{\text{oxide}}}}$ for $^{238}UO_2$ lumps (HELLSTRAND, 1957)

$R_{28} = 3{\cdot}91 + 24{\cdot}7\sqrt{\frac{\gamma S}{M}}$ for ^{238}U metal lumps (HELLSTRAND, 1957)

$R_{28} = 3{\cdot}8\left(\frac{\Sigma_s}{N_{28}}\right)^{0{\cdot}42}$ for homogeneous mixtures of ^{238}U and water (DRESNER, 1956) (the maximum value of R_{28} is $278b$)

$R_{02} = 0{\cdot}215 + 26{\cdot}83\sqrt{\frac{\gamma S}{M_{\text{oxide}}}}$ for ThO_2 lumps (PETTUS, 1959)

$R_{02} = 7{\cdot}8\left(\frac{\Sigma_s}{N_{02}}\right)^{0{\cdot}26}$ for homogeneous mixtures of thorium and water (DRESNER, 1956) (the maximum value of R_{02} is $100b$).

S/M is the surface to-mass ratio for the fuel lumps (excluding the clad) and γ is the Dancoff factor which reduces the effective surface of the absorber lump to account for the shadowing effect of neighbouring pins. According to the work of BELL (1959) the Dancoff factor is given by

$$\gamma = \left(1 + \frac{S}{4V_M \Sigma_M}\right)^{-1}$$

where S is the surface area of the fuel pin, V_M is the volume fraction of water in the unit cell, and Σ_M is the total (epithermal) cross-section in the moderator.

Both calculations and experiments have indicated that the Fermi age τ is a linear function of metal-to-water volume ratio for a given fuel. Calculations using 40 energy groups (Selengut-Goertzel slowing-down kernel) show that the age is almost exactly a linear function of the metal-to-water volume ratio over the

VOL 14 196

entire range of interest. These 40-group calculations were fitted with the linear formula

$$\tau = 32{\cdot}0 + F\left(\rho, \frac{V_{el}}{V_{fuel}}\right) \cdot \frac{M}{W}. \qquad (10)$$

F is plotted for various fuels and cladding materials as a function of the parameter $\frac{V_{el}}{V_{fuel}}$ for a number of fuel densities in Figs. 1–4.

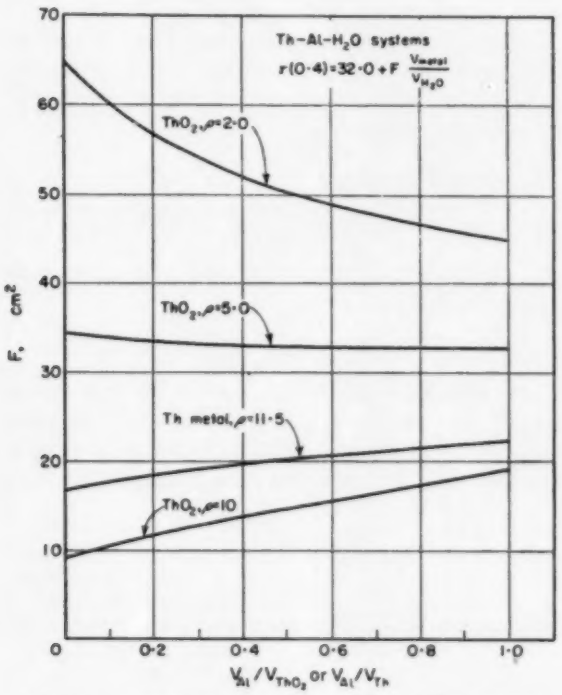

FIG. 1.—Formula to compute age—Th–Al–H_2O systems.

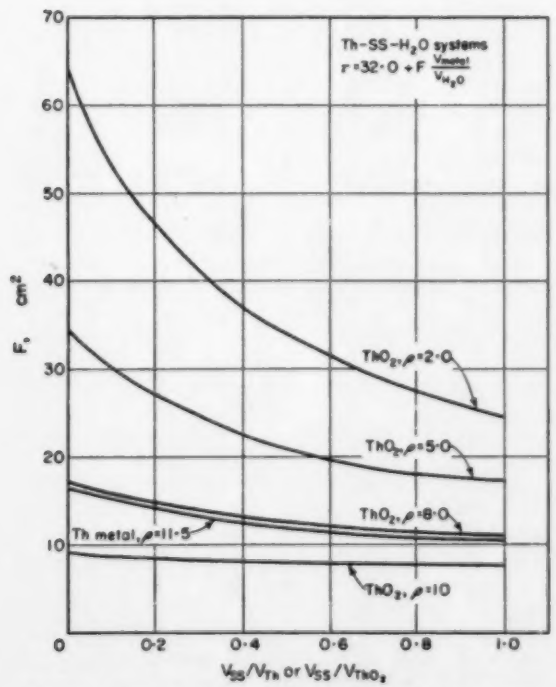

FIG. 2.—Formula to compute age—Th–SS–H_2O systems.

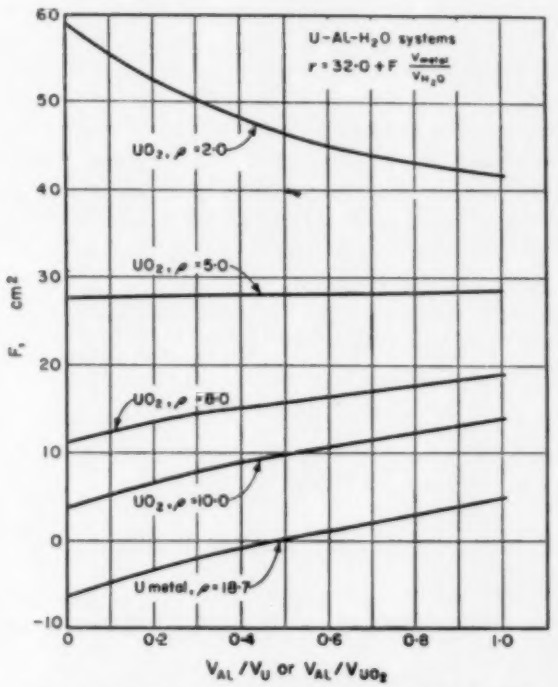

FIG. 3.—Formula to compute age—U–Al–H_2O systems.

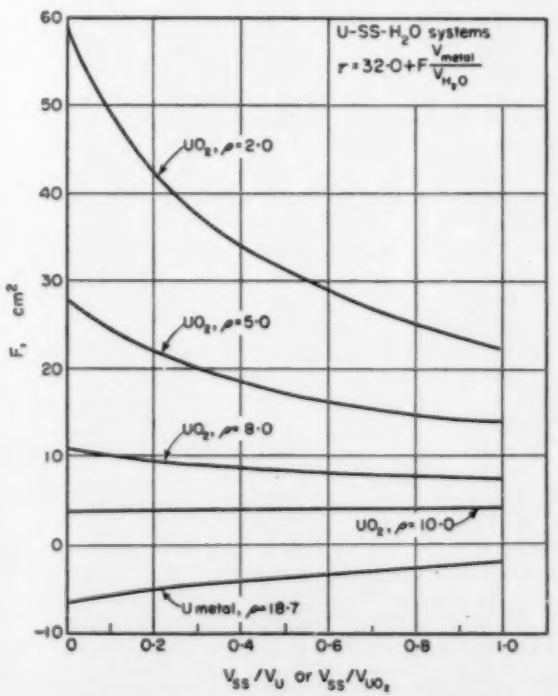

FIG. 4.—Formula to compute age—U–SS–H_2O systems.

The square of the thermal diffusion length L^2 is given by

$$L^2 = \frac{D_{\text{fuel}} V_{\text{fuel}} + D_{H_2O} V_{H_2O} \frac{\phi_w}{\phi_{25}}}{\Sigma^A_{\text{fuel}} V_{\text{fuel}} + \Sigma^A_{H_2O} V_{H_2O} \frac{\phi_w}{\phi_{25}}}. \quad (11)$$

Calculations of experimentally measured critical sizes for heterogeneous lattices using various reflector savings show that a value of 8 cm for reflector savings gives agreement between experiment and theory as calculated with the Selengut-Goertzel slowing-down kernel over a wide range of metal-to-water ratios. However, for metal-to-water ratios less than 0·358 a smaller reflector savings is required for the critical sizes to agree. The following values of reflector savings were chosen to fit one complete set of experiments over the entire range of metal-to-water ratios:

$$\delta = 8{\cdot}0 \text{ cm, for } M/W > 0{\cdot}358$$
$$\delta = 6{\cdot}0 + 9{\cdot}71\,(M/W - 0{\cdot}152) \text{ cm, for } 0{\cdot}152 < M/W < 0{\cdot}358$$
$$\delta = 6{\cdot}0 \text{ cm, for } M/W < 0{\cdot}152. \quad (12)$$

For homogeneous solutions, the best value of reflector savings was found to be nearly constant over all values of hydrogen to ^{235}U atomic ratio (H/X) that were measured:

$$\delta = 7{\cdot}0 \text{ cm (Homogeneous).} \quad (13)$$

Comparison of theoretical critical conditions with those experimentally observed, was made by setting $K_{\text{eff}} = 1$ in equation (1) and solving for B^2 in terms of all the known quantities

$$B^2 = \frac{-(\tau + L^2 - K_1 L^2) + \sqrt{(\tau + L^2 - K_1 L^2)^2 + 4\tau L^2 (K_1 + K_2 - 1)}}{2\tau L^2} \quad (14)$$

where

$$K_1 = \eta^r \epsilon P_f (1 - P_{25}), \text{ and } K_2 = \eta^{th} \epsilon f P_{25} P_f P_{el}.$$

The calculated critical cylinder radii were determined from B^2 and the known height of fuel. Computer programs DPR–144 and DPR–145 have been written to perform these calculations on a Datatron 205.

TABLE 1.—UO_2 FUEL PINS IN WATER

Reference	Fuel pin radius (cm)	Fuel pellet radius (cm)	Clad thickness (cm)	Fuel density g/cm³	N_{25}/N_{28}	Volume pins / Volume water	H/X	Fuel height (cm)	Experimental cylinder radius (cm)	Calculated cylinder radius (cm)
KOUTS *et al.* (1958)	0·8460	0·7635	0·071 Al*	7·53	0·01348	0·700 HP†	524	121·9	41·4	39·1
KOUTS *et al.* (1958)	0·8460	0·7635	0·071 Al	7·53	0·01348	0·877 HP	418	121·9	39·7	37·4
KOUTS *et al.* (1958)	0·8460	0·7635	0·071 Al	7·53	0·01348	1·150 HP	319	121·9	41·2	38·6
KOUTS *et al.* (1958)	0·5755	0·4930	0·071 Al	7·52	0·01348	0·787 HP	518	121·9	45·7	42·8
KOUTS *et al.* (1958)	0·5755	0·4930	0·071 Al	7·52	0·01348	0·980 HP	416	121·9	45·1	42·0
KOUTS *et al.* (1958)	0·5755	0·4865	0·071 Al	10·53	0·01348	0·585 HP	511	121·9	37·6	33·8
KOUTS *et al.* (1958)	0·5755	0·4865	0·071 Al	10·53	0·01348	0·787 HP	380	121·9	36·3	32·2
KOUTS *et al.* (1958)	0·5755	0·4865	0·071 Al	10·53	0·01348	0·987 HP	303	121·9	38·2	33·2
MACKINNEY and BALL (1960)	0·6350	0·5640	0·071 SS	9·45	0·03128	0·355 SP	373	168·9	24·2	24·0
MACKINNEY and BALL (1960)	0·6350	0·5640	0·071 SS	9·45	0·03128	0·807 SP	164	168·9	23·8	23·4
MACKINNEY and BALL (1960)	0·6350	0·5640	0·071 SS	9·45	0·03128	1·102 SP	120	168·9	26·7	26·6
MACKINNEY and BALL (1960)	0·6350	0·5640	0·071 SS	9·45	0·04213	0·288 SP	345	168·9	19·8	19·9
MACKINNEY and BALL (1960)	0·6350	0·5640	0·071 SS	9·45	0·04213	0·355 SP	280	168·9	18·6	18·2
MACKINNEY and BALL (1960)	0·6350	0·5640	0·071 SS	9·45	0·04213	0·807 SP	123	168·9	19·3	18·7
MACKINNEY and BALL (1960)	0·6350	0·5640	0·071 SS	9·45	0·04213	1·102 SP	90	168·9	21·7	21·2
DAVISON *et al.* (1959)	0·4329	0·3796	0·053 SS	10·20	0·0470	0·932 SP	91	142·5	20·0	18·6
DAVISON *et al.* (1959)	0·4329	0·3796	0·053 SS	10·20	0·0470	0·704 SP	121	142·5	18·5	16·9
DAVISON *et al.* (1959)	0·4298	0·3810	0·041 SS	10·20	0·0281	1·214 SP	113	121·9	32·0	29·2
DAVISON *et al.* (1959)	0·4298	0·3810	0·041 SS	10·20	0·0281	0·906 SP	151	121·9	26·8	24·5
DAVISON *et al.* (1959)	0·4298	0·3810	0·041 SS	10·20	0·0281	0·687 SP	199	121·9	24·3	22·4

* The symbol Al means aluminium cladding and the symbol SS means stainless-steel cladding.
† The symbol HP means hexagonal pitch and the symbol SP means square pitch.

VOL 14 196

CORRELATION OF EXPERIMENTS

A large number of clean critical experiments have been performed for water moderated systems. Information on 113 individual clean critical experiments with water moderator and full water reflector has been collected. Since many experimental data are as yet unpublished, a complete compilation could not be made, but all experimental data on clean critical water moderated and reflected assemblies that could be found are listed. Table 1 gives the data for low enriched uranium oxide pin lattices, Table 2 describes the experiments with mixtures of ThO_2 and fully-enriched UO_2 in pin lattices, Table 3 gives the low enriched uranium metal lattice data, and Table 4 describes the homogeneous experiments.

Since the important item measured by criticality in the lattice experiments was the critical radius, the comparison of theory and experiment in Tables 1, 2 and 3 is on values of critical core radius. Agreement between the measured radii and those calculated with the modified two-group model is reasonably good for all the heterogeneous experiments. This agreement is nearly as good as that obtained previously by ARNOLD (1959) for low-enriched uranium lattices, and has been extended over a much wider range of experiments. The agreement is particularly good for the ThO_2–UO_2 cases and for the 3 and 4 per cent enriched UO_2 cases which are shown in Figs. 5, 6 and 7.

For homogeneous systems a wide variety of geometries has been measured. The comparison of theory and experiment listed in Table 4 is on a double basis. The experimental buckling of each case is determined from the measured dimensions and the 7·0 cm reflector savings, and the calculated value from equation (14). In addition, a size comparison has been made on the smallest experimental core dimension, computing the theoretical value from the calculated B^2 and the measured other (larger) dimensions. Again, agreement is good over the entire range of experimental data. The homogeneous experiments with 2 per cent enriched uranium were performed with paraffin rather than water moderator. These calculations assumed that paraffin moderator has the same age as water with the same hydrogen density, using equation (10). This calculation assumed that the carbon in paraffin has the same moderating effect as the oxygen in water, and that the fluorine in UF_4 has similar characteristics to the oxygen in UO_2. Some further corrections to the

TABLE 2.—U-235O_2 ThO_2 FUEL PINS IN WATER

Reference	Fuel pin radius (cm)	Fuel pellet radius (cm)	Clad thickness (cm)	Fuel density g/cm³	N_{25}/N_{02}	Volume pins / Volume water	H/X	Fuel height (cm)	Experimental cylinder radius (cm)	Calculated cylinder radius (cm)
EDLUND *et al.* (1958); SNIDOW (Private communication)	0·3960	0·3300	0·048 SS*	8·36	0·0388	0·890 SP†	152	121·9	39·2	39·1
EDLUND *et al.* (1958); SNIDOW (Private communication)	0·3960	0·3300	0·048 SS	8·36	0·0388	1·116 SP	121	121·9	43·6	43·9
SNIDOW (Private communication)	0·3960	0·3300	0·048 SS	8·36	0·0667	0·152 SP	530	121·9	28·0	28·9
SNIDOW (Private communication)	0·3960	0·3300	0·048 SS	8·36	0·0667	0·358 SP	225	121·9	19·2	19·1
SNIDOW (Private communication)	0·3960	0·3300	0·048 SS	8·36	0·0667	0·656 SP	123	121·9	20·1	19·9
EDLUND *et al.* (1958); SNIDOW (Private communication)	0·3960	0·3300	0·048 SS	8·36	0·0667	0·890 SP	91	121·9	21·9	21·7
EDLUND *et al.* (1958); SNIDOW (Private communication)	0·3960	0·3300	0·048 SS	8·36	0·0667	1·116 SP	72	121·9	24·3	23·9
ANDERSON *et al.* (1960)	0·3924	0·2972	0·086 Al	8·45	0·0400	0·300 SP	524	152·4	27·3	26·6
ANDERSON *et al.* (1960)	0·3924	0·2972	0·086 Al	8·45	0·0400	0·480 SP	328	152·4	23·4	23·1
ANDERSON *et al.* (1960)	0·3924	0·3302	0·036 Al	8·35	0·0667	0·480 SP	165	152·4	15·5	15·2
ANDERSON *et al.* (1960)	0·3924	0·3302	0·036 Al	8·35	0·0667	0·860 SP	92	152·4	17·4	17·7
ANDERSON *et al.* (1960)	0·3924	0·3302	0·036 Al	8·35	0·0667	1·024 SP	77	152·4	18·1	19·1

* The symbol Al means aluminium cladding and the symbol SS means stainless steel cladding.
† The symbol SP means square pitch.

TABLE 3.—URANIUM METAL RODS IN WATER

Reference	Clad pin radius (cm)	Metal rod radius (cm)	Clad thickness (cm)	Metal density g/cm³	N_{25}/N_{28}	Volume pins / Volume water	H/X	Fuel height (cm)	Experimental cylinder radius (cm)	Calculated cylinder radius (cm)
KOUTS *et al.* (1958)	0·8460	0·7620	0·071 Al*	18·9	0·01334	0·611 HP†	214	121·9	25·1	21·4
KOUTS *et al.* (1958)	0·8460	0·7620	0·071 Al	18·9	0·01334	0·409 HP	320	121·9	25·5	22·3
KOUTS *et al.* (1958)	0·8460	0·7620	0·071 Al	18·9	0·01178	0·611 HP	242	121·9	29·6	25·0
KOUTS *et al.* (1958)	0·8460	0·7620	0·071 Al	18·9	0·01178	0·409 HP	361	121·9	30·5	26·5
KOUTS *et al.* (1958)	0·5755	0·4915	0·071 Al	18·9	0·01334	0·667 HP	215	121·9	27·2	23·4
KOUTS *et al.* (1958)	0·5755	0·4915	0·071 Al	18·9	0·01334	0·454 HP	320	121·9	25·9	22·8
LLOYD *et al.* (1959)	1·1748	1·1748	—	18·7	0·03200	0·529 HP	86	40·6	16·9	14·2
LLOYD *et al.* (1959)	1·1748	1·1748	—	18·7	0·03200	0·529 HP	86	61·0	15·5	13·0
LLOYD *et al.* (1959)	1·1748	1·1748	—	18·7	0·03200	0·437 HP	104	40·6	17·0	14·4
LLOYD *et al.* (1959)	1·1748	1·1748	—	18·7	0·03200	0·437 HP	104	61·0	15·5	13·1
LLOYD *et al.* (1959)	1·1748	1·1748	—	18·7	0·03200	0·368 HP	124	40·6	17·4	14·8
LLOYD *et al.* (1959)	1·1748	1·1748	—	18·7	0·03200	0·368 HP	124	61·0	15·9	13·5
LLOYD *et al.* (1959)	1·1748	1·1748	—	18·7	0·03200	0·316 HP	144	40·6	18·1	15·9
LLOYD *et al.* (1959)	1·1748	1·1748	—	18·7	0·03200	0·316 HP	144	61·0	16·4	14·5
LLOYD *et al.* (1959)	1·1748	1·1748	—	18·7	0·03200	0·257 HP	177	40·6	20·2	18·1
LLOYD *et al.* (1959)	1·1748	1·1748	—	18·7	0·03200	0·257 HP	177	61·0	18·1	16·2
LLOYD *et al.* (1959)	0·7620	0·7620	—	18·7	0·03200	0·485 HP	94	40·6	16·5	14·1
LLOYD *et al.* (1959)	0·7620	0·7620	—	18·7	0·03200	0·369 HP	123	40·6	16·0	14·1
LLOYD *et al.* (1959)	0·7620	0·7620	—	18·7	0·03200	0·293 HP	155	40·6	16·4	15·3
LLOYD *et al.* (1959)	0·7620	0·7620	—	18·7	0·03200	0·239 HP	190	40·6	17·2	18·4
LLOYD *et al.* (1959)	0·7620	0·7620	—	18·7	0·03200	0·193 HP	236	40·6	19·0	19·1
LLOYD *et al.* (1959)	0·7620	0·7620	—	18·7	0·03200	0·146 HP	311	40·6	23·6	24·8
LLOYD *et al.* (1959)	0·3810	0·3810	—	18·7	0·03200	0·485 HP	94	40·6	17·3	14·9
LLOYD *et al.* (1959)	0·3810	0·3810	—	18·7	0·03200	0·293 HP	155	40·6	15·8	14·8
LLOYD *et al.* (1959)	0·3810	0·3810	—	18·7	0·03200	0·200 HP	227	40·6	16·1	16·7
LLOYD *et al.* (1959)	0·3810	0·3810	—	18·7	0·03200	0·146 HP	311	40·6	17·6	19·2
LLOYD *et al.* (1959)	0·3810	0·3810	—	18·7	0·03200	0·112 HP	406	40·6	20·3	22·4

* The symbol Al means aluminium cladding.
† The symbol HP means hexagonal pitch.

age should be made for a more careful analysis of these particular experiments.

The agreement between experiment and theory is good over a wide range of water moderated systems. Tables 1 to 4 include data on

(a) low-enriched U, high-enriched U, mixtures of U and thorium
(b) homogeneous mixtures, oxide fuel pins, metal fuel pins
(c) stainless steel clad, aluminium clad, unclad fuel pins
(d) low, optimum, high moderation (H/X).

Because of the agreement of the calculated and experimental criticality over such a wide range of conditions, the theoretical model should serve well for interpolation and extrapolation of the experimental data.

DETERMINATION OF SAFE VALUES

The experimental data in Table 2 have been extrapolated using the theoretical model to determine the critical conditions for UO_2–ThO_2–H_2O systems. Figures 5 and 6 show the excellent agreement between theory and experiment for 12 critical assemblies in this system. The theoretical model was used to compute the critical buckling as a function of H/X for homogeneous mixtures, unclad fuel pellets and stainless steel clad fuel pins at five values of N_{25}/N_{02}. Using the critical B^2, the critical dimensions (∞ cylinder radius, ∞ slab thickness, sphere volume) were computed, and from these the critical mass (spherical geometry) and critical mass per cm length (∞ cylindrical geometry) were found. Some of these results are shown in Figs. 8, 9 and 10. Figure 8 shows the variation of critical mass and cylinder radius with moderation for a single fuel form and composition. The minimum critical geometry occurs at lower H/X than does the minimum critical mass, which is the general case for water moderated reactors. Figures 9 and 10 show the effect of fuel form (homogeneous vs. heterogeneous) on critical mass and cylinder radius. It should be noted that for UO_2–ThO_2 there is a region where the lumped material is more critical than the homogeneous. This effect is even more pronounced for lower values of N_{25}/N_{02} than

VOL 14 196

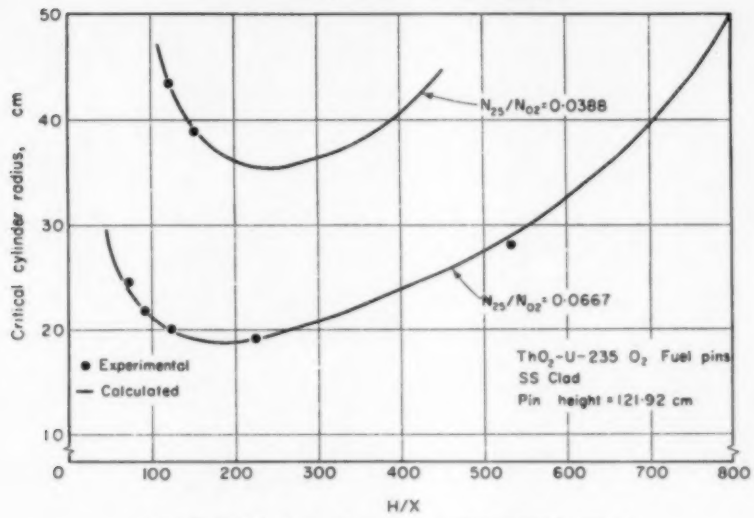

FIG. 5.—Critical experiment data—ThO $U235O_2$–SS pins.

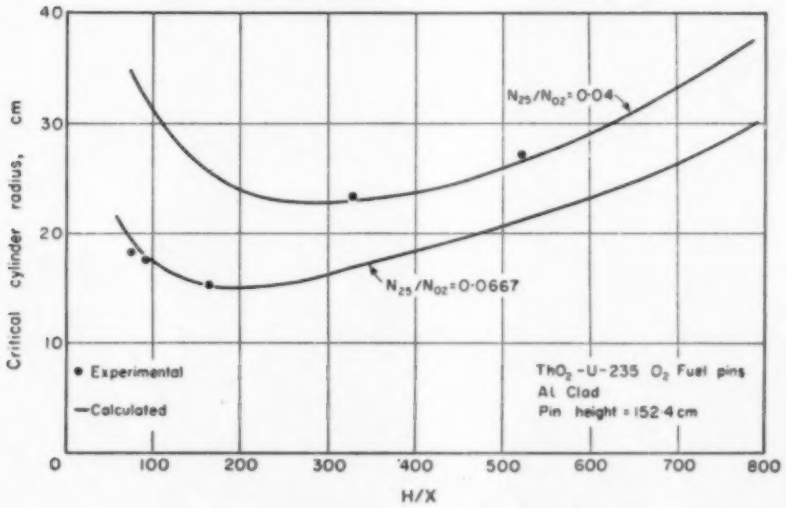

FIG. 6.—Critical experiment data—ThO_2 $U235O_2$–Al pins.

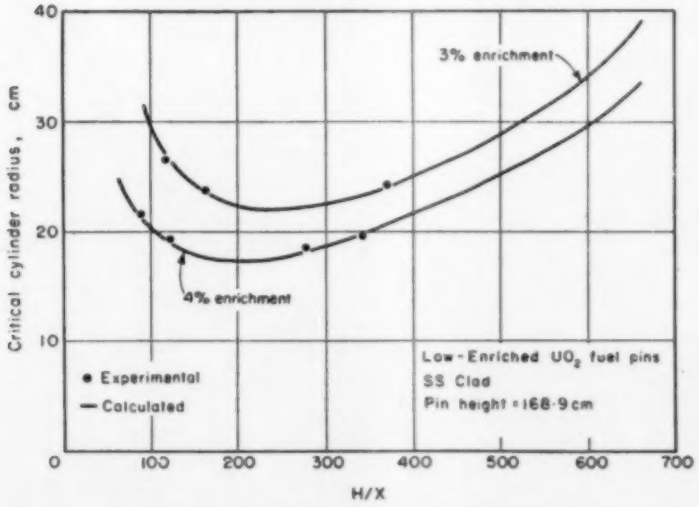

FIG. 7.—Critical experiment data—UO_2–SS pins.

TABLE 4.—HOMOGENEOUS MIXTURES OF U AND WATER

Reference	Enrichment	H/X	Geometry	Experimental			Calculated		
				Height (cm)	Radius (cm)	B^2* (cm^{-2})	Height (cm)	Radius (cm)	B^2 (cm^{-2})
BECK *et al.* (1949)	93·2	999	Cylinder	44·3	19·1	0·0114	—	19·1	0·0114
BECK *et al.* (1949)	93·2	755	Cylinder	27·1	19·1	0·0144	—	18·3	0·0149
BECK *et al.* (1949)	93·2	499	Cylinder	16·9	19·1	0·0187	16·1	—	0·0194
BECK *et al.* (1949)	93·2	499	Cylinder	35·2	12·7	0·0190	—	12·5	0·0194
BECK *et al.* (1949)	93·2	328·7	Cylinder	22·4	12·7	0·0224	—	12·3	0·0230
BECK *et al.* (1949)	93·2	290	Cylinder	40·1	10·2	0·0229	—	9·9	0·0238
BECK *et al.* (1949)	93·2	221	Cylinder	11·3	19·1	0·0239	9·9	—	0·0258
BECK *et al.* (1949)	93·2	192	Cylinder	28·1	10·2	0·0251	—	9·9	0·0260
BECK *et al.* (1949)	93·2	119	Cylinder	52·6	8·3	0·0269	—	8·2	0·0272
BECK *et al.* (1949)	93·2	99·5	Cylinder	22·4	10·2	0·0270	—	10·1	0·0273
FOX *et al.* (1958a)	93·2	72·4	Cylinder	6·2	29†	0·0286	6·9	—	0·0271
FOX *et al.* (1958a)	93·2	72·4	Cylinder	5·5	38·1	0·0288	6·2	—	0·0271
BECK *et al.* (1949)	93·2	58·8	Cylinder	20·5	10·2	0·0278	—	10·7	0·0267
BECK *et al.* (1949)	93·2	58·8	Cylinder	71·8	7·6	0·0285	—	8·1	0·0267
BECK *et al.* (1949)	93·2	56·7	Cylinder	8·5	19·1	0·0280	9·4	—	0·0266
BECK *et al.* (1949)	93·2	56·7	Cylinder	40·4	8·3	0·0280	—	8·8	0·0266
BECK *et al.* (1949)	93·2	52·9	Cylinder	7·9	19·1	0·0291	9·4	—	0·0265
BECK *et al.* (1949)	93·2	52·9	Cylinder	13·4	12·7	0·0281	—	13·8	0·0265
BECK *et al.* (1949)	93·2	52·9	Cylinder	19·5	10·2	0·0284	—	11·1	0·0265
BECK *et al.* (1949)	93·2	52·9	Cylinder	39·2	8·3	0·0282	—	8·8	0·0265
BECK *et al.* (1949)	93·2	52·9	Cylinder	70·9	7·6	0·0285	—	8·2	0·0265
FOX *et al.* (1958a)	93·2	44·3	Cylinder	4·3	29†	0·0340	7·6	—	0·0257
FOX *et al.* (1958a)	93·2	44·3	Cylinder	4·8	38·1	0·0308	6·8	—	0·0257
FOX *et al.* (1958a)	93·2	44·3	Cylinder	38·7	8·3	0·0283	—	9·2	0·0257
BECK *et al.* (1949)	93·2	29·9	Cylinder	20·7	10·2	0·0278	—	12·1	0·0241
FOX *et al.* (1958a)	93·2	27·1	Cylinder	6·3	29†	0·0285	8·6	—	0·0238
FOX *et al.* (1958a)	93·2	27·1	Cylinder	5·0	38·1	0·0302	7·7	—	0·0238
FOX *et al.* (1958a)	93·2	27·1	Cylinder	7·7	19·1	0·0295	11·4	—	0·0238
FOX *et al.* (1958a)	93·2	27·1	Cylinder	12·4	12·7	0·0291	—	17·5	0·0238
FOX *et al.* (1958a)	93·2	27·1	Cylinder	89·3	7·6	0·0281	—	8·9	0·0238
BECK *et al.* (1949)	93·2	26·2	Cylinder	21·5	10·2	0·0274	—	12·1	0·0237
BECK *et al.* (1949)	93·2	26·2	Cylinder	44·5	8·3	0·0276	—	9·6	0·0237
BLIZARD *et al.* (1958)	93·2	1270	Sphere	—	27·9	0·0081	—	28·1	0·0080
BLIZARD *et al.* (1956)	93·2	524	Sphere	—	16·0	0·0186	—	15·8	0·0190
BLIZARD *et al.* (1956)	93·2	269·8	Sphere	—	13·2	0·0241	—	13·2	0·0242
BLIZARD *et al.* (1958)	93·2	126·5	Sphere	—	11·8	0·0279	—	12·1	0·0270
BLIZARD *et al.* (1958)	93·2	76·1	Sphere	—	11·5	0·0288	—	12·0	0·0273
BLIZARD *et al.* (1956)	93·2	49·9	Sphere	—	11·5	0·0288	—	12·4	0·0262
BLIZARD *et al.* (1956)	93·2	35·8	Sphere	—	11·5	0·0288	—	13·0	0·0247
FOX *et al.* (1958b)	93·2	44·7–51·5	Slab	4·5	—	0·0288	5·5	—	0·026
BLIZARD *et al.* (1955)	4·9	1113	Sphere	—	34·6	0·0057	—	32·9	0·0062
HENRY *et al.* (1959)	4·9	530	Cylinder	44·7	19·1	0·0114	—	17·4	0·0123
HENRY *et al.* (1959)	4·9	530	Cylinder	25·4	25·4	0·0119	24·1	—	0·0123
BLIZARD *et al.* (1958)	2·0	294‡	Cylinder	122	25	0·0062	—	24	0·0065
BLIZARD *et al.* (1958)	2·0	294‡	Cylinder	58	30	0·0061	—	29	0·0065
BLIZARD *et al.* (1958)	2·0	294‡	Cylinder	46	36	0·0059	—	32	0·0065
BLIZARD *et al.* (1958)	2·0	294‡	Cylinder	38	41	0·0062	36	—	0·0065
BLIZARD *et al.* (1958)	2·0	294‡	Cylinder	33	55	0·0060	30	—	0·0065
BLIZARD *et al.* (1958)	2·0	294‡	Cylinder	30	64	0·0063	29	—	0·0065
BLIZARD *et al.* (1958)	2·0	195‡	Cylinder	122	30	0·0048	—	28	0·0052
BLIZARD *et al.* (1958)	2·0	195‡	Cylinder	64	37	0·0046	—	33	0·0052
BLIZARD *et al.* (1958)	2·0	195‡	Cylinder	58	41	0·0044	—	35	0·0052
BLIZARD *et al.* (1958)	2·0	195‡	Cylinder	48	47	0·0046	42	—	0·0052
BLIZARD *et al.* (1958)	2·0	195‡	Cylinder	43	56	0·0045	37	—	0·0052

* Computed from experimental size with reflector savings = 7 cm.
† Equivalent cylindrical radius. Cross-section is 20 × 20 inch square.
‡ All 2 per cent enriched experiments were moderated and reflected with paraffin.

VOL 14 196

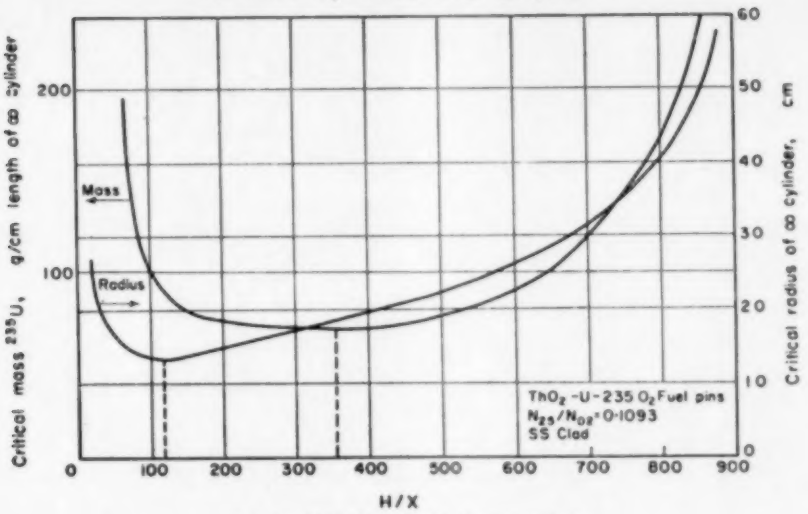

FIG. 8.—Variation of critical mass and size.

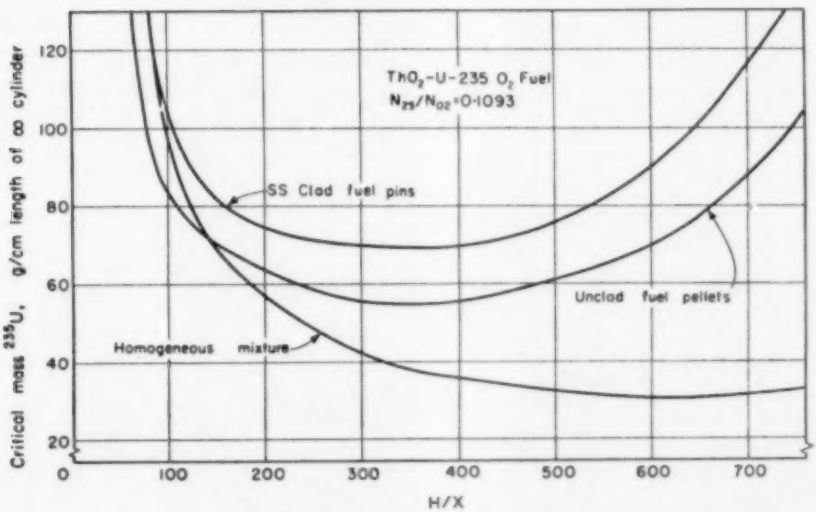

FIG. 9.—Effect of fuel form on critical mass.

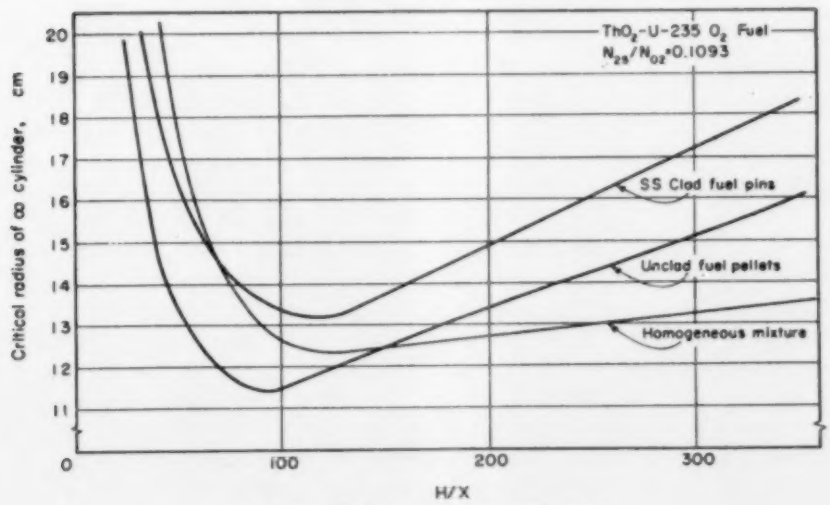

FIG. 10.—Effect of fuel form on critical size.

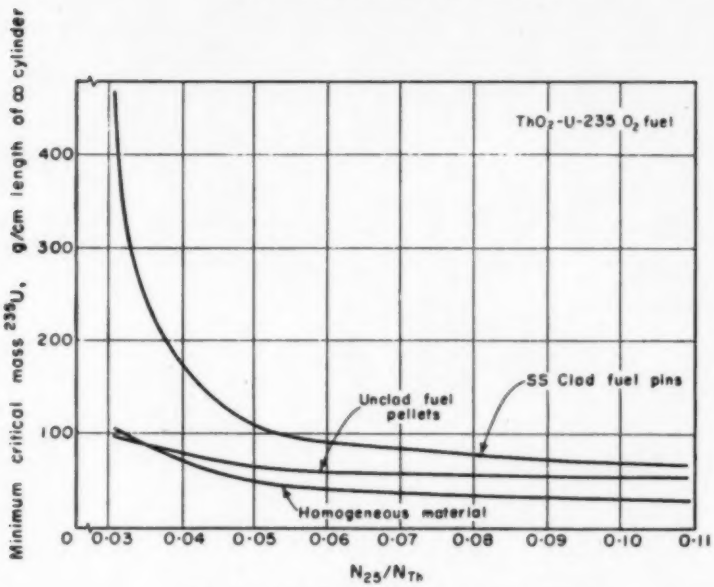

FIG. 11.—Minimum critical mass per unit length.

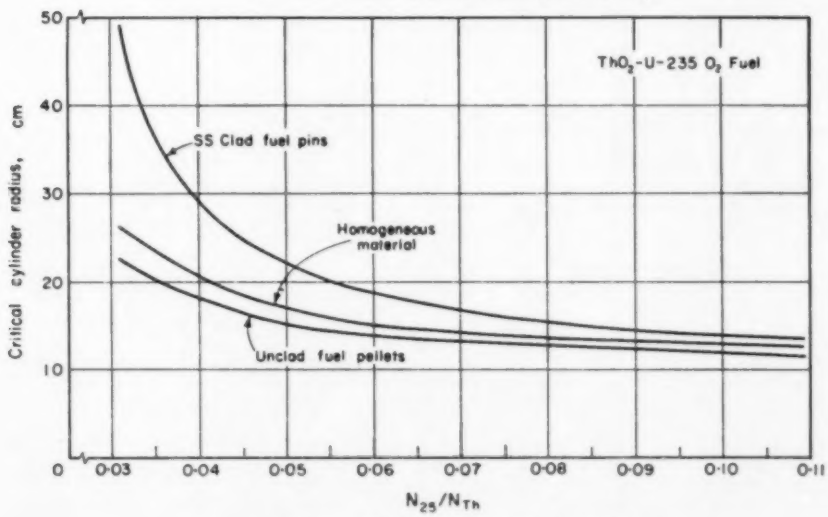

FIG. 12.—Minimum critical cylinder radius.

that shown in the figures, and is also true of low-enriched uranium systems.

The minimum critical mass and cylinder radius are plotted in Figs. 11 and 12 as functions of effective enrichment (N_{25}/N_{02}). At all N_{25}/N_{02} the value of cylinder radius is less for lumped material than for homogeneous material, and for N_{25}/N_{02} less than 0·035 the minimum critical mass of the lumped system is less than for the homogeneous case. These effects are also true for low-enriched uranium, so that careful analysis is needed to determine whether the safety limits of a process should be based on lumped or homogeneous material. The other minimum critical values for values of N_{25}/N_{02} up to 0·10 are listed in Table 5.

In order to operate a process line safely it is necessary to know more than the calculated minimum critical conditions. Estimates of the uncertainties in the basic critical data and in the theoretical model must be made, and these coupled with the additional operating safe requirements to give an overall safety factor. The critical measurements were all of cylinder radius and it is estimated that no more than 1 per cent error has been made in these data. The fit of these data with the model is good to 1 per cent for stainless steel clad and 2 per cent for aluminium clad (see Table 2). Thus it is estimated that the cylinder radius extrapolation to stainless steel clad fuel pins at other enrichments should be good to about 2½ per cent. Extrapolation to homogeneous cases is estimated to have twice this

TABLE 5.—CALCULATED MINIMUM CRITICAL PARAMETERS FOR UO_2–ThO–H_2O

N_{25}/N_{Th}	Form	Mass ^{235}U (g)		∞ Cylinder radius (cm)		∞ Slab thickness (cm)		Sphere volume (L)		Mass ^{235}U/unit length in an ∞ cylinder (g/cm)	
		Minimum critical	Safe value	Minimum critical	Safe value	Minimum critical	Safe value	Minimum critical	Safe value	Minimum critical	Safe value
0·031	Homogeneous	10,526	4,160	26·23	22·71	28·77	22·13	206·93	127·73	105·89	41·85
	Pellets*	8,831	3,345	22·32	18·45	23·61	17·11	132·26	67·83	101·42	36·75
	Fuel pins (SS clad)†	78,671	32,644	49·38	43·70	58·95	46·79	1,257·28	838·19	468·12	191·85
0·045	Homogeneous	4,609	1,822	18·32	15·86	18·44	14·18	76·50	47·22	58·98	23·31
	Pellets*	4,979	1,886	16·38	13·54	15·84	11·48	56·78	29·12	70·28	25·46
	Fuel pins (SS clad)†	12,161	5,046	24·27	21·48	26·16	20·76	166·92	111·28	131·56	53·92
0·062	Homogeneous	3,043	1,203	15·26	13·21	14·44	11·11	46·26	28·56	43·81	17·32
	Pellets*	3,932	1,489	13·85	11·45	12·55	9·09	36·24	18·58	60·55	21·94
	Fuel pins (SS clad)†	6,848	2,841	18·18	16·09	18·20	14·44	75·32	50·21	90·54	37·11
0·085	Homogeneous	2,240	885	13·35	11·56	11·96	9·20	31·97	19·73	35·41	14·00
	Pellets*	3,438	1,302	12·22	10·10	10·45	7·57	26·03	13·35	55·69	20·18
	Fuel pins (SS clad)†	5,001	2,075	14·79	13·09	13·77	10·93	43·24	28·83	75·00	30·74
0·109	Homogeneous	1,885	745	12·41	10·74	10·78	8·29	26·06	16·09	31·35	12·39
	Pellets*	3,265	1,237	11·42	9·44	9·42	6·83	21·85	11·21	55·16	19·99
	Fuel pins (SS clad)†	4,423	1,835	13·23	11·71	11·74	9·32	32·20	21·47	69·08	28·31

* Calculated for cylindrical pellets, density 9·25 g/cm³, radius 0·330 cm.
† Calculated for cylindrical fuel pins containing pellets inside SS tube with wall thickness 0·052 cm and outside radius 0·386 cm.

uncertainty (5 per cent) and, because unclad fuel pellets are more reactive, this extrapolation is estimated to have twice again the uncertainty (10 per cent). Estimated uncertainties in extrapolating to other geometries and masses range from 5 per cent to 50 per cent, all chosen to be reasonably accurate on the conservative side. These uncertainty factors (ranging from 1·025 to 1·50) are then multiplied by operating safety figures of 1·10 for dimensional control, 1·30 for volume control, and 2·30 for mass control. The resulting composite safety factors were used to compute the safe values listed in Table 5. These safe values are the maximum safe single units of mixtures of ThO_2, water and fully-enriched UO_2.

REFERENCES

ANDERSON R. C. *et al.* (1960) *Thorium-Uranium Physics Experiments-Final Report*. BAW-1191.

ARNOLD W. H. JR. (1959) *Trans. Amer. Nucl. Soc.* **2**, No. 2, 38.

BECK C. K. *et al.* (1949) *Critical Mass Studies*, Part III. K-343.

BELL G. I. (1959) *Nucl. Sci. Engng.* **5**, 138.

BLIZARD E. P. *et al.* (1955) *Physics Division Semiannual Progress Report*. ORNL-1926.

BLIZARD E. P. *et al.* (1956) *Applied Nuclear Physics Division Annual Report*. ORNL-2081.

BLIZARD E. P. *et al.* (1958) *Neutron Physics Division Annual Progress Report*. ORNL-2609.

DAVISON P. W. *et al.* (1959) *Yankee Critical Experiments*. Report YAEC-94.

DRESNER L. (1956). *Nucl. Sci. Engng.* **1**, 68.

EDLUND M. C. *et al.* (1958) *Proceedings of the Second International Conference on the Peaceful Uses of Atomic Energy, Geneva*, **13**, 482–491, Paper P/2405, United Nations, N.Y.

FOX J. K. *et al.* (1958a) *Critical Mass Studies*, Part IX. ORNL-2367.

FOX J. K. *et al.* (1958b) *Nucl. Sci. Engng.* **3**, 694.

HELLSTRAND E. (1957) *J. appl. Phys.* **28**, 1493.

HENRY H. F. *et al.* (1959) *Critically Data and Nuclear Safety Guide Applicable to the Oak Ridge Gaseous Diffusion Plant*. K-1019.

HUGHES D. J. and SCHWARTZ R. B. (1958) *Neutron Cross-Sections*, (2nd Edn.) BNL-325.

KLEIN D. *et al.* (1958) *Nucl. Sci. Engng.* **3**, 403.

KOUTS H. *et al.* (1958) *Proceedings of the Second International Conference on the Peaceful Uses of Atomic Energy, Geneva*, **12**, P/1841 446–482. United Nations, N.Y.

LLOYD R. C., SMITH R. B. and CLAYTON E. D. (1959) *Trans. Amer. Nucl. Soc.* **2**, No. 1, 62.

MACKINNEY A. L. and BALL R. M. (1960) *Trans. Amer. Nucl. Soc.* **3**, No. 1.

PETTUS W. G. (1959) *Geometric and Temperature Effects in Thorium Resonance Capture*. BAW-TM-203.

SNIDOW N. L. Private communication.

Reactor Science and Technology (J.N.E. Parts A/B), 1961, Vol. 14, pp. 200 to 208. Pergamon Press Ltd. Printed in Northern Ireland

RESONANCE ABSORPTION IN ^{239}Pu AND ITS EFFECT ON THE TEMPERATURE COEFFICIENT OF IRRADIATED URANIUM RODS

M. H. McKay
Atomic Energy Division, The General Electric Company Ltd., Erith, Kent*

(*Received* 13 *October* 1960)

Abstract—The effective resonance integral for both fission and radiative capture is first calculated for different-sized rods of pure ^{239}Pu at various temperatures in a graphite-moderated lattice. Then the contribution from ^{239}Pu to the effective resonance integral of irradiated uranium rods in a graphite moderator is evaluated for the same rod sizes and temperatures, concentrations of 0·15 per cent and 0·2 per cent ^{239}Pu being considered in turn. The fuel temperature coefficient is estimated at both concentrations and compared to the temperature coefficient of the same rods at zero irradiation. The fractional change in fuel temperature coefficient due to ^{239}Pu build-up is found to be small, in the absence of any allowance for neutron spectrum distortion in the region of the lowest ^{239}Pu resonance, due to neutron thermalization.

1. INTRODUCTION

Resonance absorption by ^{239}Pu is of interest when considering the possibility of intermediate or thermal reactors using plutonium as a fuel, either separately or mixed with uranium, and also when considering the effects of irradiated fuel rods on the reactivity of a uranium-fuelled reactor. There are three main differences from the usual treatment of resonance absorption in ^{232}Th and ^{238}U which have to be taken into account when considering ^{239}Pu.

(i) Account has to be taken of resonance fission as well as of radiative capture, so that, in addition to the resonance escape probability, one has to calculate the probability of a neutron causing resonance fission while slowing down. Moreover, fission interference may distort the normal Breit-Wigner resonance contours to a certain extent.

(ii) Since the spin of the target nucleus is not zero but equal to $\frac{1}{2}$, the statistical spin factor (g) in the Breit-Wigner formulae for the cross-sections is not unity for s-wave resonances, and so can not be neglected as in the case of the even-even nuclei. In the case of ^{239}Pu, g may be either $\frac{1}{2}$ or $\frac{3}{2}$ for reaction with neutrons of zero orbital angular momentum.

(iii) The resonances of ^{239}Pu are comparatively close together, with an average spacing of about 1·8 eV, so that the experimental resolution is not so definite as for ^{232}Th and ^{238}U, nor does it cover such a large range of neutron energies. This means that, in the case of pure ^{239}Pu, a major contribution to the resonance absorption may be expected from the unresolved resonances and practically all of the Doppler effect due to increasing temperature may be expected to occur in the unresolved region. Further, there is more mutual interference between adjacent resonances than there is when resonances are more widely spaced.

Because of these differences, one would not expect results obtained by the application of the usual theory to have the accuracy which may be claimed in the cases of ^{232}Th and ^{238}U. However, an attempt has been made in this paper to apply the theory with some modifications to obtain approximate results, which should give a useful indication of the amount of resonance fission and radiative capture in ^{239}Pu, both in pure form and in concentrations such as are likely to occur in irradiated uranium rods.

The model considered is a fuel rod immersed in a graphite moderator in which the neutron flux is considered to be uniform and isotropic, the rod consisting firstly of pure ^{239}Pu and then of two different homogeneous mixtures in turn of ^{239}Pu and natural uranium, containing 0·15 per cent and 0·2 per cent ^{239}Pu respectively. These concentrations correspond to natural uranium with an irradiation of the order of 3000 MWD/Tonne. The contribution from ^{239}Pu resonances to the effective resonance integral, including both fission and radiative capture, is calculated in each case for three different sized rods at five different temperatures, using the tables of Adler *et al.* (1958), extended where necessary. Interference between neighbouring resonances is neglected, as also is fission interference and interference between potential and resonance scattering. The contribution from the 0·3 eV resonance is not included in the main calculations, but approximate results for this resonance are given separately. The latter results are considerably less

* Attached during 1960, on leave from the University of New South Wales, Australia.

VOL
14
196

reliable than the others since there are other factors which need to be taken into account at energies so close to thermal.

The ^{239}Pu resonance escape probability is then evaluated in each case and hence the probability of absorption in each of the ^{239}Pu resolved resonances and in the whole unresolved region is evaluated. Multiplying each of the resolved absorption probabilities by the appropriate value of $1/(1 + \alpha_r)$ and the unresolved by $1/(1 + \bar{\alpha})$, where α_r is the ratio of radiative captures to fissions at resonance energy E_r and $\bar{\alpha}$ is the average value of α over the unresolved region, we obtain the fission probabilities for resolved and unresolved resonances respectively. From these probabilities the total resonance fission probability is calculated, and application of the appropriate value of ν, the average number of fast neutrons produced per fission, gives the number of second generation fast neutrons produced through resonance fission. From this we obtain what may be called the 'resonance fission increment' which should be added to the usual formula to calculate the effective reproduction constant (k_ϵ) for a reactor. Comparison of the temperature variation of the modified k_ϵ in the case of irradiated rods with that of the original k_ϵ at zero irradiation gives an indication of the effect of ^{239}Pu resonances on the fuel temperature coefficient of a reactor at different irradiation levels.

2. THEORETICAL BACKGROUND

2.1 *The narrow resonance approximation*

Let N_i be the number of atoms of the ith nuclear species present in 1 cm^3 of the fuel and let σ_{ai}, σ_{si} and σ_{pi} be respectively the microscopic resonance absorption, resonance scattering and potential scattering cross-sections of the ith nuclear species. In particular, let $i = 8$ for ^{238}U and $i = 9$ for ^{239}Pu.

Now, if we write

$$N = \sum_i N_i, \tag{1}$$

we have, for the macroscopic resonance absorption, resonance scattering and potential scattering cross-sections of the fuel,

$$N\sigma_a = \sum_i N_i\sigma_{ai}, \tag{2}$$

$$N\sigma_s = \sum_i N_i\sigma_{si} \tag{3}$$

and

$$N\sigma_p = \sum_i N_i\sigma_{pi}. \tag{4}$$

Hence, assuming that the resonances are narrow and widely spaced compared to the average energy loss of a neutron on collision with a nucleus, the effective resonance integral of a heterogeneous lattice of fuel elements, each consisting of a homogeneous mixture of uranium and plutonium, is given by the expression originally derived by WIGNER *et al.* (1955), namely

$$I = \int_{E_L}^{E_U} \frac{\sigma_a\sigma_p}{\sigma_a + \sigma_s + \sigma_p}\frac{dE}{E} + \frac{1}{N\bar{l}}\int_{E_L}^{E_U} \frac{\sigma_a(\sigma_a + \sigma_s)}{(\sigma_a + \sigma_s + \sigma_p)^2} G_0 \frac{dE}{E}. \tag{5}$$

Here E_L and E_U are respectively the lower and upper energy limits of the resonance region, $\bar{l}$ is the average length of a chord through a fuel element and G_0 is the probability that a neutron impinging on the fuel with energy E will have a collision before leaving the fuel. Thus we may write

$$G_0(E) = \int\{1 - \exp[-N\sigma(E)l]\}f(l)dl, \tag{6}$$

where $\sigma(E)$ is the total microscopic cross-section of the fuel ($= \sigma_a + \sigma_s + \sigma_p$), $f(l)$ is the distribution function for path lengths through a fuel element of neutrons traversing it without collision and the integration is over all such paths.

From equation (6) it may be seen that

$$G_0 = N\sigma\bar{l}P_0(N\sigma\bar{l}), \tag{7}$$

where P_0 is the escape probability considered by CASE, DE HOFFMAN and PLACZEK (1953) and may be evaluated from their tables.

Assuming no overlapping of resonances of the different isotopes, we may put all the σ_{ai} and σ_{si} except σ_{a9} and σ_{s9} equal to zero in the vicinity of each ^{239}Pu resonance, so that the contribution to the effective resonance integral from the plutonium resonances may be written in the form of equation (5), where now

$$\sigma_a = N_9\sigma_{a9}/N \tag{8}$$

and

$$\sigma_s = N_9\sigma_{s9}/N. \tag{9}$$

It will be noticed that, on this assumption, the total effective resonance integral of ^{239}Pu is independent of resonance absorption in ^{238}U.

If the resonances are assumed to be of Doppler-broadened Breit-Wigner form, we have, for a ^{239}Pu resonance at neutron energy E_r,

$$\sigma_a \simeq \frac{N_9(\Gamma_\gamma + \Gamma_f)}{N\Gamma}\sigma_0\psi(x, \theta) \tag{10}$$

and

$$\sigma_s \simeq \frac{N_9\Gamma_n}{N\Gamma}\sigma_0\psi(x, \theta), \tag{11}$$

where σ_0 is the total microscopic cross-section of ^{239}Pu both for resonance scattering and absorption at exact

resonance energy; Γ_γ, Γ_f and Γ_n are respectively the radiation, fission and neutron widths of the resonance, Γ is the total width ($= \Gamma_\gamma + \Gamma_f + \Gamma_n$) and

$$\psi(x, \theta) = (4\pi\theta)^{-\frac{1}{2}} \int_{-\infty}^{\infty} \exp\left\{\frac{-(x-y)^2}{4\theta}\right\} \frac{dy}{1+y^2}. \quad (12)$$

Here
$$x = 2(E - E_r)/\Gamma \quad (13)$$

and
$$\theta = 4kTE_r/A\Gamma^2, \quad (14)$$

where A is the mass number of a plutonium atom, k is Boltzmann's constant and T is the temperature on the Kelvin scale.

The peak resonance cross-section, σ_0, may be expressed in the form

$$\sigma_0 = \frac{g\hbar^2\Gamma_n}{2\pi m E_r \Gamma}, \quad (15)$$

where h is Planck's constant, m is neutron mass and g is the statistical spin factor given by

$$g = \frac{2J+1}{2(2I+1)}, \quad (16)$$

I being the spin of the target nucleus and J the spin of the compound nucleus. In the case of neutrons with zero orbital angular momentum,

$$J = I \pm \tfrac{1}{2}. \quad (17)$$

Hence, for the contribution to the effective resonance integral from a single ^{239}Pu resonance at energy E_r we have

$$I_{r0} = \frac{\sigma_p(\Gamma_\gamma + \Gamma_f)}{E_r}\left\{J(0, \beta) + \frac{1}{\beta} L(t, 0, \beta)\right\}, \quad (18)$$

where
$$\beta = N\sigma_p/N_0\sigma_0, \quad (19)$$

$$t = N\sigma_p\bar{l}, \quad (20)$$

$$J(0, \beta) = \int_0^\infty \frac{\psi(x, 0)}{\psi(x, 0) + \beta}\, dx \quad (21)$$

and

$$L(t, 0, \beta) = \int_0^\infty \frac{[\psi(x, 0)]^2}{\psi(x, 0) + \beta} P_0\left\{\frac{\psi(x, \theta) + \beta}{\beta} t\right\} dx. \quad (22)$$

The function J has been tabulated by DRESNER (1956) and by ADLER *et al.* (1958) for different values of θ and β, and the function L has also been tabulated by the latter. Thus, within the range of parameters covered by the tables, approximate values of I_{r0} may be obtained for each narrow resonance by interpolation of the tables.

2.2 *The rational approximation*

If we use the approximation

$$G_0 \approx 1 - e^{-N\sigma\bar{l}} \approx \frac{N\sigma\bar{l}}{1 + N\sigma\bar{l}}, \quad (23)$$

equation (5) may be reduced to

$$I = \int_{E_L}^{E_U} \frac{\sigma_a\sigma_m}{\sigma_a + \sigma_s + \sigma_m} \frac{dE}{E}, \quad (24)$$

where
$$\sigma_m = \sigma_p + 1/N\bar{l}. \quad (25)$$

Thus the heterogeneous lattice is effectively reduced, as far as resonance absorption is concerned, to equivalence with a homogeneous system. The error involved in this approximation has been investigated by MCKAY and KEANE (1960), who have given tables and a graph from which appropriate corrections can be made.

Hence equation (18) is replaced by

$$I_{r0} = \frac{\sigma_m(\Gamma_\gamma + \Gamma_f)}{E_r} J(\theta, \beta_m), \quad (26)$$

where
$$\beta_m = N\sigma_m/N_0\sigma_0. \quad (27)$$

2.3 *The infinite-mass-absorber approximation*

If the practical width* of a resonance exceeds the average energy loss of a neutron on collision with an absorber nucleus, but is still narrow compared to the average energy loss on collision with a moderator nucleus, it is better to use the narrow-resonance-infinite-absorber (N.R.I.A.) approximation in which scattering by absorber nuclei is neglected. This is essentially the same approach as that used by GUREVICH and POMERANCHOUK (1955) for all resonances.

In this case, provided no moderator is mixed with the absorber, equation (5) becomes

$$I = \frac{1}{N\bar{l}}\int_{E_L}^{E_U} G_0 \frac{dE}{E} = \int_{E_L}^{E_U} \sigma P_0(N\sigma\bar{l}) \frac{dE}{E}. \quad (28)$$

Thus the contribution from a 'wide' resonance at energy E_r to the effective resonance integral for pure ^{239}Pu rods isolated within a moderator is approximately given by

$$I_{r0} = \frac{\sigma_0(\Gamma_\gamma + \Gamma_f)}{E_r} L'(t_a, 0), \quad (29)$$

where
$$t_a = N\bar{l}\sigma_a(E_r) \quad (30)$$

and

$$L'(t_a, 0) = \int_0^\infty \psi(x, 0) P_0\{t_a\psi(x, 0)\}\, dx. \quad (31)$$

The function L' has also been tabulated by ADLER *et al.* (1958) for various values of t_a and θ.

* The practical width of a resonance is defined as the energy range for which the resonance cross-section exceeds the potential scattering cross-section of the fuel per absorber atom.

3. EXPERIMENTAL DATA

The ^{239}Pu resonance data used in the calculations are, in the main, those given by HUGHES *et al.* (1960) up to 52·6 eV. Exceptions, obtained by comparing the results of EGELSTAFF *et al.* (1958), SOKOLOVSKY *et al.* (1957) and FARLEY (1956) with those of BOLLINGER *et al.* (1958), are listed in Table 1. Values used for the spin factor, g, are those suggested by BOLLINGER *et al.* (1958), except that the average value, $\frac{1}{2}$, is replaced by 0·625 in view of the likelihood that there are about three times as many resonances with $g = \frac{3}{4}$ as with $g = \frac{1}{4}$ (EGELSTAFF *et al.*, 1958).

TABLE 1.—RESONANCE DATA
(Where different from those given by HUGHES *et al.*, 1960)

E_r (eV)	Γ_γ(mV)	Γ_f (mV)	$2g\Gamma'_n$ (mV)
10·95	32	115	3·34
14·3	40	79	0·64
14·7	37	33	2·7
19·2	37	22	0·25
22·3	35	61	4·0
29·9	37	10	0·4
38·5	37	40	0·6

The average values used for the unresolved resonances and the values used for the potential scattering cross-section, σ_p, and the average neutron yield per fission, ν, are set out in Table 2. Here $\overline{\Gamma}_\gamma$, $\overline{\Gamma}_f$ and $\overline{\Gamma^0_n}$ are respectively the average radiative, fission and reduced neutron widths, and $\bar{D}$ is the average level spacing. The subscripts 1 and 3 respectively refer to those unresolved resonances with spin factor $g = \frac{1}{4}$ and $g = \frac{3}{4}$.

TABLE 2.—AVERAGE PARAMETERS

$\overline{\Gamma}_\gamma = 37$ mV
$\overline{\Gamma}_f = 46$ mV

$\overline{\Gamma^0_{n1}} = 0{\cdot}7$ mV $\qquad$ $\overline{\Gamma^0_{n3}} = 0{\cdot}2$ mV
$\bar{D}_1 = 7{\cdot}2$ eV $\qquad$ $\bar{D}_3 = 2{\cdot}4$ eV
$\bar{\alpha} = 0{\cdot}8043$
$\sigma_p = 11$ barns
$\nu = 2{\cdot}92$

4. TOTAL RESONANCE ABSORPTION

4.1 *Resolved resonances*

In the case of pure ^{239}Pu rods, $N = N_9$, so that several of the equations of Section 2 are slightly simplified. In only two of the resolved resonances as specified in Table 1 is the practical width less than the average neutron loss on collision with an absorber nucleus. For these resonances, at 27·3 eV and 35·3 eV, the narrow resonance approximation has been used, I_{r9} being evaluated from (18) by using the tables of ADLER *et al.* (1958). The contribution to the effective resonance integral from each of the other resolved resonances has been evaluated by the use of equation (29). The tables of ADLER *et al.* have again been used where possible, but, as they did not cover the full range required in many cases, especially for the smaller rods, additional values of L' had to be computed.

However, in the case of very small concentrations of ^{239}Pu in uranium, the infinite-mass-absorber approximation does not apply, since account must be taken of scattering by the uranium nuclei. Indeed, because of the presence of such a large amount of uranium compared to the plutonium, the potential scattering cross-section of the fuel per atom of ^{239}Pu is so high that, by the usual definition, the practical width of nearly all of the ^{239}Pu resonances is equal to zero. Thus the concept of practical width as a criterion for specifying the narrowness of a resonance appears to break down for cases like this. Nevertheless, it remains true that the effective absorption cross-section of the ^{239}Pu is negligible outside an energy range on each side of exact resonance energy equal to half the average energy decrement of a neutron on collision with a plutonium nucleus. It seems appropriate, therefore, that the narrow-resonance approximation should be used in this case for all ^{239}Pu resonances.

4.2 *Unresolved resonances*

The following approximations have been made in evaluating the contribution to the effective resonance integral from the unresolved resonances of ^{239}Pu.

(i) The resonances have all been considered to be narrow compared to the neutron energy loss on collision with a plutonium nucleus. This would, in fact,be true in the case of small concentrations and also for the vast majority of the unresolved resonances in the case of pure ^{239}Pu.

(ii) The effective resonance integral (5) has been reduced to equivalence with a homogeneous case (24) by the use of the rational approximation (23).

(iii) Only s-wave contributions have been taken into account, so that the spin factor, g, of equation (16) has been taken as either $\frac{1}{4}$ or $\frac{3}{4}$ according as to whether the compound nucleus spin, J, is 0 or 1.

(iv) The statistical fluctuations of the reduced neutron width, the fission width and the level spacings have not been taken into account, the average values being used as set out in Table 2.

It is expected that the positive error caused by (iv) will be balanced to a considerable extent by negative errors caused by (ii) and (iii) and also by the neglect of interference effects. Thus the total contribution from

TABLE 3.—CONTRIBUTIONS TO THE EFFECTIVE RESONANCE INTEGRAL

(a) 0·15% ^{239}Pu

Rod radius (cm)		Temperature (°K)				
		0	300	600	900	1200
0·71	Resolved	0·354b	0·364b	0·367b	0·369b	0·370b
	Unresolved	0·130	0·131	0·132	0·132	0·132
	Total	0·484	0·495	0·499	0·501	0·502
1·46	Resolved	0·341	0·353	0·357	0·359	0·361
	Unresolved	0·123	0·124	0·124	0·124	0·124
	Total	0·464	0·477	0·481	0·483	0·485
2·21	Resolved	0·335	0·349	0·353	0·355	0·357
	Unresolved	0·120	0·121	0·121	0·121	0·121
	Total	0·455	0·470	0·474	0·476	0·478

(b) 0·2% ^{239}Pu

0·71	Resolved	0·459b	0·473b	0·477b	0·480b	0·482b
	Unresolved	0·169	0·172	0·172	0·172	0·172
	Total	0·628	0·645	0·649	0·652	0·654
1·46	Resolved	0·442	0·460	0·466	0·470	0·472
	Unresolved	0·158	0·160	0·160	0·160	0·160
	Total	0·600	0·620	0·626	0·630	0·632
2·21	Resolved	0·434	0·452	0·458	0·462	0·465
	Unresolved	0·155	0·157	0·157	0·157	0·157
	Total	0·589	0·609	0·615	0·619	0·622

(c) Pure ^{239}Pu

0·71	Resolved	24·4b	25·1b	25·6b	26·0b	26·3b
	Unresolved	24·8	37·4	41·1	43·4	45·1
	Total	49·2	62·5	66·7	69·4	71·4
1·46	Resolved	17·0	17·3	17·5	17·7	17·8
	Unresolved	21·3	32·6	36·0	38·3	39·9
	Total	38·3	49·9	53·5	56·0	57·7
2·21	Resolved	13·7	13·9	14·1	14·2	14·3
	Unresolved	19·9	30·7	34·0	36·2	37·9
	Total	33·6	44·6	48·1	50·4	52·2

VOL
14
196

the unresolved resonances to the effective resonance integral is approximately given by

$$I_{u9} = \frac{\sigma_m(\Gamma_\gamma + \Gamma_f)}{\bar{D}_1}\int_{E_R}^{E_U}[J(\theta, \beta_m)]_1 \frac{dE}{E} + \frac{\sigma_m(\Gamma_\gamma + \Gamma_f)}{\bar{D}_3}\int_{E_R}^{E_U}[J(\theta, \beta_m)]_3 \frac{dE}{E}, \quad (32)$$

where E_R is the energy above which resonances must be considered unresolved, σ_m is defined by (25) and the subscripts 1 and 3 refer respectively to resonances with spin factor $g = \frac{1}{4}$ and $g = \frac{3}{4}$.

4.3 *Results (excluding the 0·3 eV resonance)*

In Table 3 are set out the contributions to the total effective resonance integral of the fuel from 0·15 per cent ^{239}Pu, from 0·2 per cent ^{239}Pu and from pure ^{239}Pu. In each case the contribution from the 0·3 eV resonance is excluded. It will be observed that, in the case of 0·15 per cent ^{239}Pu in the smallest rod at temperatures above 600°K, the calculated contributions to the effective resonance integral per ^{239}Pu atom exceed the infinite dilution resonance integral as given in Section 8 by up to 1 per cent. This is due to the fact that values obtained from interpolation of the J-tables appear to be consistently a few per cent too high. This error would tend to exaggerate any effect on the fuel temperature coefficient due to the presence of ^{239}Pu, but, in fact, any allowance made to compensate for it would not lead to any significant change in the values recorded in Table 8.

5. RESONANCE ESCAPE PROBABILITIES

The probability of escaping resonance absorption in ^{239}Pu, either radiative or fission-causing, is determined by using the relation

$$p_9 = \exp\left(-\frac{V_F N}{V_M \bar{\xi}\Sigma_M} I_9\right), \quad (33)$$

where V_F/V_M is the volume ratio of fuel to moderator and $\bar{\xi}\Sigma_M$ is the slowing down power of the moderator. Taking V_F/V_M as 0·02 and $\bar{\xi}\Sigma_M$ as 0·0631 for graphite, we find values of p_9 for the different cases considered (again excluding the 0·3 eV resonance) as given in Table 4. The results for pure ^{239}Pu are academic only, since the moderating conditions specified here would not be at all appropriate in the hypothetical case of ^{239}Pu being used as fuel in pure form.

In the case of irradiated uranium rods, if we ignore resonance absorption in ^{235}U and other isotopes present in small abundance, the overall resonance escape probability is given by the product $p_8 p_9$ where p_8 is the probability of escaping resonance absorption in ^{238}U. Values of this product, based on an evaluation of the ^{238}U effective resonance integral by SCHAEFER (1960), are given in Table 5 for the two irradiation levels considered.

TABLE 4.—^{239}Pu RESONANCE ESCAPE PROBABILITIES

Rod radius (cm)	Temperature (°K)				
	0	300	600	900	1200
(a) 0·15% ^{239}Pu					
0·71	0·99274	0·99258	0·99252	0·99249	0·99247
1·46	0·99306	0·99285	0·99279	0·99276	0·99273
2·21	0·99317	0·99295	0·99289	0·99286	0·99283
(b) 0·2% ^{239}Pu					
0·71	0·99059	0·99034	0·99028	0·99024	0·99021
1·46	0·99102	0·99071	0·99062	0·99056	0·99053
2·21	0·99118	0·99088	0·99079	0·99073	0·99069
(c) Pure ^{239}Pu					
0·71	0·469	0·382	0·359	0·344	0·333
1·46	0·556	0·464	0·439	0·423	0·411
2·21	0·597	0·503	0·477	0·461	0·449

TABLE 5.—OVERALL RESONANCE ESCAPE PROBABILITIES

Rod radius (cm)	Temperature (°K)				
	0	300	600	900	1200
(a) 0·15% ^{239}Pu					
0·71	0·84166	0·81741	0·81081	0·80580	0·80161
1·46	0·87329	0·85533	0·85002	0·84597	0·84258
2·21	0·88782	0·87224	0·86753	0·86393	0·86091
(b) 0·2% ^{239}Pu					
0·71	0·83984	0·81557	0·80898	0·80397	0·79978
1·46	0·87150	0·85349	0·84816	0·84410	0·84072
2·21	0·88604	0·87042	0·86570	0·86208	0·85904

6. RESONANCE FISSION PROBABILITY

The probability that a fission neutron will cause fission while solving down through a ^{239}Pu resonance at energy E_r in the resolved region is given by

$$P_{fr} = \frac{1 - p_r}{1 + \alpha_r} p_u \prod_i p_i, \quad (34)$$

where p_r, p_u and p_i are respectively the resonance escape probabilities for the given resonance, the unresolved resonances and the resolved resonances at energies higher than E_r.

Hence the total probability of fission while slowing down through the resonance region is given by

$$P_f = P_{fu} + \sum_r P_{fr}, \quad (35)$$

where p_{fu} is the probability of fission in the unresolved region and may be taken as

$$P_{fu} = \frac{1 - p_{u9}}{1 + \bar{\alpha}}, \tag{36}$$

where p_{u9} is the probability of escaping absorption in ^{239}Pu in the unresolved region. Values of P_f for the cases considered are given in Table 6. As in the case of resonance escape probabilities, values given for pure ^{239}Pu are academic only.

TABLE 6.—RESONANCE FISSION PROBABILITIES

Rod radius (cm)	Temperature (°K)				
	0	300	600	900	1200
(a) 0·15% ^{239}Pu					
0·71	0·00387	0·00390	0·00392	0·00392	0·00392
1·46	0·00374	0·00380	0·00382	0·00383	0·00383
2·21	0·00370	0·00377	0·00379	0·00381	0·00381
(b) 0·2% ^{239}Pu					
0·71	0·00502	0·00507	0·00508	0·00509	0·00509
1·46	0·00487	0·00495	0·00498	0·00500	0·00500
2·21	0·00479	0·00490	0·00492	0·00494	0·00496
(c) Pure ^{239}Pu					
0·71	0·304	0·350	0·362	0·369	0·375
1·46	0·255	0·304	0·317	0·325	0·332
2·21	0·231	0·282	0·295	0·304	0·311

7. FUEL TEMPERATURE COEFFICIENTS

Approximate values of $(\partial I_9/\partial T)/I_9$ for the cases considered are given in Table 7. These are average values for the 3 rod sizes and may be compared with the corresponding values given by SCHAEFER (1960) of approximately $1{\cdot}4 \times 10^{-4}$, $1{\cdot}0 \times 10^{-4}$ and $0{\cdot}8 \times 10^{-4}$ for ^{238}U. The reduction in $(\partial I_9/\partial T)/I_9$ with dilution, which is seen from Table 7, is due to the reduction in resonance screening as the ^{239}Pu concentration is decreased.

TABLE 7.—APPROXIMATE VALUES OF $(\partial I_9/\partial T)/I_9$

Temperature range (°K)	0·15% ^{239}Pu	0·2% ^{239}Pu	Pure ^{239}Pu
300–600	$2{\cdot}8 \times 10^{-5}$	$2{\cdot}8 \times 10^{-5}$	$2{\cdot}4 \times 10^{-4}$
600–900	$1{\cdot}4 \times 10^{-5}$	$1{\cdot}9 \times 10^{-5}$	$1{\cdot}5 \times 10^{-4}$
900–1200	$1{\cdot}2 \times 10^{-5}$	$1{\cdot}2 \times 10^{-5}$	$1{\cdot}1 \times 10^{-4}$

However, it is very difficult to draw any significant conclusions about the temperature coefficients of irradiated rods from the above values without considering the effect of inserting the plutonium resonance escape and resonance fission probabilities into a formula for the effective reproduction constant, k_e, of a typical reactor.

For un-irradiated uranium rods, k_e is given by

$$k_e = \Lambda_f \Lambda_t \eta f \varepsilon p_8, \tag{37}$$

where Λ_f and Λ_t are respectively the fast and thermal non-leakage probabilities, η is the thermal fission factor, f the thermal utilization factor and ε the fast fission factor.

However, when significant amounts of ^{239}Pu are present, equation (37) must be replaced by

$$k_e' = \Lambda_f \Lambda_t \eta f \varepsilon R, \tag{38}$$

where

$$R = p_8 p_9 + \nu P_f / \Lambda_t \eta f, \tag{39}$$

ν being the average number of fast neutrons produced per ^{239}Pu fission. The product ηf now includes thermal fission in plutonium as well as in uranium-235.

Thus assuming Λ_f, Λ_t, η, f and ε to be independent of temperature, we have, for the un-irradiated rods,

$$(\partial k_e/\partial T)/k_e = (\partial p_8/\partial T)/p_8 \tag{40}$$

while, for the irradiated rods,

$$(\partial k_e'/\partial T)/k_e' = (\partial R/\partial T)/R, \tag{41}$$

where R is defined by (39).

Values of $(\partial p_8/\partial T)/p_8$ and $(\partial R/\partial T)/R$ in a typical reactor for each of the plutonium concentrations considered are set out in Table 8, the value of $\nu/\Lambda_t \eta f$ being taken as 2·6 in each case.

TABLE 8.—TEMPERATURE COEFFICIENTS

Rod radius (cm)	Temp. (°K)	$(\partial p_8/\partial T)/p_8$	$(\partial R/\partial T)/R$ (0·15% ^{239}Pu)	$(\partial R/\partial T)/R$ (0·2% ^{239}Pu)
0·71	450	$-2{\cdot}67 \times 10^{-5}$	$-2{\cdot}64 \times 10^{-5}$	$-2{\cdot}64 \times 10^{-5}$
	750	$-2{\cdot}05 \times 10^{-5}$	$-2{\cdot}03 \times 10^{-5}$	$-2{\cdot}02 \times 10^{-5}$
	1050	$-1{\cdot}73 \times 10^{-5}$	$-1{\cdot}71 \times 10^{-5}$	$-1{\cdot}71 \times 10^{-5}$
1·46	450	$-2{\cdot}05 \times 10^{-5}$	$-2{\cdot}03 \times 10^{-5}$	$-2{\cdot}02 \times 10^{-5}$
	750	$-1{\cdot}58 \times 10^{-5}$	$-1{\cdot}56 \times 10^{-5}$	$-1{\cdot}55 \times 10^{-5}$
	1050	$-1{\cdot}33 \times 10^{-5}$	$-1{\cdot}32 \times 10^{-5}$	$-1{\cdot}32 \times 10^{-5}$
2·21	450	$-1{\cdot}78 \times 10^{-5}$	$-1{\cdot}76 \times 10^{-5}$	$-1{\cdot}76 \times 10^{-5}$
	750	$-1{\cdot}37 \times 10^{-5}$	$-1{\cdot}35 \times 10^{-5}$	$-1{\cdot}35 \times 10^{-5}$
	1050	$-1{\cdot}16 \times 10^{-5}$	$-1{\cdot}15 \times 10^{-5}$	$-1{\cdot}14 \times 10^{-5}$

8. POSSIBLE EFFECTS OF THE 0·296 eV RESONANCE

Although it is realized that other complicating factors have considerable significance at energies as low as 0·3 eV, it is of some interest to note the results of applying the theory used in this paper to the 0·296 eV resonance.

Application of the usual formula for the infinite dilution resonance integral gives a contribution from

this resonance of 2737 barns compared to 332 barns from all other resonances. This seems to indicate that there will be a comparatively large contribution to the effective resonance integral from this resonance, especially in the case of low concentrations of ^{239}Pu, when there is very little self-screening. This is borne out by the calculation of the approximate contributions from the 0·296 eV resonance in the different cases, using the same methods as for the other resonances. Results are given for rods of radius 1·46 cm in Table 9, together with corresponding approximate values for the resonance fission probability.

TABLE 9.—CONTRIBUTIONS FROM THE 0·296 eV RESONANCE (ROD RADIUS 1·46 cm)

(a) Effective resonance integral

	Temperature (°K)			
	300	600	900	1200
0·15% ^{239}Pu	3·43b	3·44b	3·45b	3·46b
0·2% ^{239}Pu	4·36	4·38	4·39	4·40
Pure ^{239}Pu	101	101	101	101

(b) Resonance fission probability

0·15% ^{239}Pu	0·0260	0·0259	0·0258	0·0258
0·2% ^{239}Pu	0·0333	0·0332	0·0331	0·0331
Pure ^{239}Pu	0·216	0·204	0·197	0·191

It will be noticed that there is a slight decrease in P_f as the temperature rises, in spite of the fact that I_9 exhibits the usual Doppler increase. This is due to the fact that P_f depends on the probability of escaping capture in ^{238}U and in the higher ^{239}Pu resonances. As the temperature rises, absorption in these higher energy resonances of ^{238}U and ^{239}Pu increases, so that fewer neutrons reach the lowest-energy resonances of ^{239}Pu. Doppler broadening of these resonances does lead to a slightly higher proportion of these neutrons being absorbed in ^{239}Pu, but not a high enough proportion to make up for the depletion caused by the additional ^{238}U absorption in higher energy resonances.

Results obtained for the fuel temperature coefficient when the 0·296 eV resonance is included are given for rods of radius 1·46 cm in Table 10. A more exact calculation by numerical integration of the contribution to the effective resonance integral from the 0·296 eV resonance gives values somewhat higher than those of Table 9, but results for the fuel temperature coefficient are not appreciably different from those of Table 10. It should be emphasized, however, that the effect of neutron thermalization, which will cause considerable distortion of the neutron spectrum in the region of this resonance has not been considered.

TABLE 10.—FUEL TEMPERATURE COEFFICIENTS INCLUDING THE 0·296 eV RESONANCE (Rod radius 1·46 cm)

Temperature (°K)	$(\partial\rho_8/\partial T)/\rho_8$	$(\partial R/\partial T)/R$ (0·15% ^{239}Pu)	$(\partial R/\partial T)/R$ (0·2% ^{239}Pu)
450	$-2{\cdot}05 \times 10^{-5}$	$-2{\cdot}02 \times 10^{-5}$	$-2{\cdot}01 \times 10^{-5}$
750	$-1{\cdot}58 \times 10^{-5}$	$-1{\cdot}55 \times 10^{-5}$	$-1{\cdot}54 \times 10^{-5}$
1050	$-1{\cdot}33 \times 10^{-5}$	$-1{\cdot}31 \times 10^{-5}$	$-1{\cdot}30 \times 10^{-5}$

9. CONCLUSION

In the case of pure ^{239}Pu rods it is evident that much more radiative capture takes place than in corresponding rods of natural uranium, but that this is easily surpassed by the amount of resonance fission. A considerable proportion of the resonance absorption occurs in the unresolved region, but the major contribution appears to be from the 0·3 eV resonance. Almost all of the Doppler increase in the effective resonance integral occurs in the unresolved region.

In the case of irradiated uranium rods, where self-screening of the ^{239}Pu resonances is much less, the major ^{239}Pu contributors both to the effective resonance integral and to the Doppler increase are the strong low-energy resonances, particularly the 0·3 eV resonance. The small amount of self-screening causes the total Doppler increase to be quite small, so that only a small effect on the fuel temperature coefficient may be expected. However, this effect is made smaller still by the fact that Doppler broadening of the ^{238}U resonances leads to a smaller proportion of neutrons reaching the low-energy ^{239}Pu resonances as the temperature rises, so that the total fraction of neutrons absorbed in ^{239}Pu while slowing down actually decreases slightly. Thus the presence of ^{239}Pu in irradiated uranium rods has practically no effect on the fuel temperature coefficient.

It should be emphasized that no allowance has been made for spectrum distortion in the region of the 0·3 eV resonance due to neutron thermalization. It is expected that this could give rise to a further contribution to the fuel temperature coefficient of the same order of magnitude as the effect deduced in this paper.

Acknowledgments—The author wishes to express his gratitude to The General Electric Company Ltd., who made it possible for him to carry out the work reported here. He is also indebted to DRS. P. A. EGELSTAFF and G. W. SCHAEFER and to MESSRS. H. T. RICHARDSON, P. D. RUSSELL and J. J. SYRETT for helpful discussions and advice during the early stages of the preparation of this paper. Further grateful thanks are due to MR. SYRETT for several useful suggestions after a critical reading of the manuscript.

REFERENCES

Adler F. T., Hinman G. W. and Nordheim L. W. (1958) *Proceedings of the Second International Conference on the Peaceful Uses of Atomic Energy, Geneva*, P/1988. United Nations, N. Y.

Bollinger L. M., Cote R. E. and Thomas G. E. (1958) *Proceedings of the Second International Conference on the Peaceful Uses of Atomic Energy, Geneva*, P/687. United Nations, N.Y.

Case K. M., Hoffman F. de and Placzek G. (1953) *Introduction to the Theory of Neutron Diffusion*, pp. 17–42. U.S. Government Printing Office, Washington D.C.

Dresner L. (1956) *Nucl. Sci. Engng.* **1,** 68.

Egelstaff P. A., GaythER D. B. and Nicholson L. F. (1958) *J. Nucl. Energy* **6,** 303.

Farley F. J. M. (1956) *J. Nucl. Energy* **3,** 33.

Gurevich I. I. and Pomeranchouk I. Y. (1955). *Proceedings of the Second International Conference on the Peaceful Uses of Atomic Energy, Geneva*, P/649. United Nations, N.Y.

Hughes D. J., Magurno B. A. and Brussel M. K. (1960) *Neutron Cross-Sections*, Supplement No. 1. BNL-325, 2nd (Edn.) U.S. Government Printing Office, Washington D.C.

McKay M. H. and Keane A. (1960) *Aust. J. appl. Sci.* **11,** 1.

Schaeffer G. W. (1960) Private communication.

Sokolovsky V. V., Vladimirsky V. V., Radkevich I. A. and Panov A. A. (1957) *J. Nucl. Energy* **5,** 389.

Wigner E. P., Creutz E., Jupnik H. and Snyder T. (1955) *J. appl. Phys.* **26,** 260.

VOL
14
196

Reactor Science and Technology (J.N.E. Parts A/B), 1961, Vol. 14, pp. 209 to 211. Pergamon Press Ltd. Printed in Northern Ireland

A DIRECT METHOD FOR THE EVALUATION OF THE RESONANCE LINE SHAPE FUNCTIONS*

F. T. ADLER and Y. D. NALIBOFF
Department of Physics, University of Illinois, Urbana, U.S.A.

(*First received* 30 *June* 1960 *and in revised form* 23 *November* 1960)

Abstract—The determination of the line shape functions ψ and χ describing the Doppler broadening of neutron cross sections often requires lengthy numerical calculations. A direct method for calculating ψ and χ presented here is significantly faster for computer applications than procedures currently in use. The functions may be used in the usual prescriptions, or in a more accurate one based on the reaction rate.

1. EVALUATION OF THE LINE SHAPE FUNCTIONS

THE possibility of providing tables or efficient machine programmes for the calculation of Doppler-broadened cross sections, as needed in multigroup constant calculations, resonance escape problems and temperature coefficient studies, depends on the ease with which the function

$$\psi(x,t) = \frac{1}{2\sqrt{\pi t}} \int_{-\infty}^{\infty} \frac{dy}{1+y^2} e^{-(x-y)^2/4t} \qquad (1)$$

can be calculated. Various asymptotic forms are available (BORN, 1933; DRESNER, 1959) but they are not sufficient for most calculations. Much of the work done in resonance escape calculations (DRESNER, 1959; ADLER *et al.*, 1958) has been based on ψ values calculated by lengthy numerical integration.

In practical applications, ψ occurs in the integrand of several-fold integrals. Thus the calculation of ψ consumes a major part of the computing time. The method for calculating ψ presented here is significantly faster than those previously available and contains no arbitrary truncation factors.

The approximation for ψ given here depends on replacing the exponential in (1) by an accurate approximating polynomial (HASTINGS, 1955):

$$e^{-x^2/2} = \frac{\sqrt{2\pi}}{\sum_{i=1}^{5} b_{2i} x^{2i}} = \frac{\sqrt{2\pi}}{p(x)}. \qquad (2)$$

With the change of variable $z = \dfrac{x-y}{2t}$ one obtains

$$\psi(x,t) = \int_{-\infty}^{\infty} \frac{dz}{p(z)} \frac{1}{1+(x-z\sqrt{2t})^2} = \int_{-\infty}^{\infty} \frac{dz}{p(z)q(z)} \qquad (3)$$

The integral for ψ in (3) is now easily evaluated by means of the Cauchy integral formula, the result being:

$$\psi(x,t) = 2\pi i \left(\sum_{i=1}^{5} \frac{1}{p'(c_i)q(c_i)} + \frac{1}{p(c_6)q'(c_6)} \right) \qquad (4)$$

where $c_1, \ldots, c_5$ are the roots of $p(z) = 0$ in the upper half-plane, c_6 is the root of $q(z) = 0$ in the upper half-plane, and $p'(z) = \dfrac{dp}{dz}$. It should be noted that if c_6 coincides with some c_j, two first-order poles coalesce into a single second-order pole so that there is no contribution to ψ from either the term in c_j or the term in c_6. Moreover the roots c_i are constants and independent of x and t.

This method is easily extended to the function $\chi(s,t)$, which is necessary for calculating the asymmetric broadened line shape describing resonance scattering:

$$\begin{aligned}\chi(x,t) &= \frac{1}{\sqrt{2\pi t}} \int_{-\infty}^{\infty} \frac{y\,dy}{1+y^2} e^{-(x-y)^2/4t} \\ &= \int_{-\infty}^{\infty} \frac{(x - z\sqrt{2t})\,dz}{p(z)q(z)} \\ &= x\psi(x,t) - \sqrt{2t} \int_{-\infty}^{\infty} \frac{z\,dz}{p(z)q(z)} \\ &= x(\psi x,t) - \sqrt{2t} \\ &\quad \times \left[2\pi i \left(\sum_{i=1}^{5} \frac{c_i}{p'(c_i)q(c_i)} + \frac{c_6}{p(c_6)q'(c_6)} \right) \right] \end{aligned} \qquad (5)$$

We note that the two calculations for χ and ψ can be done simultaneously, and thus require little more time than the calculations of ψ alone.

For machine calculation, it is advantageous to rewrite ψ as:

$$\psi(x,t) = 2\pi \left(\sum_{i=1}^{5} \frac{(q_1 p_2' + q_2 p_1')_i}{(p_1' q_1 - p_2' q_2)_i^2 + (q_1 p_2' + q_2 p_1')_i^2} + \frac{p_6^1}{2\sqrt{2t}[(p_6^1)^2 + (p_6^2)^2]} \right) \qquad (6)$$

* This research was supported in part by the Office of Naval Research.

where

$$(q_1)_i = \mathrm{Re}\, q(c_i) = 1 + x^2 - 2x\sqrt{2t}\,\mathrm{Re}\,(c_i) + 2t[(\mathrm{Re}\,(c_i))^2 - (\mathrm{Im}\,(c_i))^2]$$

$$(q_2)_i = \mathrm{Im}\, q(c_i) = -2x\sqrt{2t}\,\mathrm{Im}\,(c_i) + 4t\,\mathrm{Re}\,(c_i)\,\mathrm{Im}\,(c_i)$$

$$p_6^1 = \mathrm{Re}\, q(c_6) \qquad p_6^2 = \mathrm{Im}\, q(c_6)$$

$$c_6^1 = \mathrm{Re}\,(c_6) = x/\sqrt{2t} \qquad c_6^2 = \mathrm{Im}\,(c_6) = 1/\sqrt{2t}$$

$$(p_1')_i = \mathrm{Re}\, p'(c_i) \qquad (p_2')_i = \mathrm{Im}\, p'(c_i)$$

$$p'(z) = \sum_{i=1}^{5} (2i) b_{2i} x^{2i-1}$$

The data necessary for evaluating ψ and χ are summarized in Tables 1 to 3, which give the HASTINGS coefficients, the roots of $p(z) = 0$ in the upper half-plane, and the values of $p'(c_i)$.

TABLE 1.—THE HASTINGS COEFFICIENTS

$b_0 = 2{\cdot}5052367$	$b_8 = 0{\cdot}1306469$
$b_2 = 1{\cdot}2831204$	$b_8 = -0{\cdot}0202490$
$b_4 = 0{\cdot}2264718$	$b_{10} = 0{\cdot}0039132$

TABLE 2.—c_i, THE ROOTS OF $p(z) = 0$ IN THE UPPER HALF-PLANE

$c_1 = 0$	$+1{\cdot}32271498\,i$
$c_2 = 1{\cdot}09147894$	$+1{\cdot}29081178\,i$
$c_3 = -2{\cdot}30555691$	$+1{\cdot}17416680\,i$
$c_4 = -1{\cdot}09147894$	$+1{\cdot}29081178\,i$
$c_5 = 2{\cdot}30555691$	$+1{\cdot}17416680\,i$

TABLE 3 —$p'(c_i)$

$p'(c_1) = 0$	$+6{\cdot}1043246\,i$
$p'(c_2) = -10{\cdot}9663038$	$+1{\cdot}1317230\,i$
$p'(c_3) = 24{\cdot}240703$	$-78{\cdot}663636\,i$
$p'(c_4) = 10{\cdot}9663038$	$+1{\cdot}1317236\,i$
$p'(c_5) = -24{\cdot}240703$	$-78{\cdot}663636\,i$

Values of ψ calculated by this approximation agree with tabulated values to within a few hundredths of a per cent over the range in which simple asymptotic forms are not applicable.

An IBM subroutine for the evaluation of ψ has been written requiring a time of less than one second per ψ value. A FORTRAN subroutine for the simultaneous evaluation of ψ and χ is also available.

2. REACTION RATES

The functions ψ and χ given here can be used directly in the standard prescription for calculating Doppler-broadened cross sections (ADLER *et al.*, 1958). In a more accurate formulation, based on the reaction rate concept, (MEGHREBLIAN and HOLMES, 1960) one obtains cross sections which can also be expressed in terms of ψ and χ. In this case, the cross section for a neutron of energy E_n in the laboratory system is given by:

$$\sigma(E_n) = \left[\left(\frac{M+1}{M}\right)^{/2} \Big/ \Delta\sqrt{\pi}\right] \int_0^\infty dE \sqrt{\frac{E}{E_n}}\,\sigma(E) \times \exp -\left[E_n - \left(\frac{M+1}{M}\right)E\right]^2 \Big/ \Delta^2 \qquad (7)$$

where

M = mass of nucleus in terms of the neutron mass,
kT = temperature of the resonance absorber, in energy units,
$\Delta = \sqrt{4kTE_n/M}$,
$\sigma(E)$ = neutron-nucleus cross section as a function of their relative energy.

The presence of the factor $\sqrt{E/E_n}$ was pointed out by COVEYOU (1951).

Aside from a few higher-order correction terms, the expressions for the cross sections given below are identical to those obtained by NEUMANN (1956). Using a single level Breit-Wigner formula, one obtains for the absorption and scattering cross sections from equation (7):

$$\sigma_a(E_n) = \frac{\sqrt{\pi}\lambda_0^2 g}{\Delta}\frac{\Gamma_n\Gamma_\gamma}{\Gamma/2}\left(\frac{M+1}{M}\right)^{3/2}\sqrt{\frac{E_0}{E_n}} \times \int_{-\infty}^{\infty}\frac{dy}{1+y^2}\,\mathrm{e}^{-(x-y)^2/4t} \qquad (8)$$

$$\sigma_s(E_n) = \frac{\sqrt{\pi}\lambda_0^2 g}{\Delta}\,2\Gamma\left(\frac{M+1}{M}\right)^{3/2} \times \sqrt{\frac{E_0}{E_n}}\left[\frac{\Gamma_n^2}{\Gamma^2}\int_{-\infty}^{\infty}\frac{dy}{1+y^2} \times\sqrt{1+\frac{\Gamma}{2E_0}y}\,\mathrm{e}^{-(x-y)^2/4t} + 2\frac{\Gamma_n}{\Gamma}\frac{R}{\lambda_0}\int_{-\infty}^{\infty}\frac{y\,dy}{1+y^2} \times\sqrt{1+\frac{\Gamma}{2E_0}y}\,\mathrm{e}^{-(x-y)^2/4t}\right] \qquad (9)$$

where

$\Gamma_n, \Gamma_\gamma, \Gamma$ = neutron, absorption, and total widths,
E_0 = resonance energy,
g = statistical factor,
λ_0 = reduced neutron wavelength at E_0,
$x = 2(E_n - E_0)/\Gamma$,
$t = 4kTE_nM/(\Gamma^2(M+1))$
and $y = (E - E_0)/(\Gamma/2)$ is the integration variable.

Actually, the lower limit of the integrals should

be $-E_0/(\Gamma/2)$. The errors introduced by setting this limit to $-\infty$ are negligible for ^{232}Th and ^{238}U, where the smallest value of $2E_0/\Gamma$ is about 600*

Equation (8) now gives the usual form for the Doppler-broadened absorption cross section:

$$\sigma_a(E_n) = \sigma_{a_0}\sqrt{\frac{\overline{E_0}}{E_n}}\,\psi(x,t) \tag{10}$$

where

$$\sigma_{a_0} = 4\pi\lambda_0^2 g\,\frac{\Gamma_n\Gamma_\gamma}{\Gamma^2}\sqrt{\frac{M+1}{M}} \tag{11}$$

We note that equation (10) is exact in this approach; in the usual procedure, it is obtained by approximating $1/\sqrt{E}$ within the integral in equation (8) with $1/\sqrt{E_0}$.

In order to express the scattering cross section in terms of ψ and χ, the radicals in equation (9) must be expanded:

$$\int_{-\infty}^{\infty}\frac{dy}{1+y^2}\sqrt{1+\frac{\Gamma}{2E_0}y}\,e^{-(x-y)^2/u} \cong \sqrt{4\pi t}\times\left[\psi+\frac{\Gamma}{4E_0}\chi-\frac{\Gamma^2}{32E_0^2}(1-\psi)\right] \tag{12}$$

$$\int_{-\infty}^{\infty}\frac{y\,dy}{1+y^2}\sqrt{1+\frac{\Gamma}{2E_0}y}\,e^{-(x-y)^2/u} \simeq \sqrt{4\pi t}\times\left[\chi+\frac{\Gamma}{4E_0}(1-\psi)-\frac{\Gamma^2}{32E_0^2}(x-\chi)\right] \tag{13}$$

* In materials with low, wide resonances (such as ^{239}Pu), $2E_0/\Gamma$ is of the order of 4 or 5, and a maximum error is of the order of 1–2 per cent. For the lowest resonances, special provision can be made for correcting the standard functions ψ and χ.

The Doppler-broadened scattering cross section can then be written in the form:

$$\sigma_s(E_n) = \sigma_p + \sigma_{s_0}\sqrt{\frac{\overline{E_0}}{E_n}}\,\psi(x,t) + \Gamma\sigma_{s_0}\sqrt{\frac{\overline{E_0}}{E_n}}\times\left[\frac{2}{\lambda_0}\frac{R}{\Gamma_n}+\frac{1}{4E_0}+\frac{\overline{R\Gamma^2}}{16\lambda_0\Gamma_n E_0^2}\right]\chi(x,t) + \sigma_{s_0}\sqrt{\frac{\overline{E_0}}{E_n}}\,\frac{R\Gamma^2}{2\lambda_0\Gamma_n E_0}\left[1-\frac{\lambda_0}{16RE_0}\right]\times(1-\psi(x,t)) - 2\sigma_{s_0}\sqrt{\frac{\overline{E_0}}{E_n}}\,\frac{\Gamma}{\Gamma_n}\frac{R}{\lambda_0}x \tag{14}$$

where

$$\sigma_{s_0} = 4\pi\lambda_0^2 g\,\frac{\Gamma_n^2}{\Gamma^2}\sqrt{\frac{M+1}{M}} \tag{15}$$

and σ_p is the constant potential scattering cross section.

REFERENCES

Adler F. T., Hinman G. W. and Nordheim L. W. (1958) *The Quantitative Evaluation of Resonance Integrals.* UN/P/1988 (GA-350).

Born M. (1933) *Optik*, Springer-Verlag, Berlin.

Coveyou R. D. (1951) *Note on the Doppler Effect.* AECD-3350.

Dresner L. (1959) *Resonance Absorption of Neutrons in Nuclear Reactors.* ORNL-2659.

Hastings C. Jr. (1955) *Approximations for Digital Computers*, Princeton University Press.

Meghreblian R. V. and Holmes D. K. (1960) *Reactor Analysis*, McGraw-Hill.

Neuman H. (1956) *Proceedings of the Brookhaven Conference on Resonance Absorption of Neutrons in Nuclear Reactors*, BNL-433 (C-24).

Reactor Science and Technology (J.N.E. Parts A/B), 1961, Vol. 14, pp. 212 to 213. Pergamon Press Ltd. Printed in Northern Ireland

LETTER TO THE EDITOR

The absorption of neutrons by the $^{16}O(n,\alpha)^{13}C$ reaction in an extended water moderator

(*Received* 9 *December* 1960)

MOST neutron source calibrations and comparisons depend on the measurement of thermal neutron densities in an extended moderator surrounding the source. To a first approximation such measurements are independent of source energy. Since the thermal neutron density is used as a measure of the source strength any process which prevents thermalization, or absorbs neutrons at energies above thermal will lead to an underestimate of the source strength.

The oxygen in water, most commonly used as a moderating material causes significant absorption of neutrons above 4 MeV by the $^{16}O(n,\alpha)^{13}C$ reaction. Sulphur (used for example as $MnSO_4$) also absorbs neutrons above 2 MeV. In an extended water moderator the absorption of neutrons from a Ra-α-Be source amounts to approximately 2 per cent.

Only two measurements of this absorption have been reported. An estimate was made by ELLIOTT (1948) during an attempt to detect an (n,2n) reaction in D_2O. DE TROYER (1954) measured the absorption during an absolute calibration of a Ra-α-Be source by means of gold foils in a water bath. Both measurements followed a similar pattern. Two neutron sources, one having a high proportion of neutrons above 4 MeV and the other emitting all its neutrons with energies less than 1 MeV, were compared by measuring the thermal neutron density around them in a large tank of paraffin oil. The same comparison in a large tank of water appeared to show that the high energy source was reduced in strength. The amount of this reduction is a measure of the fraction of neutrons absorbed by the oxygen in the water bath.

Their results are given in Table 1, and although the high energy sources used were slightly different their results are not inconsistent.

A calculation of the absorption was reported by HUBER (1950 and 1955) who interpolated the $^{16}O(n,\alpha)$ cross section between his measured values from 3·65 to 4·2 MeV and the value obtained by LILLIE (1952) at 14 MeV. This gave an absorption of 3 per cent for a Ra-α-Be source in water and agreed with the earlier experimental results given above. However, when the same cross section and Ra-α-Be neutron spectrum were used in a similar calculation at this laboratory the result obtained was much higher than the experimental value. The absorption calculated here was 7 per cent. It was inferred that the assumed $^{16}O(n,\alpha)$ cross section was too large.

TABLE 1.—$^{16}O(n,\alpha)^{13}C$ ABSORPTION IN WATER

Neutron source	Absorption % of total neutrons	Reference
Po-α-Be	3·4 ± 2·1	ELLIOTT (1948)
Ra-α-Be	2·2 ± 0·3*	DE TROYER (1954)

* DE TROYER and TAVERNIER (1954) quote 2·5 ± 0·3, but GEIGER (1959) points out that the integrals quoted in their report lead to a value of 2·2 ± 0·3.

More recently the $^{16}O(n,\alpha)$ cross section has been measured directly (WALTON *et al.*, 1956 and 1957) up to 5·2 MeV neutron energy, and values can be deduced up to 5·6 MeV by considering detailed balancing on the inverse reaction $^{13}C(\alpha,n)$ whose cross section has also been measured (BONNER *et al.*, 1956). Above 5·6 MeV the $^{16}O(n,\alpha)$ reaction can lead to excited states of ^{13}C so that although the detailed balancing can be used to estimate the $^{16}O(n,\alpha)$ cross section up to 6·2 MeV, in the range 5·6 to 6·2 MeV it does not include that part of the cross section which results in excitation of the ^{13}C nucleus. From 5·6 to 6·2 MeV the estimated values are therefore too small. Figure 1 shows the $^{16}O(n,\alpha)$ cross section and includes HUBER's interpolated values which are too high in the important energy range up to 5·2 MeV.

Using the measured and calculated values of the $^{16}O(n,\alpha)$ cross section up to 5·6 MeV and a value of 100 ± 50 mb above 5·6 MeV, the absorption calculated by the formula below for a Ra-α-Be source in water is (1·80 ± 0·40) per cent.

$$\text{Absorption} = \int_{E_t}^{\infty} \frac{N(E)\,\sigma_0(E)\,dE}{\sigma_H(E)}$$

where $N(E)\,dE$ is the number of source neutrons in the energy interval E to $E + dE$, $\sigma_0(E)$ is the oxygen capture cross section

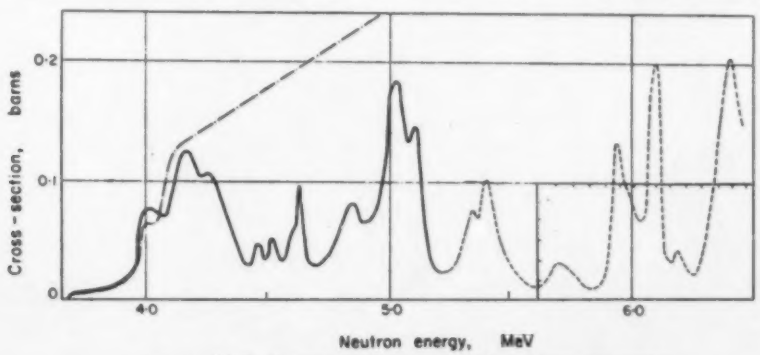

FIG. 1.—$^{16}O(n,\alpha)$ cross section as a function of neutron energy.
———— Measured values. — . — . — values from HUBER and SEITZ (1950).
– – – – – values calculated from inverse reaction. + + + + assumed extrapolation above 5·6 MeV.

in (cm)$^{-1}$ and $\sigma_H(E)$ is the hydrogen scattering cross section in (cm)$^{-1}$ E is the neutron energy and t denotes the threshold of the capture reaction. The spectrum is normalized so that

$$\int_0^\infty N(E)\,dE = 1.$$

As a check on the calculated absorption an experiment similar to the earlier ones (ELLIOTT, 1948; DE TROYER, 1954) has been performed here. The two sources were a Ra-α-Be and a 'mock fission.' They were compared in an oil bath and in a water bath. The thermal density was integrated in each by a 1 cm diameter, 5 cm long BF_3 counter. The apparent reduction in the strength of the Ra-α-Be source in the water bath was (0·4 ± 1·3) per cent. The calculated absorption for the mock fission source is small (0·26) ± 0·04) per cent and is not sensitive

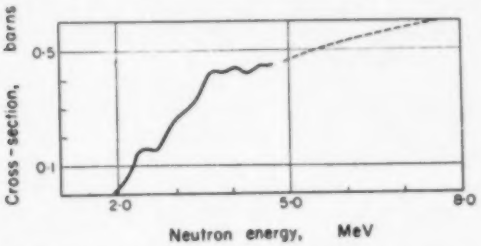

FIG. 2.—S(n,p) + S(n,α) cross section as a function of neutron energy.
———— Measured values.
- - - - - - assumed extrapolation.

to changes in the $^{16}O(n,\alpha)$ cross section above 5·2 MeV. Adding this to the apparent reduction for the Ra-α-Be source gives (0·7 ± 1·3) per cent for the total-absorption for a Ra-α-Be source in water by the $^{16}O(n,\alpha)$ reaction.

TABLE 2.—$^{16}O(n,\alpha)^{13}C$ ABSORPTION IN WATER, SUMMARY OF RESULTS (PERCENTAGE OF TOTAL NEUTRONS)

Calculated values	Reference	Experimental values	Reference
3·0	HUBER (1950)	3·4 ± 2·1	ELLIOTT (1948)
7·3	This work, using data of HUBER (1950)	2·2 ± 0·3	DE TROYER (1954)
1·8 ± 0·4	This work	0·7 ± 1·3	This work

The various results are compared below. They all refer to the absorption for a Ra-α-Be source in water, except for ELLIOTT's result which is for a Po-α-Be source which, in any case, has a similar spectrum.

TABLE 3.—ABSORPTION (PERCENTAGE) IN A $MnSO_4$ BATH

Source	Absorption S(n,p) + S(n,α)	Absorption $^{16}O(n,\alpha)$	Total absorption
Fission	0·20 ± 0·01	0·34 ± 0·05	0·54 ± 0·05
Po-α-Be	0·80 ± 0·05	2·00 ± 0·49	2·80 ± 0·50
Ra-α-Be	0·97 ± 0·05	2·39 ± 0·49	3·36 ± 0·50

The latest calculations and the most accurate experimental values are not inconsistent. Combining the results given in Table 1, omitting the calculated values based on the $^{16}O(n,\alpha)$ cross sections now known to be in error, the overall absorption is (2·0 ± 0·2) per cent. This suggests that calculated values may tend to be slightly low, but within the quoted errors the method of calculation appears to be quite reliable.

The following absorption corrections have therefore been calculated for the (concentrated) $MnSO_4$ solution bath currently used for comparing source strengths here. The S(n.p) and S(n,α) cross sections are shown together in Fig. 2.

The bath composition is:

oxygen 1060 g/litre, hydrogen 105 g/litre, manganese 189 g/litre, sulphur 111 g/litre. Its density is 1·465 g/cm^3.

M. H. MCTAGGART

Atomic Weapons Research Establishment
Aldermaston, Berks.

REFERENCES

BONNER T. W. *et al.* (1956) *Phys. Rev.* **102**, No. 5, 1348.
ELLIOTT L. G. and HINKS E. P. (1948) *Canad. J. Res.* 386.
GEIGER K. W. and WHYTE G. N. (1959) *Canad. J. Phys.* **37**, 256.
HUBER P. and SEITZ J. (1950) *Helv. Phys. Acta* **23**, 651; (1955) *Proceedings of the First International Conference on the Peaceful Uses of Atomic Energy, Geneva*, **2**, 121. United Nations, N.Y.
LILLIE A. B. (1952) *Phys. Rev.* **87**, 716.
TROYER A. DE and TAVERNIER G. C. (1954) *Bull. Acad. Roy. Belg.* **40**, 150.
WALTON R. B., CLEMENT J. D. and BORELLI F. (1956) *Bull. Acad. Phys. Soc., Series II* **1**, 326.
WALTON R. B. *et al.* (1957) *Phys. Rev.* **107**, No. 4, 1065.

VOL. 14 1961

Reactor Science and Technology (J.N.E. Parts A/B). 1961, Vol. 14, p. 214. Pergamon Press Ltd. Printed in Northern Ireland

BOOK REVIEW

High-Energy Electron Scattering Tables, ROBERT HERMAN and ROBERT HOFSTADER, Stanford University Press, Stanford, Calif., 1960. 278 pp., $8.50.

HIGH-ENERGY electron scattering yields data on the size and charge distribution of nucleons and nuclei. These data correspond to the form factors of atoms and molecules obtained by scattering of X-rays and low-energy electrons, and are of interest for various purposes of nuclear physics, and thus, indirectly, also for nuclear engineering. Rough nuclear models, discussed in this book, are sufficient, f.i., for calculations of multiple scattering. Moreover, nuclear size, entering into the cloudy-crystal-ball model, has to be in agreement with the size obtained from electron scattering. Tables in this book give the connexion between size, cross section and charge distribution. The book will naturally be of greatest use to experimental and theoretical workers in the high-energy electron field.

The first 80 pages contain the analytical foundation for the graphs and tables of the rest of the book. It gives brief discussions of the first Born approximation including its accuracy; the approximation is valid for nucleons and light nuclei. Next, the choice of nuclear models is explained. The tables and their preparation are described at some length. Proton, neutron and particularly the deuteron are discussed in some detail. The alpha particle and nuclei of the first *p*-shell are treated next very briefly, as are medium and heavy nuclei for which the first Born approximation is not adequate. Next kinematic relations are presented. The nuclear size parameters determined from experiments are summarized. Scattering of muons is briefly touched upon (the muon behaves like an electron, there is no need for a form factor).

The book is authoritative, as expected from the writers. R. Herman is a well-known and versatile experimental and theoretical physicist, presently associated with General Motors, while R. Hofstader initiated and developed the high-energy scattering method for the determination of nuclear form factors using the Stanford linear accelerators.

E. GUTH

VOL
14
196

Reactor Science and Technology (J.N.E. Parts A/B), 1961, Vol. 14, pp. 215 to 216. Pergamon Press Ltd. Printed in Northern Ireland

ABSTRACTS AND TITLES OF FUTURE PAPERS

Atomnaya Energiya

Vol. 10, No. 1

Time variation of the space and energy distributions of the neutrons from a pulsed source: I. G. DYAD'KIN and E. P. BATALINA.

A treatment is given of the time variation of the distribution and energy spectrum of neutrons from a pulsed source. (Transient states of this kind occur in geophysics, in the detection of oil-bearing strata, for example.) It is found that the time distribution for neutrons of any one energy has a Poisson distribution at almost all significant times. A formula is given for the variations in the energy spectrum in space and time; this implies that the variation of that spectrum in space is independent of the variation in time for certain ranges of distances and times. The two modes of variation are correlated in a fashion that can be allowed for outside those ranges. A formula is given for the mean-square moderation length as a function of time. All the relationships are presented as simple formulas having clear physical meanings.

The yields of fission fragments produced from ^{233}U and ^{239}Pu by fast neutrons: E. K. BONYUSHKIN, YU. S. ZAMYATNIN, V. V. SPEKTOR, V. V. RACHEV, V. R. NEGINA, and V. N. ZAMYATNINA.

Radiochemical methods have been used to measure the absolute yields of some fission products produced from ^{233}U and ^{239}Pu by 14·5-MeV neutrons and by neutrons having a fission spectrum. The shape of the curve representing the yield as a function of mass is discussed. The difference between the mean masses of the light and heavy groups is shown to be related to the mass number of the fissile isotope.

The best temperature for the regenerative water-heating system of a nuclear power station having a water-cooled and water-moderated reactor: YU. D. ARSEN'EV.

The base-point method is used to determine the best value for t_r, the temperature of regenerative heating, the best being that giving the minimum calculated consumption of electrical energy. It is shown that the t_r for a nuclear power station having a double water circuit is close to the maximum one as determined from the parameters of the steam leaving the first stage of the turbine.

Boundary conditions in the spherical-harmonic method: G. YA. RUMYANTSEV.

Equations are deduced by using spherical harmonics applied to a single-speed kinetic equation. The equations are analysed to derive the conditions at the boundary between two scattering media. It is found that those conditions define completely the solution obtained in an approximation of any order (the so-called P_N approximations are envisaged), including even orders. Great practical interest attaches to the possibility of using approximations of even order; for example, the method needed for P_2 is not very laborious, being the elementary theory of diffusion revised without substantial increase in complexity. (So far, even-order approximations, in particular P_4, have not been used in calculations.)

The reddening of minerals in uranium-bearing veins: YU. M. DYMKOV and B. V. BRODIN.

Descriptions are given of the various types of hematitization shown by siderite, ankerite, and iron manganocalcite in veins containing uraninite. It is found that the process can occur without relation in space to the uraninite either before or after orogenesis and for various reasons. The carbonates may be oxidized as a result of contact with hydro-thermal solutions; alternatively, the solutions may bring in hematite formed elsewhere in finely divided form. The process is radiogenic in origin when it occurs in regions surrounding lenses containing uraninite. Attention is directed to the practical importance of the various types of hematitization as signs of the presence of uranium in regions containing hydro-thermal veins.

The relation of structure to anisotropy in the thermal expansion for uranium, neptunium, and plutonium: N. T. CHEBOTAREV.

It is shown that the anisotropy in the thermal expansion of some modifications of U, Np, and Pu is related to changes in the structures of those modifications. It is found that in every case the anisotropy is caused by the weakening of four covalent bonds as the temperature rises, those bonds being variously placed with respect to the crystallographic directions. The relationships give a clearer conception of some properties peculiar to these three metals.

Structure and thermal expansion of δ and η plutonium: S. T. KONOBEEVSKII and N. T. CHEBOTAREV.

New ideas on the structures of the δ and η forms of plutonium are presented on the supposition that the bonds become increasingly covalent as the temperature decreases. The structures are considered as resulting from quite small deviations from an ideal face-centred lattice, the deviations being produced by four covalent bonds. It is found possible to explain some of the anomalous properties of the δ and η forms, in particular the increased atomic volumes and the negative values for the volume thermal-expansion coefficients.

Some aspects of means of locating radioisotopes and the problem of safe storage: P. V. ZIMAKOV and V. V. KULICHENKO.

It is claimed that fission products can be stored or disposed of quite safely if liquid wastes are transformed to solids. Materials such as glasses have considerable advantages as regards firmness of binding in minimum volumes. An analysis is given of the chemical basis of such modes of disposal, and a discussion is given of some aspects of the behaviour and state of fission fragments trapped by fusion in such materials. Results are given from fractional chemical and X-ray analyses to show that such materials are inhomogeneous, and that some features of the response to leaching can be explained on that basis. It is found that the radiation tends to favour an increase in the proportion of crystalline fractions.

VOL. 14 1961

Method of determining the dose received from inhaled decay products derived from radon: I. I. GUSAROV and V. K. LYAPIDEVSKII.

A new method is presented for use in determining the energy absorbed as a result of the inhalation of the decay products of radon; the method is based on the number of α particles emitted in the complete decay of the daughter products isolated from 1 litre of air. A method is proposed for determining the concentration of radon in terms of the number of α particles emitted in the complete decay of the daughter products collected on a filter from a continuously purified volume.

Letters to the Editor

The mean numbers $\bar{\nu}$ and η of neutrons produced in fission of ^{233}U and ^{239}Pu by 14 MeV neutrons: N. N. FLEROV and V. M. TALYZIN.

The effectiveness of a waveguide as the accelerating system of an electron synchrotron: A. N. DIDENKO and E. S. KOVALENKO.

Transformation of the energy of short-lived isotopes: M. G. MITEL'MAN, R. S. EROFEEV, and N. D. ROZENBLYUM.

Data on the separation of the isotopes of boron by means of volatile compounds: I. KISCH, I. OPAUSKI, and L. MATUS.

Measurement of self-absorption along the axis for a ^{60}Co preparation of cylindrical shape: K. K. AGLINTSEV, G. P. OSTROMUKHOVA, and E. A. KHOL'NOVA.

The attenuation of gamma rays by concrete and by certain soils: P. N. V'YUGOV, K. S. GONCHAROV, V. S. DEMENTII, and A. M. MANDRICHENKO.

News of Science and Technology

Bibliography

VOL.
14
196.

NOTICE

Journal of Nuclear Energy Part A: *Reactor Science* Vol. 12, Nos. 3/4

SINCE the publication of the translated article *Extracts from the Visitors' Book of the First Atomic Power Station* on page 193 of the above issue, it has been pointed out that the reference to S. G. REASON (included in the article, and queried in a footnote) probably refers to S. G. RISON who worked in the Department of Atomic Energy, London, during 1946–1947, and subsequently transferred to UNO. It is therefore feasible that he was in Moscow with a UN party.

Reprinted by Lithography in Poland
by Zakład Graficzny PWN w Łodzi

VOL.
14
961